NASA CR-
160404

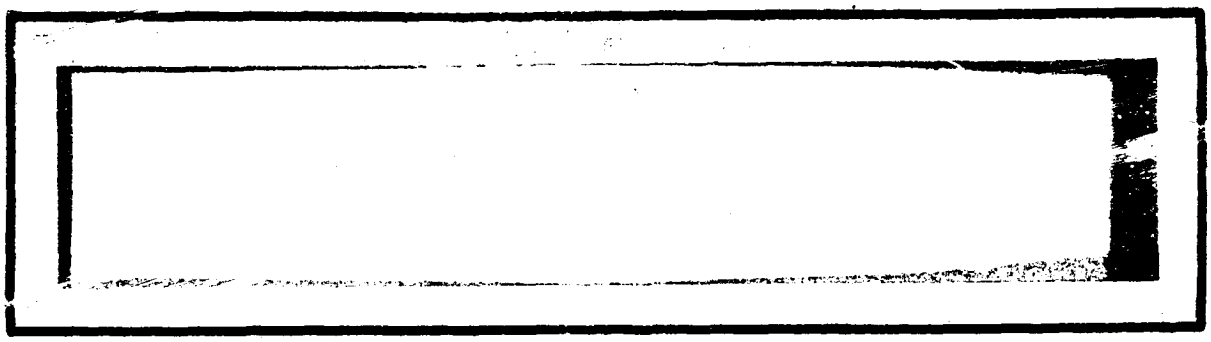

Axiomatix

(NASA-CR-160404) ORBITER CIU/IUS COMMUNICATIONS HARDWARE EVALUATION Summary Report no. 2 (Axiomatix, Los Angeles, Calif.) 411 p HC A18/MF A01 CSCL 17B

N80-13334

Unclas
G3/32 46342

ORBITER CIU/IUS COMMUNICATIONS HARDWARE EVALUATION

SECOND SUMMARY REPORT

Contract NAS 9-15409C

Technical Monitor: Don Pusch

Prepared for

NASA Lyndon B. Johnson Space Center
Houston, Texas 77058

Prepared by

S. Udalov

Contributions by

G. K. Huth
E. Kopp
R. G. Maronde
M. K. Simon

Axiomatix
9841 Airport Blvd., Suite 912
Los Angeles, California 90045

Axiomatix Report No. R7911-5
November 30, 1979

TABLE OF CONTENTS

LIST OF TABLES

LIST OF FIGURES

1.0 EXECUTIVE SUMMARY

This is a Second Summary Report for NASA Contract NAS 9-15409C. The effort period covered by this report extends from May 18, 1979 to November 30, 1979. The First Summary Report (Axiomatix Report R7906-8) was completed in May 1979.

1.1 Purpose of Effort and Degree of Performance

The primary effort of this study task is to provide for an evaluation of the DOD and NASA IUS communication system design, hardware specifications and interfaces to determine their compatibility with the Orbiter payload communications equipment (i.e., Payload Interrogator, PI, Payload Signal Processor, PSP, Communications Interface Unit, CIU) and the Orbiter operational communications equipment (i.e., the S-Band and Ku-band systems). The task requirements call for analysis of the design and test data and for the identification of potential problem areas, followed by suggestions of possible solutions.

The original contract statement of work identifies the following specific tasks that were to be performed:

Task 1: ICD Review and Interface Characterization
Task 2: Communication System Performance Analysis
Task 3: ESTL Test Requirements Update
Task 4: Final Report* Preparation

These four tasks were supplemented, along with a two-month contract period extension, by two add-on tasks listed below:

Task 5: SGLS Transponder Qualification Test Data Evaluation
Task 6: CIU and IUS Transponder Interface Issues.

During the contract period to be covered by this Summary Report (June to September 1979), two major design reviews were supported by Axiomatix. One was the Preliminary Design Review (PDR) of the STDN/TDRS S-band transponder (for use with NASA IUS); the second was the Critical Design Review (CDR) of the Communication Interface Unit (CIU) to be used for communication with DOD IUS. Consequently, a major portion of this

---

*Because of the continuing nature of the program, this "Final Report" is actually a Second Summary Report, the first report having been submitted at the end of June 1979.

summary report deals with Axiomatix's review, analysis, commentaries and recommendations pertaining to the technical material of the transponder PDR and CIU CDR data. Such emphasis is consistent with Tasks 1 and 2 of the contract.

Another major effort performed during the contract period was the preparation of an updated and detailed ESTL Test Requirements Plan. This activity was in accordance with Task 3 of the statement of work.

Of the two tasks (5 and 6) planned for the two-month extension, only task 6 could be worked on because of schedule slippage in the SGLS transponder qualification testing. With the approval of NASA, however, Axiomatix has performed extra work on Task 6 to compensate for not being able to proceed with Task 5. Thus, this report also contains a considerable amount of material pertaining to Task 6.

1.2 General Approach to the Activity

Development of the IUS, CIU and Orbiter payload communication equipment was a continuing activity in CY79. The general approach has been to work with the cognizant NASA personnel, USAF SAMSO personnel, Aerospace Corporation personnel, and individuals at the IUS prime contractor (Boeing Aerospace Company), the Orbiter prime contractor (Rockwell Int'l) and the IUS, CIU and Orbiter payload communication equipment subcontractor (TRW Defense and Space Group) to ascertain directions taken. A vital part of this activity has involved Axiomatix attendance and participation in design reviews (preliminary and critical) as well as special interface meetings. During the performance of the FY79 effort, Axiomatix provided technical support to the CIU Preliminary Design Review, the IUS SGLS Transponder Critical Design Review (CDR), the IUS Transponder Preliminary Review (PDR) and CIU Critical Design Review, as shown in Figure 1.1. Also shown in Figure 1.1 is a schedule for future design reviews and related activities which Axiomatix plans to support.

1.3 Contents of the Final Report

In addition to the Introduction section, there are three sections which address various specific aspects and details of the work performed.

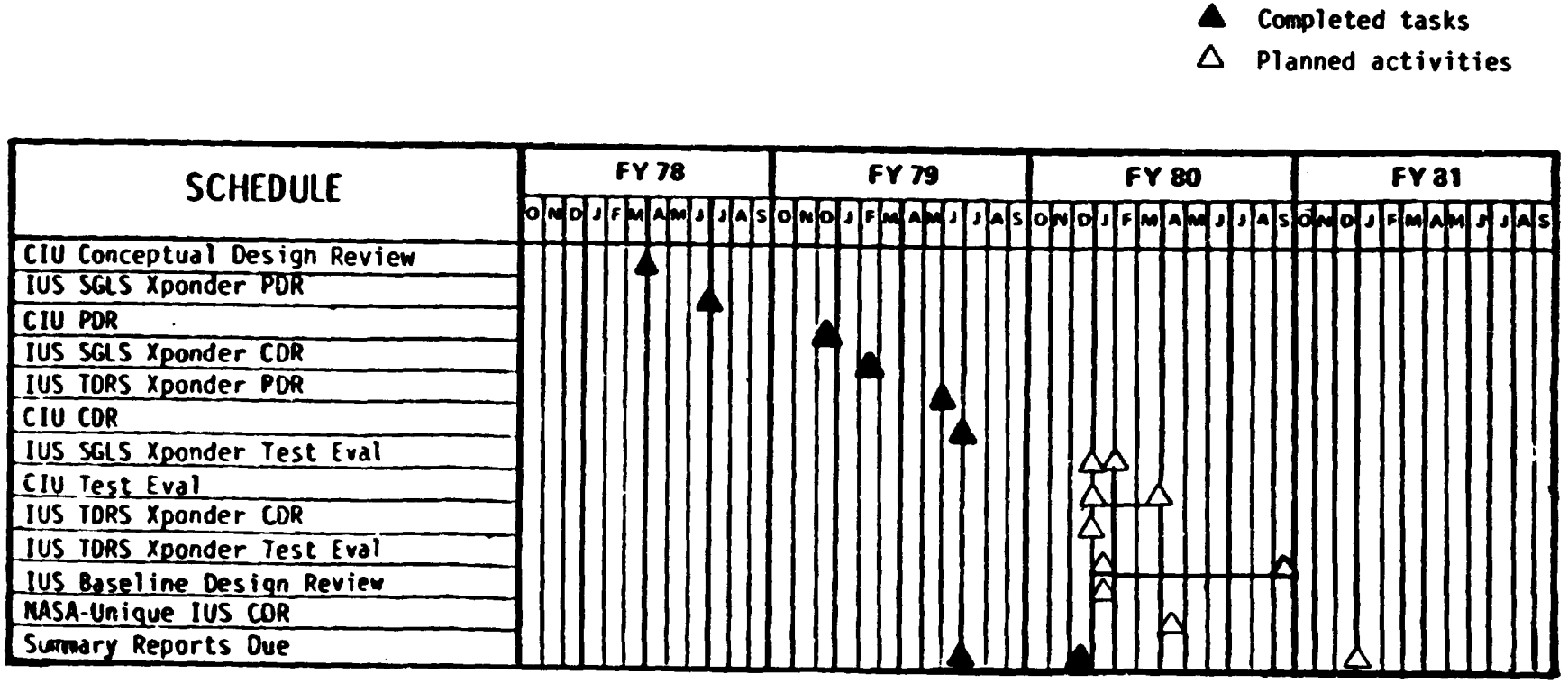

Figure ?.1. Orbiter CIU/IUS Communications Hardware Evaluation Program Schedule

Section 3.0 contains an overview of the IUS/Shuttle Orbiter communication equipment, with particular emphasis on the equipment serving the RF link. Included in this section are the considerations of close range operation of the IUS and Orbiter RF equipment. The predicted range capability is also presented.

Section 4.0 addresses the status of the IUS/Orbiter communication system development. It also provides a description of Axiomatix support activities. Issues closed and pending are enumerated and future activities are outlined.

Section 5.0 presents the description of the ESTL Test Plan.

Finally, Appendices A through F provide the detailed support material for Sections 4.0 and 5.0.

1.4 Principal Activities, Studies, Results and Assessments

Although the overall IUS/Orbiter communication system is progressing gradually towards a finalized design, there are still many areas which require additional attention in the technical sense.

Axiomatix has been following these areas and, wherever applicable, has responded with technical analysis and recommendations. On this program, Axiomatix has also been providing major original contributions such as action item responses and ESTL test plan preparation. Some of the major activities and studies, as well as the corresponding results and assessments, are described below.

1.4.1 STDN/TDRS S-Band Transponder-Related Activities

1.4.1.1 Action item regarding possible spurious components on downlink due to AM on 1.024 MHz PSK subcarrier

During the S-band STDN/TDRS transponder CDR of June 11-13, 1979 at Boeing, Seattle, NASA Goddard personnel expressed concern regarding the possible effects of AM on the 1.024 MHz PSK-modulated subcarrier. The concern was specifically directed towards the possibility of false locking the ground receiver to the RF spectral lines generated by AM on this subcarrier. Axiomatix took on the action item (Action Item 8) to investigate the causes and potential deleterious effects, if any, of AM on the 1.024 MHz PSK subcarrier.

In the course of our investigation, we established that the dominant cause of AM on the 1.024 MHz subcarrier is filtering this PSK-modulated subcarrier with a bandpass filter placed ahead of the linear phase modulator. The worst case of such AM occurs when a continuous stream of either "ones" or zeros" is PSK-modulated on the subcarrier.

However, the effect of the skirt selectivity provided by the subcarrier bandpass filter is definitely beneficial to the RF spur suppression while the AM caused by the filtering process does not, according to Axiomatix analysis, introduce any spurs into the RF spectrum of the phase-modulated carrier. In fact, the skirt selectivity of the bandpass filter helps to keep the potential false lock-up spurs far below the -60 dBc level, which is currently considered to be the threshold of lock-free operation. Specifically, our analysis indicates that, because of the filter selectivity, the ±64 kHz spur (worst case) in the vicinity of the downlink carrier can be kept down as low as -80 dBc.

Therefore, Axiomatix's conclusion is that the bandpass filter used for controlling the spectrum splatter of the PSK-modulated subcarrier within the baseband is indeed necessary and that the incidental AM caused by the filter has no deleterious effects on the RF spectrum.

The details of Axiomatix's analysis suporting this action item are given in Appendix A of this report.

1.4.1.2 Subanalyses Review

The STDN/TDRS S-band transponder PDR data package contained a number of subanalyses pertaining to the various aspects of the transponder performance. Axiomatix has reviewed all of these subanalyses and, where required, has carried out an independent analysis to verify, check and expand upon the analysis performed by the transponder contractor (TRW). Most of the subanalyses, after detailed examination by Axiomatix, were found to be valid and in agreement with our line of reasoning. Section 4.2.2 provides the summaries and conclusions resulting from our examination of these subanalyses. The subanalyses which required additional work by Axiomatix are summarized below:

1. Tracking Performance Analysis of a Filter/Square-Law Type Clock Recovery Loop

The IUS STDN/TDRSS transponder incorporates a command detector unit (CDU), part of whose function is to recover a 2 kbps clock from the received command data signal. A candidate configuration proposed by TRW to perform this function is configured as a baseband version of a squaring loop commonly used for carrier recovery. The contractor (TRW) for the NASA IUS transponder has analyzed the performance of this clock recovery loop for data transition density of 50% only. Axiomatix, therefore, has undertaken an independent analysis of the performance of this clock squaring loop to reflect the dependence on the data transition density.

As a result of our analysis, we have determined the optimum parameters for the command clock demodulator as functions of data transition density and signal-to-noise ratio. The detailed results are documented in Appendix C of this report.

2. Time-Shared Code Loop Performance Analysis

In the PN code reception mode, the NASA STDN/TDRS transponder has to first acquire the code and then track it. The method used for code tracking is that known as "tau-dither" mode. Having examined the contractor's (TRW) analysis of this tracking loop, Axiomatix personnel decided that a more detailed analysis is in order. Thus, we have carried out an independent analysis which provides an exact description of the PN tracker performance under various conditions. This analysis was one of the major tasks performed in place of Task 5. The results are included in Appendix F of this report.

3. Review of Spurious Analysis of STDN/TDRS Transponder Receiver and SGLS Transponder Receiver

A spurious response analysis of these receivers is valuable since they are of the double-conversion type and it is well-known that such receivers often have undesirable spurious responses. Moreover, the STDN and SGLS receivers are designed such that the second intermediate-frequency amplifier is part of a narrowband tracking loop which may give rise to additional spurious responses. Therefore, Axiomatix has reviewed the TRW analysis of the spurious responses of the STDN and SGLS transponder receivers to examine the possible spurs of these receivers and review the TRW analysis.

Specifically, for each of the spurs, we have computed all the relevant frequencies that appear in the signal path since these are necessary for a full understanding of the nature of the spurious responses. Axiomatix finds it satisfactory that only one spur arises from the use of a mixer not in the path and that this spur is not of a particularly troublesome level. Details of our analysis are given in Appendix B.

1.4.2 CIU-Related Activity

In the course of our participation in the CIU CDR (July 1979), Axiomatix acquired an extensive design package which it has been reviewing since then. Certain aspects of the CIU design have already been reviewed. The others remain to be analyzed. Specifically, the 1.024 MHz PSK demodulator design has been considered in detail as summarized below. The design of the analog FM demodulator has been reviewed, but remains to be analyzed in detail.

1.4.2.1 Review of CIU PSK demodulator performance analysis

Parts of the Orbiter avionics equipment serving the IUS are the CIU (communication interface unit) and the PSP (payload signal processor). The former is for DOD transponder (SGLS) communication and the latter is for NASA transponder (STDN/TDRS) communication. Because the PSP unit was developed prior to the CIU, a considerable amount of PSP technology has been applied by the PSP/CIU contractor (TRW) to the CIU implementation. Specifically, with respect to the demodulation of the PSK data received from the IUS SGLS transponder on a 1.024 MHz subcarrier, the implementation of the demodulator is identical to that of the PSP unit. In fact, TRW has included in their CIU CDR (critical design review) package the analysis of the PSP demodulator for the support of the predicted performance of a similar demodulator employed by the CIU.

Because of the importance of the PSK demodulator in determining the IUS/Orbiter link performance, Axiomatix has undertaken a close examination of the PSK demodulator analysis. As the result of this examination, we have determined certain limitations of the CDR analysis and have thus "filled in the gaps" by providing our inputs. The significance of our analysis is that it describes the expected PSK demodulator performance over the wider range of signal-to-noise (SNR) ratios, thus

providing information with regard to demodulator optimization at various SNR's. The details of this Axiomatix analysis are included in Appendix E of this report.

1.4.3 ESTL Test Requirements Plan

One of the major tasks accomplished by Axiomatix during the reporting period was the preparation of the ESTL Test Requirements Plan document. This document presents a plan for performing verification tests between the Inertial Upper Stage (IUS) and the DOD Communication Interface Unit (CIU) or NASA Payload Signal Processor (PSP) communication systems. These tests, which will be performed in the NASA Lyndon B. Johnson Space Center (JSC) Electronic System Test Laboratory (ESTL), are designed to establish that the communications link between the IUS and CIU or PSP is compatible and that the system performance will meet the requirements of the Shuttle program. Both DOD and NASA IUS configurations will be verified during the ESTL testing.

To implement these tests, Orbiter and IUS communications hardware must be obtained and installed in a representative mission configuration in the ESTL. Therefore, the communication links to be evaluated during these tests are equivalent to those which will be used during an Orbiter mission. The only significant difference is that the RF paths will be through hard-line, space-loss simulators.

As part of the ESTL test plan, Axiomatix's document discusses the following items:

- Communication links to be tested
- Operational modes to be tested
- Operating parameters to be verified
- Special test equipment requirements.

Appendix D of this report presents the ESTL Test Requirements Plan developed for NASA by Axiomatix on this contract.

1.4.4 Current CIU/Orbiter Interface Issues

The CIU interfaces with the following Orbiter avionic subsystems: Payload MDM, GN&C MDM, PI, KuSP, FMSP, PDI and PR. Each of the Orbiter avionic subsystems have different interface requirements. While

most of the CIU output signals are digital, the Orbiter avionic subsystem specifications tend to be more analog oriented than standard digital. In fact, the digital interfaces have conflicting requirements such as rise/fall times, DATA/$\overline{\text{DATA}}$ skew, DATA/clock skew, bit jitter, bit asymmetry, and signal amplitude specifications.

Section 4.2.3 of this report provides a tabulated summary of the CIU/Orbiter interface parameters. The interfaces which indicate incompatibilities are being worked on now by Boeing and the IUS/Orbiter Working Group. However, more analyses have to be performed on the various aspects of the IUS/Orbiter interface implementation before the final designs are arrived at and frozen. As a part of the ongoing effort, Axiomatix will continue to monitor and provide support to the resolution of the IUS/Orbiter interface issues.

2.0 INTRODUCTION

2.1 Statement of Work

2.1.1 Background

The Inertial Upper Stage (IUS) is being developed by DOD for joint DOD/NASA use. Two Orbiter/IUS communication configurations will be used for the DOD and NASA IUS missions. Operational constraints, however, may require the use of a DOD IUS for NASA payload missions such as the Tracking and Data Relay Satellite (TDRS) launch. The NASA IUS/Orbiter communications will use the Payload Interrogator (PI) radio equipment and Payload Signal Processor (PSP) for baseband signal processing and recovery. The DOD IUS/Orbiter communications will use the Communication Interface Unit (CIU) in place of the PSP to perform the functions of baseband signal processing and recovery. Both DOD and NASA IUS missions will require the support of the Orbiter operational S-band and Ku-band communication systems.

The DOD and NASA IUS communication hardware will be tested for performance verification and interface compatibility with the Orbiter avionic subsystems in the Electronic Systems Test Laboratory (ESTL) and the Shuttle Avionics Integration Laboratory (SAIL).

2.1.2 Effort Objectives

The overall objectives of this continuing effort are twofold:

(1) To evaluate the DOD and NASA IUS and CIU communication system design, hardware specifications and interfaces to determine their compatibility with the Orbiter payload communications equipment (the PSP and PI) and the Orbiter operational communications equipment (the S-band and Ku-band systems),

(2) Upon the identification of potential problem areas as stated in (1) above, to suggest possible solutions.

In order to carry out the above tasks, Axiomatix participated in those reviews and interface meetings of the CIU and Orbiter communications equipment conducted within the local Los Angeles area. Axiomatix also supported other reviews as directed by the Contracting Officer. Preliminary working reports covering results of meetings, conferences

and reviews pertaining to the IUS and CIU interfaces with the Orbiter were included as part of the monthly reports following the conferences.

During the contract period (June through September 1979), the IUS, CIU and Orbiter communication equipment concepts and implementation continued to develop. Some of the previous issues have been resolved, some remain open and some new issues became apparent. Thus, a considerable effort was devoted to Tasks #1 and #2. Furthermore, the ESTL test requirements preparation activity (Task #3) continued at Axiomatix at an increased rate and within a widened scope. Consequently, the ESTL test requirements material constitutes the major portion of this report.

The add-on task #6* was also one of the major activity tasks during the program. Task #5** could not be initiated yet because of delays in the SGLS transponder test-gathering by TRW.

2.1.3 General Approach to the Activity

Development of the IUS, CIU and Orbiter payload communication equipment was a continuing activity in CY79. The general approach has been to work with the cognizant NASA personnel, USAF SAMSO personnel, Aerospace Corporation personnel, and individuals at the IUS prime contractor (Boeing Aerospace Company), the Orbiter prime contractor (Rockwell Int'l) and the IUS, CIU and Orbiter payload communication equipment subcontractor (TRW Defense and Space Group) to ascertain directions taken. A vital part of this activity has involved Axiomatix attendance and participation in design reviews (preliminary and critical) as well as special interface meetings. During the performance of the FY79 effort, Axiomatix provided technical support to the CIU Preliminary Design Review, the IUS SGLS Transponder Critical Design Review (CDR), the IUS Transponder Preliminary Review (PDR) and CIU Critical Design Review, as shown in Figure 2.1. Also shown in Figure 2.1 is a schedule for future design reviews that Axiomatix plans to support.

---

*CIU and IUS transponder interface issues

**SGLS transponder qualification test data evaluation

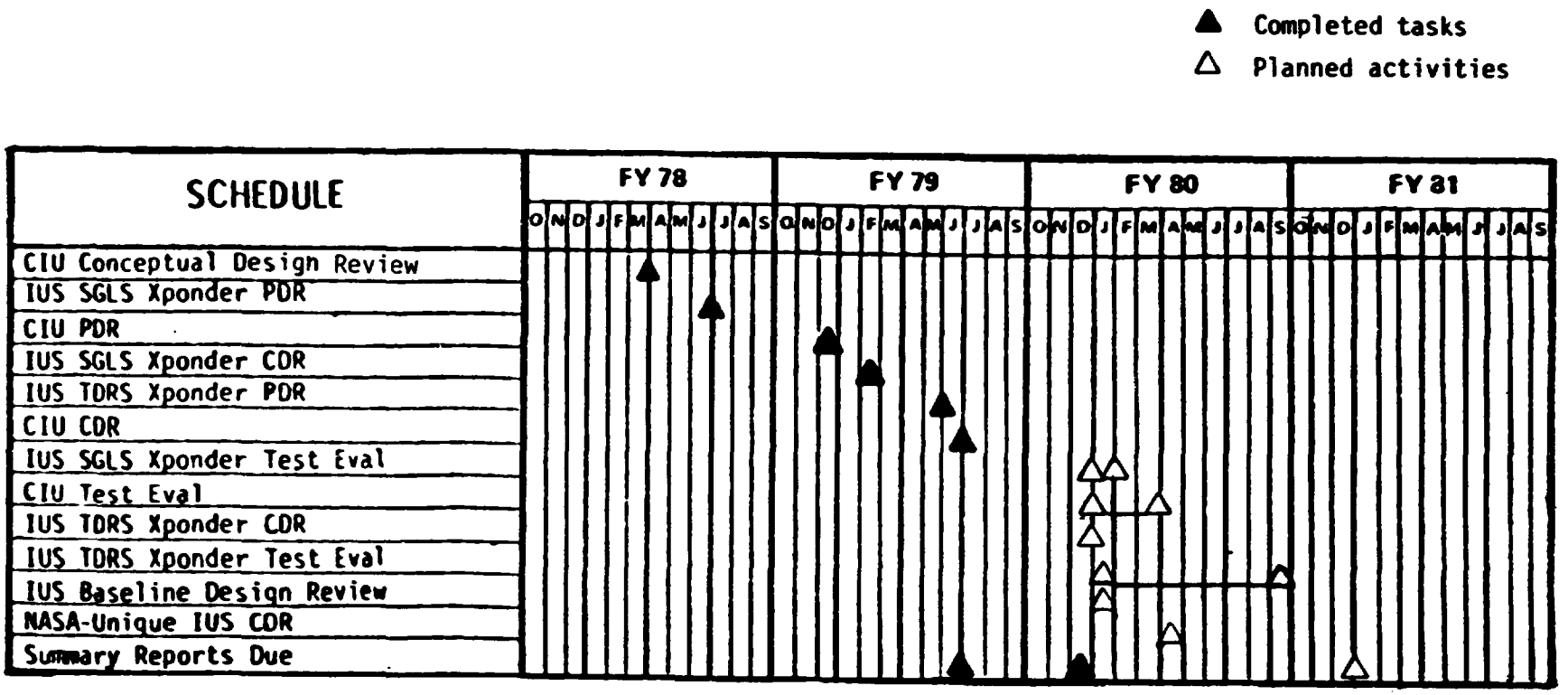

Figure 2.1. Orbiter CIU/IUS Communications Hardware Evaluation Program Schedule

2.1.4 Relationship to Parallel Work

The work performed under the subject contract was strongly interrelated to parallel efforts. Contract NAS 9-15792, "Evaluate and Assess the Shuttle S-band Communications and Design", provided support to critique the design and assess the performance of the individual NASA Orbiter S-band communication equipment (excluding the DOD CIU). Contract NAS 9-15240E/F, "Shuttle Ku-band and S-band Communications Implementation Study", forms the overall communications system framework which ties together the various payload-related equipment (excluding the IUS and CIU). Under Contract NAS 9-15604C, "Shuttle/Payload Communications and Data System Interface Analysis", the IUS, the CIU and the Orbiter equipment related to payloads are analyzed from a system design point of view to determine overall system performance and system interface problem areas.

2.2 Contents of the Final Report

There are three sections which address various aspects and details of the work performed.

Section 3.0 contains an overview of the IUS/Shuttle Orbiter communication equipment, with particular emphasis on the equipment serving the RF link. Included in this section are the considerations of close range operation of the IUS and Orbiter RF equipment. The predicted range capability is also presented.

Section 4.0 addresses the status of the IUS/Orbiter communication system development. It also provides a description of Axiomatix support activities. Issues closed and pending are enumerated and future activities are outlined.

Section 5.0 presents the description of the ESTL Test Plan.

Conclusions are given in Section 6.0.

Finally, Appendices A through F provide the detailed support material for Sections 4.0 and 5.0.

3.0 INERTIAL UPPER STAGE/SHUTTLE ORBITER COMMUNICATIONS EQUIPMENT OVERVIEW

3.1 Introduction

The Inertial Upper Stage (IUS) system is a part of the Space Transportation System (STS). The IUS is intended for carrying out both the DOD missions and the NASA missions. The STS missions involving the IUS include (1) launching payloads into earth orbits and planetary trajectories, (2) recovering payloads from low-earth orbits, and (3) performing other space missions as required.

Because of the versatility of the IUS system, the telemetry, tracking and command (TT&C) subsystems carried by the IUS must be compatible with both DOD and NASA formats. This applies to both the IUS/Orbiter links and to IUS/ground links. Consequently, the avionics equipment carried by the IUS and on board the Orbiter must be compatible with both DOD SGLS and NASA STDN/TDRS systems.

The purpose of the material presented in this section is to provide the description of the IUS/Orbiter radio link with specific emphasis on the TT&C equipment carried by the Orbiter for the purpose of communicating with the IUS during both the DOD and NASA missions. The corresponding equipment carried by the IUS is also described.

3.2 IUS/Shuttle Orbiter Communication Interface Definition

The block diagram representation of the IUS/Shuttle Orbiter avionics subsystems is shown in Figure 3.1. This figure applies to both the hardline and RF links. The Orbiter avionics equipment shown in this figure can be logically subdivided into four categories. The first category includes the equipment which performs payload RF and baseband signal processing functions. This category includes the Payload Interrogator (PI), Payload Signal Processor (PSP), Communication Interface Unit (CIU), and Ku-Band Signal Processor (KuSP). The second category consists of the equipment which handles and processes the IUS commands and telemetry on the actual data format level. Included in this category are the Payload Data Interleaver (PDI), PCM Master Unit (PCMMU), Network Signal Processor (NSP), and General-Purpose Computer (GPC). The third category includes the radio equipment used for communicating the IUS data to and from the

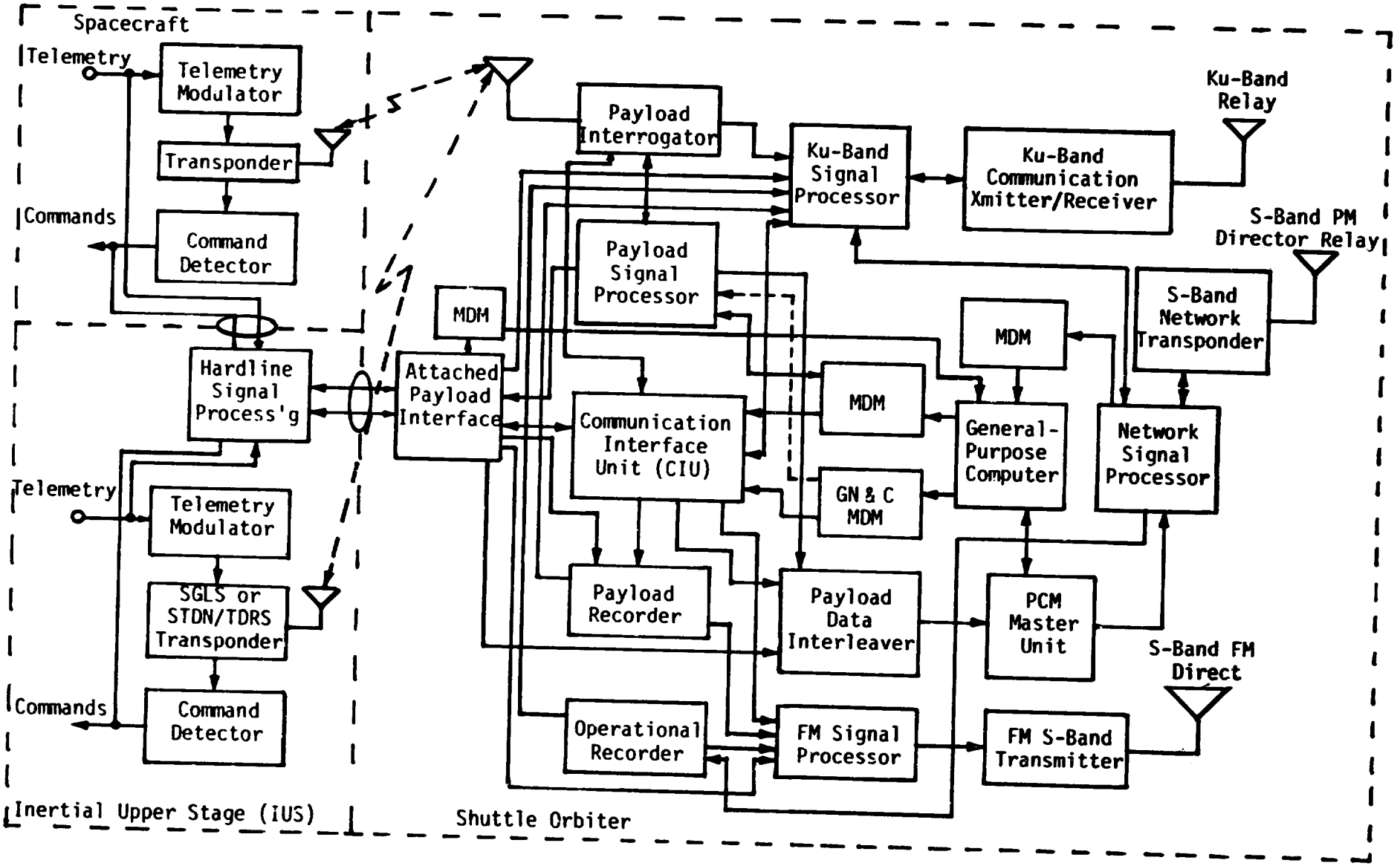

Figure 3.1. Inertial Upper Stage/Shuttle Orbiter Subsystems and Interfaces

ground. The Ku-band communication transmitter/receiver, the S-band network transponder and the FM S-band transmitter belong in this category. Into the fourth category we have arbitrarily included the support equipment such as payload recorder, multiplexer/demultiplexer units (MDM's) and the associated interface equipment.

The IUS avionics equipment consists of either an SGLS transponder for the DOD missions or an STDN/TDRS transponder for the NASA missions. The hardline signal processing equipment on board the IUS provides for the communication with the Orbiter during the attached phase.

As stated earlier, the emphasis of this overview is on the RF communications between the Orbiter and the IUS when the latter is in the detached configuration. Therefore, from the standpoint of the avionics system description, this section dwells on the Shuttle avionics equipment in the first category and the SGLS as well as STDN/TDRS transponders on board the IUS. The performance of the RF link is described in terms of this equipment. The attached mode is discussed only briefly for the purpose of completeness.

3.2.1 Attached IUS Communication

In the attached mode, a hard line (umbilical) provides two-way communication between the IUS and the Orbiter. Scientific data, engineering data, guidance, navigation and attitude control data (GN&C) are received by the Orbiter from the IUS. Alternately, command data, GN&C, and uplink data are transmitted to the IUS from the Orbiter.

For the scientific data, only limited processing (i.e., as required to throughput data to a ground terminal) is provided for IUS medium-gain and wideband data inputs (inputs in the range of 16-256 kbps). For data rates below 64 kbps, the scientific data can be routed through the PDI to the PCMMU, where it is made available to the general-purpose computers (GPC) for processing and on-board display. A payload specialist crew member may then interface directly with a specific experiment, as required. Medium-band scientific data is routed to the receiving ground terminal via either the S-band FM link or the Ku-band system, as follows:

(1) S-band FM

Analog: 300 Hz - 4 MHz

or

Digital: 200 bps - 5 Mbps NRZ-L, or
or 200 bps - 2 Mbps biphase-L

(2) Ku-band

Analog: DC - 4.5 MHz BW
or
Digital: 16 kbps - 1024 Mbps biphase-L
or 16 kbps - 2 Mbps NRZ-L, M or S.

The Ku-band wideband analog channel input (DC - 4.5 MHz) can be used by the IUS or CIU for analog telemtry as a transparent throughput channel, which provides flexibility and minimum Orbiter processing. Capability is constrained only by the KuSP bandwidth.

The PDI provides the capability to receive engineering data from up to five attached payloads simultaneously. The PDI then decommutates up to four of these inputs and provides time-tagged, time-homogenous data from these four payloads simultaneously to the Orbiter data processing subsystem (DPS) for on-board display and/or transmission to the ground via PI downlink. The throughput data rate (composite PDI output to the PCMMU) is limited to 64 kbps maximum on-orbit and 5 kbps for ascent.

A capability for direct recording of certain types of payload data is also provided on board the Orbiter. The payload recorder has 14 tracks capable of serial or parallel recording of digital and analog data. Data rates from 25.5 kbps to 1.024 Mbps and analog data of 1.9 kHz to 2 MHz may be recorded. A minimum record time of 56 minutes is provided at the maximum data rate. Simultaneous analog/digital parallel recording is limited to the first record pass. Subsequent passes are restricted to sequential single-channel digital records. A total of 14 tape speeds (four per mission) are available and selectable by on-board or ground control.

Guidance, navigation and attitude control services are provided for the IUS by the CIU or PSP using an MDM/GPC/MDM interface. Over this interface, the Orbiter provides state vector update data words to the IUS. The CIU transmits the Orbiter state vector data to the IUS using the SGLS command format of ternary frequency-shift-keying (FSK) with "S" tones of 64 kHz, "0" tones of 76 kHz, and "1" tones of 95 kHz. The PSP transmits

the Orbiter state vector data to the NASA IUS on a 16-kHz sine wave subcarrier at a binary command data rate of 2 kbps.

3.2.2 Detached IUS Communication

The basic low rate data-processing/display services provided for the attached IUS are also provided for detached or deployed IUS via an S-band RF communications link between the IUS and the Orbiter. Figure 3.1 shows the interfacing hardware that supports this link. Note that, when a spacecraft is launched by the IUS, the spacecraft communicates only in the attached mode through the IUS, as indicated in Figure 3.1. Also note that the PI cannot communicate with the IUS and the spacecraft simultaneously. The Orbiter S-band transceiver (PI) supporting RF communications with detached payloads is compatible frequency-wise with STDN, SGLS, and DSN-compatible payloads. The PI is capable of operating at approximately 850 selectable frequencies in the 2200-2300 MHz range.

Telemetry signals in the Orbiter standard mode of operation are routed from the PI, after carrier demodulation, to the PSP or CIU, where the data is demodulated off of a 1.024 MHz GPC for decommutation processing, display and downlinking in the same manner as the attached IUS or payload.

Data rates that can be accommodated by the PSP in the standard mode are 16, 8,4,2 and 1 kbps. Processing of 16 kbps may be provided by the CIU. When the CIU is used for DOD missions, the PSP is bypassed.

3.3 Orbiter Avionics Equipment Serving the IUS

3.3.1 Payload Interrogator (PI)

The function of the PI is to provide the RF communication link between the Orbiter and detached payloads. For communication with the NASA payloads and the NASA IUS, the PI operates in conjunction with the PSP. During DOD missions, the PI is interfaced with the CIU. Nonstandard (bent-pipe) data received by the PI from either NASA or DOD payloads is delivered to the KuSP, where it is processed for transmission to the ground via the Shuttle/TDRSS link.

Simultaneous RF transmission and reception is the primary mode of PI operation with NASA IUS, DOD IUS, and payloads. The Orbiter-to-payload link carries the commands while the payload-to-Orbiter link communicates

the telemetry data. In addition to this duplex operation, the PI provides the "transmit only" and "receive only" modes of communication with some payloads.

Figure 3.2 shows the functional block diagram for the PI. The antenna connects to an input/output RF port which is common to the receiver and transmitter of the PI unit. Because of a requirement to operate the PI simultaneously with the Shuttle/ground S-band network transponder which radiates and receives on the same frequency bands, a dual triplexer is employed.

The receiver frequency and phase-tracking loop begins at the second mixer. As shown in Figure 3.2, the output of the first IF amplifier is down-converted to the second IF as a result of mixing with a variable second LO frequency, f_{LO2}. Demodulation to baseband of the second IF signal is accomplished by mixing with a reference frequency, f_R. The output of the tracking phase detector, after proper filtering, is applied to the control terminals of a VCO which provides the second local oscillator signal, thereby closing the tracking loop.

For the purposes of frequency acquisition, the local oscillator frequency may be swept over a ±80 kHz (minimum) uncertainty region. Sweep is terminated when the output of a coherent amplitude detector (CAD) exceeds a preset threshold, indicating that the carrier-tracking loop has attained lock. The output of the CAD also provides the AGC to the first IF amplifier.

A wideband phase detector is used to demodulate the telemetry signals from the carrier. The output of this detector is filtered, envelope level controlled, and buffered for delivery to the PSP, CIU and KuSP.

The PI receiver frequency synthesizer provides the tunable first LO frequency and the corresponding exciter frequency to the transmitter synthesizer. It also delivers a reference signal to the transmitter phase modulator. Baseband NASA or DOD command signals modulate the phase of this reference signal which, in turn, is supplied to the transmitter synthesizer. There it is upconverted to either the NASA or DOD transmit frequency and applied to the power amplifier.

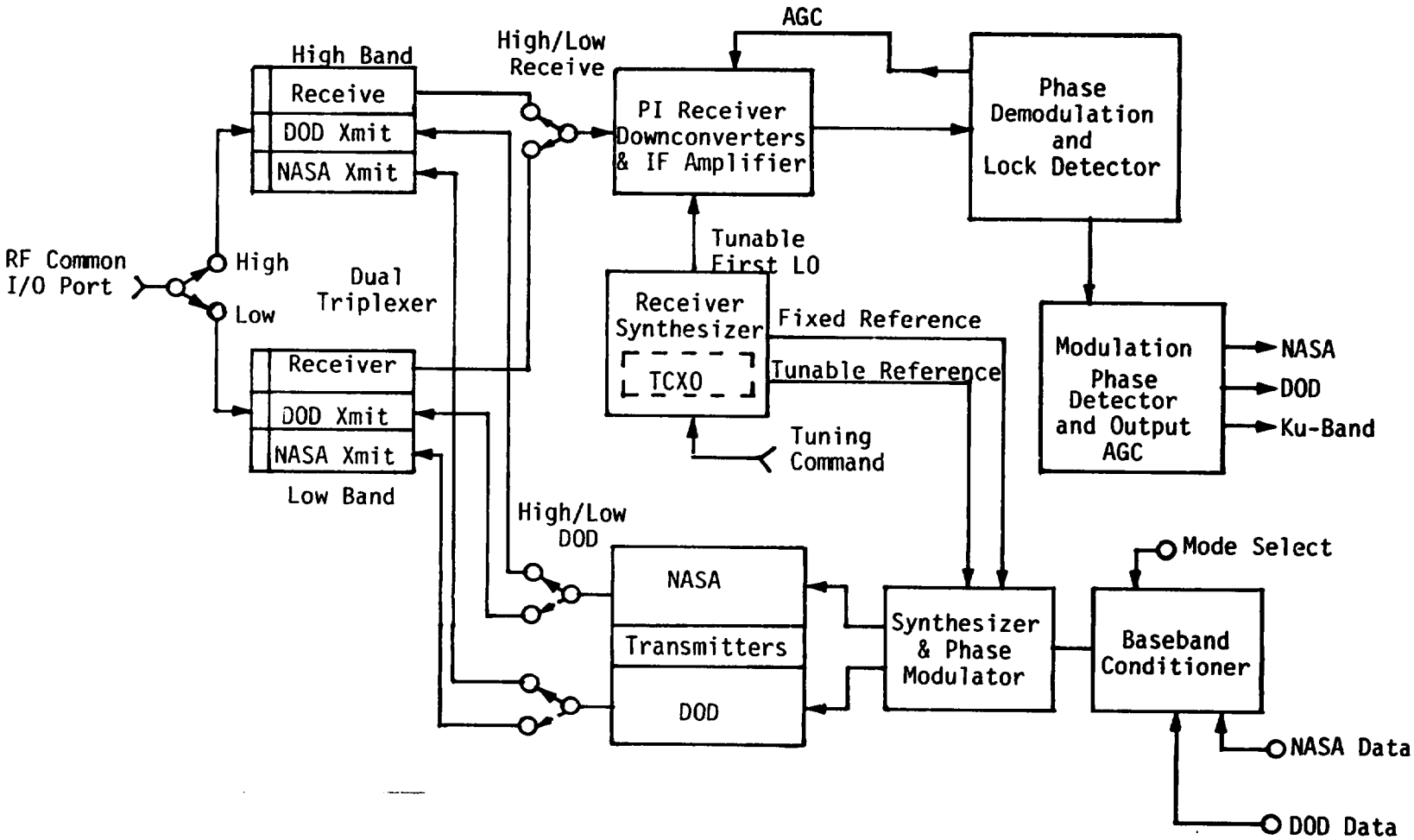

Figure 3.2. Payload Interrogator Functional Block Diagram

3.3.2 Payload Signal Processor (PSP)

The PSP performs the following functions: (1) it modulates NASA IUS and payload commands onto a 16 kHz sinusoidal subcarrier and delivers the resultant signal to the PI and attached payload umbilical, (2) it demodulates the NASA IUS and payload telemetry data from the 1.024 MHz subcarrier signal provided by the PI, and (3) it performs bit and frame synchronization of demodulated telemetry data and delivers this data and its clock to the PDI. The PSP also transmits status messages to the Orbiter GPC; the status messages allow the GPC to control and configure the PSP and validate command messages prior to transmission.

The functional block diagram for the PSP is shown in Figure 3.3. The PSP configuration and payload command data are input to the PSP via a bidirectional serial interface. Transfer of data in either direction is initiated by discrete control signals. Data words 20 bits in length (16 information, 1 parity, 3 synchronization) are transferred across the bidirectional interface at a burst rate of 1 Mbps, and the serial words received by the PSP are applied to word validation logic which examines their structure. Failure of the incoming message to pass a validation test results in a request for a repeat of the message from the GPC.

Command data is further processed and validated as to content and the number of command words. The function of the command buffers is to perform data rate conversion from the 1 Mbps bursts to one of the selected standard command rates (see Table 3.1). Command rate and format are specified through the configuration message control subunit.

Table 3.1. NASA Command System Parameters

Subcarrier Frequency	16 kHz, sinewave
Bit Rates	2000 : 2^N bps, N = 0,1,2,...,8
E_b/N_0 for $P_e^b = 1 \times 10^{-5}$	10.5 dB

From the message buffers, the command bits are fed via the idle pattern selector and generator to the subcarrier biphase modulator. The idle pattern (which, in many cases, consists of alternating "ones" and "zeros")

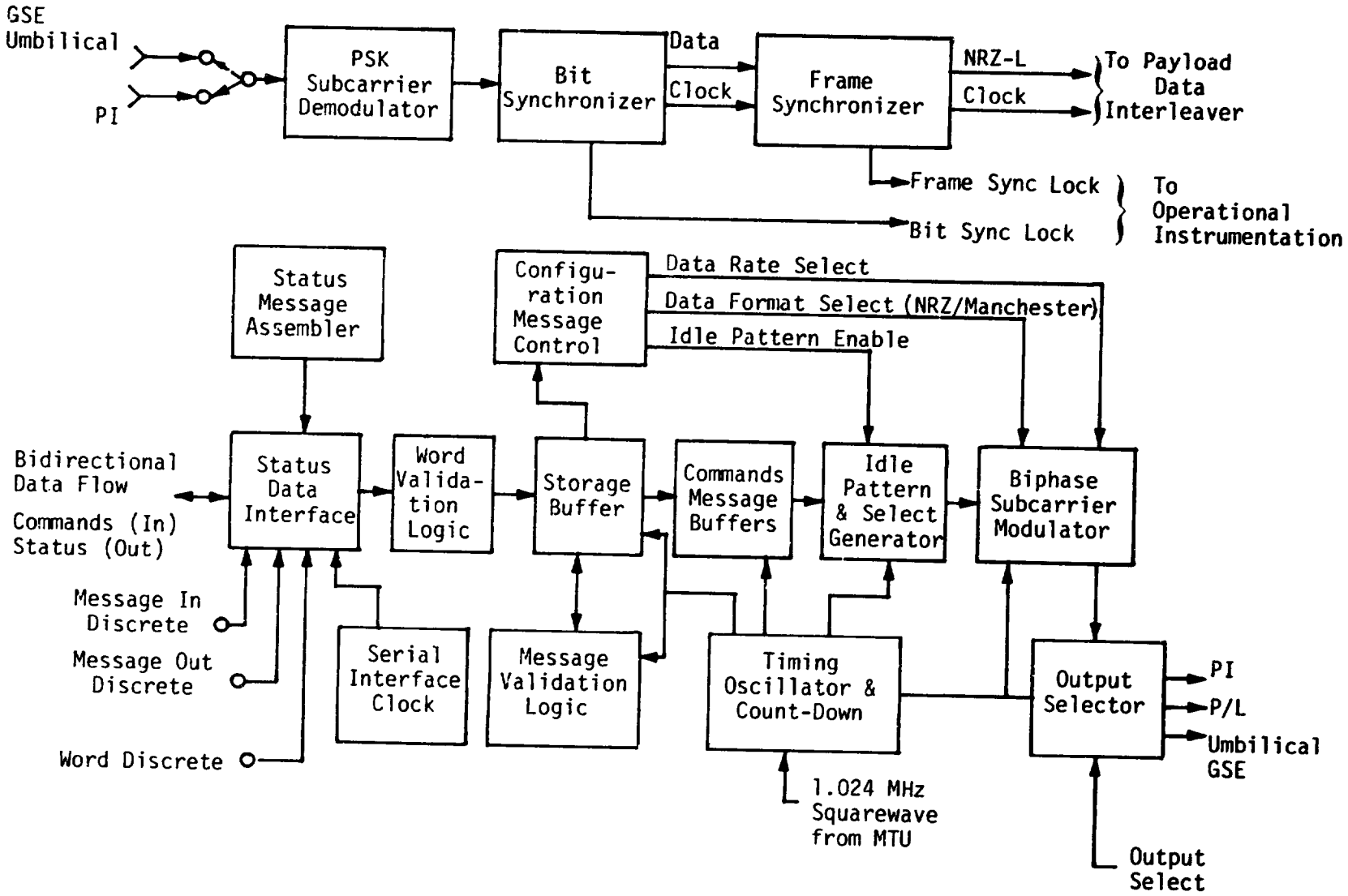

Figure 3.3. NASA Payload Signal Processor Functional Block Diagram

precedes the actual command word, and is usually also transmitted in lieu of command messages. Subcarrier modulation is PSK NRZ-L only.

The 1.024 MHz telemetry subcarrier from the PI is applied to the PSK subcarrier demodulator. The demodulated bit stream is input to the bit synchronizer subunit, where a DTTL* bit synchronization loop provides timing to an integrate-and-dump matched filter. This filter optimally detects and reclocks the telemetry data. From the frame synchronizer, the telemetry data with corrected frame synchronization words and clock are fed to the PDI.

3.3.3 Communication Interface Unit (CIU)

The primary function of the CIU is to provide command and telemetry data conditioning between the Orbiter and the IUS transponder. The CIU consists physically of four boxes and two control panels mounted in an Orbiter standard console. The CIU accepts command data from one of five sources, as follows:

(1) S-band MDM
(2) KuSP
(3) GN&C MDM
(4) Crew-generated data from control panel
(5) T-0 umbilical.

Input command data is validated, formatted, modulated on an SGLS baseband carrier (see Figure 3.4) at 1 k baud, and forwarded to one of six destinations. In the attached mode, the CIU forwards the conditional command data directly over hard line to one of two redundant IUS transponders on one of two IUS's in the Orbiter payload bay. In the detached mode, the CIU forwards the conditioned command data to one of two redundant PI's for RF transmission to the IUS transponder.

The CIU receives IUS telemetry over hard line (attached) and from the PI (detached). In the attached or hard-line mode, the CIU receives data from one of two IUS's and provides selected telemetry data (NRZ-L) to the COMSEC and the PDI. The CIU provides the same telemetry data after NRZ-L to biphase-L conversion for selection to the Payload Recorder (PR),

*Digital Transition Tracking Loop

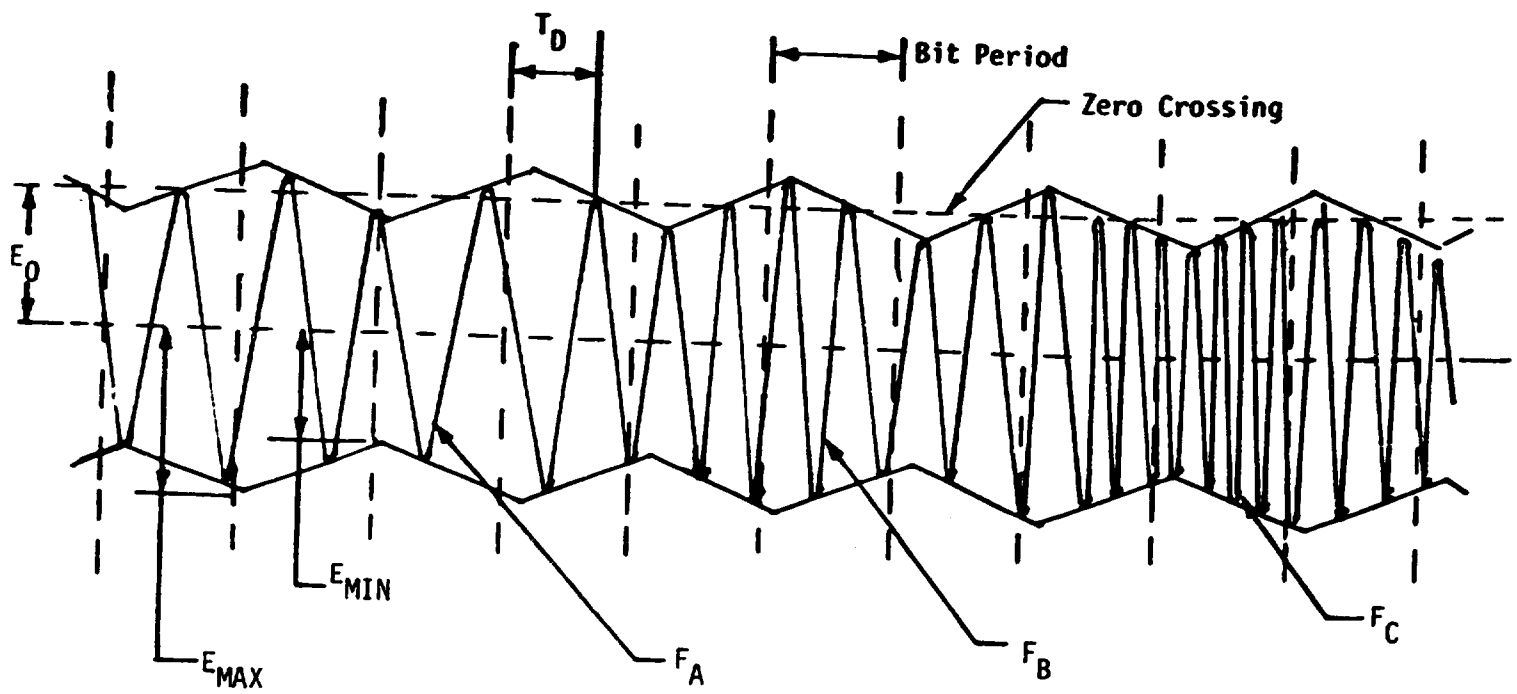

T_D = Delay Time = 600 microseconds

$$\text{Percent Modulation} = \frac{E_{MAX} - E_{MIN}}{E_{MAX} + E_{MIN}} \times 100 = 50\% \pm 10\%$$

F_A = 65 kHz nominal = "S"

F_B = 76 kHz nominal = "0"

F_C = 95 kHz nominal = "1"

Figure 3.4. Command Tone Modulation Envelope

FMSP or KuSP. The CIU also receives NRZ-L data from the Wideband Data Interleaver (WBDI) on the CIU and performs NRZ-L to biphase-L conversion. The WBDI data is selected to be supplied to the PI, FMSP or KuSP. The IUS EMU analog environmental data is received by the CIU for selection to the PR. In the detached or RF mode, the CIU receives telemetry data from one of the two PI's as a PSK subcarrier (1.024 MHz) frequency multiplexed with FM/FM environmental data on a 1.7 MHz subcarrier. The CIU performs PSK demodulation and bit synchronization to generate NRZ-L telemetry data and clock to be supplied to the PDI. The same telemetry data is NRZ-L to biphase-L converted to selection to the PR, FMSP or KuSP. The CIU performs FM demodulation on the 1.7 MHz subcarrier to generate three-channel FM (16, 24 and 32 kHz). The CIU provides the three-channel FM plus a 100 kHz reference for selection to the PR.

Figure 3.5 shows a simplified block diagram of the CIU. Microprocessor technology is fundamental to the CIU operation. The microprocessor performs the bit synchronization function on the telemetry data for processing by a COMSEC and receives telemetry data (NRZ-L) and clock from the COMSEC. The microprocessor performs frame synchronization, VCC extraction (required for DOD commands), command authentication, and determines command rejection. The microprocessor also accepts GN&C data and provides the command generator function to send GN&C or crew-generated command data to the FM/AM modulator. The required binary-to-ternary conversion on the command data is also performed by the microprocessor. Additional functions performed by the microprocessor are CIU mode control and status display.

3.3.4 Ku-Band Signal Processor (KuSP)

The KuSP receives IUS and payload data from the PI, PSP, CIU, PR, operational recorder (OR), and attached payload interface (API). Similarly, the KuSP transmits data to the IUS and payload via the CIU or NSP/GPC/PSP (or CIU). Table 3.2 presents the characteristics of the data that are handled by the KuSP. The 216 kbps data shown for the forward link originates at the TDRSS ground station and can be 72 kbps command data to the NSP, 128 kbps DOD command data to the CIU, 128 kbps text and graphics data and 216 kbps data containing 72 kbps command data plus digital voice data that is sent directly to the NSP.

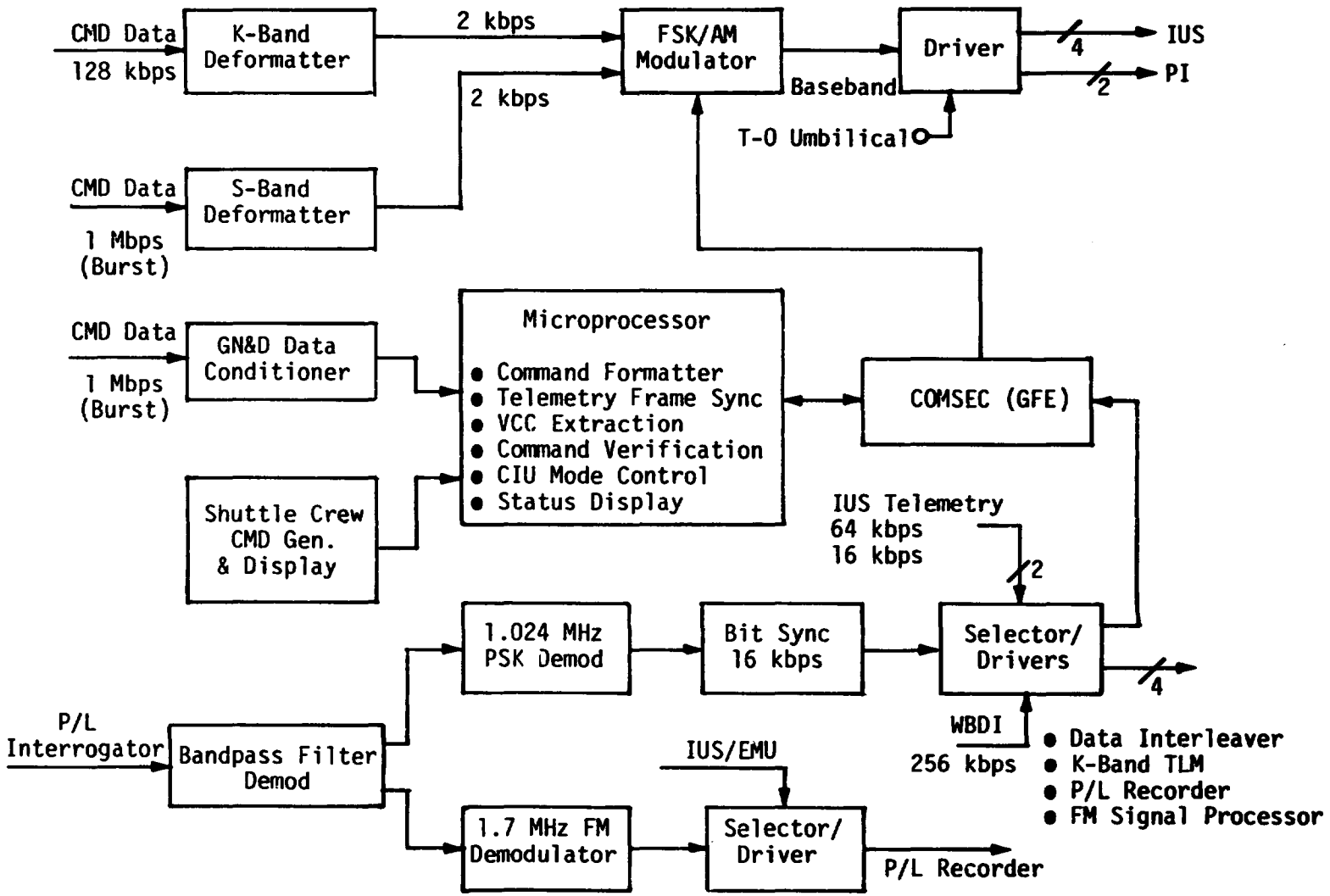

Figure 3.5. Communication Interface Unit Functional Biock Diagram

Table 3.2. Ku-Band Signal Processor Data Characteristics

Processor Interface	Type	Rate or Bandwidth
FORWARD LINK		
Operations Data - NSP(1,2)	Digital	32,72,96,219 kbps (Manchester)
Command/Text & Graphics - NSP (1,2) and Test & Graphics	Digital	72 kbps Command 128 kbps Text & Graphics 16 kbps Frame Sync (Manchester)
Command/DOD Payload Command Data - NSP(1,2)/CIU	Digital	72 kbps Command 128 kbps DOD Payload 16 kbps Frame Sync (Manchester)
RETURN LINK		
CHANNEL 1 (MODE 1/MODE 2)		
Operations Data - NSP(1,2)	Digital	129 kbps (Manchester)
CHANNEL 2 (MODE 1/MODE 2)		
Payload Recorder (PR)	Digital	25.4-1024 kbps (Manchester)
Operations Recorder (OR)	Digital	25.5-1024 kbps (Manchester)
Payload low data rate - PSP (1,2) or Attached Payload Interface (API)	Digital	16-2000 kbps (NRZ) 16-1024 kbps (Manchester)
PI(1,2) low data rate	Digital/Analog	16-2000 kbps (NRZ) 16-1024 kbps (Manchester) 0-2 MHz
CHANNEL 3 (MODE 1)		
Attached Payload Interface (API)	Digital	2-50 Mbps (NRZ)
CHANNEL 3 (MODE 2)		
PI(1,2) high data rate	Digital/Analog	16-4000 kbps (NRZ) 0-4.5 MHz
Attached Payload Interface	Digital/Analog	16-4000 kbps (NRZ) 0-4.5 MHz
Video Interface Unit	Analog	0-4.5 MHz

Figure 3.6 illustrates the functional processing of the KuSP for data to be transmitted to the IUS and payload (i.e., the forward link). When the forward link contains the normal S-band 216 kbps operational data of the 72 kbps command data plus digital voice data, the data mode select is set to transfer the data directly to NSP1 and NSP2 without any processing in the KuSP. Note that, in this data select position, the possible data rates are 32, 72, 96 and 216 kbps. When the 216 kbps forward link data contains either text and graphics data or DOD command data, then data mode select is set to transfer the 72 kbps command data to NSP1 and NSP2. The 128 kbps DOD command data is actually 2 kbps which has been coded to use the available 128 kbps data rate without having to modify the KuSP bit synchronizer or frame synchronizer design.

The characteristics of the data that must be processed by the KuSP on the return link are quite varied, as shown in Table 3.2. The return link is transmitted in one or two modes which are identified by the type of carrier modulation utilized. Mode 1 implements unbalanced quadriphase-shift-keying (UQPSK) while Mode 2 implements FM. In both modes of operation, two of the channels (1 and 2) UQPSK modulate a subcarrier, as shown in Figure 3.7. Mode 2 linearly sums the modulated subcarrier with the third channel and frequency modulates the carrier with the resultant summed signal, as shown in Figure 3.8.

Channel 1 always (Modes 1 and 2) carries the operations data of 192 kbps consisting of 128 kbps telemetry data and two kbps delta-modulated voice channels. Similarly, the data on Channel 2 does not change from Mode 1 to Mode 2. Channel 2 carries the output from the PR, the OR and the PSP as well as low rate data for the API and narrowband bent-pipe data from the PI. The range of data rates handled by the KuSP Channel 2 is shown in Table 3.2 to be 16-1024 kbps Manchester-coded data, 16-2000 kbps NRZ-coded data or DC-2 MHz analog bent-pipe data.

The data carried on Channel 3 in Mode 1 is digital data of 2-50 Mbps (NRZ) which is rate 1/2-constraint length 7, convolutionally encoded by the KuSP to maintain adequate performance margin at bit error probability of 10^{-6}. Because the output data rate of the convolutional encoder is twice the input, the input data clock must be doubled by the KuSP.

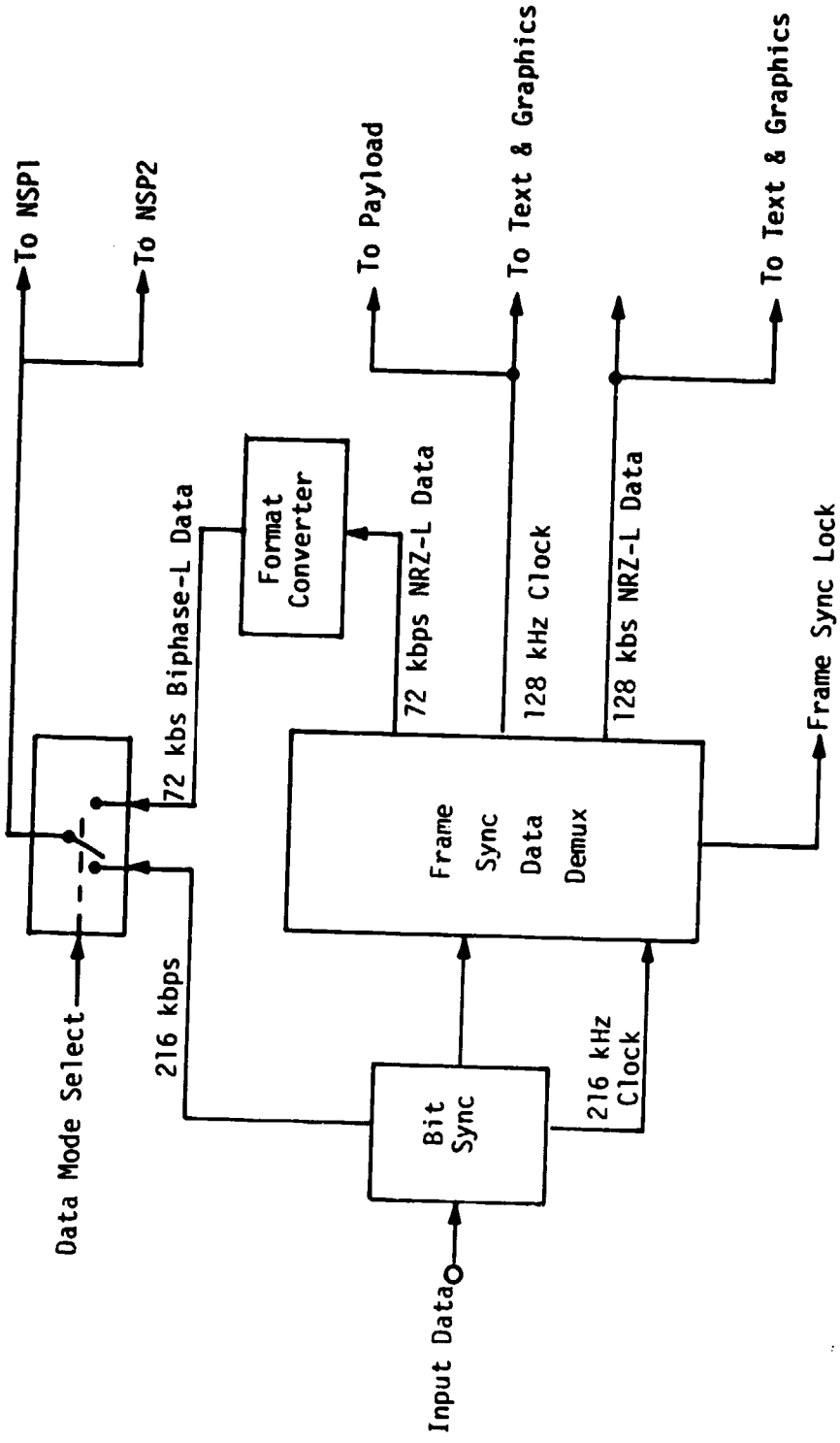

Figure 3.6. Ku-Band Signal Processor Forward Link Functional Block Diagram

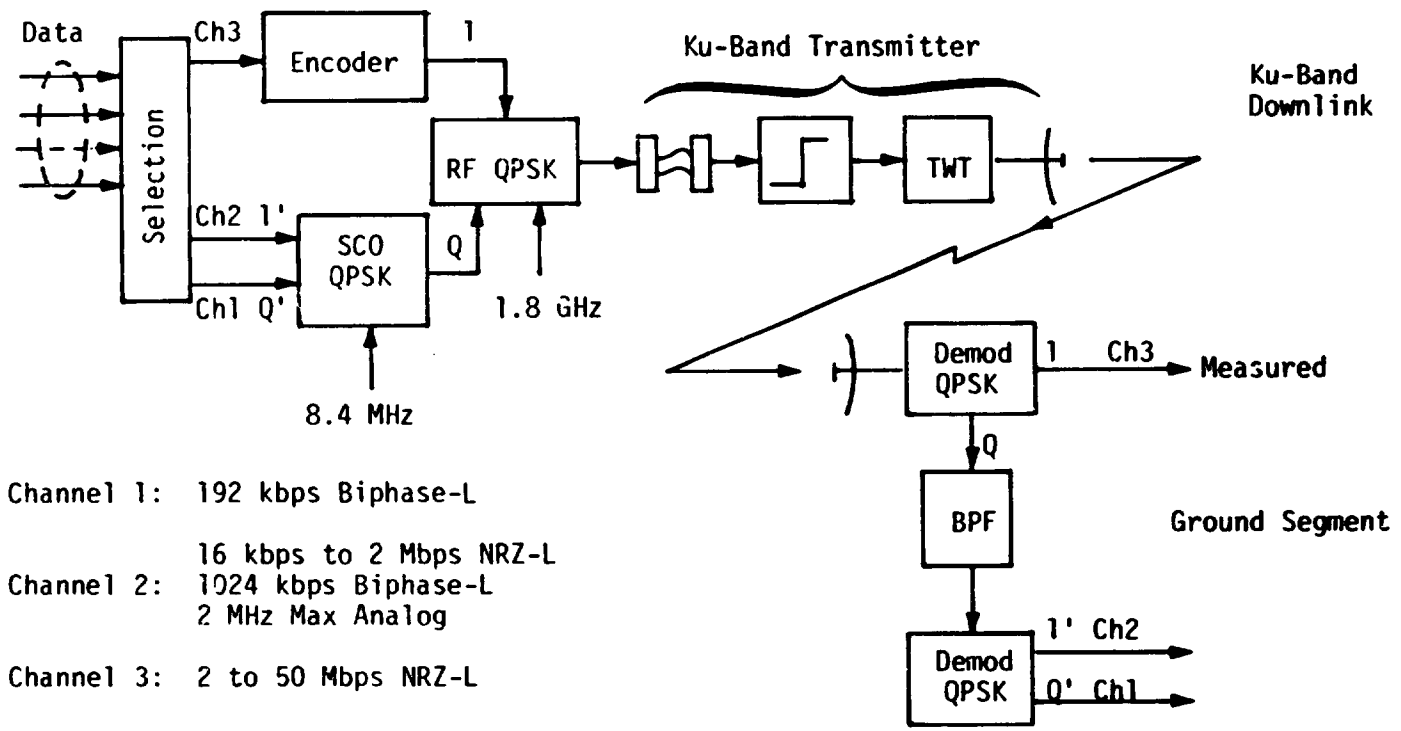

Figure 3.7. Ku-Band MODE 1 Three-Channel Downlink Modulation

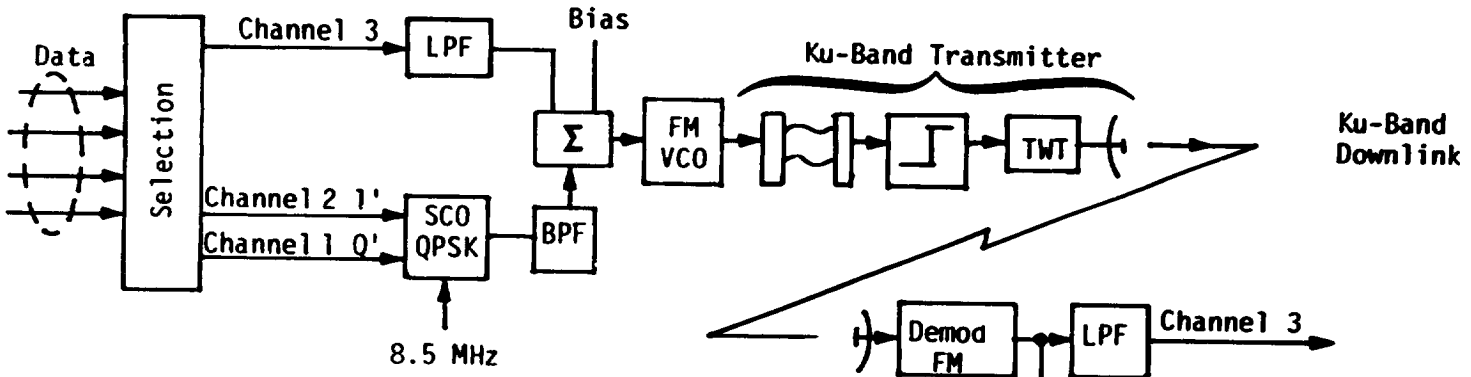

Channel 1: 192 kbps Biphase-L

Channel 2: 16 kbps to 2 Mbps NRZ-L
1024 kbps Biphase-L
2 MHz Max Analog

Channel 3: 4.5 MHz CCTV
4.5 MHz Max Analog
4 Mbps Max NRZ-L

QPSK Power Split: I/O = 4:1 Nominal

FM Power Split: Channel 3 FM Deviation: 11 MHz Nominal
Sub C_x FM Deviation: 6 MHz Nominal

Figure 3.8. Ku-Band MODE 2 Three-Channel Downlink Modulation

3.4 IUS Communication Equipment

Two Orbiter/IUS communication configurations will be used for the DOD and NASA IUS missions. Operational constraints, however, may require the use of a DOD IUS for NASA payload missions such as the TDRS launch. The DOD IUS uses the SGLS transponder for communications with the Orbiter. Alternately, the NASA IUS uses the STDN/TDRS transponder in the STDN mode for communications with the Orbiter.

3.4.1 IUS SGLS Transponder

The telemetry, tracking and command (TT&C) SGLS transponder acquires and tracks, with a phase-locked loop, an incoming S-band signal and provides demodulated spacecraft commands to the decoder. The transponder also receives data and telemetry from the spacecraft and phase modulates this information and the internally demodulated ranging tones onto an S-band 3W carrier which is provided to the antenna for downlink transmission.

The transponder shown in a functional block diagram, Figure 3.9, is a single unit consisting of an S-band receiver, transmitter and the auxiliary circuitry. This transponder configuration performs the following functions:

- Searches and acquires an SGLS-compatible S-band signal with modulation
- Provides a coherent link, when in the VCXO mode, with a fixed 256/205 transmit-to-receive frequency ratio
- Provides a noncoherent stable return link signal when in the auxiliary oscillator mode
- Receives, demodulates command signals, outputting commands and clock signals
- Receives, demodulates to baseband, and remodulates ranging signals on the return link carrier to provide coherent turn-around ranging
- Accepts, modulates and transmits various analog and digital telemetry data on the return link
- Provides telemetry outputs of key transponder parameters and operational status of the transponder
- Operates in the receive and transmit modes independent by way of having separate dc-to-dc converters.

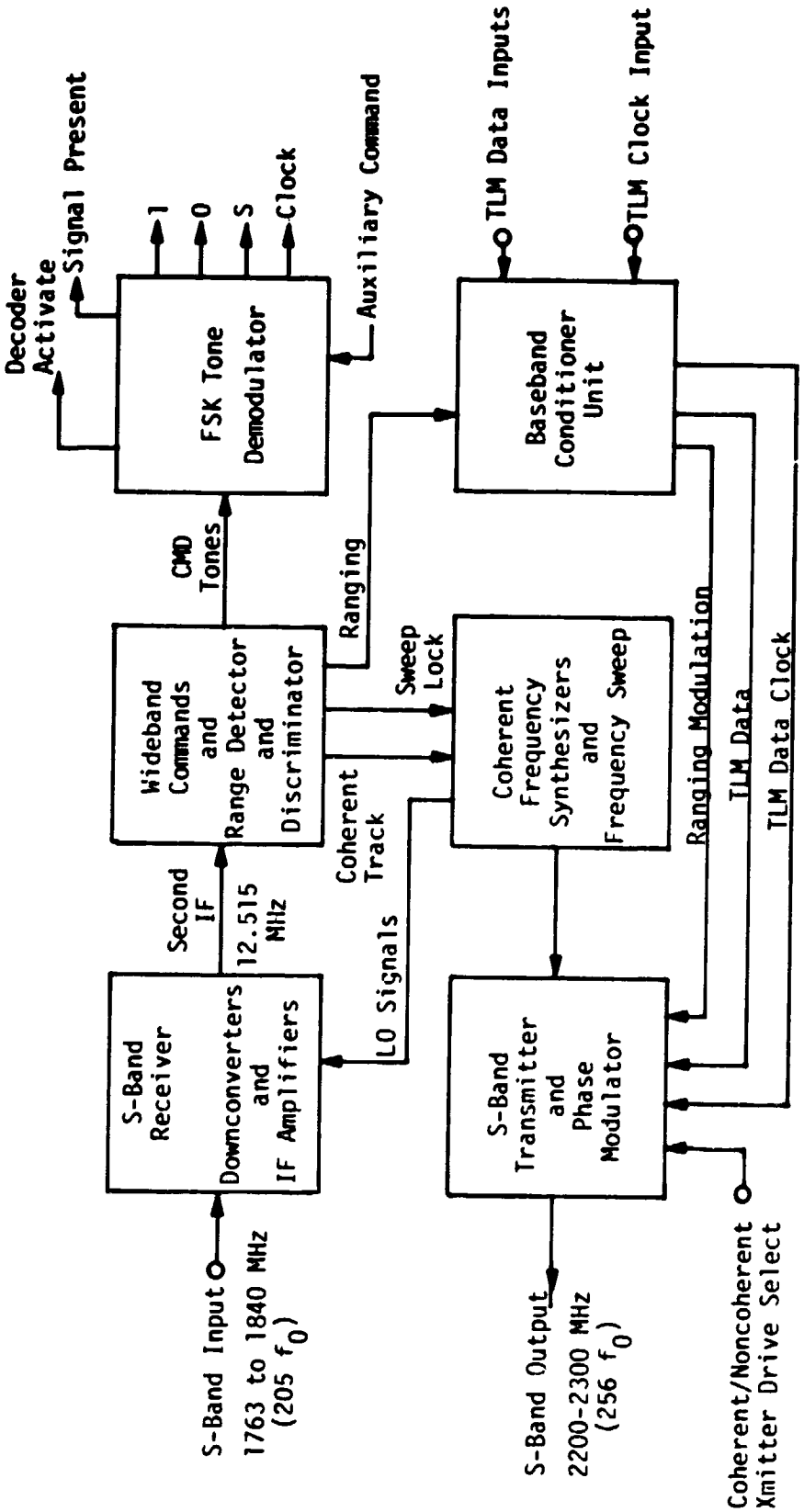

Figure 3.9. IUS SGLS Transponder Functional Block Diagram

The receiver utilizes a dual downconversion, fully phase-coherent design, incorporating a second-order phase-lock loop. S-band input signals in the frequency range of 1763-1840 MHz are amplified in a low noise preamplifier before downconversion to a first IF frequency of approximately 44 MHz. Amplification, gain control and bandwidth limiting are accomplished in the first IF circuits before further downconversion to 12.515 MHz. Then the signal is further amplified and sent to the demodulator module circuits. Here four functions are performed:

(1) Acquisition. Operates in conjunction with the discriminator module to acquire an SGLS signal (including modulation).

(2) Phase detection. A predetection filter (30 kHz crystal filter) reduces the noise spectrum before phase detection takes place in the carrier-tracking phase-lock loop. Loop bandwidth (B_L) is 2 kHz.

(3) Coherent amplitude detection. Another detector, using a 90° phase-shifted reference, produces an output proportional to the RF carrier amplitude. This output forms the correction signal in the automatic gain control (AGC) loop and signal strength information for telemetry.

(4) Wideband detection. A wideband detector/frequency discriminator which, unlike the above two detectors, is not preceded by a narrowband filter, is used to demodulate the phase modulation from the uplink carrier. The output of this demodulator provides the wideband data output to the baseband circuits where filtering separates ranging and command data. The discriminator function of this module does not allow the receiver to acquire to a sideband and, upon carrier acquisition, commands the sweep off in the demodulator. The module supplies the command tones to the FSK tone demodulator and the ranging information to the baseband conditioner.

The S-band transmitter operates from an internal auxiliary oscillator in the noncoherent mode, or from a VCXO output provided by the receiver (coherent mode). Selection of the source can be determined by command or will be automatically set by the phase lock status of the receiver. Both sources are at a frequency of $2f_0$, approximately 17.5 MHz. Frequency multipliers utilizing SAW filters increase the output frequency to S-band at 256 f_0. Phase modulation is performed at 1/4 the output frequency, approximately 560 MHz. The modulator utilizes a quadrature hybrid terminated in voltage variable reactances to achieve linear phase modulation.

Digital telemetry and data are biphase modulated on a 1.024 MHz subcarrier while the analog data is FM modulated onto a 1.7 MHz subcarrier. These signals are summed with the turn-around ranging tones before they are provided to the linear phase modulator. An option is available to replace the 1.7 MHz FM subcarrier with a 1.7 MHz biphase modulated subcarrier. The transmitter also provides variable modulation indices of the subcarrier automatically when either of the subcarriers are commanded off. The S-band power amplifiers are wideband circuits culiminating in a circulator protecting the 2.5 to 3.5W output from shorted or open loads. A separate high-efficiency dc-dc power converter provides operating power to the transmitter upon command.

3.4.2 IUS STDN/TDRS Transponder

The STDN/TDRS transponder is a multimode device capable of receiving and transmitting signals compatible with both the STDN and TDRS operational modes and signal formats. An abbreviated block diagram of the transponder is shown in Figure 3.10. A summary of transponder functions is given below:

- Provides two-way coherent communications with the Orbiter, STDN ground station or TDRS satellites at the appropriate S-band frequency
- Transponds with a coherency ratio of 240/221
- Acquires and demodulates STDN signals in 1/2 second ($>$ -117 dBm) when commanded to the STDN ONLY false acquisition mode
- Recognizes, acquires and demodulates either STDN or TDRS signals when commanded to the DUAL mode; transponder recognizes signals based on the signal structure rather than on the signal level
- Incorporates a command decoder unit which demodulates the STDN subcarrier and recovers the 2 kbps clock and data signals in either mode; a data squelch circuit based on the measurement of E_b/N_0 is also included
- Removes the 3 Mbps spread spectrum code from the TDRS command channel signal and recovers the range synchronization from the TDRS spread spectrum range channel signal
- QPSK or PM modulates the coherent S-band transmit carrier with telemetry and ranging data; in TDRS, the carrier is also coherently spread at about 3 Mbps
- Provides noncoherent telemetry transmission in the absence of received signals or when commanded.

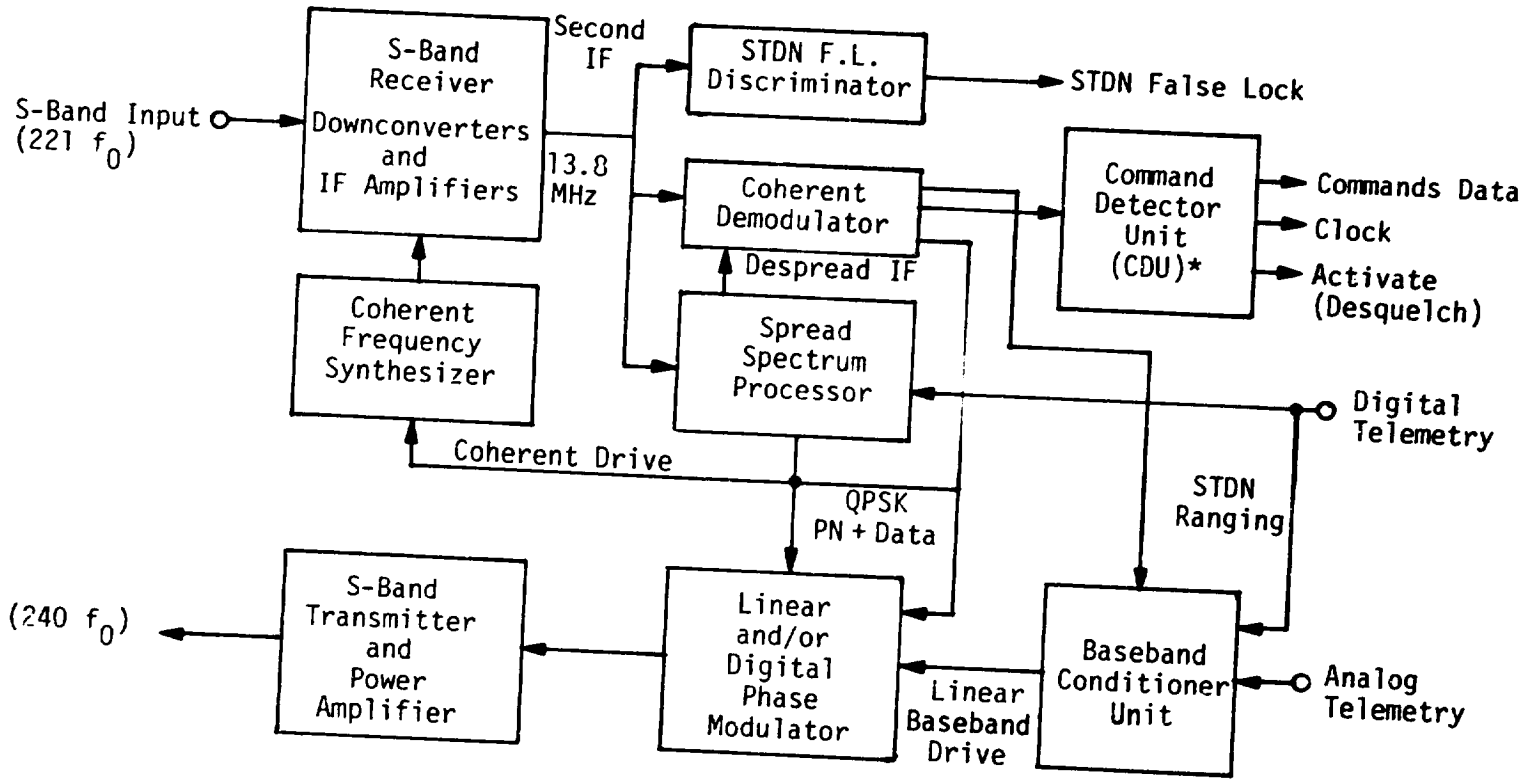

*Includes Bit Synchronizer

Figure 3.10. IUS STDN/TDRS Transponder Functional Block Diagram

The basic transponder configuration is the same for both the STDN and TDRS modes; that is, both are configured to utilize the same frequency plan, receiver and transmitter RF and IF modules. When communicating with the Orbiter, the transponder is configured to the STDN mode.

The received signal is amplified by a low noise preamplifier to a first downconversion to approximately 47 MHz. A second coherent downconversion brings the signal to the second IF (F_R = 13.8 MHz); due to the design of the frequency plan, this second IF operates at a fixed frequency regardless of the input frequency. The second IF signal is divided three ways and is simultaneously sent to the discriminator, the carrier (coherent) demodulator and the spread spectrum processor. The discriminator is employed as an aid to fast acquisition of modulated STDN signals; its sole purpose is to prevent the receiver from locking onto the STDN 16 kHz subcarrier.

The coherent demodulater is employed to recover the data signals which are modulated onto the received carrier. It can be configured as either a linear demodulator (STDN signals) or a Costas PSK demodulator (TDRS signals). Demodulation also generates the phase error signal used to lock up the receiver VCXO; it also generates the coherent amplitude detector (CAD) signal which indicates receiver lock. The TDRS signals are demodulated using a conventional linear phase-lock loop.

In the normal configuration, the demodulated data (baseband) signals are sent to the command detector unit. This unit contains a subcarrier demodulator and a bit synchronizer. The subcarrier demodulator recovers the 2 kbps data from the STDN 16-kHz PSK subcarrier; it employs a frequency-doubling subcarrier recovery loop. The bit synchronizer is an advanced design capable of recovering and reclocking data at three different selectable data rates (2 kbps, 2 kbps/N and 2 kbps/M), where N and M may be an integer from 1 to 16. Only 2 kbps is used for the IUS program.

The bit synchronizer also includes a combined squelch and bit synchronization lock circuit which is insensitive to bit transition density. The outputs of the CDU are the data and clock and an ACTIVATE (desquelch) signal. Upon command, the CDU is also capable of demodulating an auxiliary 16-kHz PSK subcarrier signal.

The return link signal is provided by the transmitter, shown in the lower portion of Figure 3.10. The STDN mode service consists of a 1.024 MHz PSK subcarrier for digital telemetry, a 1.7 MHz subcarrier for

analog telemetry, and the ranging signal. These signals are assembled at baseband in the baseband conditioner unit and are used to modulate a linear phase modulator operating at 1/4 the output frequency. This signal is frequency multiplied x4; in the STDN mode, the inputs to the digital modulator are held to a logical one. The signal is amplified to 3.0W nominal and passed through an isolator to the output.

One of the salient features of the STDN/TDRS transponder is the capability to automatically identify the format of the received signal (i.e., STDN versus TDRS) and to configure the transponder to the appropriate mode. For example, if an STDN (or Orbiter) signal appears and is recognized, the receiver VCXO select switch is switched to allow the carrier loop to commence tracking. In either event, the receiver control algorithm configures the command detector unit (CDU) to match the received signal (TDRS or STDN), and also sends the lock-up information to the transmitter control algorithm circuit. The transmitter is then reconfigured and switched to coherent, assuming that the external TXR command is COHERENT. In the TDRS mode, this does not occur until long (range) code lockup is verified.

In the STDN (and Orbiter) mode only, the requirement is to correctly acquire an STDN signal modulated with a 16-kHz command subcarrier (but no range tones) and to achieve this within 1/2 second at signal levels $\geq$ -117 dBm. The STDN signal may be swept or it may be stationary. In this mode, the receiver VCXO select switch is set to permit the receiver to sweep ±150 kHz every 300 ms. The demodulator is configured for LINEAR. A true lock indication is declared when both of the following conditions are achieved:

- The demodulator CAD indicates the presence of a CW signal within the acquisition loop bandwidth (±4 kHz)
- The discriminator indicates that this CW signal is not a sideband of the received carrier.

The discriminator is thus used to prevent false lock on the STDN (or Orbiter) subcarrier. It is equipped with a dual (±) threshold which indicates if the incoming carrier is ±16 kHz from the true receiver center frequency, as it would be if the receiver was attempting to lock on to a subcarrier sideband. If both of the above conditions are satisfied, the Receiver Select switch is positioned so that coherent tracking commences. When tracking is verified, the carrier loop bandwidth is narrowed to 800 Hz to prevent tracking out the 4 kHz range tone when it is turned on.

3.5 IUS/Shuttle Orbiter RF Links

One of the requirements for the RF link between the IUS and the Orbiter is that the link be operational from a minimum range equivalent to IUS being in the payload bay of the Orbiter to a range of 10 nmi. The resulting wide range in the RF signal levels requires special considerations for protecting the STDN/TDRS and the SGLS transponder when they are in the payload bay. Conversely, the PI receiver must also be protected. The considerations pertaining to the short-range operation are discussed below.

3.5.1 Payload Interrogator (PI) Transmitter to the IUS Receiver Link

The transmitter for the PI has the capability of being switched to a power output compatible with the distance to the IUS. The power steps are 5W, 0.5W, and 0.0025W. Since the cable loss is of the order of 9.8 dB, the payload antenna EIRP is +29.7 dBm, +19.7 dBm, and -3.3 dBm. For the case of the IUS in the payload bay, the output power should be set at the lowest power level (-3.3 dBm) to avoid the possibility of saturating or damaging any of the IUS SGLS or STDN/TDRS transponders. At this level, the received power at the SGLS receiver is -56.8 dBm, which is within the operating dynamic range of threshold (approximately -120 dBm) to -40 dBm maximum. However, the other two output power levels are -23.8 and-33.8 dBm, which exceed the upper limit of the SGLS transponder specified dynamic range. Similar examination of the received signal power for the NASA IUS with the STDN/TDRS transponder shows that the lowest PI output power level must be used so that the IUS received power (-52.5 dBm) is less than -40 dBm (i.e., the upper limit of the specified dynamic range for the STDN/TDRS transponder.

3.5.2 IUS Transmitter to Payload Interrogator Receiver Link

No adjustments are possible for controlling the output power of the IUS transmitter so that the 20W (13 dBW) from the TWT results in 13.2W (11.2 dBW) being radiated into the bay. Above -20 dBm, however, the receiver IF amplifier circuits begin to saturate. Although this would not adversely affect demodulation of constant envelope signals, it may cause receiver false lock under certain conditions. Therefore, receiver operation with signals higher than above -20 dBm is not recommended. At input signal levels of +10 dBm and higher, a preamplifier protective diode breakdown limiter becomes operative. Thus, intentional receiver operation above +10 dBm is not recommended.

The PI received power from the IUS SGLS transponder at 3 m is estimated at -19.4 dBm. Thus, the receiver IF amplifier will begin to saturate. Furthermore, this estimate of the received power was calculated based on a -4.0 dB IUS pointing loss (worst case). If there is no pointing loss, the received power is -15.4 dBm and the PI IF amplifier could be in saturation but there will be no damage to the PI receiver. Similarly, the PI received power from the IUS STDN/TDRS transponder at 3 m is estimated to be at -13.6 dBm including a -3.4 dB IUS pointing loss. Therefore, when at close range, the antenna selection on IUS will be such as to keep the PI receiver out of saturation. Thus, there will be no damage to the PI receiver at close ranges.

3.5.3 IUS and Orbiter Received Power Versus Range

Figures 3.11 and 3.12 present, respectively, the IUS and Orbiter received power as a function of range. Figure 3.11 presents the received power at the IUS SGLS and STDN/TDRS transponders versus range for the three PI output power levels. The IUS transponders are specified to achieve acquisition at a received power of -117 dBm in 0.5 seconds with a probability of 0.9 for a modulated signal. In terms of the Orbiter acquisition procedure, a modulated signal would be present only during reacquisition. Therefore, the reacquisition threshold for the SGLS transponder is reached at 5 nmi in the low-power mode, while the STDN/TDRS transponder reaches the reacquisition threshold at 8.5 nmi in the low-power mode. In the medium-power mode, the SGLS and STDN/TDRS transponders reach the reacquisition threshold at 24 nmi and 36 nmi, respectively. Considering the range limitations due to performance, one determines the received power at which the system operates with zero margin. We call such points ZPMO in Figures 3.11 and 3.12. Thus, as seen from Figure 3.11, the ZPMO for the STDN transponder is outside the range for acquisition. Thus, the STDN range is reacquisition limited rather than performance limited.

For the SGLS, we have a ZPMO range of 14 nmi with medium-power PI transmission. Therefore, for either transponder, the 10 nmi operating range requirement can be met with medium-power PI transmissions.

The power received by the PI versus the range to IUS is presented in Figure 3.12. As can be seen from the figure, the reacquisition threshold is far above the zero margin performance (ZPMO) for both the SGLS and STDN/TDRS transponder transmissions. It can also be seen from Figure 3.12 that

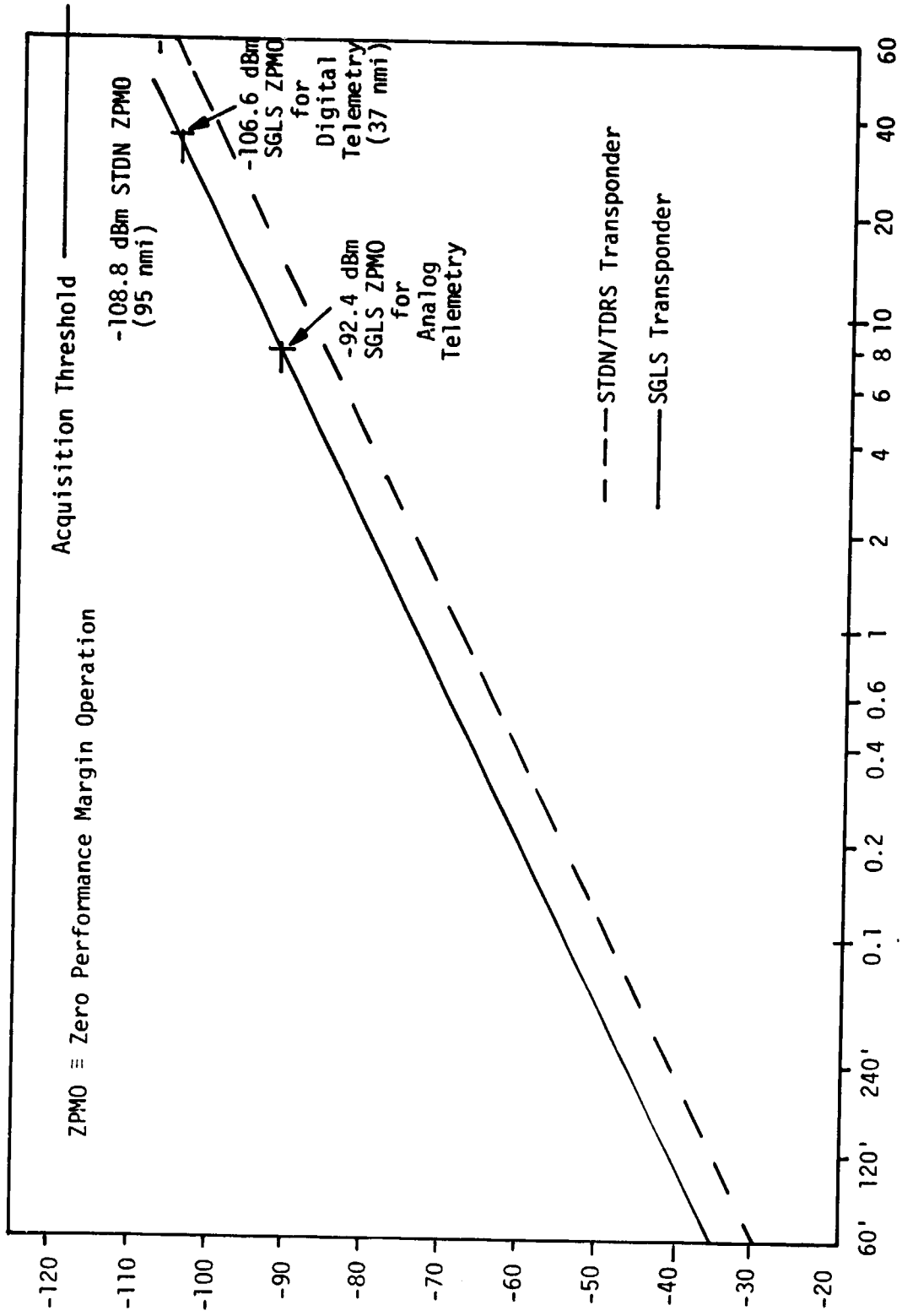

Figure 3.11. PI Received Power versus Range from IUS

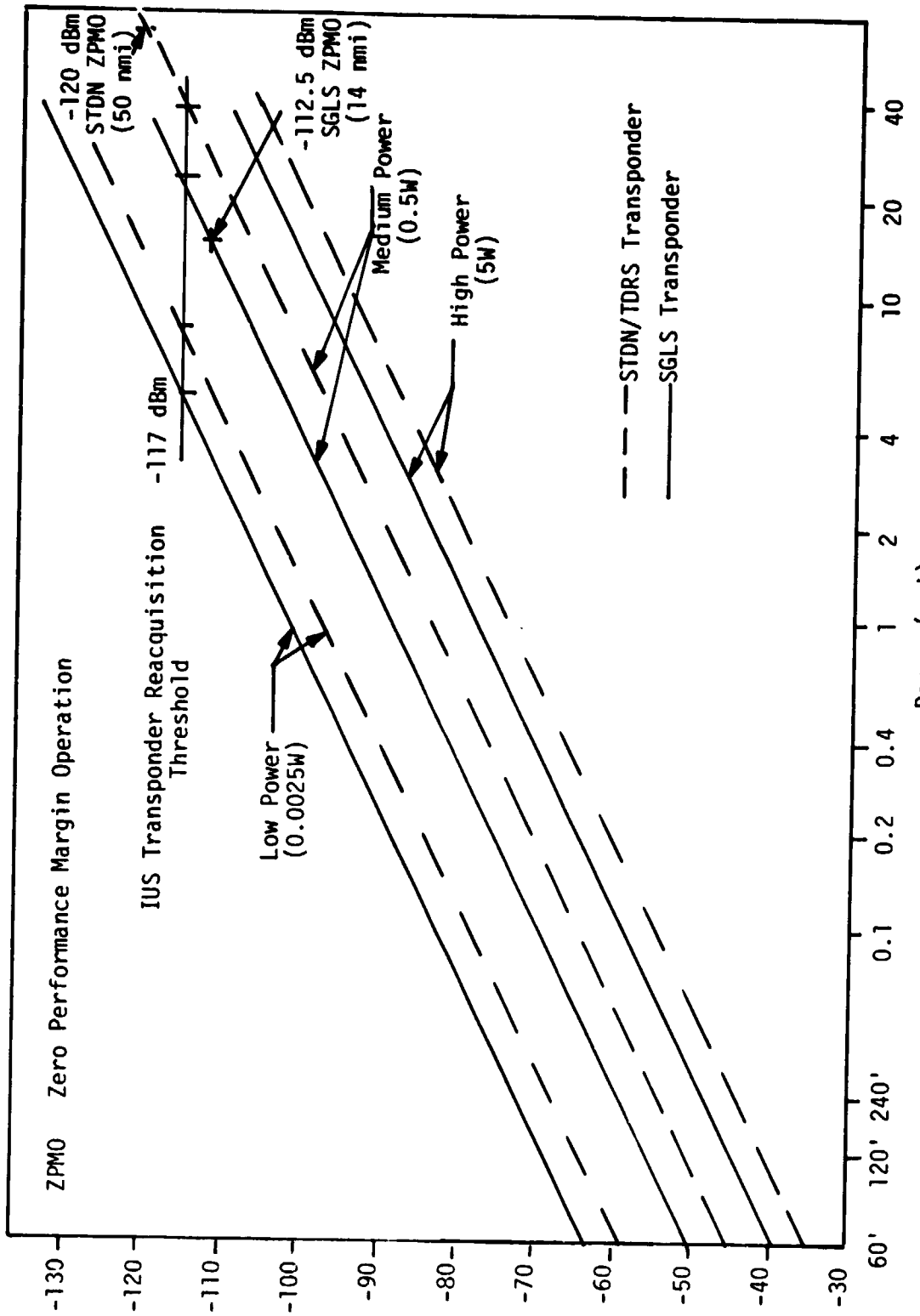

Figure 3.12. IUS Received Power versus Range for Each PI Output Power Setting

the 10 nmi operating range requirement is met for both transponders in the digital telemetry mode. In the analog FM mode, the performance is limited to 7 nmi.

3.6 Summary

The Inertial Upper Stage (IUS) system will be used by DOD and NASA for space vehicle (S/V) launches from the Shuttle Orbiter. The communication equipment to support these launch missions consists of (1) Shuttle Orbiter on-board equipment, and (2) IUS on-board transponders compatible with either SGLS (DOD) or STDN (NASA) signal formats. This equipment has, as described herein, sufficient capability to provide two-way transponded communication for an IUS/Orbiter range of 10 nmi (minimum) for commands and digital telemetry modes.

4.0 PROGRAM/SYSTEM DEVELOPMENT STATUS

4.1 Summary of ICD and Design Reviews Attended

As one of the major tasks of the contractual effort, Axiomatix is required to support the ICD's and the Design Review meetings pertaining to the IUS/Orbiter communication equipment development program. The purpose of such attendance is to permit Axiomatix to track equipment specification changes and provide assistance in resolving specification inconsistencies and conflicts whenever such action is required or warranted.

Listed below is the summary of the technical meetings which Axiomatix supported during this program interval.

1. S-Band STDN/TDRS transponder preliminary design review.

During June 11-13, a preliminary design review of the S-band STDN/TDRS transponder took place at The Boeing Company, Seattle, Washington. Axiomatix supported this meeting. The following companies and agencies were represented:

- Boeing (prime contractor)
- TRW (transponder subcontractor)
- SAMSO
- Aerospace Corporation
- NASA JSC
- NASA Goddard
- NASA Marshall.

As a result of this meeting, 17 RID's and 10 action items were generated. The RID's were assigned to TRW and Boeing. The action items were distributed between TRW and Boeing, with Axiomatix picking one action item as the one most appropriate to our function.

Most of the RID's dealt with inconsistencies within the transponder specifications; so did most of the action items.

Among the specific problem areas were such items as:

1. Inability of TRW to meet the length specification for the transponder enclosure (18.1" versus 17.6" specified)

2. Critically high power consumption with the transponder module

3. Requirement to telemeter the temperature of the VCXO to ground for the purpose of compensating the uplink RF carrier

4. Spurious radiation levels of the S-band transmitter.

The first two problem areas are hardware design-related items; they are to be resolved between TRW and Boeing. Item 3 is a systems problem and may require NASA to determine the impact on the operational scenario.

The impact of spurious responses and the associated phenomenon on the system operation are subject to analysis and, thus, Axiomatix has performed the related analyses to determine the severity of their impacts. Specifically, the action item taken by Axiomatix involved analyzing the effects of (1) spurious low-frequency AM modulation of the subcarrier, and (2) bandpass filtering of the 1.027 MHz subcarrier on the spectral components of the radiated signal. (Goddard is concerned with spurs that can cause a potential false lock.) Section 4.2.1 and Appendix A provide details pertaining to the nature of this action item.

Furthermore, Axiomatix has examined the analysis included in the PDR package to determine if there are inconsistencies with the required performance. Details of Axiomatix's review are presented in Section 4.2.2 and also in Appendix A.

2. COMSEC CIU/NSP Meeting

During June 20-21, a COMSEC equipment-related ICD conference took place at Motorola's facility in Scottsdale, Arizona. The purpose of this conference was twofold: (1) to define the ICD pertaining to the CIU COMSEC equipment, and (2) to review the ICD pertaining to the COMSEC equipment interfacing with the Network Signal Processor (NSP) of the Shuttle Orbiter avionics equipment.

Besides Axiomatix, the representation of other companies and agencies was as follows:

- Motorola (subcontractor)
- Boeing (prime contractor for CIU)
- Aerospace Corporation
- NASA JSC
- DOD
- SAMSO
- USAF
- Rockwell (Shuttle contractor)

The first day of the conference was devoted to the discussion of the ICD defining the interfaces between the CIU and the KGT-60/KGR-60 equipment group. The latter equipment group is being manufactured by Motorola for ultimate incorporation into the CIU. (The CIU is built by TRW under subcontract to Boeing.) The two ICD's--one for the KGT-60 and the second for the KGR-60--were generated by Motorola. As a result of the review of the ICD's, several action items were generated. Most of these action items dealt with mechanical aspects of the KGT/R-60 packaging. The execution of these action items was left to Motorola/TRW/Boeing complex, with Rockwell providing the overall packaging guidelines for the Shuttle-borne avionics equipment.

A major action item resulting from the review of the KGT/R-60 ICD's was to resolve an apparent electrical interface inconsistency between the CIU unit and the KG boxes. Specifically, the CIU, as conceived by TRW at the time of this meeting, provides about five parallel control lines which select the various modes of the CIU operation. The signals carried by these parallel control lines consist of either 0V or +24 V ±4 V (Orbiter power level) discretes. In comparison, Motorola's KG boxes at the time of the meeting were being designed to be controlled by a serial digital word over 10 bits long, with bit levels being defined by the standard T^2L [-0V (logic zero) to +5 V (logic one)] levels.

The resolution of this action item was left to the DOD supplier of the KG boxes and the SAMSO user.

During the second day of the conference, the ICD pertaining to KGX-60 equipment was reviewed. This particular ICD was prepared by Rockwell, and its purpose is to establish the hardware interface requirements between the Orbiter and network COMSEC equipment. The network COMSEC equipment will provide a capability to encrypt the Orbiter 92/192 kbps downlink data and decrypt the 32/72 kbps uplink data.

The review of this ICD did not result in any major action items, with the exception of certain connector pin reassignments and minor ICD format modifications. These action items were taken up by Rockwell personnel who will reissue the updated ICD.

3. Communication Interface Unit (CIU) CDR

The CIU critical design review (CDR) was held at the TRW facility, Redondo Beach, California, July 10-11, 1979. Mr. Udalov represented Axiomatix at this CDR.

Because of the reproduction problems caused by the immense volume of the CDR, the distribution of this CDR package was delayed until only a few days before the review. Axiomatix personnel, therefore, did not have an opportunity to examine in detail the CIU CDR package prior to the actual review. However, because of Axiomatix's familiarity with the CIU development program, the belated acquisition of the CDR package did not hamper our interactive participation in the design review. With the CIU CDR package in our possession, we have proceeded with the examination of its contents.

The principal participants of the CIU CDR were the Boeing Aerospace Company (BAC), TRW, and SAMSO, the latter being supported by technical personnel from Aerospace Corporation. NASA was represented by personnel from JSC, Rockwell and Axiomatix. Because of the large amount of technical material required to be covered, the two days allotted for the CDR were sufficient only for the presentation of the technical material but were not adequate to complete the preparation of all the action items and RID's. Thus, the disposition of the RID's continued on the morning of July 12.

In all, 24 action items and 32 RID's have resulted from this CDR. Most of these appear to be caused by either (1) inadequately defined specifications, or (2) misinterpretation of certain specification statements. In general, however, no unresolvable major electrical performance issues seem to have been uncovered as a result of the CDR. In other words, it appears that most of the debatable issues can be resolved by either additional test data and/or specification rewording.

At the time of the CIU CDR, the interface discrepancy with respect to KG boxes was not discussed. Axiomatix learned, however, that the action to resolve the discrepancy was assigned to Boeing and TRW, with the former taking it upon themselves to prepare an updated ICD.

In the mechanical/packaging area, the major issue during the CIU CDR was the location of the fill connector. The presented TRW design placed the connector behind the kick panel which has to be removed to

allow access to the connector. This makes access to the connector difficult, particularly when the Shuttle is in a vertical position. Thus, the relocation of the connector to the front panel of the CIU unit is now being considered by BAC and TRW as per SAMSO's request. Other mechanical/packaging problem areas did not appear critical and, thus, were treated as minor modifications. Upon receipt of the CDR meeting minutes,* Axiomatix will review these once again to determine if some inconsistencies still exist.

Section 4.2 contains some of the discussions of CIU CDR material as interpreted by Axiomatix as a result of reviewing the CIU CDR package material.

4. COMSEC Equipment PDR

A PDR meeting dealing with both the spaceborne and ground segments of Shuttle COMSEC equipment took place at Motorola, Phoenix, during August 14-15. Axiomatix supported this meeting as a part of the ongoing participation in the overall IUS/CIU communication equipment development effort.

4.2 STDN/TDRS S-Band Related Activities

4.2.1 Action Item Description

4.2.1.1 Background and conclusions

During the S-band STDN/TDRS transponder CDR of June 11-13, at Boeing, Seattle, NASA Goddard personnel expressed concern regarding the possible effects of AM on the 1.024 MHz PSK-modulated subcarrier. The concern was specifically directed towards the possibility of false locking the ground receiver to the RF spectral lines generated by AM on this subcarrier. Axiomatix took on the action item (Action Item #8) to investigate the causes and potential deleterious effects, if any, of AM on the 1.024 MHz subcarrier. Appendix A contains the detailed analysis of this item.

In the course of our investigation, we established that the dominant cause of AM on the 1.024 MHz subcarrier is filtering this PSK-modulated subcarrier with a bandpass filter placed ahead of the linear

*At the time of this report writing, Axiomatix still had not receive the minutes of the CIU CDR.

phase modulator. The worst case of such AM occurs when a continuous stream of either "ones" or "zeros" is PSK-modulated on the subcarrier.

However, the effect of the skirt selectivity provided by the subcarrier bandpass filter is definitely beneficial to the RF spur suppression while the AM caused by the filtering process does not, according to Axiomatix analysis, introduce any spurs into the RF spectrum of the phase-modulated carrier. In fact, the skirt selectivity of the bandpass filter helps to keep the potential false lock-up spurs far below the -60 dBc level, which is currently considered to be the threshold of lock-free operation. Specifically, our analysis indicates that, because of the filter selectivity, the ±64 kHz spur (worst case) in the vicinity of the downlink carrier can be kept down as low as -80 dBc.

Therefore, one concludes that the bandpass filter used for controlling the spectrum splatter of the PSK-modulated subcarrier within the baseband is indeed necessary and that the incidental AM caused by the filter has no deleterious effects on the RF spectrum.

Presented below is an overview and summary of the detailed analysis contained in Appendix A.

4.2.1.2 Overview and analysis summary

This subsection summarizes the results of our analytical investigation of the effects of bandpass filtering the PSK-modulated 1.024 MHz subcarrier prior to carrier phase modulation. The specific goals of the analysis are (1) to establish the impact of the bandpass filtering on the magnitude of the spurious components within the RF spectra, and (2) to define the impact of these spurious components on the false lock.

Our analysis indicates that, for the worst-case data pattern, i.e., all "ones" or "zeros", at 64 kbps, the theoretical level of the f_c ±64 kHz spur is about -90 dBc for a peak deviation of 1.0 radian. Relative to the modulated carrier, this spurious component is -88 dB.

These numbers include about 60 dB of subcarrier bandpass filter attenuation and apply to the case where the 1.024 MHz PSK-modulated subcarrier is the only baseband signal contributing to the RF spectrum structure. The following paragraphs provide the description of our analytical model and its role in the development of the desired hardware and system performance parameters.

4.2.1.2.1 Description of the analytical model

Figure 4.1 provides a qualitative illustration of the key subelements addressed in our analysis. Part (a) of the figure shows the simplified block diagram of the 1.024 MHz PSK subcarrier modulator and the linear RF carrier phase modulator. The PSK modulator consists of a balanced mixer which accepts either a 16 or 64 kbps biphase-L telemetry data stream, f(t), and superimposes it on a 1.024 MHz sinusoidal subcarrier as an antipodal (0°, 180°) phase modulation. This results in a suppressed subcarrier, biphase-modulated signal, g(t).

A qualitative representation of such a spectrum is shown in the left-hand portion of part (b) of Figure 4.1. The spectrum shown is that of a continuous stream of either "ones" or "zeros" which, for the case of the biphase-L modulation, results in spectral lines located at odd multiples (i.e., 64, 192, 320 kHz, etc.) away from the subcarrier frequency of 1.024 MHz.

The modulated subcarrier is then passed through a bandpass filter which has the nominal two-way bandwidth (i.e., -3 dB points) of 330 kHz and the out-of-band rolloff of at least 18 dB/octave. The maximum specified out-of-passband attenuation of this S/C filter is 60 dB with respect to the center frequency insertion loss. Thus, the data sidebands are attenuated by a factor of $\alpha(\Delta f)$, where $\alpha \leq 1.0$ and Δf is frequency offset away from the filter's nominal center frequency of 1.024 MHz. The filter selectivity characteristic therefore attenuates the sidebands of the PSK-modulated subcarrier a(t), as shown in the right-hand portion of part (b) of Figure 4.1.

The filtered PSK subcarrier is then applied to the input of a linear phase modulator. The modulator then converts the waveform information contained in the PSK-modulated subcarrier into a phase deviation of the RF carrier. The term "linear phase" modulator implies, in this case, that there is a linear relationship between the modulating voltage at the input to the modulator and the phase deviation of the modulated RF carrier. Phase modulation of an RF carrier, however, is not a linear process by any means, and it leads to various cross product terms between the modulating frequency components, usually expressed by Bessel functions.

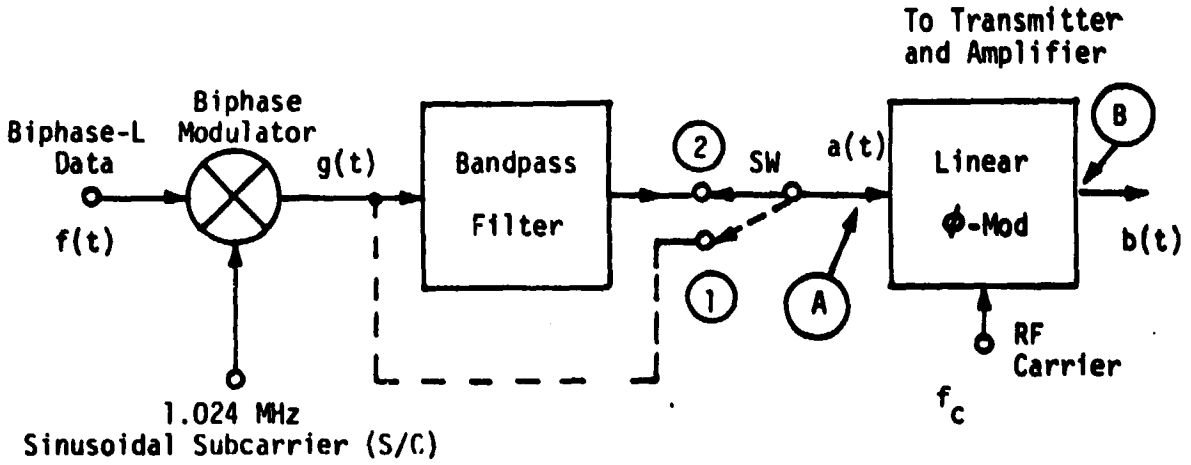

Part (a). Block Diagram for 1.024 MHz S/C Modulator

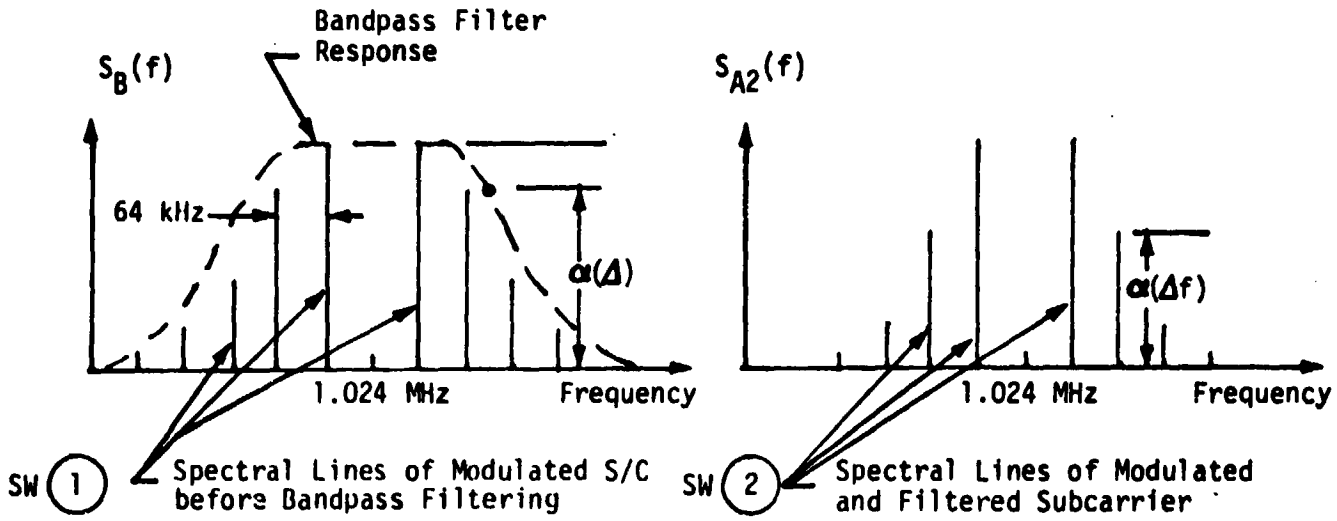

Part (b). Baseband Spectra of Modulated S/C Before and After Filtering
(Not to scale)

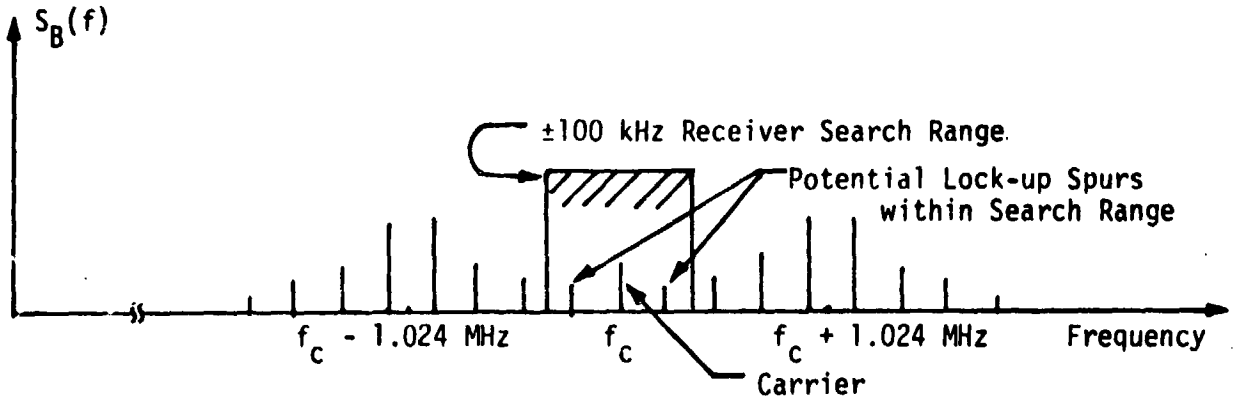

Part (c). Spectrum of Phase-Modulated RF Carrier

Figure 4.1. Effect of 1.024 MHz S/C Filter on Baseband and RF
Spectra of the Telemetry Signal

4.2.1.2.2 Spectral considerations

Part (c) of Figure 4.1 qualitatively shows the spectral distribution of the phase-modulated RF carrier. As indicated in the figure, the main spectral lines are distributed around a frequency offset of ±1.024 MHz away from the carrier. Note that the carrier line is also present. It is the presence of this carrier line which provides for the acquisition of the transponder signal by the frequency-swept STDN receiver at the ground. For the case of the 1.024 kHz PSK-modulated subcarrier being the only baseband signal determining the RF signal structure, the magnitude of the carrier component is only about 2 dB below the unmodulated carrier for a phase deviation of 1.0 radian peak.

4.2.1.2.3 False lock-up threat

Unfortunately, as indicated in part (c) of the figure, two of the sidebands generated by the subcarrier modulation fall within the ±100 kHz frequency search range of the STDN receiver. These sidebands are located ±64 kHz around the carrier when the data stream is 64 kbps and consists of only "ones" or "zeros." In order for the receiver not to lock up to the spurious sideband component, the magnitude of the sideband must be at least at or, preferably, below the acquisition threshold of the STDN receiver. Whether or not this condition is met depends on both the hardware and the system aspects of the problem.

The hardware aspect includes such factors as (1) modulation index used, (2) subcarrier bandpass filter characteristics, and (3) coherency of the subcarrier and the data clock signals. For example, for peak phase deviation of 1 radian, the magnitude of the spurious sideband will have an upper bound of -28 dB below the carrier component and a lower bound of -34 dB, the two cases representing the extremes of phase coherency between the subcarrier signal and the data clock. Without coherency, the relative phases will change and the sidebands will "beat", thus varying the amplitude of the spurious sideband between the limits. We consider, therefore, the "worst case" as -28 dB below the carrier component.

The next hardware factor to consider is the attenuation provided by the bandpass filter. Our analysis indicates that the effect of the bandpass filtering on the subcarrier reduces the f_c ±64 kHz spurs

by a factor of 60 dB. Consequently, the -28 dB and -34 dB attenuation (with respect to carrier term) values become -88 dB and -94 dB, respectively.

The system aspect of the spur lock-up problem involves such factors as (1) system geometry, and (2) the corresponding link budget. The worst-case geometry is when:

(1) The IUS is in the lowest orbit, i.e., 100 nmi (185.3 km)

(2) It is right overhead the STDN station

(3) The antennas of both the IUS and STDN are pointing directly at each other, i.e., boresight alignment.

Our link budget for this case indicates that the C/N_0 value of the ground station is 121.1 dB-Hz. For the phase deviation of 1.0 radian peak, the carrier suppression is 2 dB. Also, for a 2 B_L of 6000 Hz (i.e., B_L = 3000 Hz) and the minimum carrier acquisition SNR of +6 dB, the requirement for carrier acquisition is a C/N_0 of 45.8 dB-Hz. A comparison of this requirement with the available C/N_0 of 121.1 dB-Hz indicates a positive carrier acquisition margin of 75.3 dB. This means that the spurious cross-term should be at least 3 dB (margin) below the carrier component in order to provide spurious-free acquisition over the ±100 kHz range. But we predict the level of the spur, after filtering by the subcarrier filter, to be at -88 dB below the modulated carrier level. Thus, our false lock-up margin is

$$\text{False lock-up margin} = 75.3 \text{ dB} + 3 \text{ dB} - 88 \text{ dB} = 9.7 \text{ dB}.$$

With this margin, the acquisition loop bandwidth can be narrowed down to about 300 Hz (B_L) and still not cause a false lock-up.

We conclude, therefore, that the filtering of the PSK-modulated 1.024 MHz subcarrier does not present a potential problem, even for the worst case of data modulation and system geometry.

---

*Lowest orbit of the Space Shuttle.

4.2.2 Subanalysis Review and Verification

The preliminary design review (PDR) data package* for the S-band STDN/TDRS transponder included several subanalyses pertaining to the performance of this NASA IUS transponder. These detailed electrical design analyses were performed by the transponder contractor (TRW) to ensure that the transponder meets the performance specifications imposed by its use for NASA missions of the IUS.

The analyses which were 100% completed at the time of the PDR can be logically divided according to the subject, as shown in Table 4.1. Axiomatix has reviewed these subanalyses and, wherever applicable, has provided additional detailed analysis of our own. Presented below are the summaries and conclusions pertaining to the aforementioned subanalyses.

Subanalysis #5: IUS-TDRS Code Lock Detector for Code Lock Verification to Signal Acquisition

Overview

When the STDN/TDRS IUS transponder communicates with the ground via the TDRS relay, the transponder must establish a PN range code lock as the first step in establishing the communication link. Figure 4.2 shows the functional block diagram of the range code acquisition and lock detector. As shown in the figure, the locally generated range code is correlated with the incoming signal during the code search phase. The signal resulting from correlation (or lack of it) is applied to a band-pass filter and square law detector unit. The output of the detector is compared against the bias and the difference voltage is integrated for a certain period of time. If there is a correlation between the incoming and reference codes, a threshold comparator generates a signal which initiates the signal acquisition verification phase. The purpose of this verification phase is to distinguish between the true acquisition or false output of the threshold comparator caused by a random noise. Subanalysis #5 predicts the detection and false alarm probability performance of an "n out of N type" lock detector used for ranging code lock verification. This stage in the range channel detection process

---

*Dated April 1979 and reviewed June 11-13, 1979 meeting at Boeing, Seattle, Washington.

Table 4.1. Subanalyses Listing

Subject	Subanalysis No.	Title
PN Code Search and Lock Detection	#5	IUS-TDRSS code lock detector for code lock verification to signal acquisition
PN Code Tracking	#7	Time-shared code loop performance including an additional filter
	#11	Frequency noise of the time-shared code loop oscillator due to thermal noise
	#6	IUS-TDRS code loop acquisition and tracking bandwidth
Carrier Tracking	#12	Costas loop cycle slipping due to IUS antenna switching
Data Clock Tracking	#18	Squaring type clock recovery loop preliminary analysis of tracking performance (50% transition density)
Commands Data Performance	#20	IUS-TDRS probability of false commands
Command detection and Squelch	#21	IUS signal-to-noise ratio estimator processing
	#22	IUS decoder activation and deactivation by signal-to-noise ratio monitoring
	#19	Squelch circuit performance with and without range tone interference
Transponder frequency plan	#13	Spur analysis

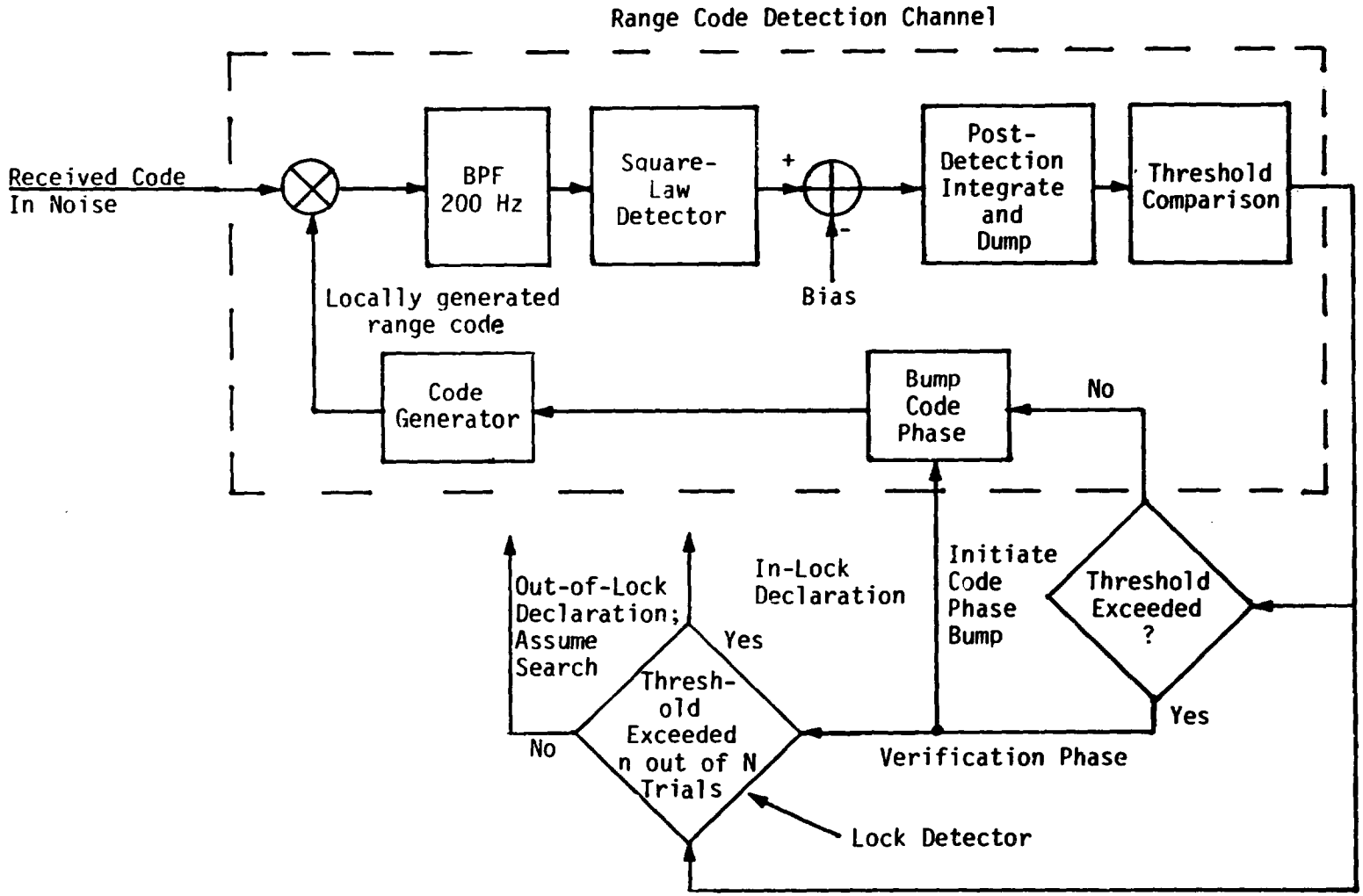

Figure 4.2. Range Code Acquisition and Lock Detection

occurs immediately after the first hit is declared while searching the 256 possible synchronization points of the locally generated range code relative to that of the received code in noise. With the locally generated code fixed in this synchronization position, the analysis determines the probability of an in-lock declaration corresponding to the probability that n out of N successive threshold comparisons in the range code detection channel produce detection decisions i.e., the threshold is exceeded.

Since, as mentioned above, the range code synchronization position is held fixed during the verification phase, a "false alarm hit" during the acquisition search would result in a false in-lock declaration while a "true hit" (correct code phase) during acquisition search would result in a true in-lock declaration. Furthermore, since the N repeated trials during the verification stage are performed independently (the post-detection integrate-and-dump intervals are disjoint), then the probability of false and true in-lock detection, $(P_{FA})_{LD}$ and $(P_D)_{LD}$ associated with the lock detector are related to the individual search cell probabilities of false alarm and true detection, P_{FA} and P_D, by simple binominal distributions, namely,

$$(P_D)_{LD} = \sum_{k=n}^{N} \binom{N}{k} P_D{}^k (1 - P_D)^{N-k}$$

$$(P_{FA})_{LD} = \sum_{k=n}^{N} \binom{N}{k} P_{FA}{}^k (1 - P_{FA})^{N-k} \qquad (1)$$

The analysis correctly identifies these relationships and tabulates (for $P_D = 0.33$, $P_{FA} = 0.0035$, both determined by simulation) $(P_{FA})_{LD}$ and $(P_D)L_D$ for various values of N (e.g., 8, 15, 25 and 30) and n = 1,2,3,4. For example, with n = 3 and N = 25 (three hits in 25 verification attempts), $(P_D)_{LD} = 0.996$ and $(P_{FA})_{LD} = 0.001$ and, with n = 4 and N = 30, we get $(P_D)_{LD} = 0.996$ (the same value) and $(P_{FA})_{LD} = 4 \times 10^{-6}$, both of which appear to give satisfactory performance.

Conclusions

Axiomatix concludes from these results that subanalysis #5 correctly provides the necessary analysis to assess the code lock detection performance and suggests that no further analysis is needed along these lines.

Subanalysis #7: Time-Shared Code Loop Performance Including an Additional Filter

Overview

Upon acquiring the PN range signal from the TDRS, the transponder will go into a tracking mode. The type of code tracking loop utilized by the STDN/TDRS transponder is known as a "tau-dither" loop. A functional block diagram of this type of loop is shown in Figure 4.3. It has been suggested that a "dither filter" (see Figure 4.2) be inserted into the loop just prior to remultiplication by the dither signal for the purpose of reducing the noise into this post-dither multiplier. Subanalysis #7 examines the effect of such a filter on the tracking performance (timing error variance) of the loop. In particular, an idealized lowpass dither filter is assumed having zero DC response and a bandwidth such as to exactly pass the first n harmonics of the square wave dither signal.

The result of the TRW analysis concludes that the timing error variance with such a dither filter present is identically equivalent to that in the absence of the dither filter multiplied by a factor $1/\gamma^2$, which accounts only for the additional SxS degradation produced by the dither filter. For the TRW analysis, the dither filter is assumed to have no effect on the SxN and NxN components into the loop filter.

The rationale provided behind this assumption is that, since the loop filter is much narrower in bandwidth than the dither filter, the dither filter's effect on determining the equivalent noise spectral density at work in the loop can be ignored. In reality, however, the dither filter and loop filter are not directly in cascade but, rather, are separated by the nonlinear operation of post-dither multiplication. This operation causes frequency translation of spectral components within the dither filter bandwidth down to DC, thus affecting the equivalent noise spectral density seen by the loop.

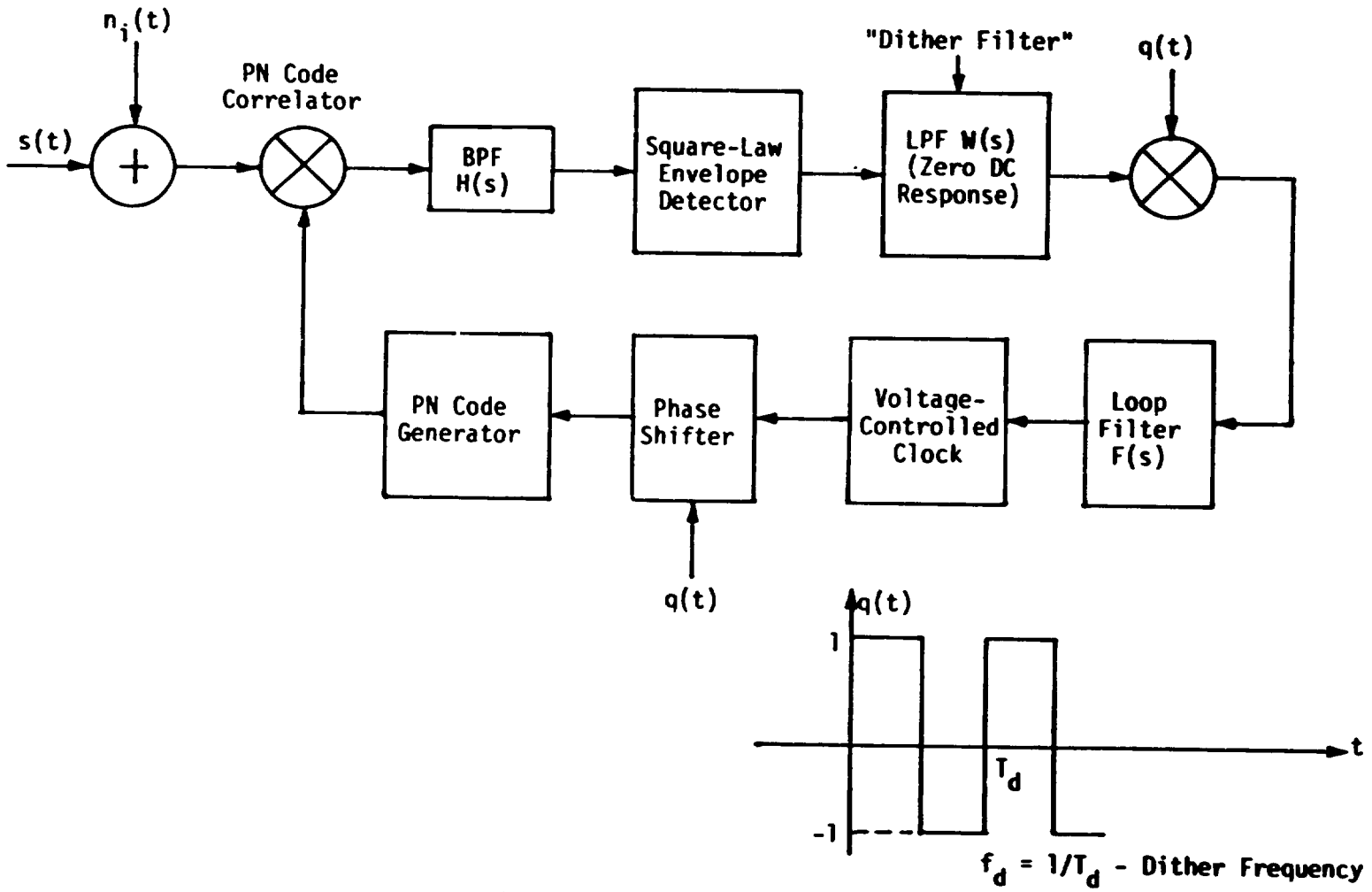

Figure 4.3. A Noncoherent "One-Δ" τ-Dither Loop with Dither Filter

To verify the validity of this assumption, Axiomatix has carried out an independent analysis of the effect of the dither filter on the tracking performance of the loop. This analysis is given in Appendix F of this report. Specifically, this appendix refines the theoretical results of TRW's analysis by including the effects of the dither filter on the above-mentioned noise components. In particular, it will be demonstrated that the additional SxS distortion (power loss) caused by the addition of the dither filter is partially compensated by an attendant reduction in SxN and NxN power, thus resulting in an even smaller performance degradation than that predicted in the TRW analysis. For a dither filter which passes only the first and third harmonics of the dither signal, it is shown that the increase in mean-square tracking jitter caused by the addition of this filter to the loop is only about 11%, rather than 23%, as indicated by neglecting the filter effect on the (SxN) and (NxN) components.

Conclusion

Using an independent analytical approach, Axiomatix has confirmed that the addition of a dither filter imposes a negligible tracking performance penalty relative to the potential advantage gained in terms of total power reduction into the post-dither multiplier.

Subanalysis #11: Frequency Noise of the Time-Shared Code Loop Oscillator Clock due to Thermal Noise

Overview

Analogous to the development in subanalysis #7 which leads to a characterization of the mean-square phase-tracking jitter (due to thermal noise) of the time-shared code loop, this subanalysis uses the same tau-dither loop model to determine the frequency noise of the code loop clock. Although it is stated in the summary and introductory sections of the subanalysis that the lowpass dither filter will be neglected, the results derived in subanalysis #11 do include the effect of this filter much in the same manner as that which was done in subanalysis #7. However, since Axiomatix has independently shown that, if anything, the results of using the TRW model for the filter effect are more pessimistic than reality, we proceed to review this subanalysis in its unaltered form.

The frequency noise of the code loop clock due to thermal noise is defined as the variance (mean-square value) of its instantaneous frequency, the latter being nothing more than the time derivative of the timing phase estimate discussed in subanalysis #7. Thus, if $\tau(t)$ denotes the unknown epoch of the received code and $\hat{\tau}(t)$ denotes its estimate produced by the code loop oscillator clock, then

$$\varepsilon(t) = \frac{\tau(t) - \hat{\tau}(t)}{T_c} \tag{2}$$

is the loop timing error (normalized to the chip interval, T_c), and

$$f(t) = \frac{d\varepsilon(t)}{dt} = \frac{1}{T_c}\left[\frac{d\tau(t)}{dt} - \frac{d\hat{\tau}(t)}{dt}\right] \tag{3}$$

is the corresponding normalized frequency error of the loop. In the absence of code doppler ($d\tau(t)/dt = 0$), this error is equal to the negative of the normalized instantaneous clock frequency.

The mean-square timing phase tracking jitter σ_ε^2 can be computed from

$$\sigma_\varepsilon^2 = \overline{\varepsilon^2(t)} = \frac{\int_{-\infty}^{\infty} |H(f)|^2 S_N(f)\,df}{(\alpha C)^2} \cong \frac{S_N(0)(2B_L)}{(\alpha C)^2} \tag{4}$$

where $S_N(f)$ is the power spectral density of the equivalent noise $N(t) = n_1(t) + n_2(t)$ [see equation (15) of subanalysis #7, reference 15 for definitions of $n_1(t)$ and $n_2(t)$] perturbing the loop, C is the received signal power, α is a data modulation filtering loss [equation (16) of subanalysis #7], B_L is the single-sided loop noise bandwidth, and H(s) is the closed-loop transfer function.

Using (3), the mean-square frequency noise is then

$$\sigma_f^2 = \overline{f^2(t)} = \frac{\int_{-\infty}^{\infty} (2\pi f)^2 |H(f)|^2 S_N(f)\,df}{(\alpha C)^2} \tag{5}$$

For a second-order code loop with a perfect integrating loop filter and 0.707 damping, the magnitude squared transfer function $|H(f)|^2$ is given by (36) of [15]

$$|H(f)|^2 = \frac{1 + 2\left(\frac{f}{f_n}\right)^2}{1 + \left(\frac{f}{f_n}\right)^4} \tag{6}$$

where $f_n = \omega_n/2\pi$ is the loop natural frequency. Making suitable approximations to the integral evaluation required in (5), in particular, the assumption $f_n << B$, where B is the predetection filter bandwidth, then the TRW analysis arrives at the final result:

$$\sigma_f^2 = \left(\frac{N_0 B}{\alpha C}\right)\left[1 + 6\left(\frac{N_0 B}{\alpha C}\right)\right]\omega_n^2 = \left(\frac{N_0 B}{\alpha C}\right)\left[1 + 6\left(\frac{N_0 B}{\alpha C}\right)\right]\left(\frac{32}{9} B_L^2\right) \tag{7}$$

The equivalent result from subanalysis #7 for σ_ε^2 is:

$$\sigma_\varepsilon^2 = \left(\frac{N_0 B_L}{\alpha C}\right)\left[1 + 2\left(\frac{N_0 B}{\alpha C}\right)\right] \tag{8}$$

Conclusion

Aside from the dither filter effects, Axiomatix agrees with the result [(8) above] derived in the TRW analysis for characterizing the frequency noise of the code loop oscillator.

Subanalysis #6: IUS-TDRS Code Loop Acquisition and Tracking Bandwidth

Overview

In this analysis, the IUS-TDRSS code loop acquisition and tracking bandwidths are specified both for operation at threshold (C/N_0 = 34 dB-Hz) and strong signal [$(C/N_0)_{max}$ = 59 dB-Hz]. In determining the bandwidth expansion with power level from threshold to strong signal, the effect of the wideband noncoherent AGC, which precedes the code loop, is accounted for.

The principal result used in this analysis to relate the acquisition and tracking performance to the corresponding loop bandwidth specifications is the relation for mean-square phase-tracking jitter as a function of the various system parameters [see equation (51) of subanalysis #7].

First, the acquisition behavior of the code loop is investigated under strong signal conditions, thus allowing use of the phase plane as an analysis tool. For a maximum carrier frequency uncertainty of ±1400 Hz (±700 Hz doppler) ±700 Hz IUS oscillator instability) corresponding to a code rate uncertainty of ±2 chips/s (the ratio of carrier frequency to code rate is 700), it is shown that, for an acquisition loop bandwidth B_L = 6 Hz, almost all valid hits (i.e., code phase coincidences) will be pulled into lock.

Second, using the above-mentioned relation from subanalysis #7, namely, (ignoring the dither filter)

$$\sigma_\varepsilon = \left\{ \frac{N_0 B_L}{\alpha C} \left[1 + 2 \frac{N_0 B}{\alpha C} \right] \right\}^{1/2} \tag{9}$$

the tracking jitter in the acquisition mode can be evaluated. In particular, at threshold with α = -0.9 dB and B = 5 kHz, we obtain σ_ε = 0.132 chips.

In the tracking mode, the filtering loss α becomes reduced to -0.46 dB since part of the code loop frequency uncertainty, namely, the code doppler, is tracked out. Thus using (9), we conclude that, at threshold, a tracking loop bandwidth B_{LO} = 4.16 Hz is required to meet the specification of σ_ε = 0.1 chips. At strong signal, taking into account the AGC action, the threshold tracking bandwidth will expand by the factor

$$\frac{B_L}{B_{LO}} = \frac{2 \frac{P_2}{P_1} + 1}{3} \tag{10}$$

where P_2/P_1 reflects the change in signal power out of the noncoherent AGC and is given by

$$\frac{P_2}{P_1} = \left(\frac{1 + SNR_{min}}{SNR_{min}}\right)\left(\frac{SNR_{max}}{1 + SNR_{max}}\right) \qquad (11)$$

with

$$(SNR)_{min} = \left(\frac{C}{N_0}\right)_{thresh}\left(\frac{1}{B_{AGC}}\right)$$

$$(SNR)_{max} = \left(\frac{C}{N_0}\right)_{max}\left(\frac{1}{B_{AGC}}\right)$$

$$B_{AGC} = \text{pre-AGC bandwidth} = 7 \text{ MHz} \qquad (12)$$

Using the design values of threshold and strong signal C/N_0, we have from (11) and (12) that $P_2/P_1 = 284.4$, whereupon $B_L/B_{LO} = 190$.

Also considered in the analysis is the question of whether or not bandwidth switching is necessary when handing over from acquisition to tracking. In order to still meet the specification on RMS tracking jitter, it has been suggested that the tracking loop bandwidth be used during acquisition. Doing so would reduce the maximum code phase error allowable to achieve pull-in and potentially cause an increase in acquisition time for valid hits with an initial error greater than this amount.

Conclusion

In summary, Axiomatix feels that TRW subanalysis #6 contains the necessary theoretical results to predict code acquisition and tracking bandwidths.

Subanalysis #12: Costas Loop Cycle Slipping due to IUS Antenna Switching

Overview

In this analysis, the potential of one or more cycle slips occurring in the carrier tracking Costas loop due to a large step change in phase at its input is examined. Such a situation occurs when switching from one IUS antenna to another produces an electrical phase shift (due to the difference in path lengths between the two) having a maximum

value of 84° in the phase of the RF carrier. Since a Costas loop tracks twice the phase error of a residual carrier loop (such as a PLL), it, in effect, sees a phase jump of 2 x 84 = 168°.

Using the phase plane technique which inherently assumes high (theoretically infinite) loop SNR, the analysis demonstrates that a negative phase change of 84° causes the loop to pull back into lock without a cycle slip. On the other hand, a positive phase step of 84° causes a single cycle slip before the loop once again returns to its locked condition. Such a cycle slip will cause the Costas loop demodulation reference signals to shift by π radians, thus inverting the demodulated data.

The particular example chosen for illustration in the analysis assumed a 0.707 loop damping and a static phase error corresponding to a normalized loop detuning $\Omega_0/A^2K = 0.4$. Thus, since the stable lock point occurs at $\Phi = \sin^{-1} \Omega_0/A^2K = 23.58°$, the ±168° phase changes should be made relative to $\Phi = 23.58°$--not $\Phi = 0°$--as is done in the TRW analysis. Fortunately for this example, doing such does not alter the conclusions stated above; however, larger values of detuning could, for a positive phase change, cause more than a single cycle slip.

Conclusion

Further analysis explaining the cycle slip behavior of the Costas loop due tc antenna switching at low values of loop SNR cannot be performed due to the lack of a theory to predict the mean time to loss of lock performance. Thus, Axiomatix, in agreement with TRW, believes that predicting loss of lock behavior under such conditions will have to be determined from experimental measurements.

Subanalysis #18: Squaring-Type Clock Recovery Loop Preliminary Analysis of Tracking Performance (50% Transition Density)

Overview

The IUS STDN/TDRS transponder incorporates a bit synchronization loop in its command detector unit (CDU) whose function is to recover a 2 kbps clock from the received command data signal. One candidate that has been suggested for this loop is configured as a baseband version of a squaring loop commonly used for carrier recovery (see Figure 4.4).

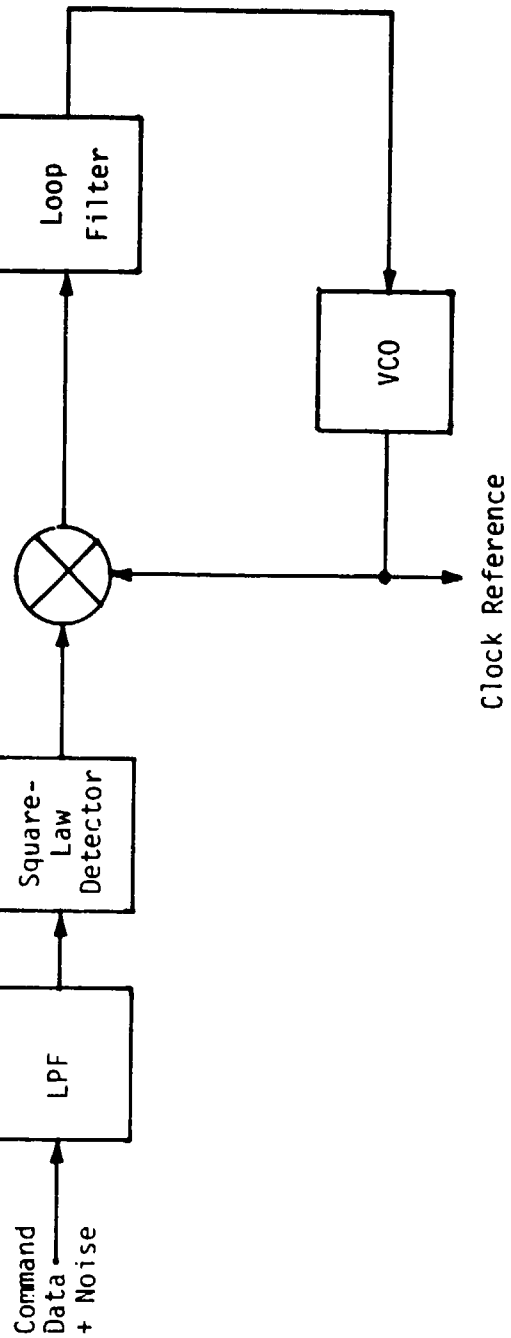

Figure 4.4. A Filter Square-Law Type Clock Recovery Loop

In particular, the baseband signal-plus-noise is heavily filtered and square-law detected, thus generating a clock component at the command data rate. Finally, the square-law detector is followed by a sinusoidal phased-lock loop (PLL) which tracks this component, thus producing the desired bit rate clock.

It must be pointed out that the derivation, as it appears in the first version of subanalysis #18, has been subsequently updated by TRW to reflect the changes in the initial assumptions.

In anticipation of these changes, Axiomatix has carried out an independent analysis of the clock loop performance. Our analysis of the bit synchronization loop, given in Appendix C, indicates that, for a fixed value of symbol-to-noise ratio E_S/N_0, there is an optimum value of R.* Furthermore, as R approaches zero or infinity, the normalized timing error variance increases without bound.

Appendix C of this report also considers the behavior of the loop as a function of bit transition density, whereas the TRW subanalysis considers only the performance for 50% transition density, i.e., random data. It is interesting to note from the results in the appendix that, for random data, the minimum normalized timing error variance is relatively insensitive to symbol energy-to-noise ratio over a large (on the order of 10 dB) range and the optimum value of R is virtually fixed at 0.2 over this same ratio of E_s/N_0 values. For large transition densities, on the other hand, the optimum filter bandwidth becomes much more sensitive to E_s/N_0.

Conclusion

Axiomatix feels that the analysis in Appendix C is both necessary and sufficient to assess the performance of the filter square-law type bit synchronization loop both absolutely and relative to published results for more commonly used loops.

Furthermore, in our analysis, consideration is also given to the possibility of designing the PLL to track a higher harmonic of the clock since these harmonics are also present in the square-law detector output. The desired data rate clock would then be obtained by counting down the PLL reference by the appropriate multiple, along with an attendant timing ambiguity caused by the frequency division.

---

*R is the product of filter cutoff frequency f_c and data symbol duration T.

Subanalysis #19: Squelch Circuit Performance With and Without Range Tone Interference

Overview

The command detector unit (CDU) of the IUS STDN/TDRS transponder will contain a squelch circuit whose purpose is to inhibit command data when the received signal-to-noise ratio (SNR) drops below a preset value, e.g., 6 dB. In subanalysis #21, the performance of an SNR estimator formed from the ratio of the square of the sample mean to the sample variance of the magnitude of the CDU integrate-and-dump (data detector) output was considered. Here in subanalysis #19, an alternate squelch circuit is considered wherein hard decisions on the CDU I&D output are correlated (multiplied) with "single sample" hard decisions made on the received command data waveform and accumulated over M bit intervals. The resultant accumulation of hard decision (±1) products is compared to a preset threshold to determine whether or not the received command data should be squelched. The primary purpose of the subanalysis is to determine suppression of the squelch circuit output caused by the presence of a 20 kHz range tone in addition to the received 16 kHz biphase-modulated command data subcarrier.

While Axiomatix agrees with the fundamental analysis approach taken by TRW to predict this degradation, our own calculations indicate a factor of two difference in assessing the SNR in the "single sample" decision channel. This difference seems to come as a result of the TRW analysis not accounting for the factor of two reduction in equivalent single-sided noise bandwidth when demodulating the subcarrier, i.e., while the BPF filter preceding the subcarrier demodulation has a single-sided noise bandwidth B = 8 kHz, the effective single-sided lowpass noise bandwidth, which affects the hard decisions in the "single sample" channel of the squelch circuit, is B/2 = 4 kHz. Thus, the result of subanalysis #19 should be modified as follows:

If the input to the BPF preceding the subcarrier demodulation is given by

$$y(t) = \sqrt{2}\,A\,d(t)\,\sin(2\pi(16000)t) + \sqrt{2}\,A_I\,\sin(2\pi(20{,}000)t) + n(t) \qquad (13)$$

where the first term is the command data subcarrier with RMS amplitude A and command modulation d(t), the second term is the interfering 20 kHz ranging tone with RMS amplitude A_I, and n(t) is bandpass Gaussian noise of power N_0B, then the mean $\bar{z}$ of the squelch circuit output, z, $\bar{z}$, is approximately given by

$$\bar{z} = \frac{1}{2\pi}\int_{-\pi}^{\pi} \operatorname{erf}\left[\sqrt{\frac{A^2}{N_0B}}\left(1+\frac{A_I}{A}\sin\phi\right)\right]d\phi$$

$$= \frac{1}{2\pi}\int_{-\pi}^{\pi} \operatorname{erf}\left[\sqrt{\frac{E_b}{N_0}}\left(\frac{1}{BT}\right)\left(1+\frac{A_I}{A}\sin\phi\right)\right]d\phi \qquad (14)$$

where $E_b/N_0 = A^2R/N_0$ is the data detection SNR. The TRW analysis obtains the result in (14) with, however, B replaced by 2B.

Since the variance σ_z^2, of the squelch circut output, z, can be shown to be essentially unchanged by the additional presence of the ranging tone, the effective SNR suppression caused by this tone is simply the reduction of $\bar{z}^2$ relative to its value when $A_I = 0$, i.e.,

$$\text{suppression (dB)} = 20\log_{10}\left\{\frac{\operatorname{erf}\left[\sqrt{\frac{E_b}{N_0}}\left(\frac{1}{BT}\right)\right]}{\frac{1}{2\pi}\int_{-\pi}^{\pi}\operatorname{erf}\left[\sqrt{\frac{E_b}{N_0}}\left(\frac{1}{BT}\right)\left(1+\frac{A_I}{A}\sin\phi\right)\right]d\phi}\right\} \qquad (15)$$

For a command data rate 1/T = 2 kbps and B = 8 kHz, BT = 4. Figure 4.5 plots the suppression as computed from (15) versus the interference-to-command data RMS amplitude ratio A_I/A for E_b/N_0 = 6 dB and the above value of BT.

Conclusion

Since the signal of (13) is phase modulated on a carrier, A_I/A also represents the ratio of ranging modulation angle to command data modulation angle. Thus, when modulation angles of 1.0 radian for the data and 0.3 radian for the range tone are used (A_I/A = 0.3), then, from

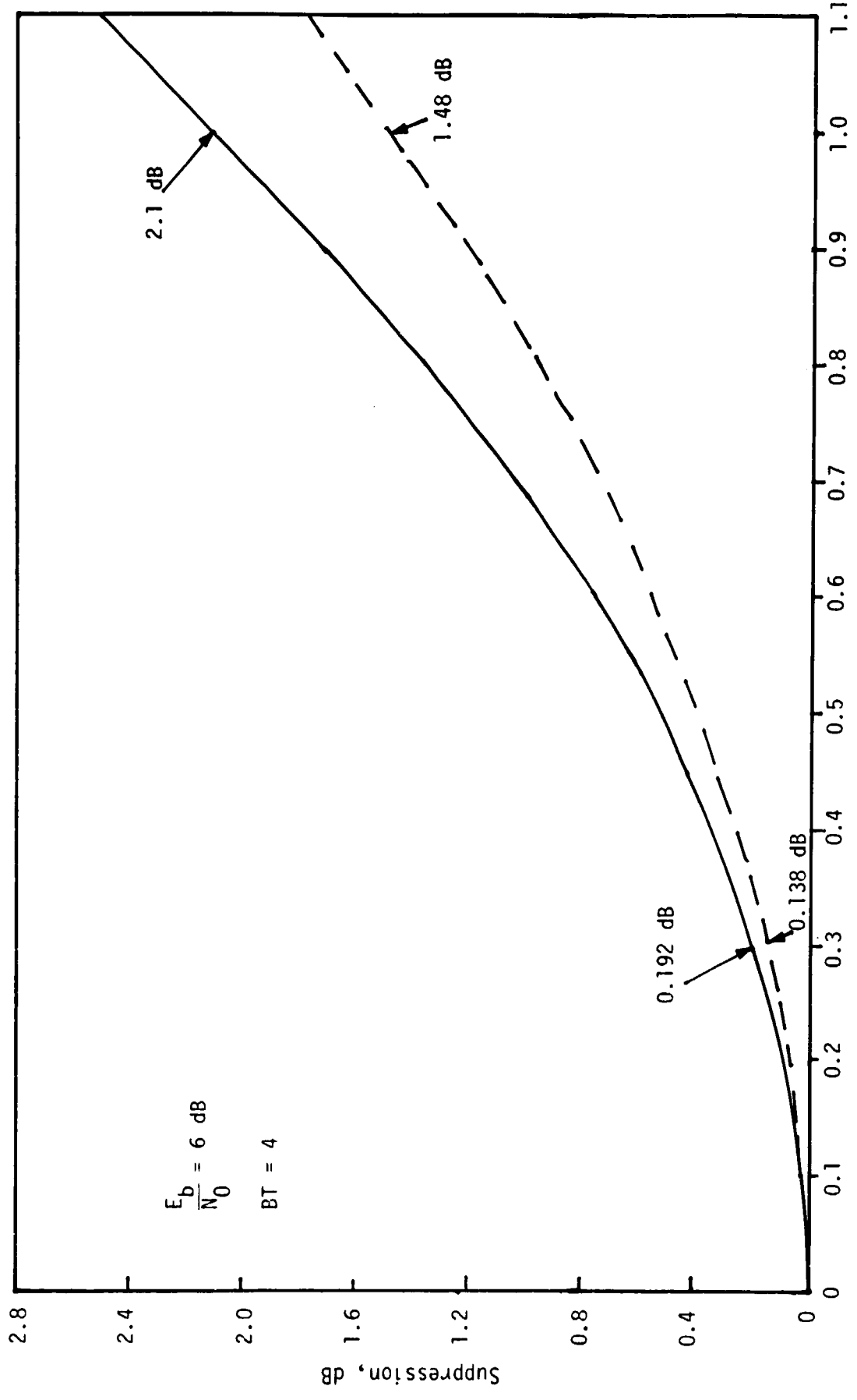

Figure 4.5. Squelch Output Signal Suppression versus Interference to Command Data RMS Amplitude Ratio

Figure 4.5, we observe that a 0.192 dB suppression of the squelch circuit output occurs relative to its value when the range tone is absent. When the modulation angles are both 0.5 radian ($A_I/A = 1$), as has more recently been proposed, the suppression increases to 2.1 dB. The corresponding results from the TRW analysis are superimposed on Figure 4.5 in dashed lines and, because of the factor of two discrepancy as previously identified, are clearly optimistic. However, it appears that the utilization of the squelch circuit is such that the overall operation is not highly sensitive to this discrepancy.

Subanalysis #13: Transponder Frequency Plan

Overview

Axiomatix has reviewed the TRW analysis of the spurious responses of the STDN and SGLS transponder receivers (STDN/TDRS Transponder PDR Package, "Subanalysis No. 13," pp 5-75 to 5-80).

A spurious response analysis of these receivers is valuable since they are of the double-conversion type and it is well-known that such receivers often have undesirable spurious responses. Moreover, the STDN and SGLS receivers are designed such that the second intermediate-frequency amplifier is part of a narrowband tracking loop which may give rise to additional spurious responses. It is therefore useful to understand the possible spurs of these receivers and to review the TRW analysis.

Block diagrams of the STDN/TDRS and SGLS receivers are shown in Figures 4.6 and 4.7, respectively. Although three mixers are shown for each receiver (M1, M2 and M3), only M1 and M2 are mixers in the conventional sense of operating in the signal path. Mixer M3, the starting point for the TRW spurious analysis, is part of the tracking loop, and neither the "inputs" nor the "outputs" of this mixer are in the signal path. The analysis of mixer M3 for spurious responses is therefore inherently different from the more conventional analyses of mixers M1 and M2; one purpose of this report is to explicate TRW's analysis of mixer M3.

The TRW subanalysis includes results of the spur analysis for each transponder (STDN/TDRS and SGLS) at both low and high ends of the respective input radio frequency ranges. TRW's approach begins by considering the third mixer, M3. TRW uses conventional mixer nomenclature

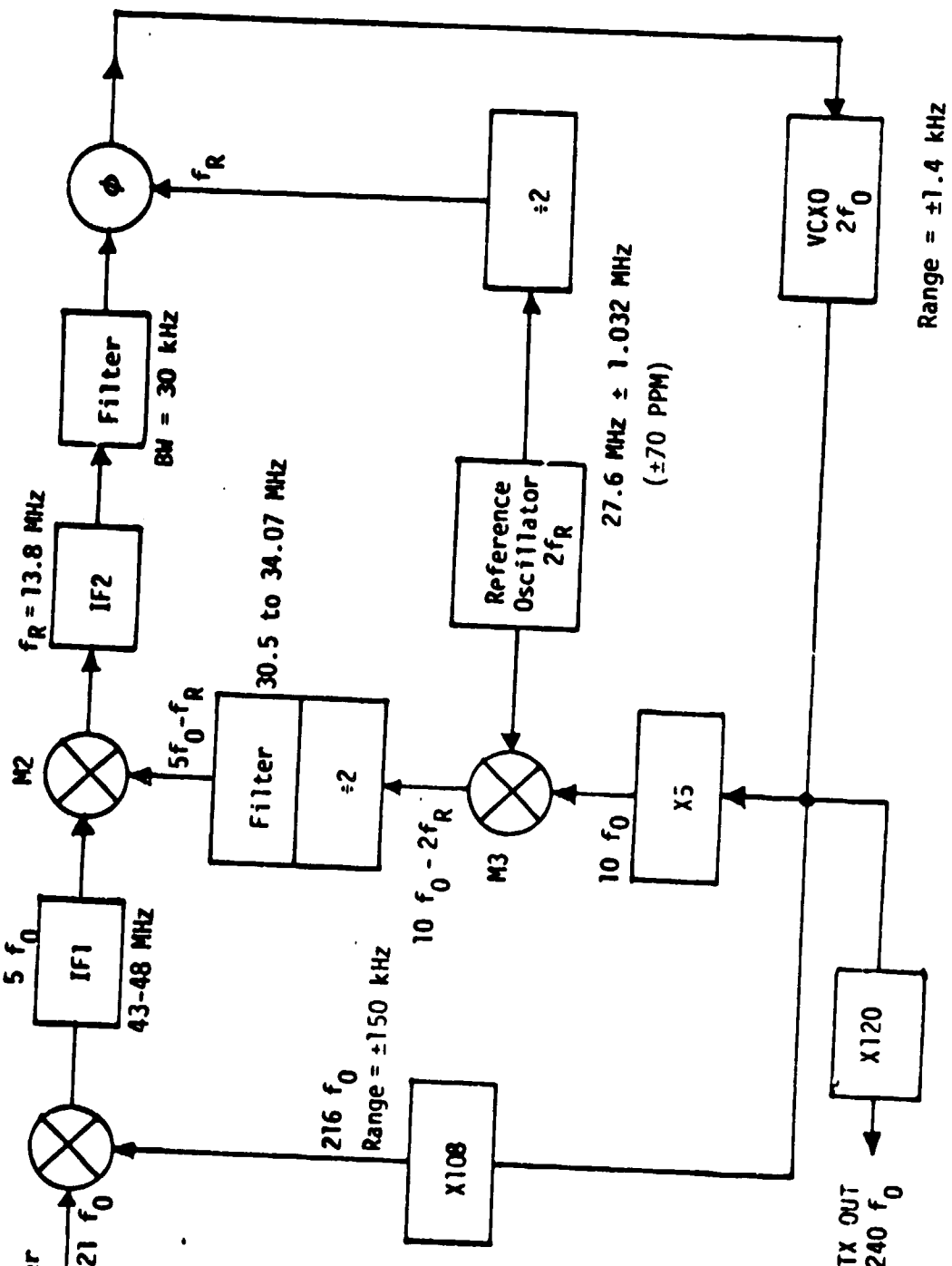

Figure 4.6. STDN/TDRS Transponder Receiver

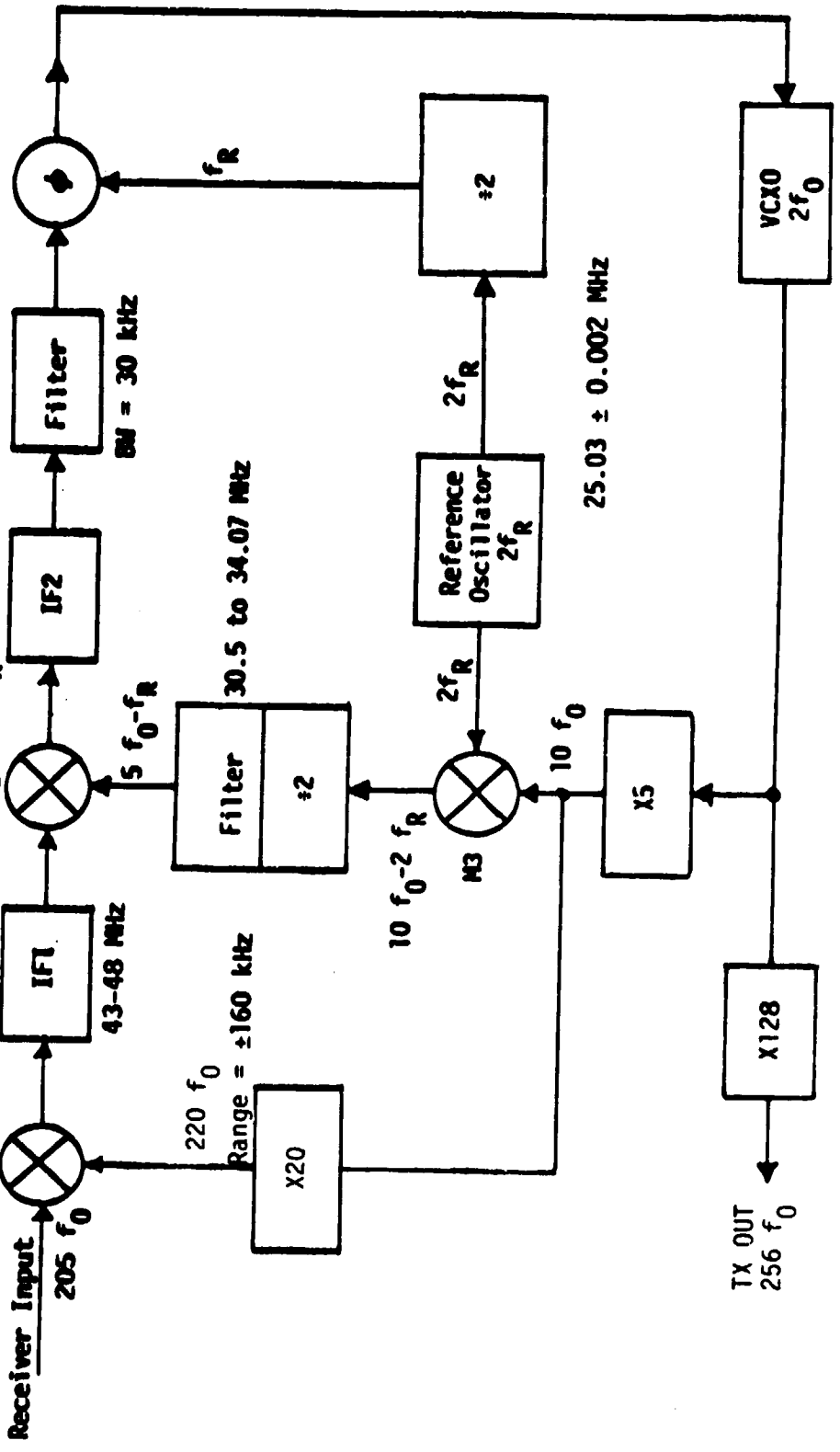

Figure 4.7. SGLS Transponder Receiver

although, as we have noted, this mixer is not part of the signal path. A detailed block diagram of M3 and the associated circuits applicable to both the STDN and SGLS receivers, is shown in Figure 4.8.

Axiomatix's detailed review and examination of TRW's spur analysis is presented in Appendix B of this report.

Conclusion

The TRW spur analysis of the STDN/TDRS and SGLS transponders have been reviewed and explicated in moderate detail, as shown in Appendix B. For each of the spurs, we have computed all the relevant frequencies that appear in the signal path since these are necessary for a full understanding of the nature of the spurious responses. Axiomatix finds it satisfying that only one spur ("FREQ F") arises from the use of a mixer M3 not in the path and that this spur is not of a particularly troublesome level.

Subanalysis #20: IUS-TDRS Probability of False Commands

Overview

The probability, P_{FC}, of executing a false command, i.e., a command word which, due to noise during transmission, was detected as another valid command word, is an important consideration in evaluating the IUS/TDRS system. This subanalysis provides upper bounds for this probability corresponding to the different types of commands which are distinguished from one another by the manner in which verification of the command is accomplished.

Single-word, one-stage commands (used only in an emergency mode) require only one stage of verification for execution, wherein the execute word which follows the actual command word and the actual command word itself must agree exactly. In single-word, two-stage commands (the standard operating command mode), the command sent to the IUS is decoded on board, first compared with the transmitted execute word, then transmitted as downlink telemetry to the sending station for comparison with the original transmitted command.

Both of these checks (verifications) must be successfully accomplished before the command is indeed implemented. Although there is presently no on-board capability for one-stage, multiword commands, their false command probability is also upper bounded.

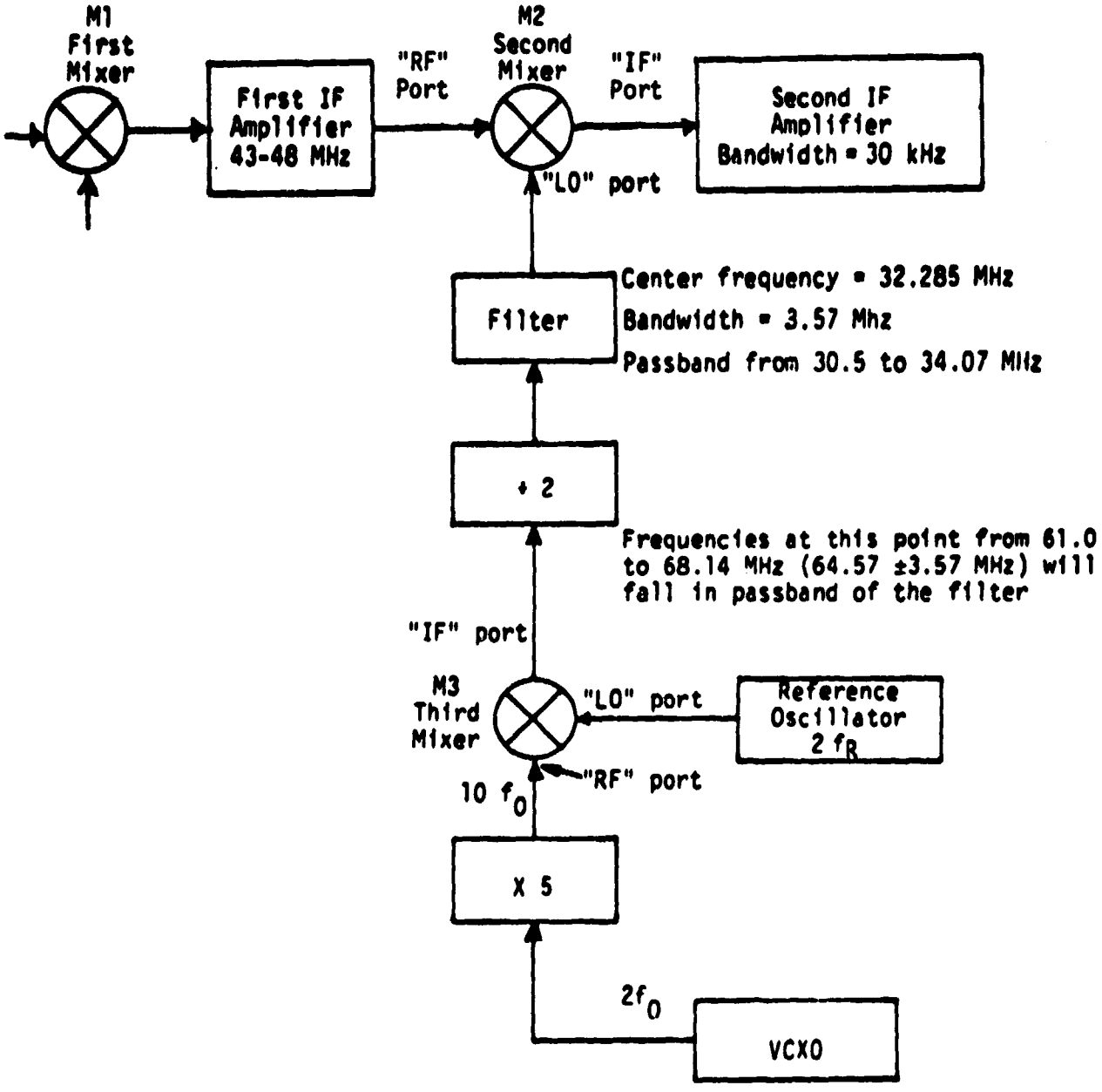

Figure 4.8. Mixer M3 and Associated Circuits
(STDN/TDRS and SGLS Receivers)

Letting P_b denote the channel bit error probability, the various results (upper bounds on P_{FC}) are summarized below. In calculating these bounds, only two bit errors are considered except in the multiple-command-word case where two and four errors are considered.

(1) Single-stage, single-word commands

Case a--Bits 1-11 plus the ambiguity word, plus the address, plus the overall parity bit (bit 20), plus the execute word are used to determine if the command word is valid

$$P_{FC} \leq 136\ (1 - P_b)^{58}\ P_b^{\ 4} \tag{16}$$

Case b--Same as case a except that the 12th bit (a subparity bit on bits 9-11) is used in addition for determining the validity of the command

$$P_{FC} \leq 84\ (1 - P_b)^{58}\ P_b^{\ 4} \tag{17}$$

Case c--Same as case b except that the 16th bit (a subparity bit on bits 13-15) is used in addition for determining the validity of the command

$$P_{FC} \leq 48\ (1 - P_b)^{58}\ P_b^{\ 4} \tag{18}$$

$$\text{Mean time between false commands} = \frac{1}{RP_{FC}} \tag{19}$$

where R is the command word rate.

(2) Single-stage, multiword commands (Axiomatix's results)

Two-word commands:

$$P_{FC} \leq 190\ P_b^{\ 2}\ (1 - P_b)^{87} + 4981\ P_b^{\ 4}\ (1 - P_b)^{85} \tag{20}$$

25-word commands:

$$P_{FC} \leq 4560\ P_b^{\ 2}\ (1 - P_b)^{708} + 10{,}080{,}016\ P_b^{\ 4}\ (1 - P_b)^{706}. \tag{21}$$

It must be pointed out that the coefficients of the second terms in (20) and (21) are different from those in the TRW subanalysis. This is due to a numerical error in TRW's computation. The final results, however, are not affected because of the small contribution these secondary terms provide.

Conclusion

Because of the assumption that $P_b \leq 10^{-3}$, the computational errors appearing in TRW's subanalysis #20 do not significantly alter the final result given by this subanalysis.

Subanalysis #21: IUS Signal-to-Noise Ratio Estimator Processing

Overview

The command detector unit (CDU) of the IUS STDN/TDRS transponder will contain a squelch circuit whose purpose is to inhibit command data when the received signal-to-noise ratio (SNR) drops below a preset value. The squelch is nothing other than an SNR estimator formed from the ratio of the square of the sample mean to the sample variance of the magnitude of the CDU matched filter [integrate-and-dump (I&D)] output. The sample size, n (i.e., the number of consecutive I&D output samples, one per command data bit), is a parameter which determines the accuracy (for a fixed confidence level) of the estimate. The accuracy of the estimate is also dependent on the actual SNR itself, although to a lesser extent.

The subanalysis first reviews the form and statistics of the well-known SNR estimator mentioned above, namely,

$$\widehat{SNR} = \frac{(\hat{\mu})^2}{\hat{\sigma}^2} = \frac{\left(\frac{1}{n}\sum_{i=1}^{n}|x_i|\right)^2}{\frac{1}{n-1}\sum_{i=1}^{n}\left(|x_i| - \hat{\mu}\right)^2} \qquad (22)$$

where x_i is the CDU I&D output sample corresponding to the ith transmitted command data bit. From the form of (22), it appears that the n samples must be stored to compute $\hat{\mu}$ before $\hat{\sigma}^2$ can be computed. By rewriting (21) in the form

$$\widehat{SNR} = \frac{\left(\frac{1}{n}\sum_{i=1}^{n}|x_i|\right)^2}{\frac{1}{n-1}\left[\sum_{i=1}^{n}|x_i|^2 - n\left(\frac{1}{n}\sum_{i=1}^{n}|x_i|\right)^2\right]} \tag{23}$$

the analysis demonstrates that it is not necessary to store the n values of x_i before computing $\hat{\sigma}^2$ and, thus, SNR.

Finally, the subanalysis shows that the SNR estimator of (23) can be computed by processing the n output sample magnitudes in subgroups of, say, 16 bits. Then, after M = n/16 subgroups are processed, the first SNR estimate may be made according to

$$\widehat{SNR} = \frac{\left(\frac{1}{M}\sum_{k=1}^{M}\mu_{16}^{(k)}\right)^2}{\frac{1}{n-1}\left[\sum_{k=1}^{M}M_{16}^{(k)} - n\left(\frac{1}{M}\sum_{k=1}^{M}\mu_{16}^{(k)}\right)^2\right]} \tag{24}$$

where $\mu_{16}^{(k)}$ and $M_{16}^{(k)}$ are the kth subgroup mean and mean-square values, namely,

$$\mu_{16}^{(k)} = \frac{1}{16}\sum_{16(k-1)+1}^{16k}|x_i|$$

$$M_{16}^{(k)} = \sum_{16(k-1)+1}^{16k}|x_i|^2 \tag{25}$$

The next SNR estimate can be obtained by updating with a new 16 bits, i.e., the sums in (24) now run from k=2 to k=M+1, etc. An alternate method of subgroup processing is to use (23) and update the summations one bit at a time, i.e., the ℓth estimate is obtained by summing from $i=\ell$ to $i=n+\ell-1$.

Conclusion

Since the SNR estimation technique presented in this subanalysis is well-known and convenient and because efficient processing algorithms have already been suggested for its evaluation, Axiomatix accepts this subanalysis as being an adequate solution to the problem of IUS SNR estimation.

Subanalysis #22: IUS Decoder Activation and Deactivation by Signal-to-Noise Ratio Monitoring

Overview

This analysis continues the discussion of the SNR monitoring function given in subanalysis #21 by presenting results for its performance as a function of the number of bits, n, used in processing (sample size) and the actual SNR value, E_b/N_0, being estimated. Specifically, for signal-to-noise ratios of 7 and 10 dB, the 90% confidence limits (the values of SNR between which $\hat{SNR}$ will lie with a probability equal to 0.9) are determined as a function of n.

In comparison with the SNR estimator discussed in subanalysis #21, two modifications were made here. First, the previous SNR estimator was divided by two and the second sample variance was scaled by the factor (n-1)/(n-3). Thus, the SNR estimator now takes the form

$$\widehat{SNR} = \frac{1}{2}\left[\frac{(\hat{\mu})^2}{\left(\frac{n-1}{n-3}\right)\hat{\sigma}^2}\right] = \frac{1}{2}\left[\frac{\frac{1}{n}\sum_{i=1}^{n}(|x_i|)^2}{\frac{1}{n-3}\sum_{i=1}^{n}(|x_i|-\hat{\mu})^2}\right] \qquad (26)$$

The reason for the latter change is that it results in an estimator with a smaller variance and a mean which is less biased.

Although an exact expression for the probability density function of $\widehat{SNR}$ of (26) is known, it was found convenient and a good approximation (e.g., for $n \geq 50$) to fit a Gaussian distribution to this estimator using the mean and variance as computed from the exact probability density function. Since, for a Gaussian distribution with mean μ and variance σ^2 the 90% confidence limits are given by $\mu \pm 1.65\sigma$, then for the estimator of (26) these limits become

$$E\{\widehat{SNR}\} \pm 1.65\sigma(\widehat{SNR}) \qquad (27)$$

where

$$E\{\widehat{SNR}\} = \frac{1}{2n} + \frac{E_b}{N_0}$$

$$\sigma^2(\widehat{SNR}) = \left(\frac{2}{n-5}\right)\left[\left(\frac{E_b}{N_0}\right)^2 + \left(\frac{E_b}{N_0}\right)\left(1 - \frac{1}{n}\right) + \frac{1}{2n}\left(1 - \frac{1}{n}\right)\right] \qquad (28)$$

As an example of the use of (27) and (28), it was found in the analysis that using, say, n = 450 bits, the 90% confidence limits were about ±0.5 dB about the true values of SNR for either value of E_b/N_0 (i.e., 7 or 10 dB). Beyond this point, large increases in n produce only small improvements in estimator accuracy (decrease in confidence region).

The final section of the subanalysis relates the way in which the SNR estimator is used to activate and deactivate the command decoder. For example, for a command data rate of 2000 bps and a processing delay time T_p = 10 ms, an SNR estimate based upon, say, 200 bits, would require a total delay time of 200/2000 + 10 x 10^{-3}, or 110 ms before the decoder could be deactivated based on the SNR estimator producing the correct SNR. Thus, in order to squelch bad command data, we would require a buffer to delay the data by 110 ms.

Conclusion

In the opinion of Axiomatix, the analysis and numerical results provided by TRW in subanalysis #22 are correct and adequate to assess the IUS decoder activation and deactivation performance using SNR monitoring.

4.2.3 Major STDN/TDRS Transponder/Orbiter Communication Interface Issues

During the subject contract, a number of major interface issues between the STDN/TDRS transponder and the Orbiter communication equipment were addressed. Some of these interface issues were resolved, while others are still in the process of being worked.

4.2.3.1 STDN/TDRS transponder auxiliary oscillator stability

The STDN/TDRS transponder auxiliary oscillator stability of 29 parts per million (0.0029%) exceeds the original PI specification and ICD (Interface Control Document) of 0.001%. In order to accommodate the additional transmitted frequency uncertainty of the STDN/TDRS transponder during independent transmitter/receiver operation, the acquisition sweep range of the PI receiver was increased. Therefore, this interface issue has been resolved by modification to the PI design.

4.2.3.2 Phase noise and communications turn-around characteristics

The effect of transmitter receiver and transponder turn-around phase noise on the STDN/TDRS transponder performance and the PI performance has yet to be analyzed. Initial PI transmitter and receiver phase noise have been released from TRW during the PI PDR in October 1979. However, these results do not reflect the change in design of the reference oscillator that drives the PI frequency synthesizer. The final PI phase noise results will not be available until the middle of 1980. Therefore, a preliminary assessment of the PI performance is being made by TRW and Axiomatix (under Contract NAS 9-15604C) using the results of the PI PDR data. To complete the assessment of the PI performance, the spectrum of the turn-around phase noise and the auxiliary oscillator phase noise of the STDN/TDRS (and SGLS) transponders is needed.

The SGLS transponder phase noise analysis, as part of the SGLS CDR data package, shows that the performance is less than 3.5° RMS except during vibration, where the phase noise is slightly less than 11.5° RMS. However, the vibration environment used for the 11.5° RMS phase noise value is not for the environment of the IUS launch from the Orbiter. Therefore, the vibration for the IUS launch from the Orbiter needs to be used to determine the phase noise, and the phase noise spectrum is needed to properly determine the effect of turn-around characteristics on the PI performance.

Similar to the analysis of the PI performance degradation due to phase noise, it is equally important to determine the STDN/TDRS (SGLS) transponder performance degradation due to the PI transmitted phase noise as well as the phase noise generated by the STDN/TDRS (SGLS) receiver. This analysis has not been performed due to the lack of phase noise

spectrum data from either the PI or the STDN/TDRS (SGLS) transponder. Therefore, this is a future task that must still be performed to determine the overall communication system performance.

4.2.3.3 False acquisition susceptibility

The data presented at the PI PDR indicates that the PI will not false lock if all transmitted sidebands and spurs within ±242 kHz of the carrier are below -26 dBc. This is true for transmitted signals all the way from threshold to saturation of the PI receiver protection diode (+10 dBm). The initial TRW analysis of the frequency discriminator-aided lock detectors in the STDN/TDRS and SGLS transponders will not false lock (negligible probability) over the range from threshold to receiver saturation.

There is some concern that a false lock could occur during periods when the signal is not within the normal operating range (either below threshold or above receiver saturation) and remain false locked when the signal reaches the normal operating range. The question to be answered is if false lock does occur (even with low probability), what can be done operationally to break lock and correctly acquire the signal.

4.2.3.4 PI sensitivity

The current PI design has only a single sensitivity rather than the previous three manually controlled sensitivities. The PI sensitivity is from -122 dBm to +10 dBm, with a protection diode in the PI front end to prevent burnout from large received signal levels. The PI receiver itself begins to saturate at -10 dBm but, from initial test results, there appears to be negligible performance degradation between -20 dBm and +10 dBm input level.

4.3 Communication Interface Unit (CIU) Related Activities

4.3.1 CIU Critical Design Review

4.3.1.1 General

The CIU Critical Design Review (CDR) was held at the TRW facility, Redondo Beach, California, July 10-11, 1979. The principal participants of the CIU CDR were the Boeing Aerospace Company (BAC), TRW and

SAMSO, the latter being supported by technical personnel from Aerospace Corporation. NASA was represented by personnel from JSC, Rockwell International and Axiomatix.

In all, 24 action items and 32 RID's have resulted from this CDR. Most of these appeared to be caused by either inadequately defined specifications or misinterpretation of certain specification statements. In general, however, it appeared that no major unresolvable electrical performance issues seem to have been uncovered as a result of the CDR. In other words, it seems that most of the debatable issues could be resolved by either additional test data and/or specification rewording.

In the mechanical/packaging area, the major issue during the CIU CDR was the location of the fill connector. The presented TRW design placed the connector behind the kick panel which has to be removed to allow access to the connector. This makes access to the connector difficult, particularly when the Shuttle is in a vertical position. Thus, the relocation of the connector to the front panel of the CIU units is now being considered by BAC and TRW as per SAMSO's request. Other mechanical/packaging problem areas did not appear critical and, thus, were treated as minor modifications. Upon receipt of the CDR meeting minutes, Axiomatix will review these once again to determine if some inconsistencies still exist.

4.3.1.2 Follow-up on RID's from the CIU PDR

During the CIU PDR held November 28-29, 1978, there were 26 RID's generated. Table 34, page 112 of Axiomatix Report No. R7906-8 (i.e., [9]) describes these RID's. Of 26 RID's listed in that table, nine were scheduled to be completed by the CDR in July 1979. Table 4.2 lists these nine RID's.

As the result of Axiomatix's examination of the CIU CDR package, it was established that all of the RID's listed in Table 4.2, except CIU-35 and CIU-46, have been completed/answered by the CDR data as scheduled. Item #35 was eliminated prior to the CDR and item #46 has been carried over as CDR's RID #23 (CDR-23).

Axiomatix will follow up on the resolution of this RID as well as others generated as the result of this CDR.

Table 4.2. Listing of RID's Generated at the CIU PDR (November 1978) and Scheduled to be Completed by CDR (July 1979)

Item	RID No.	Subject	Assigned To
1	CIU-03	Tempest Test Plan Submittal	TRW
2	CIU-11	EMC Test Plan	TRW
3	CIU-12	EMC Control Plan	TRW
4	CIU-25	Test Plan	TRW
5	CIU-35	S-Band Commands Variable Format	BAC
6	CIU-37	Revise Control Panel Layout	TRW
7	CIU-39	Revise KG Panel Design	TRW
8	CIU-42	Classify TBD's on T-0 Umbilical	BAC
		Provide Switching for Redundant T-0 Umbilical	TRW
9	CIU-46	Clear Up CIU Specification TBD's	BAC

4.3.1.3 Follow-up on action items generated at the CIU PDR

In addition to the 26 RID's generated during the CIU PDR, there were 20 action items (AI's) generated. Table 34 of [9] describes these action items. Of 20 AI's listed in that table, six were specially listed for completion by the CDR. Table 4.3 lists these AI's.

Table 4.3. Listing of AI's Generated at the CIU PDR (November 1978) and Scheduled to be Completed by CDR (July 1979)

Item	AI No.	Action Item	Assigned To
1	CIU-AI02	Switch CIU and KG Panels	TRW
2	CIU-AI07	CIU Worst-Case Propagation Delay Analysis	TRW
3	CIU-AI14	Remove LH002H from Design	
4	CIU-AI15	Measure Integrated PSK Demod-Bit Sync Acquisition Time	TRW
5	CIU-AI16	Measured Integrated PSK Demod-Bit Sync BER	TRW
6	CIU-AI20	Ensure Power "On" Maintenance for Crypto	BAC

Axiomatix examined the CIU PDR package and determined that all of the aforementioned action items, with the exception of AI #20, were answered by the time of the CDR. The handling of AI #20 remains to be pursued, unless it has been eliminated without official notice to all participants of the CDR, including Axiomatix.

4.3.2 Review of CIU PSK Demodulator Performance Analysis

Parts of the Orbiter avionics equipment serving the IUS include the communication interface unit (CIU) and the payload signal processor (PSP). The former is for DOD transponder (SGLS) communication and the latter is for NASA transponder (STDN/TDRS) communication. Because the PSP unit was developed prior to the CIU, a considerable amount of PSP technology has been applied by the PSP/CIU contractor (TRW) to the CIU implementation. Specifically, with respect to the demodulation of the PSK data received from the IUS SGLS transponder on a 1.024 MHz subcarrier, the implementation of the demodulator is identical to that of the PSP unit. In fact, TRW has included in their CIU critical design review (CDR) package the analysis of the PSP demodulator for the support of the predicted performance of a similar demodulator employed by the CIU.

Because of the importance of the PSK demodulator in determining the IUS/Orbiter link performance, Axiomatix has undertaken a close examination of the PSK demodulator analysis. As the result of this examination, we have determined certain limitations of the CDR analysis and have thus "filled in the gaps" by providing our analysis. The significance of our analysis is that it describes the expected PSK demodulator performance over the wider range of signal-to-noise ratios (SNR), thus providing information with regard to demodulator optimization at various SNR's. The details of this Axiomatix analysis is included in Appendix E of this report. An overview of our analysis is provided in subsection 4.3.2.1 following.

4.3.2.1 Costas loop PSK demodulation with a limiter in the in-phase arm

Figure 4.9 shows the functional block diagram of a Costas loop PSK demodulator with a hard-limited in-phase channel. Such a demodulator is used in both the PSP and CIU equipment for the purpose of demodulating the telemetry data on the 1.024 MHz subcarrier. The only difference between the PSP and CIU demodulators is that the former is designed to handle multiple rates of 1, 2, 4, 8 or 16 kbps, while the CIU demodulator is optimized for a single rate of 16 kbps. However, because the subsequent analysis applies equally well to the CIU and the PSP, we will refer to it as a PSP/CIU performance analysis and, in some cases, as "PSP" analysis, keeping in mind, of course, that this analysis applies equally well to the CIU PSK demodulator working at 16 kbps.

Referring back to Figure 4.9, we see a telemetry demodulator which is configured as a Costas loop with a hard-limiter in-phase arm (sometimes referred to as a polarity-type Costas loop). Such a loop, when compared with a conventional (analog-type third multiplier) loop, offers simpler hardware implementation and exhibits less unwanted DC offset voltages, both of which stem from using a chopper-type third multiplier. Also, when compared with squaring loops, Costas loops in general have an advantage of being implemented with lowpass (as opposed to bandpass) arm filters which are easier to program for operation over a variety of data rates and formats. Indeed, the latter is a prime consideration in the PSP/CIU design which is required to demodulate the 1.024 MHz subcarrier when PSK modulated by NRZ or Manchester formatted data at either 1, 2, 4, 8 or 16 kbps (PSP) and 16 kbps (CIU).

An analysis of the tracking performance of the Costas loop with hard-limited in-phase channel was performed by Simon [10] wherein detailed theoretical and numerical results were given for the case of NRZ data and single-pole (RC) arm filters. In particular, closed-form expressions were obtained, under the assumptions of low and high data signal-to-noise ratios, for loop squaring loss and equivalent loop signal-to noise ratio, thus enabling calculation of mean-square tracking jitter.

It was shown there that the polarity-type loop offers superior tracking performance, when compared with the conventional Costas loop, at high data signal-to-noise ratios, which are characteristic of typical uncoded telemetry data bit error rates.

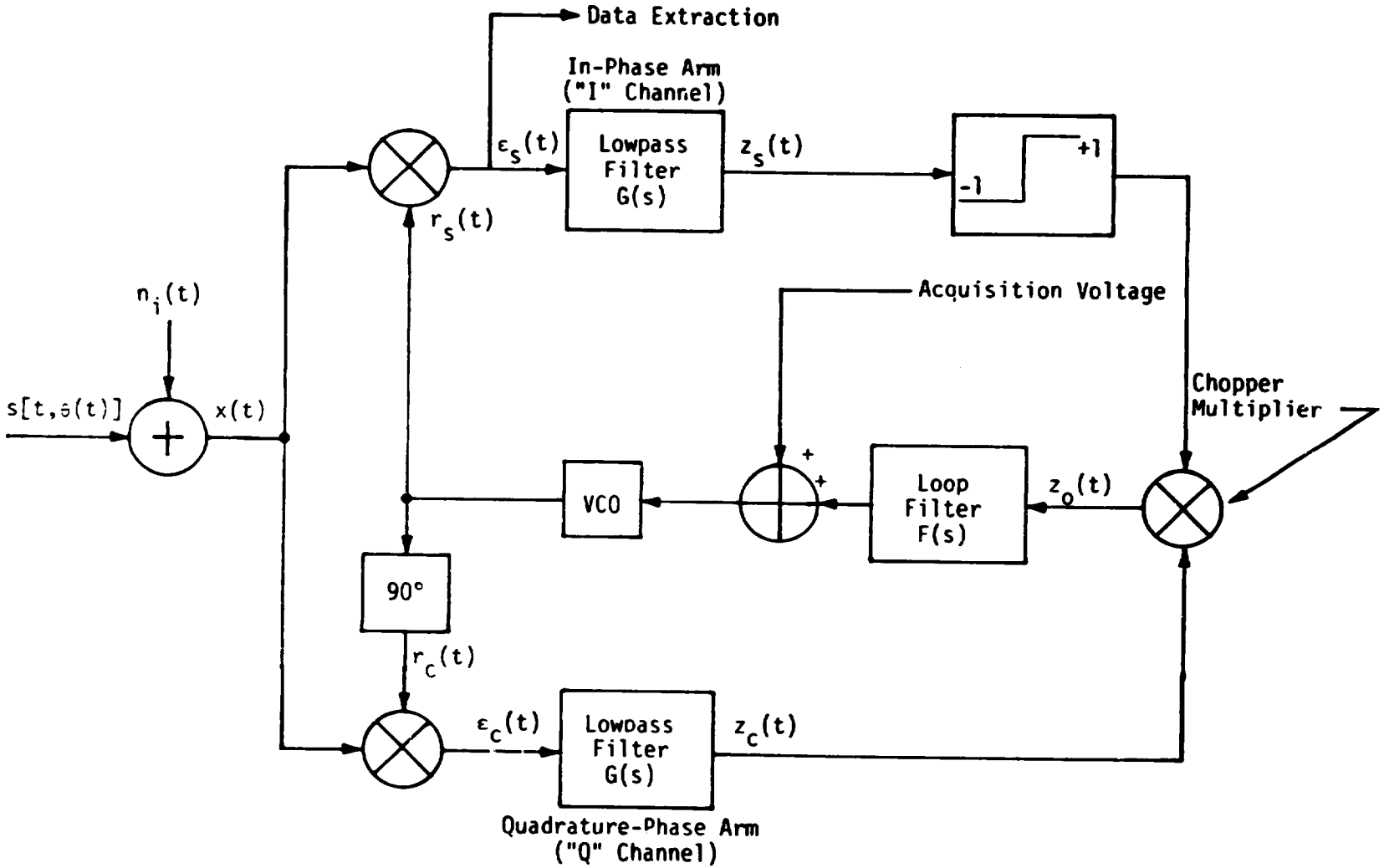

Figure 4.9. Costas Loop Functional Diagram with Hard-Limited In-Phase Channel

Since the PSP/CIU telemetry demodulators must, as mentioned above, demodulate the subcarrier from either an NRZ or Manchester PSK modulation, section 1.1.2 of the TRW report* extends the analysis in [10] to the case of Manchester data. Indeed, the identical approaches taken in [10] are repeated for this case and the nature of the results obtained is not all too (suprisingly) different. In particular, it is shown that once again, the inclusion of the hard limiter produces a tracking performance degradation at small signal-to-noise ratios whereas, for large signal-to-noise ratios, the hard-limited loop outperforms the conventional loop. Also, as was previously demonstrated for the conventional loop by Simon [11,12], the performance of the polarity-type loop, when tracking a Manchester data-modulated subcarrier, is worse than that achieved when tracking a same data-rate NRZ-modulated subcarrier assuming that, in the former case, the arm filters are appropriately widened to accommodate the wider spectrum.

The loop noise bandwidth of the PSP/CIU subcarrier demodulator depends on both the closed-loop gain and the input signal power level. Any alteration in either of these two quantities causes a change in the loop noise bandwidth relative, say, to its value at a given design point. By virtue of the presence of a hard limiter in the in-phase arm of the polarity-type Costas loop, the closed-loop gain includes an amplitude suppression factor which is a function of the signal-to-noise ratio in the arm filter bandwidth. In addition, the 1.024 MHz subcarrier, prior to crossing the PI and PSP/CIU interface, undergoes a noncoherent total power AGC operation which, in the process of trying to maintain a constant total power (signal-plus-noise) level at the PSP/CIU input, causes a variation in the demodulator input signal level.

4.3.2.2 Analytical considerations

Section 1.1.3 of the TRW report presents an analysis of the effects of the hard-limiting and AGC on the loop noise bandwidth. This allows analytical determination of loop noise bandwidths at low signal-to-noise conditions from loop bandwidth measurements performed at high signal-to-noise ratio (essentially no-noise conditions). The principal result is given as follows:

*Appendix A2 of CDR Data Package.

$$\frac{B_L}{B_{LO}} = \frac{\frac{\tilde{\alpha}}{\tilde{\alpha}_0}\left[\left(\frac{SNR}{1+SNR}\right)\left(\frac{1+SNR_0}{SNR_0}\right)\right]^{\frac{1}{2}} + \frac{1}{4\zeta_0^2}}{1+\frac{1}{4\zeta_0^2}} \tag{29}$$

where

B_L = single-sided loop noise bandwidth

$\tilde{\alpha}$ = the limiter suppression factor

ζ = the loop damping factor

SNR = signal-to-noise ratio in the noise bandwidth of the lowpass filter preceding the AGC in the PI

subscript 0 = parameter values at the chosen design point, e.g., no noise.

Ordinarily, the limiter suppression factor depends on both the bit energy-to-noise ratio E_b/N_0 (data SNR) and the ratio of two-sided arm filter bandwidth to data rate B_i/R [10]. Since, however, the arm filters are modified as a function of data rate to keep the latter ratio fixed (e.g., equal to 3.0 for NRZ and 6.0 for Manchester), then $\tilde{\alpha}$ is only a function of data format and E_b/N_0. Plots of $\tilde{\alpha}/\tilde{\alpha}_0$ versus E_b/N_0 are given in the TRW report where it is also noted that

$$\tilde{\alpha}_0 \triangleq \tilde{\alpha}\Big|_{E_b/N_0=\infty} = \begin{cases} 0.8849 & \text{NRZ} \\ 0.8273 & \text{Manchester} \end{cases} \tag{30}$$

In the absence of AGC, (30) simplifies to

$$\frac{B_L'}{B_{LO}} = \frac{\frac{\tilde{\alpha}}{\tilde{\alpha}_0}\left[\frac{SNR}{SNR_0}\right]^{\frac{1}{2}} + \frac{1}{4\zeta_0^2}}{1+\frac{1}{4\zeta_0^2}} \tag{31}$$

where the prime denotes this absence. Since, for the PSP/CIU demodulator, $\zeta = 0.707$ and $SNR_0 = -31.4$ dB (a minimum subcarrier signal-to-noise density ratio of 36 dB-Hz and a pre-AGC bandwidth of 5.5 MHz)*, the first terms in the numerators of (29) and (31) dominate. Thus, the ratio of loop bandwidth with AGC to loop bandwidth without AGC is approximately given by

$$\frac{B_L}{B_L'} \cong \left[\frac{1 + SNR_0}{1 + SNR}\right]^{\frac{1}{2}} = \left[\frac{\frac{1}{SNR_0} + 1}{\frac{1}{SNR_0} + \frac{SNR}{SNR_0}}\right]^{\frac{1}{2}} \tag{32}$$

Finally, if the dynamic range SNR/SNR_0 is less than 20 dB (the dynamic range of interest in the PSP is approximately 10-12 dB), then, for all practical purposes, $B_L = B_L'$, and the AGC need not be accounted for in acquisition and tracking threshold measurements. Indeed, this is the principal conclusion reached in Section 1.1.3 of the TRW analysis.

In Section 1.1.4 of the TRW analysis, the results of Sections 1.1.2 and 1.1.3 are used to determine the condition (specific combination of data format and data rate) for which the minimum loop noise bandwidth (corresponding to a specified tracking threshold requirement) occurs. This is necessary to assure that the loop bandwidth at all other combinations of data format and data is larger than this minimum value, thus guaranteeing that the frequency instability of the incoming 1.024 MHz subcarrier is always accommodated. This instability could be as much as 0.01% which, for a frequency of 1.024 MHz, is 100 Hz. Thus, the minimum one-sided loop bandwidth should have at least this value.

The first step in carrying the above is to determine the SNR ρ_0 in the loop bandwidth at threshold which is defined, for the PSP demodulator, as the condition wherein the mean time to slip a cycle $\bar{T}$ is 60 seconds. This threshold loop SNR is first computed in the TRW analysis by using a formula suitable for a first-order conventional Costas loop, namely,

$$\bar{T} = \left(\frac{1}{2B_{L0}}\right)\left[\pi^2 \rho_0' I_0^2(\rho_0')\right] \tag{33}$$

*Note the design point is now taken as the maximum noise rather than the no-noise condition.

where $I_0(x)$ is the zero-order modified Bessel function of the first kind and ρ_0' is the effective loop SNR at threshold and is related to the actual threshold loop SNR ρ_0 by

$$\rho_0' = \frac{\rho_0}{4} \mathscr{A}_L^2 \tag{34}$$

where $\mathscr{A}_L$ is the loop "squaring loss". Using a threshold bandwidth B_{LO} = 100 Hz and $\bar{T}$ = 60 seconds results in ρ_0' = 6.9 dB, as computed from (29).

The analysis to determine the theoretical threshold for the polarity-type Costas loop was pointed out, in the TRW report, as not having been performed. This void has now been filled by the analysis presented in Appendix E of this report. Indeed, it is shown there that the threshold loop SNR is both a function of E_b/N_0 and data format for fixed values of $\bar{T}$ and B_{LO}. In fact, for B_{LO} = 100 Hz and $\bar{T}$ = 60 seconds, the effective loop SNR at threshold ρ_0' for the polarity-type loop varies between 5.63 and 6.37 dB for Manchester and 5.27 and 6.29 dB for NRZ when E_b/N_0 varies over the range 0 to 10 dB (see Figures 3 and 4 of Appendix E). In both cases, the ratio of two-sided arm filter bandwidth to data rate is held fixed at 3.0 for NRZ and 6.0 for Manchester. We note that, for both NRZ and Manchester data, the polarity-type Costas loop has a lower threshold loop SNR than the conventional Costas loop although the difference between the two is only on the order of 1 to 2 dB.

It should also be pointed out that all of these numerical results have been computed for first-order loops. Nevertheless, the relative performance of two equivalent second-order loops should remain virtually unchanged, keeping in mind, however, that, for a fixed damping, a second-order loop has a higher threshold loop SNR than a first-order loop. This phenomenon has been verified by simulation results [13]. Appendix E also discusses an approximate theoretical approach to computing the mean-time-to-cycle-slip performance of second-order Costas loops, both of the conventional and polarity-type.

4.3.2.3 Discussion of results

In the absence of the aforementioned theoretical results, TRW used a hybrid of PSP demodulator breadboard measurements and analysis to arrive at a threshold value of ρ_0' for the polarity-type Costas loop equal to 10.5 dB, essentially independent of all data formats and rates. Based upon the above discussion, one must conclude that, somehow, this numerical value is in error. Furthermore, since this value of 10.5 dB was used as the tracking threshold SNR throughout the remainder of Section 1.1.4, the validity of the numerical results carried out there must be held with suspicion until this discrepancy can be resolved. In particular, the determination of 16 kbps NRZ as being the data rate/format combination resulting in minimum loop bandwidth should perhaps be reexamined in light of the above.

The final subsection (1.1.5) of the PSP demodulator discussion presents a routine analysis of the bit error rate (BER) degradation due to the noisy demodulation reference supplied by the polarity-type Costas loop. Since the PSK must process both PSK and differentially encoded PSK data, the degradations on both of these data types are considered. The results taken from [14] can be summarized as follows:

$$P_E = \int_{-\pi}^{\pi} P_E\left(\frac{\Phi}{2}\right) p(\Phi)\,d \tag{35}$$

where $\Phi = 2\phi$ is the phase error tracked by the loop and

$$P_E\left(\frac{\Phi}{2}\right) = \begin{cases} \frac{1}{2}\,\mathrm{erfc}\left[\sqrt{\frac{E_b}{N_0}}\cos\frac{\Phi}{2}\right]; & \text{PSK} \\ \mathrm{erfc}\left[\sqrt{\frac{E_b}{N_0}}\cos\frac{\Phi}{2}\right]\left\{1 - \frac{1}{2}\,\mathrm{erfc}\left[\sqrt{\frac{E_b}{N_0}}\cos\frac{\Phi}{2}\right]\right\}; & \text{differentially encoded PSK} \end{cases} \tag{36}$$

$$p(\Phi) = \frac{\exp(\rho'\cos\ )}{2\pi I_0(\rho')} \quad ; \quad |\Phi| \le \pi \tag{37}$$

In (37), ρ' is the effective loop SNR at the operating point and is related to the actual loop SNR, ρ, at the operating point by an expression analogous to (34). Also, (37) assumes a first-order loop model.

Again assuming a tracking threshold $\rho' = \rho_0' = 10.5$ dB, the TRW calculation of (35) yields a very small (less than 0.2 dB) degradation for the five data rates and E_b/N_0 values from -2 to +8 dB. It should be noted that the BER degradation at a value of $\rho_0' \cong 6$ dB, as predicted by the results of Appendix E of this report, can, on the other hand, be quite large depending on the value of E_b/N_0 (see Figures 2 and 4 of Section 1.1.5 of the TRW report). Thus, once again, the true tracking threshold of the polarity-type Costas loop plays a significant role.

4.3.3 FM Demodulator

In addition to the PSK demodulator used for the recovery of a 16 kbps telemetry data stream, the CIU utilizes an FM demodulator centered at 1.7 MHz. This demodulator is used for recovery on the analog telemetry data transmitted by the IUS. Specifically, the requirements for the demodulator are as follows:

(1) Accept a 1.7 MHz FM/FM modulated subcarrier from the Payload Interrogator (PI)

(2) Extract baseband signals from the subcarrier and transmit the data to an analog track on the Payload Recorder (PR)

(3) Operate at an input SNR down to 15 dB

(4) Modulation index to be less than or equal to 1.0 radians.

The corresponding demodulated signal characteristics are as follows:

Channel	Frequency	Frequency Deviation
1	16 kHz	± 2 kHz
2	24 kHz	± 2 kHz
3	32 kHz	± 2 kHz

The TRW considerations of potential candidates for an FM discriminator implementation has considered several candidates such as:

(1) Hybrid detection and inverse-limiting

(2) Phased-lock loop (PLL) and frequency feedback techniques

(3) Zero-crossing detector of the pulse rate type.

The latter has been selected as most easy to implement with digital, space-qualified components. A rudimentary analysis of this discriminator is presented in Appendix A2 of the CDR package.

Axiomatix, however, was not able to verify the predicted performance (as presented by TRW) because most of the analysis is based on a previous, internal technical memo by TRW.

Thus, when we obtain this memo, we will verify the predictions given by TRW with respect to FM demodulator performance.

4.3.4 CIU/Orbiter Interface Issues

The CIU interfaces with the following Orbiter avionic subsystems: Payload MDM, GN&C MDM, PI, KuSP, FMSP, PDI and PR. Each of the Orbiter avionic subsystems have different interface requirements. While most of the CIU output signals are digital, the Orbiter avionic subsystem specifications tend to be more analog oriented than standard digital. In fact, the digital interfaces have conflicting requirements such as rise/fall times, DATA/$\overline{\text{DATA}}$ skew, DATA/clock skew, bit jitter, bit asymmetry and signal amplitude specifications. Tables 4.4 through 4.7 present a comparison of digital signal interface parameters for each CIU/Orbiter avionic subsystem interface.

In Table 4.3, note that KuSP signal-level parameter is 2.3 to 5.0 V p-p, line-to-line, while a standard digital interface is 3-9 V p-p, line-to-line. Hence, a special interface circuit is required for the CIU/KuSP interface which has a significant cost impact.

In Table 4.4, the rise/fall times required are conflicting between various subsystems. Therefore, a separate interface circuit must be designed for each subsystem.

In Table 4.5, the PR specification of less than 2% of the bit duration includes data asymmetry, which makes this a difficult specification for the CIU to meet. Therefore, the CIU design needs to be analyzed further to determine if this specification can be met.

Finally, the CIU/PDI interface is a special problem area which is currently being worked by Boeing and the IUS/Orbiter Working Group. The minimum rise and fall time specifications shown in Table 4.4 require waveform filtering to slow down the maximum rise and fall time of the interface device. However, waveform filtering causes DATA/$\overline{\text{DATA}}$ skew.

Table 4.4. CIU/Orbiter Digital Interface Parameters

Parameter	Payload Recorder	Payload Data Interleaver	FM Signal Processor	Ku-Band Signal Processor
Signal Level	3.7-9 V p-p, line-to-line	2-12 V p-p, line-to-line (2.5-9.0 V open PIRN)	5.0 ± 0.5 V p-p, line-to-line (Wideband) 1.0 ± 0.5 V p-p, line-to-line (DOD)	2.3-5.0 V p-p, line-to-line
RMS SNR	-	-	45 dB p-p to RMS noise DC to 2 MHz	35 dB minimum
Data Rates	25.5 kbps to 1.024 Mbps	10 bps to 64 kbps	200 bps - 5 Mbps, NRZ-L 200 bps - 2 Mbps, Biphase-L 250 bps - 256 kbps (DOD)	16 kbps - 2 Mbps NRZ-L,M,S 16 kbps to 1.024 Mbps Biphase-L,M,S 2-50 Mbps NRZ-L,M,S 16 kbps-4 Mbps, NRZ-L,M,S
Signal Code	Biphase-L	NRZ-L,M,S Biphase-L,M,S	NRZ-L Biphase-L	NRZ-L,M,S Biphase-L,M,S

Table 4.5. CIU/Orbiter Digital Interface Parameters

Parameter	Payload Recorder	Payload Data Interleaver	FM Signal Processor	Ku-Band Signal Processor
Rise and Fall Times	10% of bit duration	Maximum: 5 μs or 10% of bit duration, whichever is less Minimum: 100 ns	Maximum: 50 ns (Wideband) 100 ns (DOD)	5% or 50 ns, whichever is less (KuSP specification) ICD: 40 ns to 1 Mbps 20 ns 1-2 Mbps 5 ns 2-4 Mbps 10% of bit duration 2-50 Mbps
DATA/$\overline{\text{DATA}}$ Skew	-	±200 ns	-	-
Data Asymmetry	Included in bit jitter specification	-	-	
			(±3% TDRSS user constraint; JSC recommends ±10%)	-
Waveform Distortion	-	Overshoot/undershoot less than 20% of signal level	-	-

Table 4.6. CIU/Orbiter Digital Interface Parameters

Parameter	Payload Recorder	Payload Data Interleaver	FM Signal Processor	Ku-Band Signal Processor
Frequency Jitter	-	-	-	±0.01% RMS of data rate at 0.01% RMS of the data rate
Bit Jitter	<2% of bit duration (p-p) (Includes data asymmetry)	-	-	- (≤0.1% TDRSS user constraint)
Bit Rate Accuracy	-	±2%	-	-
Bit Rate Stability	-	1 part in 10^5 (60 s average)	-	0.01% (long term)
Clock/Data Skew	-	5% of clock period or 10 μs, whichever is less	-	-

Table 4.7. CIU/Orbiter Digital Interface Parameters

Parameter	Payload Recorder	Payload Data Interleaver	FM Signal Processor	Ku-Band Signal Processor
Clock Duty Cycle	-	50.0 ± 5%	-	-
Load Impedance	75 ± 10% ohms	Min: 74 ohms Max: 91 ohms	75 ± 10% ohms	75 ± 5 ohms 50 ± 10% ohms (2 - 50 Mbps)
Cable Impedance @ 1 MHz	75 ± 5 ohms,	75 ± 5 ohms, TSP 2900 pf capacitance*	75 ± 5 ohms, TSP	75 ± 5 ohms, TSP 50 ohms (RF 142BU (2 - 50 Mbps)
Source Impedance	TTL-compatible (TI 5514 IR equivalent)	-	75 ± 10% ohms	-
Noise Immunity	-	150 Mv p-p** DC to 100 kHz	-	-
Common Mode Voltage (Line-to-Signal Ground)	±15 V	±3 V	-	±10 V

*18-23 pf per foot of cable

**100 Mv p-p maximum EMI, 50 Mv p-p from payload

Boeing's worst-case analysis shows that the original PDI specification of 100 ns minimum cannot be met simultaneously with the ±200 ns DATA/$\overline{\text{DATA}}$ skew specification. Preliminary Interface Revision Notice (PIRN) BAC026A resulting from the Orbiter/IUS Avionics Working Group Meeting of July 12-13, 1979 changes the PDI minimum rise and fall time specification to 30 ns. If PIRN BAC026A changes the PDI specification, Boeing feels that it is possible to meet both the specifications for rise and fall times and DATA/$\overline{\text{DATA}}$ skew, but more analysis must be performed to assure that both specifications can be met.

5.0 ESTL TEST REQUIREMENTS PLAN OVERVIEW

5.1 Motivation

A main objective of the NASA Task 501 Program is the verification testing of the various RF space-space and space-ground links of the Shuttle and Shuttle-launched payloads. A considerable portion of this verification testing will be performed by ESTL.

The functional diagram of the ESTL is shown in Figure 5.1. As can be seen from this diagram, the ESTL has the capability to simulate the direct Shuttle/earth S-band links and the indirect Orbiter/ground S-band and Ku-band links. Means are additionally provided to simulate the data generated within the Orbiter itself, along with the capability for routing it via the various space-ground links for the purpose of total systems evaluation.

The preparation of the ESTL test requirements is one of the major tasks of this Axiomatix contract. Specifically, the contract work statement calls out the following task:

> "ESTL Test Requirements. The contractor shall develop a complete set of test requirements for the IUS (DOD and NASA) communications equipment when it arrives at the ESTL for compatibility testing. The test requirements shall define all communication links, modes and parameters to be tested. Any special test equipment shall be identified."

In response to the above requirement, this Axiomatix report presents a plan for performing verification tests between the Inertial Upper Stage (IUS) and the DOD Communication Interface Unit (CIU) or NASA Payload Signal Processor (PSP) communication systems. These tests, which will be performed in the NASA Lyndon B. Johnson Space Center (JSC) Electronic System Laboratory (ESTL), are designed to establish that the communications link between the IUS and the CIU or PSP is compatible and that the system performance will meet the requirements of the Shuttle program.

The detailed ESTL Test Requirement plan is given in Appendix D of this report. The highlights of this test plan are presented in the paragraphs which follow.

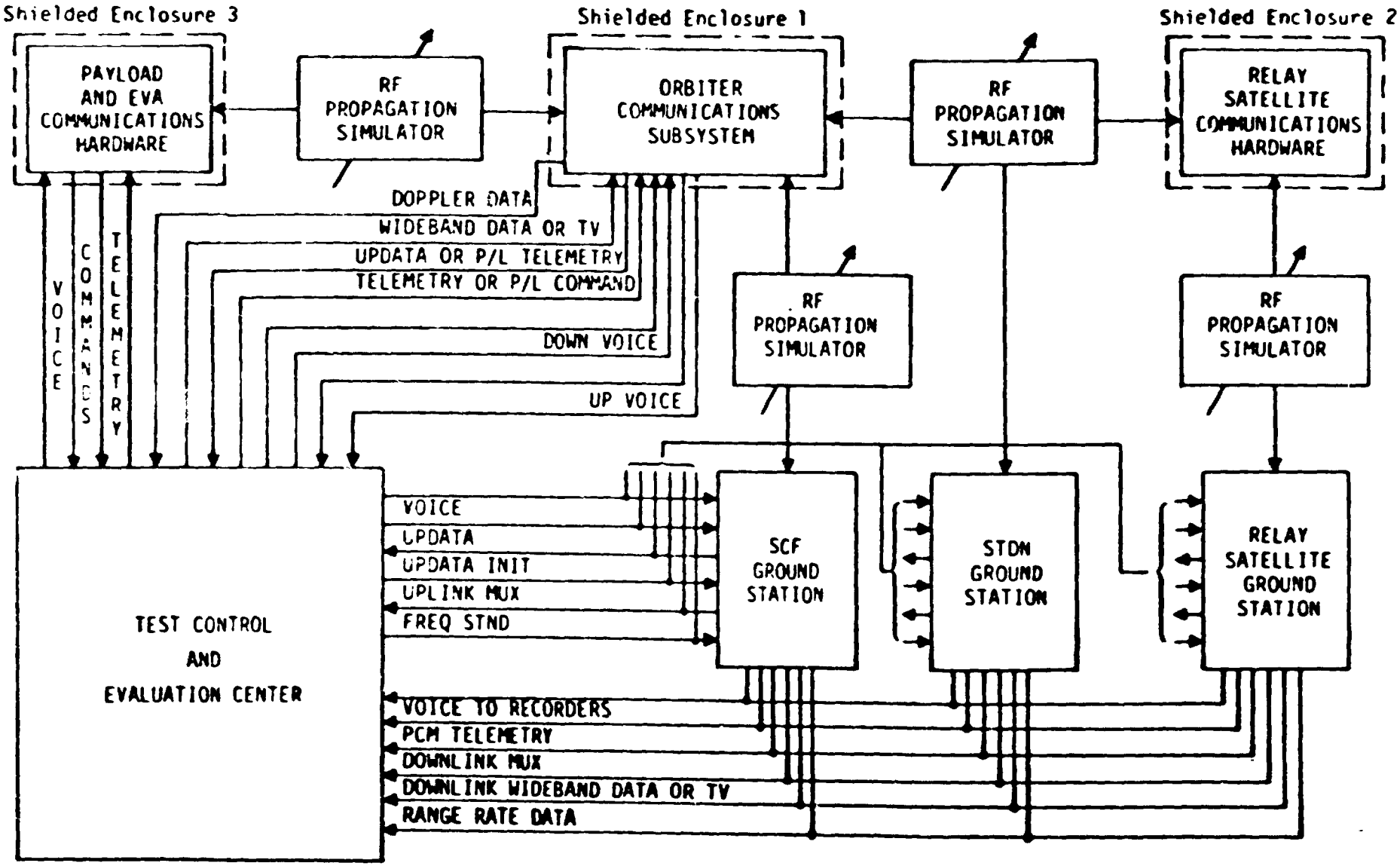

Figure 5.1. ESTL Functional Block Diagram

5.2 Background

The Orbiter communications subsystem provides a capability for establishing communication links with both the attached IUS within the Shuttle bay and the detached IUS in the near vicinity of the Orbiter. As described in Section 3.0, the communication with the attached IUS is via hardware channels, and the detached IUS RF communication is a two-way link carrying commands and telemetry. Both the hardwire and RF links with the IUS constitute a portion of the overall space-space capability of the Orbiter communication system.

The ESTL test program objectives for the IUS and CIU with the Orbiter subsystems and ground stations are to:

(1) Establish equipment/subsystem electrical compatibility

(2) Identify performance and operational limitations and constraints

(3) Verify that appropriate RF and hardware interfaces are commensurate with mission communications requirements

(4) Verify experimentally that the Orbiter/IUS forward and return RF links are signal compatible in all modes

(5) Verify experimentally those tracking, ranging, command, and telemetry channel performance characteristics required for operational mission support.

To implement these tests, Orbiter and IUS communications hardware must be obtained and installed in a representative mission configuration in the ESTL. Therefore, the communications links to be evaluated during these tests are equivalent to those which will be used during an Orbiter mission. The only significant difference is that the RF paths will be through hard-line, space-loss simulators.

The IUS is being developed by the DOD for joint DOD/NASA use and will consist of a DOD and a NASA configuration. Both IUS configurations will be verified during the ESTL testing. Operational constraints, however, may require the use of a DOD IUS for NASA payload missions such as the Tracking and Data Relay Satellite (TDRS) launch.

As part of the ESTL test plan, the following items must be addressed:

- Communication links to be tested
- Operational modes to be tested
- Operating parameters to be verified
- Special test equipment requirements.

5.3 Axiomatix' Approach to the Test Plan Preparation Activity

A number of previous reports and studies were reviewed to determine the overall end-to-end communication links to be tested. The result was a very large number of end-to-end links but, by applying the test philosophy developed by Axiomatix and described in this document, the number of test links required was greatly reduced.

Each test link was analyzed and various performance test requirements such as forward and return link and RF acquisition tests were developed. Within each test requirement, operational modes and parameters were also evolved.

5.4 Definition of IUS/Orbiter Interfaces

The function of the IUS determines the requirements for the IUS/Orbiter communication interfaces. Thus, the mission of the IUS must be considered. Specifically, one method used to deliver a payload beyond the Orbiter's operating range is to assist the payload with an inertial upper stage (IUS). Being developed by the DOD, the IUS consists primarily of a Titan 34D final stage. Two IUS vehicles with attached payloads can be carried in tandem in the Orbiter bay, with each IUS carrying up to four payloads or spacecraft.

Because of differences in communication link requirements, there is a DOD configuration and a NASA configuration. The DOD IUS will use communication link equipment compatible with the ground stations of the USAF Satellite Control Facility (SCF); the NASA IUS will use communication link equipment compatible with the ground stations of both the Spaceflight Tracking and Data Network (STDN) and the Tracking and Data Relay Satellite System (TDRSS).

As a note of clarification, what is now known as the NASA Spaceflight Tracking and Data Network (STDN) consists of the original STDN ground stations and the newer TDRS ground stations. The term GSTDN is used to differentiate the original STDN ground stations from the other, newer ground stations within the STDN system.

For the purpose of on-orbit checkout, the Shuttle is required to communicate with the IUS while the IUS is physically located within the Orbiter bay (attached) or within a range of 10 miles from the Orbiter after the IUS has been deployed (detached). In the attached mode, communication between the Orbiter and the IUS is either via a hard-line umbilical link or via the RF links. Ground stations may also communicate with the IUS in the attached mode using either a direct link or the Orbiter as a relay. In the detached mode, communication between the Orbiter and the IUS is only via the RF links. Again, the Orbiter may act as a relay for IUS/ground communication.

The Orbiter avionics equipment serving the IUS in the attached and detached modes perform two major functions. First, there are avionic equipment which perform payload RF and baseband signal processing functions. This equipment includes:

- Payload Interrogator (PI)
- Payload Signal Processor (PSP)--NASA configuration
- Communication Interface Unit (CIU)--DOD configuration
- Ku-Band Signal Processor (KuSP)
- FM Signal Processor (FMSP)

Second, there are avionic equipment which perform data handling functions. This equipment includes:

- Payload Data Interleaver (PDI)
- Payload Recorder (PR)
- PCM Master Unit (PCMMU)
- Network Signal Processor (NSP)
- Various DOD encryptor/decryptor units.

The IUS avionics equipment serving the Orbiter in the attached and detached modes also perform two major functions. First, the equipment performing the RF and baseband signal processing functions include:

- IUS Transponder
- Signal Conditioning Unit (SCU).

Second, the avionics equipment performing the data handling functions include:

- Signal Interface Unit (SIU)
- Environmental Measurement Unit (EMU)
- Wideband Data Interleaver (WBDI).

5.4.1 Attached IUS Communication

In the attached mode, a hard-line umbilical provides two-way communication between the IUS and the Orbiter. Scientific data, engineering data, guidance, navigation and attitude control data (GN&C) are received by the Orbiter from the IUS. Alternately, command data, GN&C and uplink data are transmitted to the IUS from the Orbiter.

Figure 5.2 illustrates the functional scientific data interfaces for attached payloads. Only limited processing--that required to throughput data to a ground terminal--is provided for IUS medium-band and wideband scientific data inputs (inputs in the range of 16-256 kbps). For data rates below 64 kbps, the data can be routed through the PDI to the PCMMU, where it is made available to the general-purpose computers (GPC) for processing and on-board display. A payload specialist crew member may then interface directly with a specific experiment, as required. Medium-band scientific data is routed to the receiving ground terminal via either the S-band FM link or the Ku-band system, as follows:

(1) S-band FM;

Analog:	300 Hz - 4 MHz

or

Digital:	200 bps - 5 Mbps NRZ-L, or 200 bps - 2 Mbps biphase-L

(2) Ku-band:

Analog:	DC - 4.5 MHz BW

plus

Digital:	16 kbps - 1.024 Mbps biphase-L

or

	16 kbps - 2 Mbps NRZ-L,M or S.

The Ku-band wideband analog channel input (DC - 4.5 MHz) can be used by the IUS or CIU for analog telemetry as a transparent throughput channel, which provides flexibility and minimum Orbiter processing. Capability is constrained only by the KuSP bandwidth.

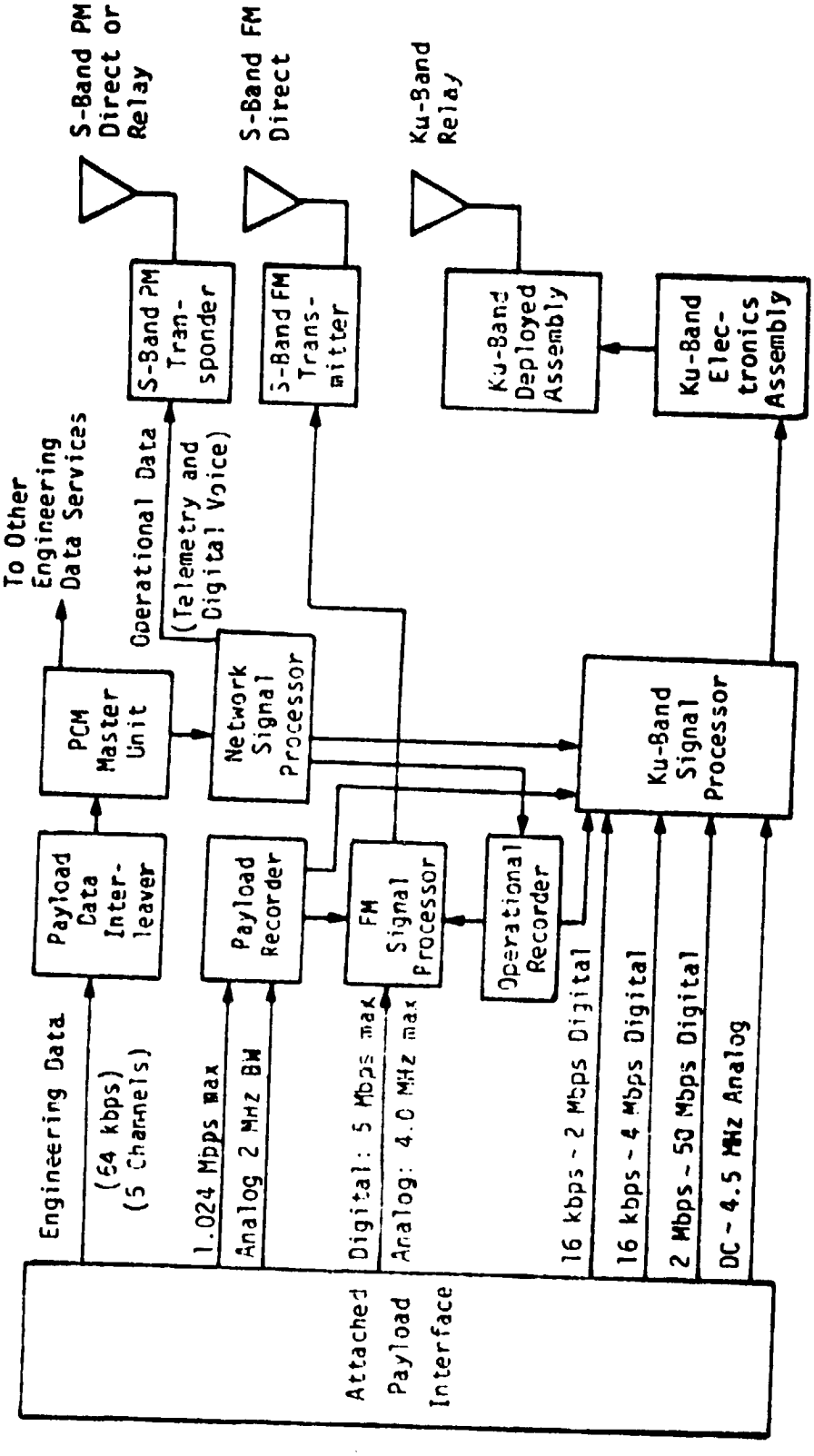

Figure 5.2. Attached Payload Scientific Data Interface

Figure 5.3 depicts the Orbiter provisions for processing, displaying and downlinking systems status data from the IUS in support of monitoring and checkout functions. Data can be accessed by the Orbiter via one of the five inputs to the PDI which makes specific parameters contained in the input PCM bit stream (0-64 kbps) available to the PCMMU for insertion into the operational instrumentation (OI) downlink and available to the GPC's for processing and display.

The PDI provides the capability to receive engineering data from up to five attached payloads simultaneously. The PDI then decommutates up to four of these inputs and provides time-tagged, time-homogeneous data from these four payloads simultaneously to the Orbiter data processing subsystem (DPS) for on-board display and/or transmission to the ground via the OI downlink.

In order to provide the data processing service, the input data to the PDI must be in a standard format, as follows:

- Bits per word: 8
- Words per frame: 1024 max
- Subframe rate groups per frame: 4 max
- Words per subframe: 128 max
- Frame rate: 200 per second max
- Bits per frame synchronization: 8, or 16, or 24, or 32
- Process data rate: up to 64 kbps

The throughput data rate (composite PDI output to the PCMMU) is limited to 64 kbps maximum on-orbit and 5 kbps for ascent.

A capability to throughput data which is in nonstandard format, or other unique data such as encrypted data, is also provided by the PDI. In this mode, the frame synchronization circuitry is bypassed and artificial data blocks are established to transfer the data to the PCMMU. No on-board processing or display of the data is available when operating in the nonstandard mode.

A capability for direct recording of certain types of payload data is provided. The payload recorder has 14 tracks which are capable of serial or parallel recording of digital and analog data. Data rates from 25.5 kbps to 1.024 Mbps and analog data of 1.9 kHz to 2 MHz may be recorded. A minimum record time of 56 minutes is provided at the maximum

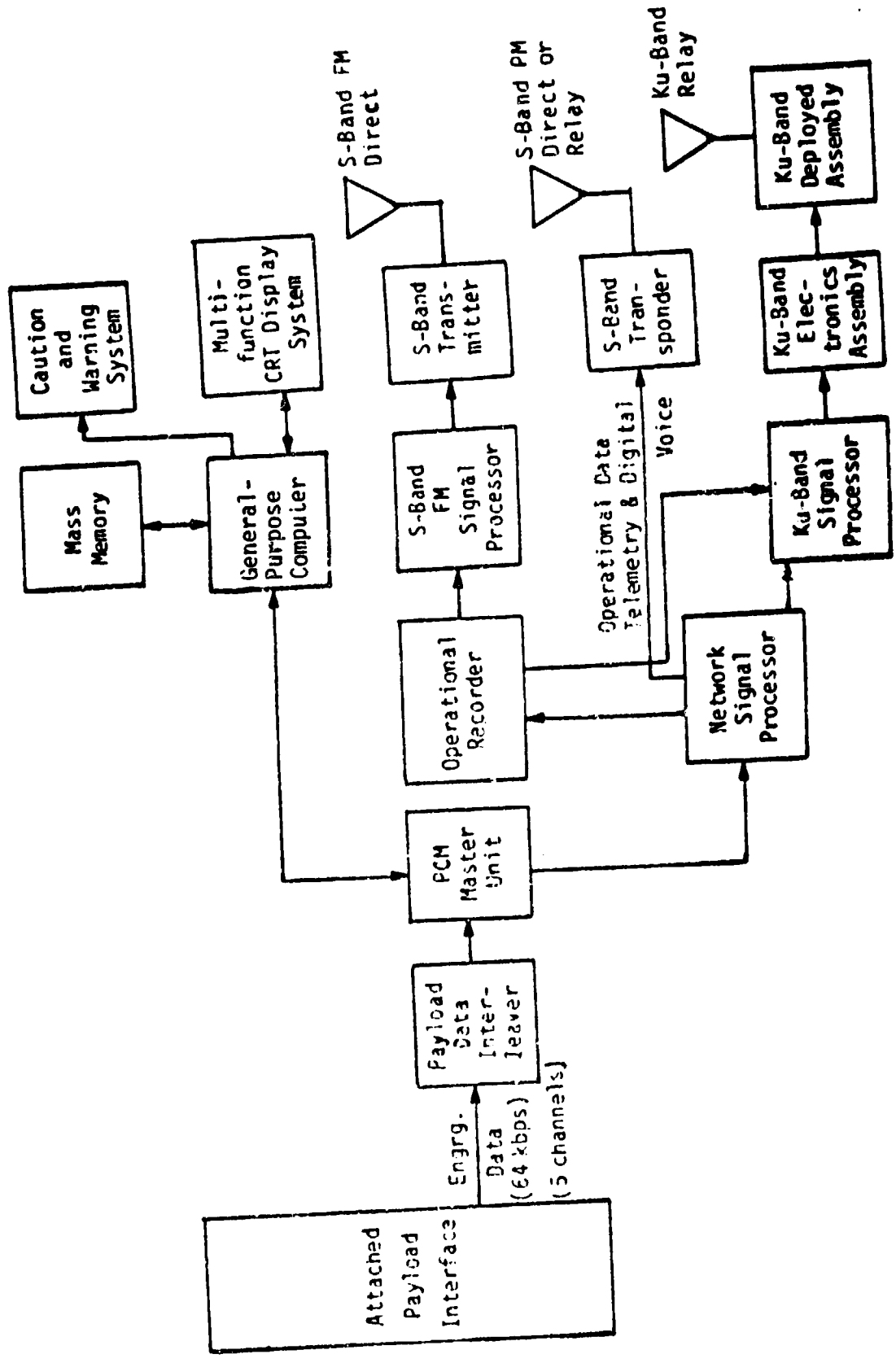

Figure 5.3. Attached Payload Engineering Data Interface

data rate. Simultaneous analog/digital parallel recording is limited to the first record pass. Subsequent passes are restricted to sequential single-channel digital record.

A total of 14 tape speeds (four per mission) are available and selectable by on-board or ground control.

Guidance, navigation and attitude control services are provided for the IUS by the CIU or PSP using the hard-line interface over which the Orbiter provides state vector update data words to the IUS. The CIU transmits the Orbiter state vector data to the IUS using the SLGS command format of ternary frequency-shift-keying (FSK) with "S" tones of 65 kHz, "0" tones of 76 kHz, and "1" tones of 95 kHz. The PSP transmits the Orbiter state vector data to the NASA IUS on a 16 kHz sine wave subcarrier at a binary command data rate of 2 kbps.

5.4.2 Detached IUS Communication

The basic low-rate data-processing/display services provided for the attached IUS are also provided for detached or deployed IUS via S-band RF communications link* between the Orbiter and IUS. Figure 5.4 shows the interfacing hardware that supports this link. Note that, when a spacecraft is launched by the IUS, as shown in Figure 5.4, the spacecraft communicates only in the attached mode through the IUS. Also note that the PI cannot communicate with the IUS and the spacecraft simultaneously.

The Orbiter S-band transceiver (PI) supporting RF communications with detached payloads is compatible frequency-wise with STDN, SGLS, and DSN-compatible payloads--capable of operating at approximately 850 selectable frequencies in the 2200-2300 MHz range.

Telemetry signals in the Orbiter standard mode of operation are routed from the PI, after carrier demodulation, to the PSP or CIU, where the data is demodulated off of a 1.024 MHz subcarrier (and a 1.7 MHz subcarrier by the CIU). The data is then routed to the PDI/PCMMU/GPC for decommutation processing, display and downlinking in the same manner as the attached IUS or payload.

---

*See Section 3.0 of this report for a detailed description of this RF communication link and the related equipment.

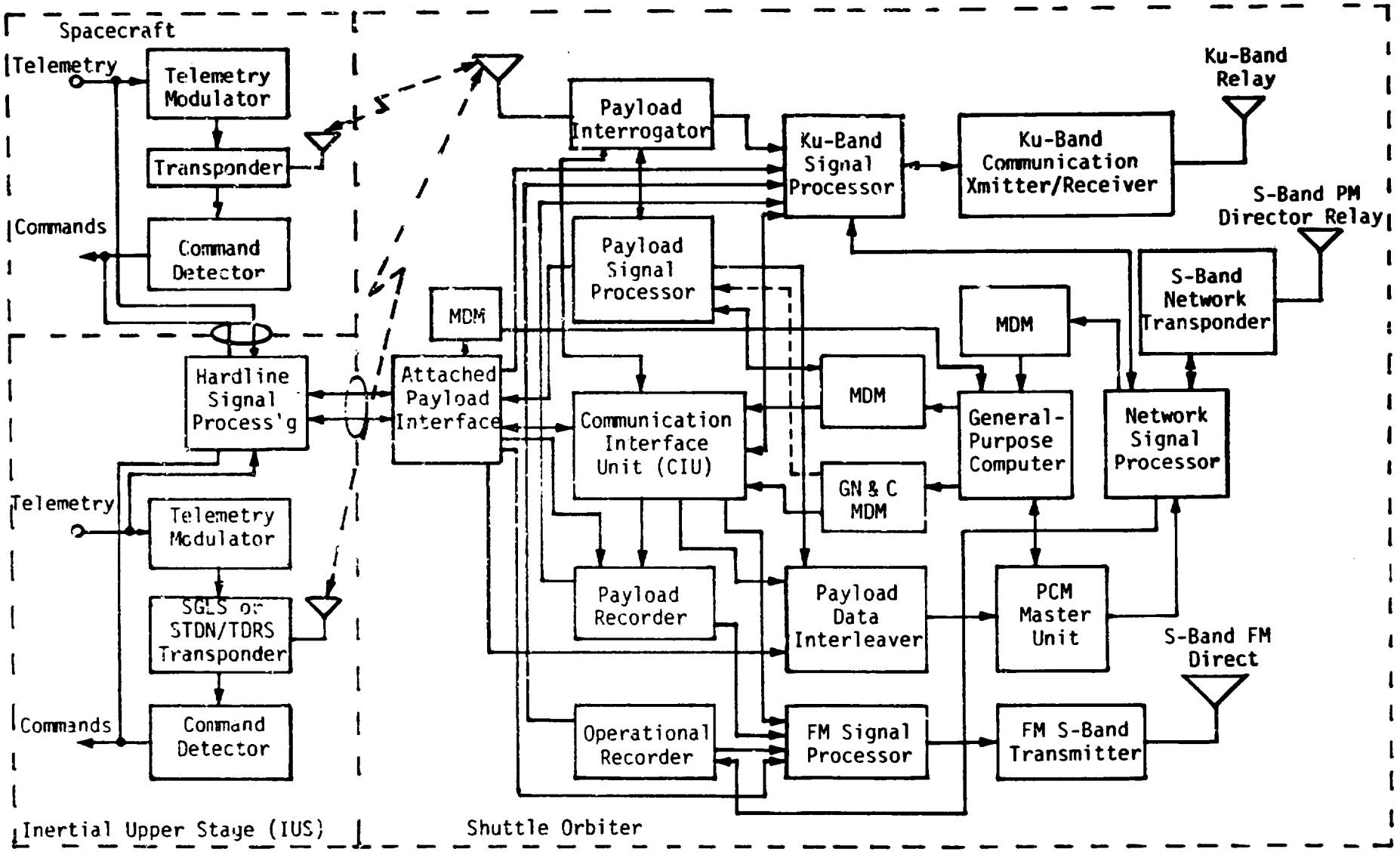

Figure 5.4. Inertial Upper Stage/Shuttle Orbiter Subsystems and Interfaces

Data rates that can be accommodated by the PSP in the standard mode are 16, 8, 4, 2 and 1 kbps. Processing the 16 kbps may be provided by the CIU located at the payload station in the aft flight deck for DOD missions. In this mode, the PSP is bypassed. The PSP is being designed to accommodate any one of six PCM code formats in the standard mode (biphase-L, M, S and NRZ-L, M, S).

The Orbiter standard mode of operation was selected to provide a degree of flexibility of operation while minimizing basic Orbiter hardware costs. Payloads that ultimately fly on the Orbiter which are incompatible with the standard in terms of data rate or subcarrier frequency will be accommodated in a transparent throughput fashion using a "bent-pipe" mode of operation. In this mode, the interrogator output, following carrier demodulation, is routed to the KuSP 4.5 MHz analog input channel or the 2 Mbps digital channel. These inputs are essentially limited only by the respective bandwidths and are capable of a wide range of data rate/subcarrier options (the 2 Mbps channel is limited to one subcarrier). Unique demodulation hardware at either the Ku-band ground station or the payload operation center currently must be provided by the payload requiring bent-pipe service. The bent-pipe channels are available for use by one detached payload at a time with the following capabilities:

- Digital data from 2 kbps to 2 Mbps, or
- Analog data from 2 kHz to 2 MHz, or
- Digital data from 16 kbps to 4 Mbps, or
- Analog data from DC to 4.5 MHz.

No onboard processing or display of data is available when operating in the bent-pipe mode.

5.5 End-to-End Communication Link Definitions

In both the DOD and NASA IUS configurations, multiple signal paths exist through which the IUS can be commanded and from which IUS telemetry may be received. Before attempting to specify any IUS communications equipment test requirements, all signal paths must be identified. This will be done by separating the command paths into the DOD and NASA configurations and further subdividing into RF and hard-line paths. The same will be done for the telemetry paths.

5.5.1 SGLS Command Signal Flow (DOD Mode)

The SGLS commanding of the IUS is presented in Figure 5.5. The various functional command signal paths are illustrated from the SCF ground station and CIU control panel. In the attached mode, commands from the SCF can be transmitted to the Orbiter using either the TDRS ground station to relay the commands via the TDRS over the Ku-band or S-band, or the direct S-band link from the SCF ground station to the S-band network transponder. On-board commands are entered using the CIU control panel.

In terms of redundant command paths, note that the S-band network transponder and the NSP are completely redundant. Also, commands can be sent from the KuSP to the two NSP's or directly to the CIU, but note that the Ku-band system is not redundant. From each NSP, commands are sent to the GPC using MDM's but, from the GPC to the CIU, there is only a single MDM path. Thus, with only the S-band network equipment, the MDM to CIU is a single-point failure that would eliminate the capability of transmitting commands to the IUS from the ground through the Orbiter.

During the first IUS flight(s) before the TDRS is operational, the Ku-band system will not be available to provide a redundant command path through the Orbiter to the IUS. The only way commands can be transmitted from the ground to the IUS is via the SCF ground station directly to the IUS in the payload bay.

When the IUS is in the payload bay, the Orbiter may have to maneuver so that the line-of-sight (LOS) from the SCF ground station to the IUS antennas is not blocked by the Orbiter. In some cases, the IUS will have to be raised on the cradle in order to assure that the LOS is not blocked by the Orbiter.

Another way to command the IUS is with crew-generated commands using the CIU control panel. A failure in the KGT-60 would eliminate the possibility of ENCRYPTED commands from the control panel. A failure in the CIU FSK/AM modulator or I/O driver and selector would eliminate all command signal paths through the Orbiter and the direct RF link from the SCF to the IUS described in the previous paragraph would have to be used.

In the attached mode, the CIU can command the IUS directly (hardline) or by using the PI for RF communications even though the IUS is still in the payload bay. In the detached mode, the CIU sends its commands through one of two redundant PI's.

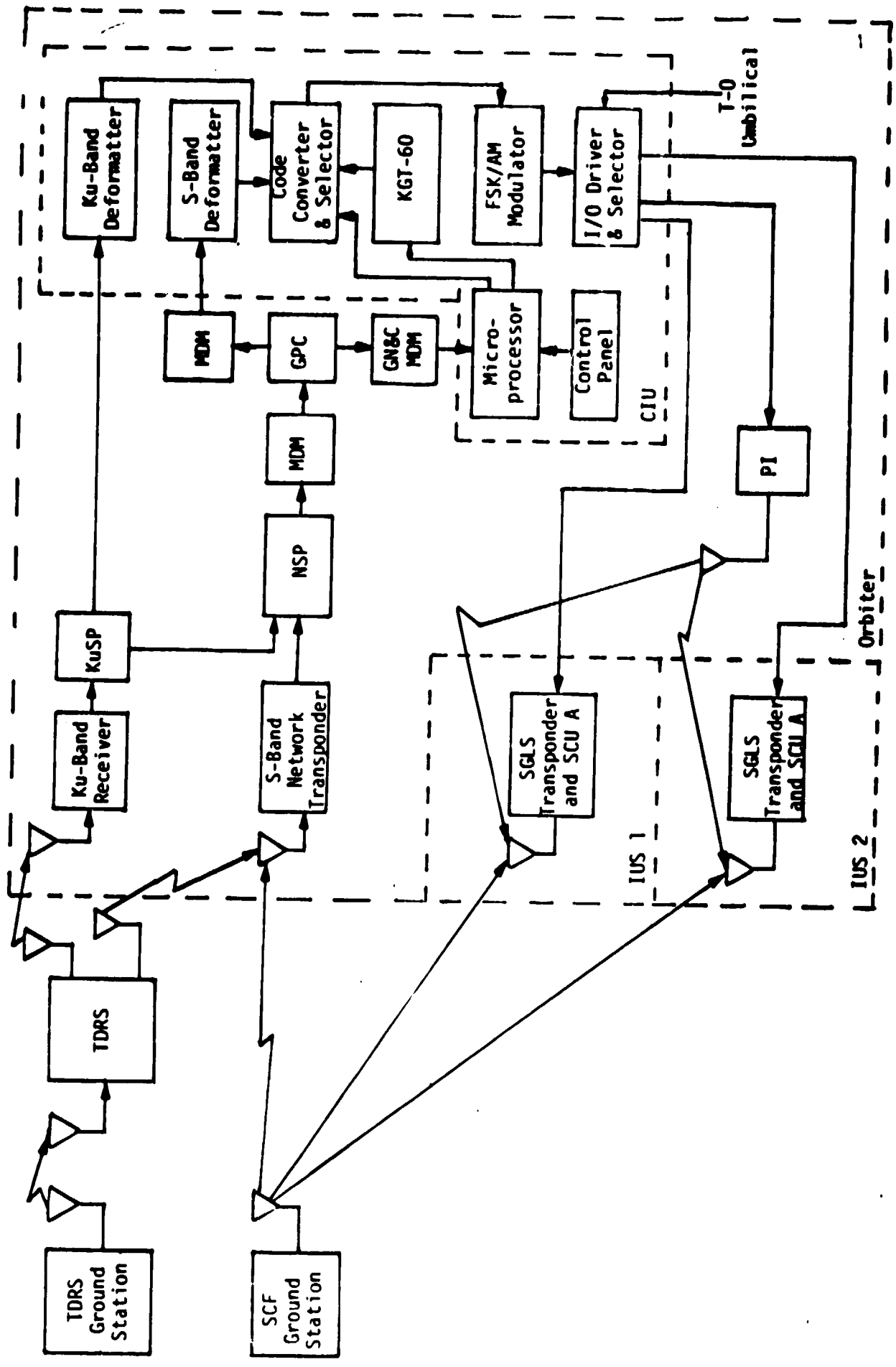

Figure 5.5. Functional SGLS Command Signal Flow (DOD Mode)

Figures 1 through 15 in Addendum A of Appendix D show each of the separate end-to-end communications paths for the DOD or SGLS commands. There are 15 separate paths over which the DOD IUS may be commanded and, while a number of elements are common in each path, notice that each path is distinctly different.

5.5.2 STDN/TDRS Command Signal Flow (NASA Mode)

The NASA IUS employs STDN/TDRS transponders. The functional command signal flow for the NASA IUS is shown in Figure 5.6. Note that the Orbiter command signal flow is completely redundant, with only a single string, using the Ku-band system. Also note that the IUS can be commanded from the GSTDN directly or from the TDRS station via the TDRS while the IUS is in the payload bay and still attached. Again, however, the Orbiter may have to maneuver so that the LOS from the GSTDN or TDRS to the IUS antennas is not blocked by the Orbiter. The maneuvers required of the Orbiter will be less demanding for the NASA IUS than the DOD IUS because of the greater coverage of the TDRS. In some cases, however, the IUS still might have to be raised on the cradle in order to make sure that the LOS is not blocked by the Orbiter.

Crew-generated commands to the IUS are via the GPC. In Figure 5.6, the payload station control panel is shown as a way to enter commands into the GPC and then into the PSP for transmission to the IUS. While a single MDM is shown from the payload station control panel to the GPC, there are several redundant keyboards with MDM that would allow the entering of commands into the GPC.

Figures 1 through 12 in Addendum B of Appendix D show each separate end-to-end communications path for the NASA or STDN/TDRS commands. There are 12 separate paths over which the NASA IUS may be commanded whereas there were 15 separate paths for the DOD IUS. As previously mentioned, each path has a number of common elements but each path is distinctly different.

5.5.3 SGLS Telemetry Signal FLow (DOD Mode)

The SGLS telemetry functional signal flow is presented in Figure 5.7. In the attached mode, IUS telemetry comes from three sources: (1) the Signal Interface unit (SIU), (2) the Environmental Measurement

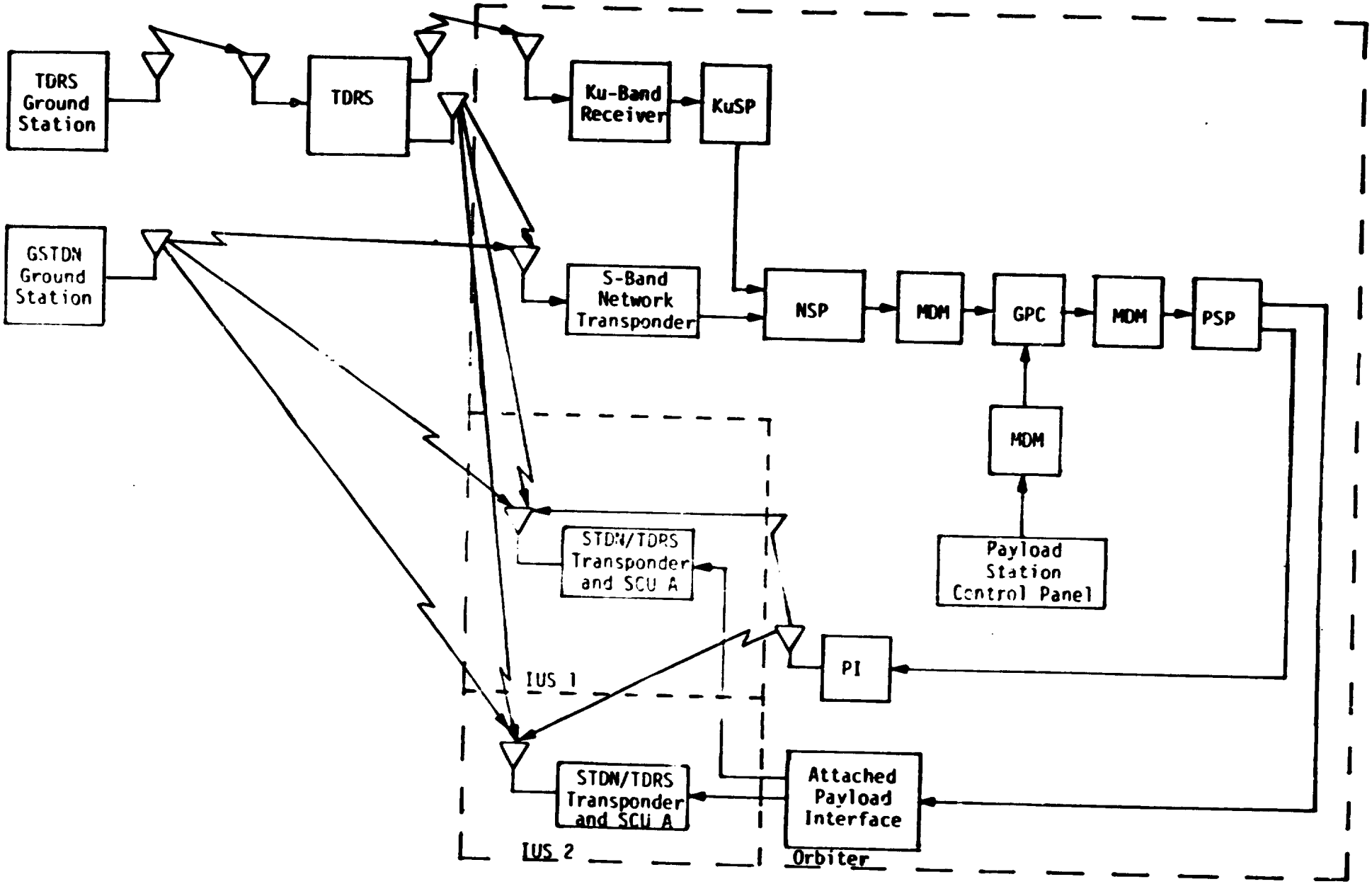

Figure 5.6. Functional STDN/TDRS IUS Command Signal Flow (NASA Mode)

Unit (EMU) and, (3) the Wideband Data Interleaver (WBDI). Note that each of these telemetry sources is nonredundant so if one of these units fails, that portion of the telemetry is lost. The SIU provides switching from the two IUS computers to the one SGLS transponder and also provides proper interfacing with the encrypter for the ENCRYPTED TEXT mode.

The FM vibration data consists of three sensors mounted on the spacecraft interface ring. Their analog output is signal conditioned to modulate three standard subcarriers in the EMU. The three subcarriers are summed together and cabled directly to the attached payload interface and the transponder 1.7 MHz input port.

The WBDI interleaves up to six separate channels of asynchronous NRZ-L telemetry data. The WBDI output is serial NRZ-L data at a rate of 256 kbps.

As shown in Figure 5.7, the output of the attached payload interface is (1) EMU data from one of two IUS's sent to the CIU for selection to the Payload Recorder (PR), (2) WBDI data from one of two IUS's sent to the CIU for NRZ-L to biphase-L conversion and selection to the KuSP, FMSP and PR and, (3) SIU data from both IUS's (labeled IUS 1 and IUS 2 data in Figure 5.7) sent to the CIU for selection to the PDI or after NRZ-L to biphase-L conversion to the KuSP, FMSP and PR.

In the detached mode, the telemetry can be received by the Orbiter via the PI or by the SCF ground station via a direct RF link. On the Orbiter, the output of one of the two PI's is selected for demodulation. If the selector fails, the Orbiter cannot process telemetry data in the detached mode. Also, following selection between the two PI's, the FM demodulator and PSK demodulator are not redundant so, if either fails, either the EMU or SIU data is not recovered by the Orbiter.

The bit synchronizer following the PSK demodulator is implemented partially in hardware and partially in software. Once the telemetry data is processed by the CIU up to the output selector, the commands on the attached mode in terms of the result of failures in the CIU apply to the detached mode.

The telemetry data has several RF paths available to the ground. Using the Ku-band system, the telemetry data is transmitted via the TDRS to the TDRS ground station. Using the S-band network transponder, the telemetry data can be transmitted via either TDRS to the TDRS ground

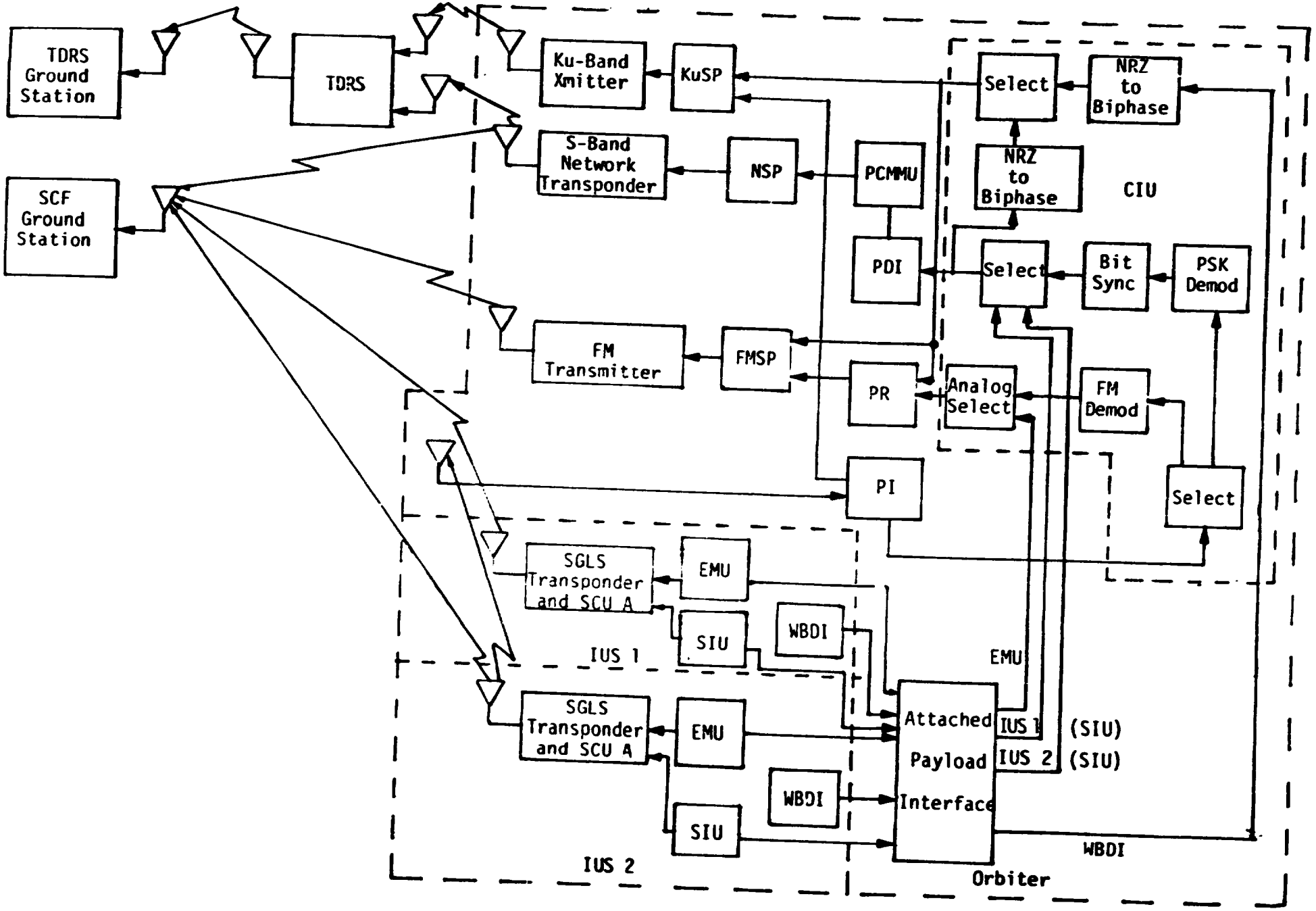

Figure 5.7. **Functional SGLS Telemetry Signal Flow (DOD Mode)**

station or directly to the SCF ground station. Finally, using the S-band FM transmitter, the telemetry data is transmitted directly to the SCF ground station.

Figures 1 through 14 in Addendum C of Appendix D show each separate end-to-end communications path for the DOD or SGLS telemetry. There are 14 separate paths over which telemetry may be received from the DOD IUS.

5.5.4 STDN/TDRS Telemetry Signal Flow (NASA Mode)

The telemetry functional signal flow for the NASA IUS is shown in Figure 5.8. Note that, as shown in the figure, the telemetry data has several RF paths to the ground. As was mentioned previously, the NASA IUS can transmit telemetry in the TDRS mode via the TDRS to the TDRS ground station or in the STDN mode directly to the GSTDN ground station. When the telemetry data is processed by the Orbiter, the telemetry data can be transmitted via the TDRS using either the Ku-band system or the S-band network transponder. Alternately, the Orbiter can transmit the data directly to the GSTDN ground station using either the S-band network transponder or the FM transmitter.

Figures 1 through 16 in Addendum D of Appendix D show each separate end-to-end communications path for the NASA or STDN/TDRS telemetry. There are 16 separate paths over which telemetry may be received from the NASA IUS whereas there were 14 separate paths over which telemetry could be received from the DOD IUS. Again note that, while the paths contain common elements, each path, from an end-to-end viewpoint, is unique.

5.6 Proposed ESTL Test Configuration Description

In this section, the overall test philosophy will be described, the required test links developed and a general description of the ESTL discussed. Also, any special test equipment will be outlined.

5.6.1 Testing Philosophy

In the previous section, all of the end-to-end signal paths were defined. Since there are 57 different end-to-end signal routes, testing all the command and telemetry paths would be extremely time-consuming, redundant and expensive. There are segments of these paths,

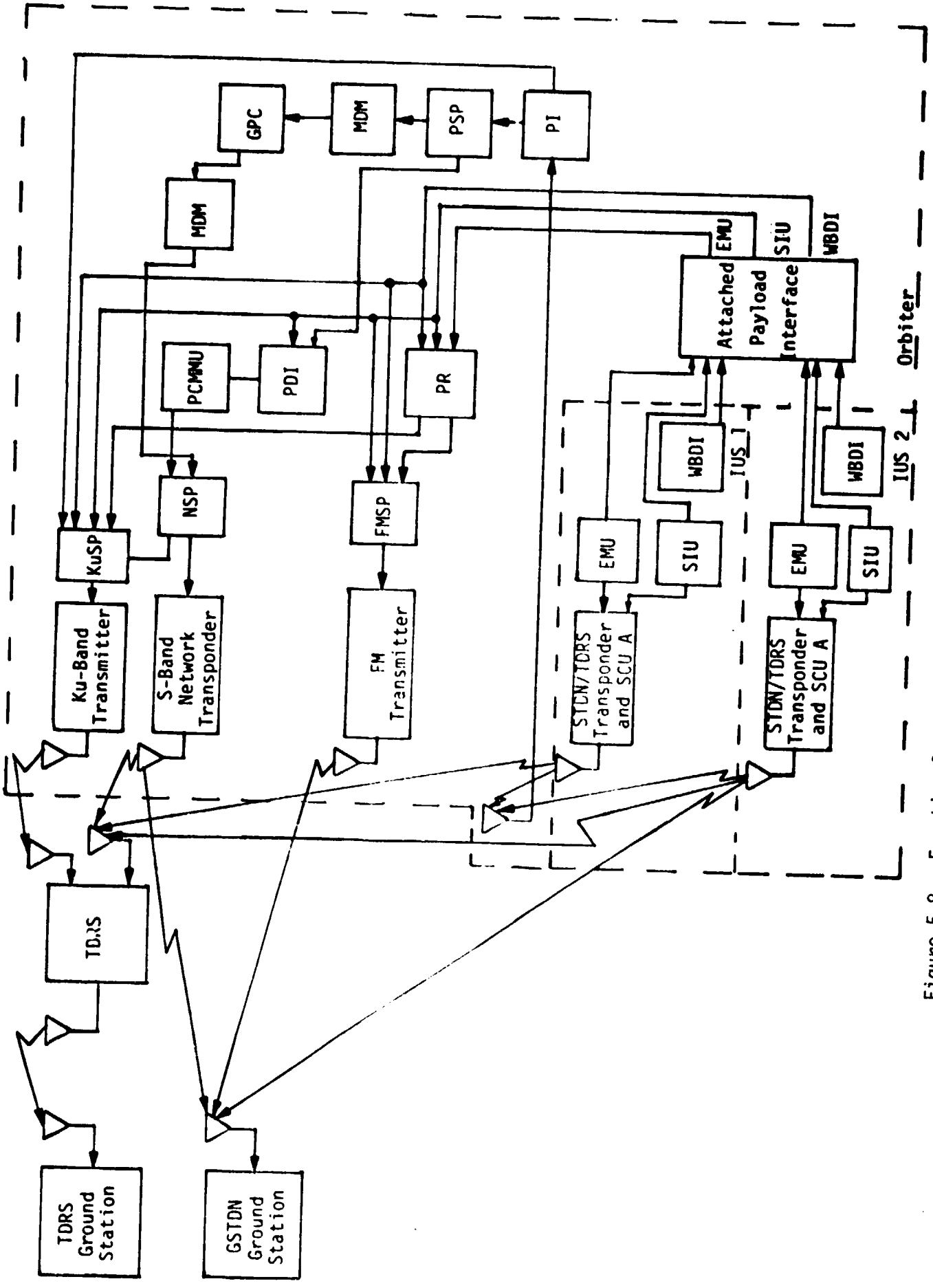

Figure 5.8. Functional STDN/TDRS Telemetry Signal Flow (NASA Mode)

however, that are being or will be tested under separate test plans. For example, there are ESTL verification test procedures being implemented for the S-band network transponder direct DOD and NASA links which include the ground stations, S-band transponder and the NSP.

By comparing those link segments which are or should be tested under separate test plans with the total end-to-end signal paths, only those unverified link segments remaining need to be discussed in this test plan. In making these correlations, any "holes" in the testing program are apparent and, at the same time, the amount of testing redundancy is minimized. To start comparing one link segment to another, the overall signal path must be separated into easily quantifiable sections.

From an end-to-end link point of view, the Orbiter and IUS communications system is essentially composed for modular equipment serially connected. For example, a command may be send from a ground station to the Orbiter S-band network transponder, processed through a number of Orbiter modules or line replaceable units (LRU's) such as the NSP, and retransmitted by the PI LRU to the IUS, where the command is received and decoded through another series of modules.

Conceptually, an end-to-end communications link may be characterized as a series of modules as represented by triangles 1 through 5 shown in Figure 5.9a. Assume that link segment I, as represented by the circled triangles 1 through 3 shown in Figure 5.9b, was tested or will be tested as part of another test plan. The link characteristics of segment I will then have been quantified, and the link will perform adequately up to and including the module or LRU 3. In testing the remaining link segment composed of modules or LRU's 4 and 5, if there is at least one LRU overlap, as shown in Figure 5.9c, both segments have a common LRU which, itself, has been quantified thorugh acceptance and qualification testing.

The basic philosophy of this test plan, therefore, is to test only those signal path segments which will not be tested under separate test plans. To have confidence that the overall link will meet mission objectives when the segments have been tested separately, some redundancy or LRU overlap in the testing program is necessary.

The one LRU overlap philosophy is applied to the NASA mode commands and telemetry; the philosophy is modified somewhat, however, for the DOD mode. All the Orbiter communication LRU's such as the PI, PR,

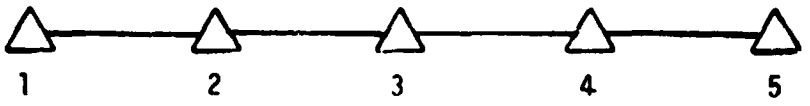

(a) Conceptual End-to-End Communication Link

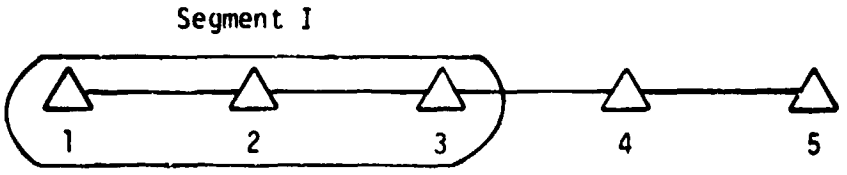

(b) Link Segment Tested Under Another Test Plan

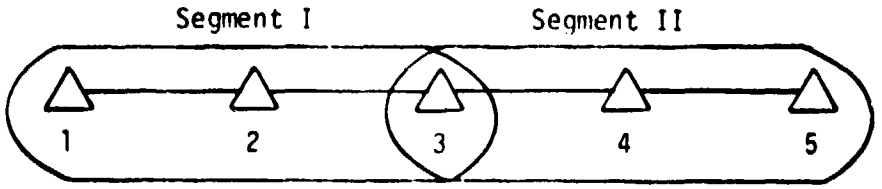

(c) Total Link Test as Tested Under Two Separate Test Plans

△ ≡ Modular Equipment or LRU's

Figure 5.9. Conceptual End-to-End Communications Link

NSP, etc., are under the direct control of the Orbiter contractor, Rockwell International (RI), where RI is responsible for performance and interface compatibility. The only exception is the CIU, which is under the control of the IUS contractor--the Boeing Company. Just as a redundant verification, any tests with the CIU will include the CIU plus at least an RI-controlled LRU. For example, the CIU output may interface with the PR, so the PR would be included in the test link.

Since this plan addresses only the IUS/Orbiter links, direct IUS/ground links should be covered in a separate test plan. Also, only telemetry linked <u>through</u> the IUS will be tested under this plan. Any direct payload/Orbiter communications and, similarly, any direct payload/ground communications will not be discussed.

The test philosophy used in this plan may be summarized as follows:

- Only IUS/Orbiter links will be tested
- Only those IUS/Orbiter link segments not addressed in other test plans will be discussed
- Test link segments will include at least one LRU which has been tested as part of another test plan
- Text links which include the CIU will also include at least one RI LRU past the CIU output.

5.6.2 General Test Configuration

The Orbiter communications subsystem provides a capability for establishing communication links with both the attached IUS within the Shuttle bay and the detached IUS in the near vicinity of the Orbiter. Communication with the attached IUS is via hardwire channels, as described in Section 3.0. The detached IUS RF communication is a two-way link carrying commands and telemetry. Both the hardwire and RF links with the IUS constitute a portion of the overall space/space capability of the Orbiter communication system.

Figure 5.10 shows the general configuration to be used for all tests involving the IUS/Orbiter subsystem, and Table 5.1 gives a summary of the ESTL test links. To accomplish the operational tests, the ESTL test setup must provide command data to the CIU or PSP and telemetry data to the IUS transponder.

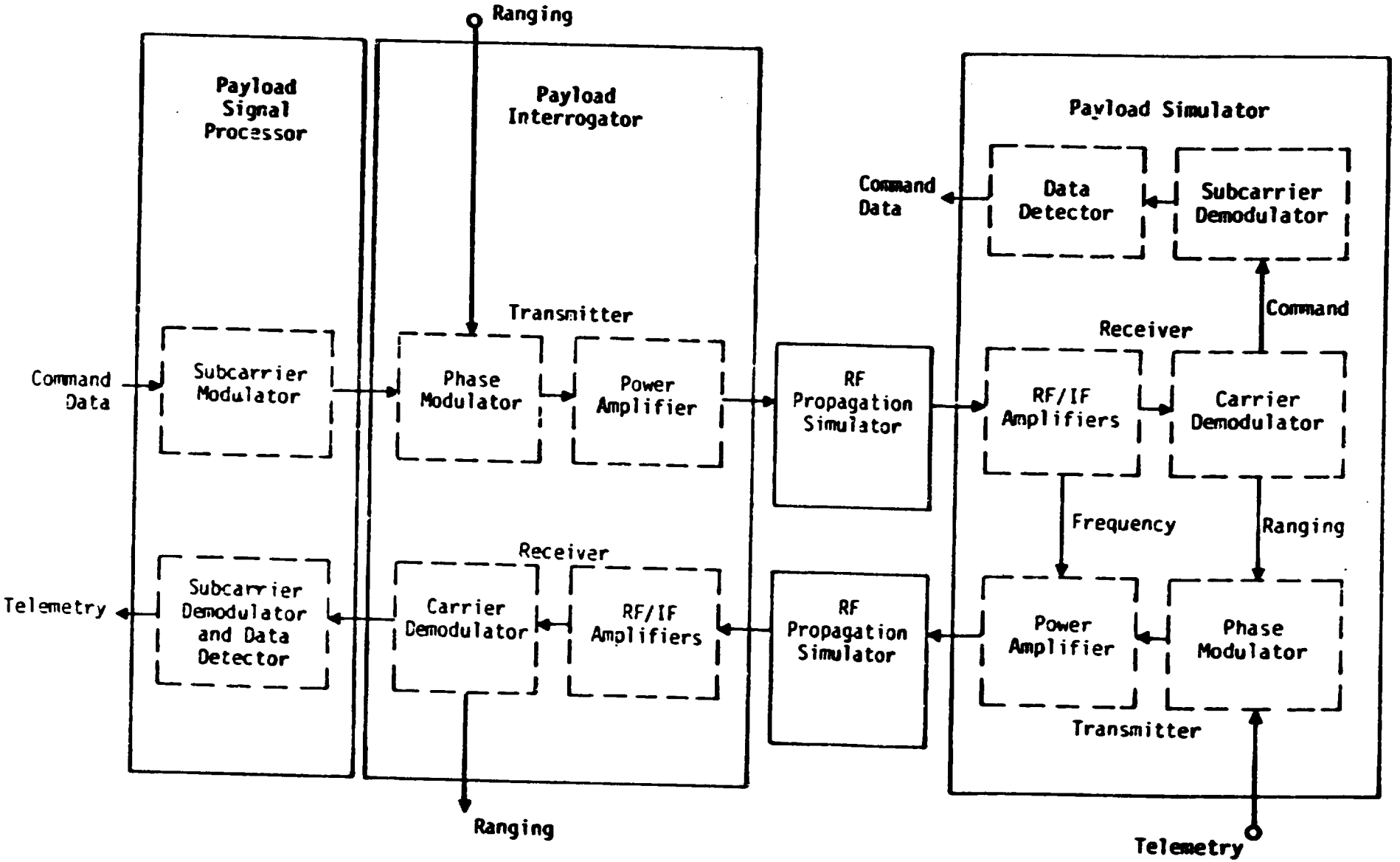

Figure 5.10. General Test Configuration

Table 5.1. ESTL Communication Link Test Configurations Summary

User	Link Type	Data	Modulation Format	Signal Flow Direction Tested (Simulated)
NASA	Hardwire	CMDS	NRZ	Orbiter to IUS
	Hardwire	CMDS	PSK	Orbiter to IUS
	Hardwire	TLM	NRZ	IUS to Orbiter
	RF	CMDS	PSK/PM	Orbiter to IUS
	RF	TLM	PSK/PM	IUS to Orbiter
DOD	Hardwire	CMDS	Ternary Symbols plus Clock	Orbiter to IUS
	Hardwire	CMDS	FSK/AM	Orbiter to IUS
	Hardwire	NAV UPDATE	FSK/AM	Orbiter to IUS
	Hardwire	TLM	NRZ	IUS to Orbiter
	Hardwire	TLM	PSK and FM	IUS to Orbiter
	RF	CMDS	FSK/AM/PM	Orbiter to IUS
	RF	TLM	PSK/PM and FM/FM	IUS to Orbiter

For testing the forward (Orbiter-to-IUS) link, a Univac M642B computer generates commands which are sent to the IUS transponder via either the hard-line cable or the simulated RF link. Command verification is accomplished by comparing the command sent to the CIU or PSP with the command output of the IUS SCU.

Return link (IUS-to-Orbiter) telemetry data is originated by a telemetry simulator and transmitted via the hard-line interface or RF link. The PCM simulated data may be verified directly by a bit error comparator, and the simulated analog telemetry may be verified by signal-to-noise ratio measurements.

Use of the M642B computer depends on the nature of the tests being carried out. Primarily, it is used to aid in the statistical evaluation of the link performance and, most importantly, the M642B provides the processing and control necessary to multiplex received commands and return telemetry data.

5.6.3 Required Test Equipment

The Orbiter and IUS communication systems will be installed in the ESTL in a representative mission configuration. The equipment will be interconnected either through a space-loss simulator which accurately controls the forward and return link total received power levels to test the RF links or via the cables to test the hard-line interface links.

To perform the verification tests, special support equipment is necessary. For example, the M642B computer has a parallel data interface whereas the CIU and PSP are serial data devices. Appropriate computer I/O converters will be needed to interface the computer with the test setup.

A telemetry simulator is required to exercise the various test links, which are summarized in Table 5.1. The simulator must be capable of producing both the PCM digital data at different rates and the analog data required for certain tests.

In most tests, the digital and analog data is at baseline frequency. There are some tests, however, where the digital and analog data must first be demodulated before verifying performance. Therefore one or two demodulators must be included in some test setups.

A summary of the required equipment is shown in Table 5.2.

Table 5.2. Required Equipment Summary

ORBITER	IUS
PI	Transponder (DOD & NASA)
CIU	SCU (DOD & NASA)
PSP	SIU (DOD & NASA)
PDI	EMU (DOD & NASA)
KuSP	WBDI (DOD & NASA)
FMSP	Decryptor
PR	Encryptor
MDM	
Encryptor	

ESTL
Space Loss Simulator
Bit Synchronizer
Bit Error Rate Detector
Frame Synchronizer
M642B Computer
Computer Input Converter (Serial/Parallel)
Computer Output Converter (Parallel/Serial)
Signal-to-Noise Ratio Meter
Decryptor
Telemetry Simulator (Digital & Analog)
Ku-Band Deliverable Test Equipment (DTE)
ESTL Range and Doppler Simulator (ERDS)
IUS Antenna Select Simulator

5.7 System Performance Evaluation Tests

5.7.1 General

There are two major test categories: calibration tests and system compatibility and performance tests. The system compatibility and performance tests include both the RF and hard-line links.

5.7.2 Calibration Tests

The purposes of the calibration tests are (1) to verify that the overall communications system configuration, consisting of the Orbiter equipment, RF or hard-line interface path and IUS equipment, is ready for the system compatibility and performance tests and (2) to measure important equipment parameters that will be needed to conduct the tests and to evaluate the test results. The calibration tests will include space-loss simulator calibration, measurement of RF power levels, noise figures, frequency responses and modulation indices. Calibration tests will be performed on both Orbiter and IUS equipment, as applicable. In addition, as a prerequisite to performing the system compatibility and performance tests, operator's certification procedures must be performed on equipment which requires certification.

5.7.3 System Compatibility and Performance Tests (RF Links)

The purposes of these tests are to verify overall system compatibility and determine channel performance. Channel performance determines the total received power-to-noise spectral density ratios required to achieve the specified data channel performance. Tables 5.3 through 5.6 show the signal combinations and performance requirements which will be used during the system RF performance evaluation. The data rates shown in these four tables represent the maximum and minimum rates for that particular RF link.

The Orbiter/IUS forward link tests will evaluate the command channel performance while the IUS/Orbiter return link tests will verify the telemetry channel performance. RF acquisition tests will first substantiate the forward and return links individually, then the two-way link. All tests will assess system performance for both the DOD and NASA IUS configurations but will not include doppler offsets since the relative velocity between the Orbiter and IUS is small.

Table 5.3. Forward Link RF Signal Combinations and Performance Requirements (DOD)

Combination	Information Transmitted	Modulation Techniques	Modulation Index (Radians)	DOD IUS Required Prec/No. (dB - Hz)
1*	2 ksps Commands	FSK/AM	0.2 - 2.5	56.5
2	1 ksps Commands	FSK/AM	0.2 - 2.5	56.5

*Current CIU design is not capable of this rate.

Table 5.4. Forward Link RF Signal Combinations and Performance Requirements (NASA)

Combination	Information Transmitted	Modulation Techniques	Modulation Index (Radians)	NASA IUS Required Prec/No. (dB - Hz)
3	2 kbps Commands	PSK	$\pi/2$	48.2
4	7.8125 bps Commands	PSK	$\pi/2$	48.2

Table 5.5. Return Link RF Signal Combinations and Performance Requirements (DOD)

Combination	Information Transmitted	Modulation Techniques	Modulation Index (Radians)	Orbiter Required Prec/No. (dB - Hz)
5	Telemetry, includes 16 kbps digital (1.024 MHz subcarrier) & Analog (IRIG 1A, 2A & 3A freq.)	PSK	π/2	60.4
	(1.7 MHz subcarrier)	FM/FM		74.5
6*	Telemetry, includes 64 kbps Digital (1.024 MHz subcarrier) & Analog (IRIG 1A, 2A & 3A freq.)	PSK	π/2	60.4
	(1.7 MHz subcarrier)	FM/FM		74.5
7*	Telemetry 256 kbps digital (1.7 MHz subcarrier)	PSK	π/2	60.4
8*	Telemetry, 0.25 kbps digital (1.024 MHz subcarrier)	PSK	π/2	60.4
9*	Telemetry Analog (IRIG 1A, 2A & 3A freq.)			
	(1.7 MHz subcarrier)	FM/FM		74.5

*Combinations 6-9 are the "bent-pipe" signals.

Table 5.6. Return Link RF Signal Combinations and Performance Requirements (NASA)

Combination	Information Transmitted	Modulation Techniques	Modulation Index (Radians)	Orbiter Required Prec/No. (dB - Hz)
10	16 kbps Telemetry	PSK	$\pi/2$	60.4
11	1 kbps Telemetry	PSK	$\pi/2$	60.6

The Orbiter/IUS forward and return links are capable of operating in any one of approximately 850 fully duplex channels, each of which is divided into two bands, designated the "high" and "low" bands. Ideally, the links should be tested at both frequency extremes of the high and low bands. While the PI is capable of operating in any one of the channels, the link operating frequency is dependent upon the IUS transponder which has two fixed frequencies. The tests in the ESTL, therefore, will not be able to exercise the links at the band extremes since the two IUS transponder frequencies are not selectable and are in the same band very close to each other.

5.7.3.1 Forward link tests (RF)

The purpose of these tests is to evaluate the capability of the Orbiter-to-IUS RF command link to meet mission requirements. The forward link tests are subdivided into the DOD and NASA command channel tests.

The command channel will be evaluated by measuring message rejection rate and command word verification as functions of total received power-to-noise spectral density ratios. To measure message rejection rate and command word verification, special test equipment will be used to interface the IUS SCU and the command computer, where a comparison will be made of the commands transmitted and those received by the SCU.

BER's cannot be measured for the command channel because test points are not available. Therefore, the command word verification and message rejection rates will be used to estimate the BER. In addition, verification will be made that 10,000 error-free commands can be received and clocked out of the IUS SCU under strong signal conditions.

The results of these tests will be compared to performance predictions to ascertain how well the measured results compared with theory. The measured results will also be compared with any program requirements to verify that the command link will support a Shuttle mission.

5.3.7.1.1 DOD command configuration

There are three RF test links used to verify that the DOD command channel meets mission requirements. The DOD command RF test link [1] shown in Figure 5.11, and test link 2, shown in Figure 5.12, assess the Orbiter-to-CIU interface. As previously mentioned, since the CIU is not under direct RF control in terms of performance and interface compatibility, an additional ESTL task will be to substantiate the performance of the Orbiter/CIU interface, after which commands may be injected directly into the CIU.

The primary DOD forward RF test link is test link 3, as shown in Figure 5.13. Test link 3 will measure message rejection rates and command word verification as functions of total received power-to-noise spectral density ratios with and without encryption.

Table 5.7 summarizes the DOD command RF tests. The signal combination shown is from Table 5.3.

5.3.7.1.2 NASA command configuration

Test link 4 is one forward RF test link used to assess the NASA command channel, as shown in Figure 5.14. Table 5.8 summarizes the NASA command RF tests, with the signal combinations shown being from Table 5.4.

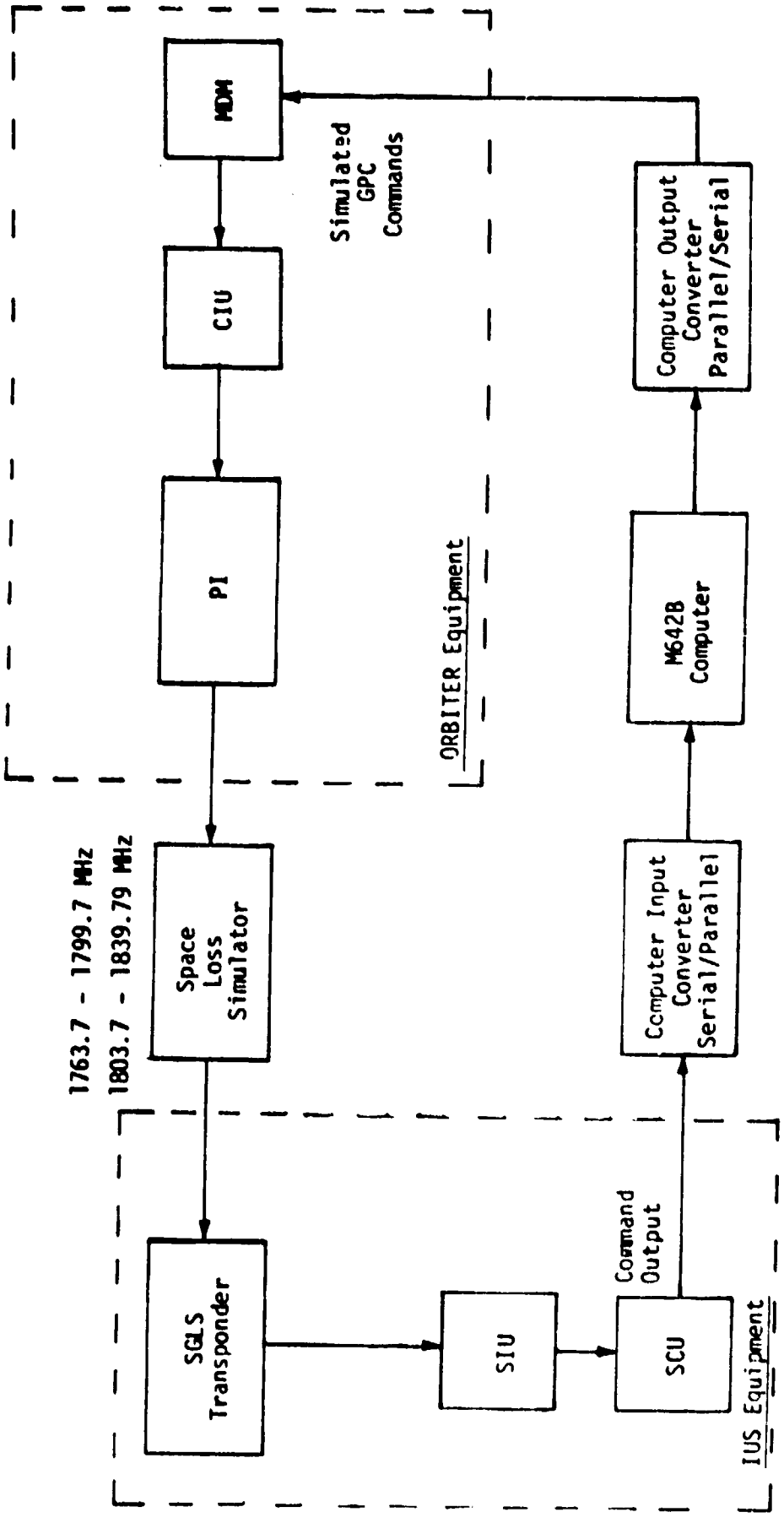

Figure 5.11. DOD Command RF Test Link 1 SGLS Commands

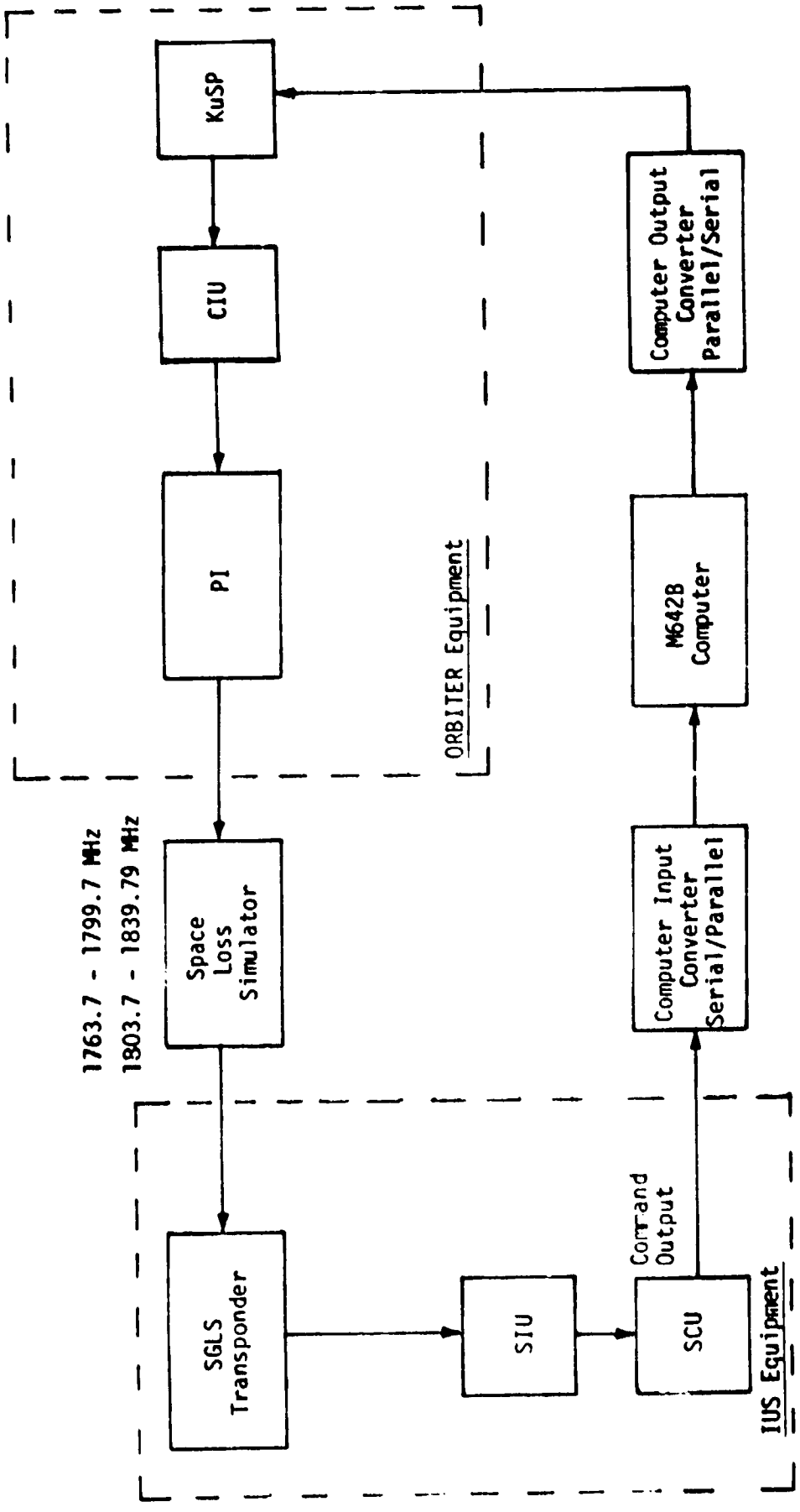

Figure 5.12. DOD Command RF Test Link 2 SGLS Commands

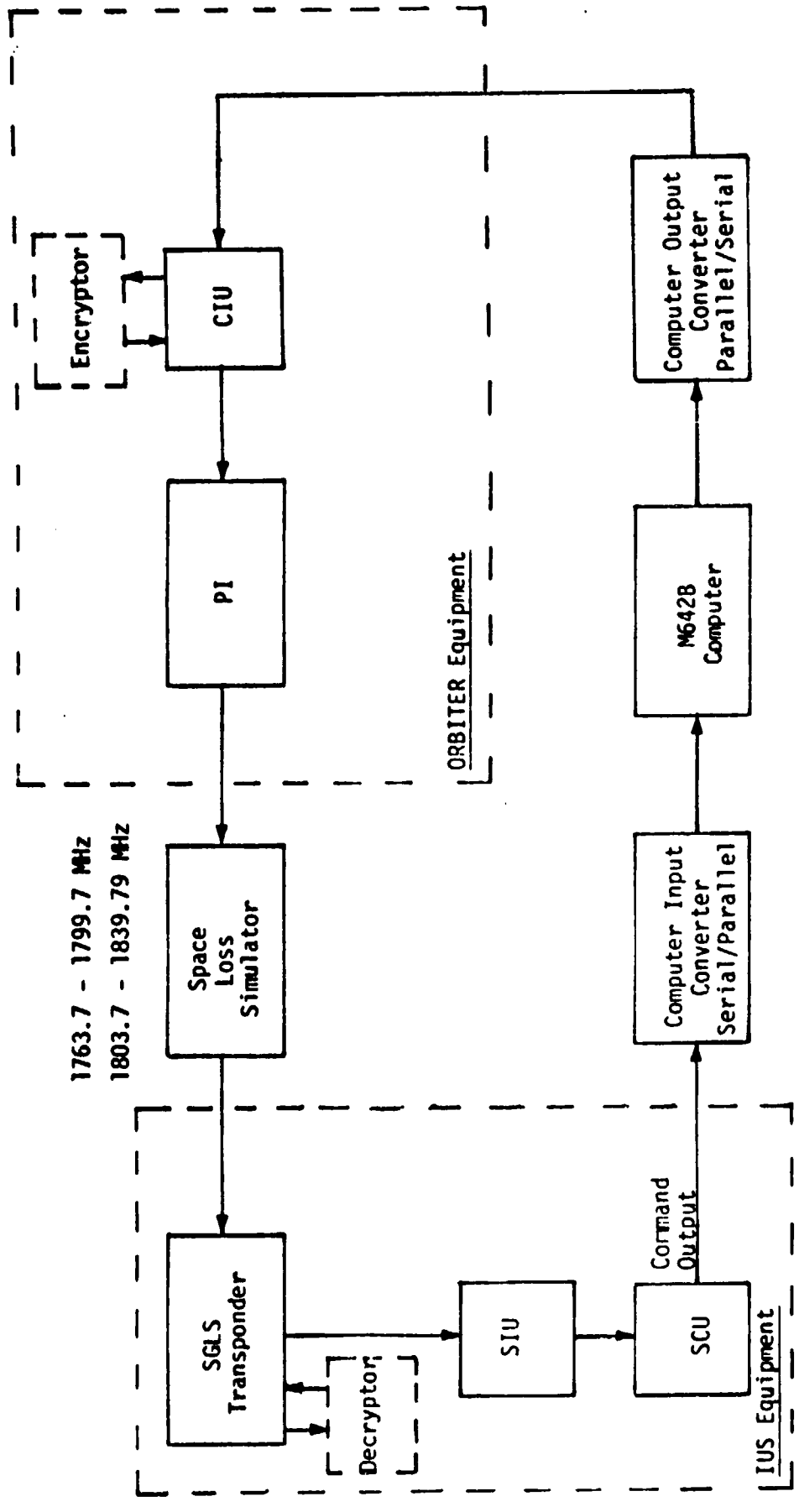

Figure 5.13. DOD Command RF Test Link 3 SGLS Commands

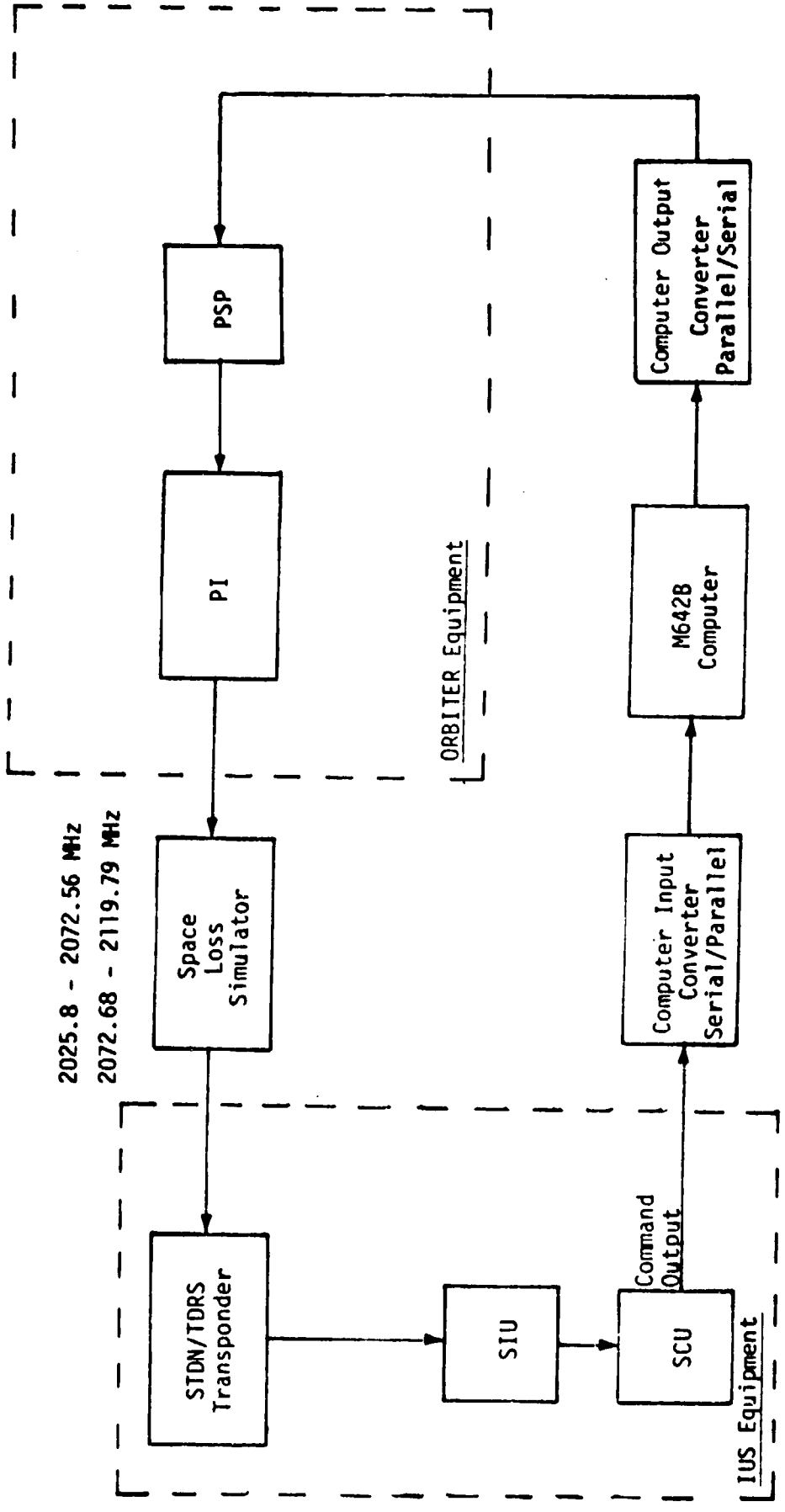

Figure 5.14. **NASA Command RF Test Link 4 STDN/TDRS Commands**

Table 5.7. DOD Command RF Test Summary
(Forward Link)

Test Link 1 (Figure 5.11)	
Measured Parameter:	Command word verification under strong signal conditions
Test Conditions:	• Either IUS transponder frequency* • Signal combination 2
Test Link 2 (Figure 5.12)	
Measured Parameter:	Command word verification under strong signal conditions
Test Conditions:	• Either IUS transponder frequency* • Signal combination 2
Test Link 3 (Figure 5.13)	
Measured Parameter:	Command word verification and message rejection rate as functions of total Prec/No.
Test Conditions:	• Either IUS transponder frequency* • Signal combination 2 • With and without encryption
Measured Parameter:	10,000 error-free commands received under strong signal conditions
Test Conditions:	• Either IUS transponder frequency* • Signal combination 2

*Both IUS frequencies are in the same band (high or low) and, typically, are very close to each other.

Table 5.8. NASA Command RF Test Summary
(Forward Link)

Test Link 4 (Figure 32)	
Measured Parameter:	Command word verification and message rejection rate as functions of total Prec/No.
Test Conditions:	• Either IUS transponder frequency*
	• Signal combinations 3 and 4
Measured Parameter:	10,000 error-free commands received under strong signal conditions
Test Conditions:	• Either IUS transponder frequency*
	• Signal combination 4

*Both IUS frequencies are in the same band (high or low) and, typically, are very close to each other.

5.7.3.2 Return link tests (RF)

The purpose of these tests is to evaluate the capability of the IUS-to-Orbiter RF telemetry link to meet mission requirements. The return links are subdivided into the DOD and NASA telemetry channel tests.

There is a variety of telemetry formats and data rates transmitted by the IUS transponder to the PI. Basically, the telemetry consists of digital information PSK modulated onto a subcarrier; however, analog information may be FM modulated onto a second subcarrier (DOD mode only). In the wideband "bent-pipe" mode, either subcarrier may be modulated with digital or analog data.

The digital telemetry channels will be evaluated by measuring bit error rates (BER) and percent data loss as functions of Orbiter total received power-to-noise spectral density ratios. The telemetry simulator will input digital information to both the IUS SIU and bit error detector. The information received by the Orbiter also will be input to the bit error detector, where the telemetry transmitted to the IUS may be compared to the telemetry received by the Orbiter. In some instances, it will be necessary to demodulate the digital information with the test equipment before performing the BER measurements.

The percent data loss tests will be performed by comparing the number of frames sent by the IUS to the number of frames received by the Orbiter. To accomplish this test, the telemetry simulator must output frame synchronization information.

The analog telemetry channels will be evaluated by measuring the Orbiter analog output signal-to-noise ratio (SNR) as a function of total received power-to-noise spectral density ratios. The telemetry simulator will input analog information to the IUS EMU for transmission to the Orbiter by the IUS transponder. As in the case with the digital telemetry, it will be necessary in some instances to demodulate the analog information with the test equipment prior to conducting the SNR measurements.

The results of these tests will be compared to performance predictions to ascertain how well the measured results compare with theory; the measured results will also be compared with any program requirements to verify that the telemetry link will support a Shuttle mission.

5.7.3.2.1 DOD telemetry test configurations (RF)

There are six RF test links used to verify that the DOD telemetry channel meets mission requirements. DOD telemetry RF test links 5-8, Figures 5.15 through 5.18, represent the primary digital test configurations. As previously stated, since the CIU is not under direct RI control in terms of performance and interface compatibility, an additional ESTL task will be to substantiate the CIU/Orbiter interface performance. Note that, in test link 8, the KuSP remodulates the digital data in preparation for transmission over the Ku-band equipment. Therefore, the information must be demodulated by the Ku-band deliverable test equipment (DTE) to baseband before performing the test measurements.

DOD telemetry RF test link 9, Figure 5.19, represents the primary analog test configuration. Both analog and digital telemetry may be simultaneously transmitted to the Orbiter, where both are recorded with the PR. The digital channel performance has already been verified with test link 7, and the analog portion is evaluated with test link 9 by making SNR measurements at the PR output.

DOD telemetry RF test link 10, Figure 5.20, tests the "bent-pipe" mode. In this situation, both the analog and digital channel performances are verified in the same test setup. Because there are both narrowband and wideband "bent-pipe" modes, many different signal combinations are required to adequately assess test link 10.

Table 5.9 summarizes the DOD telemetry RF tests. The signal combinations shown are from Table 5.5.

5.7.3.2.2 NASA telemetry test configurations (RF)

There is only one RF test link used to assess that the NASA telemetry channel meets mission requirements; as shown in Figure 5.21, NASA telemetry consists entirely of digital data unless the "bent-pipe" mode is utilized. The NASA "bent-pipe" configuration is not verified because it is identical to the DOD configuration, test link 10.

Table 5.10 summarizes the NASA telemetry RF tests. The signal combinations shown are from Table 5.6.

5.7.3.3 RF acquisition tests

The purpose of these tests will be to evaluate the capability of the Orbiter PI and the IUS transponder to provide automatic RF acquisition that meets the Shuttle mission requirements.

The RF acquisition tests will be performed under computer control. The desired number of acquisition trials will be accomplished through computer-generated commands to the ESTL ranging and doppler simulator (ERDS) which switches the RF link on and off. Even though the Orbiter/IUS link tests will require no doppler offsets or ranging, the ERDS is still needed to provide control for the test sequences.

An antenna switch simulator will be necessary for these tests to simulate the IUS switching from one antenna to another. The simulator will be controlled by the M642B computer through the ERDS.

The measurements will include acquisition threshold, acquisition time, reacquisition time after switching IUS antennas, and acquisition probability for each signal level. The RF acquisition tests are divided into forward link RF acquisition, return link RF acquisition and two-way RF acquisition tests.

5.7.3.3.1 Forward link RF acquisition tests (Orbiter to IUS)

The forward link RF acquisition capability will be evaluated by measuring acquisition threshold, acquisition time, reacquisition time after switching IUS antennas and acquisition probability, with and without encryption (DOD mode only), as functions of IUS total received power-to-noise spectral density ratios. Acquisition tests will also be performed for the modulated forward link carrier to determine the effect on acquisition time and threshold.

The results of these tests will be compared to performance predictions to ascertain how well the measured results compare with theory.

5.7.3.3.2 Return link RF acquisition tests (IUS to Orbiter)

The return link RF acquisition capability will be evaluated by measuring acquisition threshold, acquisition time, reacquisition time after switching IUS antennas and acquisition probability, with and without encryption (DOD mode only), as functions of Orbiter total received power-to noise spectral density ratios. Acquisition tests will also be performed for the modulated return link carrier to determine the effect on acquisition time and acquisition threshold.

The results of these tests will be compared to performance predictions to ascertain how well the measured results compare with theory. The measured results will also be compared with any program requirements to verify that the return link RF acquisition tests will support a Shuttle mission.

5.7.3.3.3 Two-way RF acquisition tests

The two-way RF acquisition capability will be evaluated by measuring acquisition threshold, acquisition time, reacquisition time after switching IUS antennas and acquisition probability, with and without encryption (DOD mode only), as functions of total received power-to-noise spectral density ratios. For the coherent IUS transponder mode, tests will also be performed to determine the out-of-lock time between when return link acquisition is lost because of forward link acquisition and when two-way acquisition is completed. The measured results will also be compared with any program requirements to verify that the two-way acquisition tests will support a Shuttle mission.

5.7.4 System Compatibility and Performance Tests (Hard-Line Links)

As previously stated, a hard-line umbilical provides two-way communication between the IUS and the Orbiter in the attached mode. The purpose of these tests is to verify the overall system compatibility of the IUS/Orbiter hard-line interface.

The tests outlined in this section are more go/no-go types of tests instead of qualitative in nature and are designed primarily to exercise the interfaces. No attempt has been made to simulate the actual transients or EMI which the hard-line umbilical would experience in an actual Orbiter.

The tests have been divided into forward and return link tests. The Orbiter/IUS forward link will evaluate the command channel performance while the IUS/Orbiter return link will evaluate the telemetry channel performance.

5.7.4.1 Forward link tests (hardline)

The command channel will be evaluated by verifying that 10,000 error-free commands can be received. For additional details of this test, see section 4.4.1 of Appendix D.

5.7.4.2 Return link tests (hardline)

The digital telemetry will be evaluated by verifying that 10^7 error-free bits can be received. The analog telemetry will be evaluated by measuring the Orbiter analog output signal-to-noise ratio (SNR).

Additional information on these tests is given in section 4.4.2 of Appendix D.

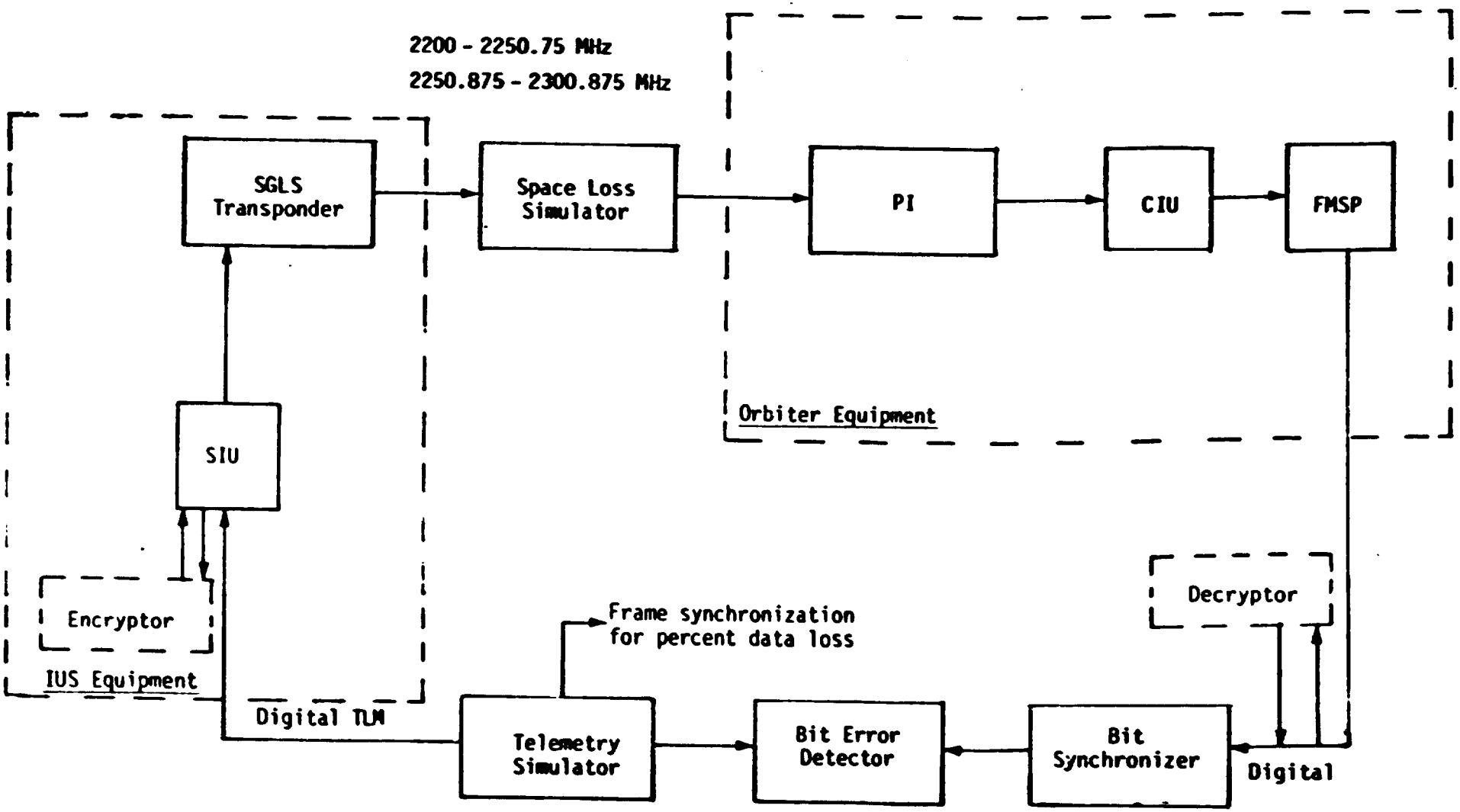

Figure 5.15. DOD Telemetry RF Test Link 5
SGLS Telemetry

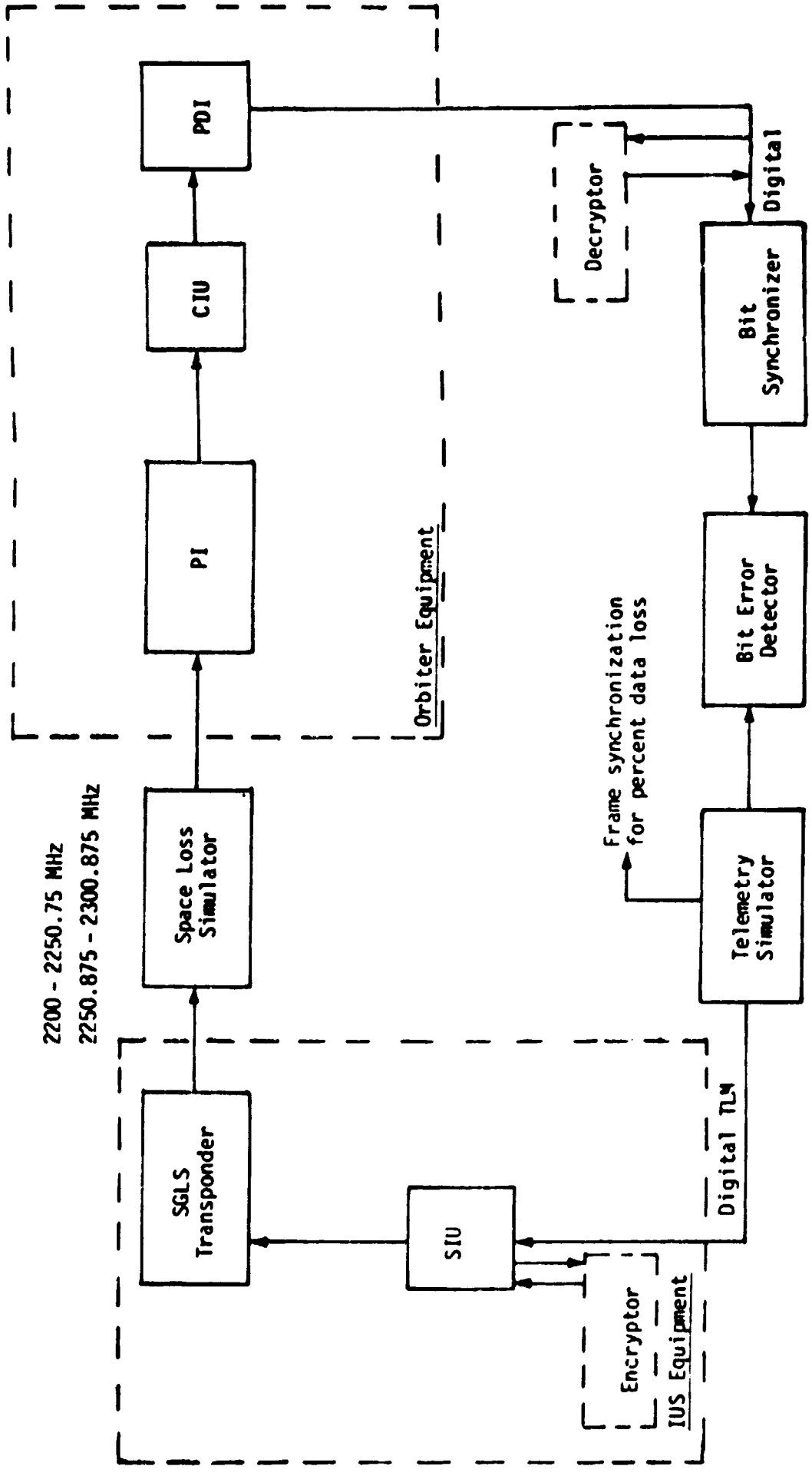

Figure 5.16. DOD Telemetry RF Test Link 6
SGLS Telemetry

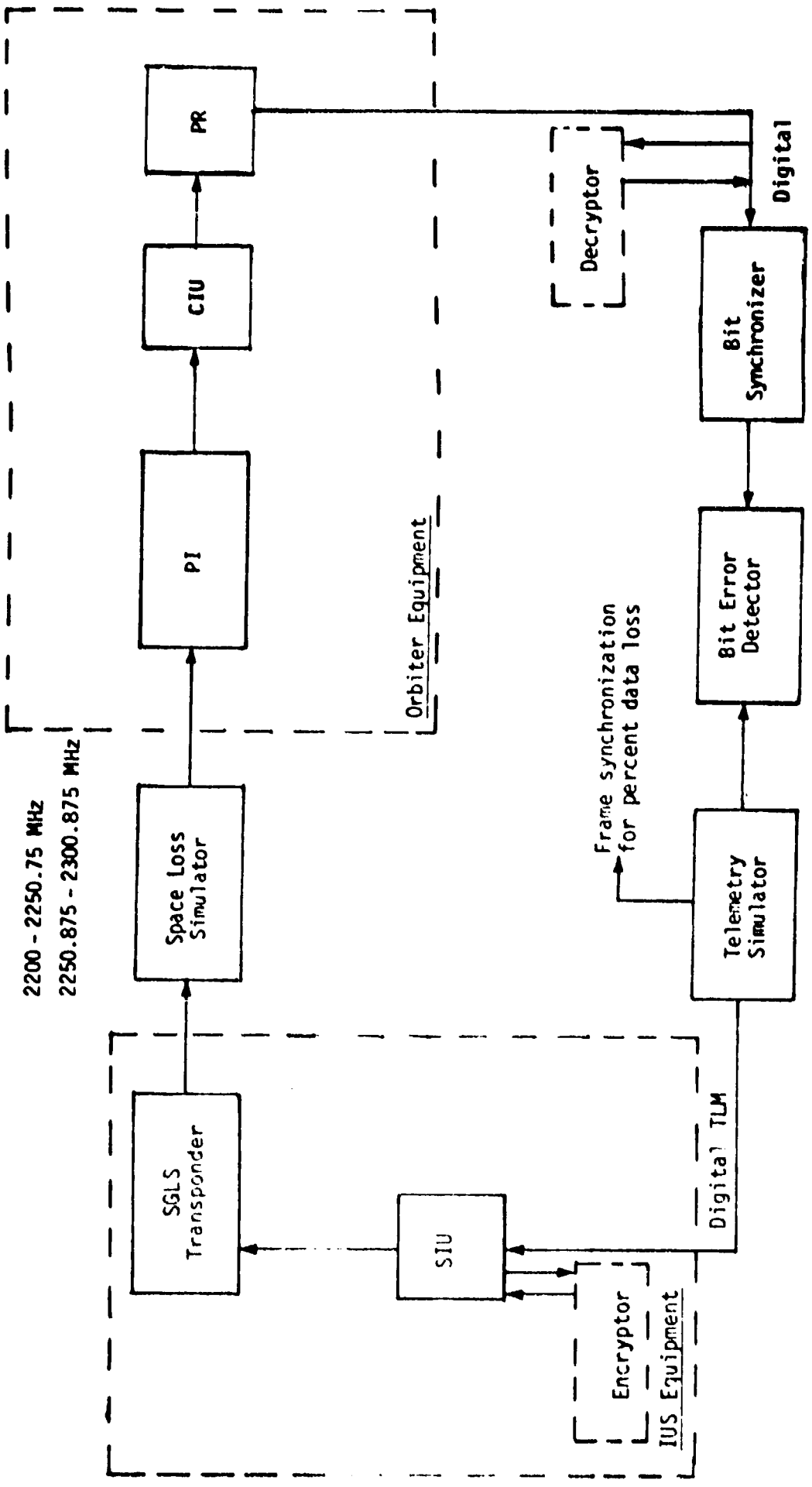

Figure 5.17. DOD Telemetry RF Test Link 7
SGLS Telemetry

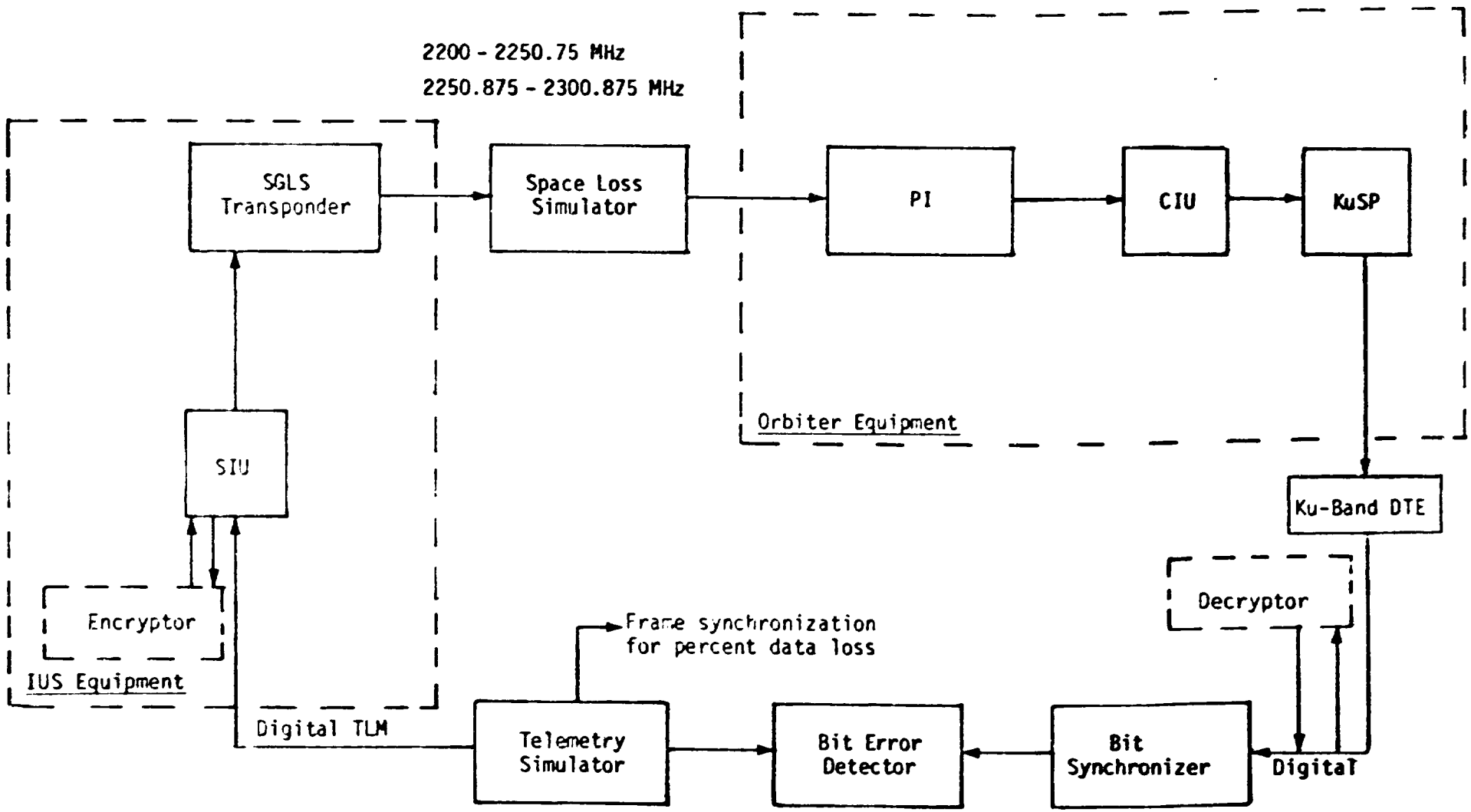

Figure 5.18. **DOD Telemetry RF Test Link 8 SGLS Telemetry**

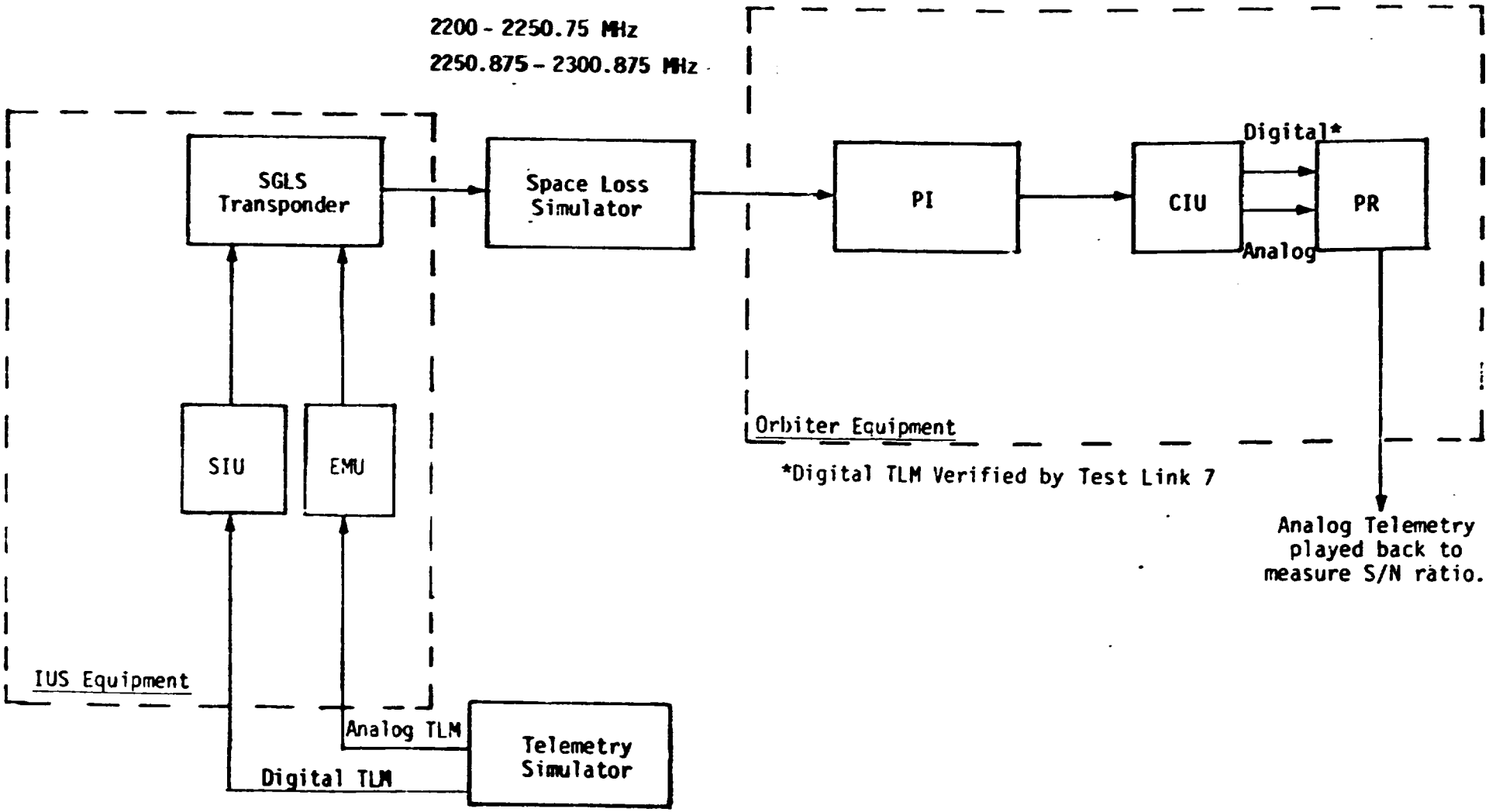

Figure 5.19. DOD Telemetry RF Test Link 9
SGLS Telemetry

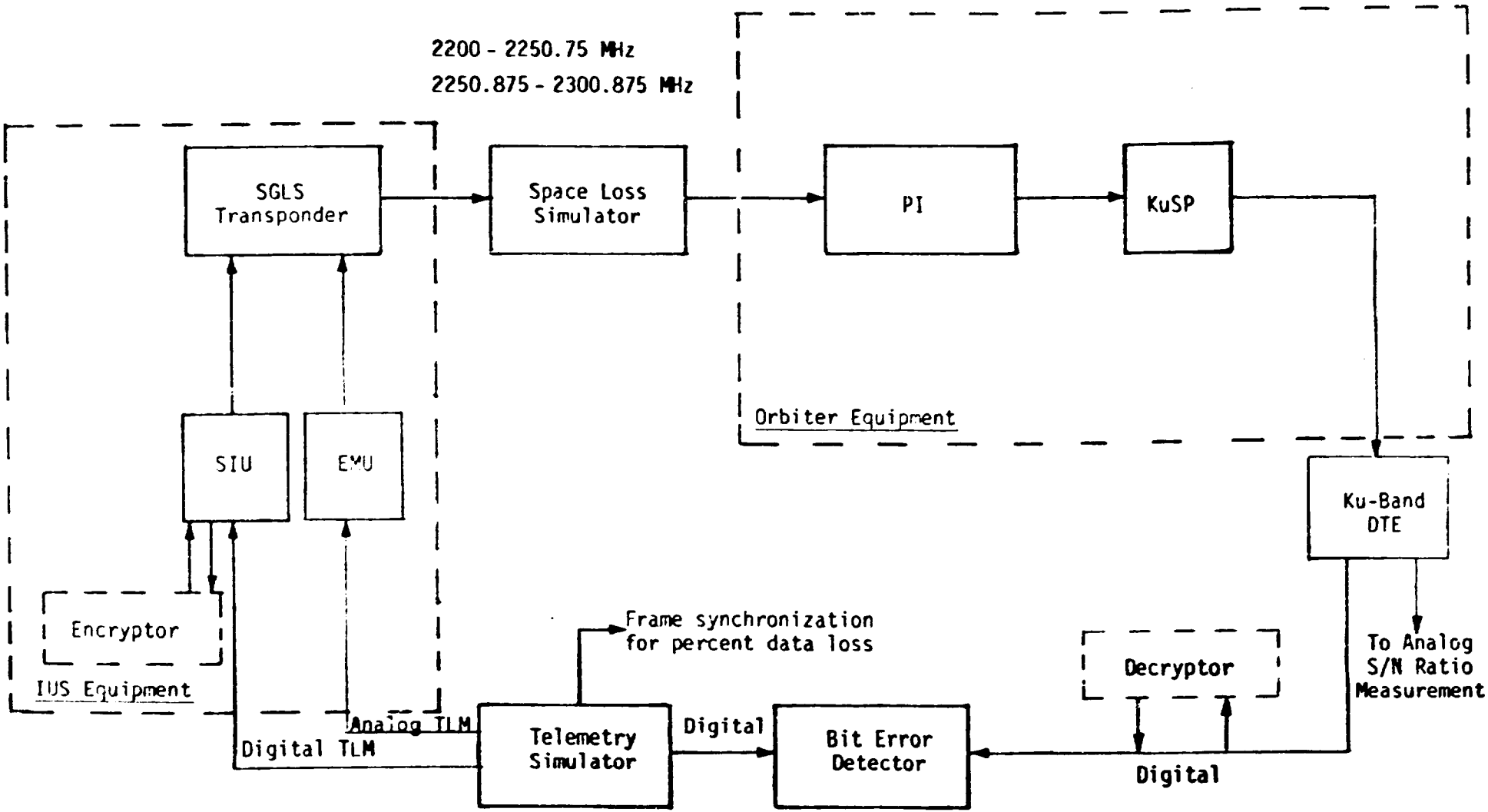

Figure 5.20. **DOD Telemetry RF Test Link 10 SGLS Telemetry**

Table 5.9. DOD Telemetry RF Test Summary (Return Link)

Test Links 5-8 (Figures 5.15 through 5.36)	
Measured parameters:	BER and percent data loss as functions of Orbiter total Prec/No.
Test conditions:	• Either IUS transponder frequency* • Signal combination 5 • With and without encryption
Test Link 9 (Figure 5.19)	
Measured parameter:	SNR as function of Orbiter total Prec/No.
Test conditions:	• Either IUS transponder frequency* • Signal combination 5
Test Link 10 (Figure 5.20)	
Measured parameters:	BER and percent data as functions of Orbiter total Prec/No.
Test conditions:	• Either IUS transponder frequency* • Signal combinations 6-8 • With and without encryption
Measured parameter:	SNR as function of Orbiter total Prec/No.
Test conditions:	• Either IUS transponder frequency* • Signal combinations 6 and 9

*Both IUS frequencies are in the same band (high or low) and, typically, are very close to each other

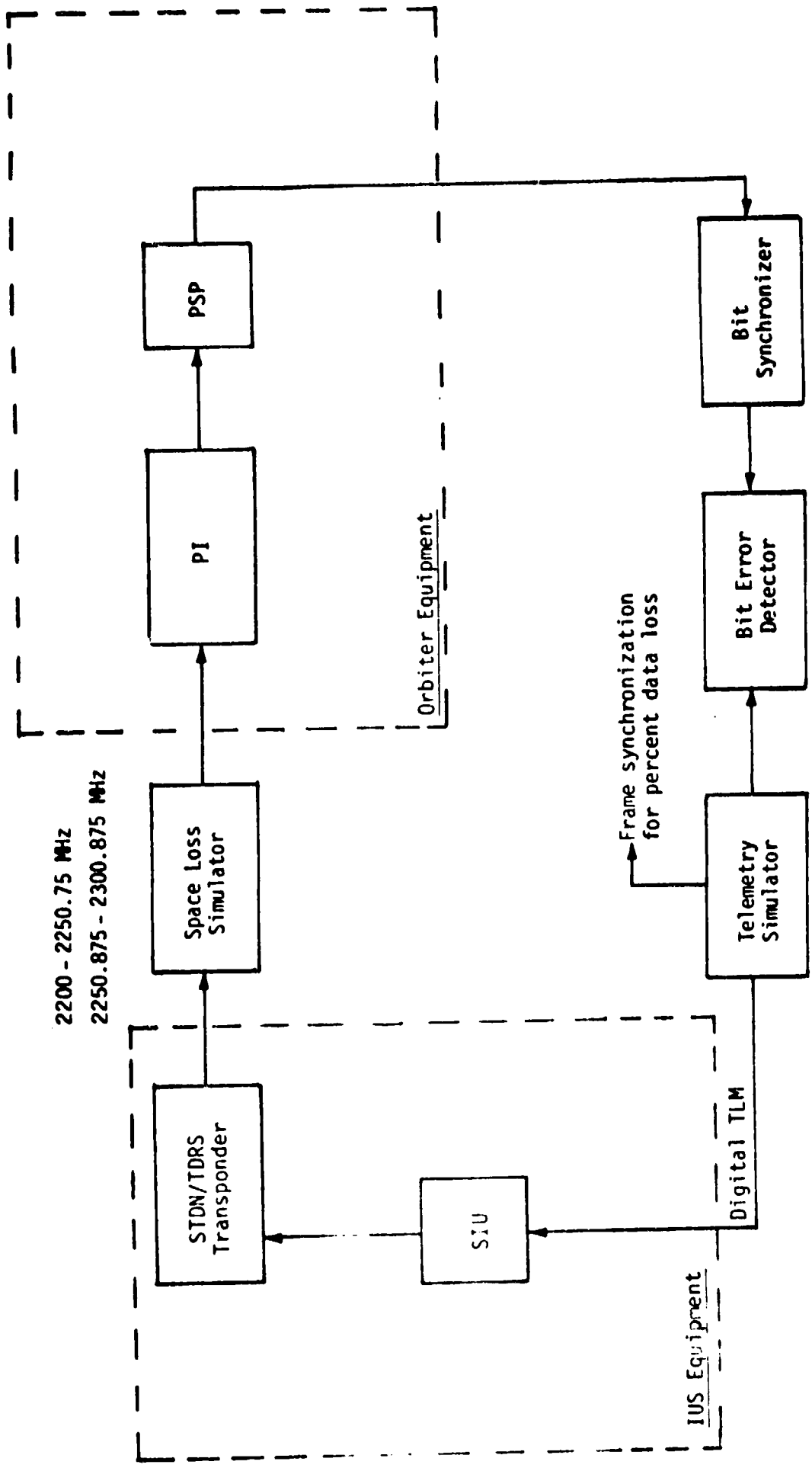

Figure 5.21. NASA Telemetry RF Test Link 11
STDN/TDRS Telemetry

Table 5.10. NASA Telemetry RF Test Summary (Return Link)

Test Link 11 (Figure 5.21)		
	Measured parameters:	BER and percent data loss as functions of Orbiter total Prec./No.
	Test conditions:	• Either IUS transponder frequency* • Signal combinations 10 and 11

Note: NASA "bent-pipe" configuration is identical to the DOD configuration, test link 10.

*Both IUS frequencies are in the same band (high or low) and, typically, are very close together.

6.0 CONCLUSIONS

This report summarizes the effort expended to date during the latter part of FY79. Figure 2.1 in Section 2.0 presented the design reviews and the tasks to be performed in the future as well as a schedule for completion of each of the tasks. The completed tasks are also indicated.

Since the overall IUS/Orbiter communication system is still evolving, direct interfacing of the avionic subsystems is in their early design stages. Consequently, it will be some time before all development problems are resolved and an accurate, up-to-date, well-defined performance can be documented.

The ESTL testing forms a vital part of the overall system performance verification. Therefore, Axiomatix provides in this report an extensive ESTL test requirements plan for the Orbiter and IUS communication equipment being developed.

REFERENCES

1. Carrier, L.M., and Pope, W.S., "An Overview of the Space Shuttle Orbiter Communication and Tracking System", IEEE Transactions on Communication, Vol. COM-26, No. 11, Special Issue on Space Shuttle Communication and Tracking, November 1978, pp 1494-1506.

2. Teasdale, W.E., "Space Shuttle Payloads and Data Handling Accommodations," IEEE Transactions on Communication, Special Issue on Space Shuttle Communication and Tracking, November 1978, pp 1557-1567.

3. Springett, J.S., and Udalov, S., "Communication with Shuttle Payloads," IEEE Transactions on Communication, Special Issue on Shuttle Communication, November 1978, pp 1584-1594.

4. Batson, B.H., Teasdale, W.E., and Huth, G.K., "Payload Data Processing for the Space Shuttle Program," NTC '77 Conference Record, Vol. 2, Los Angeles, December 1977.

5. Batson, B.H., and Moorehead, R.W., "The Space Shuttle Orbiter Telecommunication System," IEEE Communication Society Digest of News, Vol. 14, No. 3, May 1976.

6. Batson, B.H., and Johnson, J.H., "Space Shuttle Communications and Tracking System," ITC Conference Record, Los Angeles, October 1974.

7. "Space Shuttle System Payload Accommodations," Level II Program Definition and Requirements, NASA Document JSC 007700, Vol, XIV, Ref. D, Houston, Texas, November 1975.

8. "Space Transportation System User Handbook," NASA JSC, July 1977.

9. Huth, G.K., "Orbiter CIU/IUS Communications Hardware Evaluation," Axiomatix Report No. R7906-8, June 29, 1979.

10. Simon, M.K., "Tracking Performance of Costas Loops with Hard-Limited In-Phase Channel," IEEE Transactions on Communication, Vol. COM-26, No. 4, April 1978, pp 420-432.

11. Simon, M.K., and Lindsey, W.C., "Optimum Performance of Suppressed Carrier Receivers with Costas Loop Tracking," IEEE Transactions on Communication, Vol. COM-26, No. 2, February 1977, pp 215-227.

12. Simon, M.K., and Lindsey, W.C., "Optimum Design and Performance of Costas Receivers Containing Soft Bandpass Limiters," IEEE Trans. on Communication, Vol. COM-26, No. 8, August 1977, pp 822-831.

13. Lindsey, W.C., Synchronization Systems in Communication and Control, Prentice-Hall, Inc., Englewood Cliffs, New Jersey, 1973.

14. Lindsey, W.C., and Simon, M.K., Telecommunication Systems Engineering, Prentice-Hall, Inc., Englewood Cliffs, New Jersey, 1972, Chapter 6.

15. "STDN/TDRS Transponder, S-Band Preliminary Design Review Data Package," SDRL No. 32521-40, Boeing Aerospace Company, Seattle, Washington, April 1979.

APPENDIX A

ANALYSIS OF POSSIBLE SPURIOUS COMPONENTS ON DOWNLINK DUE TO AM ON 1.035 MHZ SUBCARRIER

(Action Item #8 of S-Band STDN/TDRS Transponder CDR of June 11-13, 1979)

By

Eugene Kopp

APPENDIX A

ANALYSIS OF POSSIBLE SPURIOUS COMPONENTS ON DOWNLINK DUE TO AM ON 1.024 MHZ SUBCARRIER (Action Item #8 of S-Band STDN/TDRS Transponder CDR of June 11-13, 1979)

By

Eugene Kopp

SUMMARY

During the S-Band STDN/TDRS Transponder CDR of June 11-13, 1979 at Boeing, Seattle, NASA Goddard personnel expressed concern regarding the possible effects of AM on the 1.024 MHz PSK-modulated subcarrier. The concern was specifically directed towards the possibility of false locking the ground receiver to the RF spectral lines generated by AM on this subcarrier. Axiomatix took on the action item (Action Item #8) to investigate the causes and potential deleterious effects, if any, of AM on the 1.024 MHz subcarrier.

The results of the Axiomatix analysis have been reported in Monthly Report #3, Appendix A, and in the Axiomatix Technical Memo of August 16, 1979, directed to the Orbiter IUS/CIU Communication Hardware Evaluation Project File. The purpose of this present memorandum is to provide details of the analysis for inclusion in the final report.

The analysis results, as previously reported, indicate that the primary cause of AM on the 1.024 MHz subcarrier is the result of filtering this PSK-modulated subcarrier with a bandpass filter placed ahead of the linear phase modulator. However, the detailed analysis shows that the filter is definitely beneficial to the suppression of possible spurious components and does not introduce any additional spurs into the RF spectrum. The analysis shows that, for a maximum phase deviation of 1.0 radians, a deleterious spurious sideband would be present at a level of 28 dB below the carrier in the absence of the filter; the presence of the filter, with its specification of 60 dB ultimate skirt selectivity, reduces this sideband to a level of 88 dB below the carrier. Axiomatix has shown, in the memo of August 16, that this latter level provides a margin of 9.7 dB against false lock-up for the "worst-case" geometry.

Details of the analysis follow.

1.0 INTRODUCTION

Figure 1 provides a qualitative illustration of the key subelements addressed in our analysis. Part (a) of the figure shows the simplified block diagram of the 1.024 MHz PSK subcarrier modulator (biphase modulator) and the linear RF carrier phase modulator. The PSK modulator consists of a balanced mixer which accepts either a 16 or 64 kbps biphase-L telemetry data stream, f(t), and superimposes it on a 1.024 MHz sinusoidal subcarrier as an antipodal (0°, 180°) phase modulation. This results in a suppressed subcarrier, biphase-modulated baseband signal, g(t).

The "spectral width" of this signal is proportional to the data rate, i.e., a data stream at 64 kbps occupies four times the "spectral width" of a stream at 16 kbps. In 2.0, we shall show that higher frequency components may lead to spurious components near the RF carrier and that a data stream of 64 kbps is potentially more troublesome than a stream of 16 kbps; in brief, 64 kbps constitutes one parameter of the "worst case." We therefore limit consideration, in the following, to a data stream at 64 kbps.

A qualitative representation of the spectrum of the modulated subcarrier is shown in the left-hand portion of part (b) of Figure 1. The spectrum is that of a continuous stream of either "ones" or "zeros" which, for the case of the biphase-L modulation, results in spectral lines located at odd multiples (i.e., 64, 192, 320 kHz, etc.) away from the subcarrier frequency of 1.024 MHz. It is shown in 2.0 that these particular continuous streams constitute another component of the "worst case."

The modulated subcarrier is then passed through a bandpass filter which has the nominal two-way bandwidth (i.e., -3 dB points) of 330 kHz and an out-of-band rolloff of at least 18 dB/octave. The maximum specified out-of-passband attenuation of this S/C filter is 60 dB with respect to the center frequency insertion loss. Thus, data sidebands adjacent to the subcarrier are attentuated only slightly, while those sidebands lying 330/2 = 165 kHz or more from the subcarrier are attenuated considerably. The "conceptual" switch SW shown in Figure 1 permits us to visualize operation with and without the bandpass filter; see Figure 1, parts (b) and (c).

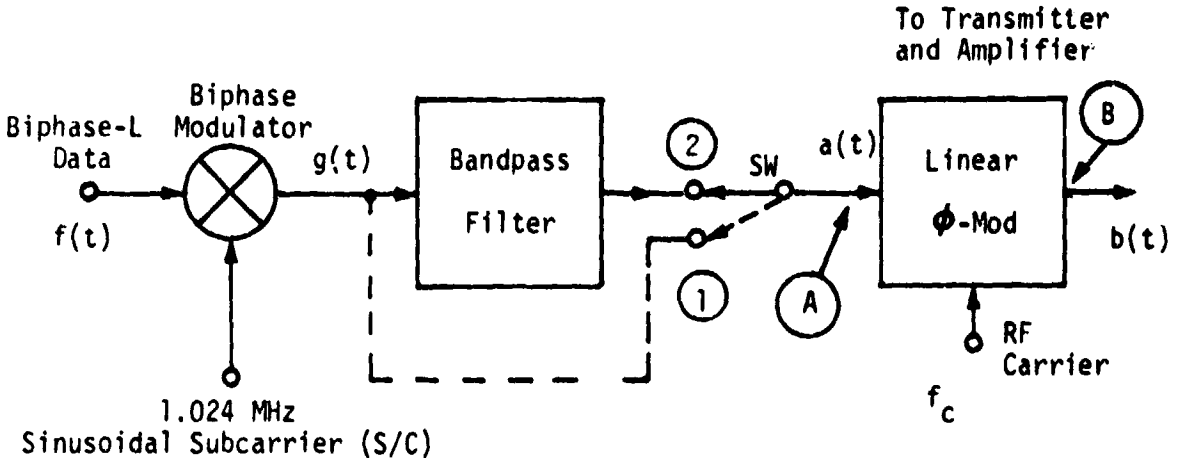

Part (a). Block Diagram for 1.024 MHz S/C Modulator

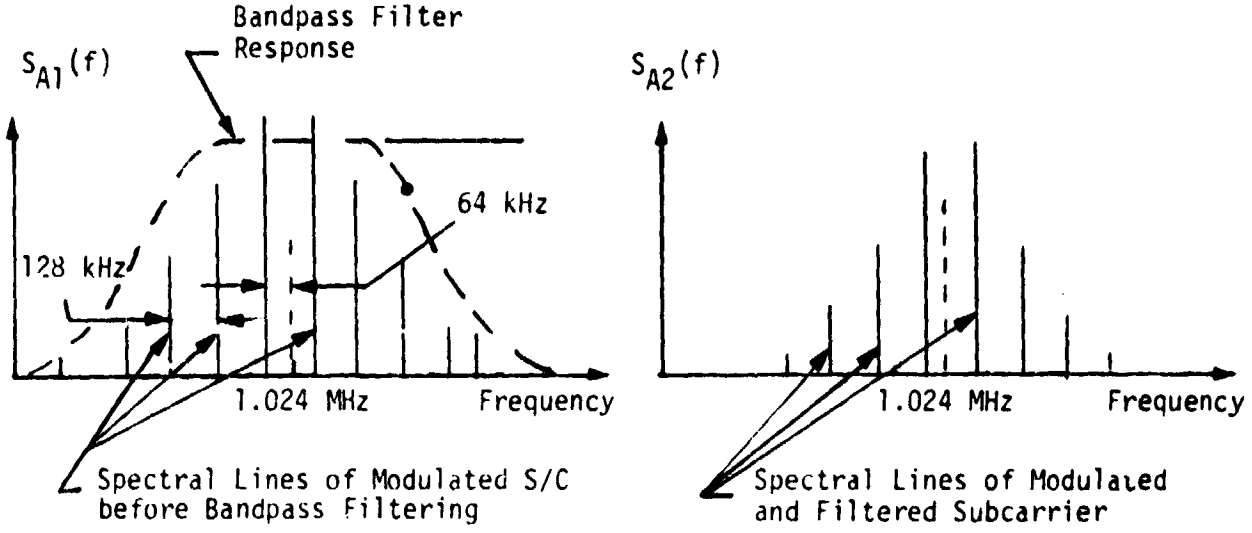

Part (b). Baseband Spectra of Modulated S/C Before and After Filtering
(Not to scale)

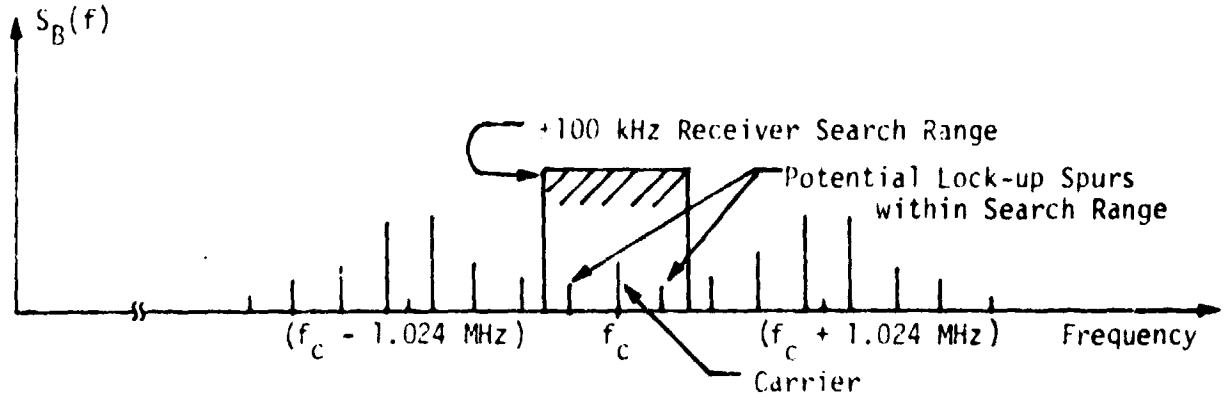

Part (c). Spectrum of Phase-Modulated RF Carrier

Figure 1. Effect of 1.024 MHz S/C Filter on Baseband and RF
Spectra of the Telemetry Signal

The filtered PSK subcarrier is then applied to the input of a linear phase modulator. The modulator converts the waveform information contained in the PSK-modulated subcarrier into a phase deviation of the RF carrier. The term "linear phase" modulator implies, in this case, that there is a linear relationship between the modulating voltage at the input to the modulator and the phase deviation of the modulated RF carrier. Phase modulation of an RF carrier, however, is not a linear process, and it leads to various cross product terms between the modulating frequency components. The action of the linear phase modulator is analyzed in Section 3.0.

Part (c) of Figure 1 qualitatively shows the spectral distribution of the phase-modulated RF carrier. As indicated in the figure, the main spectral lines are distributed around a frequency offset of ±1.024 MHz away from the carrier. Note that the carrier line is also present. It is the presence of this carrier line which provides for the acquisition of the transponder's signal by the frequency-swept STDN receiver at the ground. Unfortunately, as indicated in part (c) of the figure, two of the sidebands generated by the 64 kbps subcarrier modulation fall within the ±100 kHz frequency search range of the STDN receiver. These sidebands are located approximately ±64 kHz around the carrier for the "worst case." The primary purpose of the following analysis is to predict the level of these sidebands relative to the carrier as part of an overall system analysis of the potential for false lock.

2.0 ANALYSIS OF "WORST-CASE" DATA STREAM AND RESULTING BASEBAND SIGNAL

The telemetry data signal [f(t) in Figure 1] is formatted as biphase level pulses (Bi-ϕ-L) at a maximum bit rate of 64 kbps. Bi-ϕ-L pulses are characterized by a transition in the center of each bit interval: a positive-going transition if the bit is a "1" or a negative-going transition if the bit is a "0." An additional transition occurs at the start of the bit interval only if needed to allow the specified transition in the center of the interval. Bi-ϕ-L pulses are also known as "split phase" or "Manchester code" pulses.

Figure 2a shows a Bi-ϕ-L "1" followed by a Bi-ϕ-L "0." The remaining parts of this figure show several different data streams. Figure 2b illustrates a succession of alterate "1's" and "0's"; Figure 2c illustrates a random data sequence; and Figures 2d and 2e show, respectively, a succession of all "1's" and all "0's."

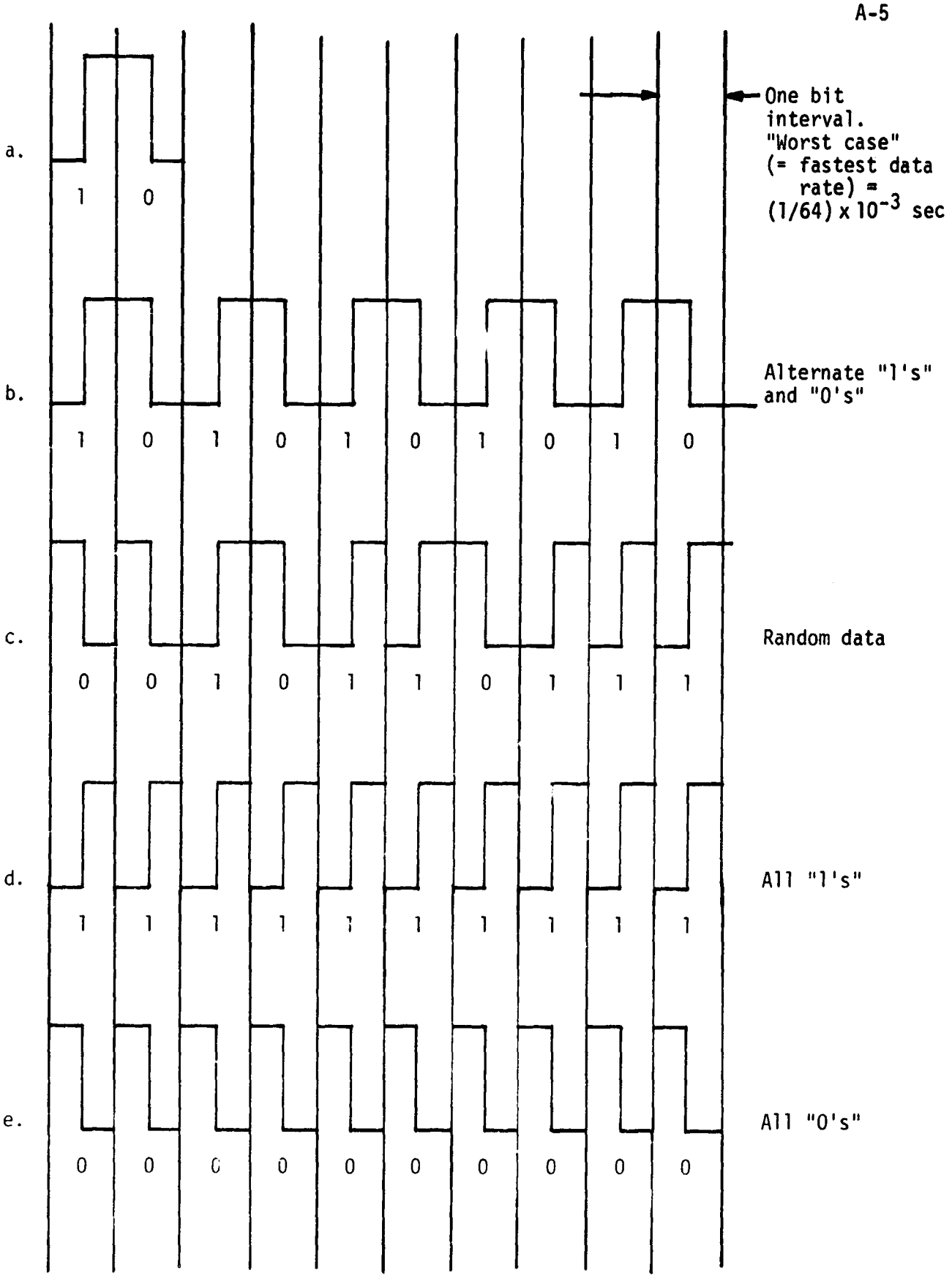

Figure 2. Biphase-Level Data Streams

It will be noted that three of these data streams represent square waves: the succession of alternate "1's" and "0's" of Figure 2b, with a period of 2-bit intervals, and the succession of all "1's" and all "0's", and Figures 2d and 2e, each of the latter with a period of one-bit interval. The high-frequency spectral content of these data streams is greatest for the latter two cases, with no spectral components <u>below</u> the fundamental square-wave frequency of 64 kHz, and all spectral energy at odd harmonics of this fundamental frequency.

We can now establish that the "worst case" corresponds to a bit rate of 64 kbps rather than 16 kbps. The frequency components which may give rise to false lock are located near the RF carrier; i.e., they are displaced from the subcarrier by about 1.024 MHz [see Figure 1, especially part (c)]. For the higher bit rate, the relevant harmonic components of the 64 kHz square-wave are the 15th and 17th, as shown in Table 1. For the 16 kbps bit rate, the relevant square-wave components would be the odd harmonics surrounding the 64th harmonic. Fourier analysis indicates that these harmonics have amplitudes approximately 12 dB below those produced by the 64 kHz wave. The harmonic components of the 64 kHz square-wave thus represent the "worst case."

The next step in our analysis is to evaluate these frequency components quantitatively. Since the magnitudes of the frequency components do not depend upon the phase of the 64 kHz square-wave, the analysis applies equally to the data streams of Figures 2d and 2e.

2.1 <u>Fourier Analysis of the Square-Wave "Worst-Case" Data Stream</u>

We express the 64 kHz "worst-case" square-wave at f(t) in the form of a Fourier series. A shift of the time exist will simplify the analysis without changing the harmonic magnitudes; we choose a time axis to yield even symmetry, as shown in Figure 3. Standard texts then give*

$$f(t) = A\left[\frac{2}{\pi}\cos\omega_b t - \frac{2}{3\pi}\cos\omega_b t + \cdots(-1)^{\frac{n-1}{2}}\cdot\frac{2}{n\pi}\cos n\,\omega_b t + \cdots\right] \qquad (1)$$

(odd n only)

*e.g., <u>Reference Data For Radio Engineers</u>, 5th Edition, page 42-12.

Table 1. Components of the Baseband Signal g(t) and the Signal a(t) After Filtering

Value of K	Amplitude of This Component of g(t) (Relative to Peak Amplitude) Numeric	dB	Frequency of this Component (MHz)	Frequency of This Component Relative to 1.024 MHz S/C	Filter Attenuation at this Frequency (A_k)	Amplitude of This Component of a(t) (Relative to Peak Input Amplitude)
+ 1	0.64	- 3.9	1.088	+0.064 MHz	0 dB	- 3.9 dB
- 1	0.64	- 3.9	0.960	-0.064	0	- 3.9
+ 3	0.21	-13.5	1.216	+0.192	3	-16.5
- 3	0.21	-13.5	0.832	-0.192	3	-16.5
- 5	0.13	-17.9	0.704	-0.320	17	-35
- 7	0.091	-20.8	0.576	-0.448	31	-52
- 9	0.071	-23.0	0.448	-0.576	45	-68
-11	0.058	-24.8	0.320	-0.704	59	-84
-13	0.049	-26.2	0.192	-0.832	60	-86
-15	0.042	-27.4	0.064	-1.088	60	-87
-17	0.037	-28.5	(-) 0.064	-1.216	60	-89

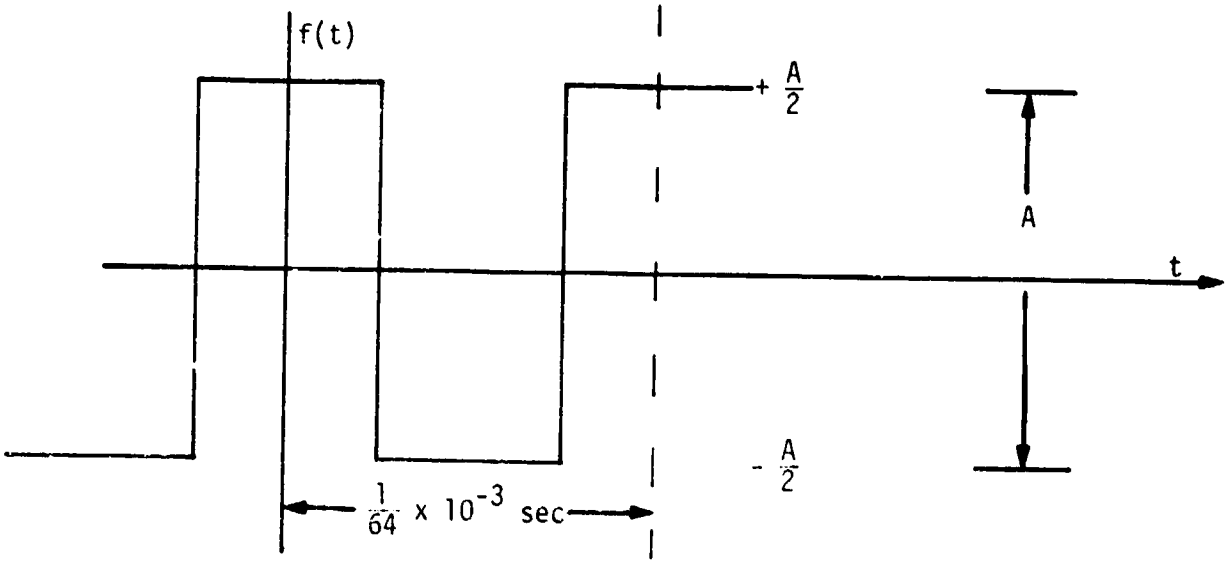

Figure 3. Square Wave for Analysis

where A $\triangleq$ peak-to-peak square-wave amplitude and $\omega_b \triangleq$ bit radian frequency = $2\pi \times 64 \times 10^3$ Hz.

2.2 Output of the Biphase Modulator

The "worst-case" data stream of section 2.1 is inputted to the biphase modulator, together with the 1.024 MHz subcarrier (see Figure 1). Assuming complete subcarrier suppression, the output of the biphase modulator is

$$g(t) = f(t) \cdot B_s \sin \omega_s t \tag{2}$$

where $B_s \triangleq$ subcarrier amplitude and $\omega_s \triangleq 2\pi \times 1.024$ MHz. Therefore,

$$g(t) = A \cdot B_s \sum_{\substack{k=1 \\ k = \text{odd integers}}}^{\infty} \frac{(-1)^{\frac{k-1}{2}} \cdot 2}{k\pi} \cos k\omega_b t \sin \omega_s t \tag{3}$$

A trig identity gives

$$g(t) = A \cdot B_s \cdot \sum_{\substack{k=1 \\ k = \text{odd integers}}}^{\infty} \frac{(-1)^{\frac{k-1}{2}}}{k\pi} \left[\sin (\omega_s - k\omega_b)t + \sin (\omega_s + k\omega_b)t\right] \tag{4}$$

The peak amplitude of the output of the biphase modulator is defined as G_0, where

$$G_0 \triangleq \left[\text{peak amplitude of } f(t)\right] \left[\text{peak subcarrier amplitude}\right] \tag{5}$$
$$= \left(\frac{A}{2}\right) \cdot (B_s) .$$

Therefore,

$$g(t) = 2G_0 \sum_{\substack{k=1 \\ k = \text{odd integers}}}^{\infty} \frac{(-1)^{\frac{k-1}{2}}}{k\pi} \left[\sin(\omega_s - k\omega_b)t + \sin(\omega_s + k\omega_b)t\right] \quad (6)$$

We note that all sidebands due to even harmonics are absent and that g(t) contains no term at the subcarrier radian frequency, ω_s, consistent with the assumption of complete subcarrier suppression. The left-hand side of Table 1 gives the amplitudes (relative to the peak amplitude G_0) of some of the components of this signal. This table also gives the frequency of these components for the "worst-case" of a 64 kHz square-wave modulating a 1.024 MHz subcarrier.

Components are listed through the 17th harmonic. It will be shown in Section 3.0 that the 15th and 17th harmonic components in this baseband signal give rise to spurs within the 100 kHz receiver search range of the RF carrier; harmonics higher than the 17th do not produce spurs within this range. The 17th harmonic is shown in Table 1 as a "negative" frequency for the baseband signal; this is a temporary mathematical artifact that is removed in the expressions which result when the baseband signal modulates the RF carrier.*

2.3 Action of the Bandpass Filter

If there were no bandpass filters in the system. the input a(t) to the linear phase modulator would be identical to the output g(t) of the biphase modulator (see Figure 1). With the filter in the system, we find a(t) from g(t) as follows.

Figure 4 shows the specified nominal frequency response of the filter (specification, section 10.4, sheet 63.1). Each frequency component of g(t) passes through the filter and undergoes attenuation, as shown toward the right-hand side of Table 1. The amplitude of each component at the output of the filter relative to the peak input amplitude is the algebraic sum (in dB) of its relative amplitude at the input and its attenuation through the filter. Thus, the components of a(t) are shown in the extreme right-hand column of Table 1. (The 1 dB filter passband ripple has been neglected since it is unimportant for the spur analysis.)

---

*S. Goldman, Frequency Analysis, Modulation and Noise, McGraw-Hill, 1978, pp 70-72.

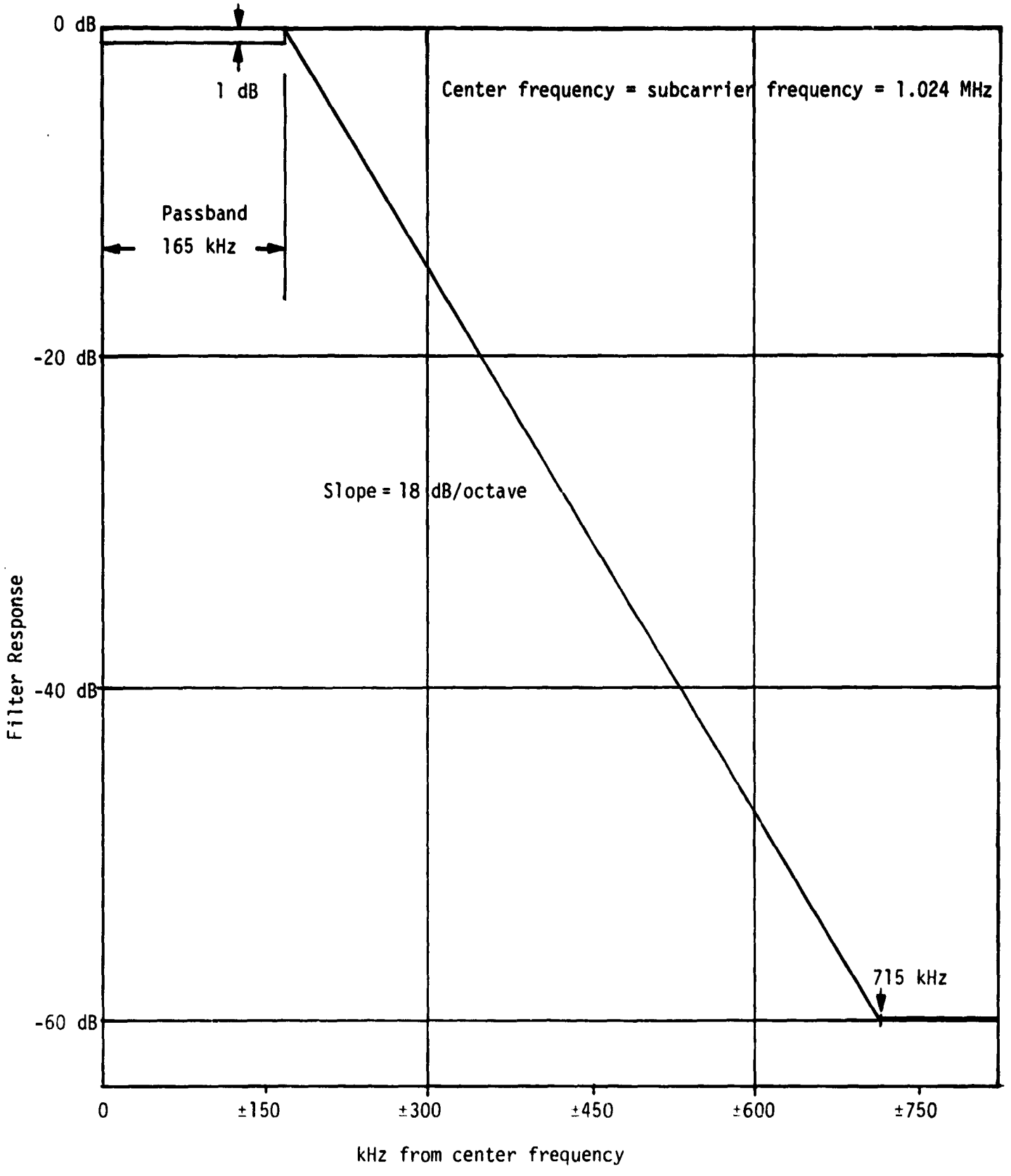

Figure 4. Bandpass Filter Characteristics

From Table 1, it may be seen that the bandpass filter has only a small effect on the relatively large frequency components (with $k = \pm 1, \pm 3$) near the subcarrier. The peak value of the time function a(t) is primarily determined by these components and, therefore, little error is introduced by assuming that the peak value of a(t) = peak value of g(t) $\triangleq G_0$ (this error is on the order of 1 dB).

3.0 ANALYSIS OF THE LINEAR PHASE MODULATOR

As shown in Figure 1, the filtered signal a(t) is applied to the linear phase modulator. The modulation sensitivity of this device will be denoted by γ; for example, γ might have a value of 1.0 radians/volt. The RF carrier b(t) is thus given by

$$b(t) = e^{j\left[\omega_c t + \psi(t)\right]} = e^{j\omega_c t}\, e^{\psi(t)} \tag{7}$$

where $\omega_c \triangleq$ RF carrier radian frequency and $\psi(t) = \gamma\, a(t)$ = phase modulation. Spurs near the RF carrier will be most severe at high modulation indices. For the STDN/TDRS transponder, the maximum value of $\psi(t)$ for the 1.024 MHz subcarrier is expected to be 1.0 radians.* Therefore,

$$[\psi(t)]_{max} = \gamma[a(t)]_{peak} = \gamma G_0 = 1.0 \text{ radians} \tag{8}$$

so that

$$\psi(t) = \frac{2}{\pi} \sum_{\substack{k=1 \\ k = \text{odd integers}}}^{\infty} \frac{(-1)^{\frac{k-1}{2}}}{k} A_k \left[\sin\,(\omega_s - k\omega_b)t + \sin\,(\omega_s + k\omega_b)t\right] \tag{9}$$

where A_k is the relative amplitude of the kth components, given (in dB) in Table 1, for k from 1 to 17.

Because phase modulation is a nonlinear process, the RF carrier contains, in principle, frequency components at all possible sum and difference

*This is generalized in Section 4.0.

frequencies. It is useful to recall that the introductory treatment of phase modulation (or frequency modulation) considers that the RF carrier is phase modulated by one sinusoidal tone or, at most, by two or three sinusoids. In the present case, as shown by (9), the RF carrier is phase modulated by a (double) countable infinity of sinusoids. The Axiomatix analysis of this modulated carrier is based on an extension of the analysis appearing in Panter's text.* Readers of this memo may wish to review the introductory treatment included as Addendum A (adapted from "Users' Handbook for Payload-Shuttle Data Communication," Axiomatix Report No. R7809-4, September 27, 1978) before proceeding with our extension of Panter's analysis.

3.1 Amplitudes of Components of the RF Spectrum

For the present case with $\psi(t)$ given by (9), the total RF phase angle (corresponding to Panter's equation 7-66) is

$$\theta(t) = \omega_c t + \psi(t) \tag{10}$$

We shall show that the RF carrier contains frequency components at

$$\omega_c \pm n_1^- (\omega_s - \omega_b) \pm n_1^+ (\omega_s + \omega_b) \pm n_3^- (\omega_s - 3\omega_b) \pm n_3^+ (\omega_s + 3\omega_b) \cdots$$

$$\pm n_k^- (\omega_s - k\omega_b) \pm n_k^+ (\omega_s + k\omega_b) \pm \cdots \tag{11}$$

where (in principle) there are a (double) countable infinity of n_k's, and the n_k's range <u>simultaneously</u> over all positive integers including zero. It is to be noted that the "carrier component" of the modulated RF wave corresponds to the frequency component when <u>all</u> n_k's are zero. If more than one or two of the n_k's are nonzero, the analysis will indicate that the corresponding frequency components are (fortunately) negligible.

The amplitude of the carrier component may be computed from Panter's analysis. However, it is known that the carrier component corresponding to a biphase modulated baseband signal (without filtering) is the same as that which results from single-tone baseband modulation with the same value of β.**

---

*Panter, P.F., <u>Modulation, Noise and Spectral Analysis</u>, McGraw-Hill 1965, p. 254.

**Axiomatix Internal Memorandum, July 30, 1979.

For single-tone modulation with $\beta = 1.0$ radians, we note from Addendum A, Figure A.4, that the carrier component given by $J_0(1.0)$ has an amplitude of 0.77 (-1.8 dB) of the unmodulated RF level. Since the filter has a small effect on the major components of the baseband signal (see section 2.3), we assume the same carrier component.

We now consider the general case. If an RF carrier is modulated by N sinusoids such that the total RF phase angle is

$$\theta(t) = \omega_c t + \beta_1 \sin \omega_1 t + \beta_2 \sin \omega_2 t + \cdots \beta_N \sin \omega_N t \quad , \tag{12}$$

Panter shows that the modulated carrier may be expressed by

$$b(t) = \left[\sum_{n_1=-\infty}^{\infty} J_{n_1}(\beta_1)\, e^{jn\omega_1 t}\right]\left[\sum_{n_2=-\infty}^{\infty} J_{n_2}(\beta_2)\, e^{jn_2\omega_2 t}\right]\cdots$$
$$\times\left[\sum_{n_N=-\infty}^{\infty} J_{n_N}(\beta_N)\, e^{jn_N\omega_N t}\right] e^{j\omega_c t} \tag{13}$$

or

$$b(t) = \left[\prod_{m=1}^{N} \sum_{n_m=-\infty}^{\infty} J_{n_m}(\beta_m)\, e^{jn_m\omega_m t}\right] e^{j\omega_c t} \tag{14}$$

for unit amplitude of the unmodulated carrier.

With $\psi(t)$ given by (9), we must extend Panter's results to the case when the carrier is modulated by a double countable infinity of sinusoids:

$$b(t) = \left[\prod_{\substack{k=1 \\ k=\text{odd integers}}}^{\infty} \sum_{n_k^-=-\infty}^{\infty} J_{n_k^-}(\beta_k)\, e^{jn_k^-(\omega_s - k\omega_b)t}\right]$$
$$\times\left[\prod_{\substack{k=1 \\ k=\text{odd integers}}}^{\infty} \sum_{n_k^+=-\infty}^{\infty} J_{n_k^+}(\beta_k)\, e^{jn_k^+(\omega_s + k\omega_b)t}\right] e^{j\omega_c t} \tag{15}$$

where $\beta_k \triangleq \frac{2\,(-1)^{\frac{k-1}{2}}}{\pi k} A_k$; values of $|\beta_k|$ are tabulated in dB in the right-hand column of Table 1.

The frequency components are given by (11). The carrier amplitude may be found by computing the value of b(t) that results when all the indices n_k are simultaneously zero:

$$[b(t)]_{\text{carrier}} = \left[\prod_{\substack{k=1 \\ k = \text{odd integers}}}^{\infty} J_0(\beta_k) \right]^2 \qquad (16)$$

and we have already shown that this is equal to $J_0(1.0)$ for the present case.

To get a "feel" for (15), consider another relatively simple case: let $n_k^+ = +1$ when $k = 1$, all other n_k's = 0. The resulting frequency component is found from (11),

$$\omega_c + (1)\,(\omega_s + 1 \cdot \omega_b)$$

and so is 1.088 MHz above the RF carrier (see Table 1). The amplitude of this component is found from (15):

$$\underbrace{\left[\prod_{\substack{k=1 \\ k = \text{odd integers}}}^{\infty} J_0(\beta_k) \right]}_{\text{product of } n_k^-\text{'s}} \underbrace{\left[\prod_{\substack{k=3 \\ k = \text{odd integers}}}^{\infty} J_0(\beta_k) \right] J_1(\beta_1)}_{\text{product of } n_k^+\text{'s}}$$

which may be expressed as

$$\left[\prod_{\substack{k=1 \\ k = \text{odd integers}}}^{\infty} J_0(\beta_k) \right]^2 \times \frac{J_1(\beta_1)}{J_0(\beta_1)} = (\text{carrier amplitude}) \times \frac{J_1(\beta_1)}{J_0(\beta_1)} \qquad (17)$$

The right-hand column of Table 1 gives β_1 as -3.9 dB ≈ 0.64; then, using Addendum A, Figure A.4,

$$J_1(\beta_1) \approx 0.25 \quad , \qquad J_0(\beta_1) \approx 0.9$$

and so this component, located near the subcarrier and 1.088 MHz above the RF carrier, has a relative amplitude of

$$\frac{0.25}{0.9} \approx -11 \text{ dBC} \tag{18}$$

(11 dB below the RF carrier level). This completes this example.

Our interest is primarily in frequency components that lie near the RF carrier, and so may produce false lock. Reference to Table 1 indicates that the expression $\omega_s - k\omega_b$ has the value 0.064 MHz (64 kHz) when k = -15. Therefore, consider (15) when n_k = +1 for k = -15, all other n_k's = 0. The resulting frequency component is found from (11),

$$\omega_c + (1)\ (\omega_s - 15\ \omega_b)$$

and so is 64 kHz above the carrier, as expected. The amplitude of the component is found from (15):

$$\left[\prod_{\substack{k=1 \\ k = \text{odd integers} \\ k \neq 15}}^{\infty} J_0(\beta_k)\right] \times J_1(\beta_{15}) \times \left[\prod_{\substack{k=1 \\ k = \text{odd integers}}}^{\infty} J_0(\beta_k)\right] \tag{19}$$

Proceeding as in the previous example, this may be expressed as

$$(\text{carrier amplitude}) \times \frac{J_1(\beta_{15})}{J_0(\beta_{15})}$$

Since β_{15} is very small (-87 dB ≈ 4.5×10^{-5}),

$$J_0(\beta_{15}) \approx 1$$

and so the magnitude of this frequency component, relative to the level of the modulated carrier, is simply

$$\left|J_1(\beta_{15})\right| = \left|J_1\left(\frac{2A_k}{k\pi}\right)\right|_{k=-15} \tag{20}$$

We now inspect the modulated spectrum carefully and generalize our results to include other components that may cause false lock. First note from (11) that a given value of k produces four frequency components located symmetrically with respect to both the RF carrier and the subcarrier (see Figure 1c); the spectrum pair close to the RF carrier is spaced from it by ±[1.024 - k(0.064)] MHz. For k = 15, these frequency components lie 64 kHz above (+ sign) and below (- sign) the carrier; we have just investigated the first case in detail. For k = 17, the frequency components coincide with those for k = 15, but the + sign corresponds to a components below the carrier and the - sign to a component above the carrier (see Table 1).

The lack of coherence between the subcarrier and the data must now be considered. As a result, the factor of 16 between the subcarrier frequency (1.024 MHz) and the data frequency (64 kHz) is only nominal. In the absence of such coherence, we expect a slow phase shift between the frequency components corresponding to k = 15 and those corresponding to k = 17, with a "beating" effect. When these two components are additive ("worst case"), they generate a pair of sidebands spaced 64 kHz from the RF carrier, with amplitude

$$\left|J_1\left(\frac{2A_{15}}{15\pi}\right)\right| + \left|J_1\left(\frac{2A_{17}}{17\pi}\right)\right| \tag{21}$$

relative to the (modulated) carrier level.

These components, produced by k = 15 and k = 17, result from a "first-order" interaction in the modulation process since they involve only one of the n_k's being nonzero; they are the only such "first-order" products spaced ±64 kHz from the RF carrier. Although there are, in principle, an infinite number of other (higher order) interactions that produce frequency components ±64 kHz from the RF carrier, these have amplitudes given by the products of Bessel functions of high orders and small arguments, and a straightforward application of (15) shows these amplitudes to be negligibly small.

For small values of x, it is known that*

$$J_1(x) \approx \frac{x}{2} \tag{22}$$

This permits convenient evaluation of (21). For the present case, with $\beta = 1.0$,

$$J_1\left(\frac{2\,A_{15}}{15\pi}\right) \text{ is } \quad -93.4 \text{ dBc} \tag{23}$$

and

$$J_1\left(\frac{2\,A_{17}}{17\pi}\right) \text{ is } \quad -94.5 \text{ dBc} \tag{24}$$

(below the modulated carrier level). Converting these to numeric values, adding them and reconverting to dB gives a final spur value of

$$-88.0 \text{ dBc}. \tag{25}$$

4.0 ACTION OF THE FILTER

The process we have analyzed involves biphase modulation of a subcarrier by data, with the resulting baseband signal filtered and applied to linearly phase-modulate an RF carrier. Despite the complexity of the general case [i.e., (15)], significant results have been obtained by considering the lowest order modulation products.

The form of the results makes it easy to verify the helpful action of the filter. In the absence of the filter

$$A_k = 1 \qquad (= 0 \text{ dB})$$

for all k. Therefore, without the filter,

$$J_1\left(\frac{2}{15\pi}\right) \text{ is } \quad -33.4 \text{ dBc}, \tag{26}$$

$$J_1\left(\frac{2}{17\pi}\right) \text{ is } \quad -34.5 \text{ dBc} \tag{27}$$

---

*M. Abramowitz and I. Stegun, Handbook of Mathematical Functions, NBS, 1964, page 360; also see Addendum B.

and the spurs are at a level of

$$-28.0 \text{ dBc.} \qquad (28)$$

Comparing with (23) through (25), the 60 dB selectivity of the filter effectively reduces the spurs by 60 dB. It is consequently important that this specification be satisfied. Axiomatix advises that the attentuation at 64 kHz (and 192 kHz) of this filter be examined during the prototype performance test.

The foregoing analysis is easily generalized. In Figure 5, we have plotted the spur level as a function of peak phase modulation index from 0.5 to 2.0 radians, although this appendix gives detailed treatment only in the case of $\beta = 1.0$ radians.

As a further generalization, consider a possible revision in the search range, say, from the present ±100 kHz to ±200 kHz. Table 1 indicates that this expanded frequency range would then include frequency components with $k = 13$ and $k = 19$ (the latter is not shown explicitly in the table). The amplitude of the "19th" component of $g(t)$ is -29.5 dB relative to the peak amplitude of $g(t)$, and the amplitude of the same component $a(t)$ is ≈ -90 dB. Applying the Bessel function approximation, the resulting spurs [analogous to (23) and (24)] would be at -92 dBc for $k = 13$ and -96 dBc for $k = 19$. Under "worst-case" conditions of additive phase, the spur at ±192 kHz from the carrier would have an amplitude [analogous to (25)] of -87.8 dBc. This spur is very slightly larger than the spur at 64 kHz from the carrier, so increasing the search range does not significantly affect the possibility of false lock (other factors being equal).

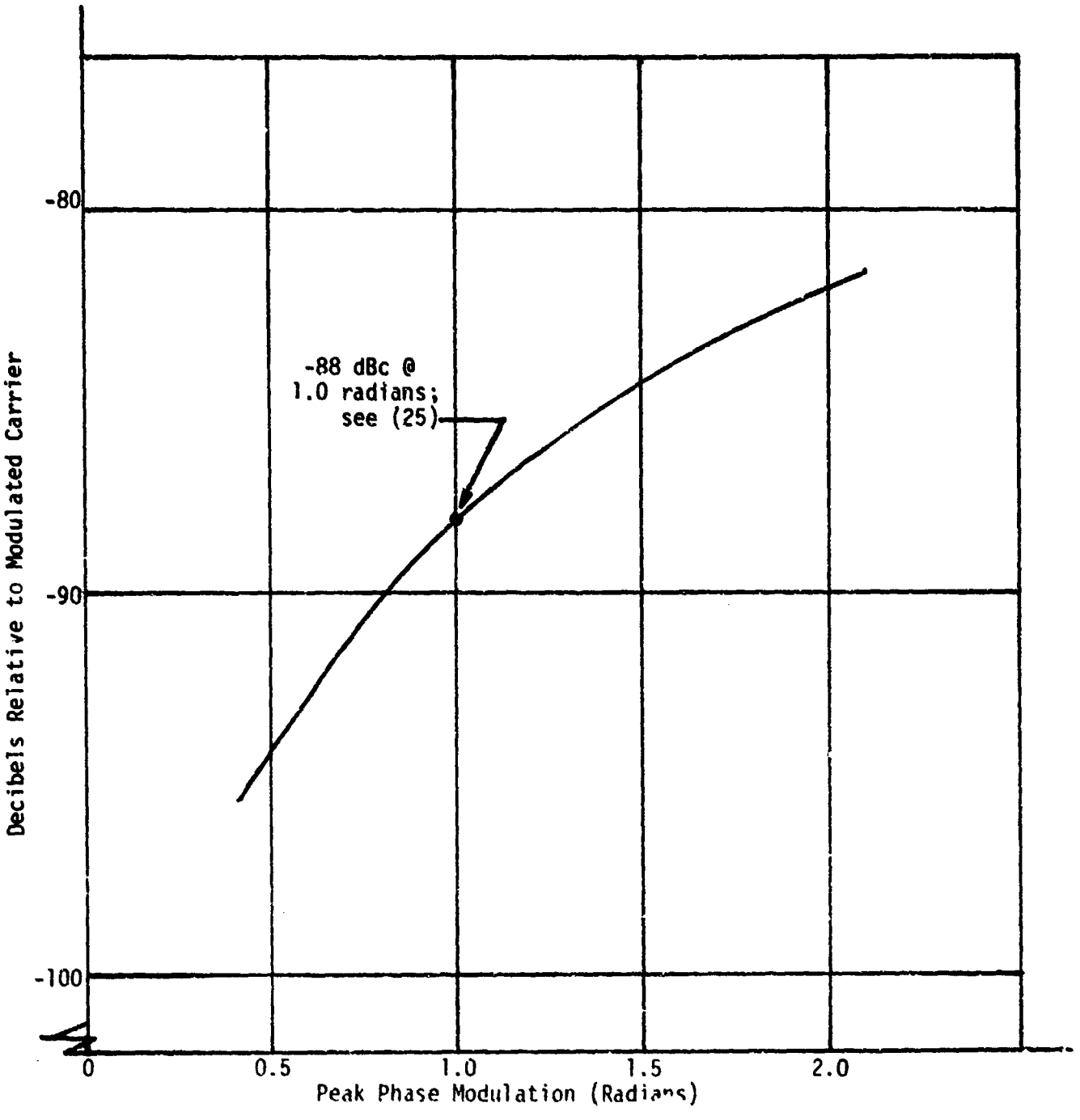

Figure 5. Spur Level Relative to Modulated RF Carrier Level as a Function of Peak Phase Modulation (Bandpass Filter of Figure 1a in the system)

ADDENDUM A
AN INTRODUCTION TO PHASE MODULATION (PM) AND FREQUENCY MODULATION (FM)

The basic signal form of PM and FM is given by

$$s(t) = \sqrt{2P}\cos(\omega_o t + \theta(t)) \tag{A-1}$$

where for an input signal $x(t)$, the instantaneous phase angle for the PM signal is

$$\theta(t) = m_p x(t) \tag{A-2}$$

with m_p defined as the phase-modulation index. For the FM signal,

$$\theta(t) = m_f \int_0^t x(t)dt \tag{A-3}$$

where m_f is defined as the modulation index for FM. Note that in PM, the instantaneous phase of the modulated signal depends linearly upon the modulating signal $x(t)$* while in FM, the instantaneous frequency varies linearly with $x(t)$, namely,

$$\omega_i(t) = \omega_o + m_f x(t) \tag{A-4}$$

which is equivalent to the statement that the phase depends linearly upon the integral of $x(t)$. As an example, when the modulating signal is a single-tone sinusoid so that $x(t) = \cos \omega_m t$, the PM signal is

$$s_p(t) = \sqrt{2P}\cos(\omega_o t + m_p \cos\omega_m t) \tag{A-5}$$

and the FM signal is

$$s_f(t) = \sqrt{2P}\cos\left(\omega_o t + \frac{m_f}{\omega_m}\sin\omega_m t\right) \tag{A-6}$$

This is illustrated in Figure A.1, where the modulating signal is a sinusoid; amplitude modulation of the carrier is also included for comparison. It should be noted here that a distinction can be made between the phase- and frequency-modulated carrier only when compared with the modulating signal, as illustrated in Figure A.1.

---

*This is the case for the RF carrier in the STDN/TDRS transponder; see page A-3.

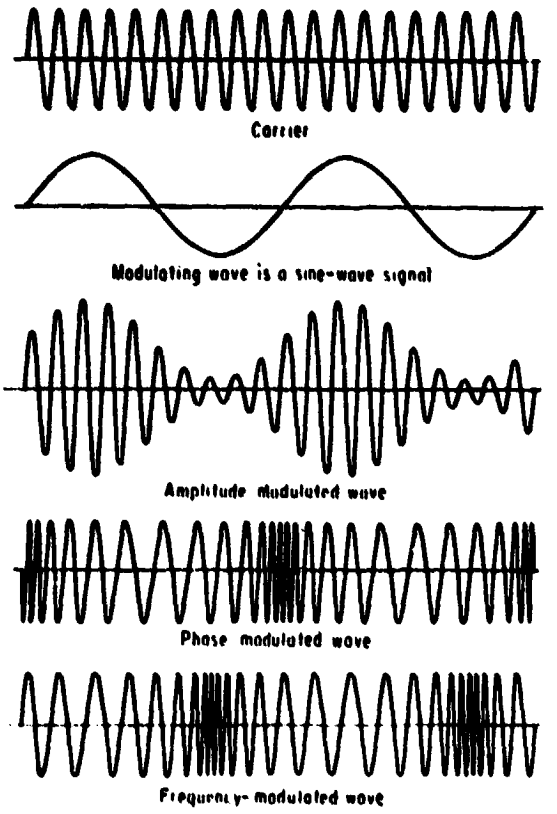

Figure A.1. Amplitude, Phase and Frequency Modulation of a Sine-Wave Carrier by a Sine-Wave Signal

Also note that, for phase modulation, the peak phase deviation or modulation index m_p is a constant, independent of the frequency of the modulating signal, and for frequency modulation, the peak phase deviation is given by m_f/ω_m, which is inversely proportional to the frequency of the modulating signal.

The spectral analysis of PM and FM can best be performed by considering specific examples of $\theta(t)$. As the first example, let $\theta(t) = \beta \sin \omega_m t$. Therefore,

$$s(t) = \sqrt{2P} \cos (\omega_0 t + \beta \sin \omega_m t) \tag{A-7}$$

where β is the peak phase deviation of the modulated signal of angular frequency ω_m. Hence, the instantaneous frequency $\omega_i(t)$ is equal to

$$\omega_i(t) = \omega_0 + \omega_m \beta \cos \omega_m t = \omega_0 + \Delta\Omega \cos \omega_m t \tag{A-8}$$

where $\omega\Omega = \beta \omega_m$ is the maximum frequency deviation of the modulated frequency ω_0. If $\beta << 1$, then $s(t)$ is a narrowband PM signal and

$$\begin{aligned} s(t) &= \sqrt{2P} \left[\cos \omega_0 t \cos (\beta \sin \omega_m t) - \sin \omega_0 t \sin (\beta \sin \omega_m t)\right] \\ &= \sqrt{2P} \left[\cos \omega_0 t - \beta \sin \omega_m t \sin \omega_0 t\right] \quad \beta << 1 \\ &= \sqrt{2P} \left[\cos \omega_0 t - \frac{\beta}{2} \cos (\omega_0 - \omega_m) t + \frac{\beta}{2} \cos (\omega_0 + \omega_m) t\right] \end{aligned} \tag{A-9}$$

From (A-9), note that the spectrum of narrowband PM consists of a carrier and two sidebands which are 180^0 out of phase.

If β is not small, then $s(t)$ is a wideband PM signal and

$$\begin{aligned} s(t) &= \sqrt{2P} \left[\cos \omega_0 t \cos (\beta \sin \omega_m t) - \sin \omega_0 t \sin (\beta \sin \omega_m t)\right] \\ &= \sqrt{2P} \left[\cos \omega_0 t \sum_{n=-\infty}^{\infty} J_n(\beta) \cos(n\omega_m t) - \sin \omega_0 t \sum_{n=-\infty}^{\infty} J_n(\beta) \sin(n\omega_m t)\right] \\ &= \sqrt{2P} \left\{J_0(\beta) \cos \omega_0 t - J_1(\beta) \left[\cos (\omega_0 - \omega_m) t - \cos (\omega_0 + \omega_m) t\right]\right. \\ &\quad + J_2(\beta) \left[\cos (\omega_0 - 2\omega_m) t + \cos (\omega_0 + 2\omega_m) t\right] \\ &\quad \left. - J_3(\beta) \left[\cos (\omega_0 - 3\omega_m) t - \cos (\omega_0 + 3\omega_m) t\right] + \cdots\right. \end{aligned} \tag{A-10}$$

Thus the wideband PM signal consists of a carrier and an infinite number of sidebands, whose amplitudes are proportional to $J_n(\beta)$* spaced at frequencies $\pm \omega_m$, $\pm 2\omega_m$, etc., away from the carrier, as shown in Figure A.2.

In practice, the spectrum of PM and FM signals are not infinite because, beyond a certain frequency range from the carrier depending on the magnitude of β, the sideband amplitudes which are proportional to $J_n(\beta)$ become negligibly small. Thus, the bandwidth of the transmitter and receiver can be restricted to encompass only the significant bands without introducing an excessive amount of harmonic distortion.

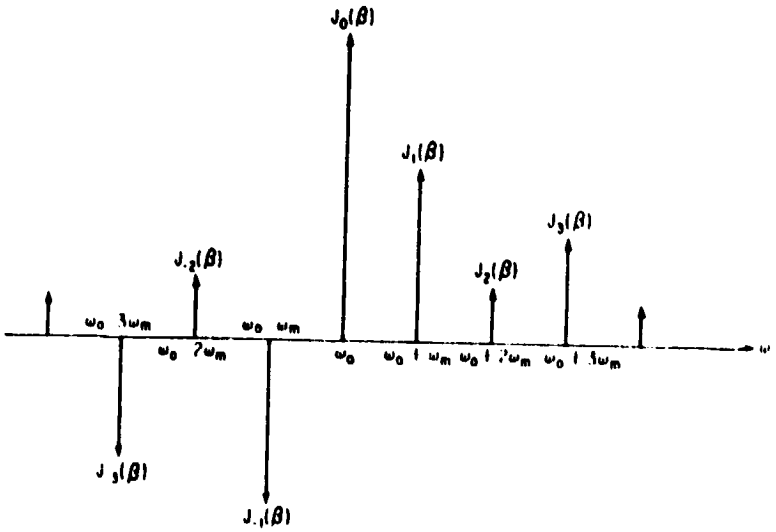

Figure A.2. Composition of FM Wave into Sidebands (Single-Tone Modulation)

*$J_n(\beta)$ is the Bessel function of the first kind of order n; also see Figure A.4.

To compare FM to the spectral analysis of PM, note that assuming a sinusoidal modulating signal cos $\omega_m t$ with maximum frequency deviation $\Delta\Omega$, the instantaneous frequency is given by

$$\omega_i(t) = \omega_o + \Delta\Omega \cos \omega_m t \qquad \Delta\Omega << \omega_o \tag{A-11}$$

where the frequency deviation $\Delta\Omega$ is independent of the modulating frequency and is proportional to the amplitude of the modulating signal.

The instantaneous phase angle $\theta(t)$ for this special case is given by

$$\omega_i(t) = \int_o^t \omega_i(t)\, dt = \omega_o t + \frac{\Delta\Omega}{\Omega_m} \sin \omega_m t + \theta_o \tag{A-12}$$

where θ_o may be taken as zero by referring to an appropriate phase reference so that the FM signal is given by

$$s(t) = \sqrt{2P} \cos(\omega_o t + \beta \sin \omega_m t) \tag{A-13}$$

where β is inversely proportional to the modulating angular frequency ω_m; namely, $\beta = \Delta\Omega/\omega_m$, which is of the same form as (A-7) for PM. It should be emphasized, however, that, while (A-13) and (A-7) are of the same form, nevertheless, the respective modulation indices β assume different significance. In PM the maximum phase deviation β is constant, independent of the modulating angular frequency ω_m, but in FM the maximum frequency deviation $\Delta\Omega$ is constant, independent of ω_m.

Since the expressions representing phase - and frequency-modulated signals are identical as given by (A-13) and (A-7), it follows therefore that, for a single modulating frequency, the spectral representations are identical. However, it is of interest to examine the spectral behavior as ω_m is varied, $\Delta\Omega$ being held constant. As shown in Figure A.3, as $\beta \to \infty$, the number of sidebands increases and the spectral components become more and more confined to the band between $\omega_o \pm \Delta\Omega$.

The bandwidth is equal to $2\Delta f_0 (\Delta\Omega = 2\pi\Delta f_0)$ only for a very large modulation index. For smaller values of β, we determine the bandwidth by counting the significant number of sidebands. The word "significant" is usually taken to mean those sidebands which have a magnitude at least 1 percent of the magnitude of the unmodulated carrier.

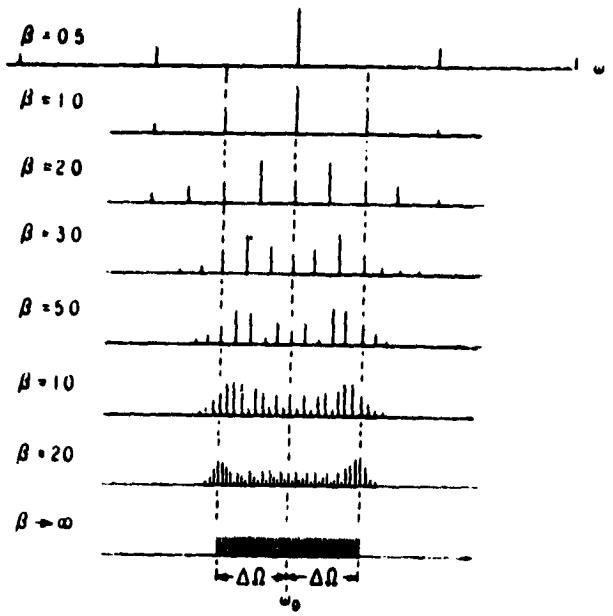

Figure A.3. FM Spectrum of Single-Tone Modulation Bandwidth versus Modulation Index β

It has been shown that for $\beta << 1$, the spectrum of an FM signal is essentially a carrier and one pair of significant sidebands. As β increases, the number of significant sidebands increases while the total average power of the sidebands plus the carrier remains constant, equal to P. Since the amplitudes of the carrier and sidebands are proportional to the Bessel function $J_n(\beta)$ where $n = 0, \pm 1, \pm 2, \ldots$, the variation of the amplitudes as a function of the

modulation index β can be obtained from the plot of the Bessel functions of the first kind, as shown in Figure A.4. The behavior of the carrier amplitude is determined from the zero-order Bessel function $J_0(\beta)$. As β is increased, the value of the Bessel function drops off rapidly until, at β = 2.404, the amplitude is zero. As seen from the plot, the zero-order Bessel function is oscillatory with decreasing peak amplitude, the spacing between zeros approaching asymptotically the constant value π. This follows from the approximation

$$J_0(\beta) = \frac{\cos(\beta - \pi/4)}{\sqrt{\pi\beta/2}} \qquad \text{(A-14)}$$

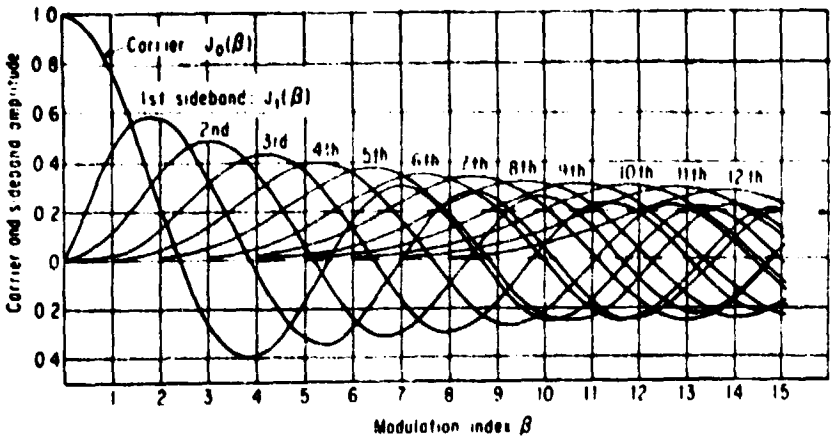

Figure A.4. Plot of Bessel Functions of First Kind as a Function of Argument β

The treatment to this point has involved only single-tone modulation. Now consider two sinusoidal tones to wideband PM a carrier. That is,

$$s(t) = \sqrt{2P}\cos[\omega_0 t + \beta_1 \sin \omega_1 t + \beta_2 \sin \omega_2 t]\,. \qquad \text{(A-15)}$$

Expanding the cosine term,

$$s(t) = \sqrt{2P}\cos\omega_0 t\,[\cos(\beta_1 \sin\omega_1 t)\cos(\beta_2 \sin\omega_2 t) - \sin(\beta_1 \sin\omega_1 t)\sin(\beta_2 \sin\omega_2 t)] - \sin\omega_0 t\,[\sin(\beta_1 \sin\omega_1 t)\cos(\beta_2 \sin\omega_2 t) + \sin(\beta_2 \sin\omega_2 t)\cos(\beta_1 \sin\omega_1 t)] \qquad \text{(A-16)}$$

and using Bessel function series expansion for the terms within the brackets,

$$s(t) = \sqrt{2P}\left\{\cos\omega_0 t\left\{\left[J_0(\beta_1) + 2\sum_{\substack{n=2\\ \text{even}}}^{\infty} J_n(\beta_1)\cos n\omega_1 t\right]\cdot\left[J_0(\beta_2) + 2\sum_{\substack{n=2\\ \text{even}}}^{\infty} J_n(\beta_2)\cos n\omega_2 t\right] - \left[2\sum_{\substack{n=1\\ \text{odd}}}^{\infty} J_n(\beta_1)\sin n\omega_1 t\right]\left[2\sum_{\substack{n=1\\ \text{odd}}}^{\infty} J_n(\beta_2)\sin n\omega_2 t\right]\right\} - \sin\omega_0 t\left\{\left[2\sum_{\substack{n=1\\ \text{odd}}}^{\infty} J_n(\beta_1)\sin n\omega_1 t\right]\left[J_0(\beta_2) + 2\sum_{\substack{n=2\\ \text{even}}}^{\infty} J_n(\beta_2)\cos n\omega_2 t\right] + \left[2\sum_{\substack{n=1\\ \text{odd}}}^{\infty} J_n(\beta_2)\sin n\omega_2 t\right]\cdot\left[J_0(\beta_1) + 2\sum_{\substack{n=2\\ \text{even}}}^{\infty} J_n(\beta_1)\cos n\omega_1 t\right]\right\}\right\}. \qquad \text{(A-17)}$$

Note that, when β_2 is zero (i.e., a single tone to PM the carrier), (A-17) reduces to the same form as (A-10). For two tones, frequency components are produced at

$$\omega_0 \pm n_1 \omega_1 \pm n_2 \omega_2 \qquad \text{(A-18)}$$

with amplitudes given by the products of appropriate Bessel functions. The general case, with N sinusoidal modulating tones, is considered in the body of this appendix (see section 3.1).

ADDENDUM B

ASYMPTOTIC FORMULAE FOR BESSEL FUNCTIONS OF SMALL ARGUMENTS

Asymptotic formulae for Bessel functions of small arguments are given in N. Abramowitz and I. Stegun, Handbook of Mathematical Functions, NBS, 1964. From page 360, no. 9.1.7,

$$J_\nu(z) \approx \left(\frac{1}{2} z\right)^\nu \Big/ \Gamma(\nu+1)$$

For $\nu = 1$,

$$J_1(z) \approx \frac{\frac{1}{2} z}{\Gamma(2)}$$

$\Gamma(2)$ is the Gamma function of argument 2. From the same handbook page 255, no. 6.1.5 and Figure 6.1,

$$\Gamma(2) = 1! = 1.0$$

so that

$$J_1(z) \approx \frac{z}{2} .$$

See (22) in the body of this report.

1.0 INTRODUCTION

Axiomatix has reviewed the TRW analysis of the spurious responses of the STDN and SGLS transponder receivers (STDN/TDRS Transponder PDR Package, "Subanalysis No. 13," pp 5-75 to 5-80).

A spurious response analysis of these receivers is valuable since they are of the double-conversion type and it is well-known that such receivers often have undesirable spurious responses. Moreover, the STDN and SGLS receivers are designed such that the second intermediate-frequency amplifier is part of a narrowband tracking loop which may give rise to additional spurious responses. It is therefore useful to understand the possible spurs of these receivers and to review the TRW analysis.

Block diagrams of the STDN/TDRS and SGLS receivers are shown in Figures 1 and 2, respectively. Although three mixers are shown for each receiver (M1, M2 and M3), only M1 and M2 are mixers in the conventional sense of operating in the signal path. Mixer M3, the starting point for the TRW spurious analysis, is part of the tracking loop, and neither the "inputs" nor the "outputs" of this mixer are in the signal path. The analysis of mixer M3 for spurious responses is therefore inherently different from the more conventional analyses of mixers M1 and M2; one purpose of this appendix is to explicate TRW's analysis of mixer M3.

2.0 ANALYSIS

The TRW memorandum includes results of the spur analysis for each transponder (STDN/TDRS and SGLS) at both low and high ends of the respective input radio frequency ranges. The analysis for each of these four conditions may be facilitated by reference to Table 1, which shows the significant frequencies, particularly those involved in the analysis of mixer M3. The overall analysis of spurs, in notation consistent with that of TRW Subanalysis No. 13, is given in Tables 2-5.

TRW's approach begins by considering the third mixer, M3. TRW uses conventional mixer nomenclature although, as we have noted, this mixer is not part of the signal path. A detailed block diagram of M3 and the associated circuits applicable to both the STDN and SGLS receivers, is shown in Figure 3. Table 1, lines 9-12, gives the various frequencies associated with M3 for the two transponders at the end frequencies.

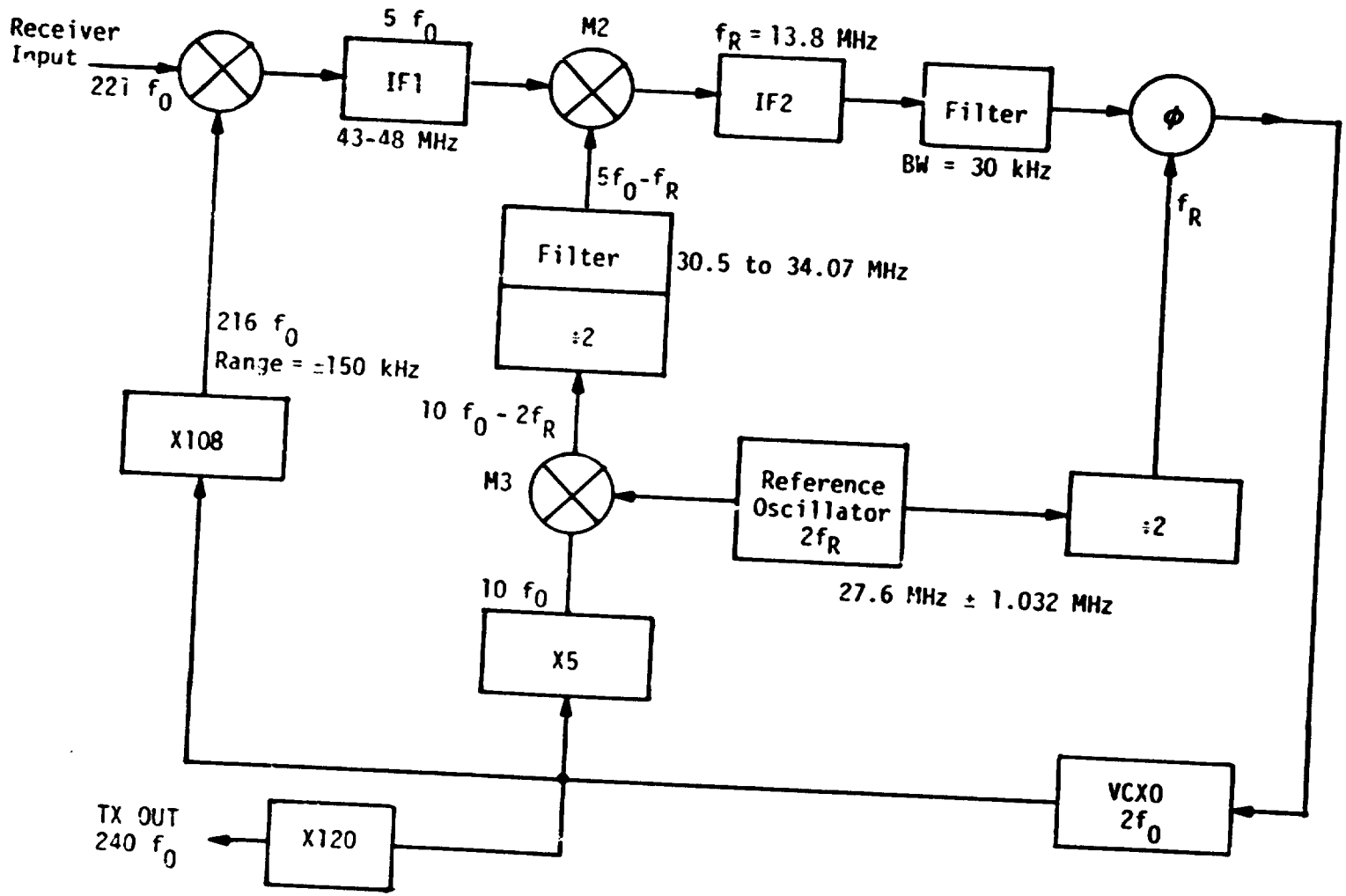

Figure 1. STDN/TDRS Transponder Receiver

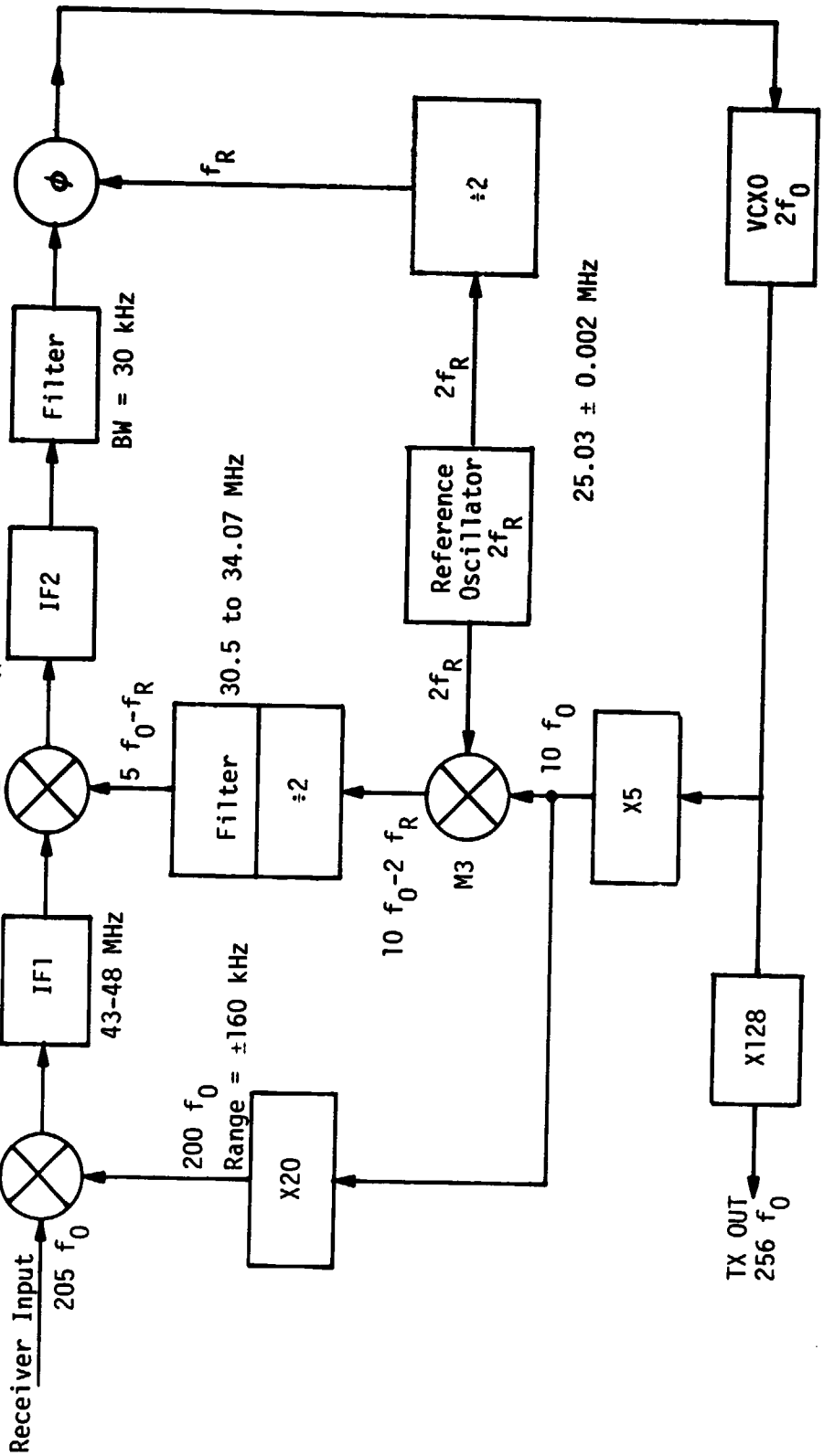

Figure 2. SGLS Transponder Receiver

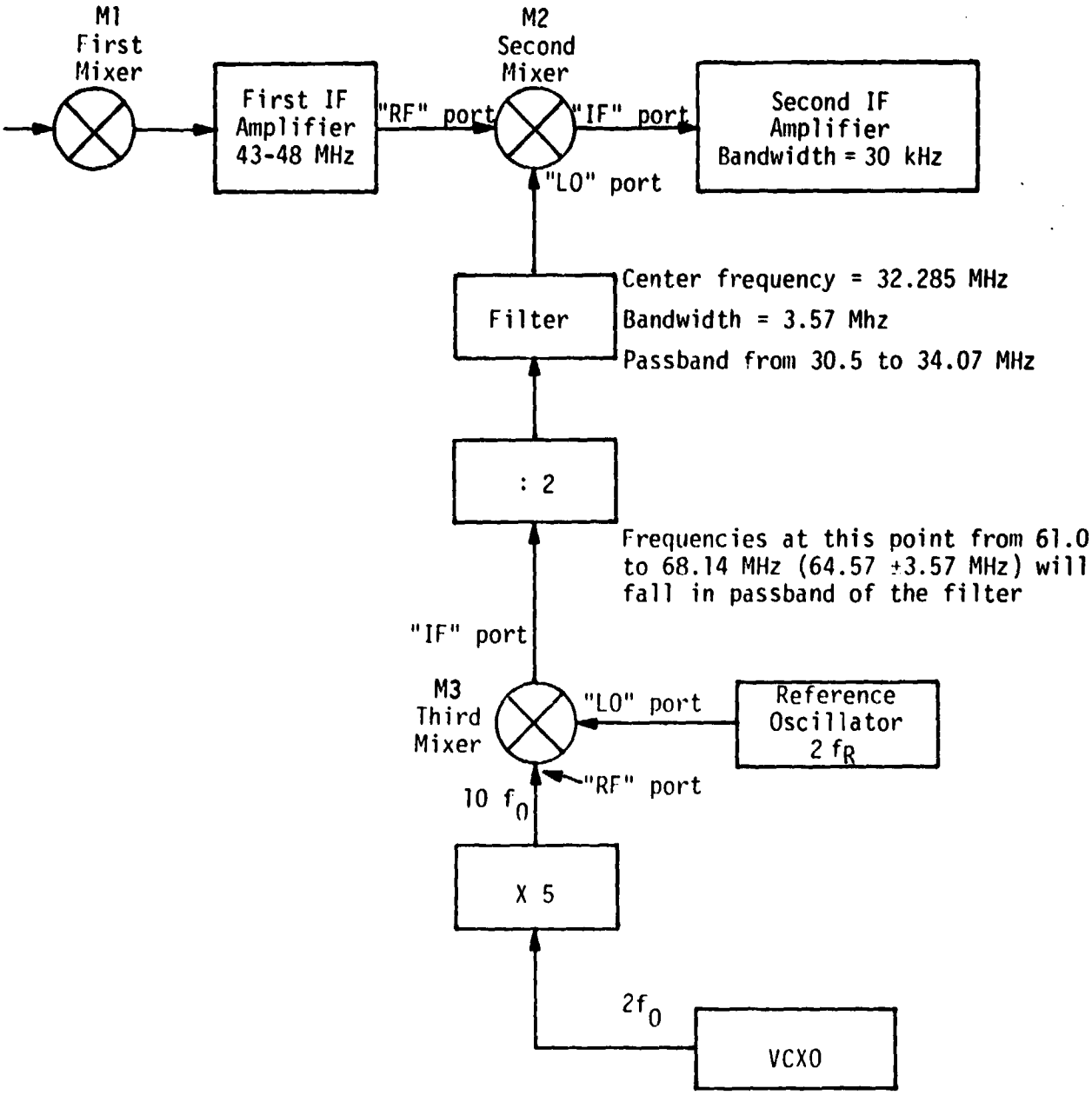

Figure 3. Mixer M3 and Associated Circuits
(STDN/TDRS and SGLS Receivers)

Table 1. Relevant Frequencies
(Refer also to Figures 1 - 3)

Line No.	(All frequencies in MHz)	STDN / TDRS Transponder		SGLS Transponder	
		Low Frequency Limit	High Frequency Limit	Low Frequency Limit	High Frequency Limit
1	Channel Assignment	NASA / STDN Channel 21	NASA/STDN Channel 781	DOD Channel 900	DOD Channel 919
2	Transponder TX Frequency	2202.500	2297.500	2202.500	2297.500
3	RCV/TX ratio	221 / 240	221 / 240	205 / 256	205 / 256
4	Nominal desired receive frequency	2028.1	2115.6	1763.7	1839.8
5	$f_0 = \frac{\text{TX frequency}}{\text{TX multiplier}}$	9.177	9.573	8.6035	8.975
6	VCXO frequency ($2f_0$)	18.354	19.146	17.207	17.949
7	f_R = reference frequency	13.8	13.8	12.515	12.515
8	Ref Osc. Freq. ($2f_R$)	27.6	27.6	25.03	25.03
	M3 (Third Mixer)				
9	"RF" input (VCXO x 5)	91.77	95.73	86.03	89.75
10	"LO" input (same as Ref Osc)	27.6	27.6	25.03	25.03
11	"IF" output	64.17	68.13	61.00	64.72
12	Desired output of ÷2 circuit (becomes LO input to mixer M2)	32.085	34.065	30.500	32.360

Table 2. STDN/TDRS Receiver at Low Frequency Limit

1.0 Desired Operation ("FREQ. A")

1.1 Desired input RF (TRW's "FREQ. A") = 2028.1 MHz

1.2 Transponder RCV/TX ratio = 221/240

1.3 Therefore, f_0 = 2028.1/221 = 9.177 MHz

1.4 Mixer M1:

"RF" = 221 f_0 = 2028.1 MHz

"LO" = 216 f_0 = 1982.2 MHz

"IF" = 221 f_0 - 216 f_0 = 5 f_0 = 45.885 MHz

1.5 Mixer M2:

"RF" = M1 "IF" = 45.885 MHz

"LO" = 32.085 MHz (See line 12, Table 1)

"IF" = f_R = 13.8 MHz = desired input frequency of second IF amplifier

2.0 Image Frequency ("FREQ. B")

2.1 Mixer M1:

"RF" = "LO" - "IF" = 216 f_0 - 5 f_0 = 211 f_0 = 1936.3 MHz
All else same as above

3.0 Spurious Response of M1 ("FREQ. C")

3.1 Input frequency = 2005.2 MHz

3.2 Mixer M1:

"RF" = 2 x input frequency = 4010.4 MHz

"LO" = 2 x 216 f_0 = 3964.4 MHz

"IF" = "RF" - "LO" = 45.885 MHz
All else same as section 1.0 above

4.0 Spurious Response of M2 ("FREQ. D")

4.1 Input frequency = 2032.6 MHz

4.2 Mixer M1:

"RF" = 2032.6 MHz

"LO" = (same as 1.4) = 1982.2 MHz

"IF" = "RF" - "LO" = 50.4 MHz

Table 2. STDN/TDRS Receiver at Low Frequency Limit (Cont'd)

4.3 Mixer M2:

"RF" = M1 "IF" = 50.4 MHz

"LO" = 2 x ("LO" of 1.5) = 64.17 MHz

"IF" = 13.8 MHz = desired input frequency of second IF amplifier

(This is termed the "1,-2" spur of M2)

5.0 Spurious Response Produced by Action of M3 ("FREQ. E")

5.1 Input frequency = 2028.3 MHz

5.2 Mixer M1:

"RF" = 2028.3 MHz

"LO" = (same as 1.4) = 1982.2 MHz

"IF" = "RF" - "LO" = 46.1 MHz

5.3 Mixer M2:

"RF" = M1 "IF" = 46.1 MHz

"LO" = 32.29 MHz (see page B-16)

"IF" = 13.8 MHz = desired input frequency of second if amplifier

6.0 Spurious Response due to Spurious LO input to Mixer M1 ("FREQ. F")

6.1 Input frequency = 2009.8 MHz

6.2 Mixer M1:

"RF" = 2009.8 MHz

"LO" = 214 f_0 (compare 216 f_0 in 1.4) = 1963.9 MHz

"IF" = "RF" - "LO" = 45.9 MHz

All else same as 1.0

Table 3. STDN/TDRS Receiver at High Frequency Limit

1.0 Desired Operation ("FREQ. A")

1.1 Desired input RF (TRW's "FREQ. A") = 2115.6 MHz

1.2 Transponder RCV/TX ratio = 221/240

1.3 Therefore, f_0 = 2115.6/221 = 9.573 MHz

1.4 Mixer M1:

"RF" = 221 f_0 = 2115.6 MHz

"LO" = 216 f_0 = 2067.7 MHz

"IF" = 221 f_0 - 216 f_0 = 5 f_0 = 47.865 MHz

1.5 Mixer M2:

"RF" = M1 "IF" = 47.865 MHz

"LO" = 34.065 MHz (see line 12, Table 1)

"IF" = f_R = 13.8 MHz = desired input frequency of second IF amplifier

2.0 Image Frequency ("FREQ. B")

2.1 Mixer M1:

"RF" = "LO" - "IF" = 216 f_0 - 5 f_0 = 211 f_0 = 2019.9 MHz

All else same as 1.0

3.0 Spurious Response of M1 ("FREQ. C")

3.1 Input frequency = 2091.7 MHz

3.2 Mixer M1:

"RF" = 2 x input frequency = 4183.4 MHz

"LO" = 2 x 216 f_0 = 4135.54 MHz

"IF" = "RF" - "LO" = 47.865 MHz

All else same as 1.0.

4.0 Spurious Response of M2 ("FREQ. D")

4.1 Input frequency = 2122.0 MHz

Table 3. STDN/TDRS Receiver at High Frequency Limit (Cont'd)

4.2 Mixer M1:

"RF" = 2122.0 MHz

"LO" = (same as 1.4) = 2067.7 MHz

"IF" = "RF" - "LO" = 54.3 MHz

4.3 Mixer M2:

"RF" = M1 "IF" = 54.3 MHz

"LO" = 2 x ("LO" of 1.5) = 68.13 MHz

"IF" = 13.8 MHz = desired input frequency of second IF amplifier

(This is termed the "-1,2" spur of M2)

5.0 Spurious Response Produced by Action of M3 ("FREQ. E")

5.1 Input frequency = 2112.2 MHz

5.2 Mixer M1:

"RF" = 2112.2 MHz

"LO" = (same as 1.4) = 2067.7

"IF" = "RF" - "LO" = 44.5 MHz

5.3 Mixer M2:

"RF" = M1 "IF" = 44.5 MHz

"LO" = 30.71 MHz (see page B-16)

"IF" = 13.8 MHz = desired input frequency of second IF amplifier

6.0 Spurious Response due to Spurious LO input to Mixer M1 ("FREQ. F")

6.1 Input frequency = 2096.46 MHz

6.2 Mixer M1:

"RF" = 2096.46 MHz

"LO" = 214 f_0 (compared 216 f_0 of 1.4) = 2048.60

"IF" = "RF" - "LO" = 47.86 MHz

All else same as 1.0.

Table 4. SGLS Receiver at Low Frequency Limit

1.0 Desired Operation ("FREQ. A")

1.1 Desired input RF (TRW's "FREQ. A") = 1763.7 MHz

1.2 Transponder RCV/TX ratio = 205/256

1.3 Therefore, f_0 = 1763.7/205 = 8.603 MHz

1.4 Mixer M1:

"RF" = 205 f_0 = 1763.7 MHz

"LO" = 200 f_0 = 1720.7 MHz

"IF" = 205 f_0 - 200 f_0 = 5 f_0 = 43.02 MHz

1.5 Mixer M2:

"RF" = M1 "IF" = 43.02 MHz

"LO" = 30.5 MHz (see line 12, Table 1)

"IF" = f_R = 12.515 MHz = desired input frequency of second IF amplifier

2.0 Image Frequency ("FREQ. B")

2.1 Mixer M1:

"RF" = "LO" - "IF" = 200 f_0 - 5 f_0 = 195 f_0 = 1677.6 MHz

All else same as 1.0

3.0 Spurious Response of M1 ("FREQ. C")

3.1 Input frequency = 1742.2 MHz

3.2 Mixer M1:

"RF" = 2 x input frequency = 3484.4 MHz

"LO" = 2 x 200 f_0 = 3441.4 MHz

"IF" = "RF" - "LO" = 43.02 MHz

All else same as 1.0

4.0 Spurious Response of M2 ("FREQ. D")

4.1 Input frequency = 1769.2 MHz

Table 4. SGLS Receiver at Low Frequency Limit (Cont'd)

4.2 Mixer M1:

"RF" = 1769.2 MHz

"LO" = (same as 1.4) = 1720.7 MHz

"IF" = "RF" - "LO" = 48.5 MHz

4.3 Mixer M2:

"RF" = M1 "IF" = 48.5 MHz

"LO" = 2 x ("LO" of 1.5) = 61.0 MHz

"IF" = 12.52 MHz = desired input frequency of second IF amplifier

(This is termed the "-1,2" spur of M2)

5.0 Spurious Response Produced by Action of M3 ("FREQ. E")

5.1 Input frequency = 1765.3 MHz

5.2 Mixer M1:

"RF" = 1765.3 MHz

"LO" = (same as 1.4) = 1720.7 MHz

"IF" = "RF" - "LO" = 44.6 MHz

5.3 Mixer M2:

"RF" = M1 "IF" = 44.6 MHz

"LO" = 32.08 MHz (see page B-17)

"IF" = 12.52 MHz = desired input frequency of second IF amplifier

6.0 Spurious Response due to Spurious LO Input to Mixer M1 ("FREQ. F")

6.1 Input frequency = 1746.5 MHz

6.2 Mixer M1:

"RF" = 1746.5 MHz

"LO" = 198 f_0 (compare 200 f_0 of 1.4) = 1703.5 MHz

"IF" = "RF" - "LO" = 43.02 MHz

All else same as 1.0.

Table 5. SGLS Receiver at High Frequency Limit

1.0 Desired Operation ("FREQ. A")

1.1 Desired input RF (TRW's "FREQ. A") = 1839.8 MHz

1.2 Transponder RCV/TX ratio = 205/256

1.3 Therefore, f_0 = 1839.8/205 = 8.975 MHz

1.4 Mixer M1:

"RF" = 205 f_0 = 1839.8 MHz

"LO" = 200 f_0 = 1794.9 MHz

"IF" = 205 f_0 - 200 f_0 = 5 f_0 = 44.9 MHz

1.5 Mixer M2:

"RF" = M1 "IF" = 44.9 MHz

"LO" = 32.360 MHz (see line 12, Table 1)

"IF" = f_R = 12.515 MHz = desired input frequency of second IF amplifier

2.0 Image Frequency ("FREQ. B")

2.1 Mixer M1:

"RF" = "LO" = 200 f_0 - 5 f_0 = 195 f_0 = 1750.0 MHz

All else same as 1.0

3.0 Spurious Response of M1 ("FREQ. C")

3.1 Input frequency = 1817.4 MHz

3.2 Mixer M1:

"RF" = 2 x input frequency = 3634.7 MHz

"LO" = 2 x 200 f_0 = 3589.8 MHz

"IF" = "RF" - "LO" = 44.9 MHz

All else same as 1.0.

4.0 Spurious Response of M2 ("FREQ. D")*

4.1 Input frequency = 1847.1 MHz

*TRW's memo indicates 1847.5 MHz--probably a typographical error.

Table 5. SGLS Receiver at High Frequency Limit (Cont'd)

4.2 Mixer M1:

"RF" = 1847.1 MHz

"LO" = (same as 1.4) = 1794.9 MHz

"IF" = "RF" - "LO" = 52.2 MHz

4.3 Mixer M2:

"RF" = M1 "IF" = 52.2 MHz

"LO" = 2 x ("LO" of 1.5) = 64.72 MHz

"IF" = 12.52 MHz = desired input frequency of second IF amplifier

(This is termed the "-1,2" spur of M2)

5.0 Spurious Response Produced by Action of M3 ("FREQ. E")

5.1 Input frequency = 1841.3 MHz

5.2 Mixer M1:

"RF" = 1841.3 MHz

"LO" = (same as 1.4) = 1794.9 MHz

"IF" = "RF" - "LO" = 46.4 MHz

5.3 Mixer M2:

"RF" = M1 "IF" = 46.4 MHz

"LO" = 33.76 MHz (see page B-17)

"IF" = 12.52 MHz = desired input frequency of second IF amplifier

6.0 Spurious Response due to Spurious LO Input to Mixer M1 ("FREQ. F")

6.1 Input frequency = 1821.8 MHz

6.2 Mixer M1:

"RF" = 1821.8 MHz

"LO" = 198 f_0 (compare 200 f_0 of 1.4) = 1776.9 MHz

"IF" = "RF" - "LO" = 44.9 MHz

All else same as 1.0.

As shown in Table 1, TRW considers the sinusoid at the frequency 10 f_0, delivered by the X5 multiplier to mixer M3, as the "RF" input to this mixer; the output of the Reference Oscillator, at frequency $2f_R$, is considered the "LO" input to this mixer. The output of M3 is termed the "IF" although this output generates the local oscillator input to mixer M2. Ths search for spurs begins by considering the possible ranges of the "RF" and "LO" frequencies into M3 and noting which of the output "IF" frequencies fall into the 30.5-34.07 MHz passband of the output filter (after processing by the "÷2" circuit). For mixer M3, the <u>desired</u> output is the difference frequency between the "RF" and "LO" inputs identified in the TRW analysis as

$$F(IF) = M\,F(RF) + N\,F(LO)$$

with M = 1, N = -1; see lines 11 and 12 of Table 1.

This output is then applied to mixer M2, where it serves as the "LO" input. The frequency of this sinusoid ($5f_0 - f_R$) varies with f_0 and therefore varies with the input radio frequency, as shown in Table 1. Working back from mixer M2 to the input, it is straightforward to find the operating frequencies of M2 and M1 for the desired RF input signals of both transponders, as has been done in part 1 of Tables 2-5. The desired radio frquency is designated as "FREQ A" in the TRW analysis.

We next consider TRW's "FREQ B", the conventional image frequency of mixer M1. Since the term "M1 image" implies that the frequencies associated with M2 and M3 are unchanged from their values when receiving the desired signal, one may easily compute this spurious response frequency. As is characteristic of images, it lies below the M1 LO frequency by the same amount ($5f_0$) that the desired frequency lies above the M1 LO frequency. Results are presented in part 2 of Tables 2-5 as "FREQ B."

The next spur to be considered is termed "FREQ C" and also arises in mixer M1. This spur is of higher order; it is termed the (2,-2) spur since its RF frequency is the solution to the equation

$$F(IF) = 2F(RF) - 2\,F(LO)$$

when F(IF) and F(LO) have the same values as for the desired signal. For

this spur, frequency doubling of both the input radio frequency and the local oscillator take place in mixer M1. Since (as with "FREQ B") the operating frequencies of M2 and M3 are unchanged from the desired signal, it is again straightforward to compute this spurious response frequency from the equation above; results are shown in Tables 2-5. Since the first IF frequency is relatively low, this spur is fairly close in frequency to the desired signal (separation is half of the first IF frequency).

"FREQ D", the next spur to the considered, arises in mixer M2. For this mixer, reference to Figures 1-3 will show that, when one applies the fundamental equation

$$F(IF) = M\,F(RF) + N\,F(LO)\ ,$$

the symbol F(RF) must be interpreted as the frequency out of the first IF amplifier, the symbol F(IF) must be interpreted as the frequency into the second IF amplifier, and F(LO) is one-half of the output frequency of mixer M3. Since this is an "M2 spur", the operation of mixer M3 is unchanged from its operation on the desired signal, which implies that F(LO) for mixer M2 is unknown. Further, the input frequency to the second IF amplifier is fixed for each receiver, so F(IF) is also known. The spur analysis consists of searching for any values of M and N which lead to a value of F(RF) within the passband of the first IF amplifier. TRW has found that such a spur exists for M = -1 and N = 2, i.e., for

$$F(IF) = -F(RF) + 2\,F(LO)$$

due to frequency doubling of the local oscillator signal in the second mixer. It is then necessary to work back through mixer M1 and find the input radio frequency that leads to this spur. Results are presented in part 4 of Tables 2-5.

The next spur considered in the TRW memorandum, termed "FREQ E," arises in an unconventional way. We have pointed out that mixer M3 is not in the signal path and that this mixer generates the local oscillator input to mixer M2. The frequency termed "FREQ E" arises from a spurious response of M3, resulting in a spurious local oscillator input to mixer M2. Moreover, the specific details of this spur differ between the STDN/TDRS and SGLS transponders.

For both transponders, it will be noted from Figure 3 that the desired "RF" input to mixer M3 is the output of the X5 circuit following the VCXO. Since this circuit is not ideal, there is a small output at four times the VCXO frequency, which is a spurious "RF" input to M3. TRW has found, for the STDN/TDRS transponder, that this input, together with a fifth-order harmonic of the "LO" input, produces an output from M3 that lies in the passband of the filter preceding the "LO" input of mixer M2.

Relevant frequencies associated with M3 are, for the STDN/TDRS transponder:

1. Low End of Frequency Range

   4 x VCXO frequency = 4 x 18.355 = 73.42 MHz
   5 x LO input = 5 x 27.6 = 138.0 MHz
   LO input to M2 = 1/2 (output frequency of M3)
   = 1/2 (138.0 - 73.42) = 39.29 MHz

2. High End of Frequency Range

   4 x VCXO frequency = 4 x 19.145 = 76.58 MHz
   5 x LO input = 5 x 27.6 = 138.0 MHz
   LO input to M2 = 1/2 (output frequency of M3)
   = 1/2 (138.0 - 76.58) = 30.71 MHz

The action of the spurious LO input to M2 is detailed in part 5 of Tables 2 and 3, indicating how the spur "FREQ E" results.

In the SGLS transponder, "FREQ E" arises in mixer M3, but in a somewhat different way than in the STDN/TDRS transponder; moreover, in the SGLS transponder, the TRW analysis indicates that the spur arises differently at the two ends of the frequency range. Because the high end spur is similar in nature to the corresponding spur for the STDN/TDRS transponder, we consider the high end first.

It will be recalled that "FREQ E" for the STDN/TDRS transponder results from imperfect filtering of the 5 x VCXO signal, producing some "4x" input to M3. For the SGLS transponder at the high frequency end, the spur results from a spurious "6x" input to M3. This frequency, considered the M3 "RF", interacts with the seventh harmonic of the M3 "LO" to produce an output that lies in the passband of the filter preceding the "LO" input of M2. Relevant frequencies are:

High End of Frequency Range (SGLS Transponder)

6 x VCXO frequency = 6 x 17.949 = 107.694 MHz
7 x LO input = 7 x 25.03 = 175.21 MHz
LO input to M2 = 1/2 (output frequency of M3)
= 1/2 (175.21 - 107.694) = 33.76 MHz

The action of this spurious input to mixer M2 is detailed in part 5 of Table 5.

At the low end of the SGLS frequency range, the "FREQ F" M3 spur arises from the desired VCXO product (i.e., the "5x" harmonic) interacting with the sixth-order harmonic of the M3 "LO" signal. Although not explicit in the TRW analysis, one may expect that this spur, because of the more direct nature of its production, will be at a higher level than the other spurs classified as "FREQ E". Relevant frequencies are:

Low End of Frequency Range (SGLS Transponder)

5 x VCXO frequency = 86.03 MHz (see Table 1)
6 x LO input = 6 x 25.03 = 150.18 MHz
LO input to M2 = 1/2 (output frequency of M3)
= 1/2 (150.18 - 86.03) = 32.08 MHz

The action of this spurious input to mixer M2 is detailed in part 5 of Table 4.

The final spur in the TRW analysis, termed "FREQ F", is more conventional that "FREQ E", occurs in the same manner in both transponders, and does not require a detailed treatment. "FREQ F" arises from a spurious LO input, but this input is into mixer M1 in the signal path and the spur origin is easily explained. It will be noted from Figures 1 and 2, respectively, that the LO input into mixer M1 is intended to be at frequency 216 f_0 for the STDN/TDRS transponder and at frequency 200 f_0 for the SGLS transponder. These frequencies have been produced by multiplication up from 2 f_0, and the residual next lower frequency products (at 214 and 198 f_0), respectively, cause the "FREQ F" spur. Details appear in part 6, Tables 2-5.

3.0 SUMMARY

The TRW spur analysis of the STDN/TDRS and SGLS transponders have been reviewed and explicated in moderate detail. For each of the spurs, we have computed all the relevant frequencies that appear in the signal path since these are necessary for a full understanding of the nature of the spurious responses. Axiomatix finds it interesting that only one spur ("FREQ F") arises from the use of a mixer (M3) not in the path and that this spur is not of a particularly troublesome level.

APPENDIX C

A TRACKING PERFORMANCE ANALYSIS OF A FILTER/SQUARE-LAW TYPE CLOCK RECOVERY LOOP

By

Marvin K. Simon

September 1979

1.0 INTRODUCTION

The IUS STDN/TDRSS transponder incorporates a command detector unit (CDU), part of whose function is to recover a 2 kbps clock from the received command data signal. One candidate for a loop to perform this function is configured as a baseband version of a squaring loop commonly used for carrier (or subcarrier) recovery. In particular, the baseband signal-plus-noise is first heavily filtered, then square-law detected, thus generating signal(clock) components at integer multiples of the command data rate. Finally, the square-law detector is followed by a sinusoidal phase-locked loop (PLL) which tracks one of these components, thus enabling recovery of a clock at the corresponding multiple of the data rate. The desired data rate clock can be obtained by counting down (if the multiple is greater than one) from the PLL reference.

This appendix analyzes the tracking performance of the above bit synchronization loop as a function of received energy per bit-to-noise spectral density ratio E_b/N_0 and input bit transition density p_t. In particular, it is demonstrated that, by fixing the above two parameters, there exists an optimum filter bandwidth (relative to the data rate) in the sense of minimizing the loop tracking jitter. The variation of this optimum performance with E_b/N_0 and p_t is graphically demonstrated for NRZ data and a single-pole RC-type filter. While tracking the signal component at the data rate (first harmonic) is, from a practical standpoint, the likely choice, consideration is given to the loop performance obtained by tracking higher harmonics of the data rate clock. In the latter case, ambiguity resolution is required because of the attendant countdown from the PLL reference.

2.0 ANALYSIS OF THE SIGNAL AND NOISE COMPONENTS IN THE LOOP

Consider the filter/square-law type of clock recovery loop illustrated in Figure 1. The input baseband signal-plus-noise x(t) is characterized by

$$x(t) = \sqrt{S}\, m(t) + n(t) \qquad (1)$$

where S is the average signal power, n(t) is additive "white" Gaussian

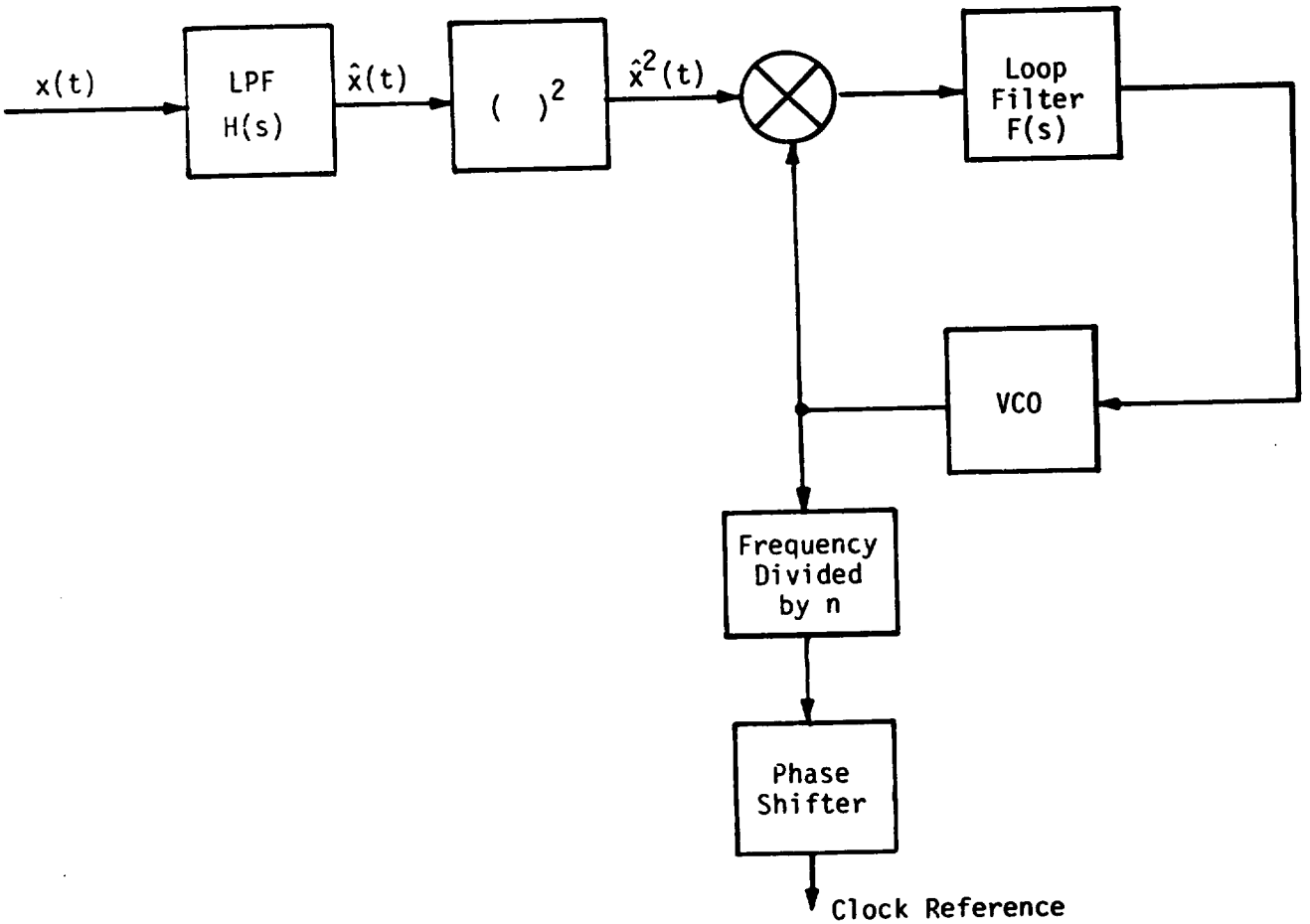

Figure 1. A Filter/Square-Law Type Clock Recovery Loop

noise with single-sided spectral density N_0 W/Hz and

$$m(t) = \sum_{n=-\infty}^{\infty} a_n \, p(t - nT) \tag{2}$$

represents the data modulation, with a_n denoting the nth data bit in the sequence and p(t) the symbol (bit) pulse shape of duration T seconds. To allow for arbitrary (between 0 and 1) transition densities, the data sequence $\{a_n\}$ will be characterized as a first-order Markov source with the properties:

$$\text{Prob}\{a_n = 1 | a_{n-1} = -1\} = \text{Prob}\{a_n = -1 | a_{n-1} = 1\} \triangleq p_t$$

$$\text{Prob}\{a_n = 1 | a_{n-1} = 1\} = \text{Prob}\{a_n = -1 | a_{n-1} = -1\} \triangleq 1 - p_t$$

$$\text{Prob}\{a_n = \pm 1 | a_{n-k} = \pm 1\} = \text{Prob}\{a_n = \pm 1\} = 1/2; \; k \geq 2 \tag{3}$$

The case of random data (i.e., 50% transition density) then becomes a special case of this model corresponding to $p_t = 0.5$.

Passing x(t) through the lowpass filter H(s) produces the output

$$\hat{x}(t) = \sqrt{S}\,\hat{m}(t) + \hat{n}(t) \tag{4}$$

where

$$\hat{m}(t) \triangleq \sum_{n=-\infty}^{\infty} a_n \, \hat{p}(t-nT)$$

$$\hat{p}(t) \triangleq H(p)\, p(t)$$

$$\hat{n}(t) \triangleq H(p)\, n(t) \tag{5}$$

and p denotes the Heaviside operator. Squaring $\hat{x}(t)$ of (4) together with the definitions of (5) yields

$$\hat{x}^2(t) = S\hat{m}^2(t) + 2\sqrt{S}\,\hat{m}(t)\,\hat{n}(t) + \hat{n}^2(t)$$

$$= S\left[\sum_{n=-\infty}^{\infty} \hat{p}^2(t - nT) + \sum_{\substack{n=-\infty \\ n\neq m}}^{\infty}\sum_{m=-\infty}^{\infty} a_n\, a_m\, \hat{p}(t - nT)\,\hat{p}(t - mT)\right]$$

$$+ N(t) \qquad (6)$$

where

$$N(t) \triangleq 2\sqrt{S}\,\hat{m}(t)\,\hat{n}(t) + \hat{n}^2(t) \qquad (7)$$

represents the SxN and NxN components in the square-law detector output.

2.1 Evaluation of the Signal Component in the Loop

Taking the ensemble average of the squared signal terms in $\hat{x}^2(t)$ of (6) gives

$$\overline{\hat{m}^2(t)} = \sum_{n=-\infty}^{\infty} \hat{p}^2(t - nT) + \sum_{\substack{n=-\infty \\ n\neq m}}^{\infty}\sum_{m=-\infty}^{\infty} \overline{a_n\, a_m}\,\hat{p}(t - nT)\,\hat{p}(t - mT) \qquad (8)$$

From the probabilistic properties of the data sequence given in (3), it is simple to show that

$$\overline{a_n\, a_m} = (1 - 2p_t)^{|m-n|} \qquad (9)$$

Thus, substituting (9) into (8) gives

$$\overline{\hat{m}^2(t)} = \sum_{n=-\infty}^{\infty} \hat{p}^2(t - nT) + \sum_{k=1}^{\infty} (1 - 2p_t)^k \sum_{n=-\infty}^{\infty} \hat{p}(t - nT)$$

$$\times \left[\hat{p}\{t - (n-k)T\} + \hat{p}\{t - (n+k)T\}\right] \qquad (10)$$

Recognizing from (10) that $\overline{\hat{m}^2(t)}$ is periodic in t with period T, it may be expanded in the Fourier series

$$\overline{\hat{m}^2(t)} = \sum_{n=-\infty}^{\infty} (C_n + D_n)\, e^{j\frac{2n\pi}{T}t} \qquad (11)$$

where

$$C_n \triangleq \frac{1}{T}\int_0^T \sum_{\ell=-\infty}^{\infty} \hat{p}^2(t-\ell T)\, e^{-j\frac{2n\pi}{T}t}\, dt$$

$$D_n \triangleq \sum_{k=1}^{\infty} d_{nk}(1-2p_t)^k \qquad (12)$$

with

$$d_{nk} \triangleq \frac{1}{T}\int_0^T \sum_{\ell=-\infty}^{\infty} \hat{p}(t-\ell T)\left[\hat{p}(t-(\ell-k)T) + \hat{p}(t-(\ell+k)T)\right] e^{-j\frac{2n\pi}{T}t}\, dt \qquad (13)$$

Through proper change of variables, the combination of finite interval integration and infinite sum in the defining expressions for C_n and d_{nk} can be replaced by a single doubly infinite integral, namely,

$$C_n = \frac{1}{T}\int_{-\infty}^{\infty} \hat{p}^2(t)\, e^{-j\frac{2n\pi}{T}t}\, dt$$

$$d_{nk} = \frac{1}{T}\int_{-\infty}^{\infty} \hat{p}(t)\left[\hat{p}(t+kT) + \hat{p}(t-kT)\right] e^{-j\frac{2n\pi}{T}t}\, dt \qquad (14)$$

Using (5), C_n and d_{nk} can be equivalently expressed in the frequency domain by

$$C_n = \frac{1}{T}\int_{-\infty}^{\infty} P\left(\omega + \frac{2\pi n}{T}\right) P(-\omega)\, H\left(\omega + \frac{2\pi n}{T}\right) H(-\omega)\, \frac{d\omega}{2\pi}$$

$$d_{nk} = \frac{2}{T}\int_{-\infty}^{\infty} P\left(\omega + \frac{2\pi n}{T}\right) P(-\omega)\, H\left(\omega + \frac{2\pi n}{T}\right) H(-\omega)\, \cos\,\omega kT\, \frac{d\omega}{2\pi} \qquad (15)$$

where $P(\omega)$ is the Fourier transform of the pulse shape $p(t)$ and $H(\omega)$ is the filter transfer function.

Recognizing from (14) that $C_n = d_{n0}/2$, the nth total Fourier coefficient $\alpha_n \triangleq C_n + D_n$ is given by

$$\alpha_n \triangleq C_n + D_n = \frac{d_{n0}}{2} + \sum_{k=1}^{\infty} d_{nk} (1 - 2p_t)^k$$

$$= \frac{1}{2} \sum_{k=0}^{\infty} \epsilon_k \, d_{nk} (1 - 2p_t)^k \tag{16}$$

where

$$\epsilon_k = \begin{cases} 1 ; & k = 0 \\ 2 & k > 0 \end{cases} \tag{17}$$

Note from (11) that $|\alpha_n|$ represents the magnitude of the clock component at n times the data rate which is to be tracked by the PLL.

2.2 Evaluation of α_n for NRZ* Data and a Single-Pole RC Filter

We now consider evaluating α_n of (16) for the case of NRZ data where the symbol pulse p(t) is rectangular, namely,

$$p(t) = \begin{cases} 1 ; & 0 \leq t \leq T \\ 0 ; & \text{otherwise} \end{cases} \tag{18}$$

and a single-pole RC filter with transfer function

$$H(\omega) = \frac{1}{1 + j\frac{\omega}{\omega_c}} \tag{19}$$

where $f_c \triangleq \omega_c/2\pi$ denotes the 3 dB cutoff frequency. Using (18) and (19) in (5) results in the following expressions for the filtered pulse and its T second translates:

$$\hat{p}(t) = \left(1 - e^{-\omega_c t}\right) u(t) - \left(1 - e^{-\omega_c (t-T)}\right) u(t - T)$$

$$= \begin{cases} 0 & t \leq 0 \\ 1 - e^{-\omega_c t}; & 0 \leq t \leq T \\ -e^{-\omega_c t}\left[1 - e^{\omega_c T}\right]; & T \leq t \leq \infty \end{cases} \tag{20}$$

---

*We use the term "NRZ" here merely to imply rectangular pulses keeping in mind, however, that the sequence $\{a_n\}$ is still first-order Markov.

$$\hat{p}(t+kT) = \begin{cases} 0\ ; & t \le -kT \\ 1 - e^{-\omega_c(t+kT)}\ ; & -kT \le t \le -(k-1)T \\ -e^{-\omega_c(t+kT)}\left[1 - e^{\omega_c T}\right]; & -(k-1)T \le t \le \infty \end{cases} \tag{21}$$

$$\hat{p}(t-kT) = \begin{cases} 0\ ; & t \le kT \\ 1 - e^{-\omega_c(t-kT)}\ ; & kT \le t \le (k+1)T \\ -e^{-\omega_c(t-kT)}\left[1 - e^{\omega_c T}\right]; & (k+1)T \le t \le \infty \end{cases} \tag{22}$$

Multiplying (20) by the sume of (21) and (22) gives the functions necessary to compute d_{nk} of (14), namely (for $k \neq 0$),

$$\hat{p}(t)\left[\hat{p}(t+kT) + \hat{p}(t-kT)\right] = \begin{cases} 0\ ; & t \le 0 \\ -\left(1 - e^{-\omega_c t}\right) e^{-\omega_c(t+kT)}\left[1 - e^{\omega_c T}\right]; & 0 \le t \le T \\ e^{-\omega_c t}\left[1 - e^{\omega_c T}\right]^2 e^{-\omega_c(t+kT)}\ ; & T \le t \le kT \\ e^{-\omega_c t}\left[1 - e^{\omega_c T}\right]\left\{e^{-\omega_c(t+kT)}\left[1 - e^{\omega_c T}\right]\right. & \\ \qquad \left. -1 + e^{-\omega_c(t-kT)}\right\}; & kT \le t \le (k+1)T \\ e^{-\omega_c t}\left[1 - e^{\omega_c T}\right]^2\left\{e^{-\omega_c(t+kT)} + e^{-\omega_c(t-kT)}\right\} & \\ \qquad (k+1)T \le t \le \infty & \end{cases} \tag{23}$$

For $k = 0$, it is simply necessary to square $\hat{p}(t)$ of (20), resulting in

$$\hat{p}^2(t) = \begin{cases} 0\ ; & t \le 0 \\ \left(1 - e^{-\omega_c t}\right)^2\ ; & 0 \le t \le T \\ e^{-2\omega_c t}\left[1 - e^{\omega_c T}\right]^2\ ; & T \le t \le \infty \end{cases} \tag{24}$$

Substituting (23) in (14) results, after much algebra, in

$$d_{nk} = e^{-k\omega_c T} \beta_n ; \qquad k \neq 0 \tag{25}$$

where

$$\beta_n = -\left(\frac{1 - e^{-\omega_c T}}{\omega_c T}\right)\left(1 - e^{\omega_c T}\right)\left[\frac{1}{\left(1 + j\frac{\pi n}{\omega_c T}\right)\left(1 + j\frac{2\pi n}{\omega_c T}\right)}\right] \tag{26}$$

Similarly, using (24) in (14), we get

$$d_{n0} = -2\frac{\left(1 - e^{-\omega_c T}\right)}{\omega_c T}\left[\frac{1}{\left(1 + j\frac{\pi n}{\omega_c T}\right)\left(1 + j\frac{2\pi n}{\omega_c T}\right)}\right] \tag{27}$$

Thus, combining (25), (26) and (27), α_n of (16) can finally be evaluated as

$$\alpha_n = -\frac{\left(1 - e^{-\omega_c T}\right)}{\omega_c T}\left[\frac{1}{\left(1 + j\frac{\pi n}{\omega_c T}\right)\left(1 + j\frac{2\pi n}{\omega_c T}\right)}\right]\left[1 + \left(1 - e^{\omega_c T}\right)\sum_{k=1}^{\infty}\left(1 - 2p_t\right)^k e^{-k\omega_c T}\right]$$

$$= -\frac{\left(1 - e^{-\omega_c T}\right)}{\omega_c T}\left[\frac{1}{\left(1 + j\frac{\pi n}{\omega_c T}\right)\left(1 + j\frac{2\pi n}{\omega_c T}\right)}\right]\left[\frac{2\,p_t}{1 - (1-2p_t)e^{-\omega_c T}}\right] \tag{28}$$

Note that, for random data ($p_t = 0.5$), the latter factor in (28) evaluates to unity; thus, this factor entirely accounts for the effect of varying transition density on the signal strength of the nth harmonic clock component. Furthermore, since from (28) $\alpha_{-n} = \alpha_n^*$, where the asterisk denotes complex conjugate, then, from (11), the nth harmonic component of $m^2(t)$ denoted by $s_n(t)$ is given by

$$s_n(t) = 2|\alpha_n| \cos\left(\frac{2n\pi}{T}t + \arg \alpha_n\right) \tag{29}$$

where

$$|\alpha_n| = \left(\frac{1 - e^{-2\pi R}}{2\pi R}\right) \left[\frac{1}{\sqrt{\left[1 + \left(\frac{n}{2R}\right)^2\right]\left[1 + \left(\frac{n}{R}\right)^2\right]}}\right] \left[\frac{2p_t}{1 - (1-2p_t)e^{-2\pi R}}\right]$$

$$\arg \alpha_n = \pi - \tan^{-1}\frac{n}{2R} - \tan^{-1}\frac{n}{R} \tag{30}$$

and we have introduced the simplfying notation $R \triangleq \omega_c T/2\pi = f_c T$. It is indeed $s_n(t)$ which the PLL of Figure 1 tries to track.

2.3 Evaluation of the Noise Components in the Loop

Since the PLL acts like a narrowband filter (with respect to the noise bandwidth at its input) around the frequency being tracked, i.e., $\omega = 2\pi n/T$, then it is sufficient to determine the equivalent single-sided noise spectral density N_0' of N(t) defined in (7) at this frequency. The total noise power affecting the loop tracking performance is then $N_0'B_L$, where B_L denotes the loop bandwidth. Consequently, from the above discussion, we are required to evaluate

$$N_0' = 2\int_{-\infty}^{\infty} R_N(\tau)\, e^{-j\frac{2\pi n}{T}\tau}\, d\tau \tag{31}$$

where

$$R_N(\tau) \triangleq \overline{\langle N(t)\, N(t+\tau)\rangle} = R_{SxN}(\tau) + R_{NxN}(\tau) \tag{32}$$

with

$$R_{SxN}(\tau) \triangleq 4S\overline{\langle \hat{m}(t)\, \hat{m}(t+\tau)\rangle}\ \overline{\hat{n}(t)\, \hat{n}(t+\tau)}$$

$$R_{NxN}(\tau) \triangleq \overline{\hat{n}^2(t)\, \hat{n}^2(t+\tau)} \tag{33}$$

Recognizing that, for Gaussian random variables $\{x_i\}$, we have that

$$\overline{x_1x_2x_3x_4} = \overline{x_1x_2}\,\overline{x_3x_4} + \overline{x_1x_3}\,\overline{x_2x_4} + \overline{x_1x_4}\,\overline{x_xx_3} \tag{34}$$

then the latter term of (33) becomes

$$R_{NxN}(\tau) = 2R_{\hat{n}}^2(\tau) + R_{\hat{n}}^2(0) \tag{35}$$

where

$$R_{\hat{n}}(\tau) \triangleq \overline{\hat{n}(t)\,\hat{n}(t+\tau)} = \frac{N_0}{2}\int_{-\infty}^{\infty}|H(\omega)|^2\, e^{j\omega\tau}\,\frac{d\omega}{2\pi} \tag{36}$$

Substituting (35) into (31), the NxN component of N_0' then becomes

$$N_{0_{NxN}}' = 4\int_{-\infty}^{\infty} R_{\hat{n}}^2(\tau)\, e^{-j\frac{2\pi n}{T}\tau}\,d\tau + 2R_{\hat{n}}^2(0)\underbrace{\int_{-\infty}^{\infty} e^{-j\frac{2\pi n}{T}\tau}\,d\tau}_{\delta\left(\frac{2\pi n}{T}\right)}$$

$$= 4\int_{-\infty}^{\infty} R_{\hat{n}}^2(\tau)\, e^{-j\frac{2\pi n}{T}\tau}\,d\tau \quad ; \quad n \neq 0 \tag{37}$$

Equivalently, using (36), $N_{0_{NxN}}'$ can be expressed in the frequency domain by

$$N_{0_{NxN}}' = 4\left(\frac{N_0}{2}\right)^2\int_{-\infty}^{\infty}|H(\omega)|^2\left|H\left(-\omega + \frac{2\pi n}{T}\right)\right|^2\frac{d\omega}{2\pi} \tag{38}$$

For the single-pole RC filter with transfer function as in (19), (38) evaluates to

$$N_{0_{NxN}}' = \frac{\omega_c\, N_0^2}{4\left[1 + \left(\frac{n}{2R}\right)^2\right]} \tag{39}$$

This result can also be obtained from (37) by noting that

$$R_{\hat{n}}(\tau) = \frac{N_0 \omega_c}{4} e^{-\omega_c|\tau|} \tag{40}$$

The SxN component of N_0' can be similarly obtained by substituting $R_{SxN}(\tau)$ of (33) into (31), namely,

$$N_{0_{SxN}}' \triangleq 2 \int_{-\infty}^{\infty} 4S\, R_{\hat{m}}(\tau)\, R_{\hat{n}}(\tau)\, e^{-j\frac{2\pi n}{T}\tau}\, d\tau \tag{41}$$

where

$$R_{\hat{m}}(\tau) \triangleq \overline{\langle \hat{m}(t)\, \hat{m}(t+\tau) \rangle} \tag{42}$$

is the correlation function of the filtered modulation. Alternately, in the frequency domain

$$N_{0_{SxN}}' = 8S \int_{-\infty}^{\infty} S_{\hat{m}}(\omega)\, S_{\hat{n}}\left(\frac{2\pi n}{T} - \omega\right) \frac{d\omega}{2\pi} \tag{43}$$

where $S_{\hat{m}}(\omega)$ and $S_{\hat{n}}(\omega)$ are, respectively, the Fourier transforms of $R_{\hat{m}}(\tau)$ and $R_{\hat{n}}(\tau)$.

For a first-order Markov source generating an NRZ-type sequence, the power spectral density is given by [1,2]

$$S_m(\omega) = T \left[\frac{\sin \omega T/2}{\omega T/2}\right]^2 \left[\frac{4\, p_t\, (1-p_t)}{1 - 2(1-2p_t)\cos \omega T + (1-2p_t)^2}\right] \tag{44}$$

Thus, passing this modulation through the RC filter characterized by (19) gives

$$S_{\hat{m}}(\omega) = S_m(\omega)|H(\omega)|^2 = S_m(\omega) \frac{1}{1 + \left(\frac{\omega}{\omega_c}\right)^2} \tag{45}$$

The filtered noise $\hat{n}(t)$ has the spectrum

$$S_{\hat{n}}(\omega) = \frac{N_0}{2} |H(\omega)|^2 = \frac{N_0}{2} \frac{1}{1 + \left(\frac{\omega}{\omega_c}\right)^2} \tag{46}$$

Thus, performing a change of variables in (46) and substituting this result together with (44) and (45) in (43) yields

$$N_{0_{SxN}}' = \frac{4SN_0}{\pi} \int_{-\infty}^{\infty} \left(\frac{\sin x}{x}\right)^2 \left[\frac{4\, p_t(1-p_t)}{1-2(1-2p_t)\cos 2x + (1-2p_t)^2}\right] \left[\frac{1}{1+\left(\frac{x}{x_c}\right)^2}\right] \left[\frac{1}{1+\left(\frac{x-n\pi}{x_c}\right)^2}\right] dx \tag{47}$$

where we have further let

$$x = \omega T/2$$

$$x_c = \omega_c T/2 = \pi R \; ; \quad R = f_c T \tag{48}$$

The integral in (47) can be solved by applying the method of partial fraction expansion. In particular, we group the polynomial factors and form the partial-fraction expansion

$$\frac{1}{x^2}\left[\frac{1}{1+\left(\frac{x}{x_c}\right)^2}\right]\left[\frac{1}{1+\left(\frac{x-n\pi}{x_c}\right)^2}\right] = \frac{1}{x^2}\left[\frac{x_c^2}{x^2+x_c^2}\right]\left[\frac{x_c^2}{(x-n\pi)^2+x_c^2}\right]$$

$$= \frac{A_1 x + A_2}{x^2} + \frac{B_1 x + B_2}{x^2 + x_c^2} + \frac{C_1(x-n\pi) + C_2}{(x-n\pi)^2 + x_c^2} \tag{49}$$

After much laborious algebra, the following solutions for the unknown coefficients emerge:

$$A_1 = \frac{2\pi n}{x_c^2\left[1+\left(\frac{n\pi}{x_c}\right)^2\right]^2}$$

$$A_2 = \frac{1}{1+\left(\frac{n\pi}{x_c}\right)^2}$$

$$B_1 = -\frac{1}{2n\pi\left[1+\left(\frac{n\pi}{2x_c}\right)^2\right]}$$

$$B_2 = -\frac{1}{4\left[1+\left(\frac{n\pi}{2x_c}\right)^2\right]}$$

$$C_1 = -\frac{2\pi n}{x_c^2\left[1+\left(\frac{n\pi}{x_c}\right)^2\right]^2} + \frac{1}{2n\pi\left[1+\left(\frac{n\pi}{2x_c}\right)^2\right]}$$

$$C_2 = -\frac{1-\left(\frac{n\pi}{x_c}\right)^2}{\left[1+\left(\frac{n\pi}{x_c}\right)^2\right]^2} - \frac{1}{4\left[1+\left(\frac{n\pi}{2x_c}\right)^2\right]} \qquad (50)$$

Since the remainder of the integrand in (47) is an even function of x, the integrals corresponding to the coefficients A_1, B_1 and C_1 will then equate to zero. Thus, it remains to evaluate only the integrals corresponding to the contributions from the partial-fraction expansion with coefficients A_2, B_2 and C_2. The first term to be evaluated is:

$$I_1 \triangleq A_2 \int_{-\infty}^{\infty} \left(\frac{\sin x}{x}\right)^2 \left[\frac{4\,p_t(1-p_t)}{1-2(1-2p_t)\cos 2x + (1-2p_t)^2}\right] dx. \qquad (51)$$

To perform this integration, we first consider the more general form

$$I = \int_{-\infty}^{\infty} \frac{\sin^2 x}{x^2+\left(\frac{\beta}{2}\right)^2}\left[\frac{1}{1-2a\cos 2x + a^2}\right] dx \qquad (52)$$

Letting $y = 2x$ and using the trigonometric identity $\sin^2(y/2) = (1-\cos y)/2$, (52) simplifies to

$$I = 2\int_0^\infty \left[\frac{1 - \cos y}{1 - 2a\cos y + a^2}\right]\left(\frac{1}{y^2 + \beta^2}\right) dy \tag{53}$$

Now from [3; p 437, Eq. 3.792-17], we have that

$$\int_0^\infty \left[\frac{\cos by}{1 - 2a\cos y + a^2}\right]\left(\frac{1}{y^2 + \beta^2}\right) dy = \frac{\pi}{2\beta}\left[\frac{e^{\beta - \beta b} + ae^{\beta b}}{(1 - a^2)(e^\beta - a)}\right] \tag{54}$$

Letting $b = 0$ and 1 in (54) and subtracting the results gives the desired result

$$I = \left(\frac{\pi}{\beta}\right)\frac{\left[e^\beta + a - (1 + ae^\beta)\right]}{(1 - a^2)(e^\beta - a)} = \left(\frac{\pi}{\beta}\right)\left[\frac{(e^\beta - 1)}{(1 + a)(e^\beta - a)}\right]$$

$$= \left(\frac{\pi}{\beta}\right)\left[\frac{1 - e^{-\beta}}{(1 + a)(1 - ae^{-\beta})}\right] \tag{55}$$

To use (55) in (51), we let $a = 1 - 2p_t$ and take the limit as β goes to zero. Thus,

$$\lim_{\beta \to 0} I = \frac{\pi}{1 - a^2} \tag{56}$$

and

$$I_1 = A_2\left[4p_t\,(1 - p_t)\right]\lim_{\beta \to 0} I\Big|_{a\,=\,1\,-\,2p_t}$$

$$= \pi\left[\frac{1}{1 + \left(\frac{n\pi}{x_c}\right)^2}\right]\left[\frac{1}{1 - (1 - 2p_t)^2}\right] \tag{57}$$

The second and third terms (coefficients B_2 and C_2) of (49) can be combined since a shift of $n\pi$ in the remainder of the integrand of (47) has no effect on the integral. Thus,

$$I_2 + I_3 \triangleq (B_2 + C_2) \int_{-\infty}^{\infty} \left(\frac{\sin^2 x}{x^2 + x_c^2} \right) \left[\frac{4p_t(1-p_t)}{1 - 2(1-2p_t)\cos x + (1-2p_t)^2} \right] dx \quad (58)$$

But this integral is precisely of the form of I in (52). Thus, we can immediately write

$$I_2 + I_3 = (B_2 + C_2) \left[4p_t(1-p_t) \right] \left(\frac{\pi}{2x_c} \right) \left[\frac{1 - e^{-2x_c}}{\left[1 + (1-2p_t) \right] \left[1 - (1-2p_t)e^{-2x_c} \right]} \right] \quad (59)$$

and using (50),

$$I_2 + I_3 = -\left[\frac{6 + \left(\frac{n\pi}{x_c} \right)^2 + \left(\frac{n\pi}{x_c} \right)^4}{4\left[1 + \left(\frac{n\pi}{2x_c} \right)^2 \right] \left[1 + \left(\frac{n\pi}{x_c} \right)^2 \right]^2} \right] \left[4p_t(1-p_t) \right] \left(\frac{\pi}{2x_c} \right)$$

$$\times \left[\frac{1 - e^{-2x_c}}{\left[1 + (1-2p_t) \right] \left[1 - (1-2p_t)e^{-2x_c} \right]} \right] \quad (60)$$

Finally, summing (57) and (60) and multiplying by $4SN_0/\pi$ gives the SxN component of N_0 characterized by (47), namely,

$$N_{0_{SxN}}' = \frac{4SN_0}{1+\left(\frac{n}{R}\right)^2} - \left(\frac{SN_0\left(1-e^{-2\pi R}\right)}{2\pi R}\right)\left[\frac{2p_t}{1-(1-2p_t)\,e^{-2\pi R}}\right] \times \left[\frac{6+\left(\frac{n}{R}\right)^2+\left(\frac{n}{R}\right)^4}{\left[1+\left(\frac{n}{R}\right)^2\right]\left[1+\left(\frac{n}{R}\right)^2\right]^2}\right] \tag{61}$$

The total equivalent noise spectral density N_0' is the sum of (39) and (61).

2.4 Mean-Square Tracking Jitter Performance

Since the square-law device in Figure 1 is followed by a conventional sinusoidal PLL, then using the well-known linear theory for such a loop, the mean-square phase tracking jitter $\sigma_{\phi_n}^2$ is given by the ratio of noise power in the loop bandwidth ($N_0'\,B_L$) to the power of the signal component being tracked. Recalling that $s_n(t)$ of (29) is indeed that signal, then

$$\sigma_{\phi_n}^2 = \frac{N_0'\,B_L}{2|\alpha_n|^2} = \frac{\left(N_{0_{NxN}}' + N_{0_{SxN}}'\right)B_L}{2|\alpha_n|^2} \tag{62}$$

Substituting (30), (39) and (61) into (62) and simplifying gives the desired result, namely,

$$\sigma_{\phi_n}^2 = \frac{(2\pi)^2}{(\xi p_t)^2}\left(\frac{N_0 B_L}{S}\right)\left[\frac{R^2+\left(\frac{n}{2}\right)^2}{\left[1-e^{-2\pi R}\right]^2}\right]\left\{2+\frac{N_0\pi f_0}{4S}\left[\frac{1+\left(\frac{n}{R}\right)^2}{1+\left(\frac{n}{2R}\right)^2}\right] - \xi p_t\,\frac{\left(1-e^{-2\pi R}\right)}{4\pi R}\left[\frac{6+\left(\frac{n}{R}\right)^2+\left(\frac{n}{R}\right)^4}{\left[1+\left(\frac{n}{2R}\right)^2\right]\left[1+\left(\frac{n}{R}\right)^2\right]}\right]\right\};$$

$$n = 1,2,\ldots \tag{63}$$

where we have introduced the simplifying notation

$$\xi_{p_t} \triangleq \frac{2 p_t}{1 - (1 - 2p_t)\, e^{-2\pi R}} \tag{64}$$

Note that, for random data ($p_t = 0.5$), $\xi_{p_t} = 1$. Since the period of the oscillation being tracked is T/n, the equivalent <u>timing</u> error in the loop is given by

$$\tau_n = \left(\frac{\phi}{2\pi}\right) \left(\frac{T}{n}\right) \tag{65}$$

with mean-square value

$$\phi_{\tau_n}^{\ 2} = \left(\frac{1}{2\pi}\right)^2 \left(\frac{T}{n}\right)^2 \sigma_{\phi_n}^{\ 2} \tag{66}$$

Finally, the clock obtained by counting down (if $n > 1$) the VCO reference by a factor n would have a relative timing error

$$\varepsilon_n \triangleq \frac{\tau_n}{T} \tag{67}$$

with a corresponding mean-square jitter

$$\sigma_{\varepsilon_n}^{\ 2} = \frac{\sigma_{\tau_n}^{\ 2}}{T^2} = \left(\frac{1}{2\pi}\right)^2 \left(\frac{1}{n}\right)^2 \sigma_{\phi_n}^{\ 2} = \frac{1}{\rho \mathcal{L}_L} \tag{68}$$

where

$$\rho \triangleq \frac{S}{N_0 B_L}$$

is the equivalent "linear loop" signal-to-noise ratio and

$$\mathcal{L}_L \triangleq (\xi p_t)^2 n^2 \left[\frac{\left[1 - e^{-2\pi R}\right]^2}{R^2 + \left(\frac{n}{2}\right)^2}\right] \left\{ 2 + \frac{\pi}{4}\left(\frac{R}{E_b/N_0}\right)\left[\frac{1 + \left(\frac{n}{R}\right)^2}{1 + \left(\frac{n}{2R}\right)^2}\right] \right.$$

$$\left. - \xi p_t \frac{\left(1 - e^{-2\pi R}\right)}{4\pi R}\left[\frac{6 + \left(\frac{n}{R}\right)^2 + \left(\frac{n}{R}\right)^4}{\left[1 + \left(\frac{n}{2R}\right)^2\right]\left[1 + \left(\frac{n}{R}\right)^2\right]}\right] \right\} \quad (70)$$

is a factor analogous to the squaring loss* of a squaring loop used for tracking a suppressed carrier. Also, in (70) we have introduced the parameter $E_b/N_0 \triangleq ST/N_0$ which denotes bit energy-to-noise ratio and is a fixed quantity for a given command data error rate.

The remainder of this report deals with various numerical interpretations of the result in (70).

2.5 Numerical Evaluations and Interpretations

Figures 2 and 3 are illustrations of $\mathcal{L}_L$ in dB versus $R = f_c T$ with E_b/N_0 as a parameter. Both figures correspond to the case where the PLL provides a reference at the data rate (i.e., n=1) with Figure 2 drawn for random data ($p_t = 0.5$) and Figure 3 for a transition density half that amount. Several important observations can be made from these results:

(1) For fixed E_b/N_0, there exists in optimum (in the sense of maximum $\mathcal{L}_L$ or, equivalently, minimum σ_ϕ^2) filter cutoff frequency (relative to the data rate).

(2) The optimum filter cutoff frequency as discussed in (1) is very insensitive to the value of E_b/N_0 for $p_t = 0.5$.

(3) The performance degrades heavily with decreasing transition density and improves moderately with increasing E_b/N_0.

A further illustration of some of these points is presented in Figure 4 where the optimum value of $\mathcal{L}_L$ is plotted versus transition density p_t

---

*Where the squaring loss associated with a squaring is a factor always less than unity, $\mathcal{L}_L$ of (70) can, as we shall shortly see, exceed unity.

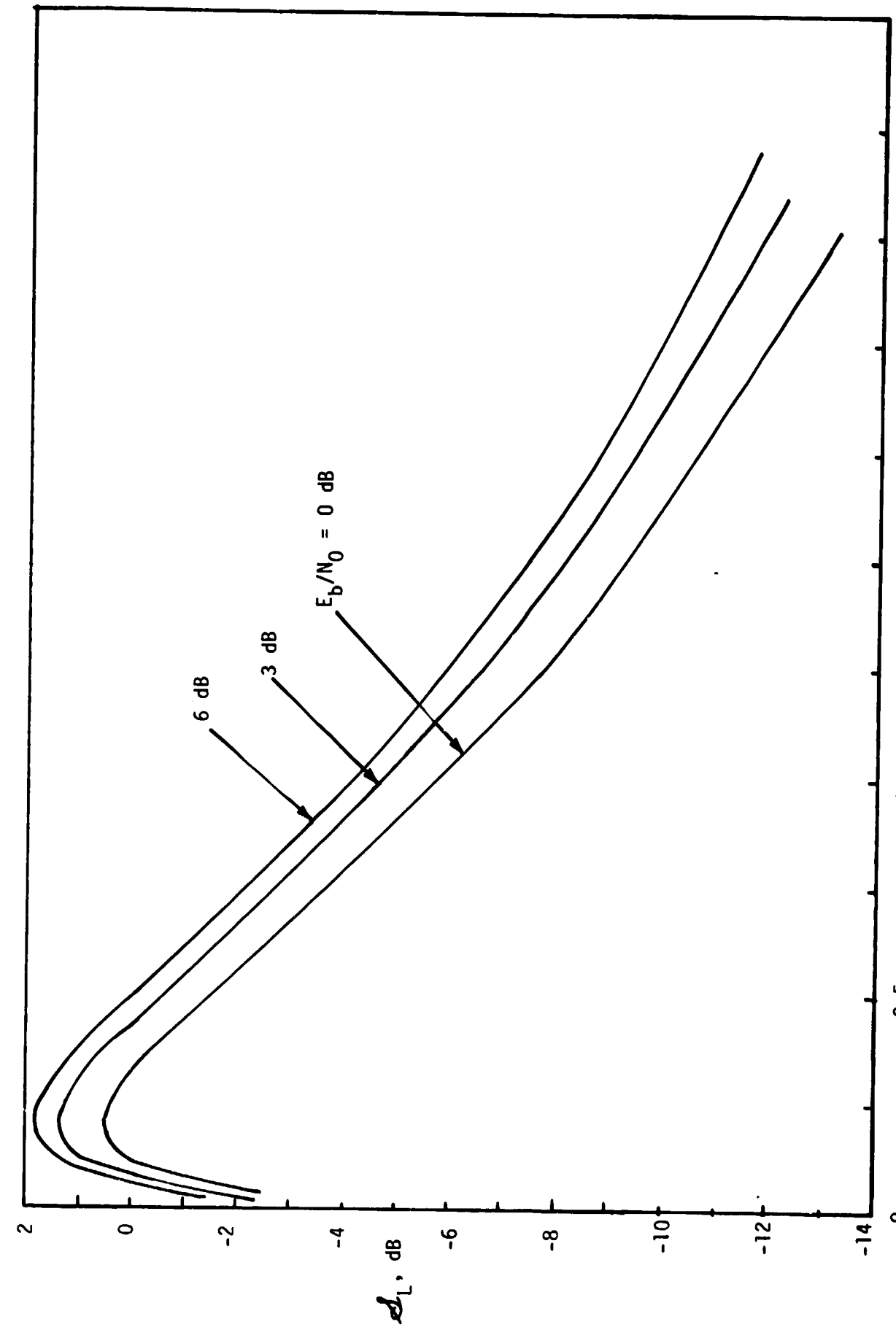

Figure 2. "Squaring Loss" versus the Ratio of Filter 3 dB Cutoff Frequency to Data Rate with Bit Energy-to-Noise Ratio as a Parameter; $n = 1$, $p_t = 0.5$

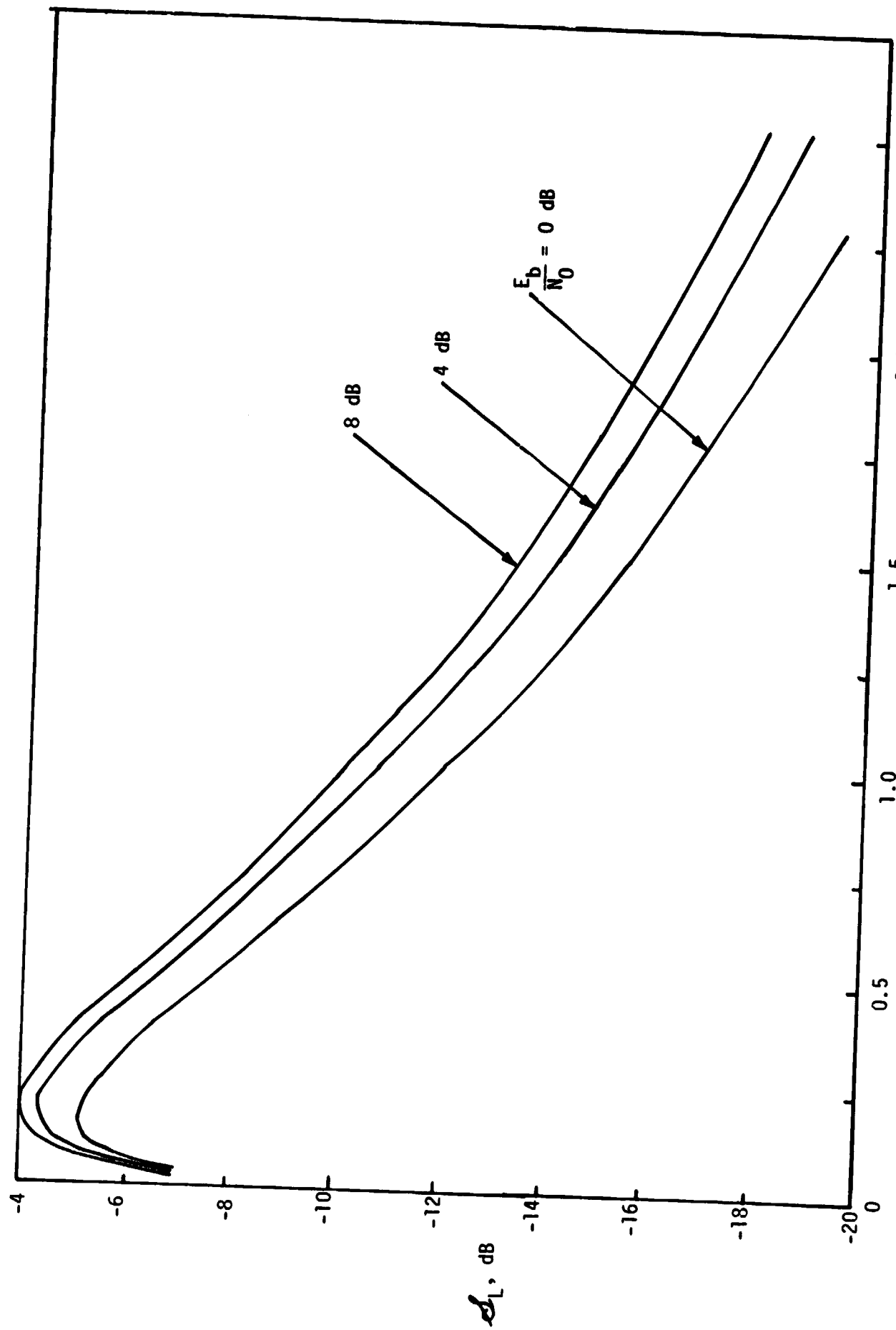

Figure 3. "Squaring Loss" versus the Ratio of Filter 3 dB Cutoff Frequency to Data Rate with Bit Energy-to-Noise Ratio as a Parameter; $n = 1$, $P_t = 0.25$

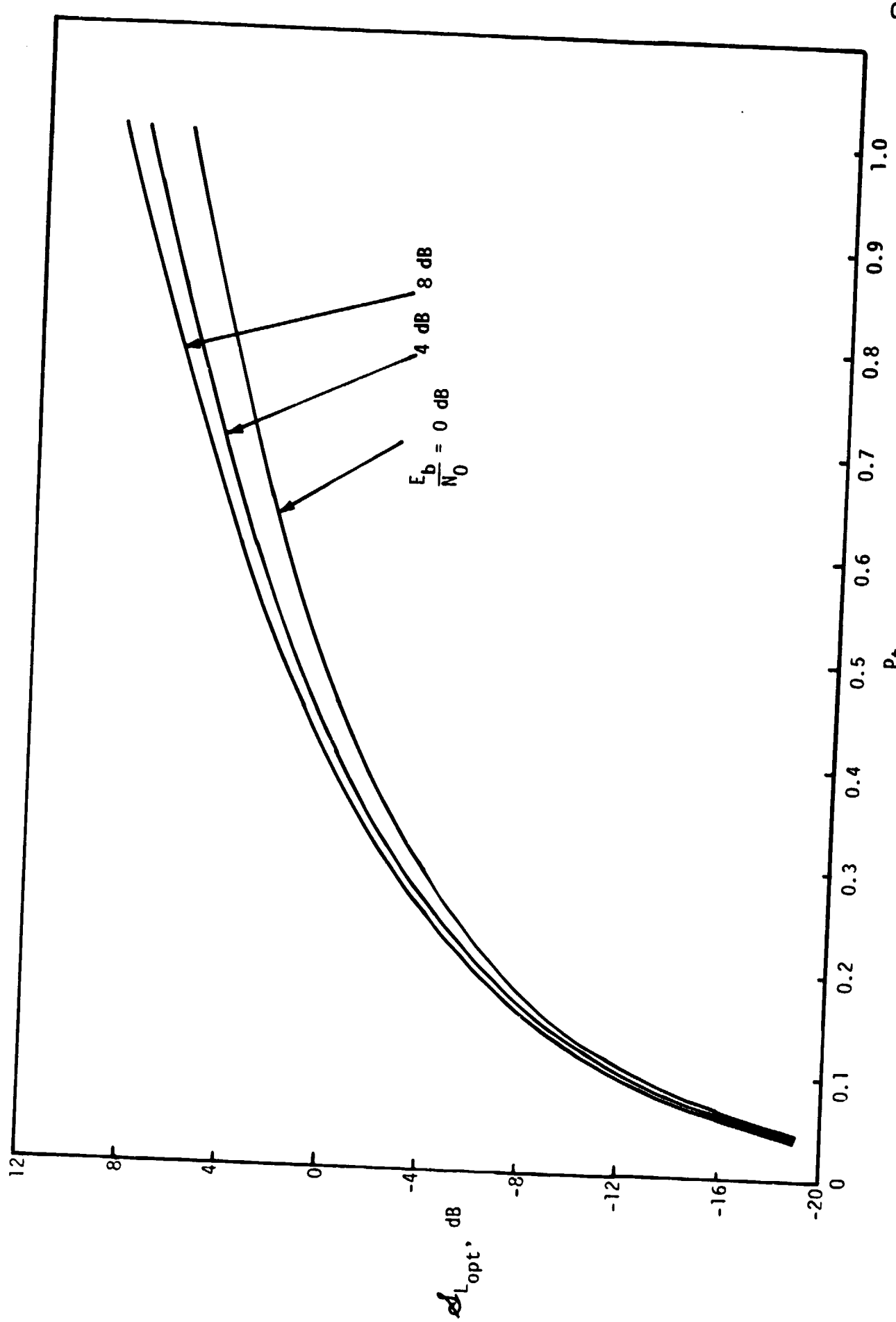

Figure 4. Optimum "Squaring Loss" versus Bit Transition Density with Bit Energy-to-Noise Ratio as a Parameter; n = 1

with E_b/N_0 as a parameter. Figure 5 is the corresponding plot of the optimum filter cutoff frequency (normalized to the data rate).

Thus far, all of the numerical results have been presented for the case n = 1 wherein the VCO sinusoidal reference has a frequency equal to the data rate. Figure 6 illustrates how the bit synchronization loop behaves as a function of n, i.e., the PLL tracks the nth harmonic of the data rate. Note that improved performance can be obtained by increasing n beyond unity. However, since the desired clock must now be obtained by frequency dividing (counting down) the VCO reference by a factor n, an n-fold timing ambiguity is created which must be resolved. Clearly, the larger the value of n, the more difficult the resolution process.

Before concluding our discussion, we draw attention to one additional consideration which heretofore has not been discussed. We recall from (29) that the PLL input $s_n(t)$ included a phase shift arg α_n which was a function of the ratio n/R. Clearly, the loop will track this phase; thus, to establish a clock in phase with the input data modulation, this phase shift must be compensated for as indicated by the box labeled "phase shifter" in Figure 1.

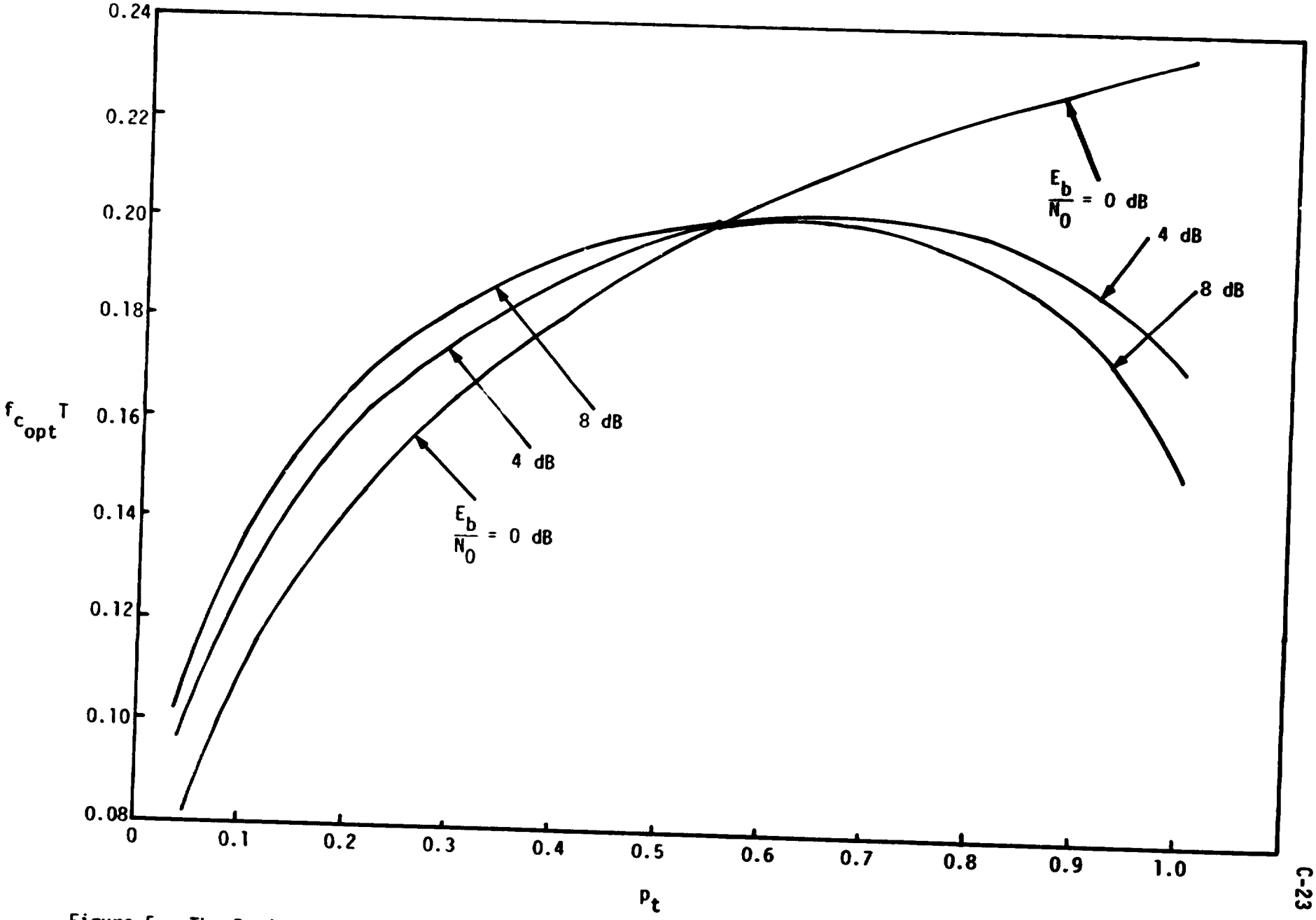

Figure 5. The Ratio of Optimum Filter 3 dB Cutoff Frequency to Data Rate versus Bit Transition Density with Bit Energy-to-Noise Ratio as a Parameter; $n = 1$

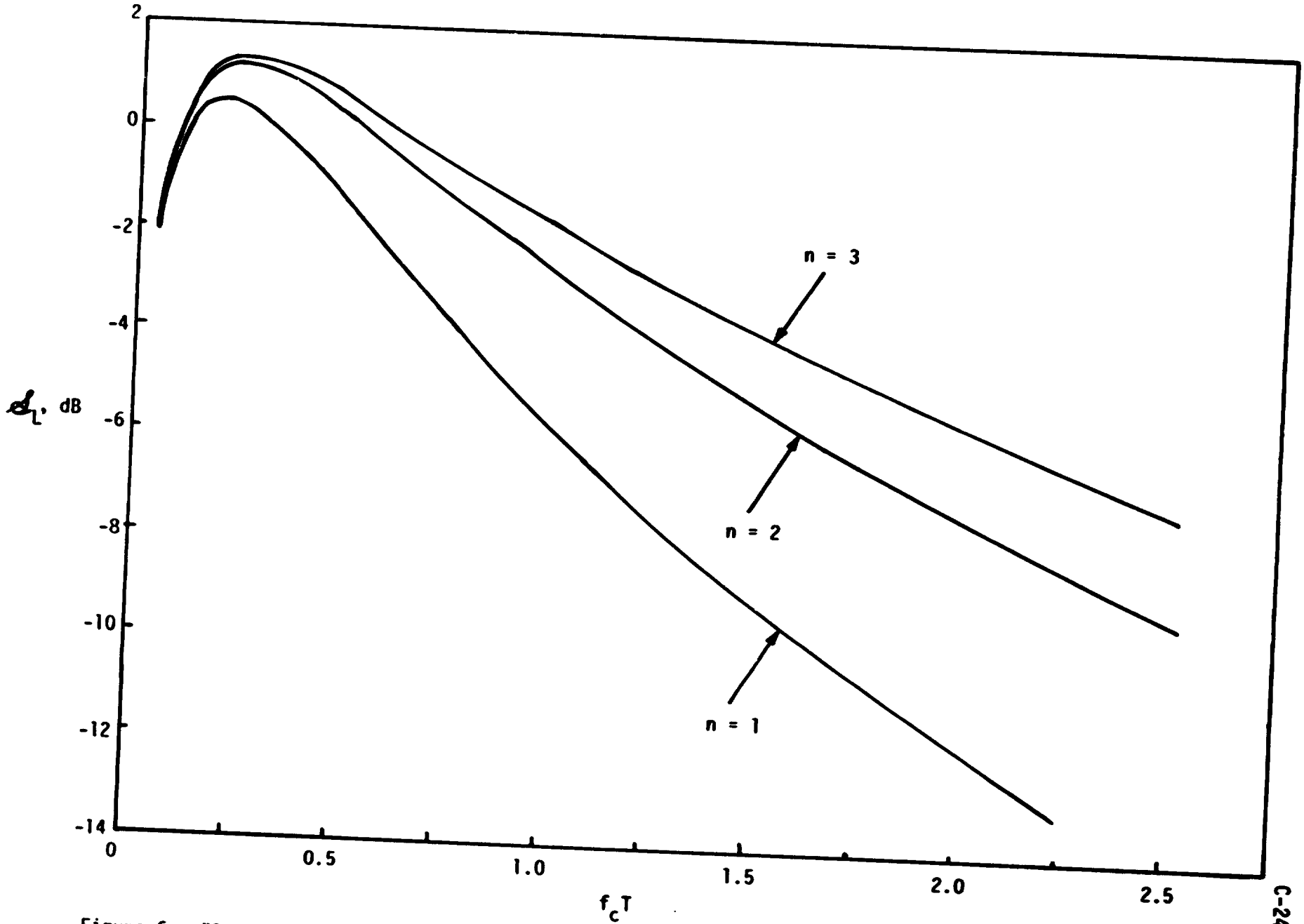

Figure 6. "Squaring Loss" versus the Ratio of Filter 3 dB Cutoff Frequency to Data Rate with Clock Frequency Harmonic as a Parameter; $E_b/N_0 = 0$ dB, $P_t = 0.5$

REFERENCES

1. Levitt, B. K., "Power Spectrum for Binary NRZ Data with Less Than 50 Percent Transitions," JPL DSN Progress Report 42-32, April 15, 1976, pp 86-89.

2. Divsalar, D., and Simon, M. K., "Spectral Characteristics of Convolutionally Coded Digital Signals," JPL Technical Report 79-93, August 1, 1979, Appendix A.

3. Gradshteyn, I. S., and Ryzhik, I. M., Table of Integrals, Series, and Products, Academic Press, New York, 1965.

APPENDIX D

ESTL TEST REQUIREMENTS PLAN

By

R.G. Maronde

1.0 INTRODUCTION

1.1 Statement of Work

1.1.1 Objectives

This document presents a plan for performing verification tests between the Inertial Upper Stage (IUS) and the DOD Communication Interface Unit (CIU) or NASA Payload Signal Processor (PSP) communication systems. These tests, which will be performed in the NASA Lyndon B. Johnson Space Center (JSC) Electronic System Laboratory (ESTL), are designed to establish that the communications link between the IUS and the CIU or PSP is compatible and that the system performance will meet the requirements of the Shuttle program.

To implement these tests, Orbiter and IUS communications hardware must be obtained and installed in a representative mission configuration in the ESTL. Therefore, the communications links to be evaluated during these tests are equivalent to those which will be used during an Orbiter mission. The only significant difference is that the RF paths will be through hard-line, space-loss simulators.

The IUS is being developed by the DOD for joint DOD/NASA use and will consist of a DOD and a NASA configuration. Both IUS configurations will be verified during the ESTL testing. Operational constraints, however, may require the use of a DOD IUS for NASA payload missions such as the Tracking and Data Relay Satellite (TDRS) launch.

As part of the ESTL test plan, this document will discuss the following items:

- Communication links to be tested
- Operational modes to be tested
- Operating parameters to be verified
- Special test equipment requirements.

1.1.2 Stipulated Tasks

The contract work statement calls out the following task:

> "Task #4--ESTL Test Requirements. The contractor shall develop a complete set of test requirements for the IUS (DOD and NASA) communications equipment when it arrives at the ESTL for compatibility testing. The test requirements shall define all communication links, modes, and parameters to be tested. Any special test equipment shall be identified."

1.1.3 General Approach to the Activity

A number of previous reports and studies were reviewed to determine the overall end-to-end communication links to be tested. The result was a very large number of end-to-end links but, by applying the test philosophy developed later in this document, the number of test links required was greatly reduced.

Each test link was analyzed and various performance test requirements such as forward and return link and RF acquisition tests were developed. Within each test requirement, operational modes and parameters were also evolved.

1.2 Contents of the Report

Three sections address various aspects and details of this work. Section 2.0 contains the numerous IUS/Orbiter communication interfaces and operating mode descriptions. Referenced in this section, but included in the Addendums, are the details outlining all the end-to-end IUS/Orbiter/Ground Station communication links. Section 3.0 discusses the test philosophy used in this report which, when applied, greatly reduces the number of IUS/Orbiter communication links that must be tested in the ESTL. The test links are outlined in this section. Section 4.0 outlines the necessary equipment calibration tests and the system compatibility/performance test required.

2.0 IUS/ORBITER COMMUNICATION INTERFACES DEFINITION

One method used to deliver a payload beyond the Orbiter's operating range is to assist the payload with an inertial upper stage (IUS). Being developed by the DOD, the IUS consists primarily of a Titan 34D final stage. Two IUS vehicles with attached payloads can be carried in tandem in the Orbiter bay with each IUS carrying up to four payloads or spacecraft.

Because of differences in communication link requirements, there is a DOD configuration and a NASA configuration. The DOD IUS will use communication link equipment compatible with the ground stations of the USAF Satellite Control Facility (SCF); the NASA IUS will use communication

link equipment compatible with the ground stations of both the Spaceflight Tracking and Data Network (STDN) and the Tracking and Data Relay Satellite System (TDRSS).

As a note of clarification, what is now known as the NASA Spaceflight Tracking and Data Network (STDN) consists of the original STDN ground stations and the newer TDRS ground stations. The term GSTDN is used to differentiate the original STDN ground stations from the other, newer ground stations within the STDN system.

For the purpose of on-orbit checkout, the Shuttle is required to communicate with the IUS while the IUS is physically located within the Orbiter bay (attached) or within a range of 10 miles from the Orbiter after the IUS has been deployed (detached). In the attached mode, communication between the Orbiter and the IUS is either via a hard-line umbilical link or via the RF links. Ground stations may also communicate with the IUS in the attached mode using either a direct RF link or the Orbiter as a relay. In the detached mode, communication between the Orbiter and the IUS is only via the RF links. Again, the Orbiter may act as a relay for IUS/ground communication.

The Orbiter avionics equipment serving the IUS in the attached and detached modes perform two major functions. First, there are avionic equipment which perform payload RF and baseband signal processing functions. This equipment includes:

- Payload Interrogator (PI)
- Payload Signal Processor (PSP)--NASA configuration
- Communication Interface Unit (CIU)--DOD configuration
- Ku-Band Signal Processor (KuSP).
- FM Signal Processor (FMSP)

Second, there are avionic equipment which perform data handling functions. This equipment includes:

- Payload Data Interleaver (PDI)
- Payload Recorder (PR)
- PCM Master Unit (PCMMU)
- Network Signal Processor (NSP)
- Various DOD encryptor/decryptor units.

The IUS avionics equipment serving the Orbiter in the attached and detached modes also perform two major functions. First, the equipment performing the RF and baseband signal processing functions includes:

- IUS Transponder
- Signal Conditioning Unit (SCU).

Second, the avionics equipment performing the data handling functions includes:

- Signal Interface Unit (SIU)
- Environmental Measurement Unit (EMU)
- Wideband Data Interleaver (WBDI).

2.1 Attached IUS Communication

In the attached mode, a hard-line umbilical provides two-way communication between the IUS and the Orbiter. Scientific data, engineering data, guidance, navigation and attitude control data (GN&C) are received by the Orbiter from the IUS. Alternately, command data, GN&C and uplink data are transmitted to the IUS from the Orbiter.

Figure 1 illustrates the functional scientific data interfaces for attached payloads. Only limited processing--that required to throughput data to a ground terminal--is provided for IUS medium-band and wideband scientific data inputs (inputs in the range of 16 to 256 kbps). For data rates below 64 kbps, the data can be routed through the PDI to the PCMMU, where it is made available to the general-purpose computers (GPC) for processing and on-board display. A payload specialist crew member may then interface directly with a specific experiment, as required. Medium-band scientific data is routed to the receiving ground terminal via either the S-band FM link or the Ku-band system, as follows:

(1) S-band FM:

	Analog:	300 Hz - 4 MHz
or		
	Digital:	200 bps - 5 Mbps NRZ-L, or 200 bps - 2 Mbps biphase-L

(2) Ku-band:

	Analog:	DC - 4.5 MHz BW
plus	Digital:	16 kbps - 1024 Mbps biphase-L
or		16 kbps - 2 Mbps NRZ-L, M or S.

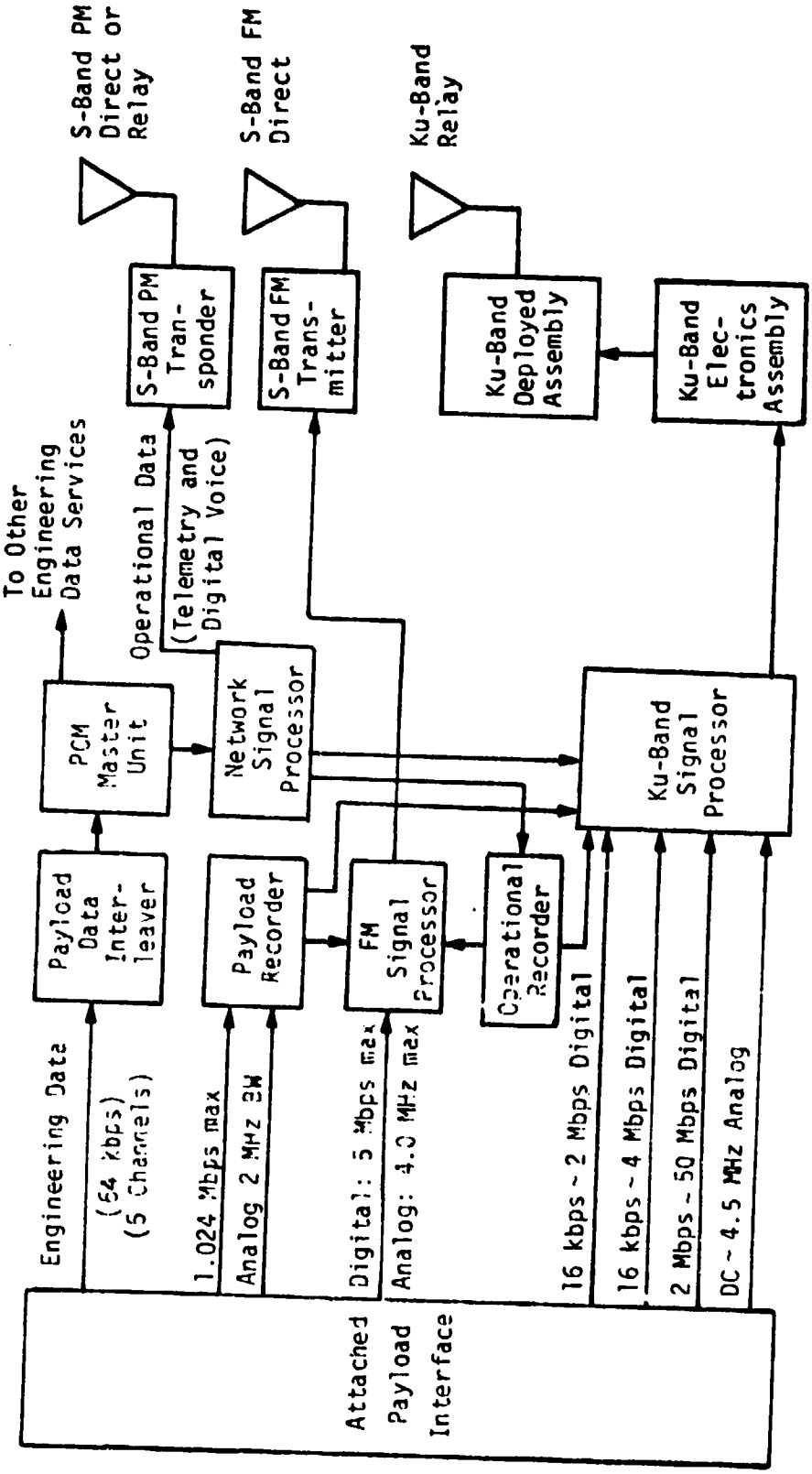

Figure 1. Attached Payload Scientific Data Interface

The Ku-band wideband analog channel input (DC - 4.5 MHz) can be used by the IUS or CIU for analog telemetry as a transparent throughput channel, which provides flexibility and minimum Orbiter processing. Capability is constrained only by the KuSP bandwidth.

Figure 2 depicts the Orbiter provisions for processing, displaying and downlinking systems status data from the IUS in support of monitoring and checkout functions. Data can be accessed by the Orbiter via one of five inputs to the PDI which makes specific parameters contained in the input PCM bit stream (0-64 kbps) available to the PCMMU for insertion into the operational instrumentation (OI) downlink and available to the GPC's for processing and display.

The PDI provides the capability to receive engineering data from up to five attached payloads simultaneously. The PDI then decommutates up to four of these inputs and provides time-tagged, time-homogeneous data from these four payloads simultaneously to the Orbiter data processing subsystem (DPS) for onboard display and/or transmission to the ground via OI downlink.

In order to provide the data processing service, the input data to the PDI must be in a standard format, as follows:

- Bits per word: 8
- Words per frame: 1024 max
- Subframe rate groups per frame: 4 max
- Words per subframe: 128 max
- Frame rate: 200 per second max
- Bits per frame synchronization: 8, or 16, or 24, or 32
- Process data rate: up to 64 kbps

The throughput data rate (composite PDI output to the PCMMU) is limited to 64 kbps maximum on-orbit and 5 kbps for ascent.

A capability to throughput data which is in nonstandard format, or other unique data such as encrypted data, is also provided by the PDI. In this mode, the frame synchronization circuitry is bypassed and artificial data blocks are established to transfer the data to the PCMMU. No onboard processing or display of the data is available when operating in the nonstandard mode.

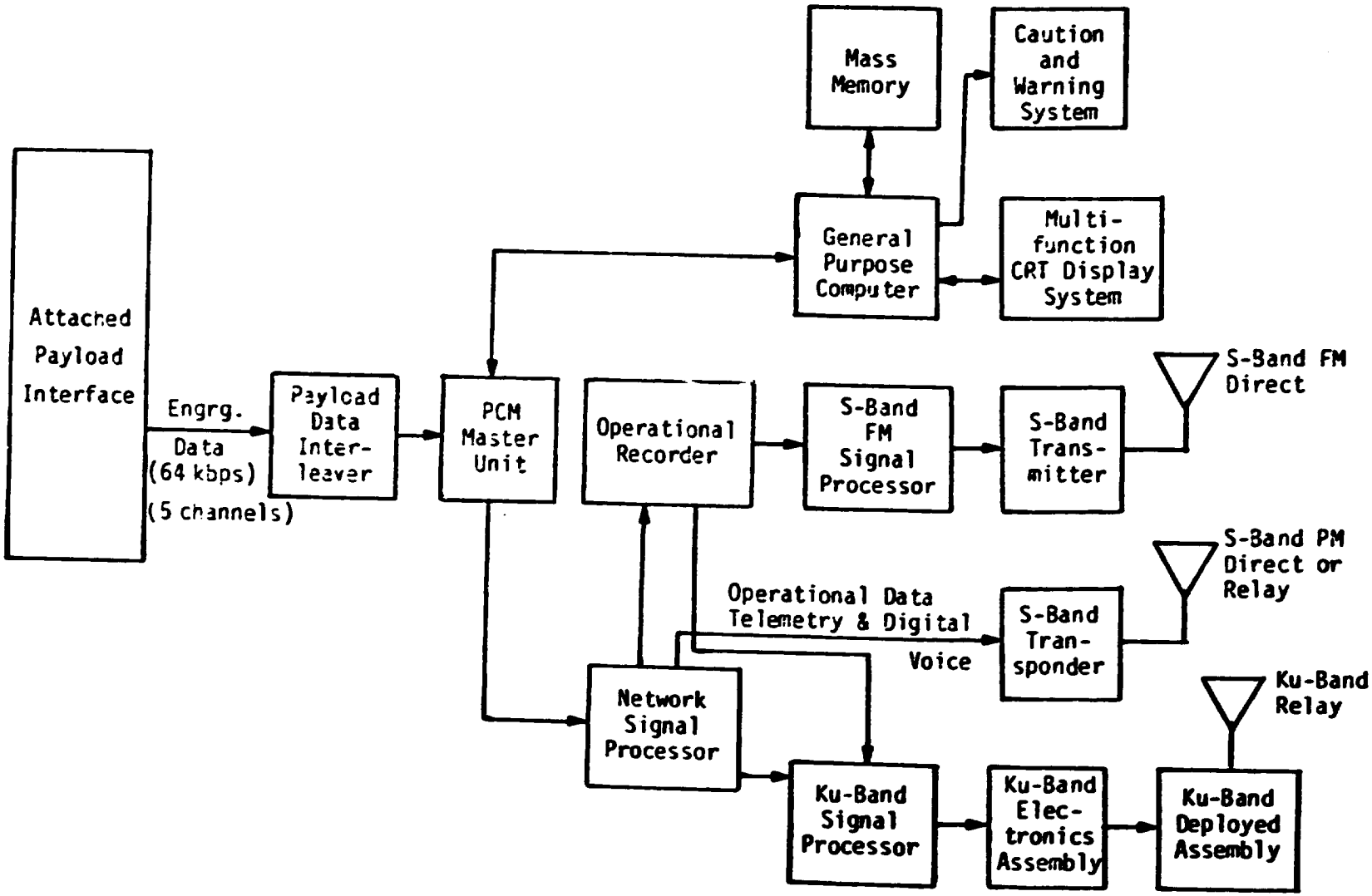

Figure 2. Attached Payload Engineering Data Interface

A capability for direct recording of certain types of payload data is provided. The payload recorder has 14 tracks which are capable of serial or parallel recording of digital and analog data. Data rates from 25.5 kbps to 1.024 Mbps and analog data of 1.9 kHz to 2 MHz may be recorded. A minimum record time of 56 minutes is provided at the maximum data rate. Simultaneous analog/digital parallel recording is limited to the first record pass. Subsequent passes are restricted to sequential single-channel digital record.

A total of 14 tape speeds (four per mission) are available and selectable by onboard or ground control.

Guidance, navigation and attitude control services are provided for the IUS by the CIU or PSP using the hard-line interface over which the Orbiter provides state vector update data words to the IUS. The CIU transmits the Orbiter state vector data to the IUS using the SGLS command format of ternary frequency-shift-keying (FSK) with "S" tones of 65 kHz, "0" tones of 76 kHz, and "1" tones of 95 kHz. The PSP transmits the Orbiter state vector data to the NASA IUS on a 16-kHz sine wave subcarrier at a binary command data rate of 2 kbps.

2.2 Detached IUS Communication

The basic low rate data-processing/display services provided for the attached IUS are also provided for detached or deployed IUS via S-band RF communications link between the Orbiter and IUS. Figure 3 shows the interfacing hardware that supports this link. Note that, when a spacecraft is launched by the IUS, as shown in Figure 3, the spacecraft communicates only in the attached mode through the IUS. Also note that the PI cannot communicate with the IUS and the spacecraft simultaneously.

The Orbiter S-band transceiver (PI) supporting RF communications with detached payloads is compatible frequency-wise with STDN, SGLS, and DSN-compatible payloads--capable of operating at approximately 850 selectable frequencies in the 2200-2300 MHz range.

Telemetry signals in the Orbiter standard mode of operation are routed from the PI, after carrier demodulation, to the PSP or CIU, where the data is demodulated off of a 1.024 MHz subcarrier (and a 1.7 MHz subcarrier by the CIU). The data is then routed to the PDI/PCMMU/GPC for decommutation processing, display and downlinking in the same manner as the attached IUS or payload.

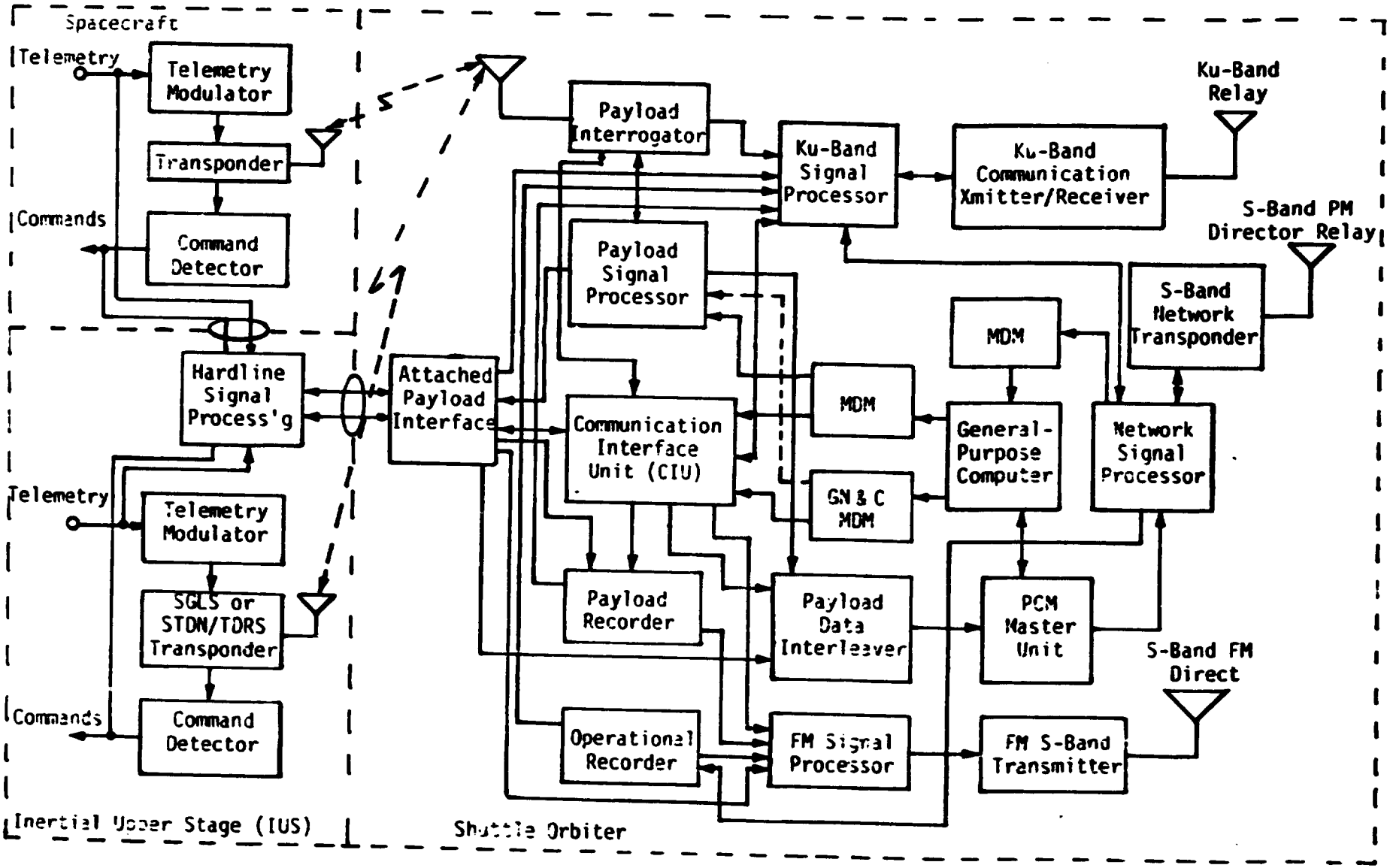

Figure 3. Inertial Upper Stage/Shuttle Orbiter Subsystems and Interfaces

Data rates that can be accommodated by the PSP in the standard mode are 16, 8, 4, 2 and 1 kbps. Processing the 16 kbps may be provided by the CIU located at the payload station in the aft flight deck for DOD missions. In this mode, the PSP is bypassed. The PSP is being designed to accommodate any one of six PCM code formats in the standard mode (biphase-L, M, S and NRZ-L, M, S).

The Orbiter standard mode of operation was selected to provide a degree of flexibility of operation while minimizing basic Orbiter hardware costs. Payloads that ultimately fly on the Orbiter which are incompatible with the standard in terms of data rate or subcarrier frequency will be accommodated in a transparent throughput fashion using a "bent-pipe" mode of operation. In this mode, the interrogator output, following carrier demodulation, is routed to the KuSP 4.5 MHz analog input channel or the 2 Mbps digital channel. These inputs are essentially limited only by the respective bandwidths and are capable of a wide range of data rate/subcarrier options (the 2 Mbps channel is limited to one subcarrier). Unique demodulation hardware at either the Ku-band ground station or the payload operation center currently must be provided by the payload requiring bent-pipe service. The bent-pipe channels are available for use by one detached payload at a time with the following capabilities:

- Digital data from 2 kbps to 2 Mbps, or
- Analog data from 2 kHz to 2 MHz, or
- Digital data from 16 kbps to 4 Mbps, or
- Analog data from DC to 4.5 MHz.

No onboard processing or display of data is available when operating in the bent-pipe mode.

2.3 End-to-End Communication Link Definitions

In both the DOD and NASA IUS configurations, multiple signal paths exist through which the IUS can be commanded and from which IUS telemetry may be received. Before attempting to specify any IUS communications equipment test requirements, all signal paths must be identified. This will be done by separating the command paths into the DOD and NASA configurations and further subdividing into RF and hard-line paths. The same will be done for the telemetry paths.

2.3.1 SGLS Command Signal Flow (DOD Mode)

The SGLS commanding of the IUS is presented in Figure 4. The various functional command signal paths are illustrated from the SCF ground station and CIU control panel. In the attached mode, commands from the SCF can be transmitted to the Orbiter using either the TDRS ground station to relay the commands via the TDRS over the Ku-band or S-band, or the direct S-band link from the SCF ground station to the S-band network transponder. On-board commands are entered using the CIU control panel.

In terms of redundant command paths, note that the S-band network transponder and the NSP are completely redundant. Also, commands can be sent from the KuSP to the two NSP's or directly to the CIU, but note that the Ku-band system is not redundant. From each NSP, commands are sent to the GPC using MDM's but, from the GPC to the CIU, there is only a single MDM path. Thus, with only the S-band network equipment, the MDM to CIU is a single-point failure that would eliminate the capability of transmitting commands to the IUS from the ground through the Orbiter.

During the first IUS flight(s) before the TDRS is operational, the Ku-band system will not be available to provide a redundant command path through the Orbiter to the IUS. The only way commands can be transmitted from the ground to the IUS is via the SCF ground station directly to the IUS in the payload bay.

When the IUS is in the payload bay, the Orbiter may have to maneuver so that the line-of-sight (LOS) from the SCF ground station to the IUS antennas is not blocked by the Orbiter. In some cases, the IUS will have to be raised on the cradle in order to assure that the LOS is not blocked by the Orbiter.

Another way to command the IUS is with crew-generated commands using the CIU control panel. A failure in the KGT-60 would eliminate the possibility of ENCRYPTED commands from the control panel. A failure in the CIU FSK/AM modulator or I/O driver and selector would eliminate all command signal paths through the Orbiter and the direct RF link from the SCF to the IUS described in the previous paragraph would have to be used.

In the attached mode, the CIU can command the IUS directly (hardline) or by using the PI for RF communications even though the IUS is still in the payload bay. In the detached mode, the CIU sends its commands through one of two redundant PI's.

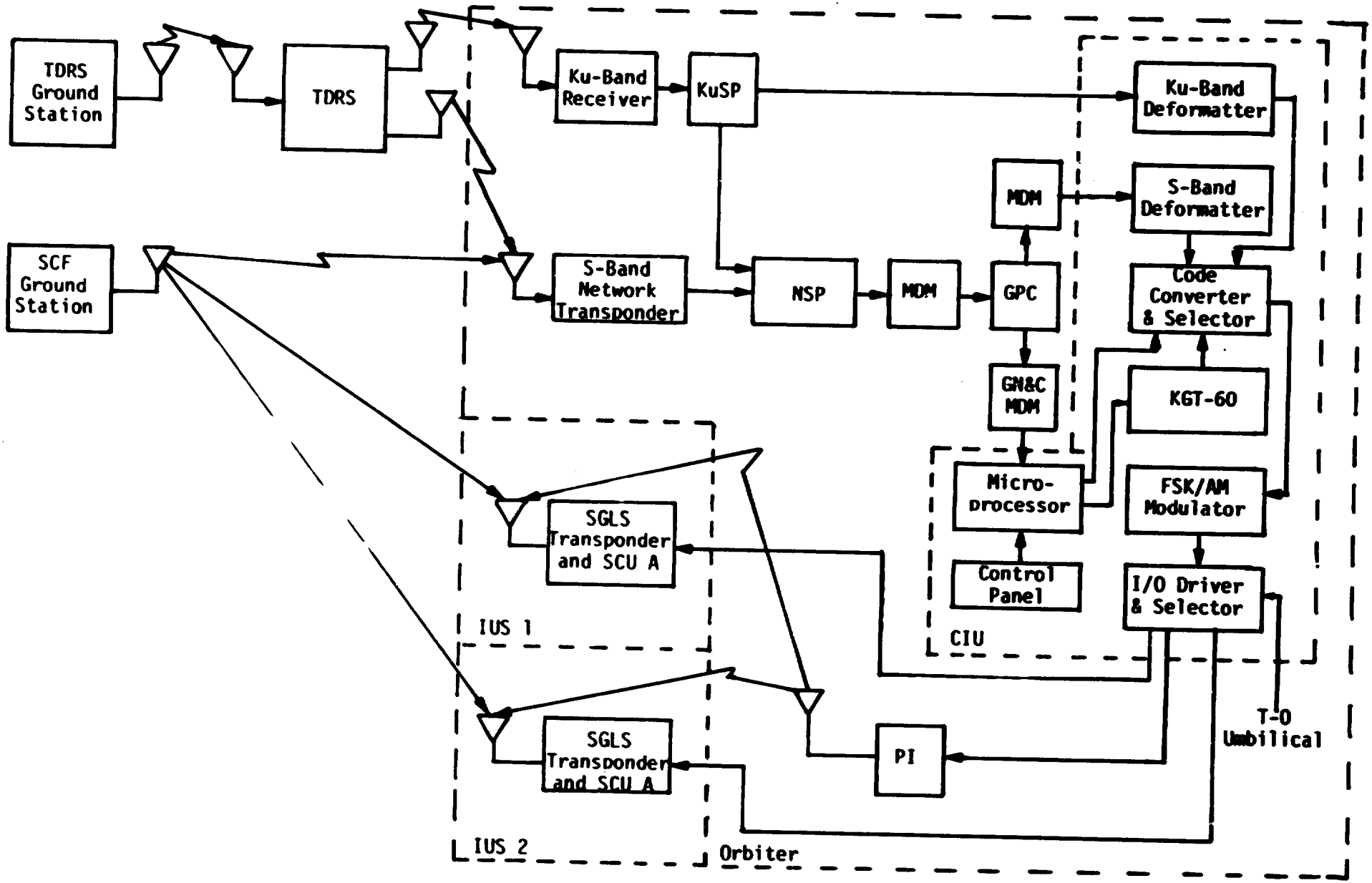

Figure 4. Functional SGLS Command Signal Flow (DOD Mode)

Figures 1-15 in Addendum A show each of the separate end-to-end communications paths for the DOD or SGLS commands. There are 15 separate paths over which the DOD IUS may be commanded and, while a number of elements are common in each path, notice that each path is distinctly different.

2.3.2 STDN/TDRS Command Signal Flow (NASA Mode)

The NASA IUS employs STDN/TDRS transponders. The functional command signal flow for the NAS IUS is shown in Figure 5. Note that the Orbiter command signal flow is completely redundant, with only a single string, using the Ku-band system. But in case of a failure in the Ku-band system, there is still a fully redundant S-band system as backup. Therefore, any single failure in the Orbiter communication system would not affect the command signal flow. Also note that the IUS can be commanded from the GSTDN directly or from the TDRS station via the TDRS while the IUS is in the payload bay and still attached. Again, however, the Orbiter may have to maneuver so that the LOS from the GSTDN or TDRS to the IUS antennas is not blocked by the Orbiter. The maneuvers required of the Orbiter will be less demanding for the NASA IUS than the DOD IUS because of the greater coverage of the TDRS. In come cases, however, the IUS still might have to be raised on the cradle in order to make sure that the LOS is not blocked by the Orbiter.

Crew-generated commands to the IUS are via the GPC. In Figure 5, the payload station control panel is shown as a way to enter commands into the GPC and then into the PSP for transmission to the IUS. While a single MDM is shown from the payload station control panel to the GPC, there are several redundant keyboards with MDM that would allow the entering of commands into the GPC.

Figures 1-12 in Addendum B show each separate end-to-end communications path for the NASA or STDN/TDRS commands. There are 12 separate paths over which the NASA IUS may be commanded whereas there were 15 separate paths for the DOD IUS. As previously mentioned, each path has a number of common elements but each path is distinctly different.

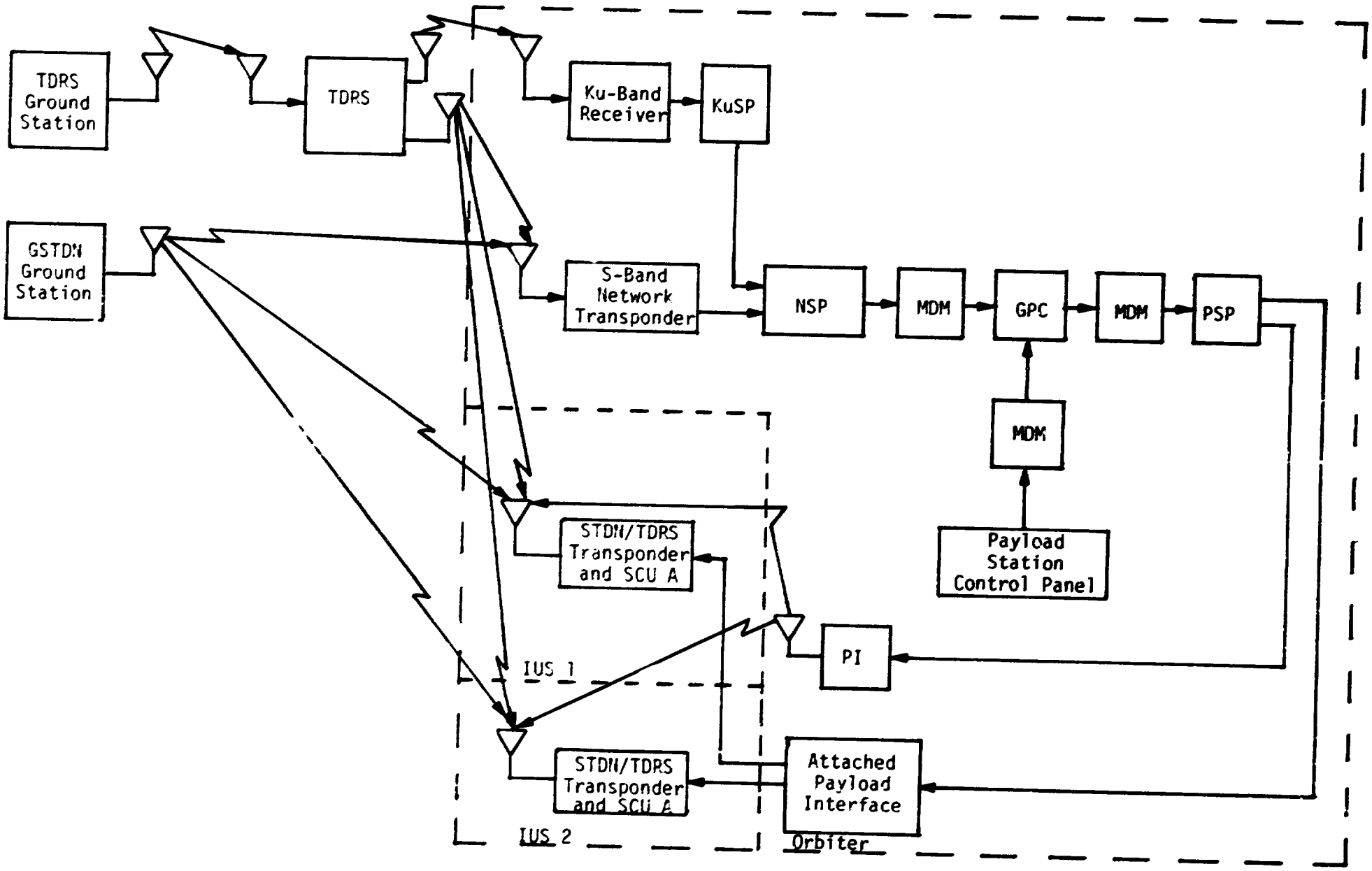

Figure 5. Functional STDN/TDRS IUS Command Signal Flow (NASA Mode)

2.3.3 SGLS Telemetry Signal Flow (DOD Mode)

The SGLS telemetry functional signal flow is presented in Figure 6. In the attached mode, IUS telemetry comes from three sources: (1) the Signal Interface Unit (SIU), (2) the Environmental Measurement Unit (EMU) and, (3) the Wideband Data Interleaver (WBDI). Note that each of these telemtry sources is nonredundant; so if one of these units fails, that portion of the telemetry is lost. The SIU provides switching from the two IUS computers to the one SGLS transponder and also provides proper interfacing with the encrypter for the ENCRYPTED TEXT mode.

The FM vibration data consists of three sensors mounted on the spacecraft interface ring. Their analog output is signal conditioned to modulate three standard subcarriers in the EMU. The three subcarriers are summed together and cabled directly to the attached payload interface and the transponder 1.7 MHz input port.

The WBDI interleaves up to six separate channels of asynchronous NRZ-L telemetry data. The WBDI output is serial NRZ-L data at a rate of 256 kbps.

As shown in Figure 6, the output of the attached payload interface is (1) EMU data from one of two IUS's sent to the CIU for selection to the Payload Recorder (PR), (2) WBDI data from one of two IUS's sent to the CIU for NRZ-L to biphase-L conversion and selection to the KuSP, FMSP and PR and, (3) SIU data from both IUS's (labeled IUS 1 and IUS 2 data in Figure 6) sent to the CIU for selection to the PDI or after NRZ-L to biphase-L conversion to the KuSP, FMSP and PR. If the NRZ-L to biphase-L convertor or selector for the WBDI fails, the WBDI data cannot be transmitted or recorded. If the selector between IUS 1 and IUS 2 data fails, this telemetry cannot be processed through the Orbiter. However, if the NRZ-L to biphase-L convertor used for this data failed, the data would still be sent to the PDI for downlinking. Also, the data from the SIU (IUS 1 or 2) can be transmitted directly to the SCF ground station with the restriction(s) on Orbiter maneuvers described in connection with the command data signal flow. It should be noted that, even in the attached mode, the SIU and EMU data are available by using the RF link from the SGLS transponder to the Orbiter PI.

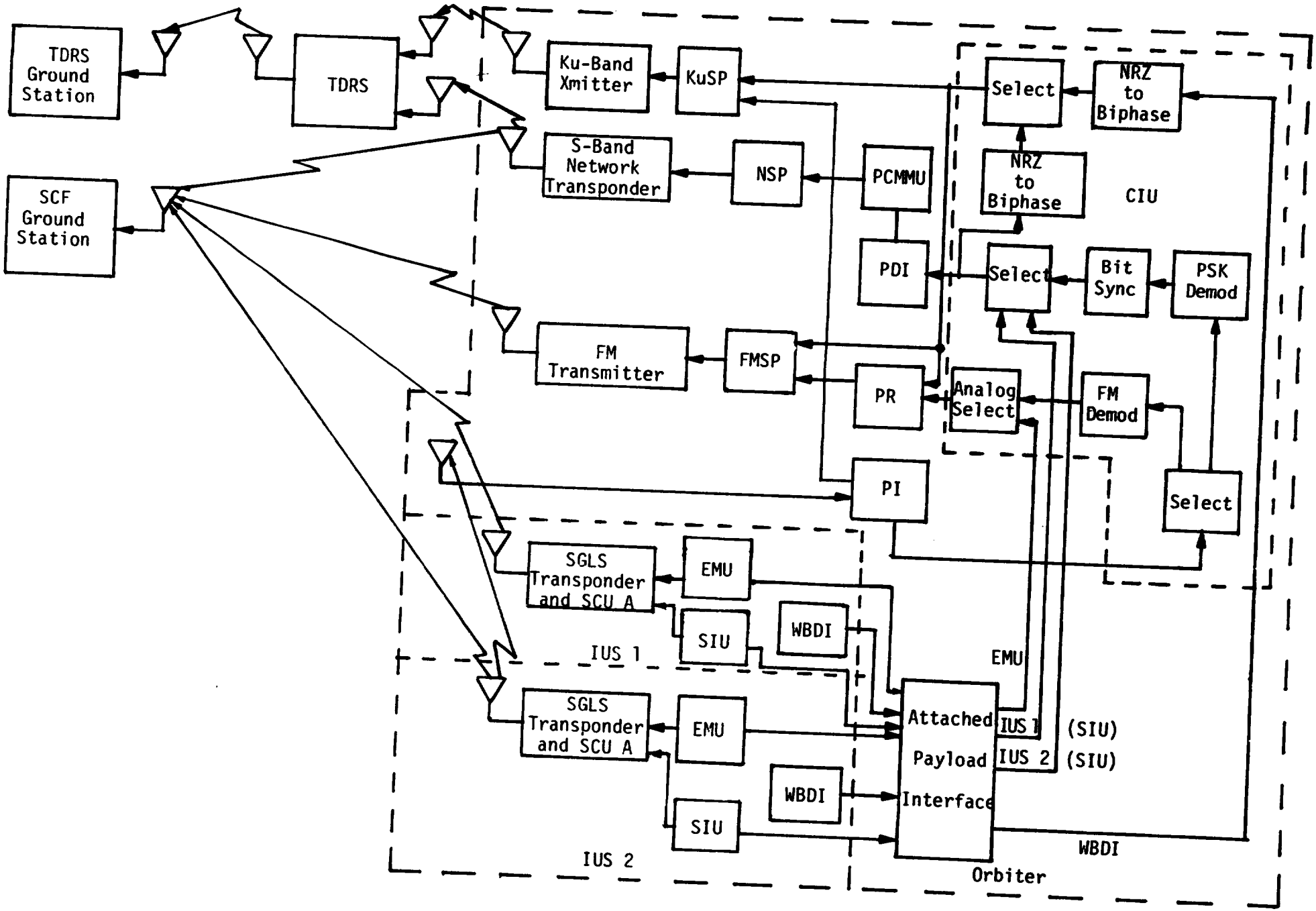

Figure 6. Functional SGLS Telemetry Signal Flow (DOD Mode)

In the detached mode, the telemetry can be received by the Orbiter via the PI or by the SCF ground station via a direct RF link. On the Orbiter, the output of one of the two PI's is selected for demodulation. If the selector fails, the Orbiter cannot process telemetry data in the detached mode. Also, following selection between the two PI's, the FM demodulator and PSK demodulator are not redundant so, if either fails, either the EMU or SIU data is not recovered by the Orbiter.

The bit synchronizer following the PSK demodulator is implemented partially in hardware and partially in software. Here again, if the hardware portion of the bit synchronizer fails, the SIU data is not processed by the Orbiter. If the software portion of the bit syncrhonizer fails because of a microprocessor failure, the whole CIU will probably not function. Once the telemetry data is processed by the CIU up to the output selector, the commands on the attached mode in terms of the result of failures in the CIU apply to the detached mode.

Following telemetry processing by the CIU, the only nonredundant Orbiter subsystems are the PDI, PCMMU and PR. Failure of the PR means that no EMU data will be available for transmission to the SCF ground station via the S-band FM link. The PDI and PCMMU are internally redundant, and the only failure that would disable the PDI is one of the input switch matrix. Alternate paths, however, (i.e., KuSP, FMSP and PR) for the same data sent to the PDI are used to provide redundancy such that a single failure in the Orbiter subsystems other than the CIU will not cause loss of telemetry data.

The telemetry data has several RF paths available to the ground. Using the Ku-band system, the telemetry data is transmitted via the TDRS to the TDRS ground station. Using the S-band network transponder, the telemetry data can be transmitted via either TDRS to the TDRS ground station or directly to the SCF ground station. Finally, using the S-band FM transmitter, the telemetry data is transmitted directly to the SCF ground station.

Figures 1-14 in Addendum C show each separate end-to-end communications path for the DOD or SGLS telemetry. There are 14 separate paths over which telemetry may be received from the DOD IUS.

2.3.4 STDN/TDRS Telemetry Signal Flow (NASA Mode)

The telemetry functional signal flow for the NASA IUS is shown in Figure 7. Note that the Orbiter telemetry signal flow is completely redundant except for the PDI, PCMMU and PR. Failures in these subsystems have exactly the same impacts as those discussed for the SGLS telemetry; however, alternate paths (i.e., KuSP and FMSP) for the same data provide redundancy for these subsystems as well. Therefore, in the attached mode, there are no single failures in the Orbiter that would cause loss of the telemetry data. The only way that portions of the telemetry data could be lost in the attached mode is failure of the telemetry sources (i.e., SIU, EMU and WBDI) on the IUS. In the detached mode, the telemetry could be lost if there were a failure in the baseline single-string transponder.

Another area of concern in the detached mode is that the EMU data is modulated on the 1.7 MHz subcarrier; the PSP, however, cannot demodulate FM data. Thus, if the EMU data is to be presented by the Orbiter in the detached mode, the CIU must be used with the PSP bypassed. Since the STDN/TDRS transponder expects command data from the PSP on a 16 kHz subcarrier, the PSP cannot be turned off (bypassed) unless command data transmission and telemetry processing are not to be performed simultaneously. Without the sequential use of the PSP and CIU, the only way the EMU data can be processed is at the ground station via the TDRS or direct RF transmission to the GSTDN.

The telemetry data has several RF paths to the ground. As was mentioned previously, the NASA IUS can transmit telemetry in the TDRS mode via the TDRS to the TDRS ground station or in the STDN mode directly to the GSTDN ground station. When the telemetry data is processed by the Orbiter, the telemetry data can be transmitted via the TDRS using either the Ku-band system or the S-band network transponder. Alternately, the Orbiter can transmit the data directly to the GSTDN ground station using either the S-band network transponder or the FM transmitter.

Figures 1-16 in Addendum D show each separate end-to-end communications path for the NASA or STDN/TDRS telemetry. There are 16 separate paths over which telemetry may be received from the NASA IUS whereas there were 14 separate paths over which telemetry could be received from the DOD IUS. Again note that, while the paths contain common elements, each path, from an end-to-end point of view, is unique.

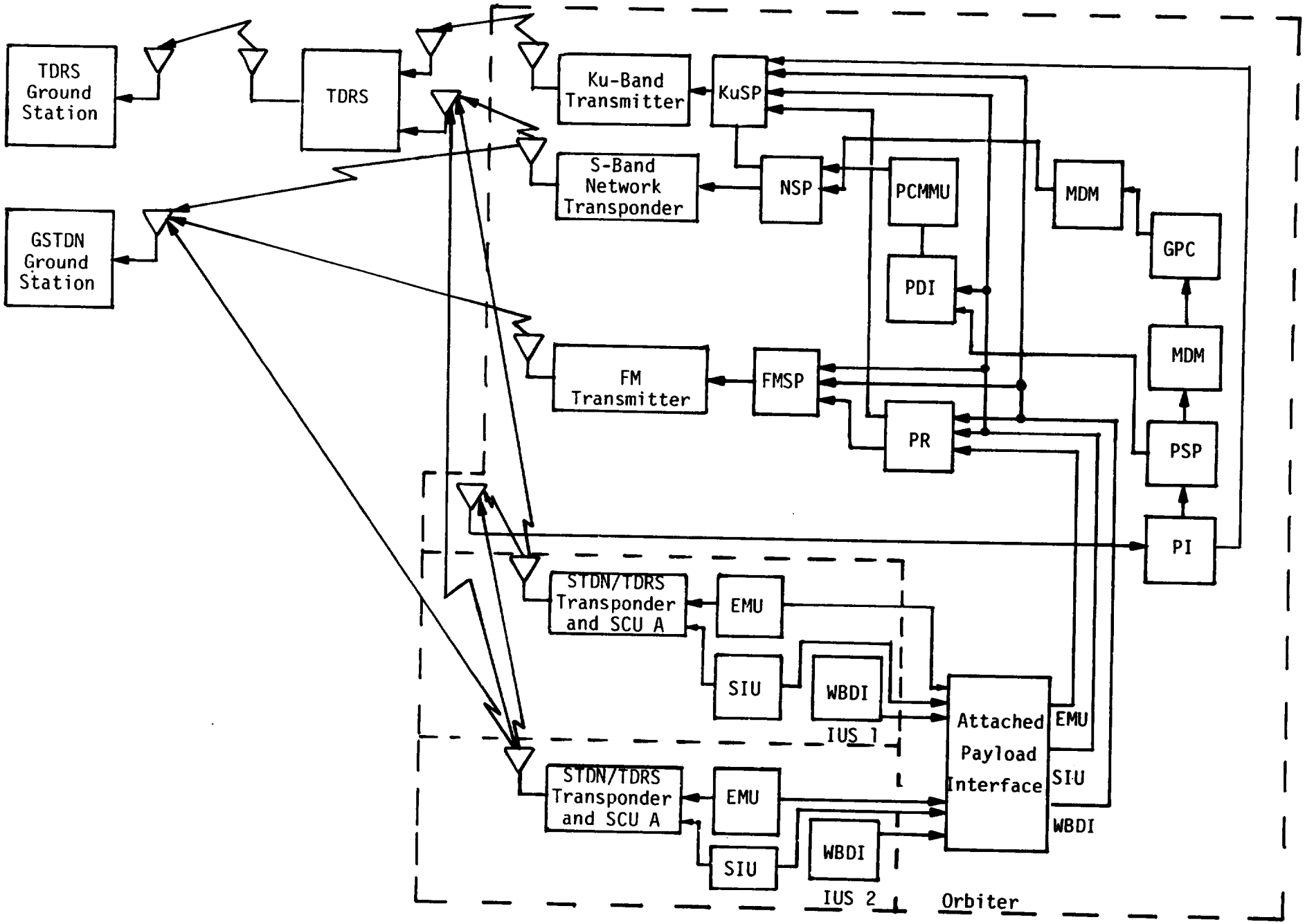

Figure 7. Functional STDN/TDRS Telemetry Signal Flow (NASA Mode)

3.0 TEST CONFIGURATION DESCRIPTION

In this section, the overall test philosophy will be described, the required test links developed and a general description of the ESTL discussed. Also, any special test equipment will be outlined.

3.1 Testing Philosophy

In the previous section, all of the end-to-end signal paths were defined. Since there are 57 different end-to-end signal routes, testing all the command and telemetry paths would be extremely time-consuming, redundant and expensive. There are segments of these paths, however, that are being or will be tested under separate test plans. For example, there are ESTL verification test procedures being implemented for the S-band network transponder direct DOD and NASA links which include the ground stations, S-band transponder and the NSP.

By comparing those link segments which are or should be tested under separate test plans with the total end-to-end signal paths, only those unverified link segments remaining need to be discussed in this test plan. In making these correlations, any "holes" in the testing program are apparent and, at the same time, the amount of testing redundancy is minimized. To start comparing one link segment to another, the overall signal path must be separated into easily quantifiable sections.

From an end-to-end link point of view, the Orbiter and IUS communications system is essentially composed of modular equipment serially connected. For example, a command may be sent from a ground station to the Orbiter S-band network transponder, processed through a number of Orbiter modules or line replaceable units (LRU's) such as the NSP, and retransmitted by the PI LRU to the IUS, where the command is received and decoded through another series of modules.

Conceptually, an end-to-end communications link may be characterized as a series of modules as represented by triangles 1-5 shown in Figure 8(a). Assume that link segment I, as represented by the circled triangles 1-3 shown in Figure 8(b), was tested or will be tested as part of another test plan. The link characteristics of segment I will then have been quantified, and the link will perform adequately up to and including the module or LRU 3. In testing the remaining link segment composed of

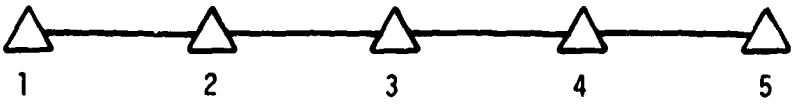

(a) Conceptual End-to-End Communication Link

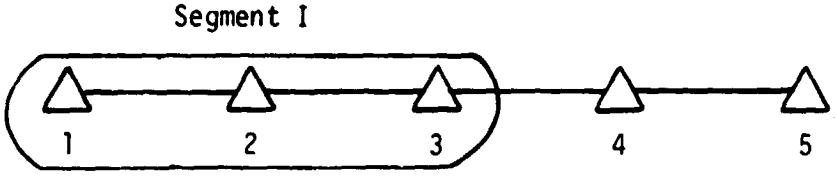

(b) Link Segment Tested Under Another Test Plan

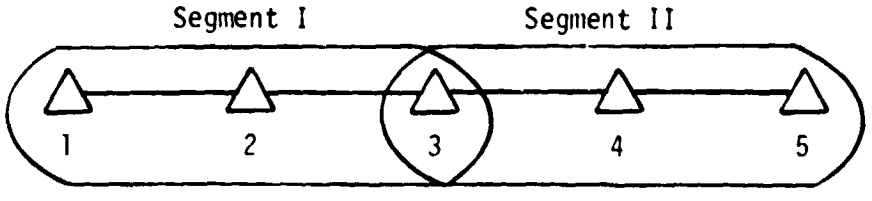

(c) Total Link Test as Tested Under Two Separate Test Plans

△ = Modular Equipment or LRU's

Figure 8. Conceptual End-to-End Communications Link

modules or LRU's 4 and 5, if there is at least one LRU overlap, as shown in Figure 8(c), both segments have a common LRU which, itself, has been quantified through acceptance and qualification testing.

The basic philosophy of this test plan, therefore, is to test only those signal path segments which will not be tested under separate test plans. To have confidence that the overall link will meet mission objectives when the segments have been tested separately, some redundancy or LRU overlap in the testing program is necessary.

The one LRU overlap philosophy is applied to the NASA mode commands and telemetry; the philosophy is modified somewhat, however, for the DOD mode. All the Orbiter communication LRU's such as the PI, PR, NSP, etc., are under the direct control of the Orbiter contractor, Rockwell International (RI), where RI is responsible for performance and interface compatibility. The only exception is the CIU, which is under the control of the IUS contractor--the Boeing Company. Just as a redundant verification, any tests with the CIU will include the CIU plus at least an RI-controlled LRU. For example, the CIU output may interface with the PR, so the PR would be included in the test link.

Since this plan addresses only the IUS/Orbiter links, direct IUS/ground links should be covered in a separate test plan. Also, only telemetry linked <u>through</u> the IUS will be tested under this plan. Any direct payload/Orbiter communications and, similarly, any direct payload/ground communications will not be discussed.

The test philosophy used in this plan may be summarized as follows:

- Only IUS/Orbiter links will be tested
- Only those IUS/Orbiter link segments not addressed in other test plans will be discussed
- Test link segments will include at least one LRU which has been tested as part of another test plan
- Test links which include the CIU will also include at least one RI LRU past the CIU output.

3.2 SGLS Command Test Links (DOD Mode)

The 15 separate end-to-end DOD or SGLS command signal paths shown in Figures 1-15 in Addendum A may be reduced to four test links. Since part of the testing philosophy is to verify that the CIU functions properly with other Orbiter communication LRU's, two of the four test links are one-time tests.

The test link shown in Figure 9 verifies the interface between the general-purpose computer (GPC) and the CIU and, similarly, the test link shown in Figure 10 verifies the interface between the KuSP and the CIU. Both of the test links in Figures 9 and 10 are one-time-only tests. After the interfaces are verified, the majority of the link verification may be performed by injecting the command signals directly into the CIU, as shown in Figure 11. Figure 12 simply verifies the hard-line interface.

3.3 STDN/TDRS Command Test Links (NASA Mode)

The 12 separate end-to-end NASA or STDN/TDRS command signal paths shown in Figures 1-12 in Addendum B may be reduced to two test links.

The test link shown in Figure 13 verifies the NASA command link by injecting the commands into the PSP. The PSP is included in this test link since the command data at this point is an easily generated baseband digital signal. The test link shown in Figure 14 verifies the hard-line interface in the same manner as with the DOD or SGLS commands.

3.4 SGLS Telemetry Test Links (DOD Mode)

The 14 separate end-to-end DOD or SGLS telemetry paths shown in Figures 1-14 in Addendum C may now be reduced to seven test links. Figures 15, 16 and 17 are the RF telemetry links. Since the CIU output characteristics are different for the KuSP, FMSP and PDI, all three need to be tested with the CIU, as shown in Figure 15. Figure 16 shows the addition of the EMU data which is recorded by the PR.

The CIU is capable of handling an SIU data rate of only 16 kbps on the RF link. Figure 17 shows the "bent-pipe" mode, where different data rates may be handled.

There is a variety of data transmitted from the IUS to the Orbiter via the hard-line interface. Figures 18-20 show the test links required to verify the various types of hard-line interface data.

3.5 STDN/TDRS Telemetry Test Links (NASA Mode)

The 16 separate end-to-end NASA or STDN/TDRS telemetry signal paths shown in Figures 1-16 in Addendum D may be reduced to six test links.

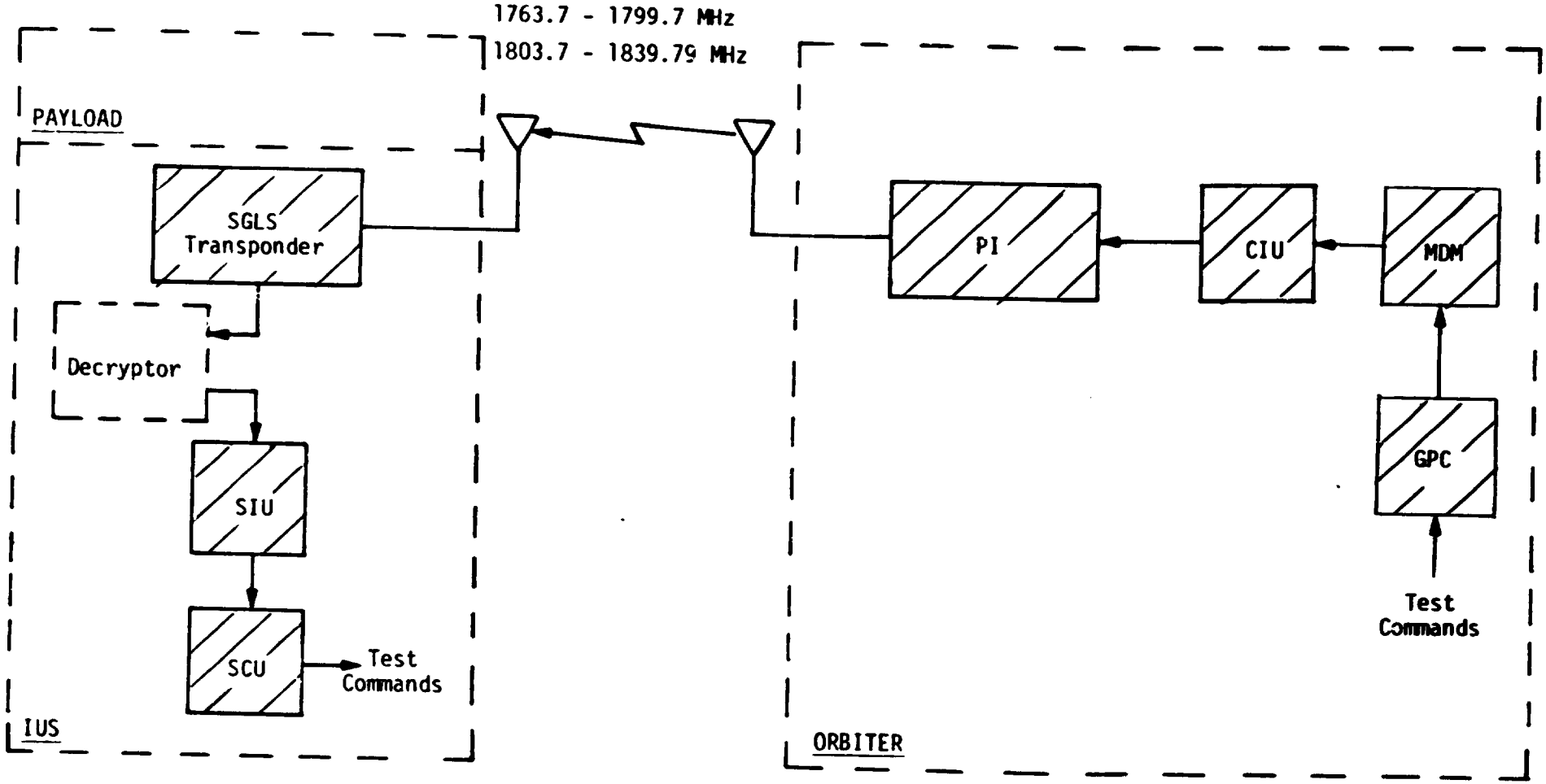

Figure 9. Attached/Detached IUS Command RF ESTL Test Link
SGLS Commands (DOD Mode)

(One-time test)

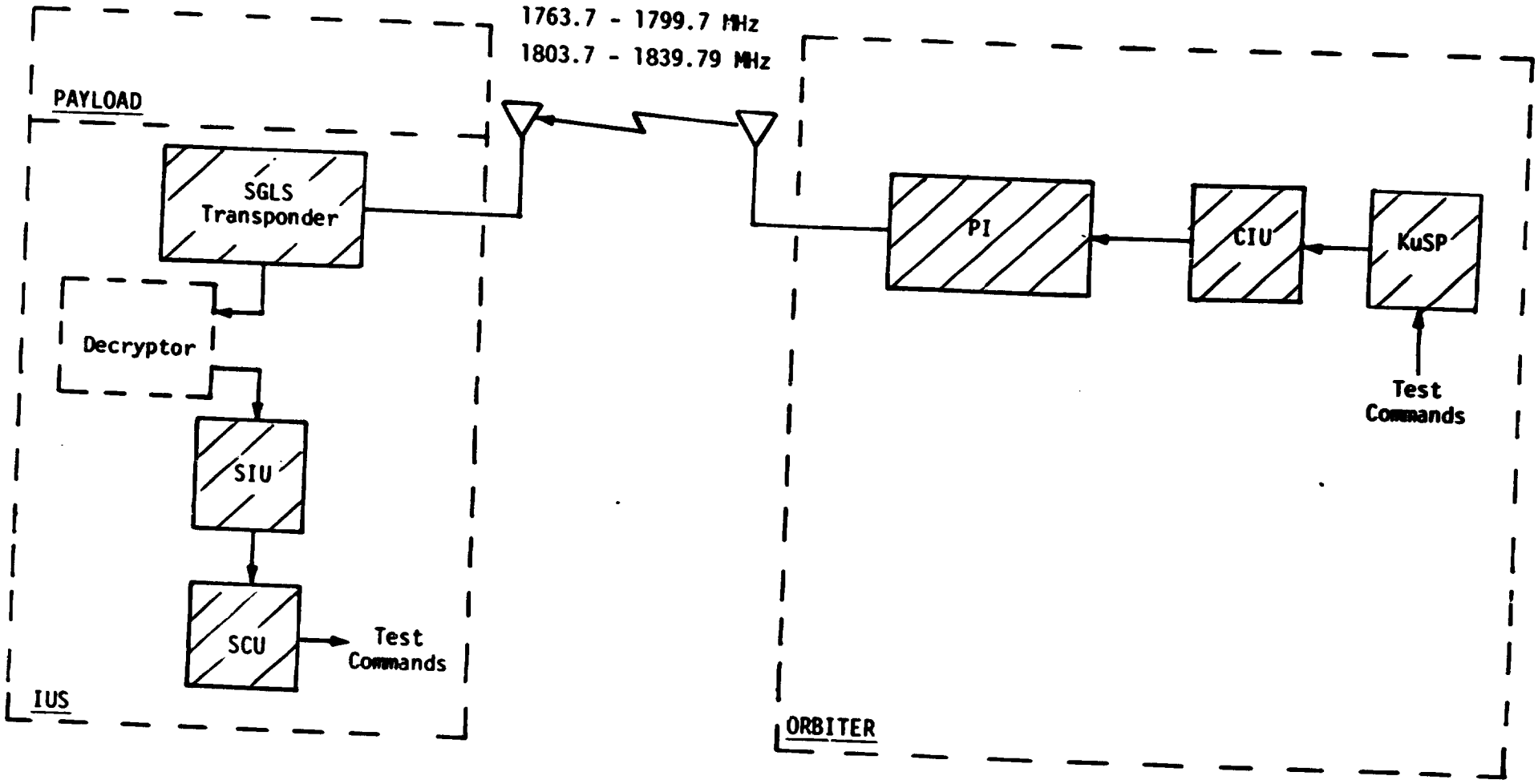

Figure 10. Attached/Detached IUS Command RF ESTL Test Link SGLS Commands (DOD Mode)

(One-time test)

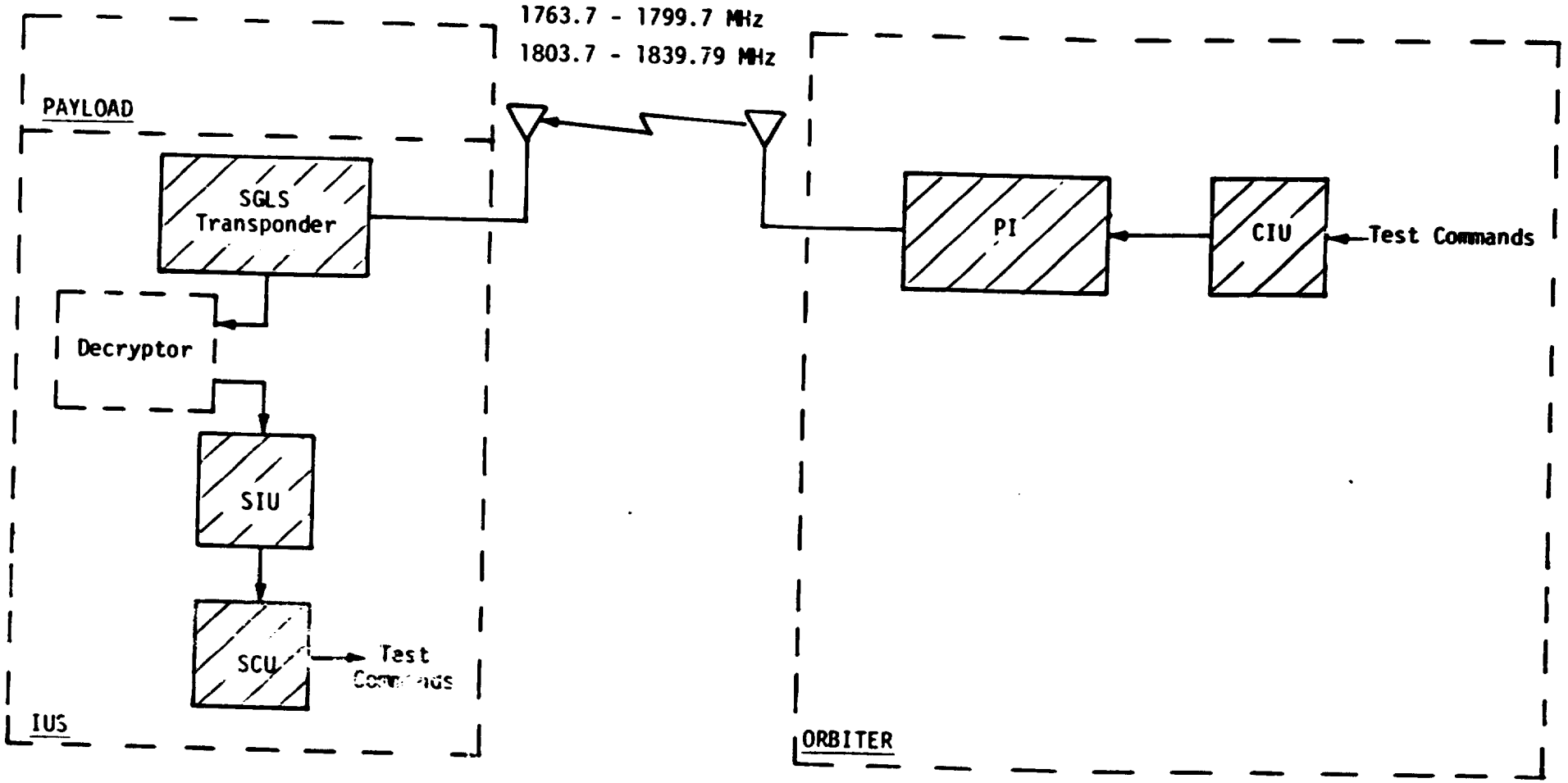

Figure 11. Attached/Detached IUS Command RF ESTL Test Link SGLS Commands (DOD Mode)

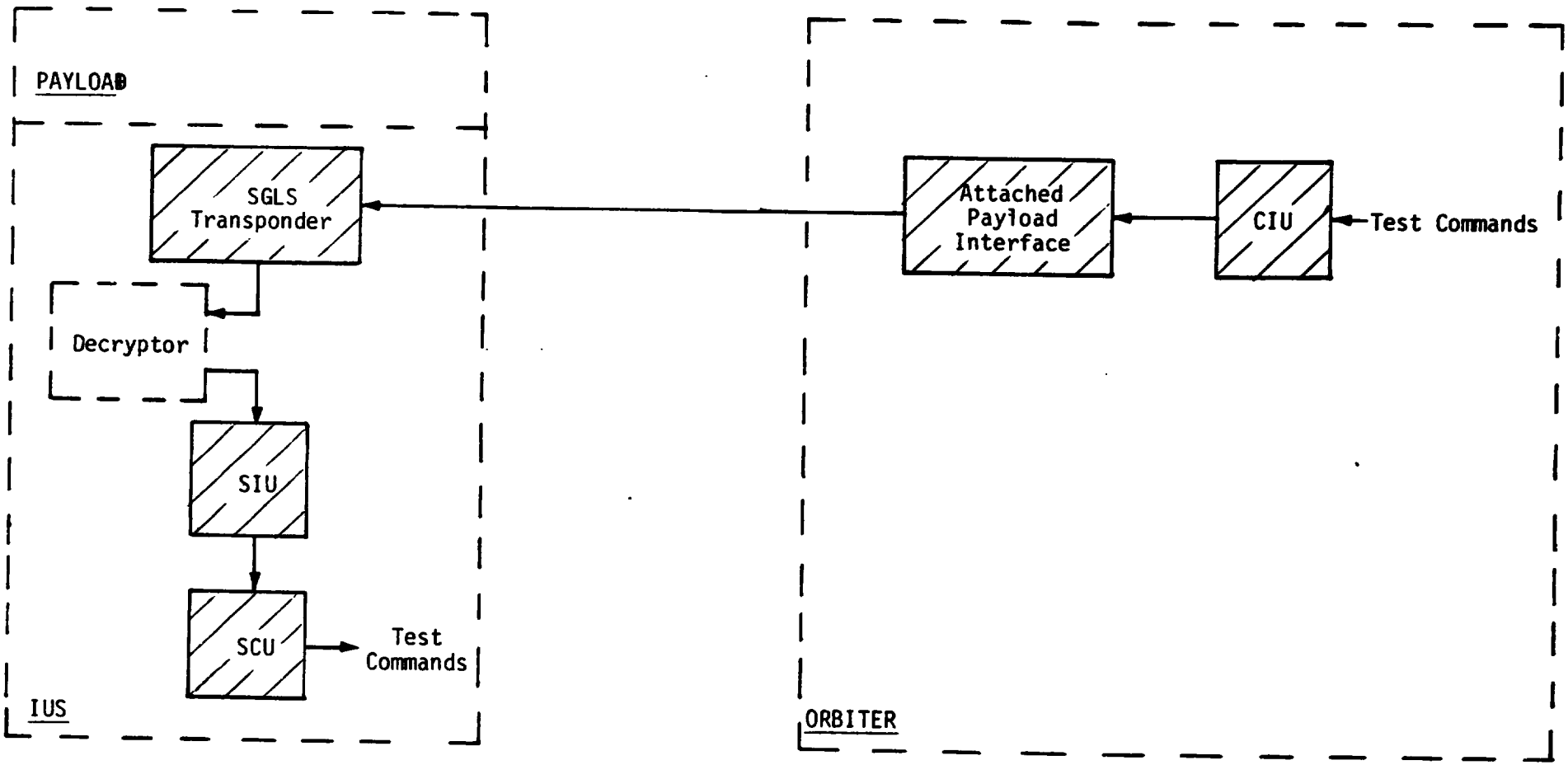

Figure 12. Attached IUS Command Hard-Line ESTL Test Link SGLS Commands (DOD Mode)

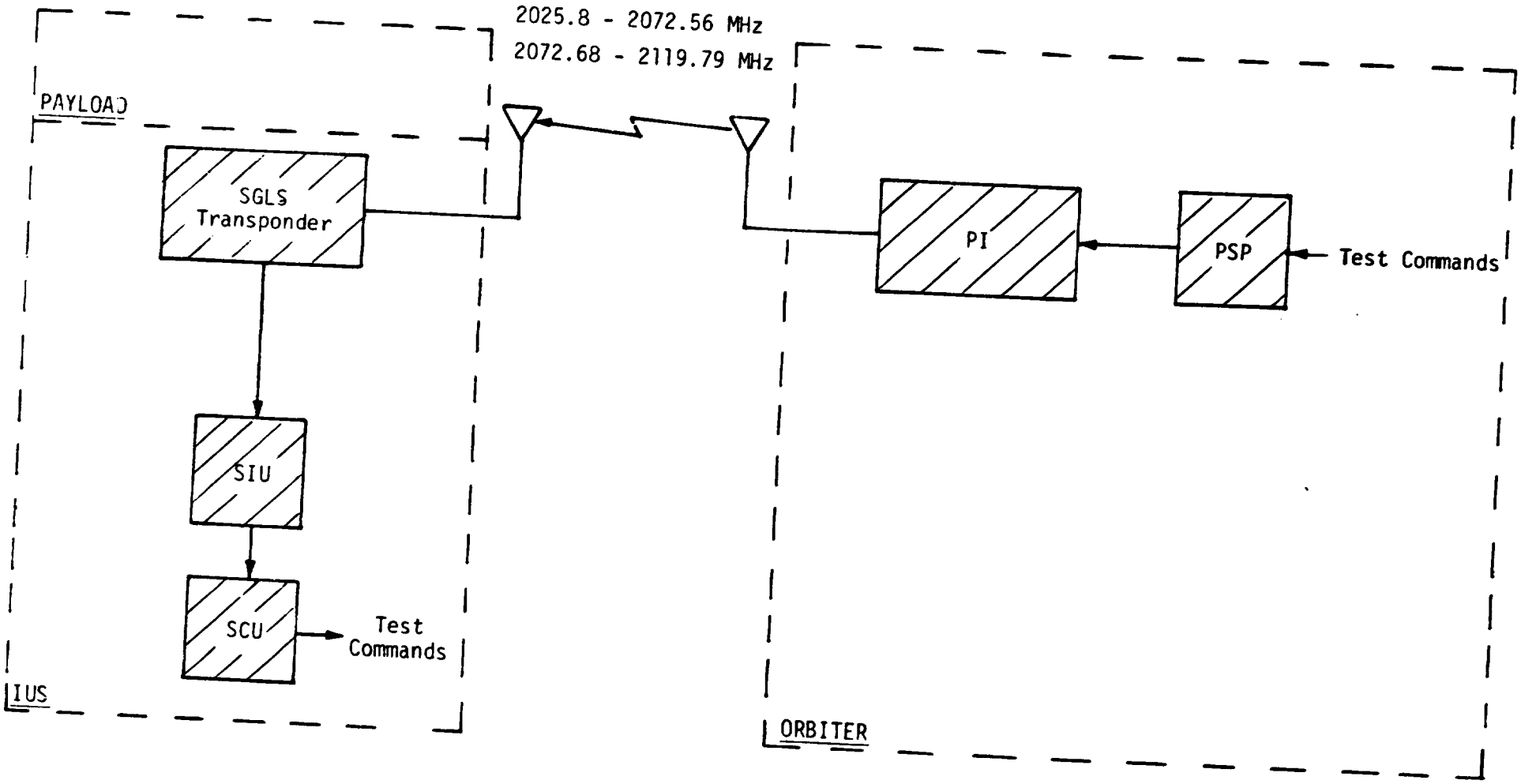

Figure 13. Attached/Detached IUS Command RF ESTL Test Link STDN/TDRS Commands (NASA Mode)

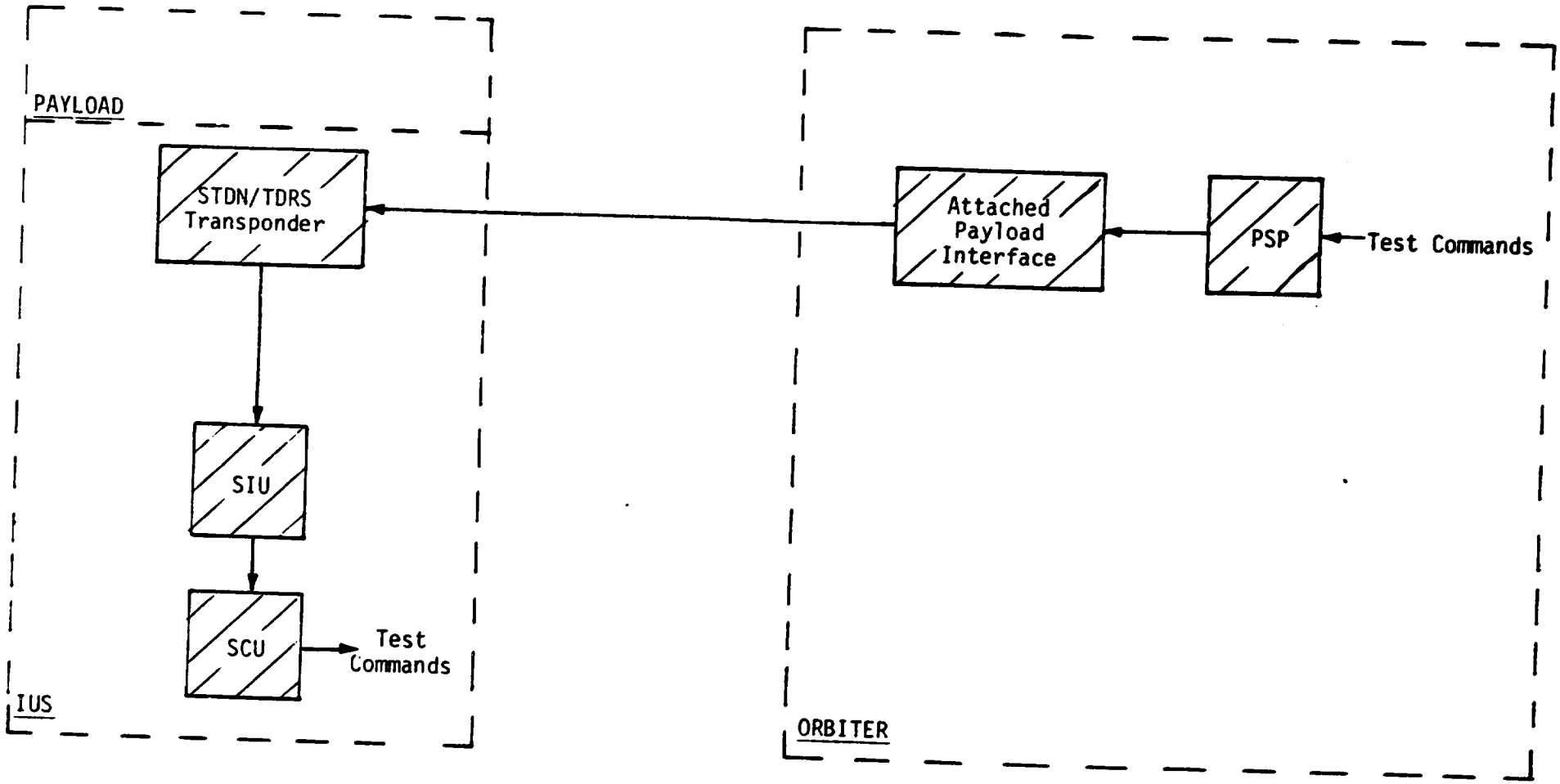

Figure 14. Attached IUS Command Hard-Line ESTL Test Link STDN/TDRS Commands (NASA Mode)

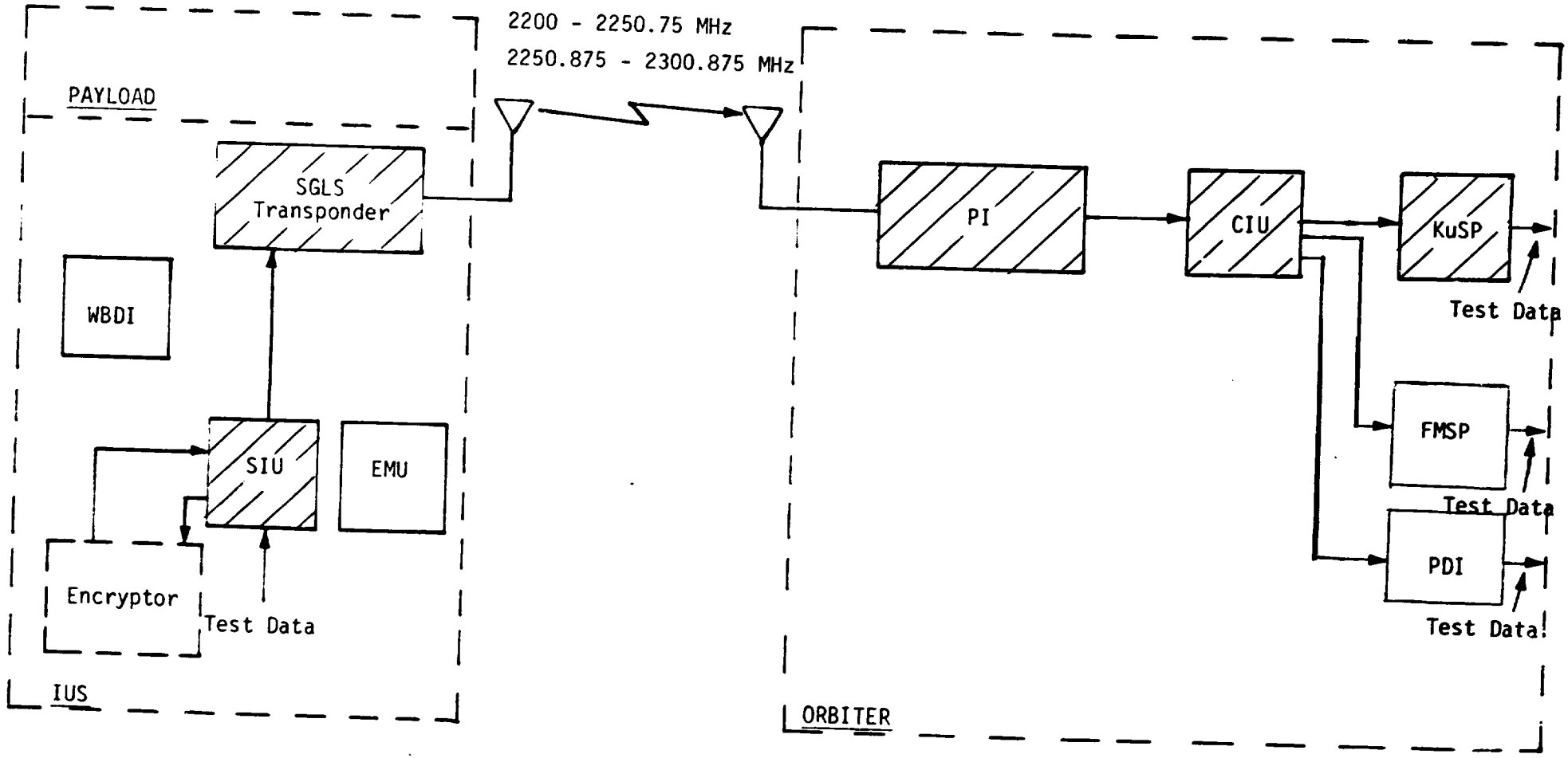

Figure 15. Attached/Detached IUS Telemetry RF ESTL Test Link SGLS Telemetry (DOD Mode)

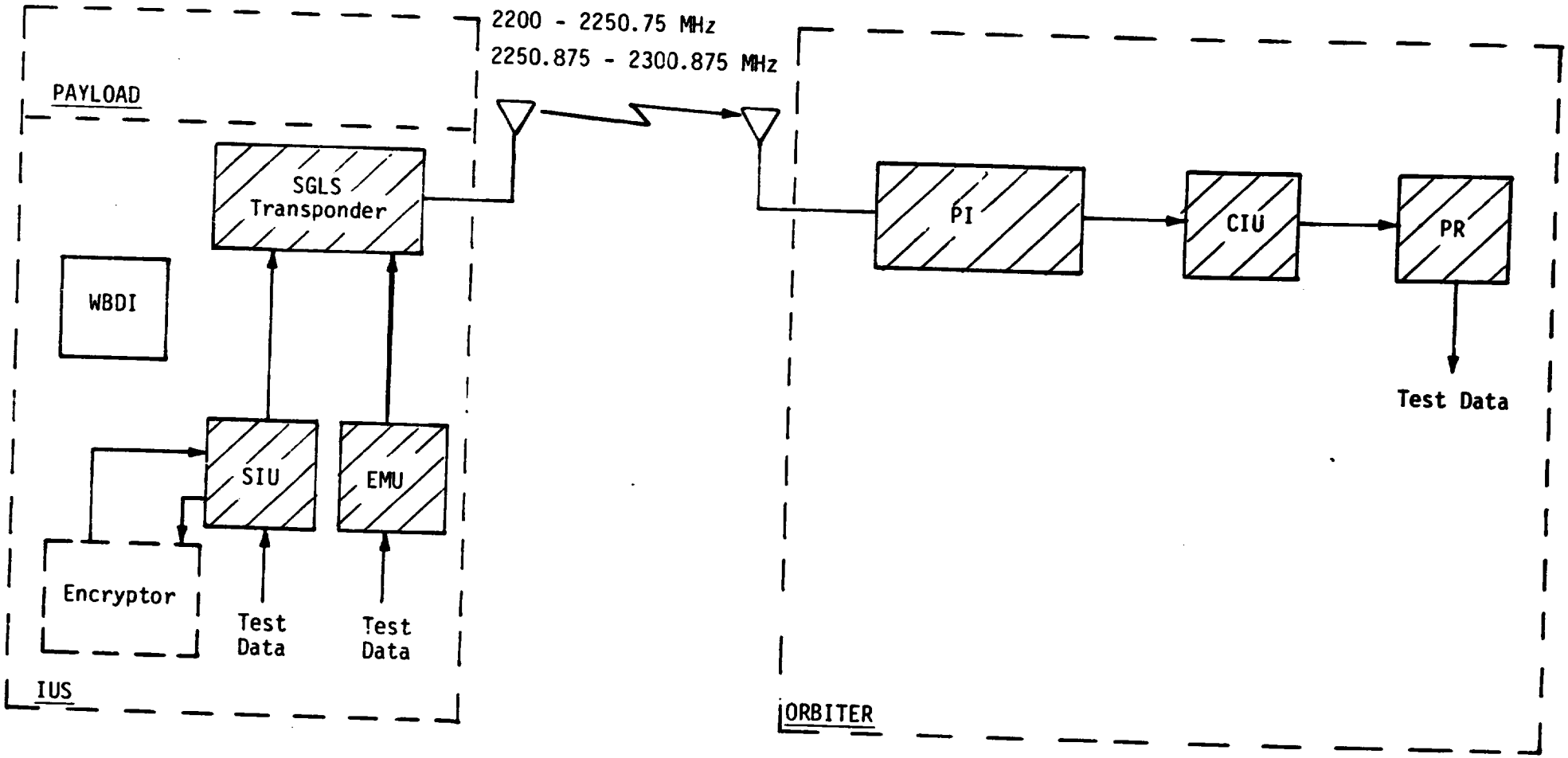

Figure 16. Attached/Detached IUS Telemetry RF ESTL Test Link SGLS Telemetry (DOD Mode)

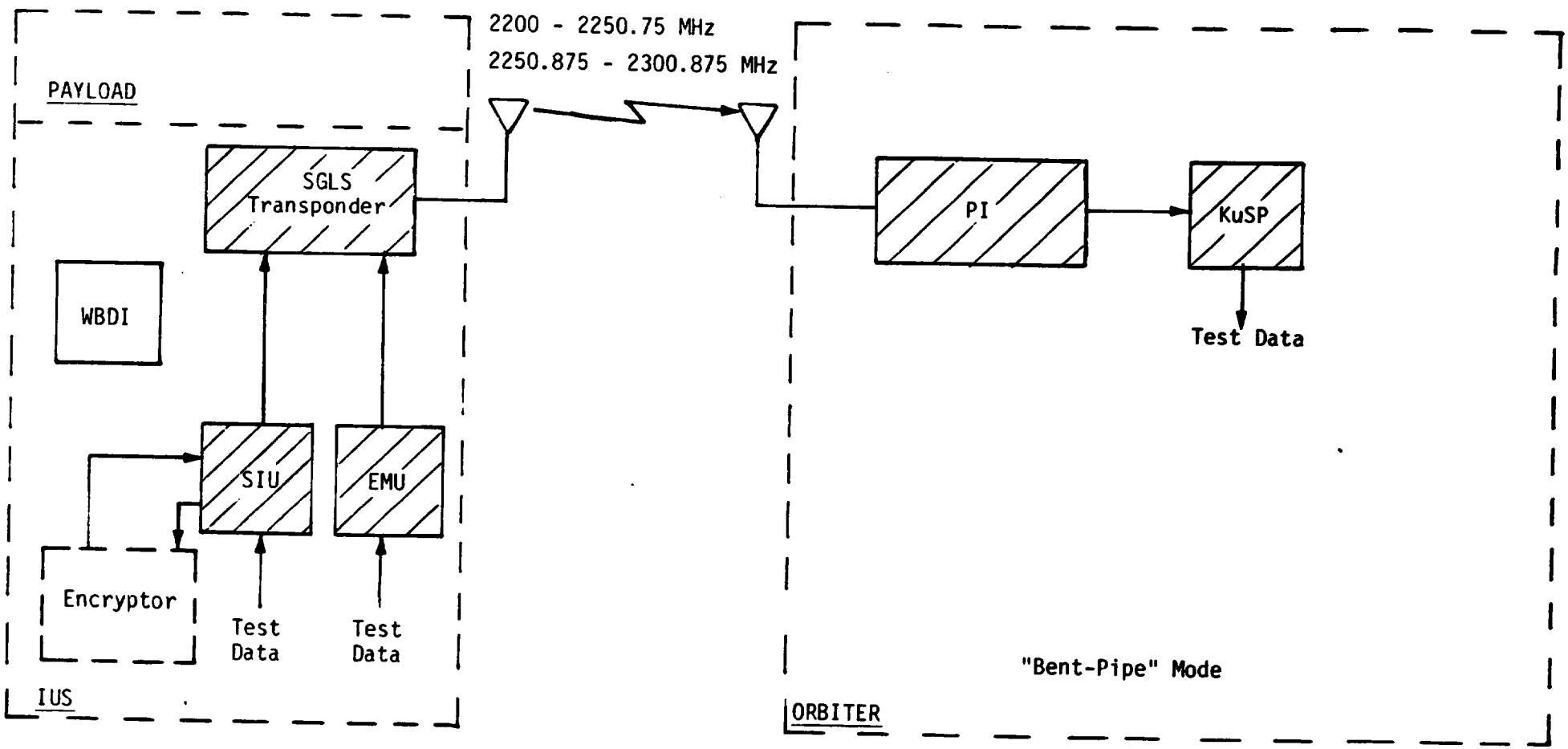

Figure 17. Attached/Detached IUS Telemetry RF ESTL Test Link
SGLS Telemetry (DOD Mode)

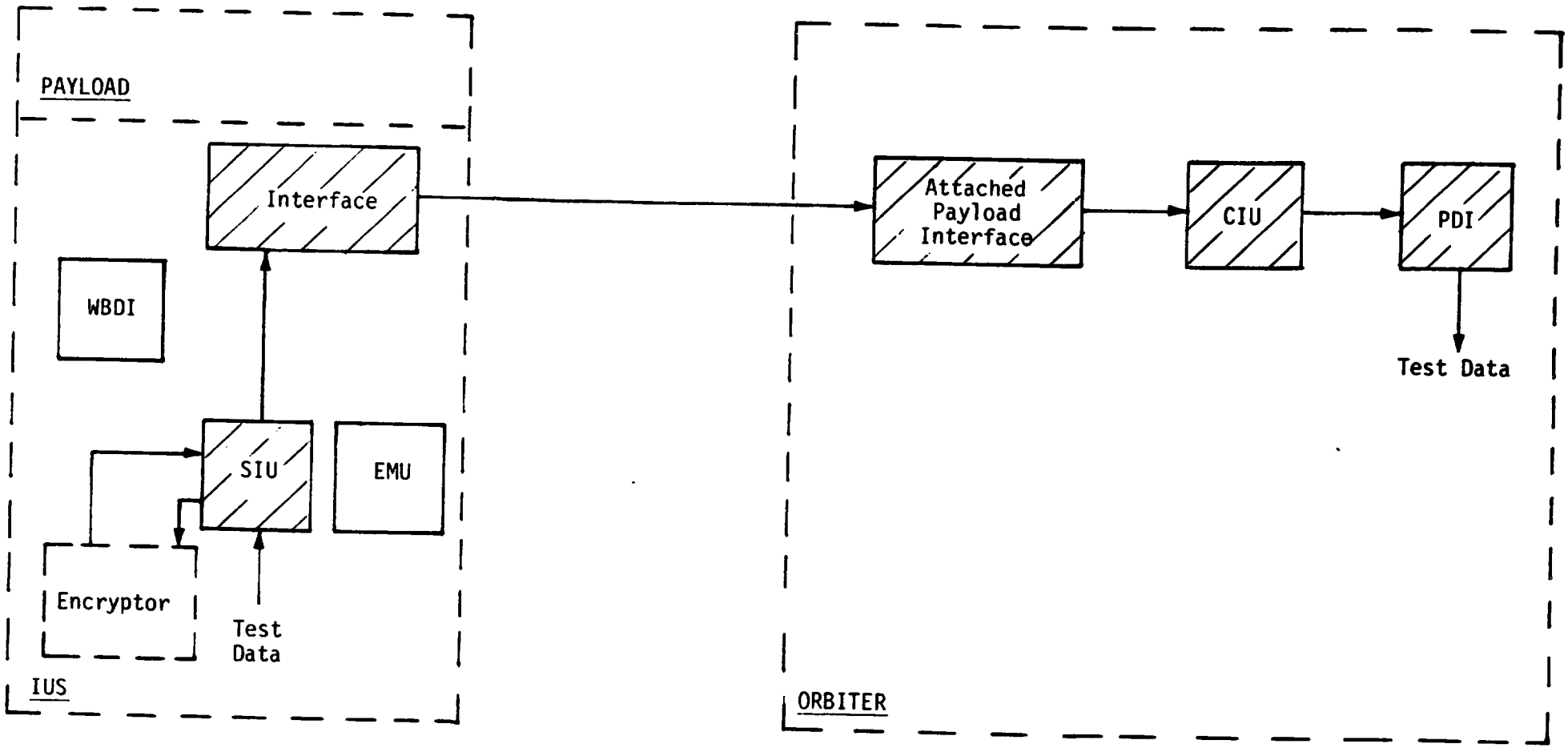

Figure 18. Attached IUS Telemetry Hard-Line ESTL Test Link
SGLS Telemetry (DOD Mode)

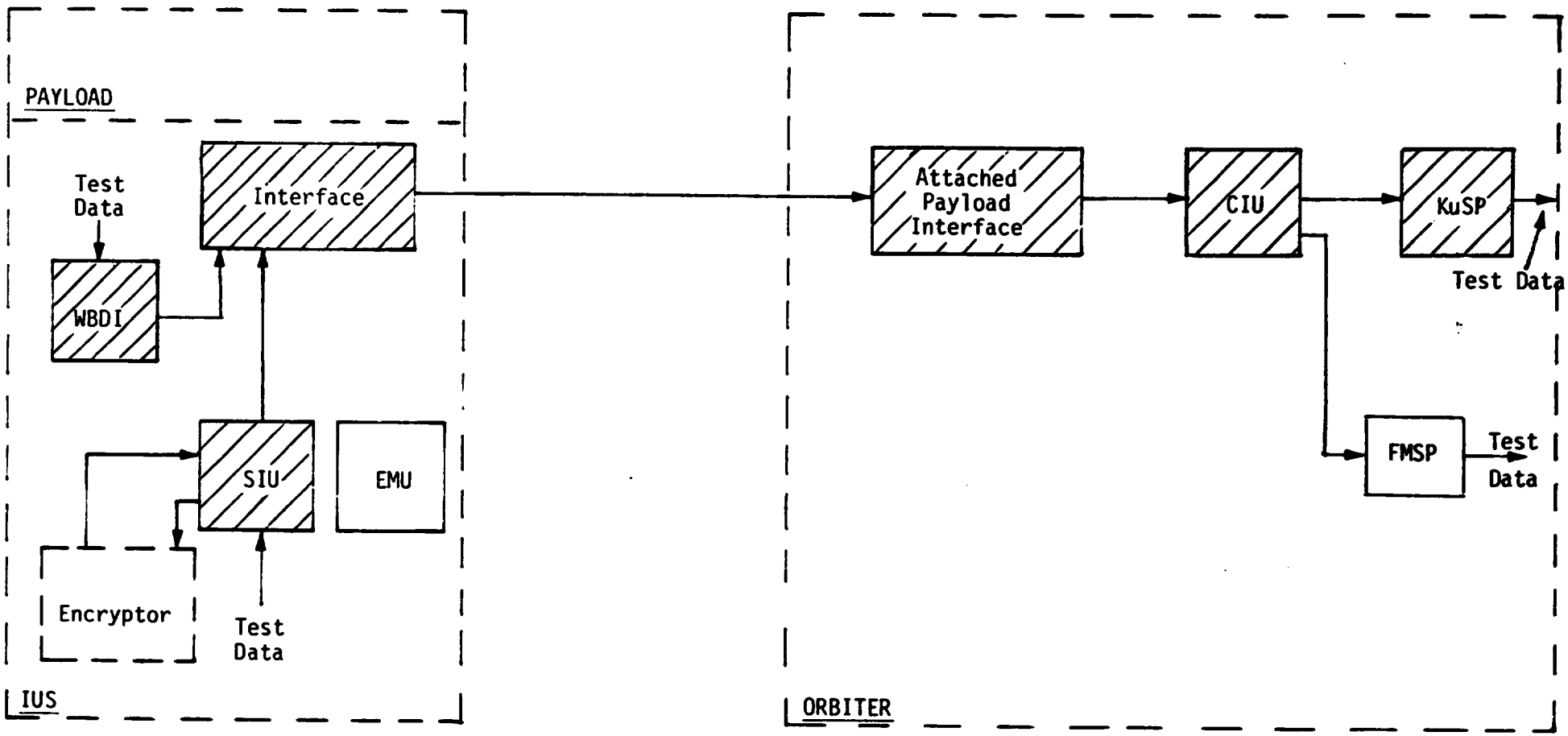

Figure 19. Attached IUS Telemetry Hard-Line ESTL Test Link SGLS Telemetry (DOD Mode)

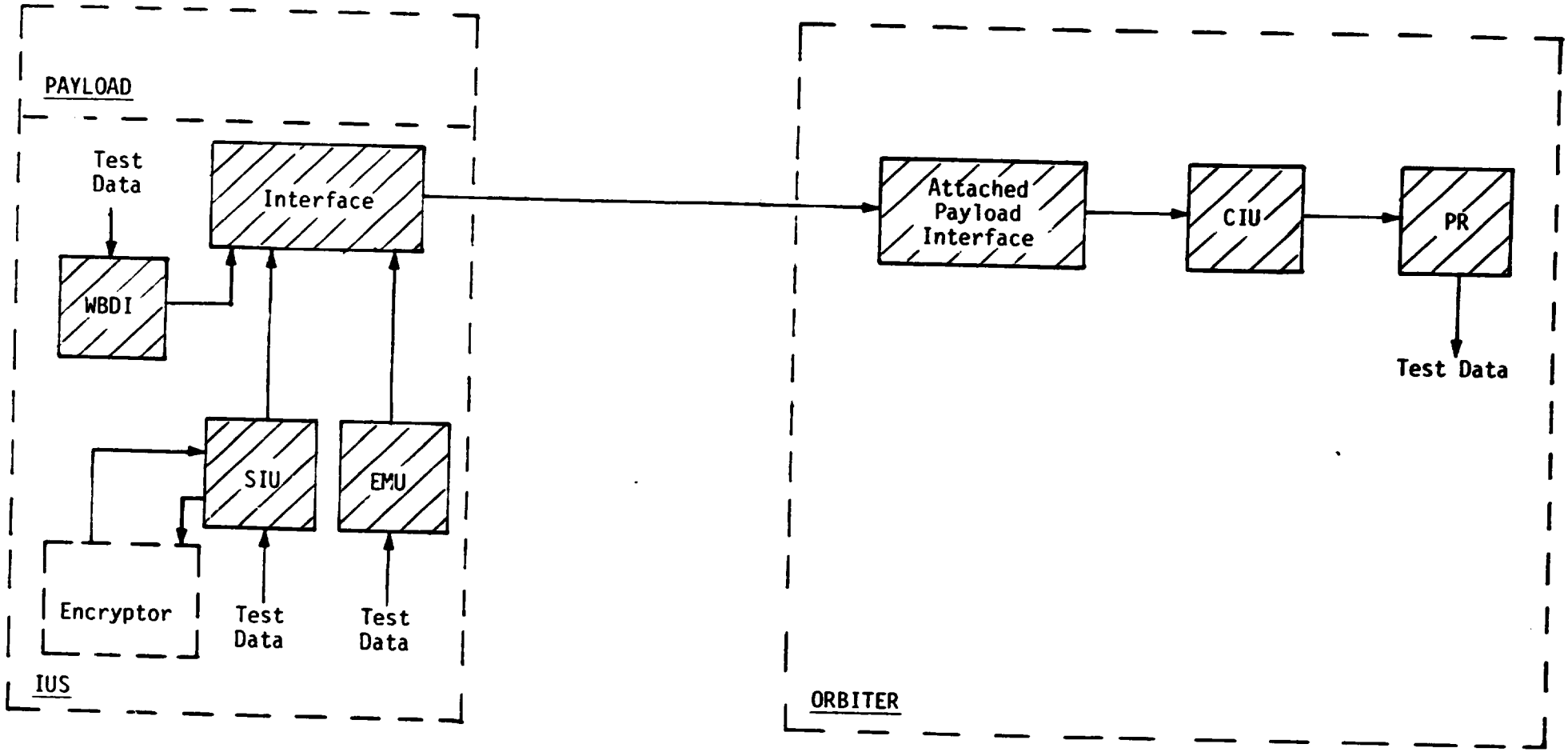

Figure 20. Attached IUS Telemetry Hard-Line ESTL Test Link SGLS Telemetry (DOD Mode)

Figures 21 and 22 outline the RF test lines. Since the PSP, like the CIU, is limited to a 16 kbps data rate, Figure 22 is the "bent-pipe" mode used to handle higher data rates. Figures 23-26 are to test the various types of data transmitted to the Orbiter via the hardwire interface.

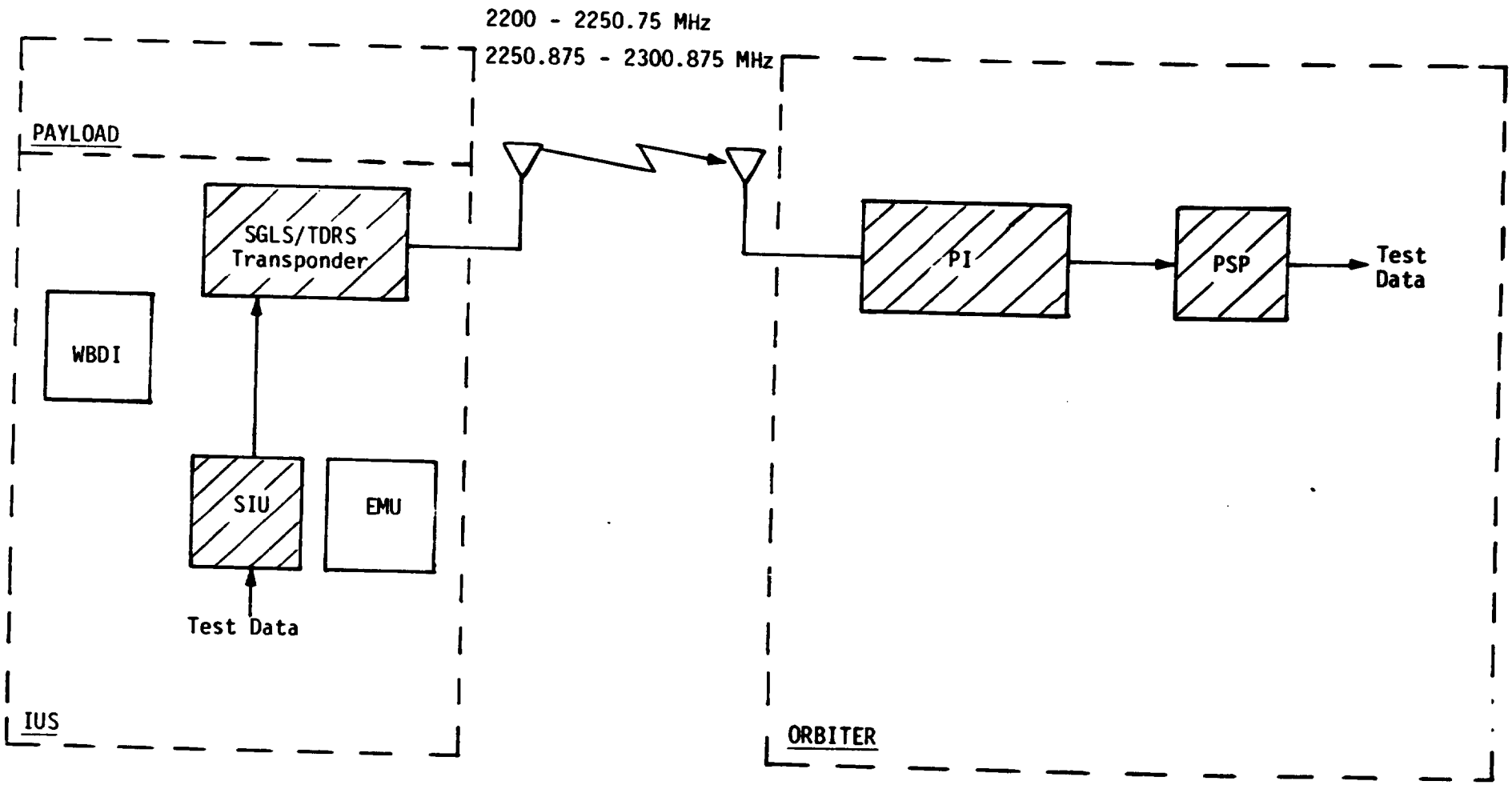

Figure 21. Attached/Detached IUS Telemetry RF ESTL Test Link
STDN/TDRS Telemetry (NASA Mode)

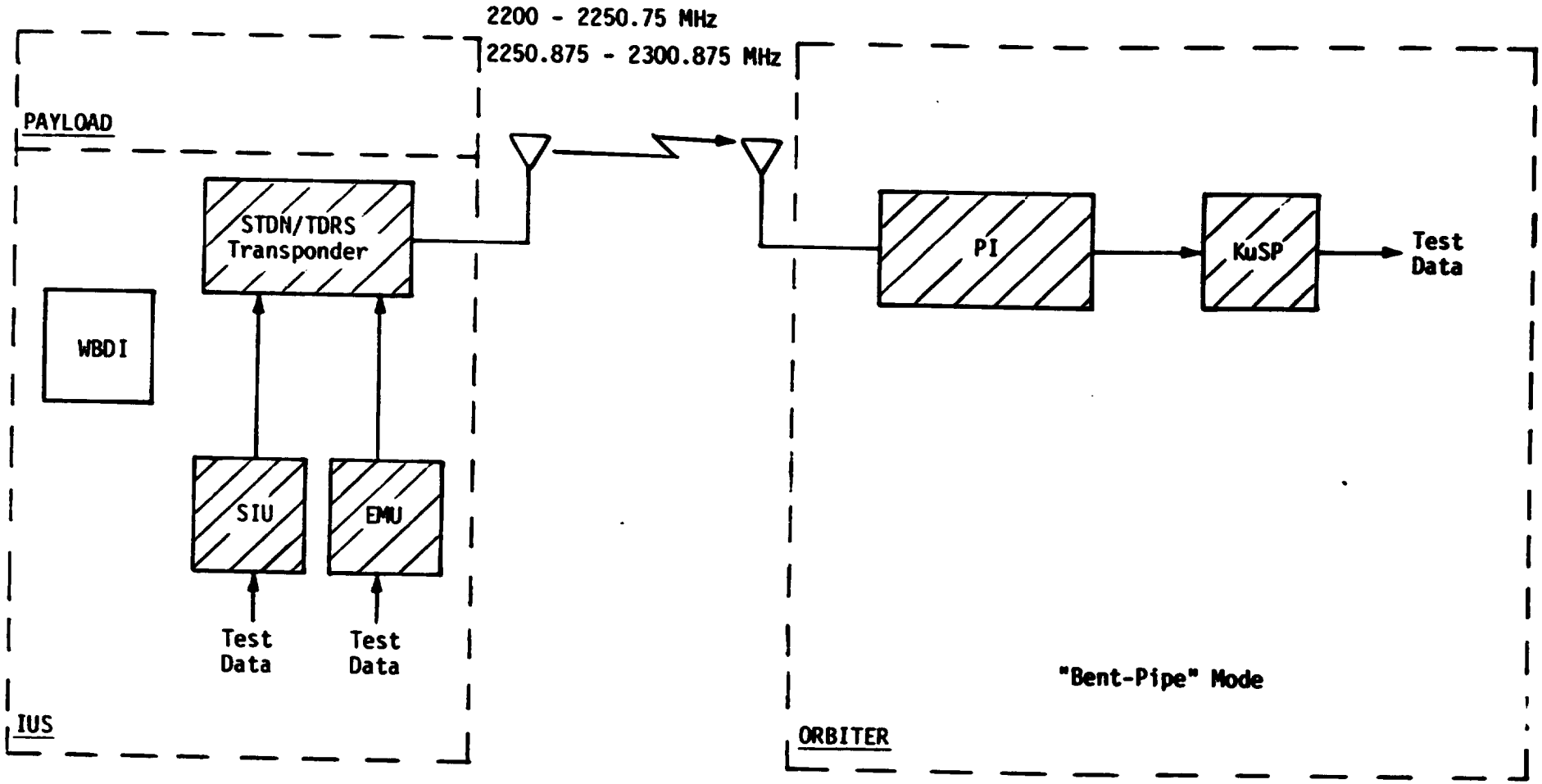

Figure 22. Attached/Detached IUS Telemetry RF ESTL Test Link STDN/TDRS Telemetry (NASA Mode)

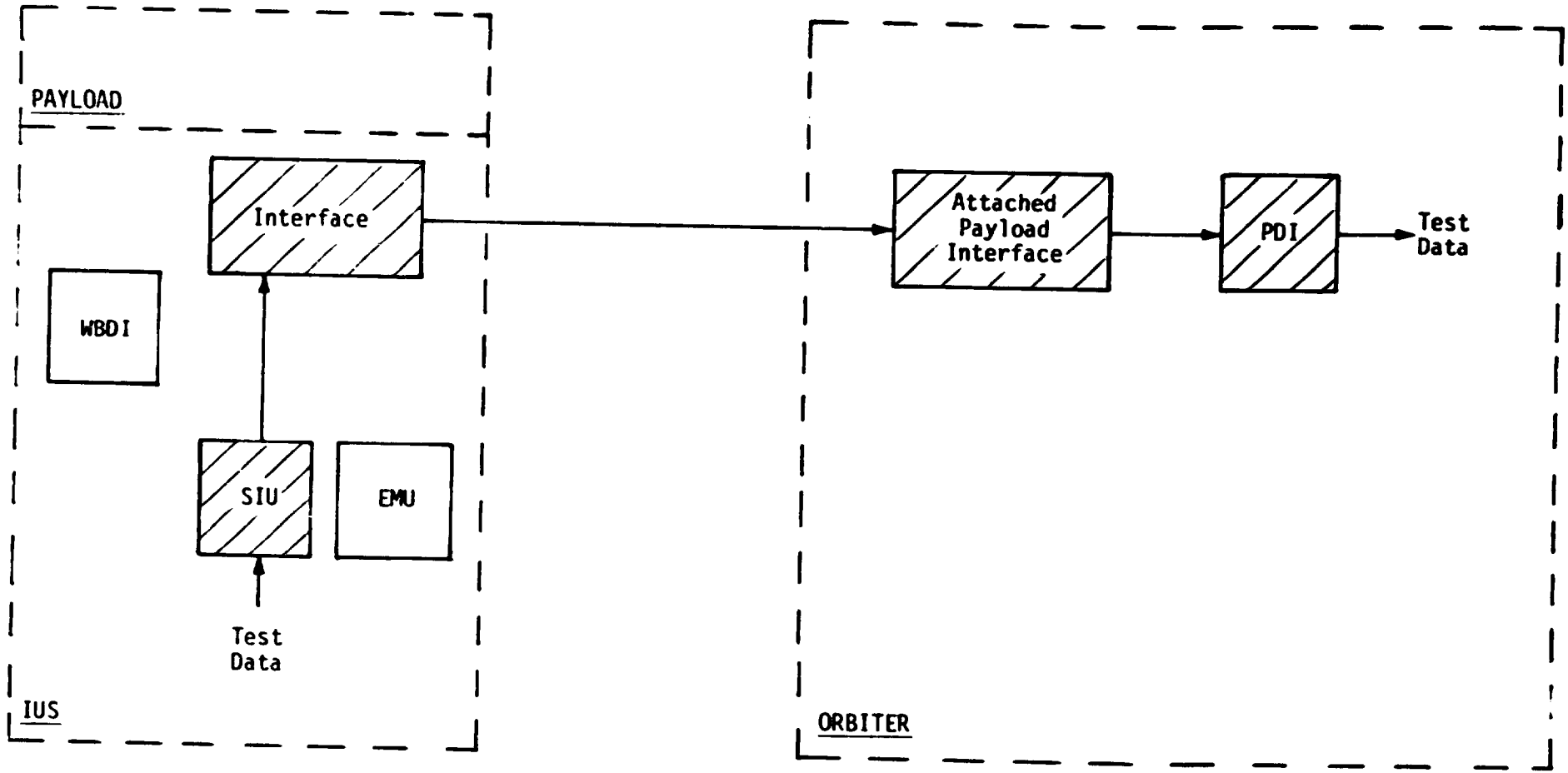

Figure 23. Attached IUS Telemetry Hard-Line ESTL Test Link
STDN/TDRS Telemetry (NASA Mode)

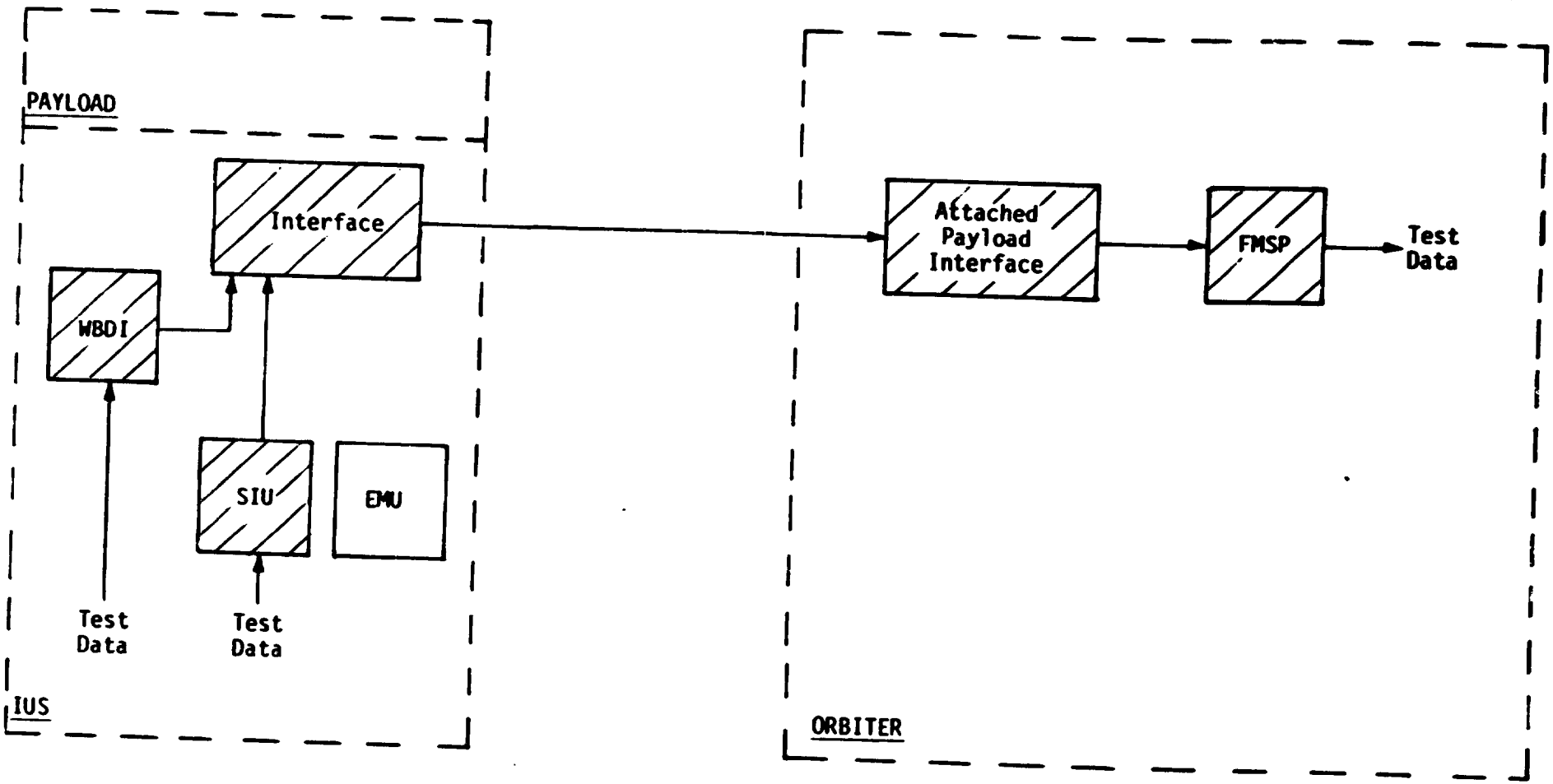

Figure 24. Attached IUS Telemetry Hard-Line ESTL Test Link STDN/TDRS Telemetry (NASA Mode)

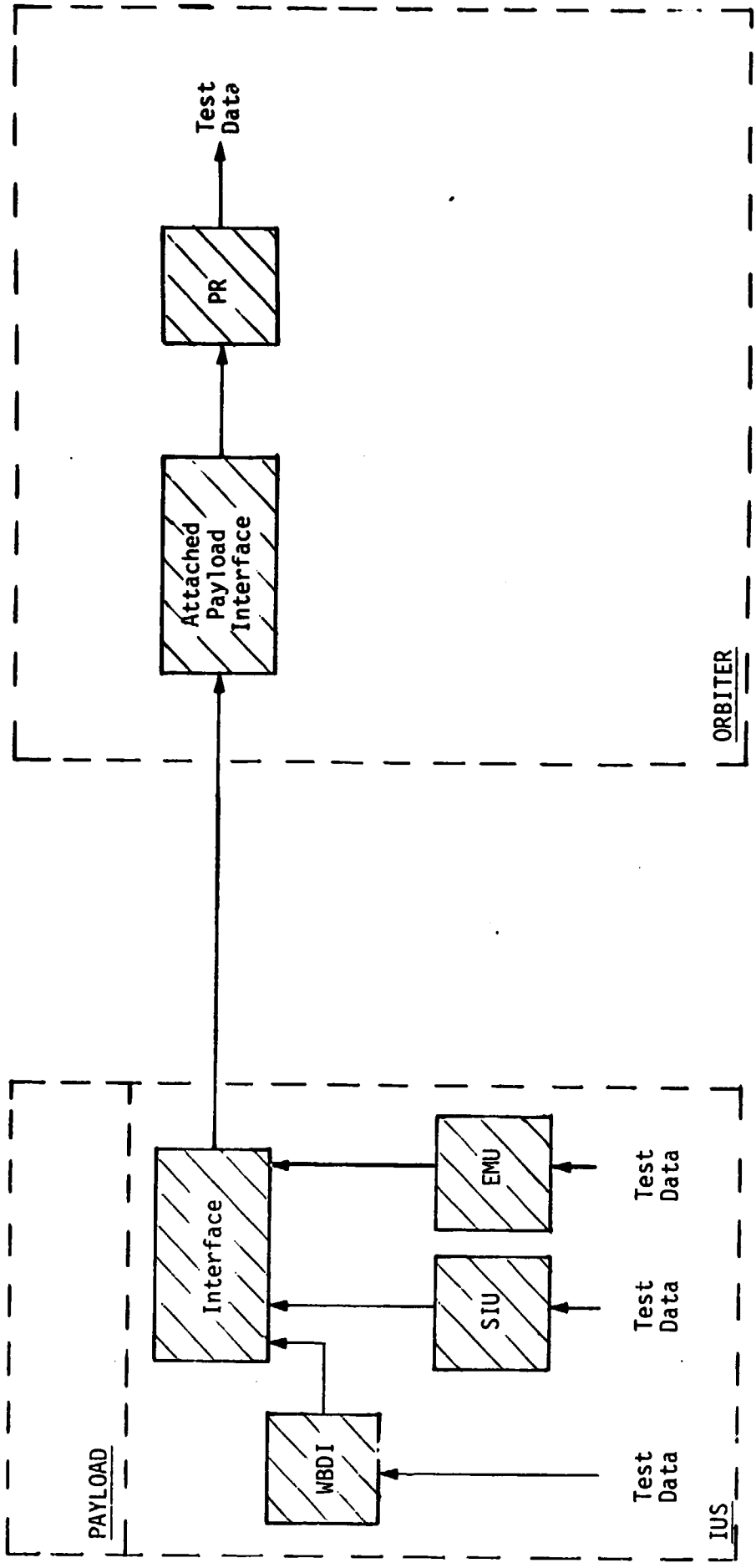

Figure 25. Attached IUS Telemetry Hard-Line ESTL Test Link STDN/TDRS Telemetry (NASA Mode)

Figure 26. Attached IUS Telemetry Hard-Line ESTL Test Link
STDN/TDRS Telemetry (NASA Mode)

3.6 ESTL Test Configuration

As previously mentioned, the main objective of this document is to present a test plan to assess the performance of the IUS/Orbiter communication links. The earlier sections discussed all of the possible signal paths between the IUS, Orbiter and ground stations for both the RF and hard-line interface modes. Of the 57 possible signal paths, 38 should or will be verified under separate test plans, which leaves 19 test links to be addressed in this report. Since the IUS/Orbiter communication link verification tests will be performed in the NASA Lyndon B. Johnson Space Center (JSC) Electronics Systems Laboratory (ESTL), a basic description of the ESTL is in order.

3.6.1 ESTL Description

The ESTL test program objectives for the IUS and CIU with the Orbiter subsystems and ground stations are:

(1) To establish equipment/subsystem electrical compatibility

(2) To identify performance and operational limitations and constraints

(3) To verify that appropriate RF and hardwire interfaces are commensurate with mission communications requirements

(4) To verify experimentally that the Orbiter/IUS forward and return RF links are signal compatible in all modes

(5) To verify experimentally those tracking, command and telemetry channel performance characteristics required for operational mission support.

The functional diagram of the ESTL is shown in Figure 27. As can be seen from this diagram, the ESTL has the capability to simulate the direct Shuttle/earth S-band links and the indirect Orbiter/ground S-band and Ku-band links. Means are additionally provided to simulate the data generated within the Orbiter itself, along with the capability for routing it via the various space/ground links for the purpose of total systems evaluation.

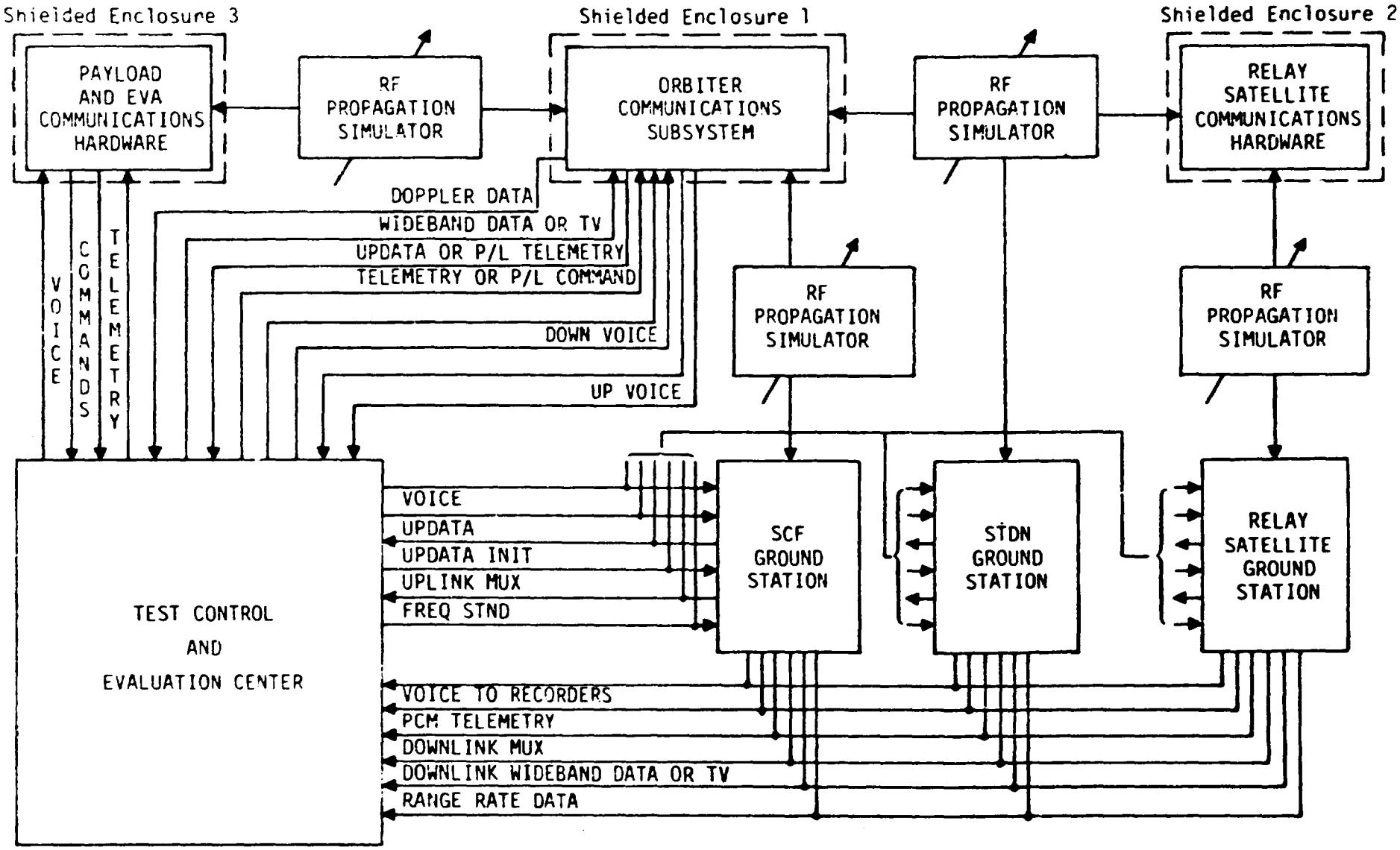

Figure 27. ESTL Functional Block Diagram

The Orbiter communications subsystem provides a capability for establishing communication links with both the attached IUS within the Shuttle bay and the detached IUS in the near vicinity of the Orbiter. Communication with the attached IUS is via hardwire channels, as described in Section 2.0. The detached IUS RF communication is a two-way link carrying commands and telemetry. Both the hardwire and RF links with the IUS constitute a portion of the overall space/space capability of the Orbiter communication system.

Figure 28 shows the general configuration to be used for all tests involving the IUS/Orbiter subsystem, and Table 1 gives a summary of the ESTL test links. To accomplish the operational tests, the ESTL test setup must provide command data to the CIU or PSP and telemetry data to the IUS transponder.

For testing the forward (Orbiter-to-IUS) link, a Univac M642B computer generates commands which are sent to the IUS transponder via either the hard-line cable or the simulated RF link. Command verification is accomplished by comparing the command sent to the CIU or PSP with the command output of the IUS SCU.

Return link (IUS-to-Orbiter) telemetry data is originated by a telemetry simulator and transmitted via the hard-line interface or RF link. The PCM simulated data may be verified directly by a bit error comparator, and the simulated analog telemetry may be verified by signal-to-noise ratio ratio measurements.

Use of the M642B computer depends on the nature of the tests being carried out. Primarily, it is used to aid in the statistical evaluation of the link performance and, most importantly, the M642B provides the processing and control necessary to multiplex received commands and return telemetry data.

3.6.2 Required Test Equipment

The Orbiter and IUS communication systems will be installed in the ESTL in a representative mission configuration. The equipment will be interconnected either through a space-loss simulator which accurately controls the forward and return link total received power levels to test the RF links or via the cables to test the hard-line interface links.

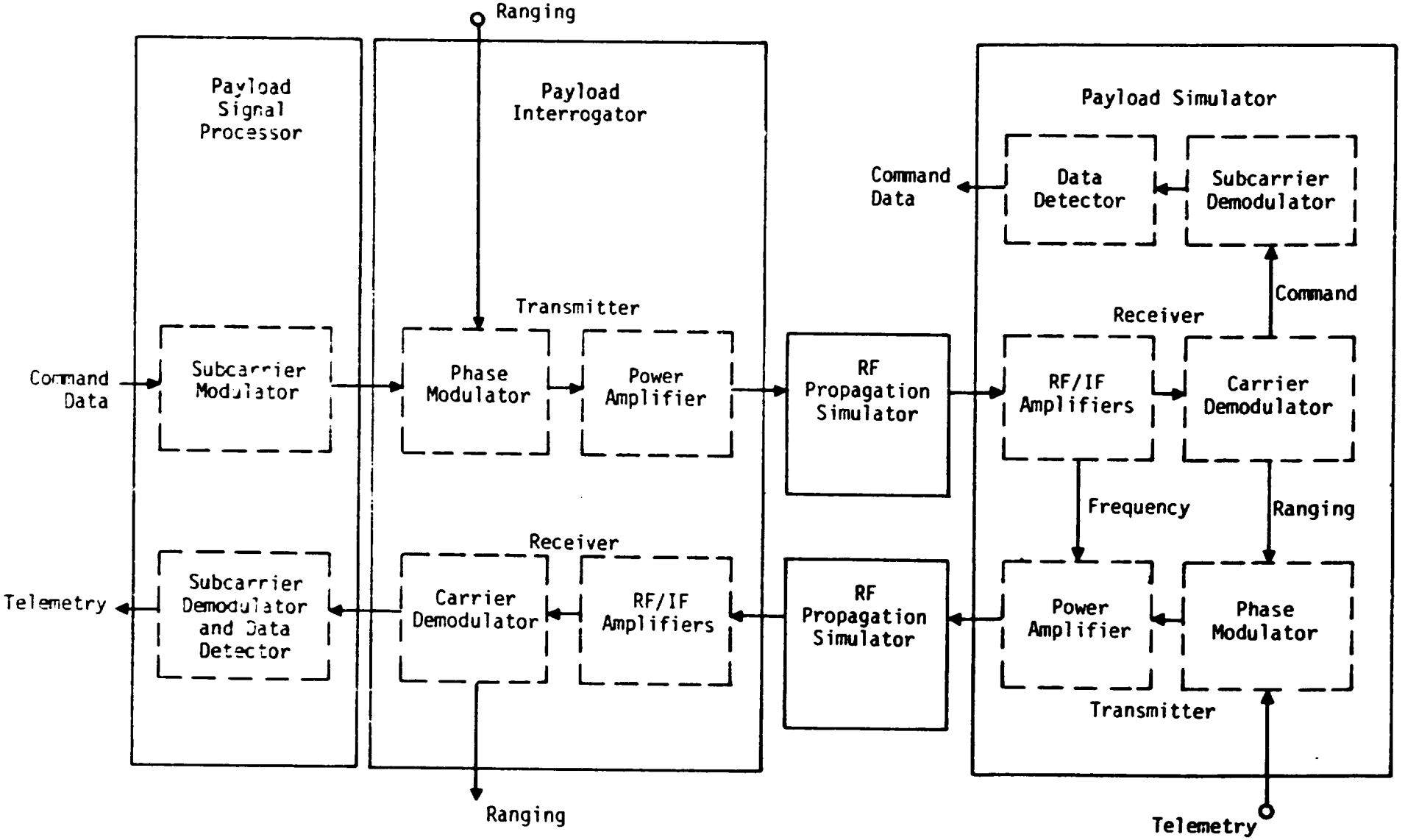

Figure 28. General Test Configuration

Table 1. ESTL Communication Link Test Configurations Summary

User	Link Type	Data	Modulation Format	Signal Flow Direction Tested (Simulated)
NASA	Hardwire	CMDS	NRZ	Orbiter to IUS
	Hardwire	CMDS	PSK	Orbiter to IUS
	Hardwire	TLM	NRZ	IUS to Orbiter
	RF	CMDS	PSK/PM	Orbiter to IUS
	RF	TLM	PSK/PM	IUS to Orbiter
DOD	Hardwire	CMDS	Ternary Symbols plus Clock	Orbiter to IUS
	Hardwure	CMDS	FSK/AM	Orbiter to IUS
	Hardwire	NAV UPDATE	FSK/AM	Orbiter to IUS
	Hardwire	TLM	NRZ	IUS to Orbiter
	Hardwire	TLM	PSK and FM	IUS to Orbiter
	RF	CMDS	FSK/AM/PM	Orbiter to IUS
	RF	TLM	PSK/PM and FM/FM	IUS to Orbiter

To perform the verification tests, special support equipment is necessary. For example, the M642B computer has a parallel data interface whereas the CIU and PSP are serial data devices. Appropriate computer I/O converters will be needed to interface the computer with the test setup.

A telemetry simulator is required to exercise the various test links, which are summarized in Table 1. The simulator must be capable of producing both the PCM digital data at different rates and the analog data required for certain tests.

In most tests, the digital and analog data is at baseline frequency. There are some tests, however, where the digital and analog data must first be demodulated before verifying performance. Therefore, one or two demodulators must be included in some test setups.

A summary of the required equipment is shown in Table 2.

4.0 SYSTEM PERFORMANCE EVALUATION TESTS

4.1 General

There are two major test categories: calibration tests and system compatibility and performance tests. The system compatibility and performance tests include both the RF and hard-line links.

4.2 Calibration Tests

The purposes of the calibration tests are (1) to verify that the overall communications system configuration, consisting of the Orbiter equipment, RF or hard-line interface path and IUS equipment, is ready for the system compatibility and performance tests and, (2) to measure important equipment parameters that will be needed to conduct the tests and to evaluate the test results. The calibration tests will include space-loss simulator calibration, measurement of RF power levels, noise figures, frequency responses and modulation indices. Calibration tests will be performed on both Orbiter and IUS equipment, as applicable. In addition, as a prerequisite to performing the system compatibility and perfomance tests, operator's certification procedures must be performed on equipment which requires certification.

Table 2. Required Equipment Summary

ORBITER	IUS
PI	Transponder (DOD & NASA)
CIU	SCU (DOD & NASA)
PSP	SIU (DOD & NASA)
PDI	EMU (DOD & NASA)
KuSP	WBDI (DOD & NASA)
FMSP	Decryptor
PR	Encryptor
MDM	
Encryptor	

ESTL
Space Loss Simulator
Bit Synchronizer
Bit Error Rate Detector
Frame Synchronizer
M642B Computer
Computer Input Converter (Serial/Parallel)
Computer Output Converter (Parallel/Serial)
Signal-to-Noise Ratio Meter
Decryptor
Telemetry Simulator (Digital & Analog)
Ku-Band Deliverable Test Equipment (DTE)
ESTL Range and Doppler Simulator (ERDS)
IUS Antenna Select Simulator

4.3 System Compatibility and Performance Tests (RF Links)

The purposes of these tests are to verify overall system compatibility and determine channel performance. Channel performance determines the total received power-to-noise spectral density ratios required to achieve the specified data channel performance. Tables 3-6 show the signal combinations and performance requirements which will be used during the system RF performance evaluation. The data rates shown in these four tables represent the maximum and minimum rates for that particular RF link.

The Orbiter/IUS forward link tests will evaluate the command channel performance while the IUS/Orbiter return link tests will verify the telemetry channel performance. RF acquisition tests will first substantiate the forward and return links individually, then the two-way link. All tests will assess system performance for both the DOD and NASA IUS configurations but will not include doppler offsets since the relative velocity between the Orbiter and IUS is small.

The Orbiter/IUS forward and return links are capable of operating in any one of approx. 850 fully duplex channels, each of which is divided into two bands, designated the "high" and "low" bands. Ideally, the links should be tested at both frequency extremes of the high and low bands. While the PI is capable of operating in any one of the channels, the link operating frequency is dependent upon the IUS transponder, which has two fixed frequencies. The tests in the ESTL, therefore, will not be able to exercise the links at the band extremes since the two IUS transponder frequencies are not selectable and are in the same band very close to each other.

4.3.1 Forward Link Tests (RF)

The purpose of these tests is to evaluate the capability of the Orbiter-to-IUS RF command link to meet mission requirements. The forward link tests are subdivided into the DOD and NASA command channel tests.

The command channel will be evaluated by measuring measage rejection rate and command word verification as functions of total received power-to-noise spectral density ratios. To measure message rejection rate and command word verification, special test equipment will be used to interface the IUS SCU and the command computer, where a comparison will be made of the commands transmitted and those received by the SCU.

Table 3. Forward Link RF Signal Combinations and Performance Requirements (DOD)

Combination	Information Transmitted	Modulation Techniques	Modulation Index (Radians)	DOD IUS Required Prec/No. (dB - Hz)
1*	2 ksps Commands	FSK/AM	0.2 - 2.5	56.5
2	1 ksps Commands	FSK/AM	0.2 - 2.5	56.5

*Current CIU design is not capable of this rate.

Table 4. Forward Link RF Signal Combinations and Performance Requirements (NASA)

Combination	Information Transmitted	Modulation Techniques	Modulation Index (Radians)	NASA IUS Required Prec/No. (dB - Hz)
3	2 kbps Commands	PSK	$\pi/2$	48.2
4	7.8125 bps Commands	PSK	$\pi/2$	48.2

Table 5. Return Link RF Signal Combinations and Performance Requirements (DOD)

Combination	Information Transmitted	Modulation Techniques	Modulation Index (Radians)	Orbiter Required Prec/No. (dB - Hz)
5	Telemetry, includes 16 kbps digital (1.024 MHz subcarrier) & Analog (IRIG 1A, 2A & 3A freq.)	PSK	π/2	60.4
	(1.7 MHz subcarrier)	FM/FM		74.5
6*	Telemetry, includes 64 kbps Digital (1.024 MHz subcarrier) & Analog (IRIG 1A, 2A & 3A freq.)	PSK	π/2	60.4
	(1.7 MHz subcarrier)	FM/FM		74.5
7*	Telemetry 256 kbps digital (1.7 MHz subcarrier)	PSK	π/2	60.4
8*	Telemetry, 0.25 kbps digital (1.024 MHz subcarrier)	PSK	π/2	60.4
9*	Telemetry Analog (IRIG 1A, 2A & 3A freq.)			
	(1.7 MHz subcarrier)	FM/FM		74.5

*Combinations 6-9 are the "bent-pipe" signals.

Table 6. Return Link RF Signal Combinations and Performance Requirements (NASA)

Combination	Information Transmitted	Modulation Techniques	Modulation Index (Radians)	Orbiter Required Prec/No. (dB - Hz)
10	16 kbps Telemetry	PSK	$\pi/2$	60.4
11	1 kbps Telemetry	PSK	$\pi/2$	60.4

BER's cannot be measured for the command channel because test points are not available. Therefore, the command word verification and message rejection rates will be used to estimate the BER. In addition, verification will be made that 10,000 error-free commands can be received and clocked out of the IUS SCU under strong signal conditions.

The results of these tests will be compared to performance predictions to ascertain how well the measured results compared with theory. The measured results will also be compared with any program requirements to verify that the command link will support a Shuttle mission.

4.3.1.1 DOD command configuration

There are three RF test links used to verify that the DOD command channel meets mission requirements. The DOD command RF test link, shown in Figure 29, and test link 2, shown in Figure 30, assess the Orbiter-to-CIU interface. As previously mentioned, since the CIU is not under direct RF control in terms of performance and interface compatibility, an additional ESTL task will be to substantiate the performance of the Orbiter/CIU interface, after which commands may be injected directly into the CIU.

The primary DOD forward RF test link is test link 3, as shown in Figure 31. Test link 3 will measure message rejection rates and command word verification as functions of total received power-to-noise spectral density ratios with and without encryption.

Table 7 summarizes the DOD command RF tests. The signal combination shown is from Table 3.

4.3.1.2 NASA command configuration

Test link 4 is one forward RF test link used to assess the NASA command channel, as shown in Figure 32. Table 8 summarizes the NASA command RF tests, with the signal combinations shown being from Table 4.

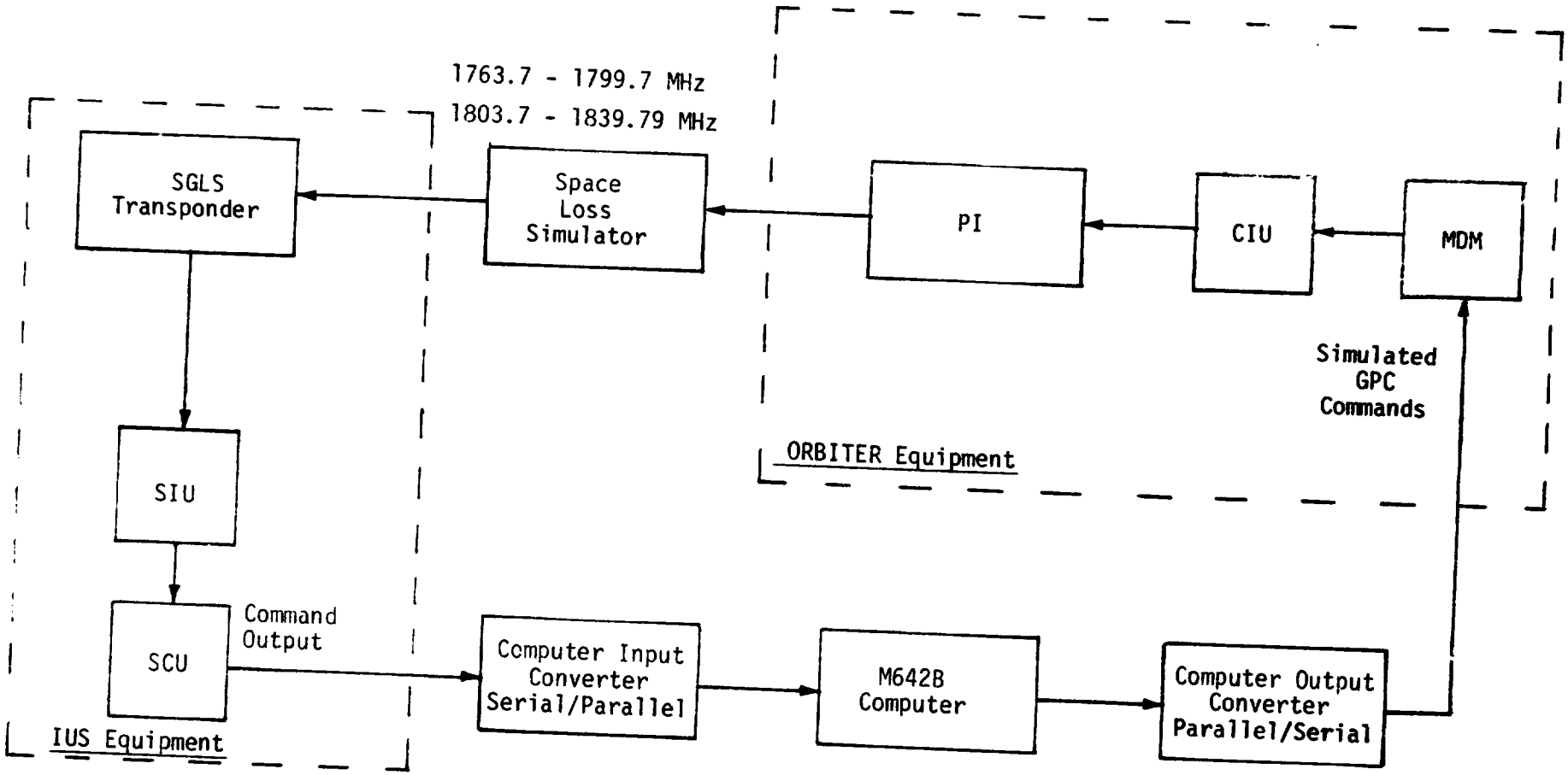

Figure 29. DOD Command RF Test Link 1 SGLS Commands

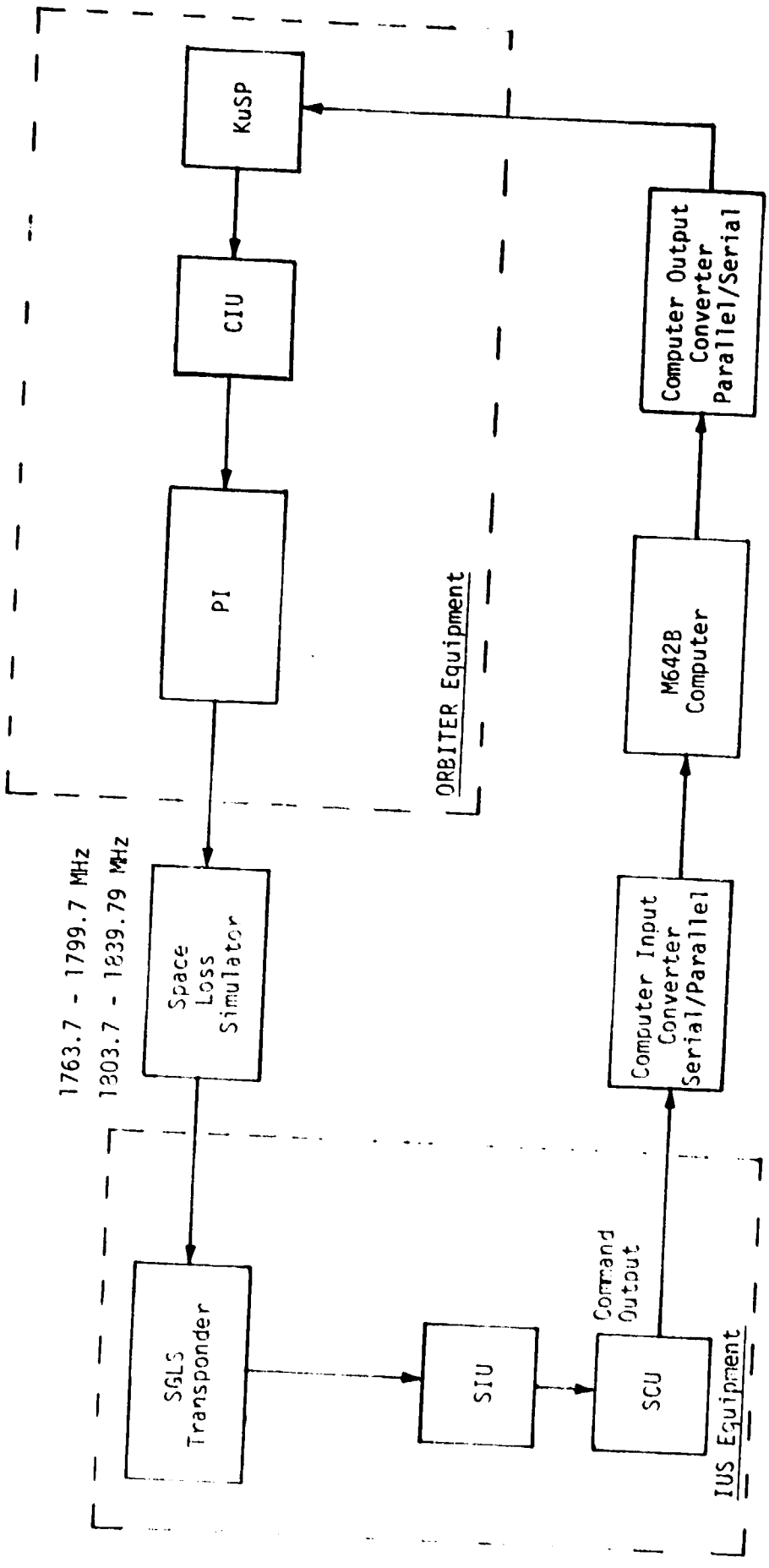

Figure 30. DOD Command RF Test Link 2 SGLS Commands

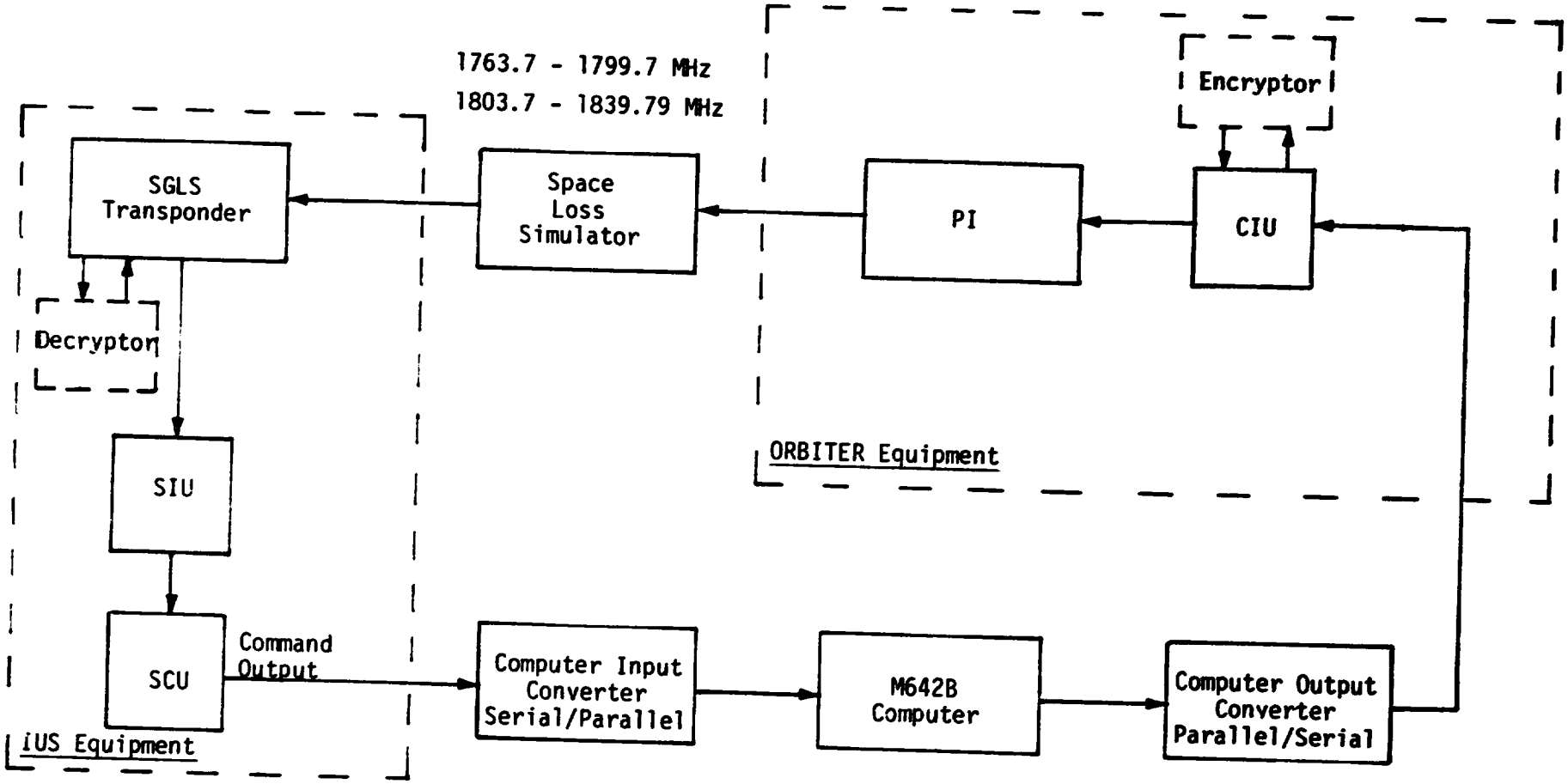

Figure 31. DOD Command RF Test Link 3 SGLS Commands

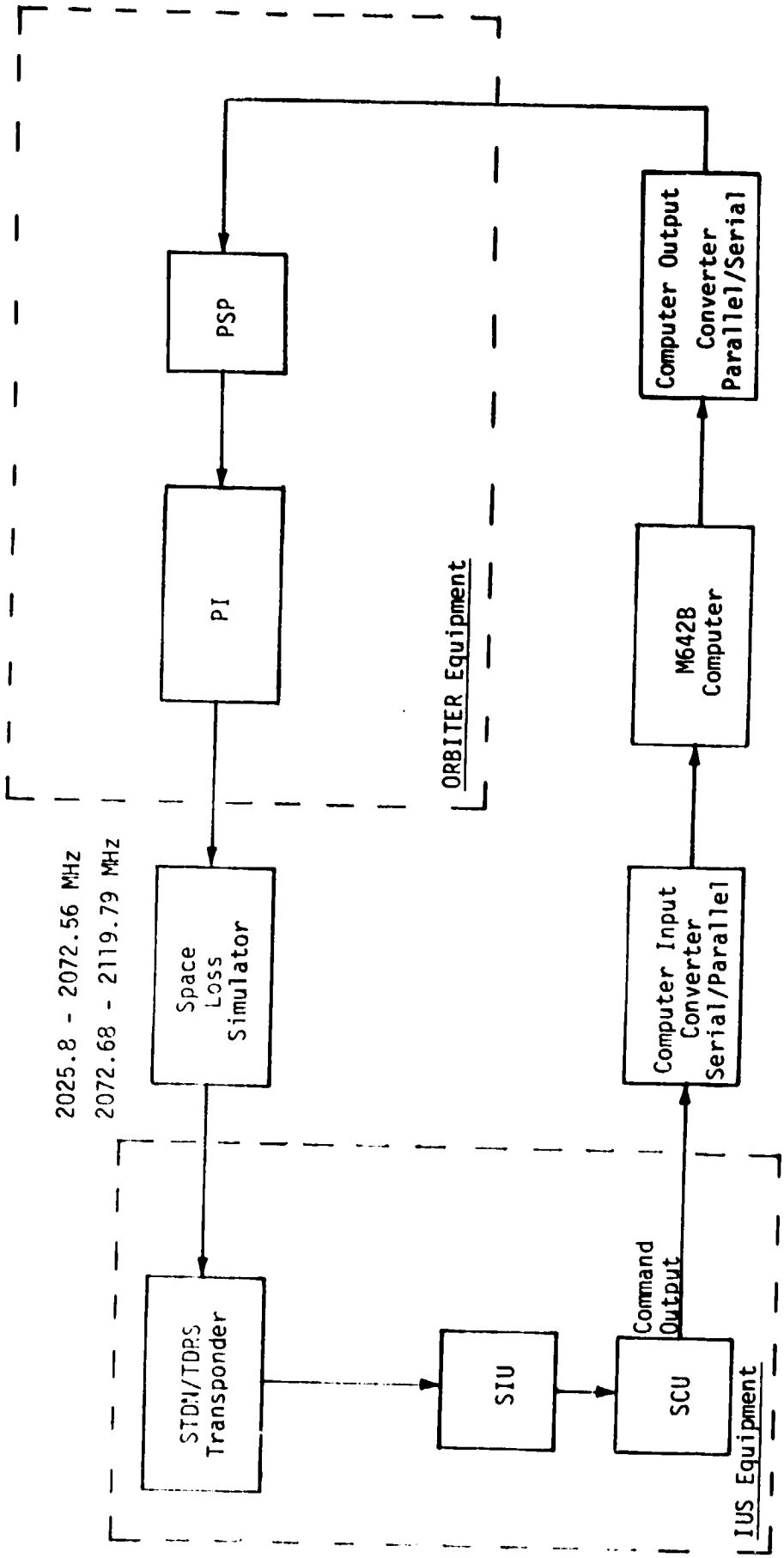

Figure 32. NASA Command RF Test Link 4 STDN/TDRS Commands

Table 7. DOD Command RF Test Summary
(Forward Link)

Test Link 1 (Figure 29)	
Measured Parameter:	Command word verification under strong signal conditions
Test Conditions:	• Either IUS transponder frequency* • Signal combination 2
Test Link 2 (Figure 30)	
Measured Parameter:	Command word verification under strong signal conditions
Test Conditions:	• Either IUS transponder frequency* • Signal combination 2
Test Link 3 (Figure 31)	
Measured Parameter:	Command word verification and message rejection rate as functions of total Prec/No.
Test Conditions:	• Either IUS transponder frequency* • Signal combination 2 • With and without encryption
Measured Parameter:	10,000 error-free commands received under strong signal conditions
Test Conditions:	• Either IUS transponder frequency* • Signal combination 2

*Both IUS frequencies are in the same band (high or low) and, typically, are very close to each other.

Table 8. NASA Command RF Test Summary
(Forward Link)

Test Link 4 (Figure 32)	
Measured Parameter:	**Command word verification and message rejection rate as functions of total Prec/No.**
Test Conditions:	**• Either IUS transponder frequency***
	• Signal combinations 3 and 4
Measured Parameter:	**10,000 error-free commands received under strong signal conditions**
Test Conditions:	**• Either IUS transponder frequency***
	• Signal combination 4

*Both IUS frequencies are in the same band (high or low) and, typically, are very close to each other.

4.3.2 Return Link Tests (RF)

The purpose of these tests is to evaluate the capability of the IUS-to-Orbiter RF telemetry link to meet mission requirements. The return links are subdivided into the DOD and NASA telemetry channel tests.

There is a variety of telemetry formats and data rates transmitted by the IUS transponder to the PI. Basically, the telemetry consists of digital information PSK modulated onto a subcarrier; however, analog information may be FM modulated onto a second subcarrier (DOD mode only). In the wideband "bent-pipe" mode, either subcarrier may be modulated with digital or analog data.

The digital telemetry channels will be evaluated by measuring bit error rates (BER) and percent data loss as functions of Orbiter total received power-to-noise spectral density ratios. The telemetry simulator will input digital information to both the IUS SIU and bit error detector. The information received by the Orbiter also will be input to the bit error detector, where the telemetry transmitted to the IUS may be compared to the telemetry received by the Orbiter. In some instances, it will be necessary to demodulate the digital information with the test equipment before performing the BER measurements.

The percent data loss tests will be performed by comparing the number of frames sent by the IUS to the number of frames received by the Orbiter. To accomplish this test, the telemetry simulator must output frame synchronization information.

The analog telemetry channels will be evaluated by measuring the Orbiter analog output signal-to-noise ratio (SNR) as a function of total received power-to-noise spectral density ratios. The telemetry simulator will input analog information to the IUS EMU for transmission to the Orbiter by the IUS transponder. As in the case with the digital telemetry, it will be necessary in some instances to demodulate the analog information with the test equipment prior to conducting the SNR measurements.

The results of these tests will be compared to performance predictions to ascertain how well the measured results compare with theory; the measured results will also be compared with any program requirements to verify that the telemetry link will support a Shuttle mission.

4.3.2.1 DOD telemetry test configurations (RF)

There are six RF test links used to verify that the DOD telemetry channel meets mission requirements. DOD telemetry RF test links 5-8, Figures 33-36, represent the primary digital test configurations. As previously stated, since the CIU is not under direct RI control in terms of performance and interface compatibility, an additional ESTL task will be to substantiate the CIU/Orbiter interface performance. Note that, in test link 8, the KuSP remodulates the digital data in preparation for transmission over the Ku-band equipment. Therefore, the information must be demodulated by the Ku-band deliverable test equipment (DTE) to baseband before performing the test measurements.

DOD telemetry RF test link 9, Figure 37, represents the primary analog test configuration. Both analog and digital telemetry may be simultaneously transmitted to the Orbiter, where both are recorded with the PR. The digital channel performance has already been verified with test link 7, and the analog portion is evaluated with test link 9 by making SNR measurements at the PR output.

DOD telemetry RF test link 10, Figure 38, tests the "bent-pipe" mode. In this situation, both the analog and digital channel performances are verified in the same test setup. Because there are both narrowband and wideband "bent-pipe" modes, many different signal combinations are required to adequately assess test link 10.

Table 9 summarizes the DOD telemetry RF tests. The signal combinations shown are from Table 5.

4.3.2.2 NASA telemetry test configurations (RF)

There is only one RF test link used to assess that the NASA telemetry channel meets mission requirements; as shown in Figure 39, NASA telemetry consists entirely of digital data unless the "bent-pipe" mode is utilized. The NASA "bent-pipe" configurations is not verified because it is identical to the DOD configuration, test link 10.

Table 10 summarizes the NASA telemetry RF tests. The signal combinations shown are from Table 6.

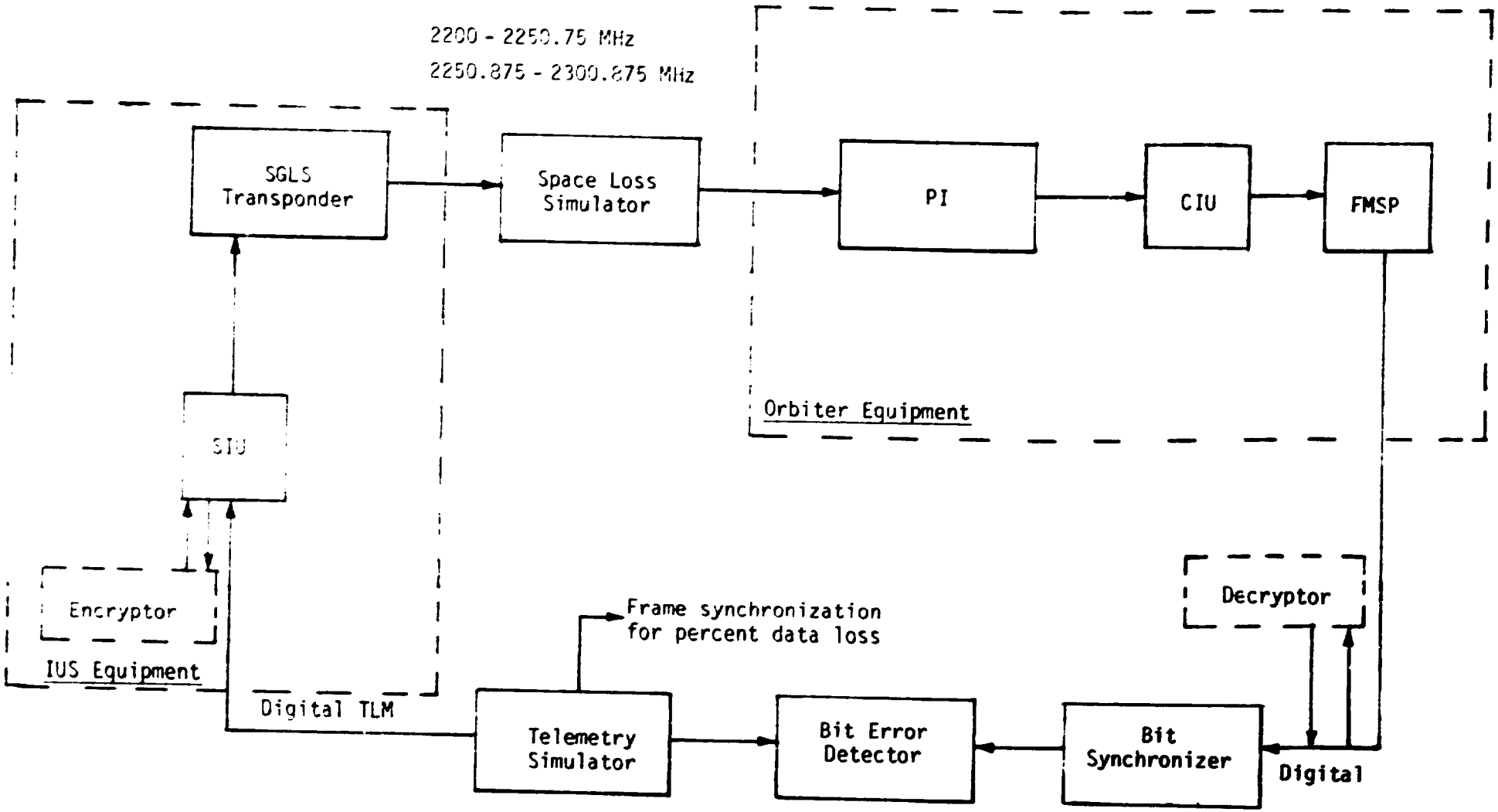

Figure 33. DOD Telemetry RF Test Link 5
SGLS Telemetry

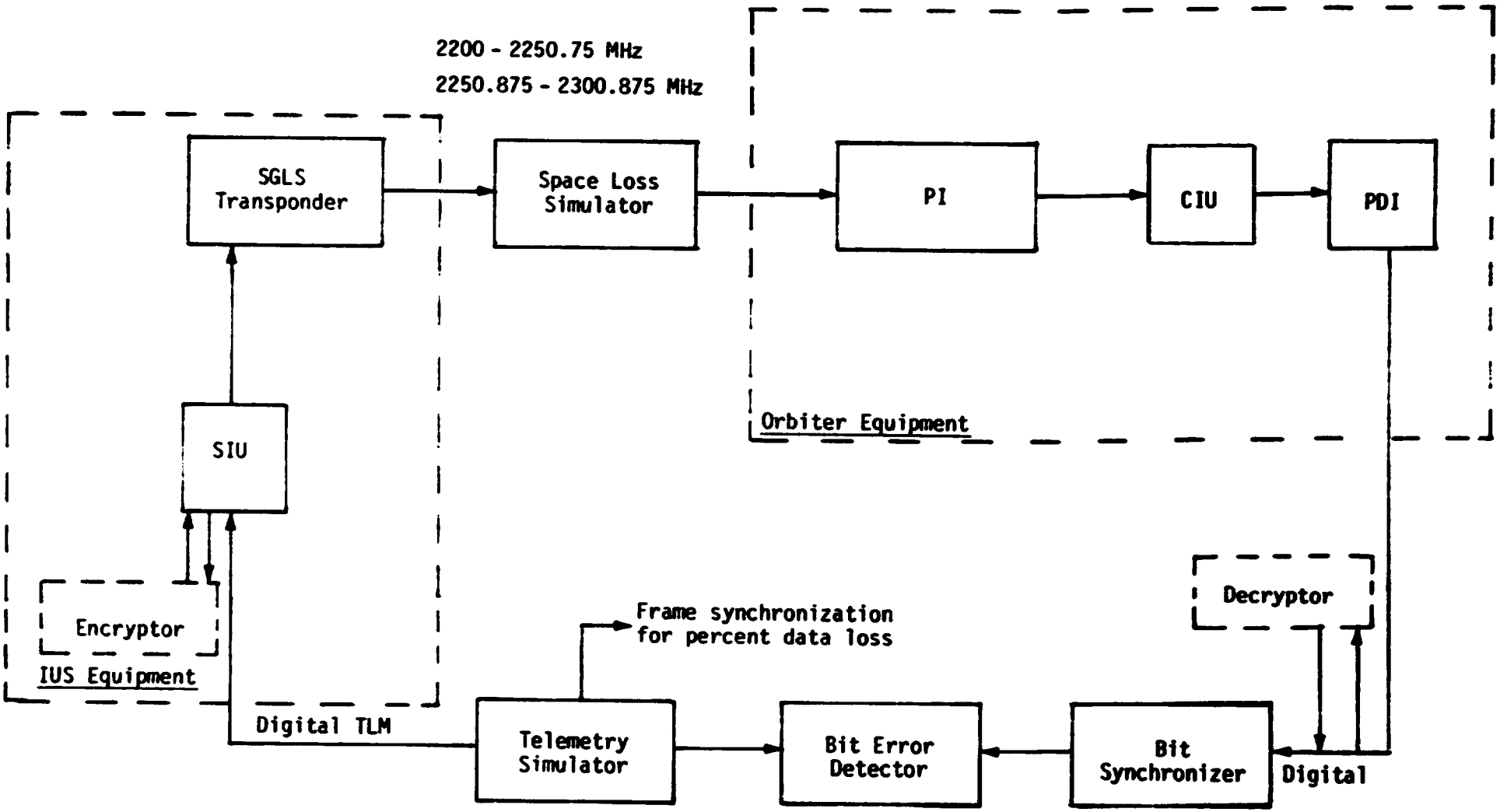

Figure 34. DOD Telemetry RF Test Link 6
SGLS Telemetry

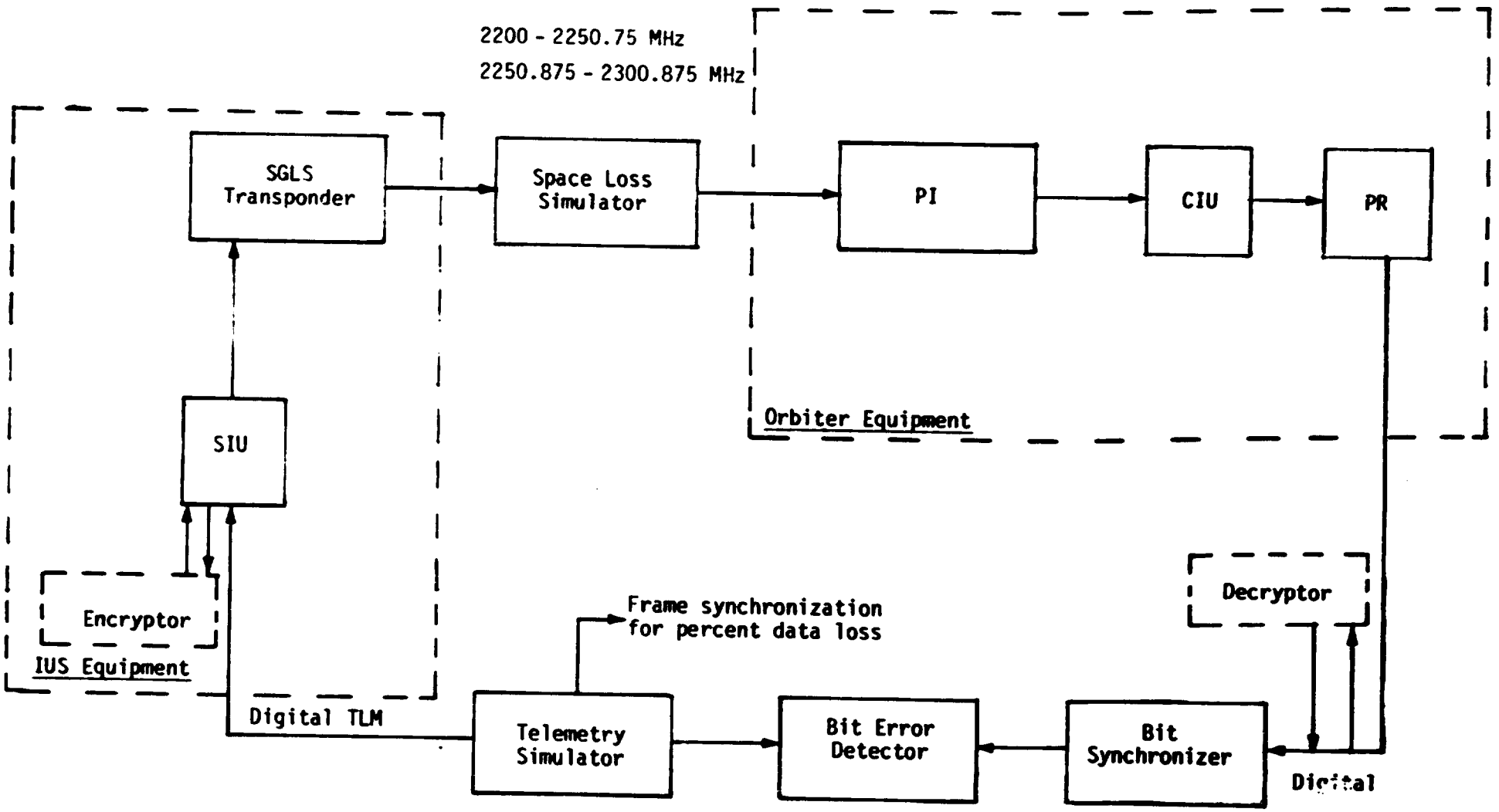

Figure 35. DOD Telemetry RF Test Link 7
SGLS Telemetry

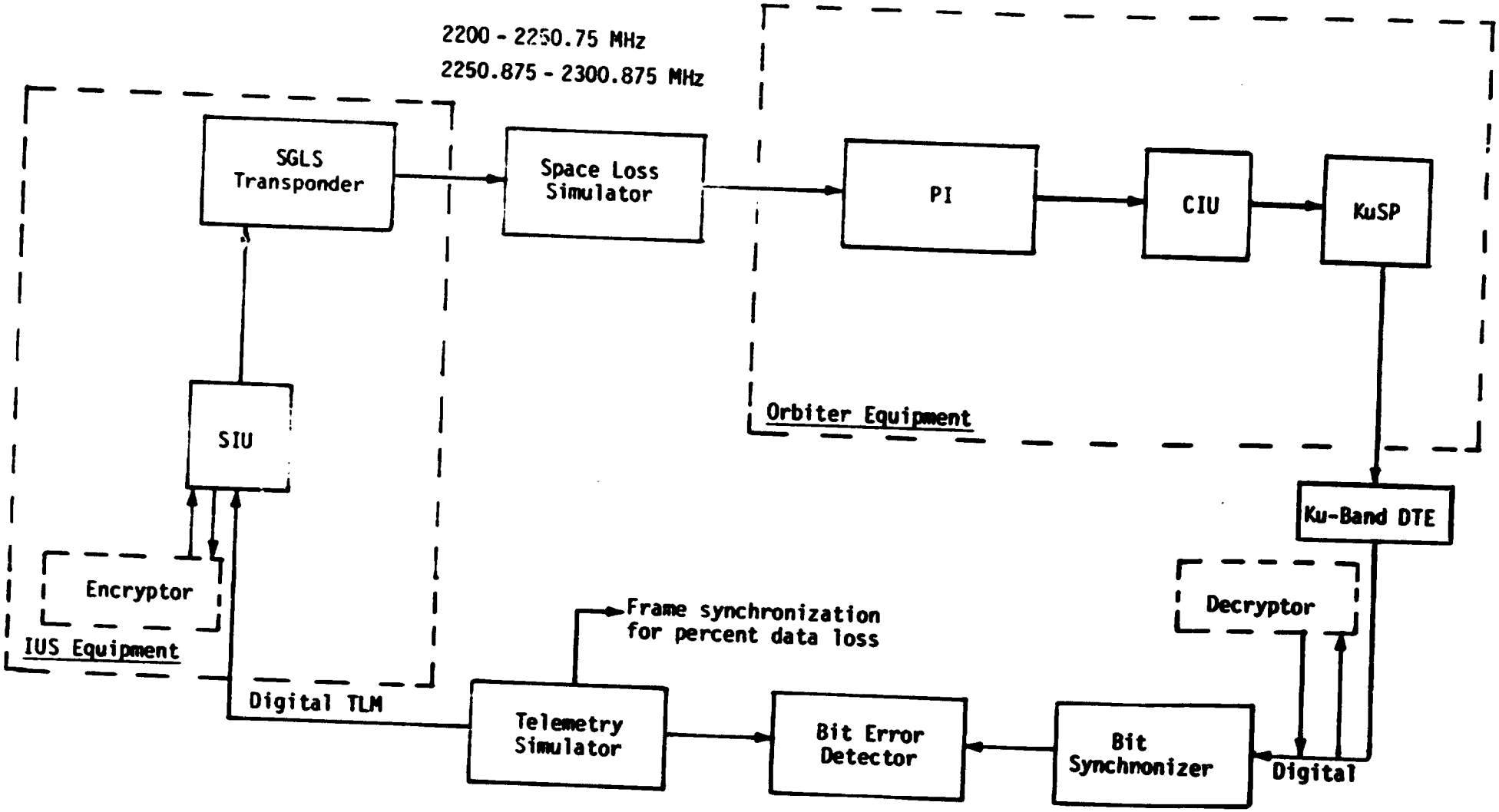

Figure 36. DOD Telemetry RF Test Link 8
SGLS Telemetry

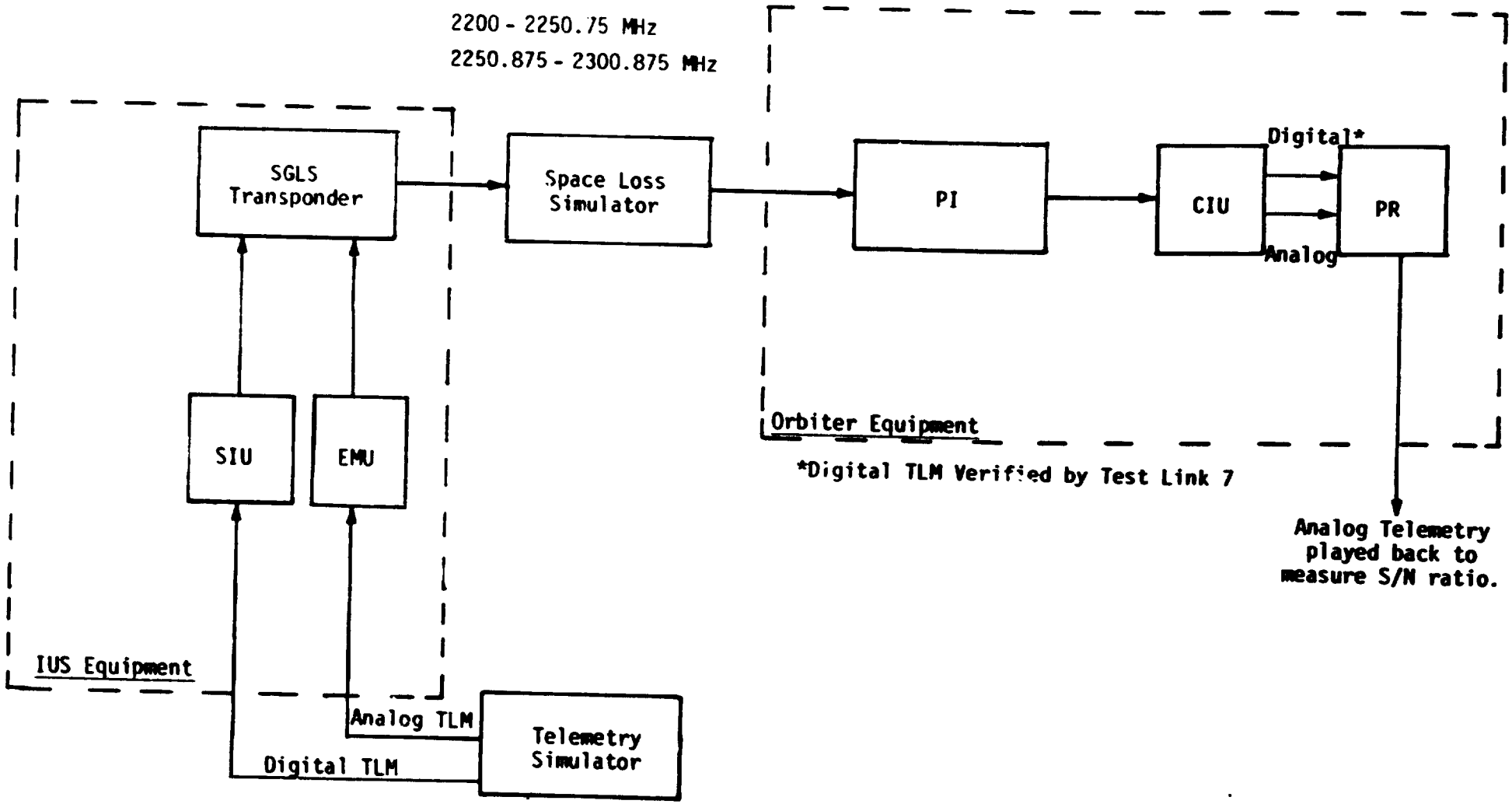

Figure 37. DOD Telemetry RF Test Link 9
SGLS Telemetry

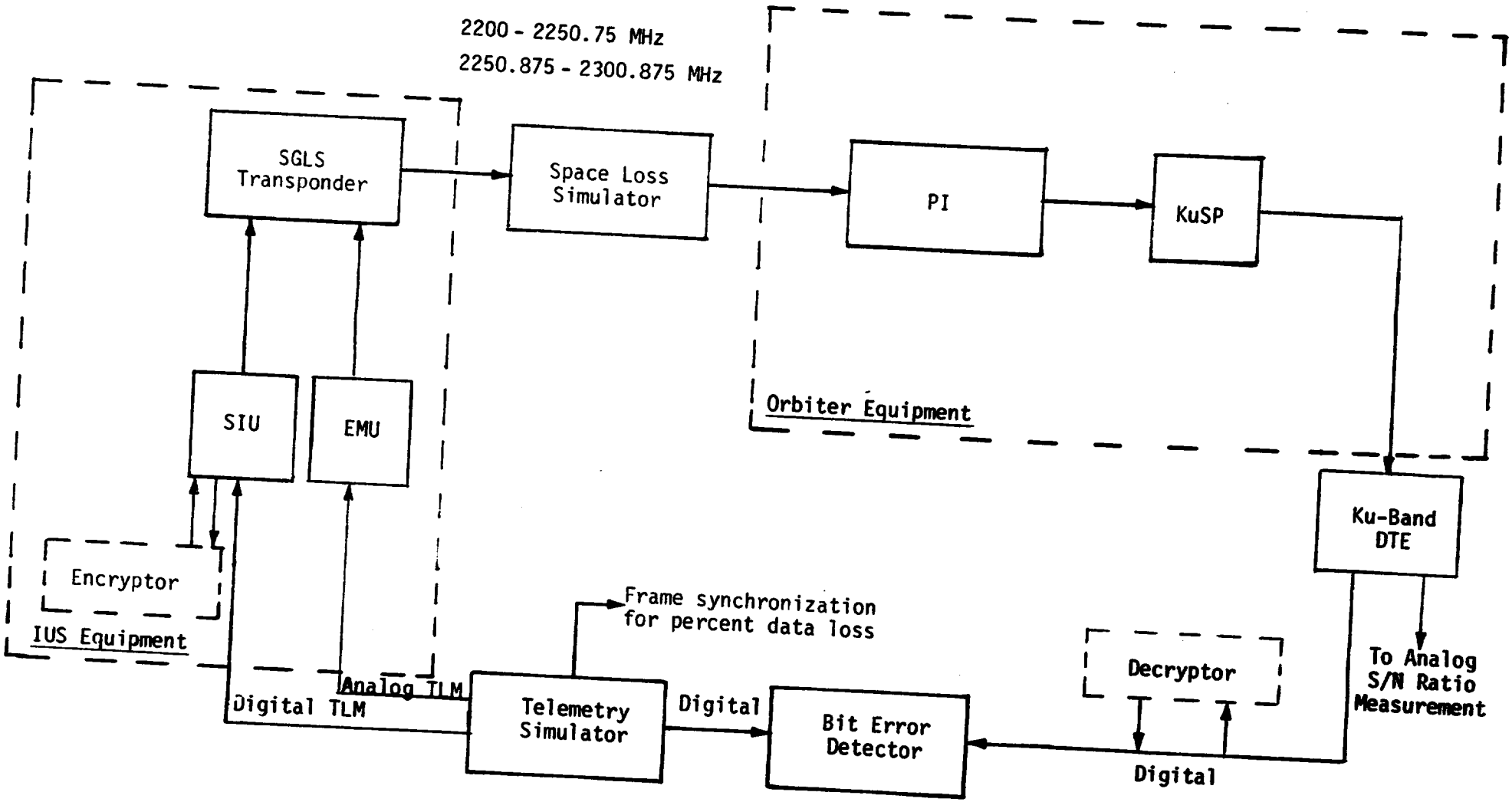

Figure 38. DOD Telemetry RF Test Link 10
SGLS Telemetry

Table 9. DOD Telemetry RF Test Summary (Return Link)

Test Links 5-8 (Figures 33-36)	
Measured parameters:	BER and percent data loss as functions of Orbiter total Prec/No.
Test conditions:	• Either IUS transponder frequency* • Signal combination 5 • With and without encryption
Test Link 9 (Figure 37)	
Measured parameter:	SNR as function of Orbiter total Prec/No.
Test conditions:	• Either IUS transponder frequency* • Signal combination 5
Test Link 10 (Figure 38)	
Measured parameters:	BER and percent data as functions of Orbiter total Prec/No.
Test conditions:	• Either IUS transponder frequency* • Signal combinations 6-8 • With and without encryption
Measured parameter:	SNR as function of Orbiter total Prec/No.
Test conditions:	• Either IUS transponder frequency* • Signal combinations 6 and 9

*Both IUS frequencies are in the same band (high or low) and, typically, are very close to each other.

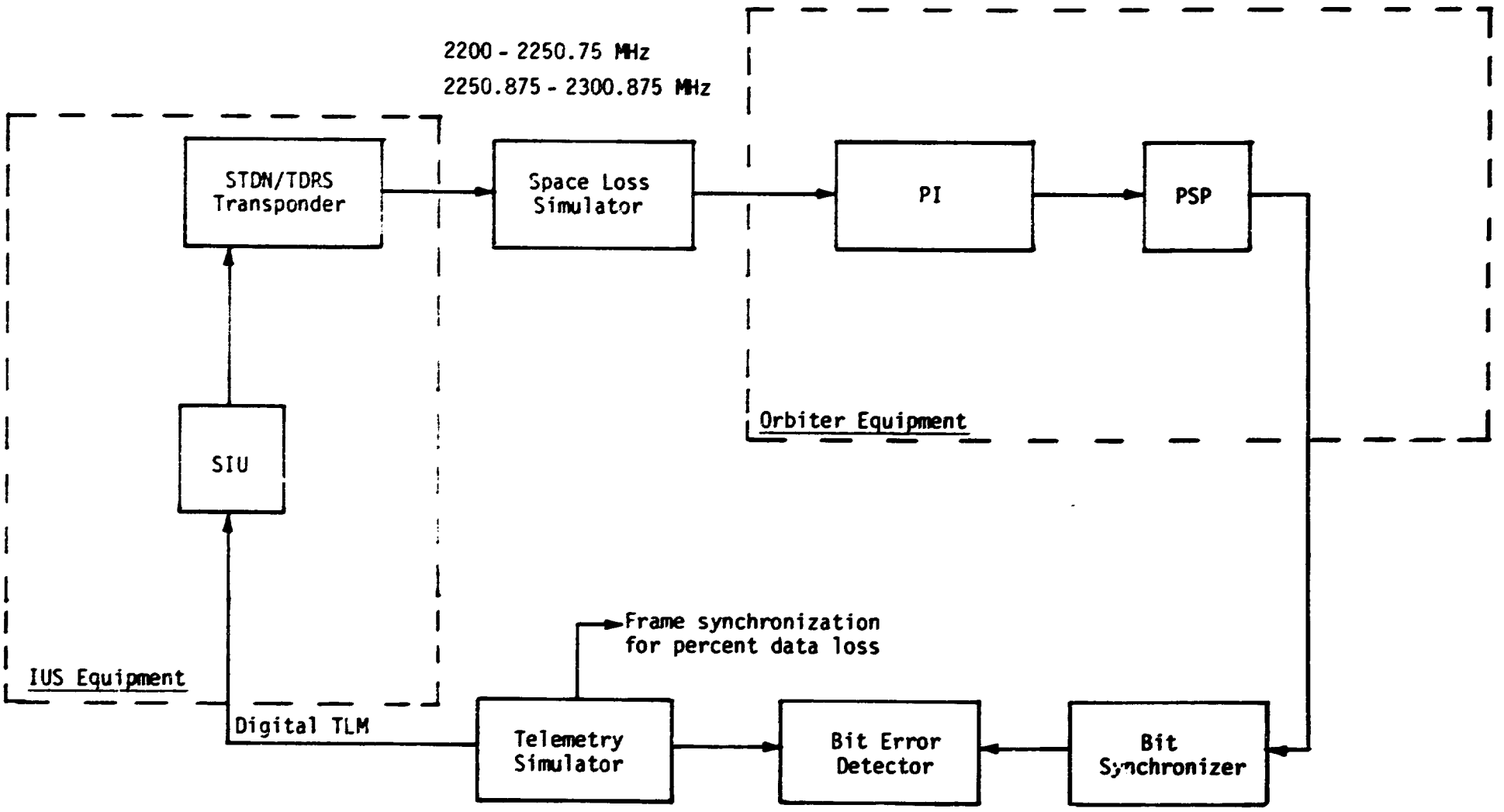

Figure 39. NASA Telemetry RF Test Link 11
STDN/TDRS Telemetry

Table 10. NASA Telemetry RF Test Summary (Return Link)

Test Link 11 (Figure 39)	
Measured parameters:	BER and percent data loss as functions of Orbiter total Prec./No.
Test conditions:	• Either IUS transponder frequency* • Signal combinations 10 and 11

Note: NASA "bent-pipe" configuration is identical to the DOD configuration, test link 10.

*Both IUS frequencies are in the same band (high or low) and, typically, are very close together.

4.3.3 RF Acquisition Tests

The purpose of these tests will be to evaluate the capability of the Orbiter PI and the IUS transponder to provide automatic RF acquisition that meets the Shuttle mission requirements.

The RF acquisition tests will be performed under computer control. The desired number of acquisition trials will be accomplished through computer-generated commands to the ESTL ranging and doppler simulator (ERDS) which switches the RF link on and off. Even though the Orbiter/IUS link tests will require no doppler offsets or ranging, the ERDS is still needed to provide control for the test sequences.

An antenna switch simulator will be necessary for these tests to simulate the IUS switching from one antenna to another. The simulator will be controlled by the M642B computer through the ERDS.

The measurements will include acquisition threshold, acquisition time, reacquisition time after switching IUS antennas, and acquisition probability for each signal level. The RF acquisition tests are divided into forward link RF acquisition, return link RF acquisition and two-way RF acquisition tests.

4.3.3.1 Forward link RF acquisition tests (Orbiter to IUS)

The forward link RF acquisition capability will be evaluated by measuring acquisition threshold, acquisition time, reacquisition time after switching IUS antennas and acquisition probability, with and without encryption (DOD mode only), as functions of IUS total received power-to-noise-spectral density ratios. Acquisition tests will also be performed for the modulated forward link carrier to determine the effect on acquisition time and threshold.

Figure 40 shows the DOD forward link RF acquisition functional configuration, test link 12, and Table 11 summarizes the tests. The signal combinations shown in Table 11 are from Table 3.

Figure 41 shows the NASA forward link RF acquisition functional configuration, test link 13, and Table 12 summarizes the tests, with the signal combinations shown being from Table 4.

The results of these tests will be compared to performance predictions to ascertain how well the measured results compare with theory.

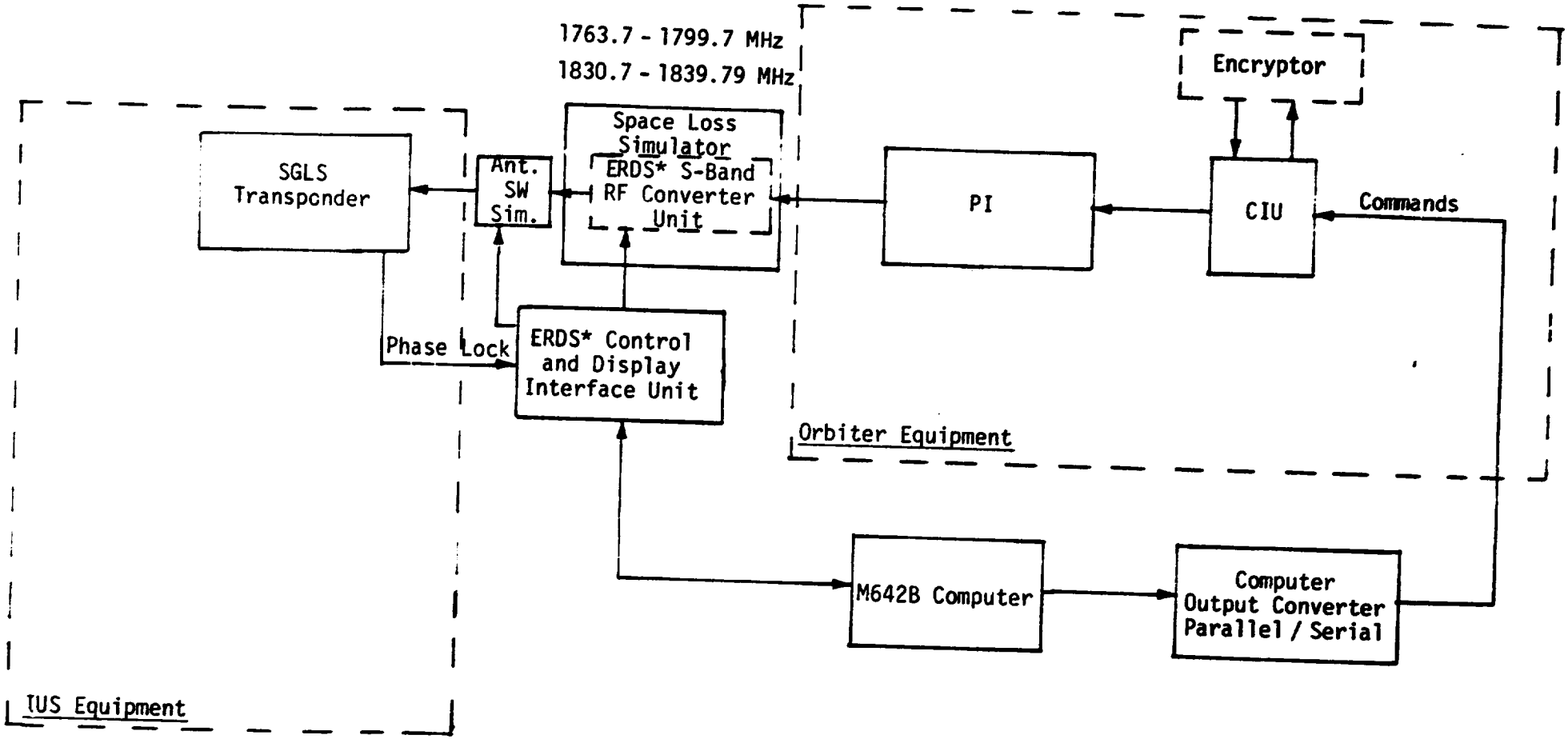

*ERDS (ESTL Range and Doppler Simulator)

Figure 40. DOD Forward Link RF Acquisition--Test Link 12 SGLS Commands

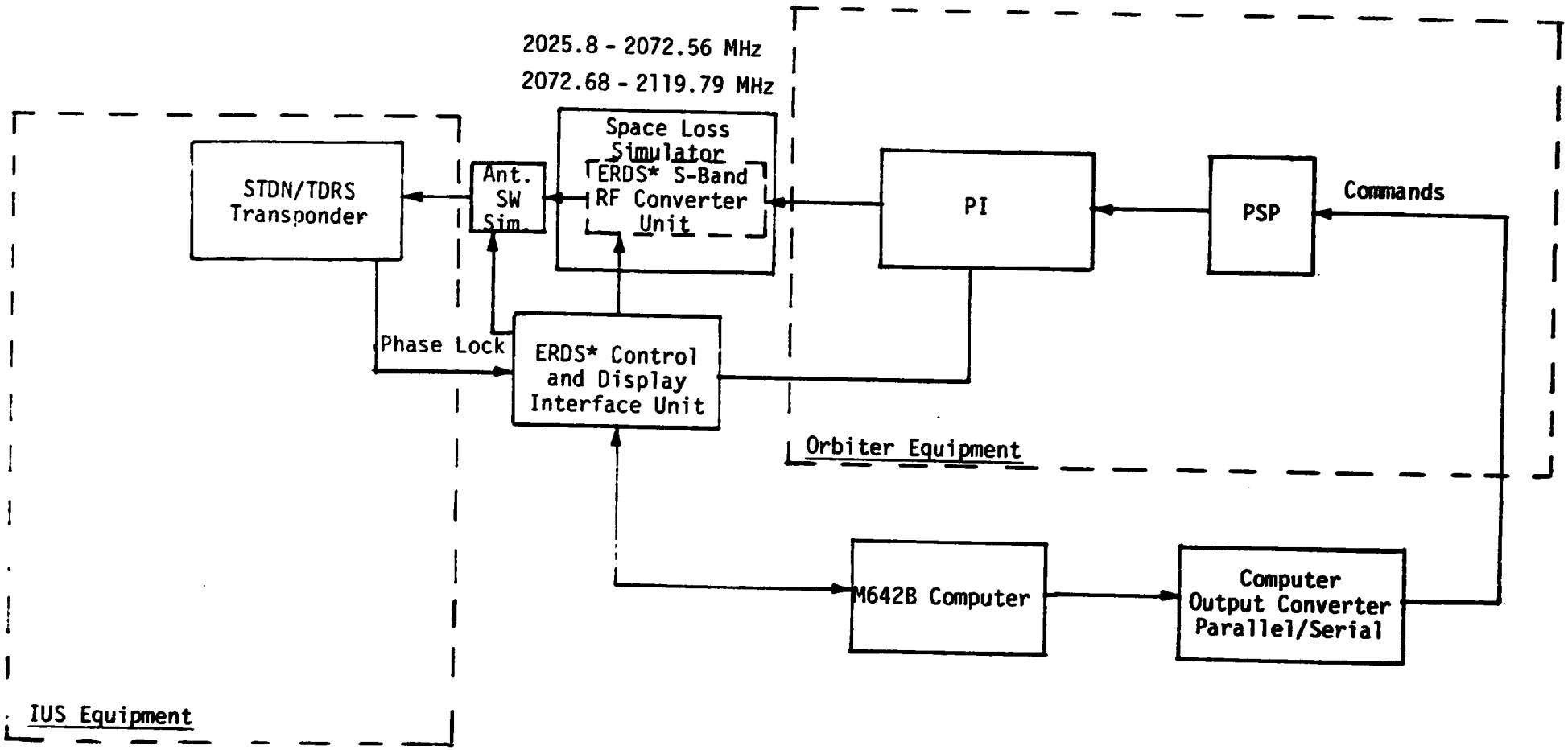

*ERDS (ESTL Range and Doppler Simulator)

Figure 41. NASA Forward Link RF Acquisition--Test Link 13 STDN/TDRS Commands

Table 11. DOD Forward Link RF Acquisition Test Summary

Test Link 12 (Figure 40)	
Measured parameters:	Acquisition threshold, acquisition time, reacquisition time after switching IUS antennas and acquisition probability as functions of IUS total Prec/No.
Test conditions:	• Either IUS transponder frequency* • Coherent and noncoherent modes • Carrier only and signal combination 2 • With and without encryption

Table 12. NASA Forward Link RF Acquisition Test Summary

Test Link 13 (Figure 41)	
Measured parameters:	Acquisition threshold, acquisition time, reacquisition time after switch IUS antennas and acquisition probability as functions of IUS total Prec/No.
Test conditions:	• Either IUS transponder frequency* • Coherent and noncoherent modes • Carrier only and signal combinations 3 and 4

*Both IUS frequencies are in the same band (high or low) and, typically, are very close together.

The measured results will also be compared with any program requirements to verify that the forward link RF acquisition will support a Shuttle mission.

4.3.3.2 Return link RF acquisition tests (IUS to Orbiter)

The return link RF acquisition capability will be evaluated by measuring acquisition threshold, acquisition time, reacquisition time after switching IUS antennas and acquisition probability, with and without encryption (DOD mode only), as functions of Orbiter total received power-to-noise spectral density ratios. Acquisition tests will also be performed for the modulated return link carrier to determine the effect on acquisition time and acquisition threshold.

Figure 42 shows the DOD return link RF acquisition functional configuration, test link 14, and Table 13 summarizes the tests. The signal combinations shown in Table 13 are from Table 5.

Figure 43 shows the NASA return link RF acquisition functional configuration, test link 15, and Table 14 summarizes the tests, with the signal combinations shown being from Table 6.

The results of these tests will be compared to performance predictions to ascertain how well the measured results compare with theory. The measured results will also be compared with any program requirements to verify that the return link RF acquisition tests will support a Shuttle mission.

4.3.3.3 Two-way RF acquisition tests

The two-way RF acquisition capability will be evaluated by measuring acquisition threshold, acquisition time, reacquisition time after switching IUS antennas and acquisition probability, with and without encryption (DOD mode only), as functions of total received power-to-noise spectral density ratios. For the coherent IUS transponder mode, tests will also be performed to determine the out-of-lock time between when return link acquisition is lost because of forward link acquisition and when two-way acquisition is completed.

Figure 44 shows the DOD two-way RF acquisition functional configuration, test link 16, and Table 15 summarizes the tests. The signal combinations shown in Table 15 are from Tables 3 and 5.

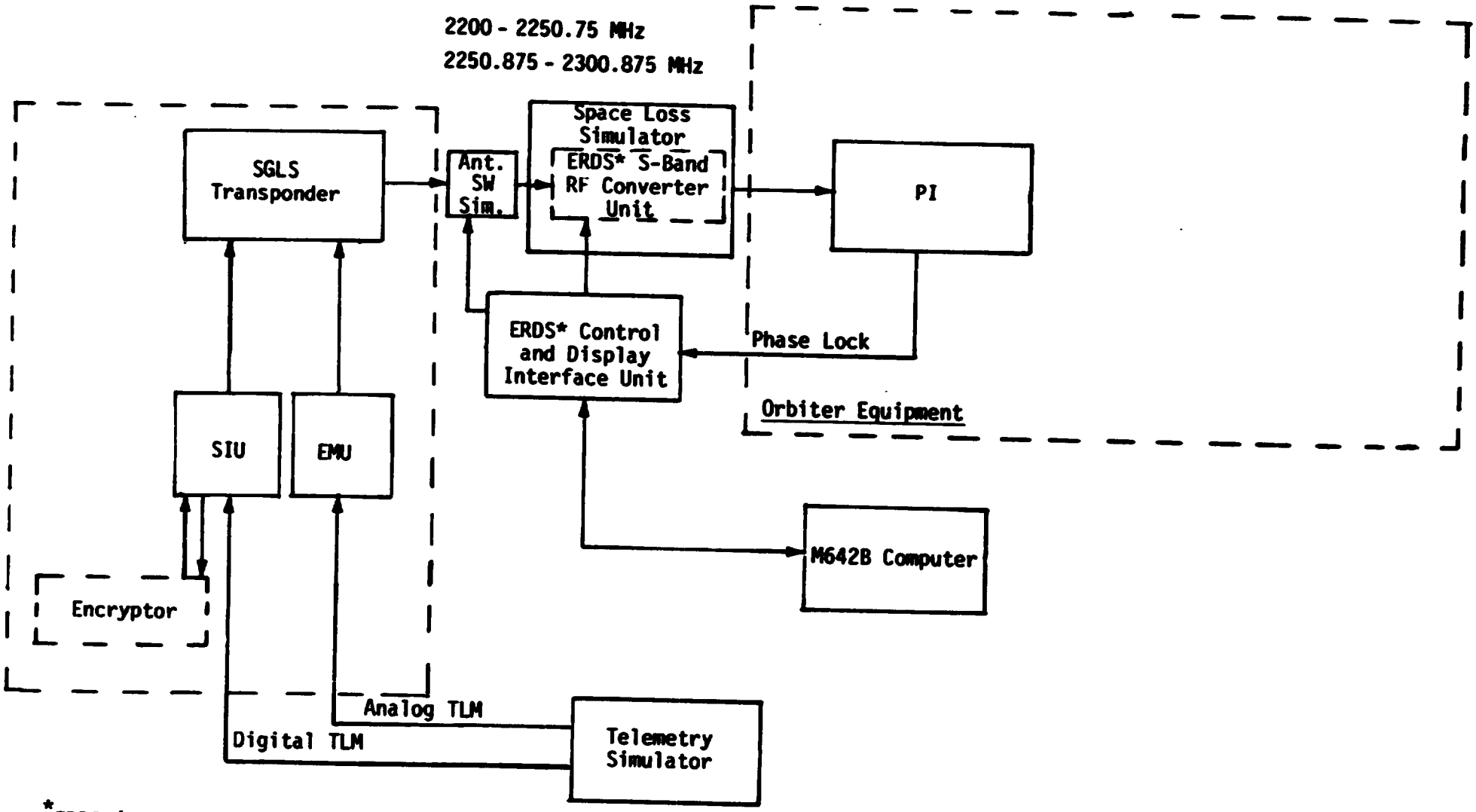

Figure 42. DOD Return Link RF Acquisition--Test Link 14 SGLS Telemetry

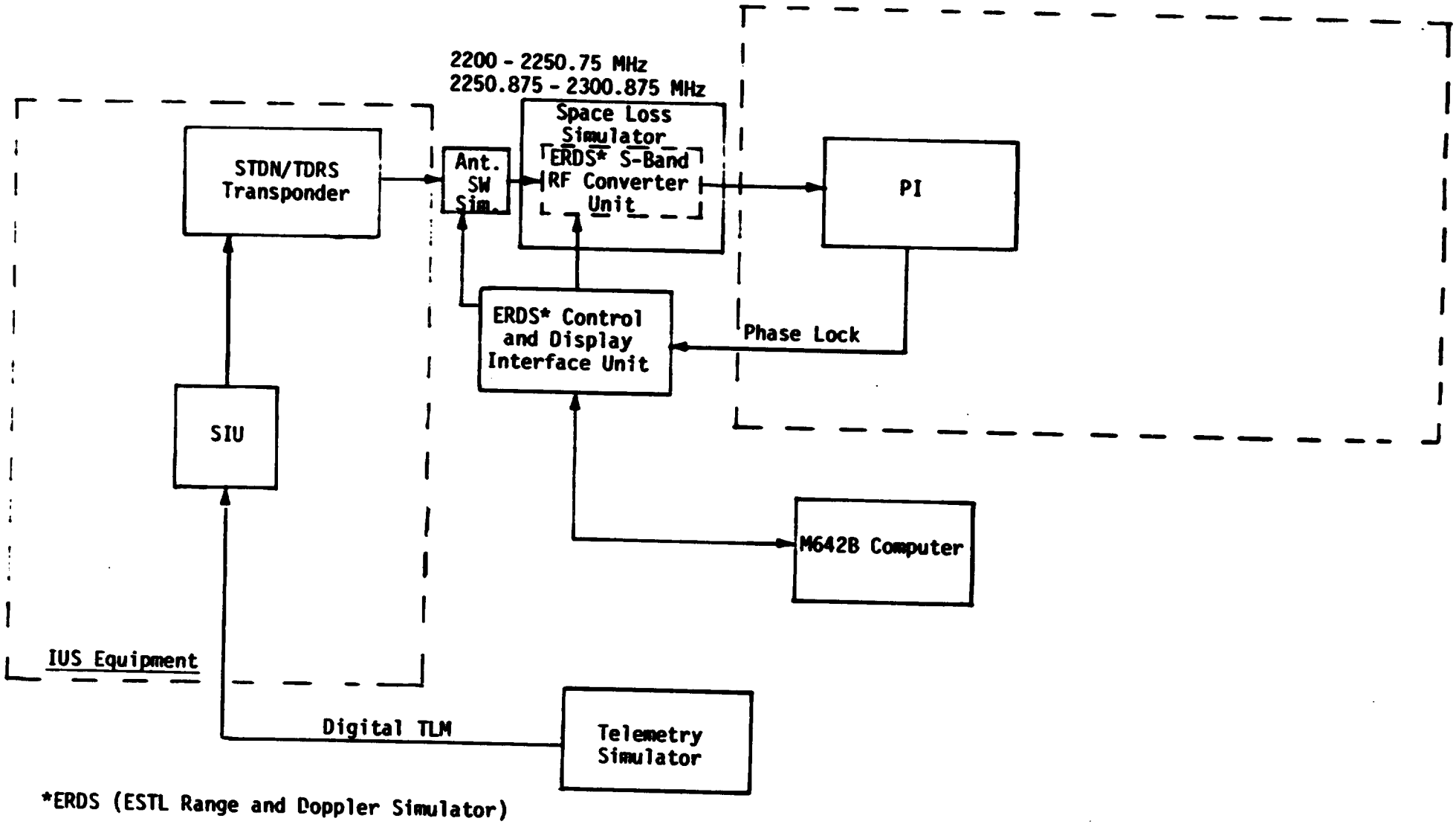

Figure 43. NASA Return Link RF Acquisition--Test Link 15 STDN/TDRS Telemetry

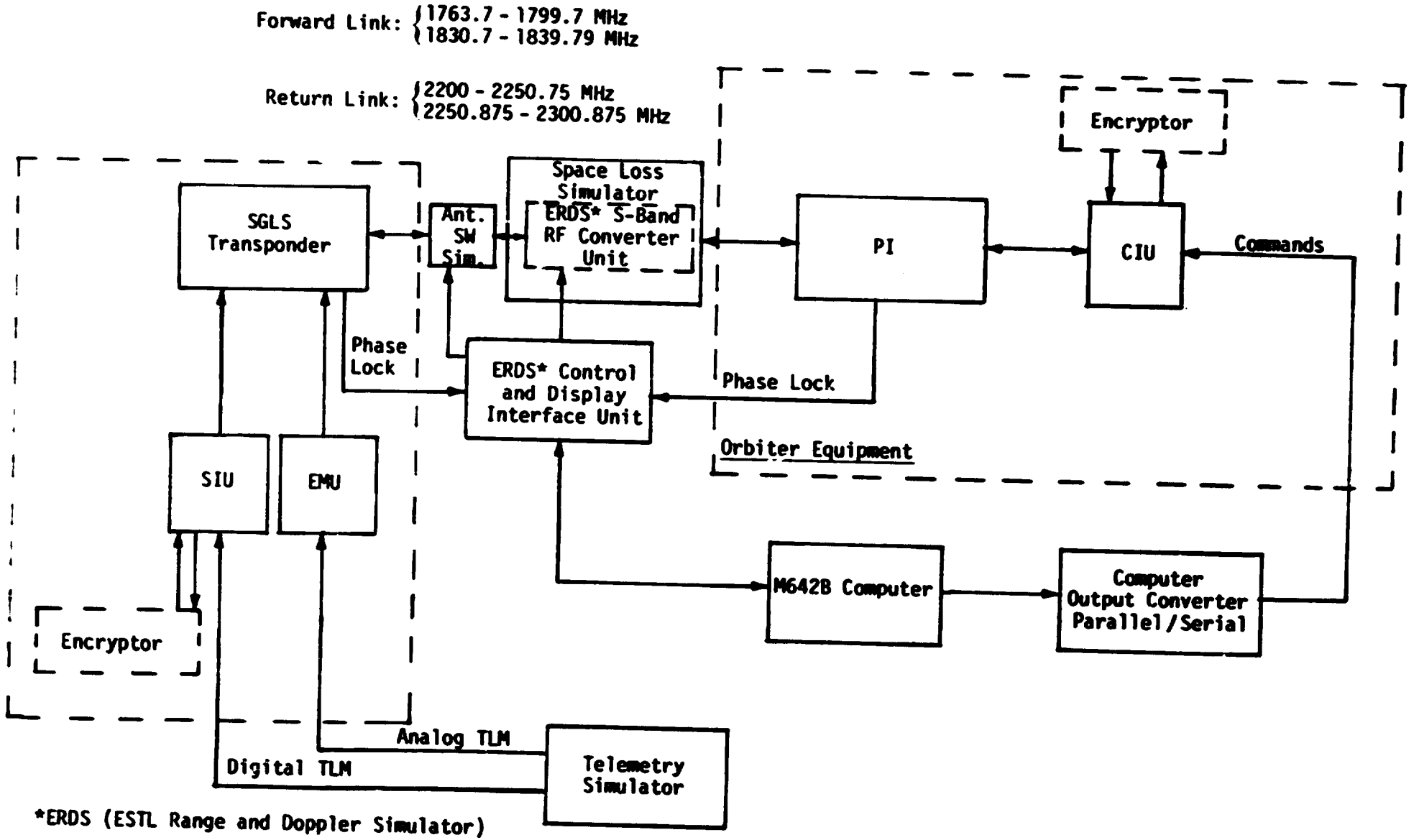

Figure 44. DOD Two-Way RF Acquisition--Test Link 16 SGLS Commands/Telemetry

Table 13. DOD Return Link RF Acquisition Test Summary

Test Link 14 (Figure 42)	
Measured parameters:	Acquisition threshold, acquisition time, reacquisition time after switching IUS antennas and acquisition probability as functions or Orbiter total Prec/No.
Test conditions:	• Either IUS transponder frequency* • Coherent and noncoherent modes • Carrier only and signal combination 5 • With and without encryption

Table 14. NASA Return Link RF Acquisition Test Summary

Test Link 15 (Figure 43)	
Measured parameters:	Acquisition threshold, acquisition time, reacquisition time after switching IUS antennas and acquisition probability as a function of Orbiter total Prec/No.
Test conditions:	• Either IUS transponder frequency* • Coherent and noncoherent modes • Carrier only and signal combinations 10 and 11

*Both IUS frequencies are in the same band (high or low) and, typically, are very close together.

Table 15. DOD Two-Way RF Acquisition Test Summary

Test Link 16 (Figure 44)

Measured parameters: Acquisition threshold, acquisition time, reacquisition time after switching IUS antennas and acquisition probability as functions of total Prec/No.

Test conditions:

- Either IUS transponder frequency*
- Coherent and noncoherent modes
Forward	Return
Carrier only	Carrier only
Carrier only	Combination 5
Combination 2	Combination 5
- With and without encryption

Measured parameter: Reacquisition time after losing return link acquisition as a function of total Prec/No.

Test conditions:

- Either IUS transponder frequency*
- Coherent mode
Forward	Return
Combination 2	Combination 5

*Both IUS frequencies are in the same band (high or low) and, typically, are very close together.

Figure 45 shows the NASA two-way RF acquisition functional configuration, test link 17, and Table 16 summarizes the tests, with the signal combinations shown being from Tables 4 and 6.

The results of these tests will be compared to performance predictions to ascertain how well the measured results compare with theory. The measured results will also be compared with any program requirements to verify that the two-way acquisition tests will support a Shuttle mission.

4.4 System Compatibility and Performance Tests (Hardline Links)

As previously stated, a hardline umbilical provides two-way communication between the IUS and the Orbiter in the attached mode. The purpose of these tests is to verify the overall system compatibility of the IUS/Orbiter hardline interface.

The tests outlined in this section are more go/no-go types of tests instead of qualitative in nature and are designed primarily to exercise the interfaces. No attempt has been made to simulate the actual transients or EMI which the hardline umbilical would experience in an actual Orbiter.

The tests have been divided into forward and return link tests. The Orbiter/IUS forward link will evaluate the command channel performance while the IUS/Orbiter return link will evaluate the telemetry channel performance. Tables 17-20 outline the signal combinations which will be used during the system hardline interface verifications.

4.4.1 Forward Link Tests (Hardline)

The command channel will be evaluated by verifying that 10,000 error-free commands can be received. Figure 46 shows the DOD command hardline test configuration, test link 18, and Table 21 summarizes the tests. The signal combination shown in Table 21 is from Table 17.

Figure 47 shows the NASA command hardline test configuration, test link 19, with Table 22 summarizing the tests. The signal combinations shown in Table 22 are from Table 18.

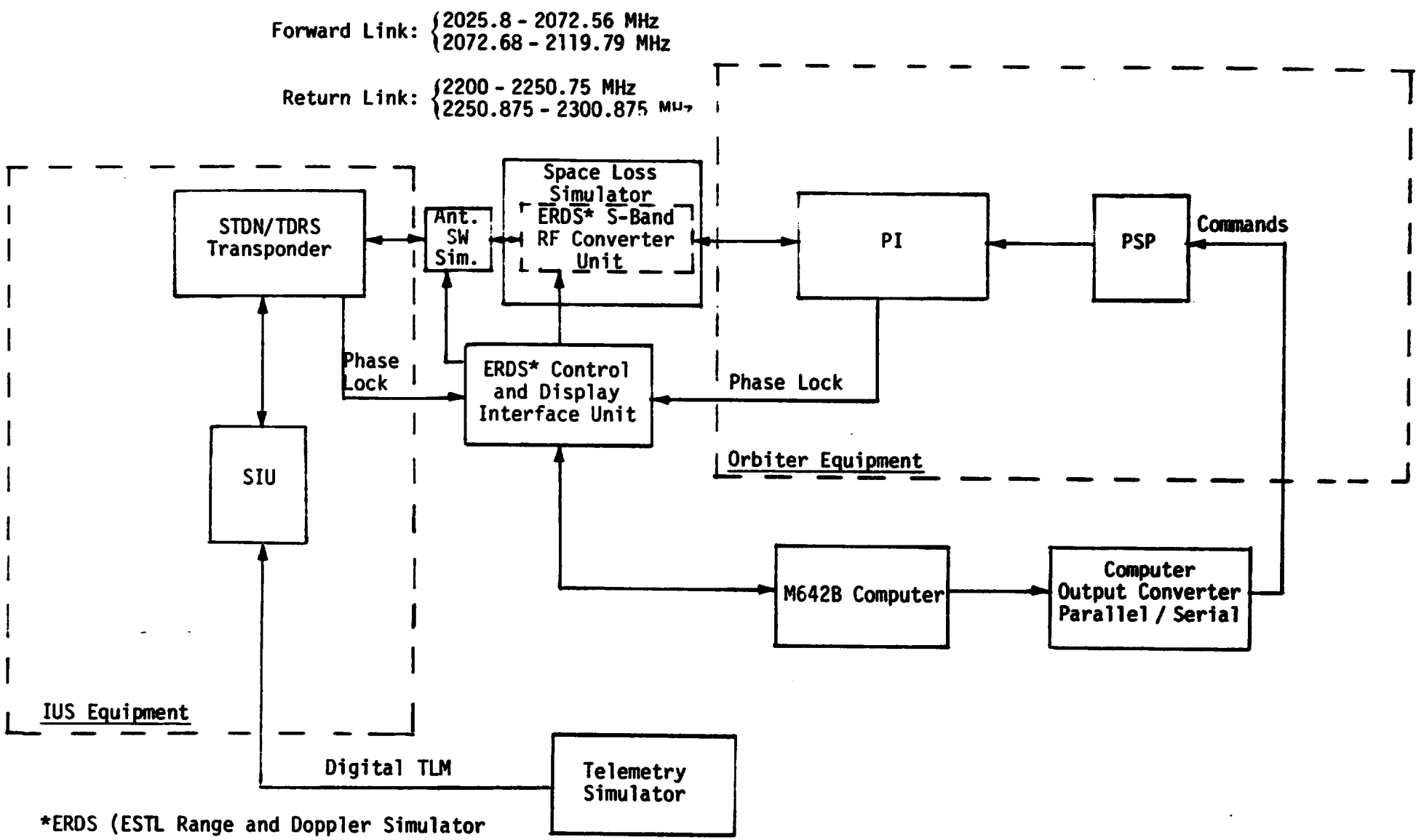

Figure 45. NASA Two-Way RF Acquisition--Test Link 17 STDN/TDRS Commands/Telemetry

Table 16. NASA Two-Way RF Acquisition Test Summary

Test Link 17 (Figure 45)

Measured parameters: Acquisition threshold, acquisition time, reacquisition time after switching IUS antennas and acquisition probability as functions of total Prec/No.

Test conditions:

- Either band IUS transponder
- Coherent and noncoherent modes
- Forward / Return

  Carrier only / Carrier only
  Carrier only / Combination 10
  Carrier only / Combination 11
  Combination 3 / Combination 10
  Combination 4 / Combination 11
  Combination 3 / Combination 11

Measured parameters: Reacquisition time after losing return link acquisition as a function of total Prec/No.

Test conditions:

- Either IUS transponder frequency*
- Coherent mode
- Forward / Return

  Combination 3 / Combination 11

*Both IUS frequencies are in the same band (high or low) and, typically, are very close together.

Table 17. Forward Link Hardline Signal Combinations and Performance Requirements (DOD)

Combination	Information Transmitted	Modulation Techniques
1A*	2 ksps commands	FSK/AM
2A	1 ksps commands	FSK/AM

*Current CIU design is not capable of this rate.

Table 18. Forward Link Hardline Signal Combinations and Performance Requirements (NASA)

Combination	Information Transmitted	Modulation Techniques
3A	2 kbps commands	PSK
4A	7.8125 bps commands	PSK

Table 19. Return Link Hardline Signal Combinations and Performance Requirements (DOD)

Combination	Information Transmitted	Signal Coding	Modulation Techniques
6A	Telemetry 64 kbps digital	NRZ-L	--
5A	Telemetry 256 kbps digital	NRZ-L	--
6A	Telemetry, Analog (IRIG 1A, 2A and 3A Frequency)	--	FM

Table 20. Return Link Hardline Signal Combinations and Performance Requirements (NASA)

Combination	Information Transmitted	Signal Coding	Modulation Techniques
8A	Telemetry 16 kbps digital	NRZ-L	--
9A	Telemetry, 256 kbps digital	NRZ-L	--
10A	Telemetry, Analog (IRIG 1A, 2A and 3A Frequency)	--	FM

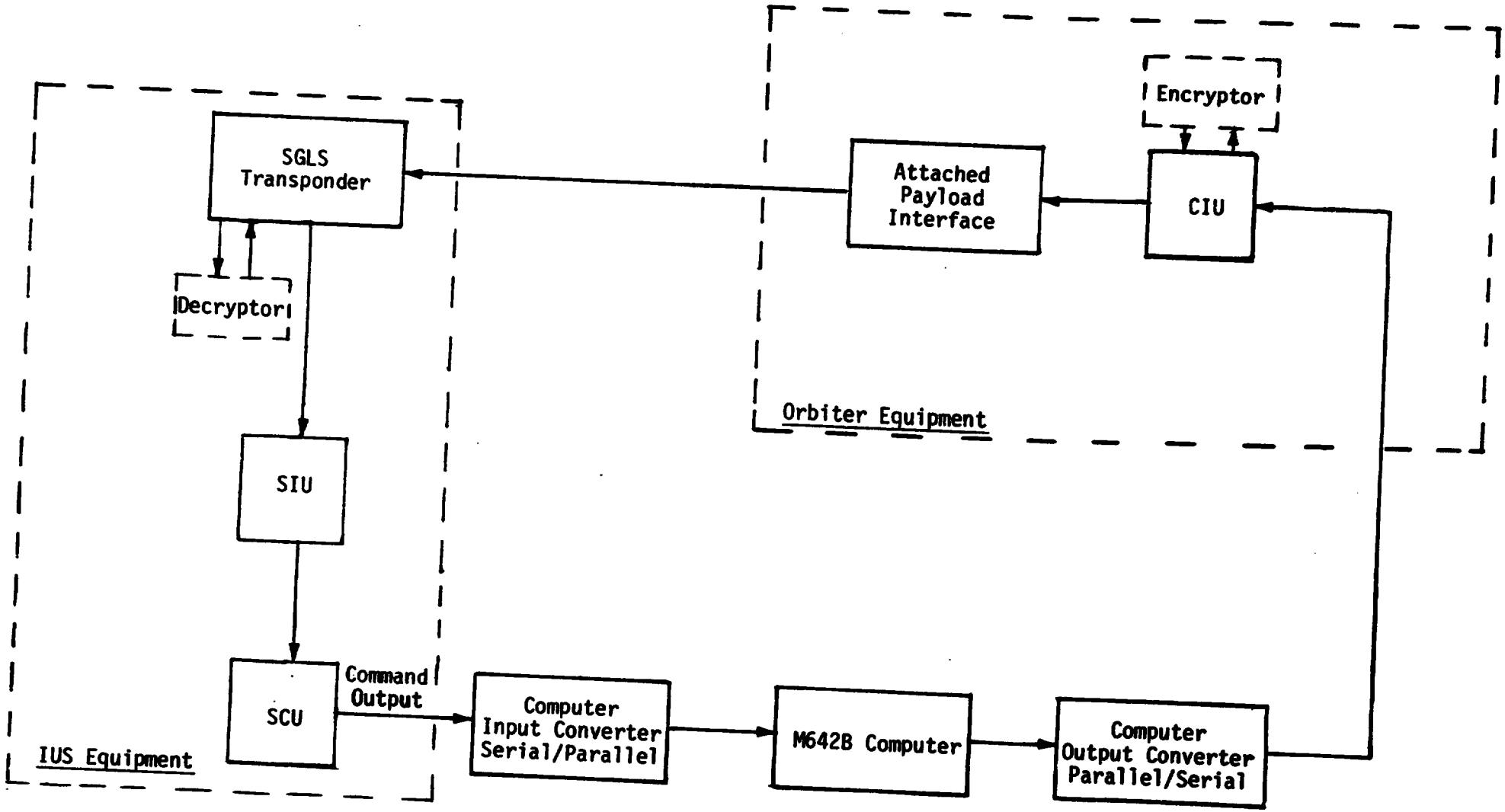

Figure 46. DOD Command Hardline Test Link 18
SGLS Commands

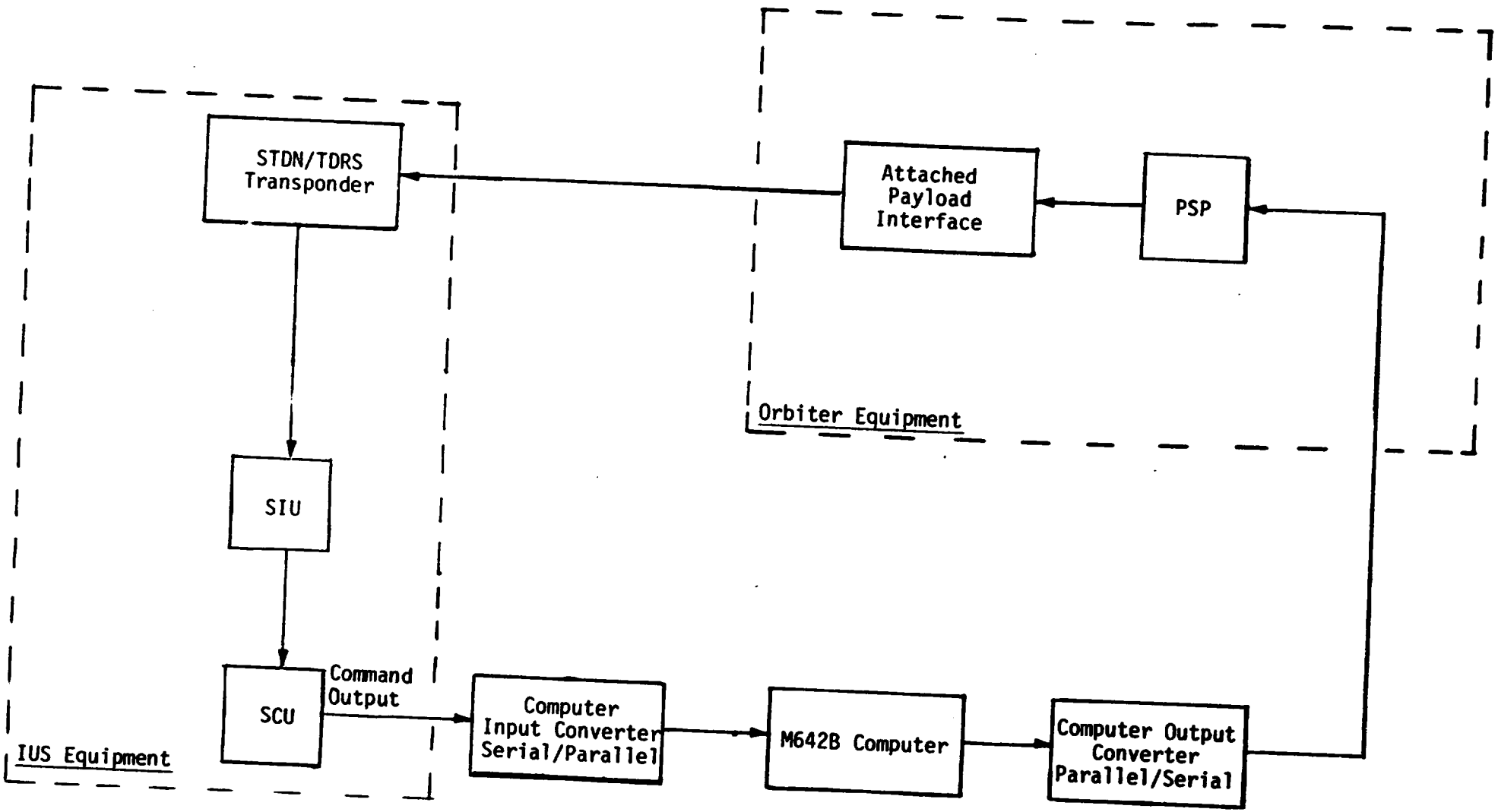

Figure 47. NASA Command Hardline Test Link 19
STDN/TDRS Commands

Table 21. DOD Command Hardline Test Summary
(Forward Link)

Test Link 18 (Figure 46)	
Measured parameter:	10,000 error-free commands received
Test conditions:	• Signal combination 2A

Table 22. NASA Command Hardline Test Summary
(Forward Link)

Test Link 19 (Figure 47)	
Measured parameter:	10,000 error-free commands received
Test conditions:	• Signal combinations 3A and 4A

4.4.2 Return Link Tests (Hardline)

The digital telemetry will be evaluated by verifying that 10^7 error-free bits can be received. The analog telemetry will be evaluated by measuring the Orbiter analog output signal-to-noise ratio (SNR).

Figures 48-54, test links 19-25, evaluate the DOD digital telemetry hardline performance and Figure 55, test link 26, evaluates the DOD analog hardline telemetry. Table 23 summarizes the DOD test results, and the signal combinations shown are from Table 19.

Figure 56-62, test links 27-33, evaluate the NASA digital telemetry hardline performance and Figure 63, test link 34, evaluates the NASA analog hardline telemetry. Table 24 summarizes the NASA test results. The signal combinations shown in Table 24 are from Table 20.

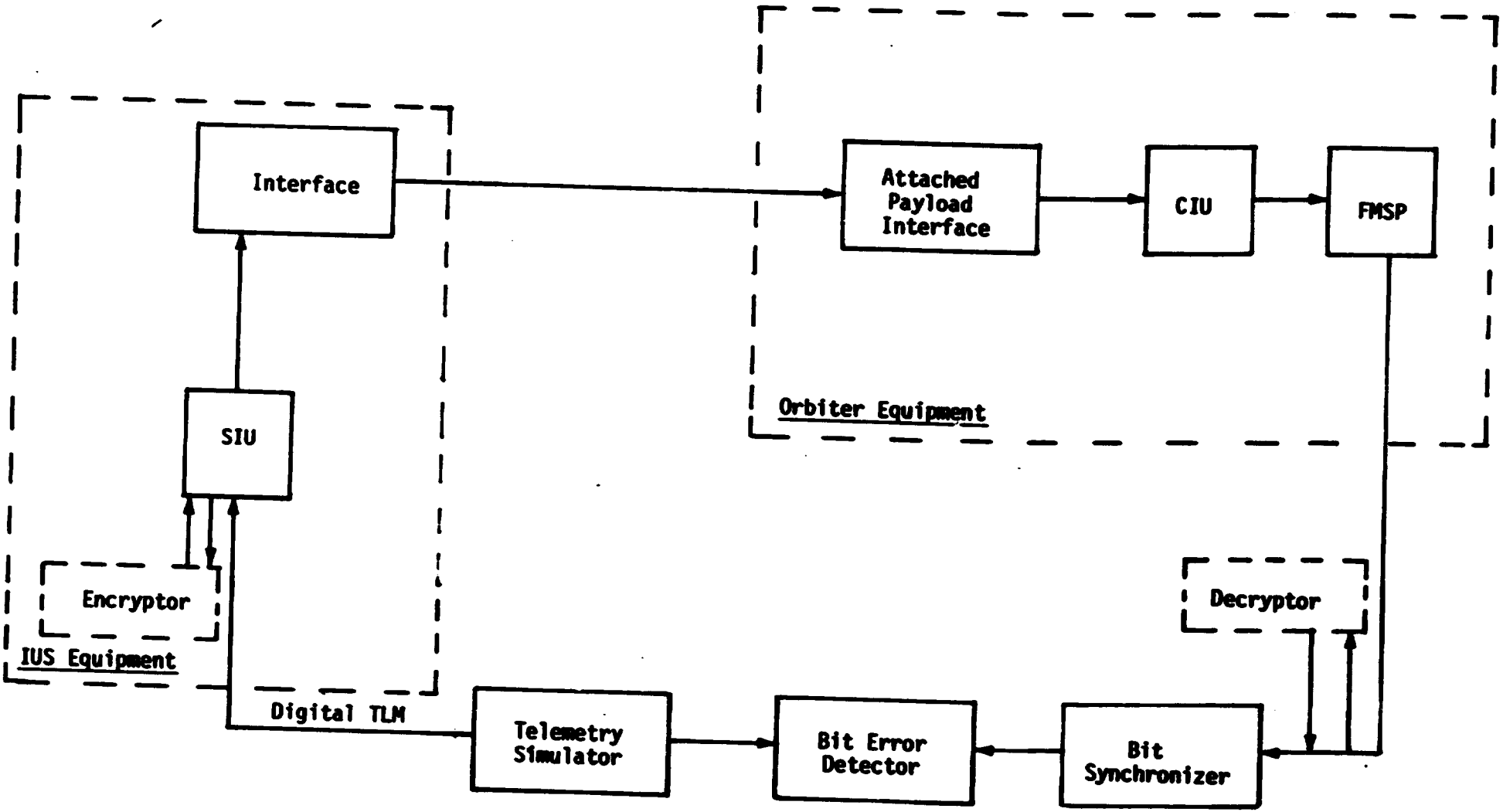

Figure 48. DOD Telemetry Hardline Test Link 19
SGLS Telemetry

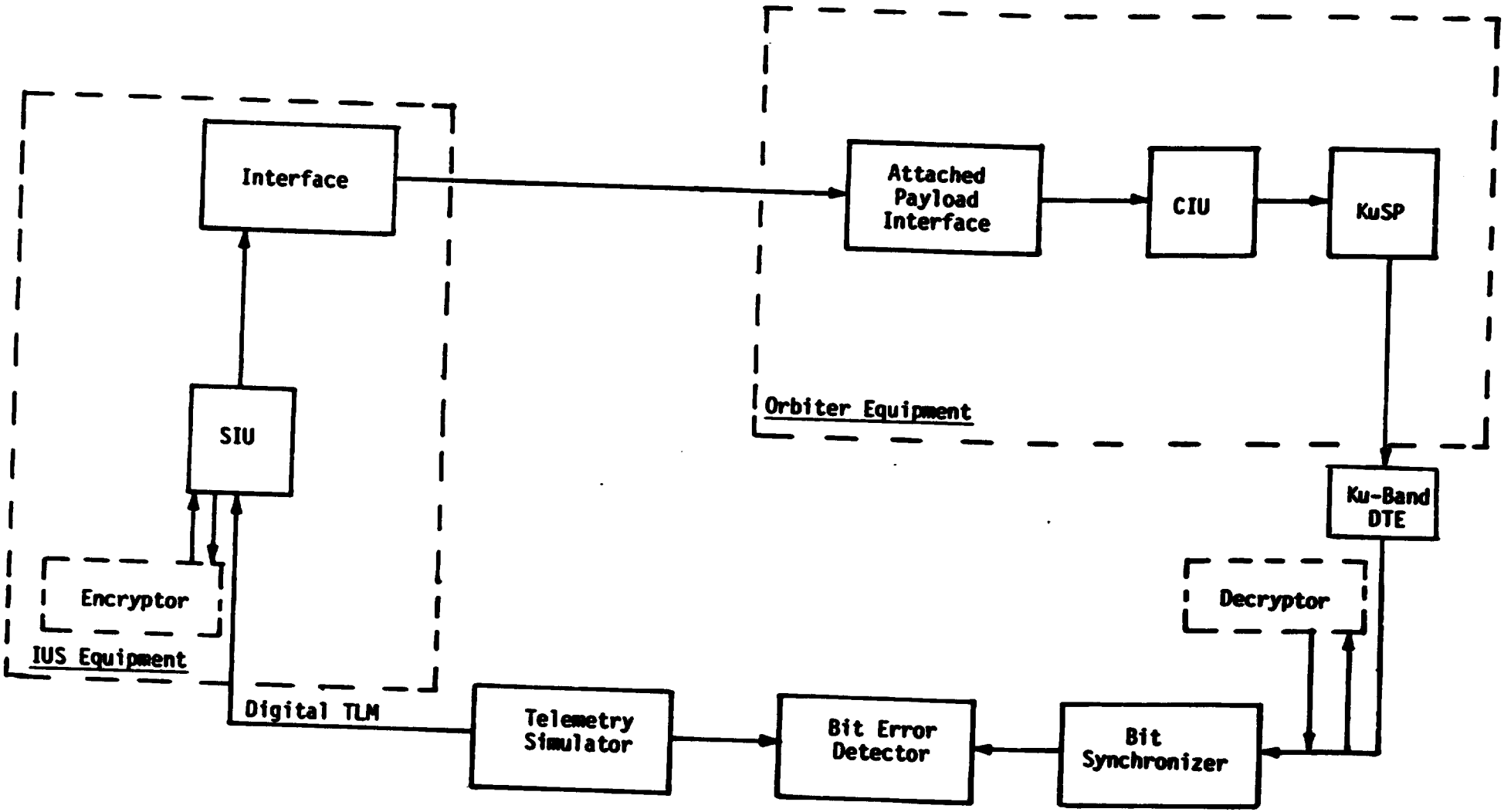

Figure 49. DOD Telemetry Hardline Test Link 20
SGLS Telemetry

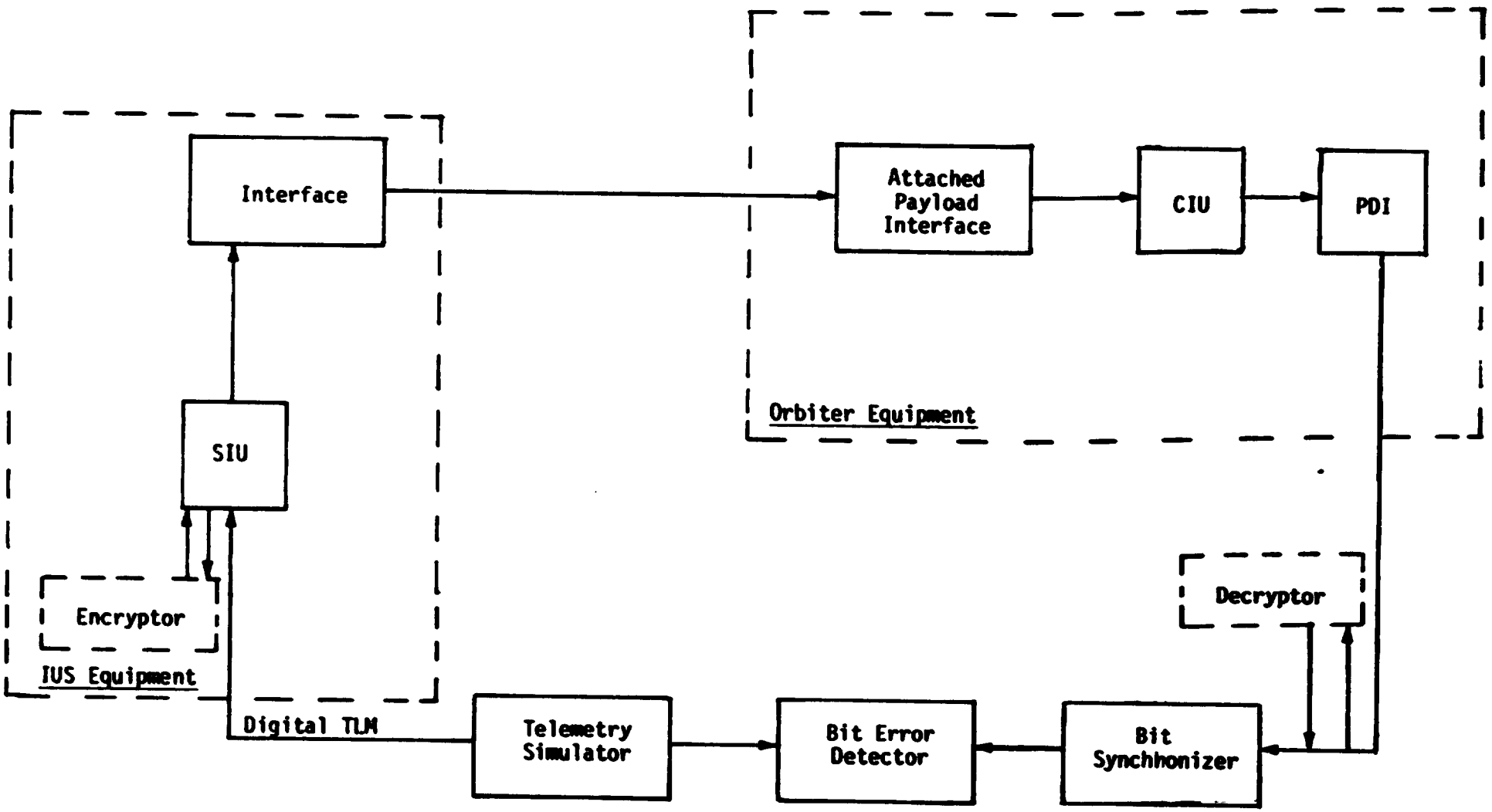

Figure 50. DOD Telemetry Hardline Test Link 21
SGLS Telemetry

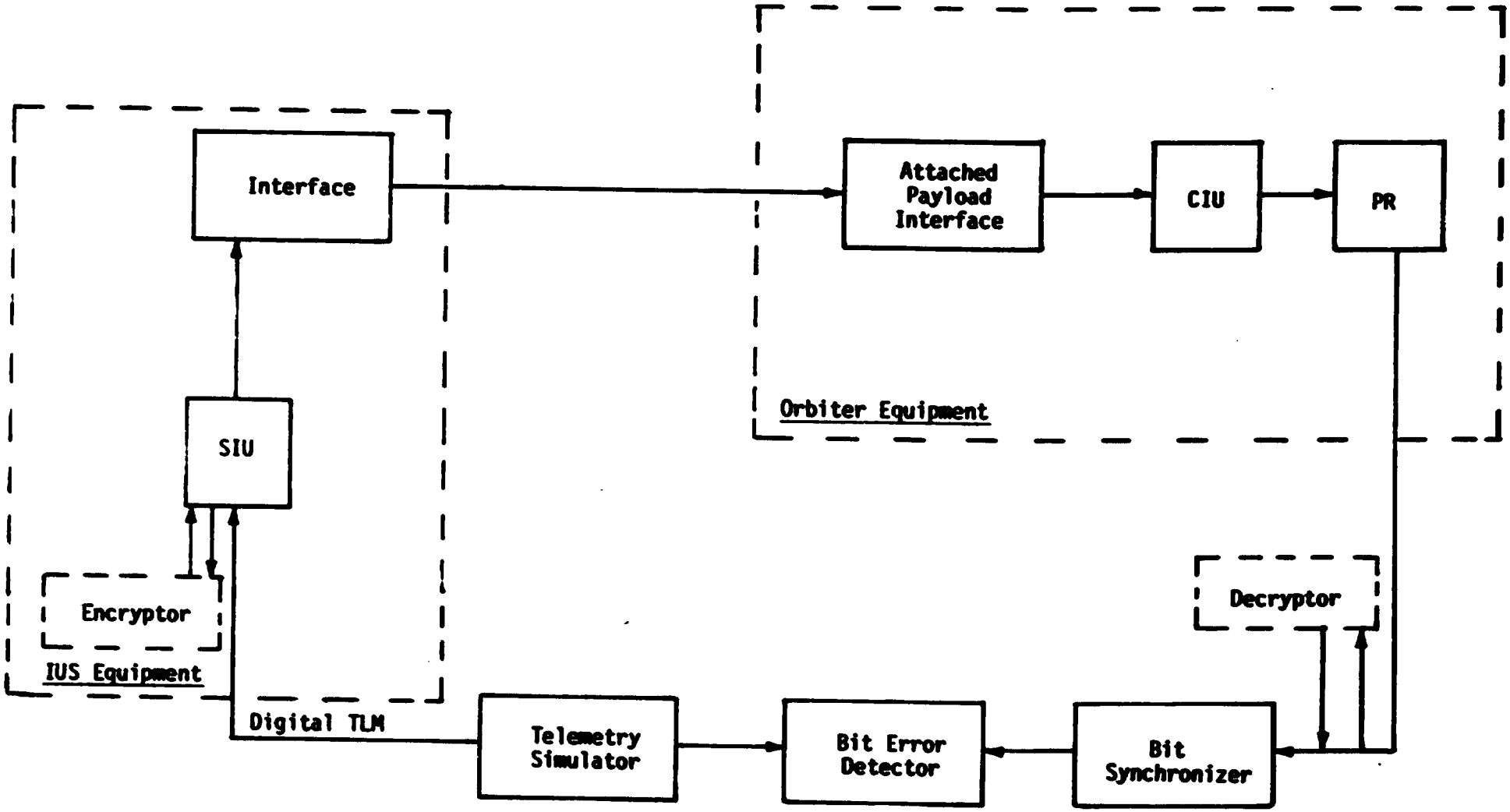

Figure 51. DOD Telemetry Hardline Test Link 22
SGLS Telemetry

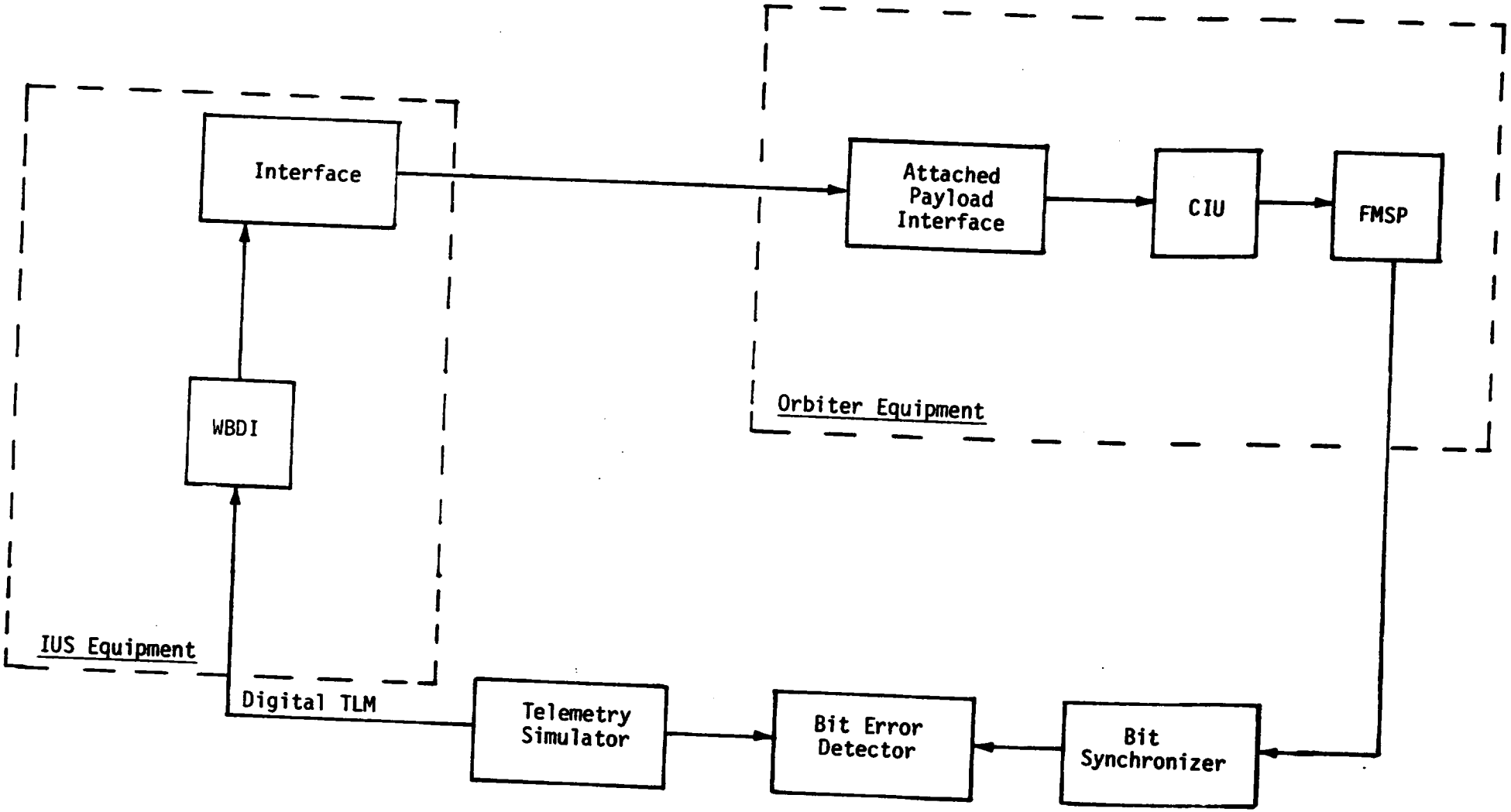

Figure 52. DOD Telemetry Hardware Test Link 23
SGLS Telemetry

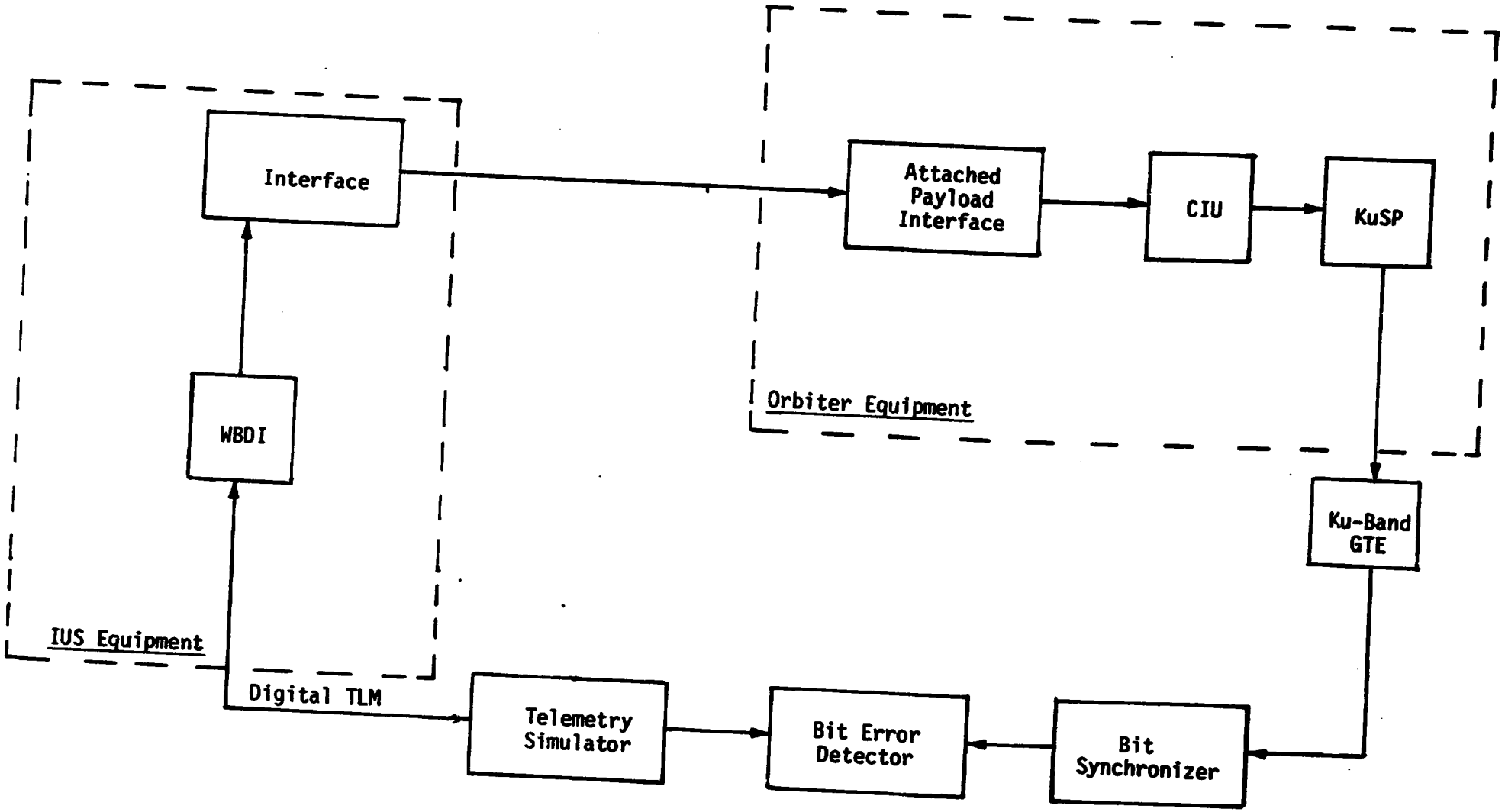

Figure 53. DOD Telemetry Hardline Test Link 24
SGLS Telemetry

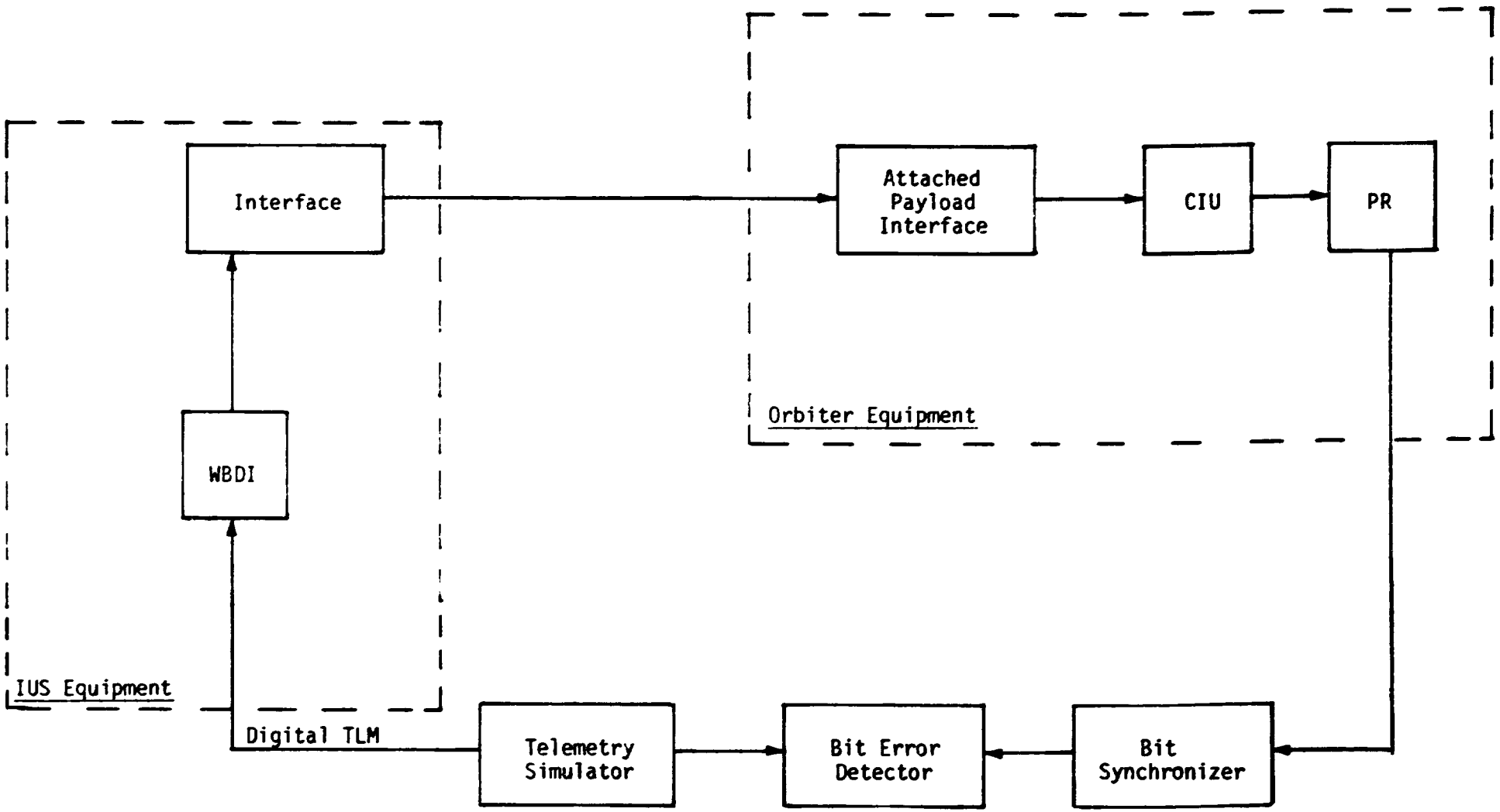

Figure 54. DOD Telemetry Hardline Test Link 25
SGLS Telemetry

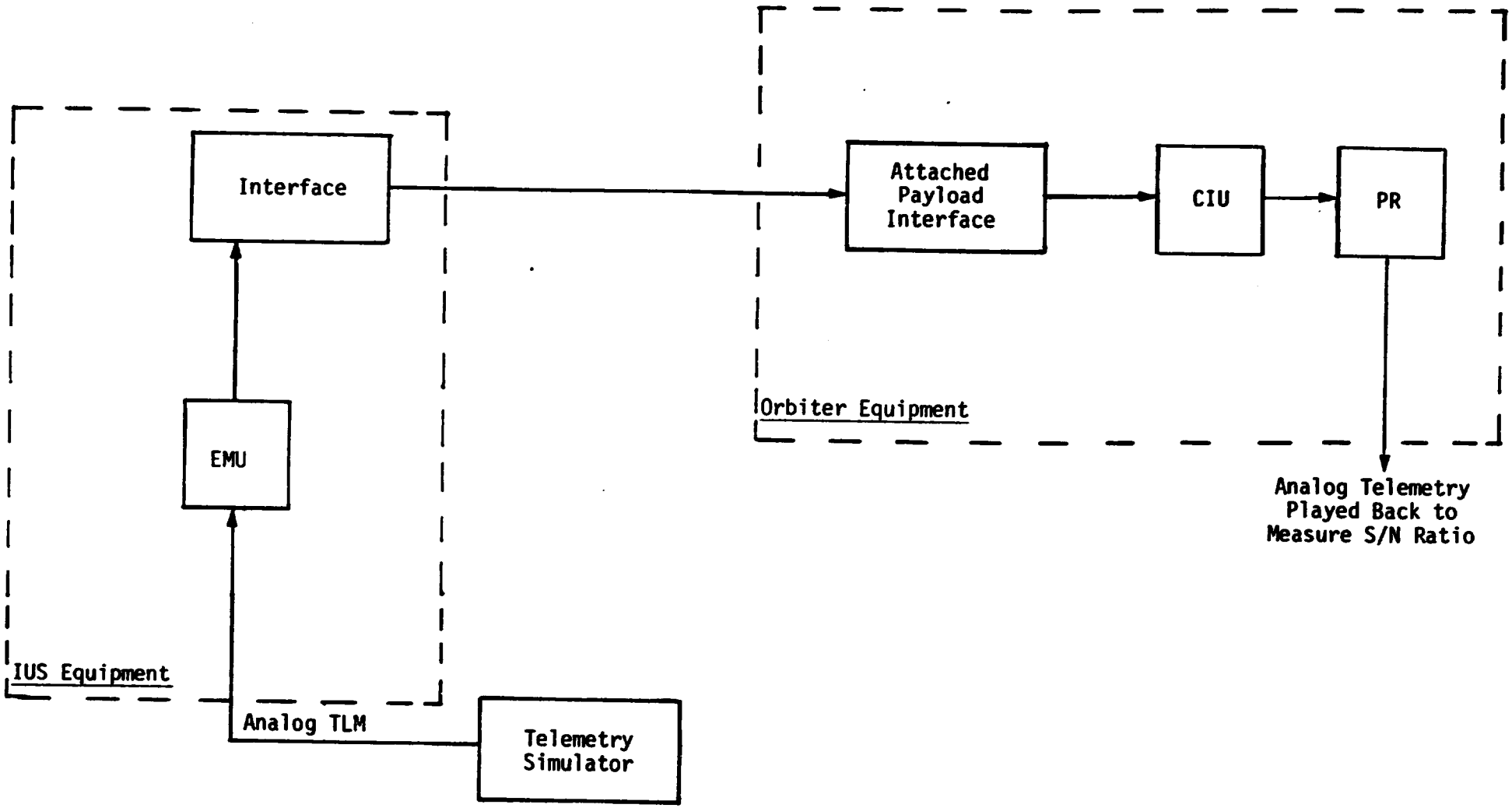

Figure 55. DOD Telemetry Hardline Test Link 26
SGLS Telemetry

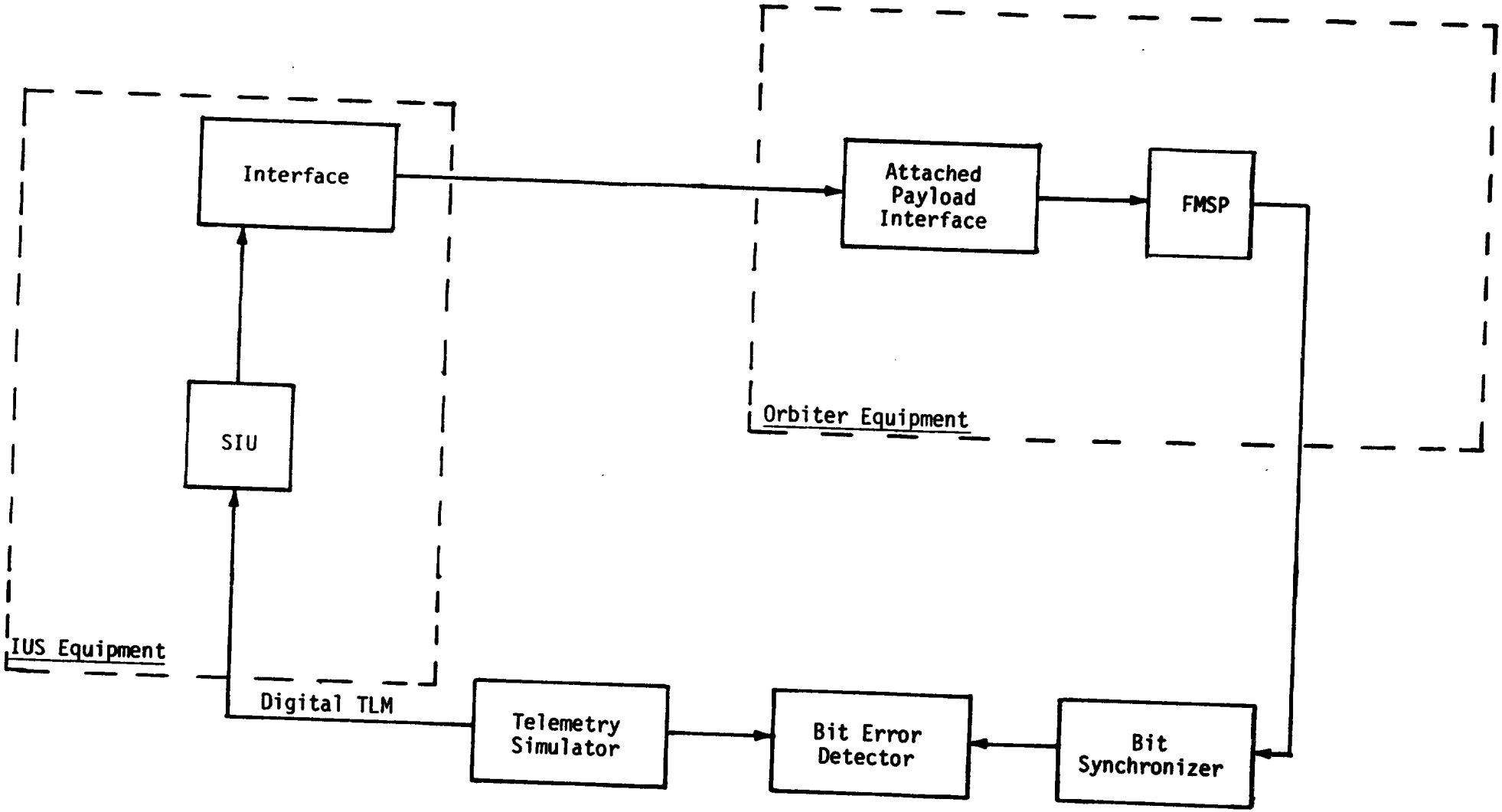

Figure 56. NASA Telemetry Hardline Test Link 27
STDN/TDRS Telemetry

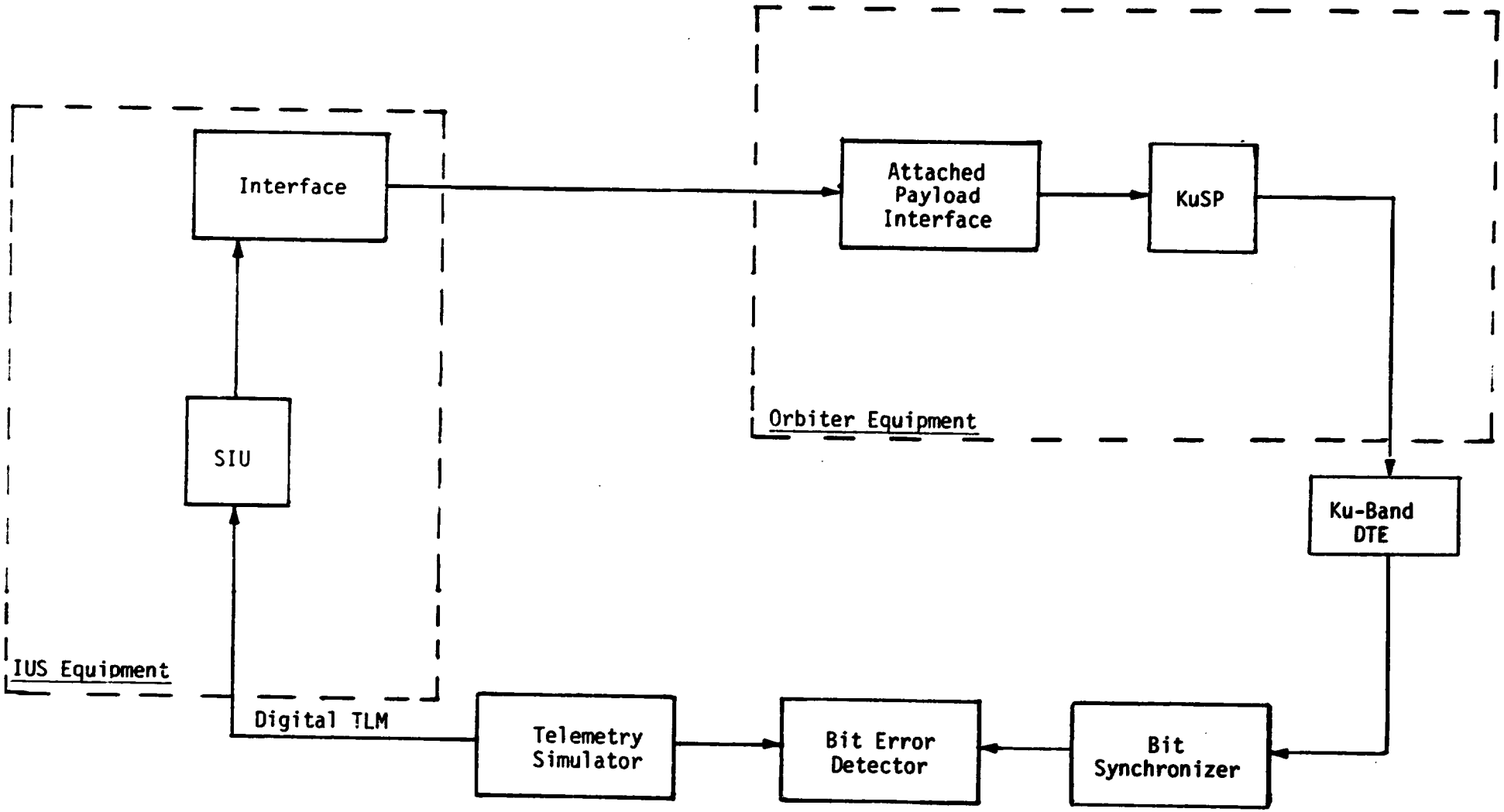

Figure 57. NASA Telemetry Hardline Test Link 28
STDN/TDRS Telemetry

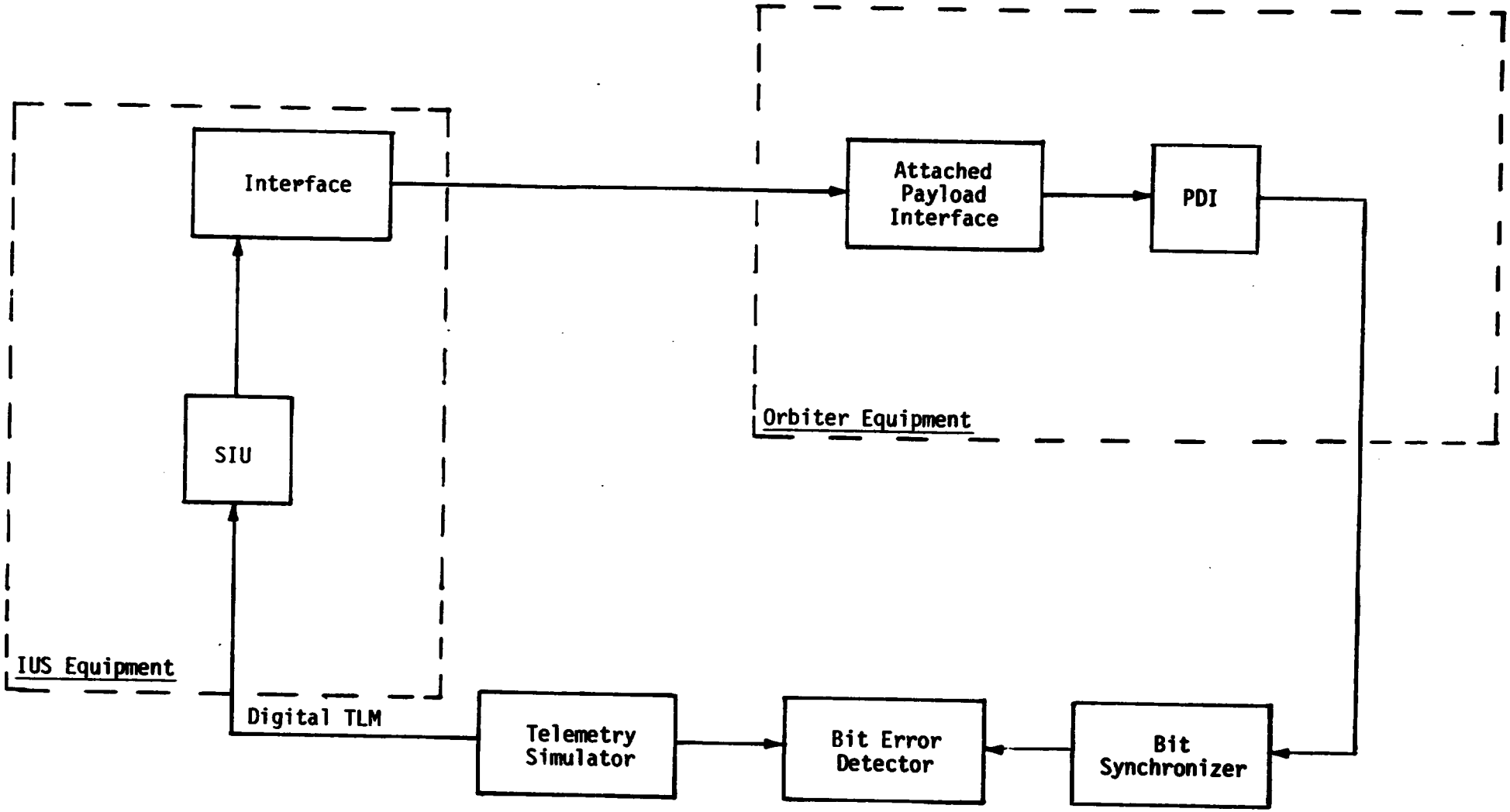

Figure 58. NASA Telemetry Hardline Test Link 29
STDN/TDRS Telemetry

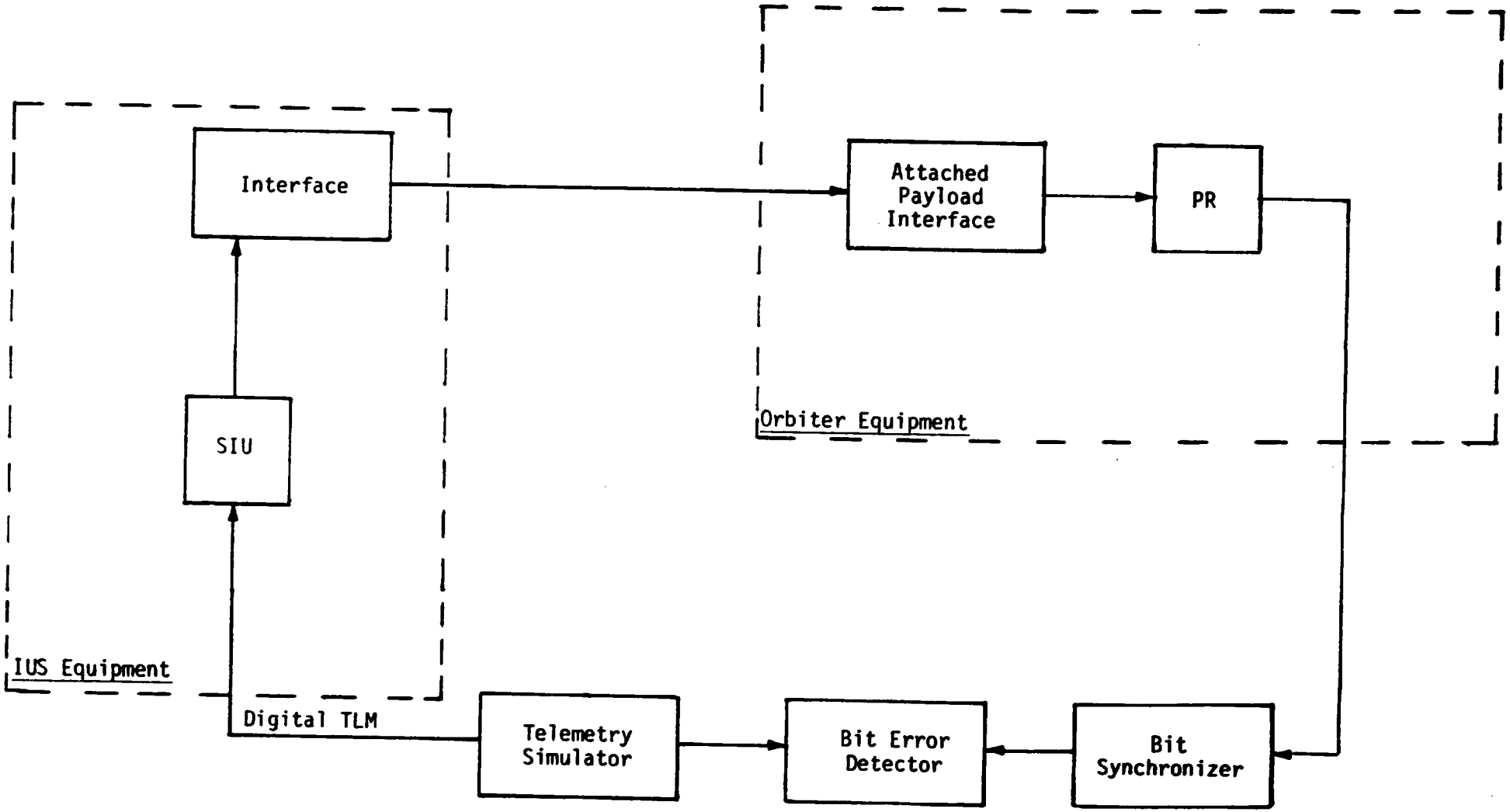

Figure 59. NASA Telemetry Hardline Test Link 30
STDN/TDRS Telemetry

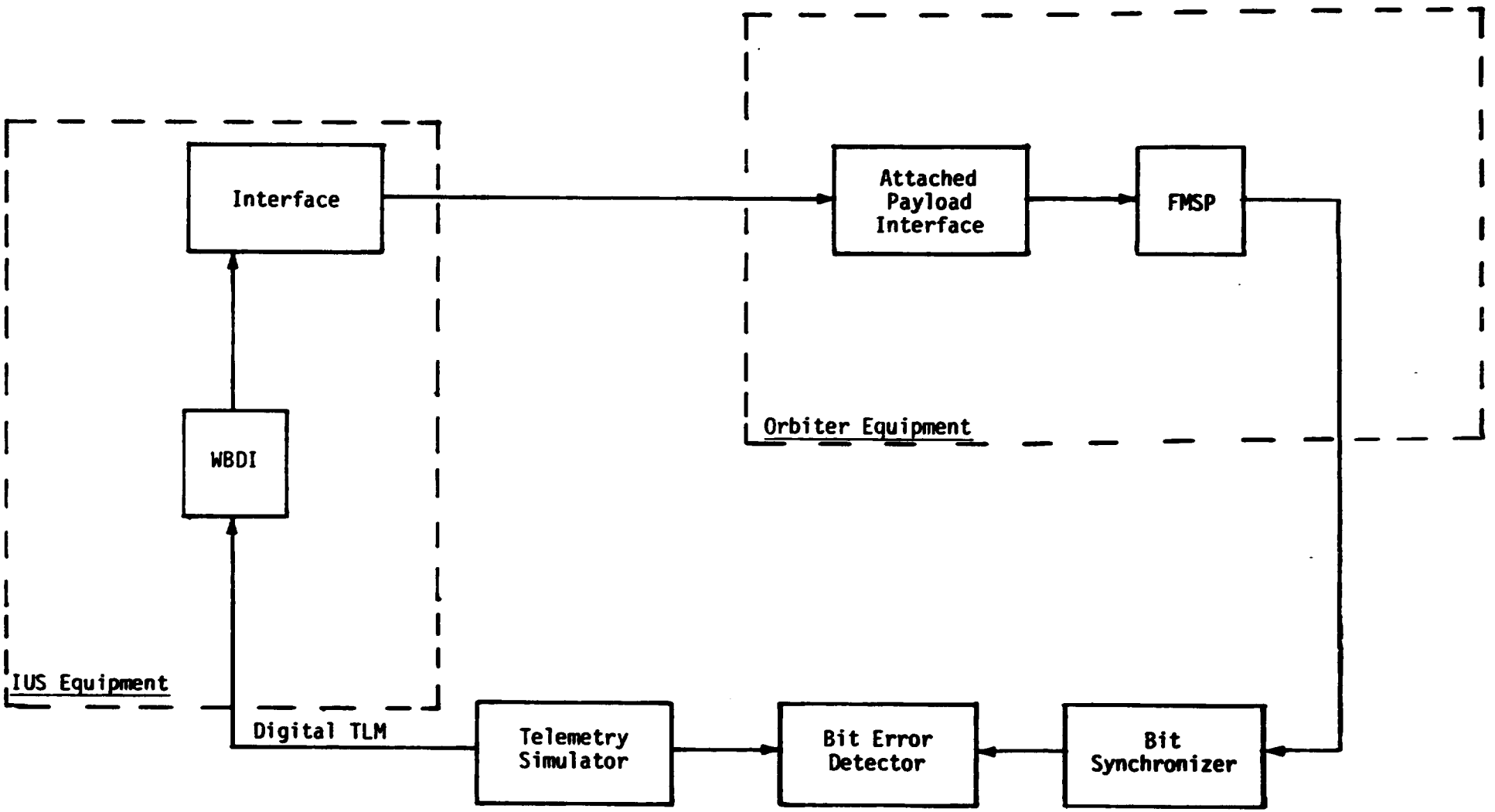

Figure 60. NASA Telemetry Hardline Test Link 31
STDN/TDRS Telemetry

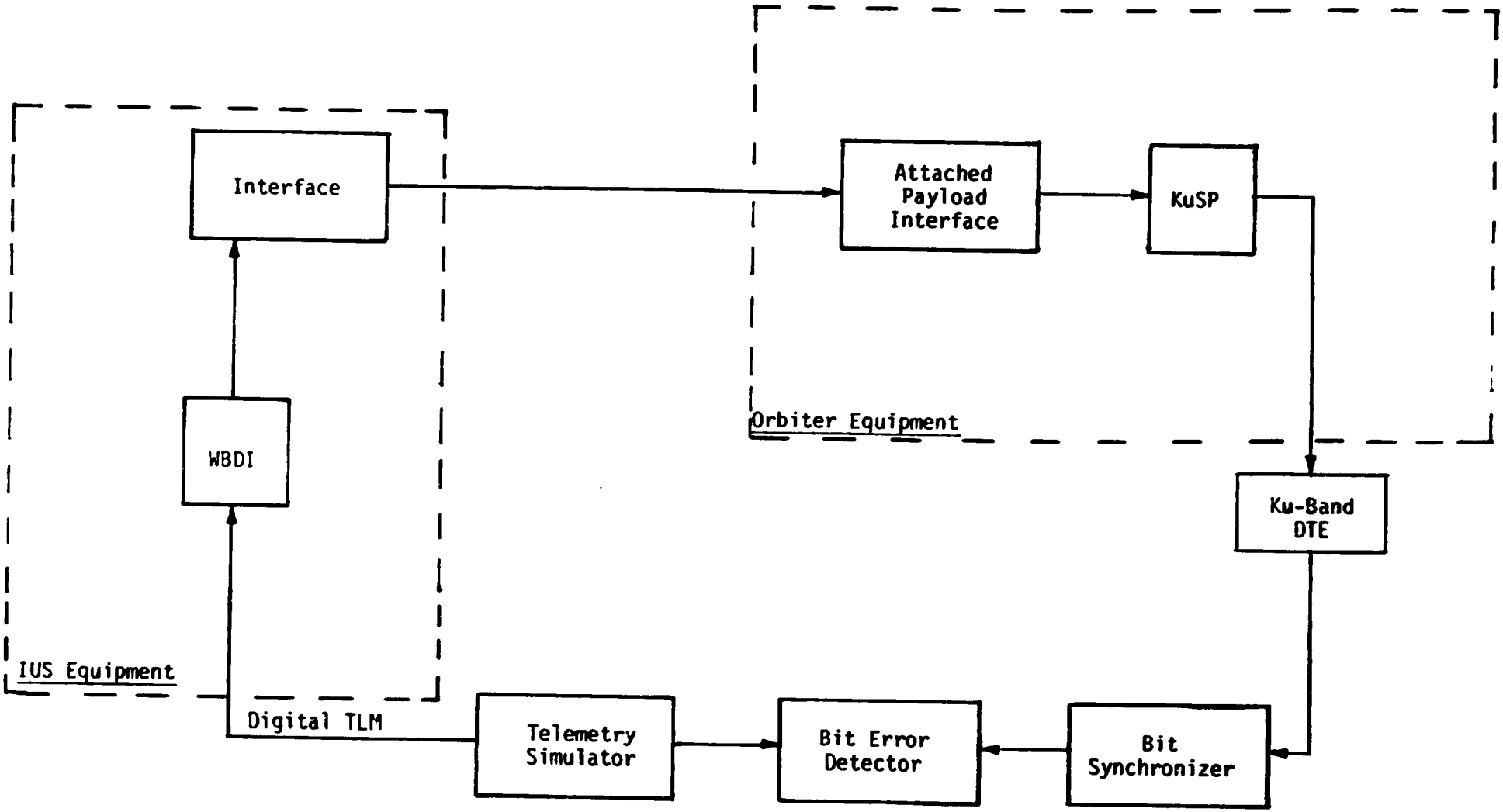

Figure 61. NASA Telemetry Hardline Test Link 32
STDN/TDRS Telemetry

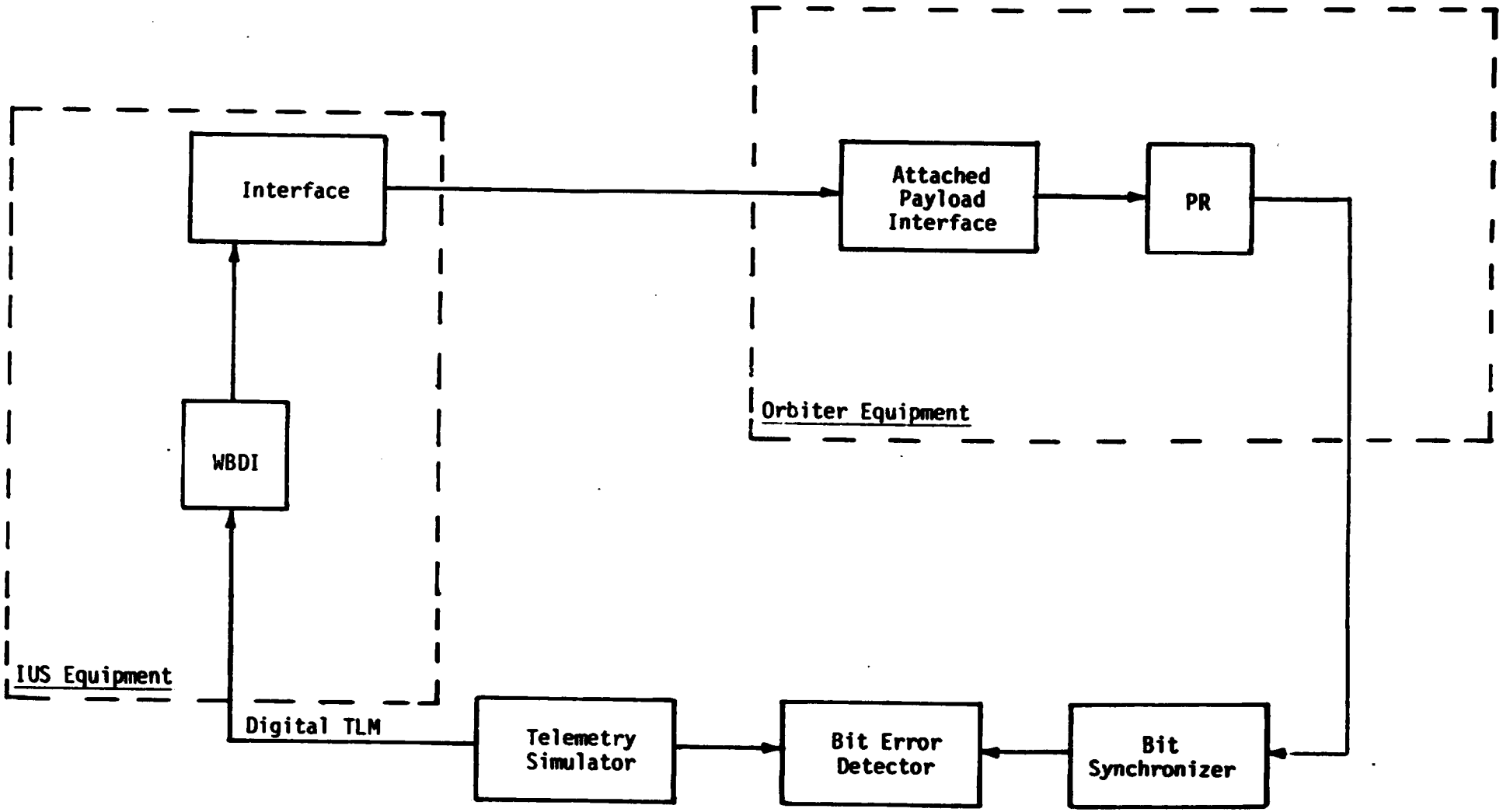

Figure 62. NASA Telemetry Hardline Test Link 33
STDN/TDRS Telemetry

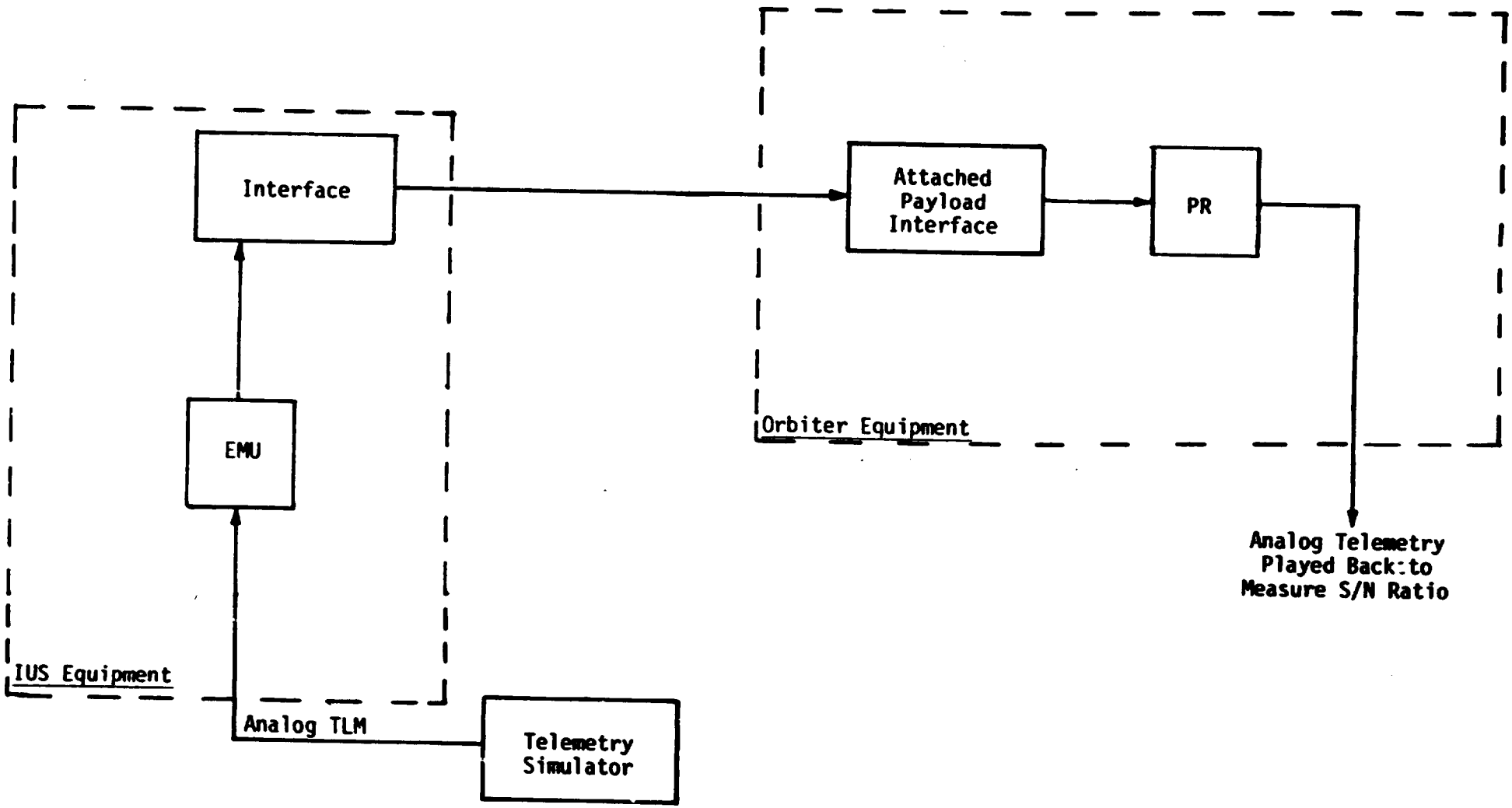

Figure 63. NASA Telemetry Hardline Test Link 34
STDN/TDRS Telemetry

Table 23. DOD Telemetry Hardline Test Summary (Return Link)

Test Links 19-22 (Figures 48-51)	
Measured parameter:	10^7 error-free bits
Test conditions:	• Signal combination 5A
Test Links 23-25 (Figures 52-54)	
Measured parameter:	10^7 error-free bits
Test conditions:	• Signal combination 6A
Test Link 26 (Figure 55)	
Measured parameter:	SNR
Test conditions:	• Signal combination 7A

Table 24. NASA Telemetry Hardline Test Summary (Return Link)

Test Links 27-30 (Figures 56-59)	
Measured parameter:	10^7 error-free bits
Test conditions:	• Signal combination 8A
Test Links 31-33 (Figures 60-62)	
Measured parameter:	10^7 error-free bits
Test conditions:	• Signal combination 9A
Test Link 34 (Figure 63	
Measured parameter:	SNR
Test conditions:	• Signal combination 10A

ADDENDUM A

END-TO-END DOD OR SGLS COMMAND SIGNAL PATHS

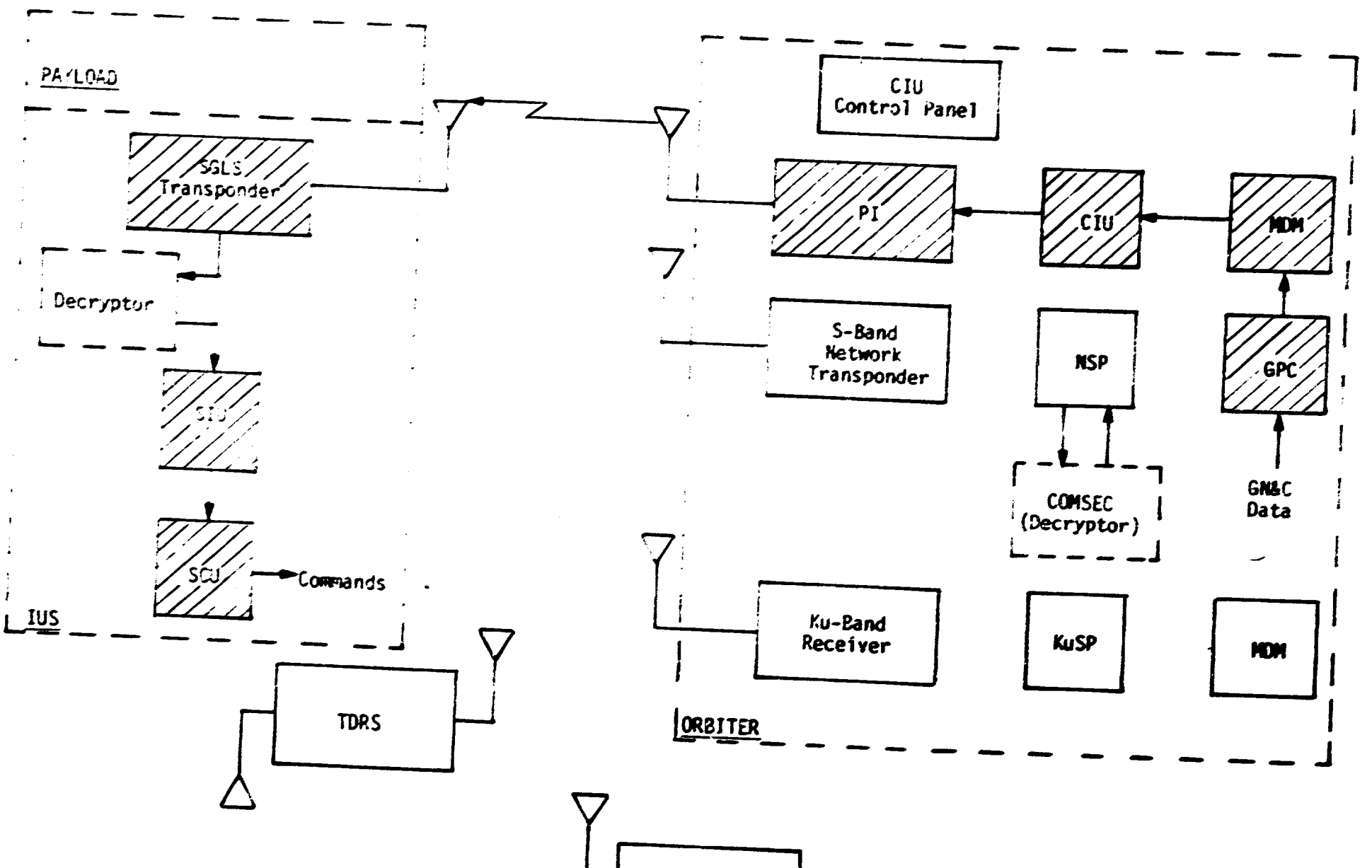

Figure 1. Attached/Detached IUS RF Command Link SGLS Commands (DOD Mode)

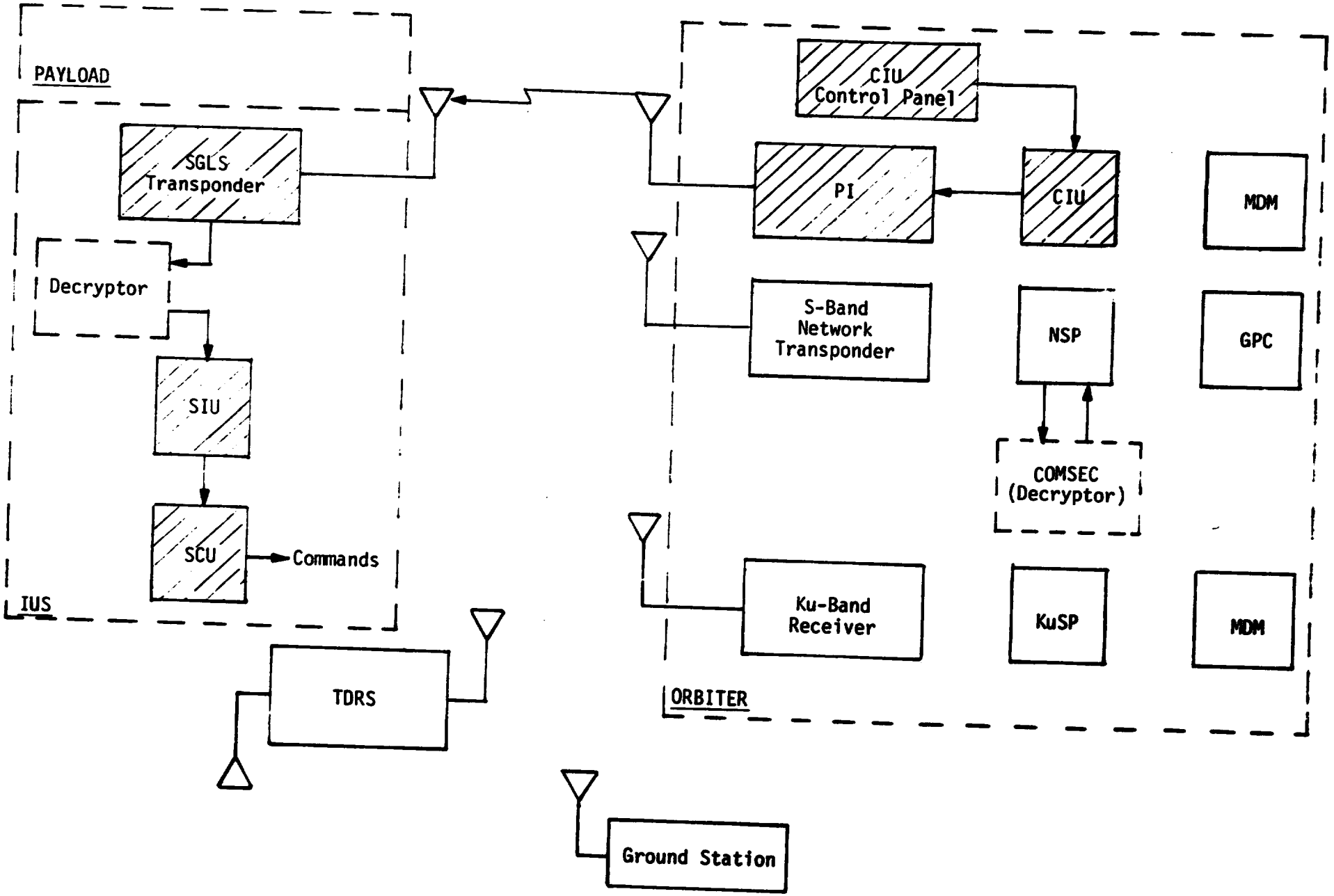

Figure 2. Attached/Detached IUS RF Command Link SGLS Commands (DOD Mode)

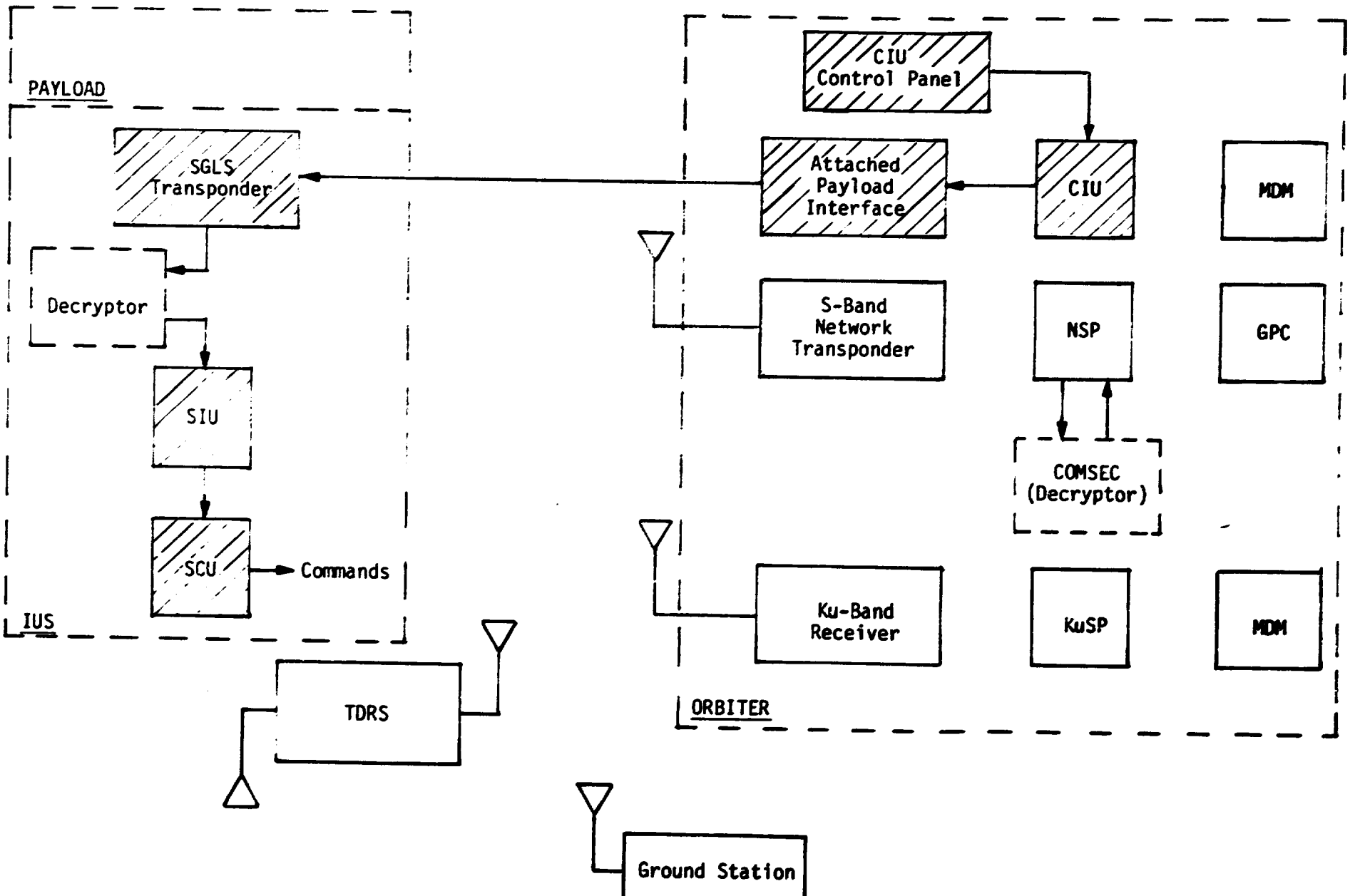

Figure 3. Attached IUS Hard-Line Command Link SGLS Commands (DOD Mode)

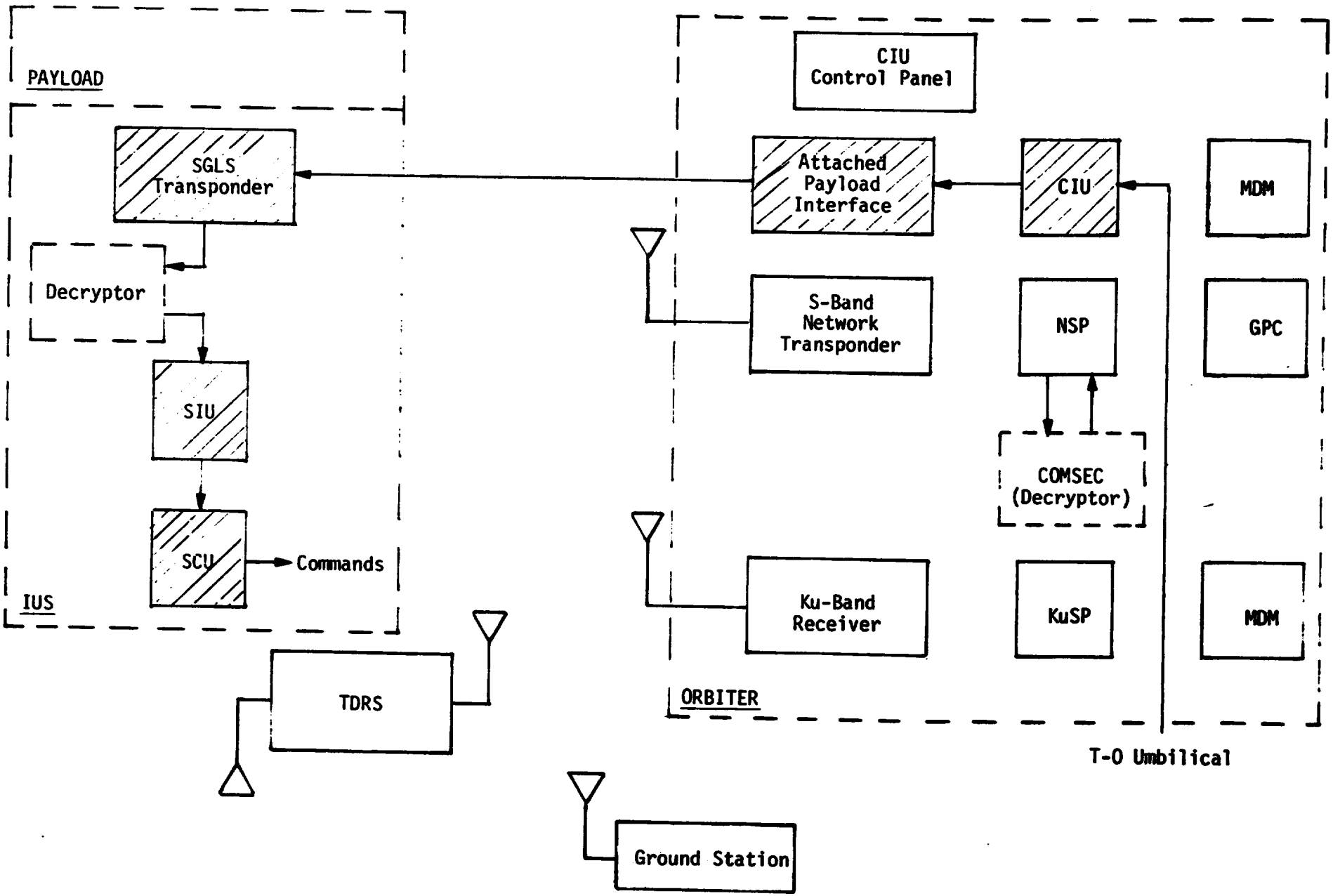

Figure 4. Attached IUS Hard-Line Command Link SGLS Commands (DOD Mode)

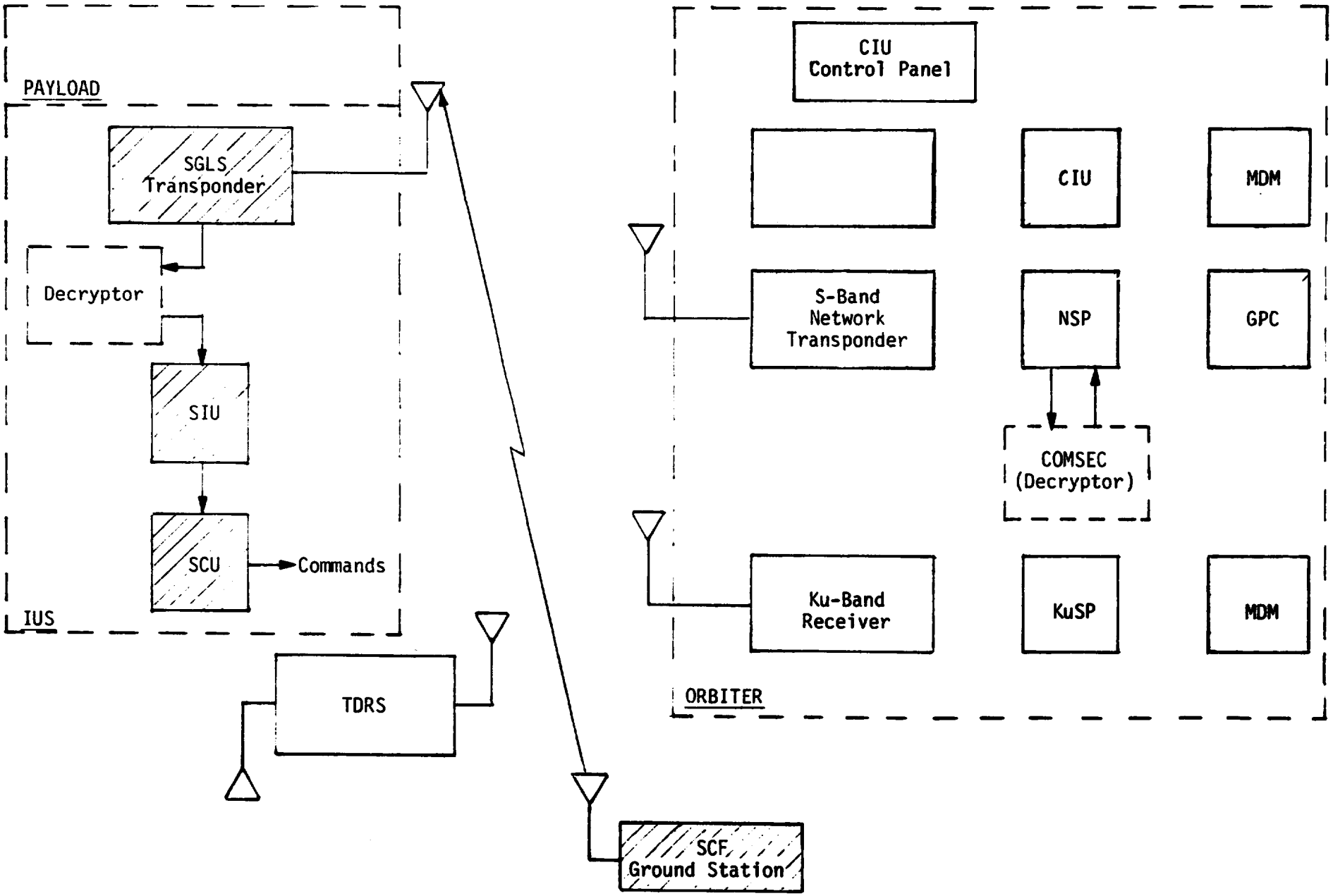

Figure 5. Attached/Detached IUS RF Command Link SGLS Commands (DOD Mode)

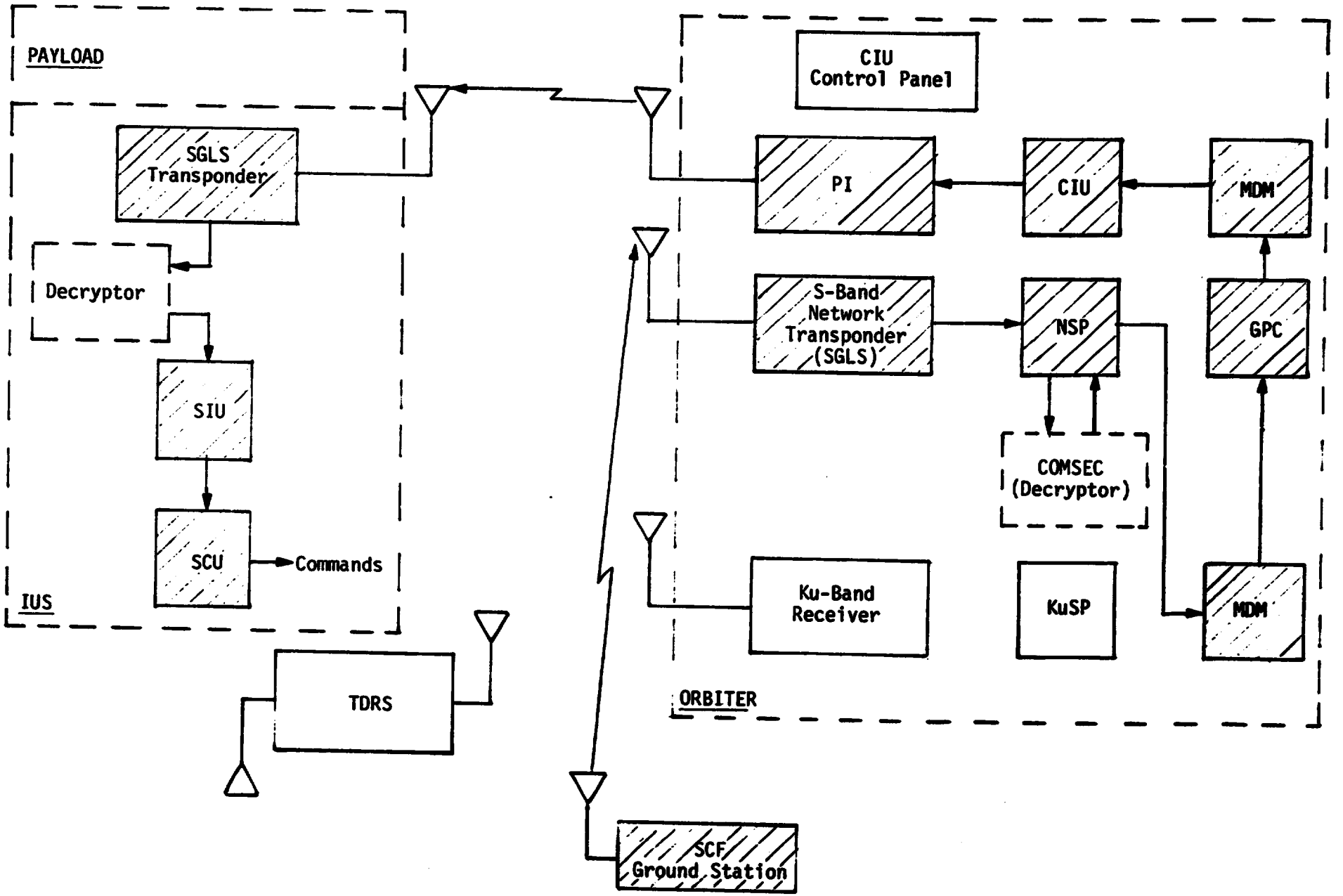

Figure 6. Attached/Detached IUS RF Command Link SGLS Commands (DOD Mode)

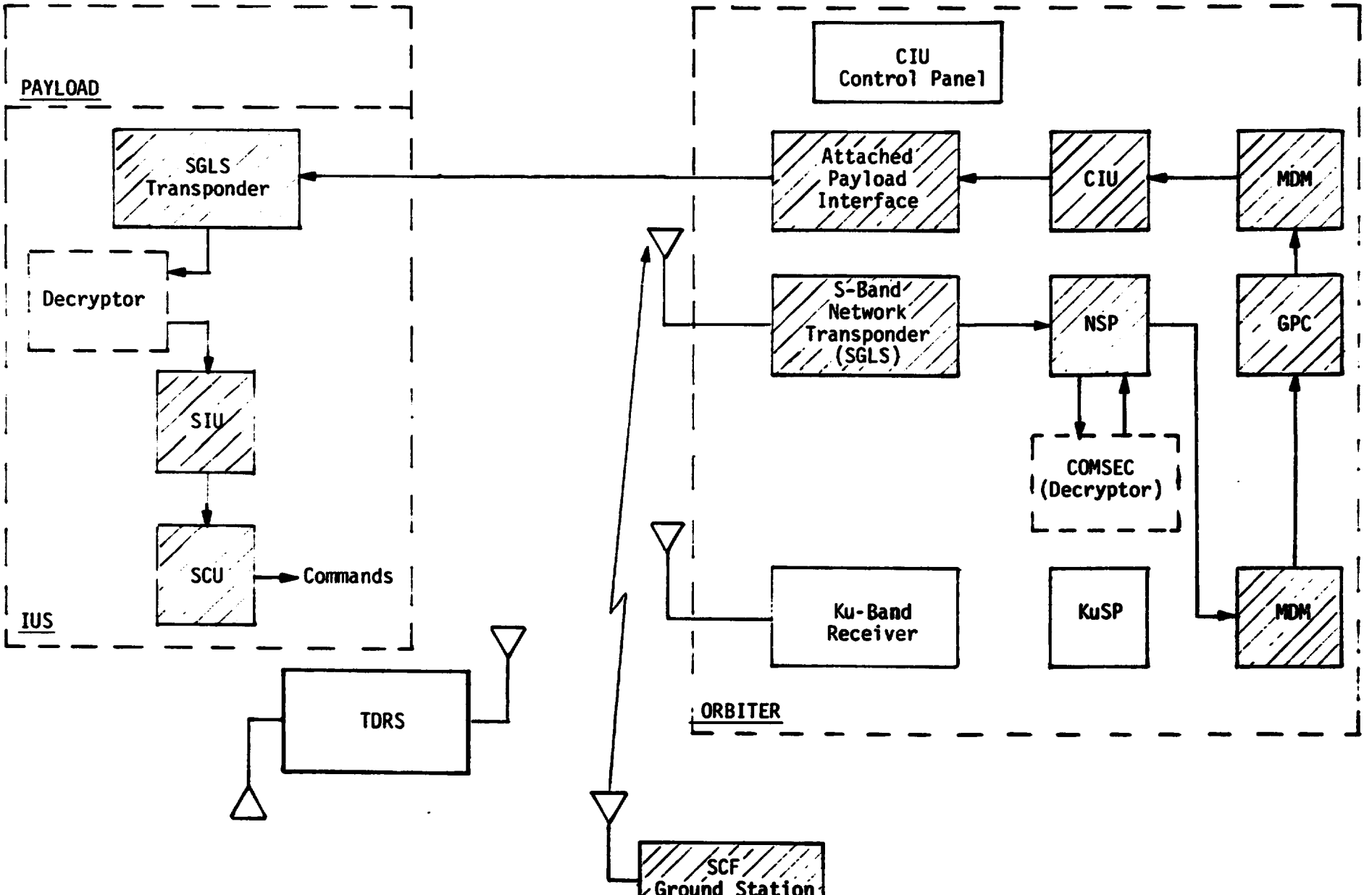

Figure 7. Attached IUS Hard-Line Command Link SGLS Commands (DOD Mode)

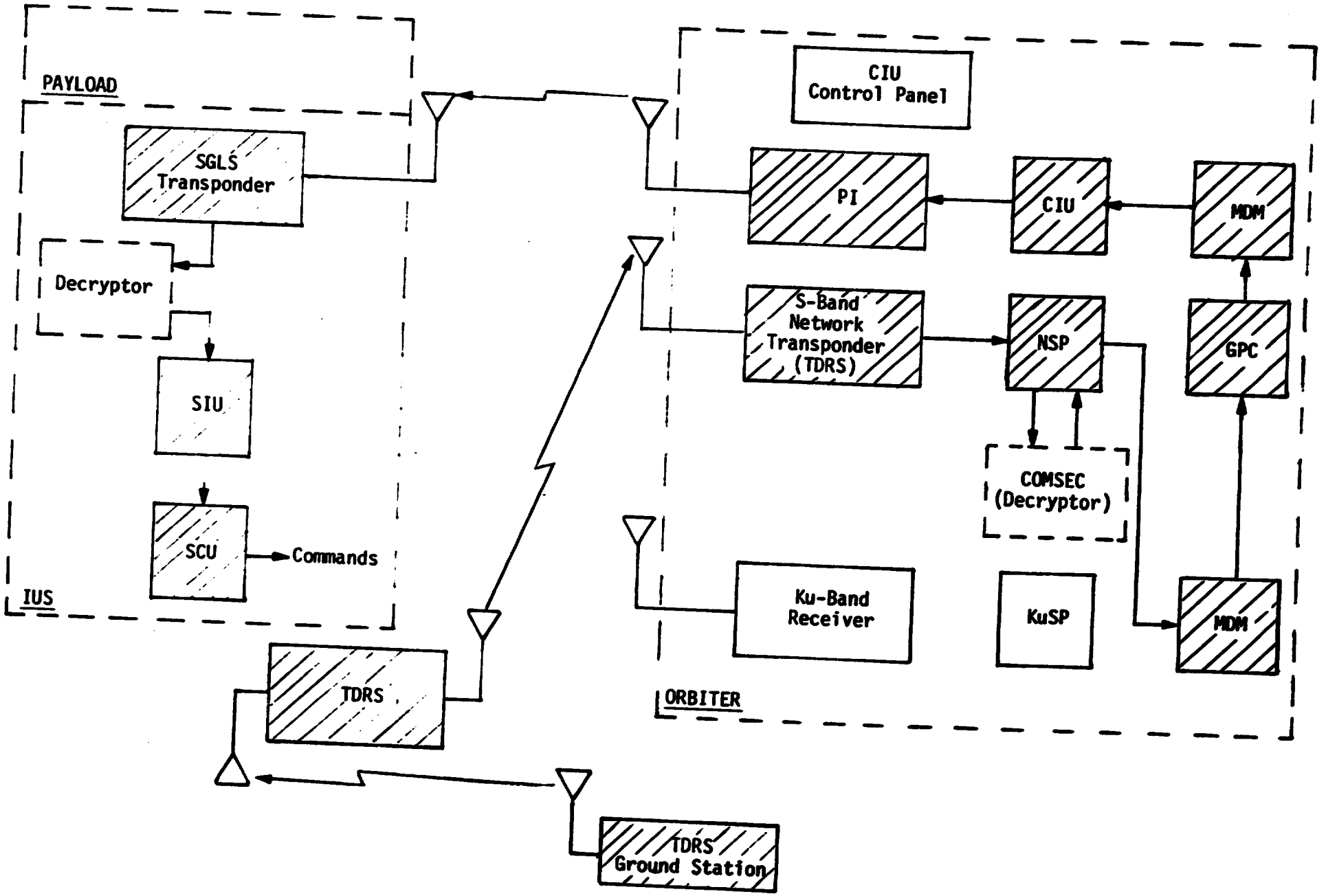

Figure 8. Attached/Detached IUS RF Command Link SGLS Commands (DOD Mode)

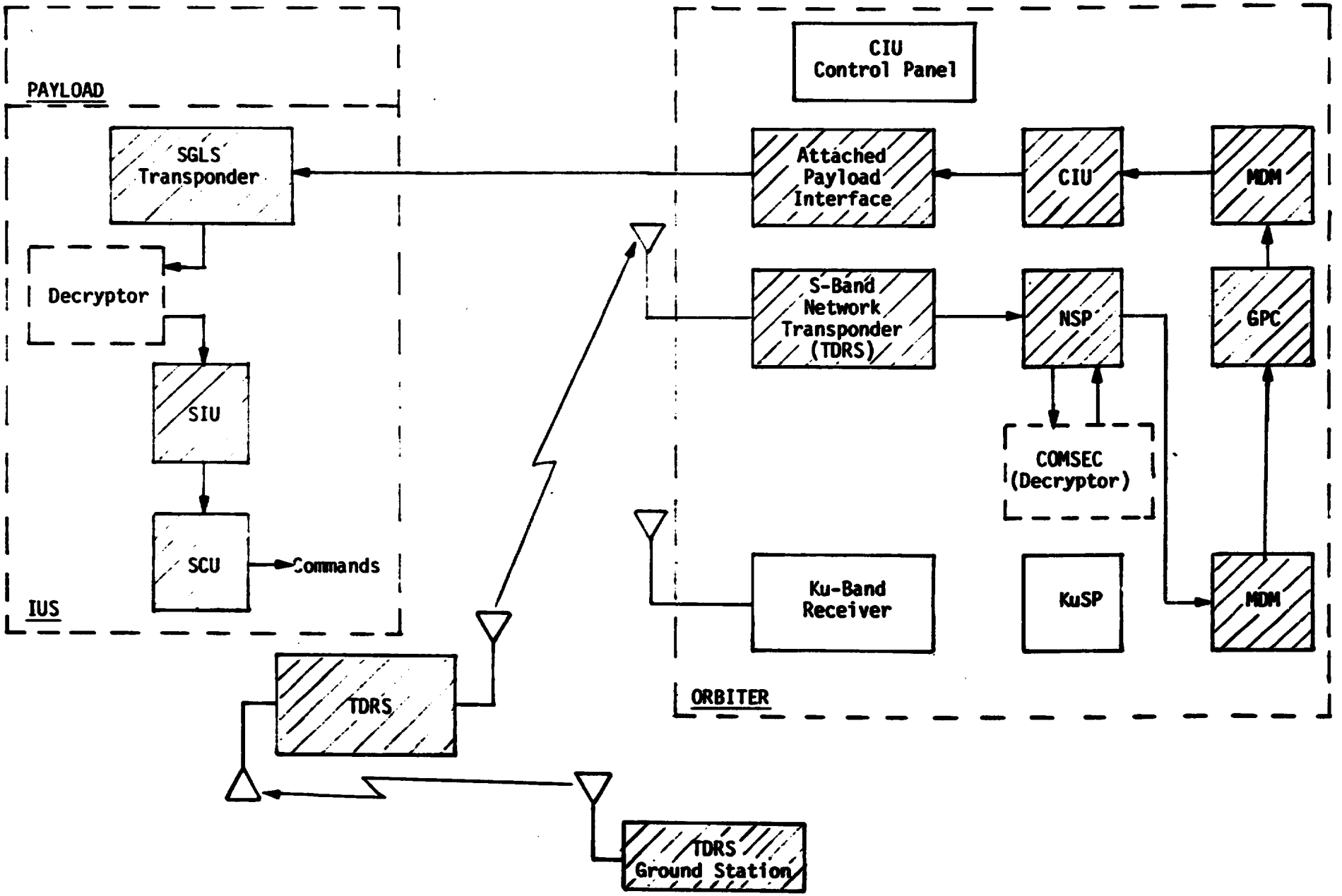

Figure 9. Attached IUS Hard-Line Command Link SGLS Commands (DOD Mode)

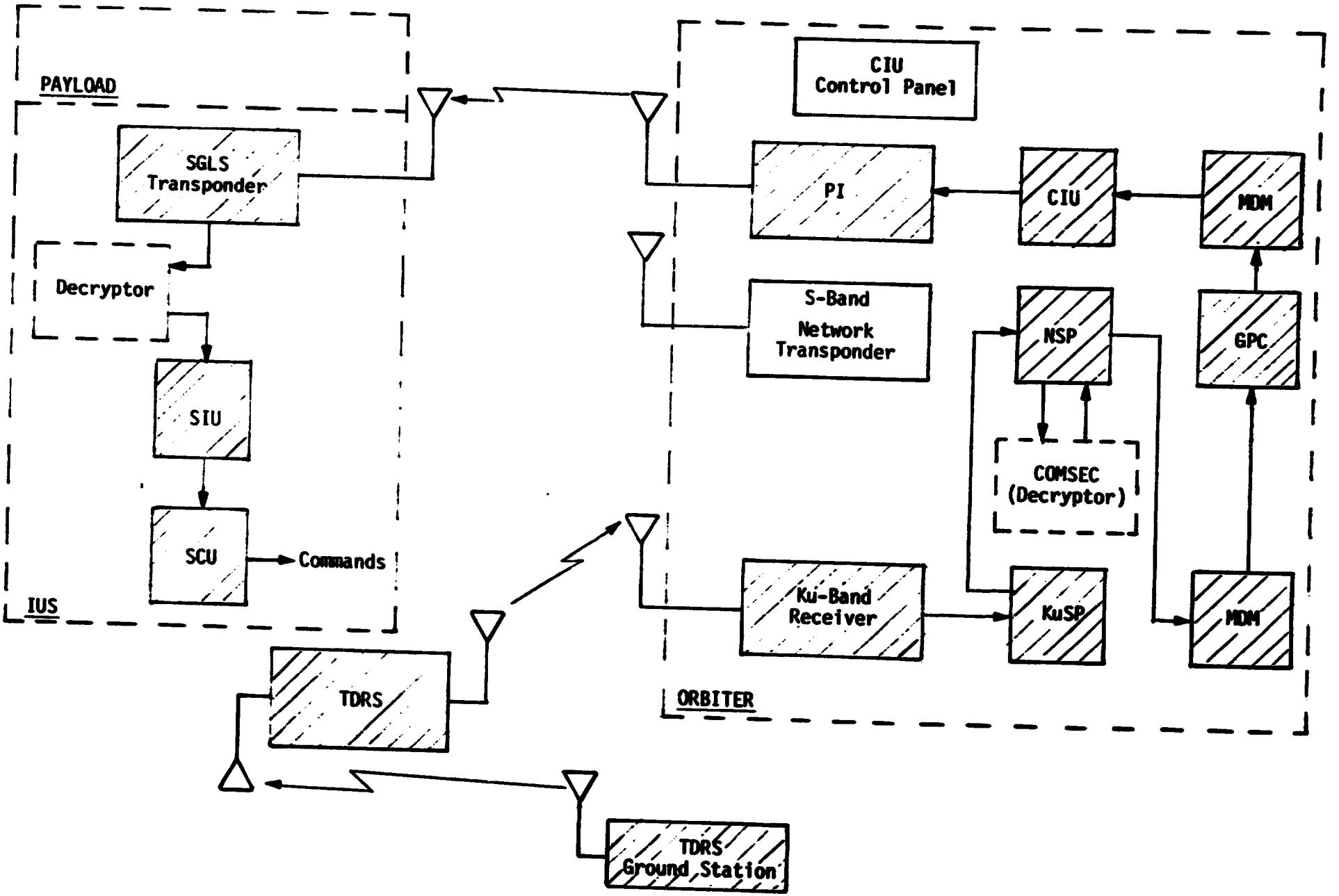

Figure 10. Attached/Detached IUS RF Command Link SGLS Commands (DOD Mode)

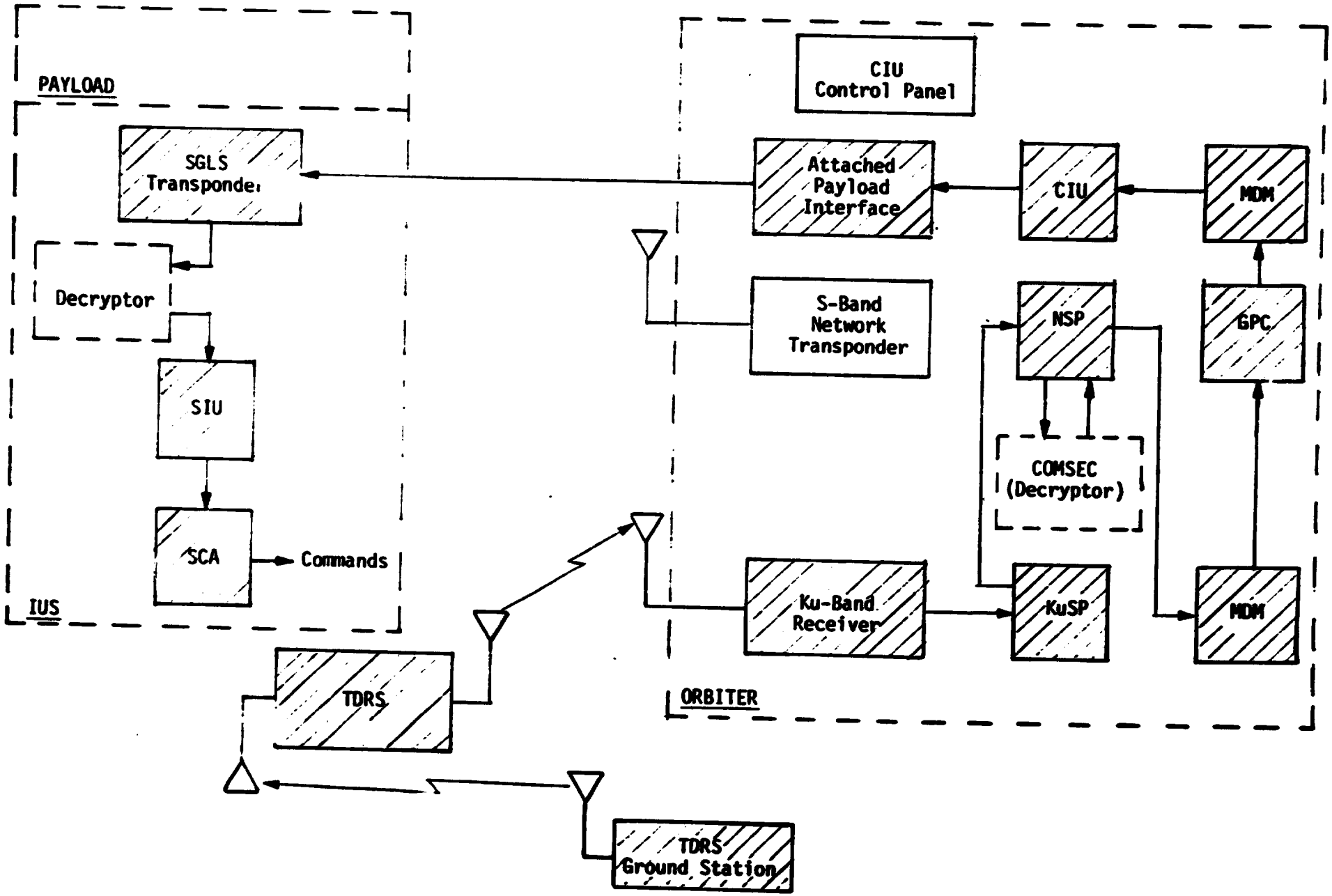

Figure 11. Attached IUS Hard-Line Command Link SGLS Commands (DOD Mode)

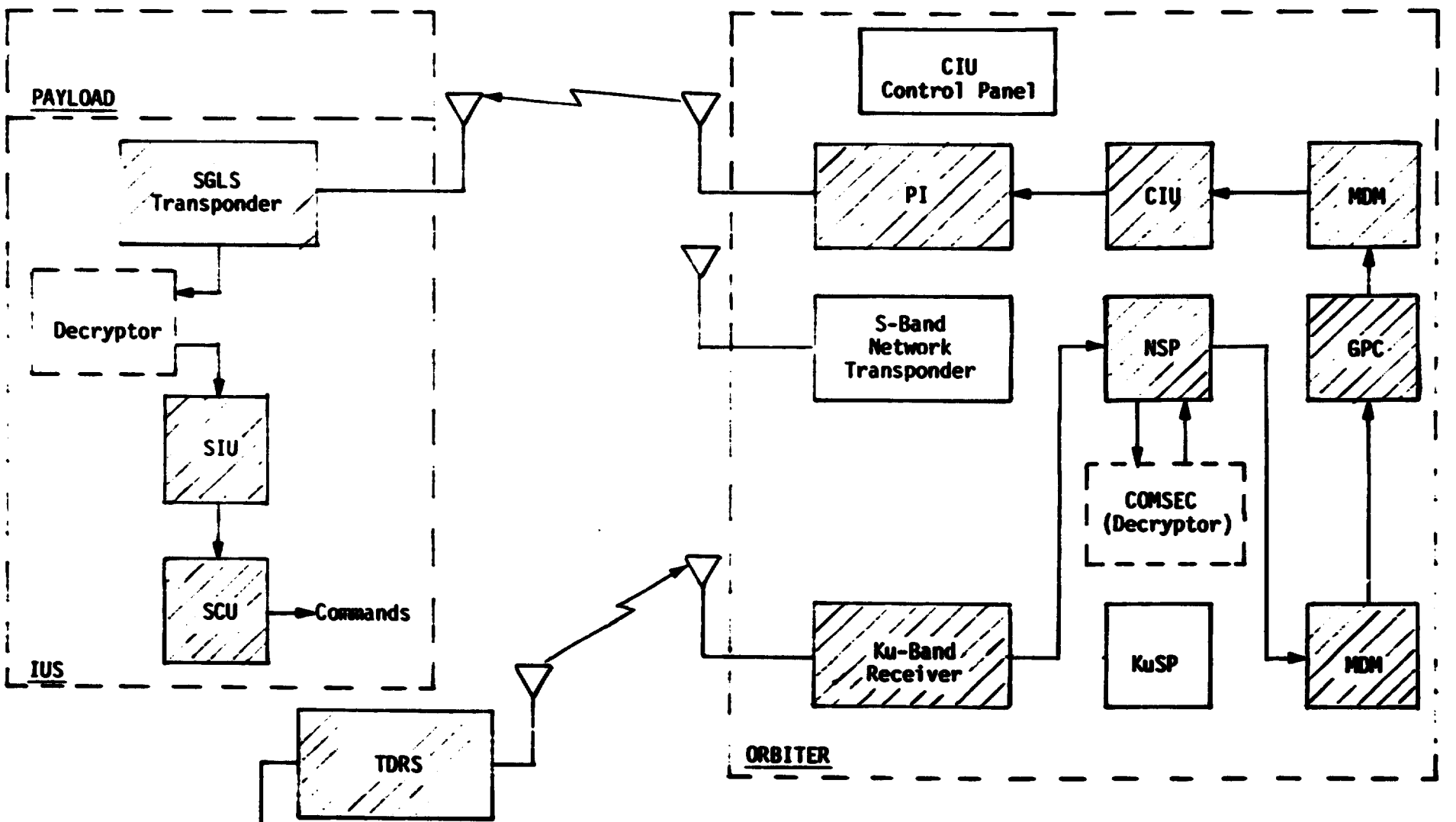

Figure 12. Attached/Detached IUS RF Command Link SGLS Commands (DOD Mode)

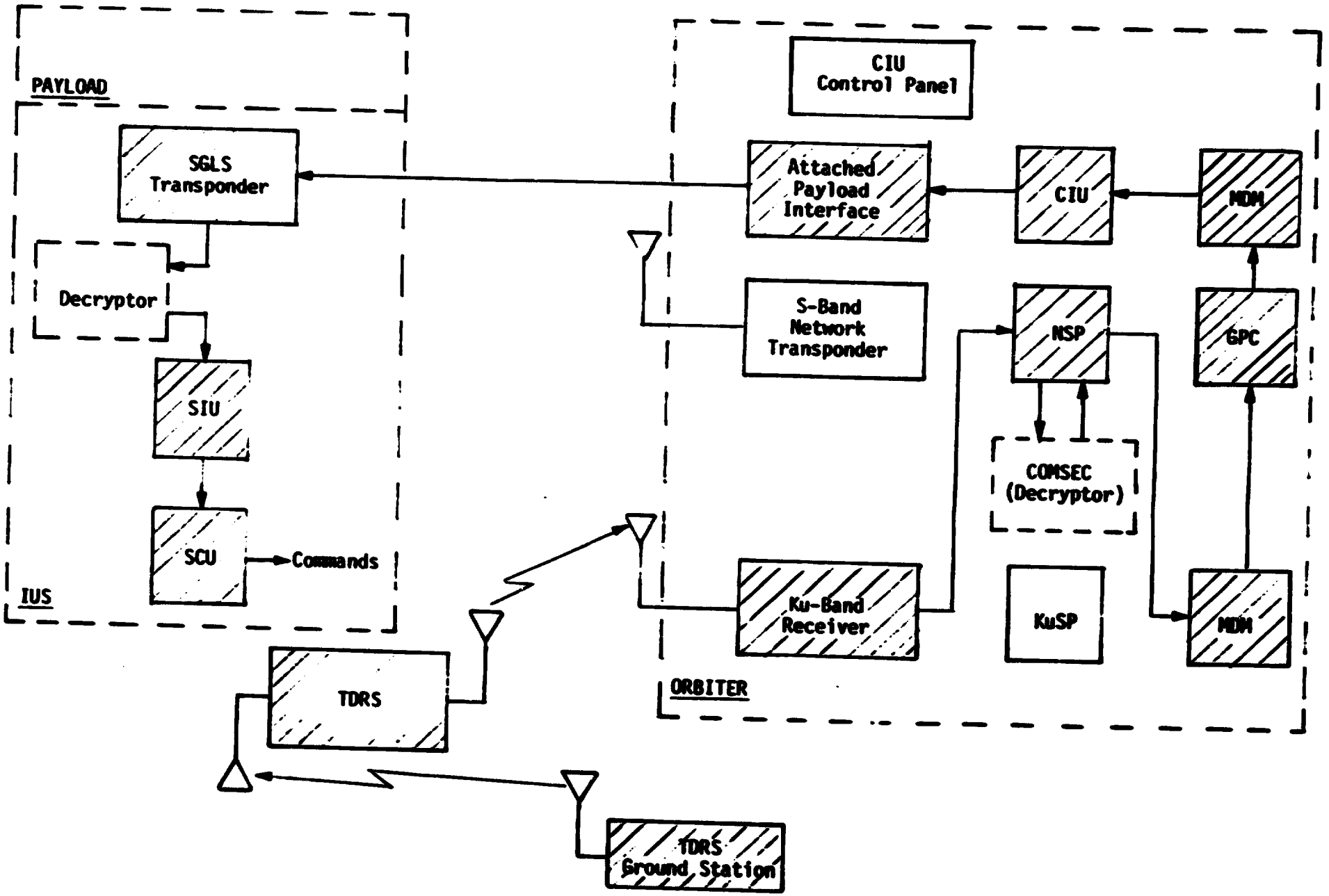

Figure 13. Attached IUS Hard-Line Command Link SGLS Commands (DOD Mode)

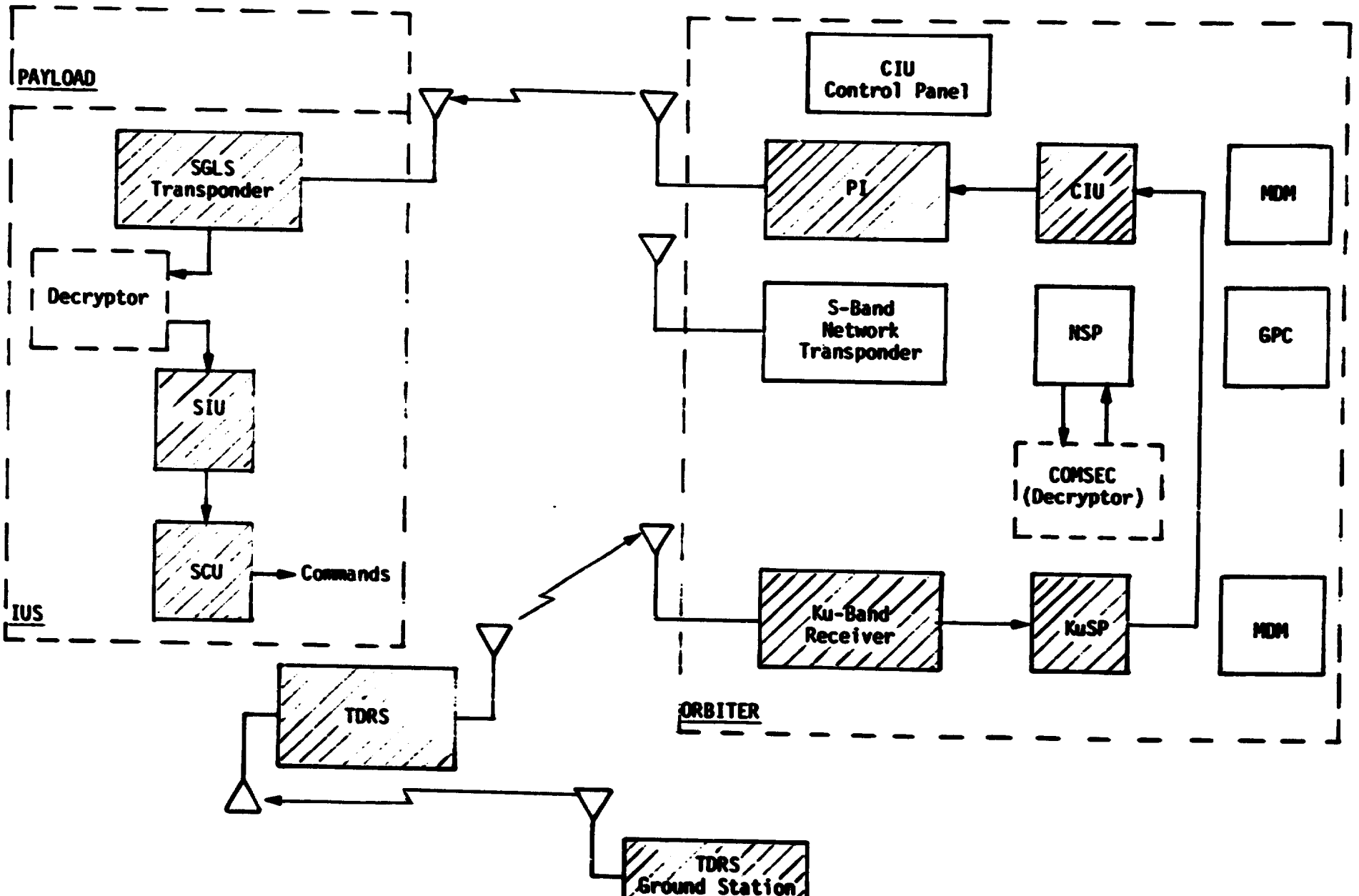

Figure 14. Attached/Detached IUS RF Command Link SGLS Commands (DOD Mode)

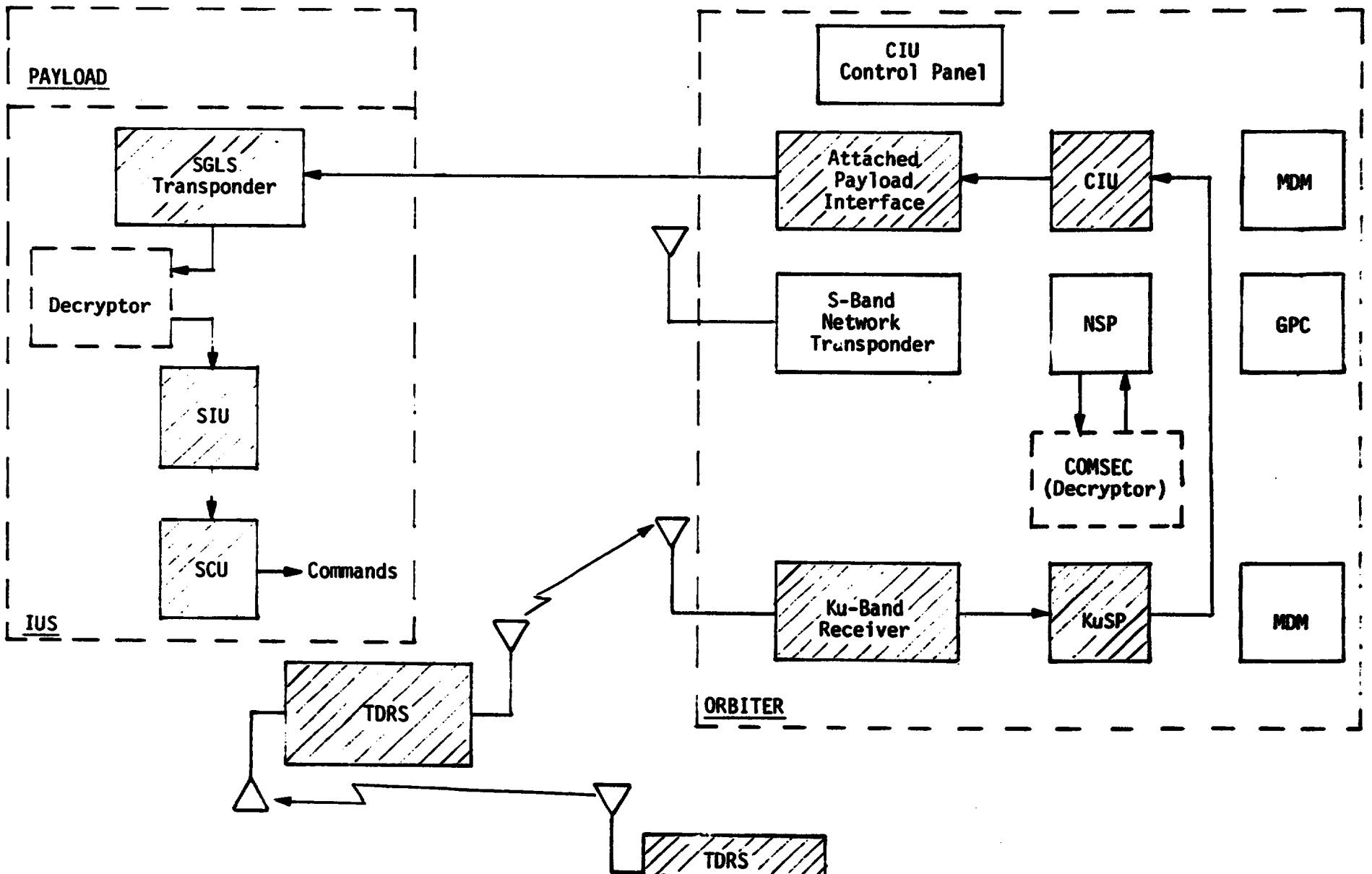

Figure 15. Attached IUS Hard-Line Command Link SGLS Commands (DOD Mode)

ADDENDUM B

END-TO-END NASA OR STDN/TDRS COMMAND SIGNAL PATHS

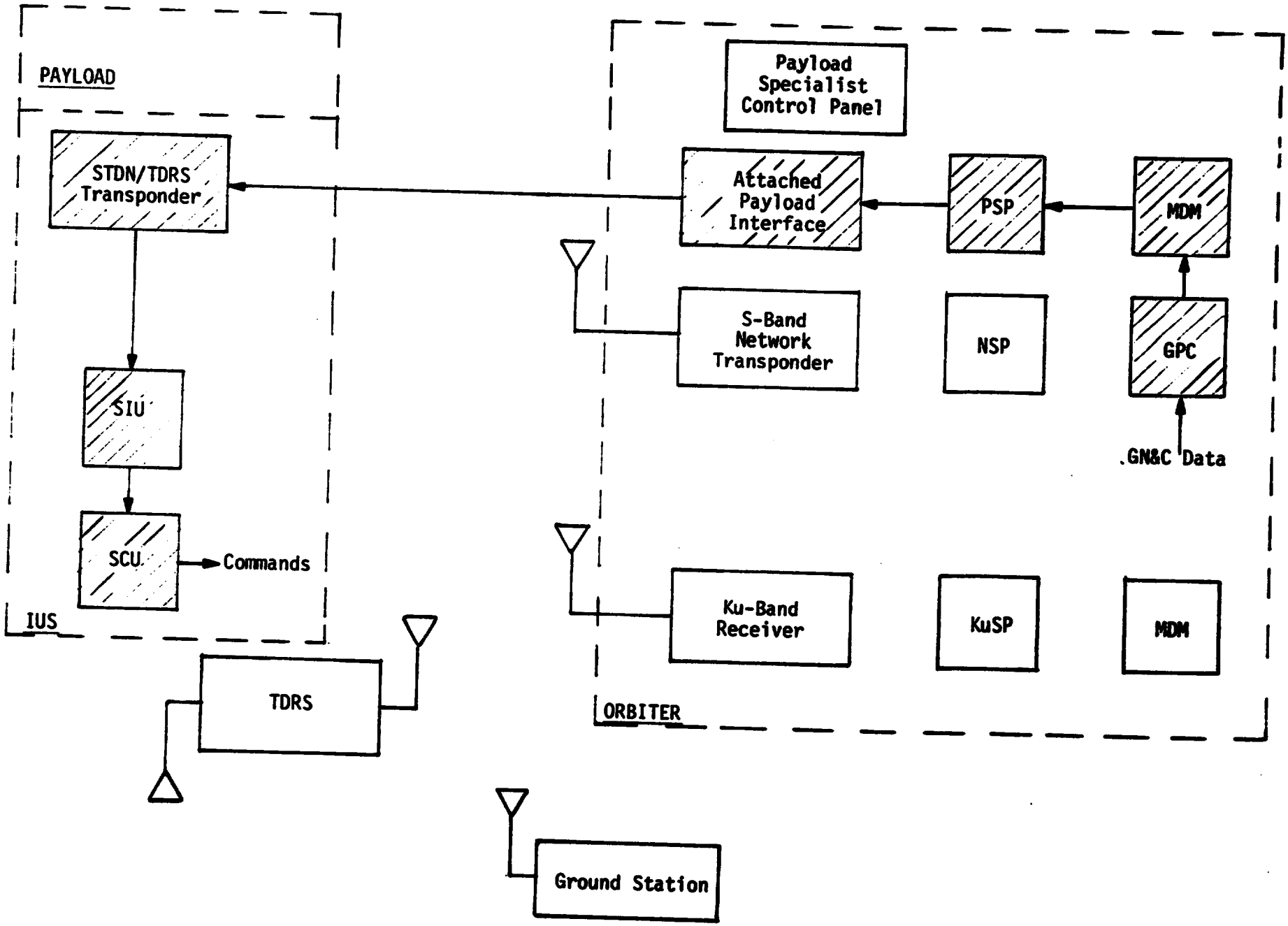

Figure 1. Attached IUS Hard-Line Command Link STDN/TDRS Commands (NASA Mode)

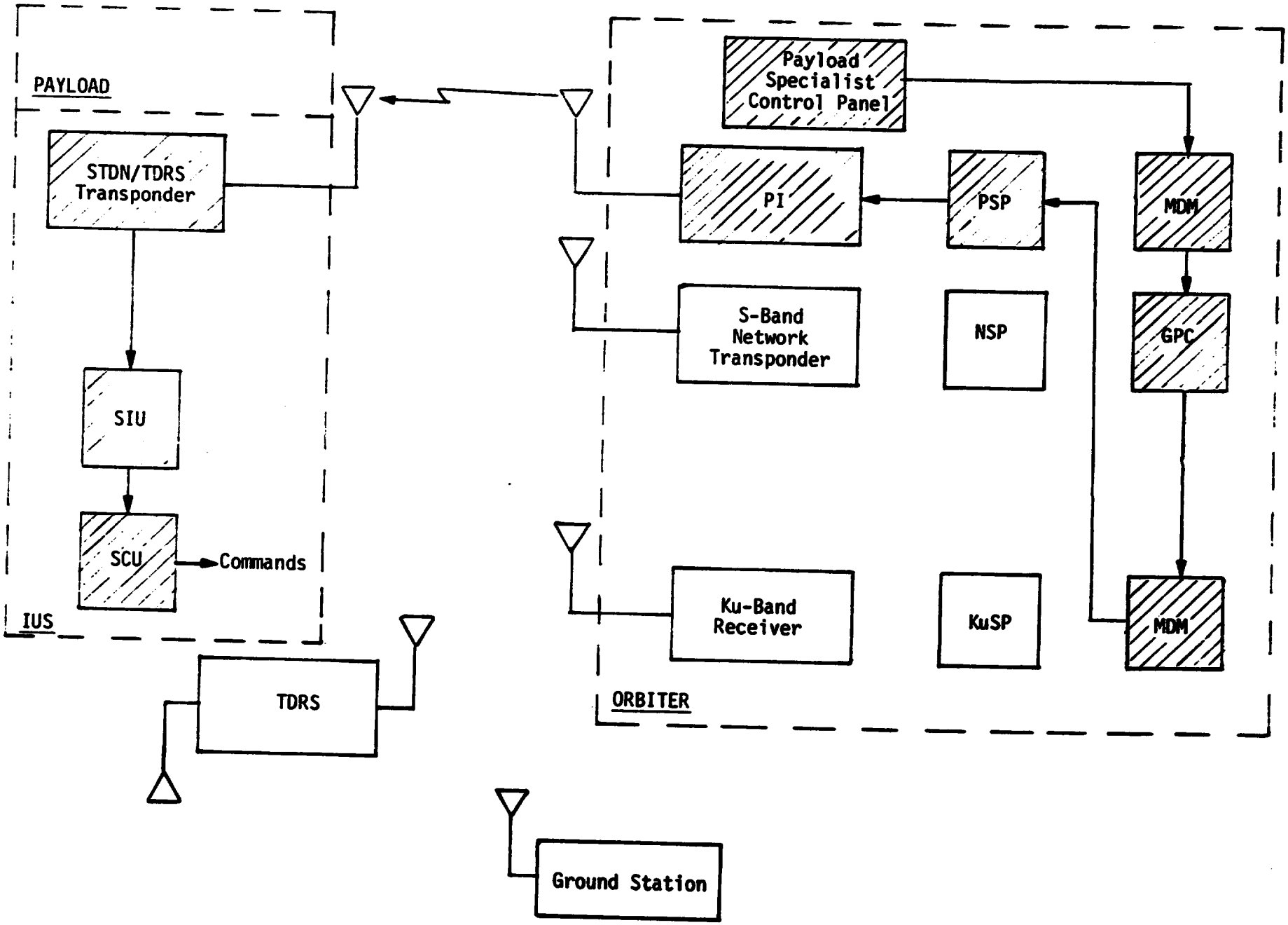

Figure 2. Attached/Detached IUS RF Command Link STDN/TDRS Commands (NASA Mode)

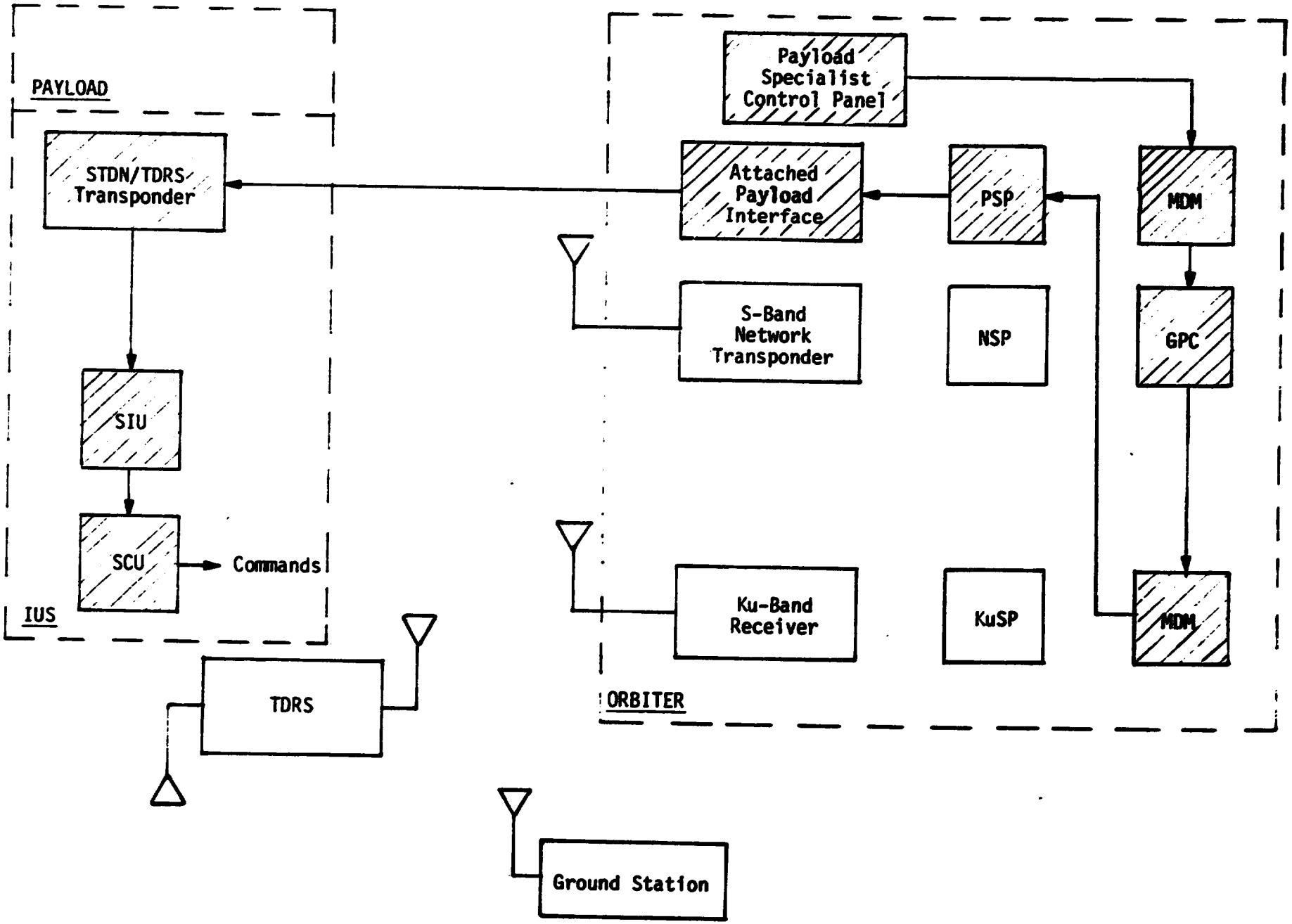

Figure 3. Attached IUS Hard-Line Command Link STDN/TDRS Commands (NASA Mode)

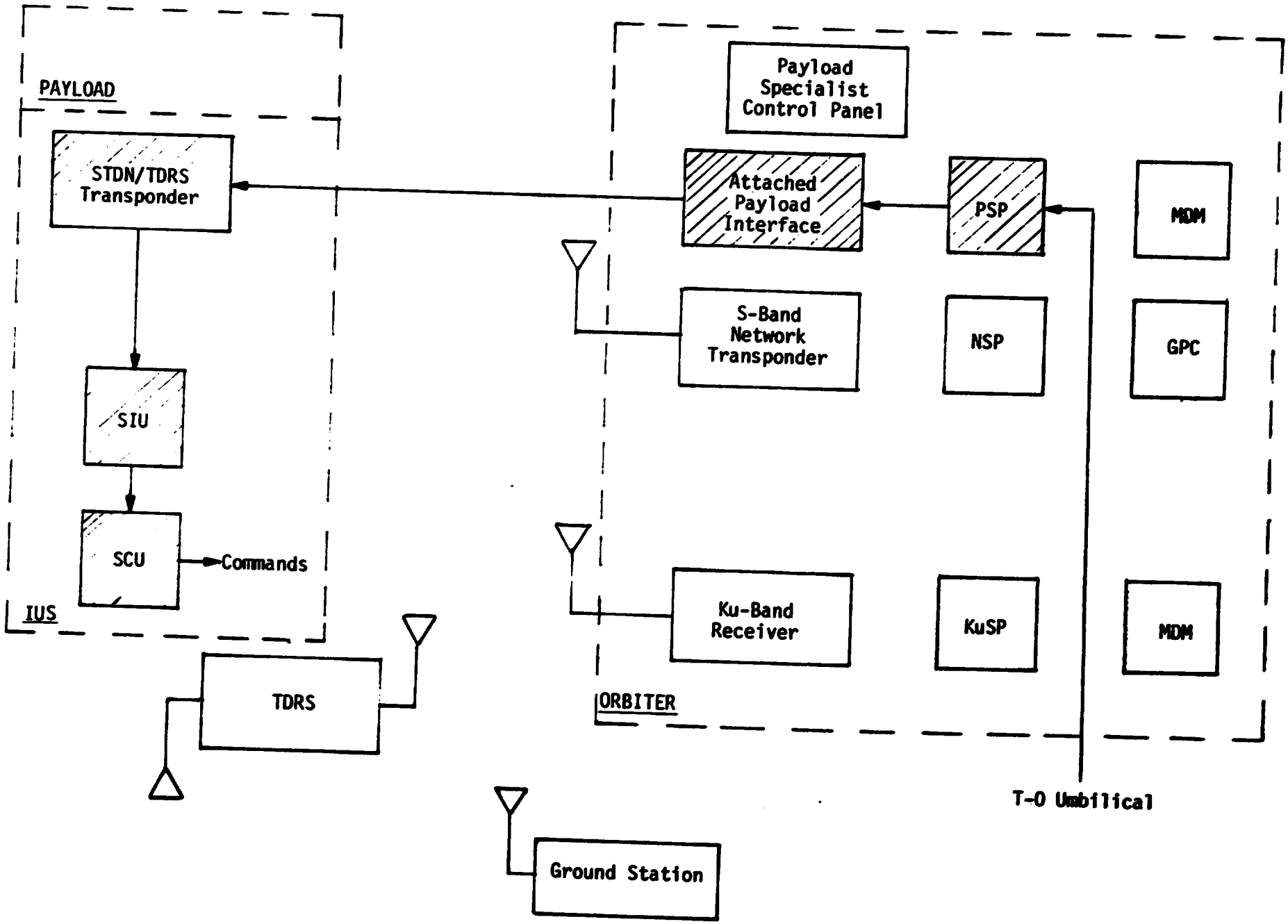

Figure 4. Attached IUS Hard-Line Command Link STDN/TDRS Commands (NASA Mode)

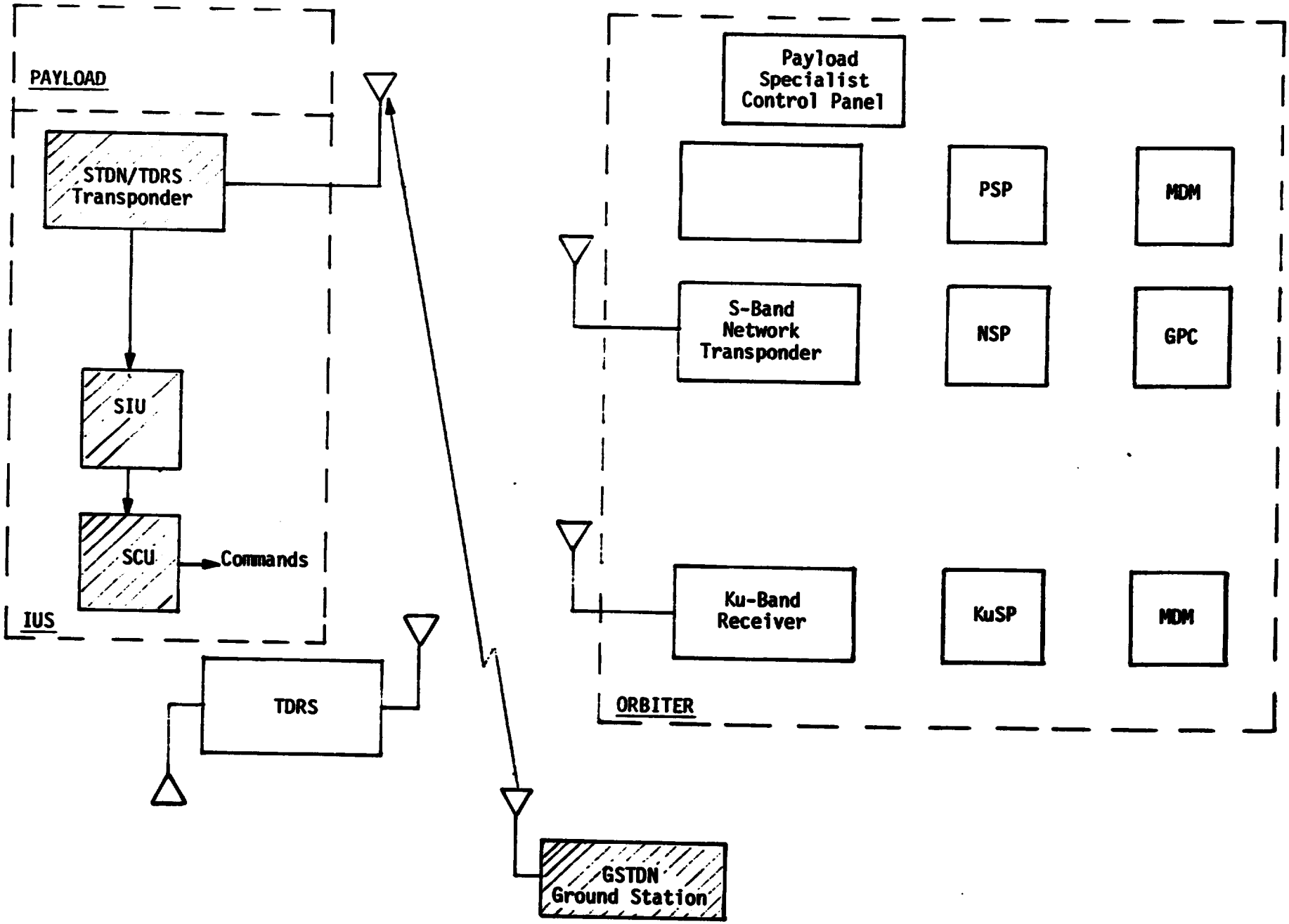

Figure 5. Attached/Detached IUS RF Command Link STDN/TDRS Commands (NASA Mode)

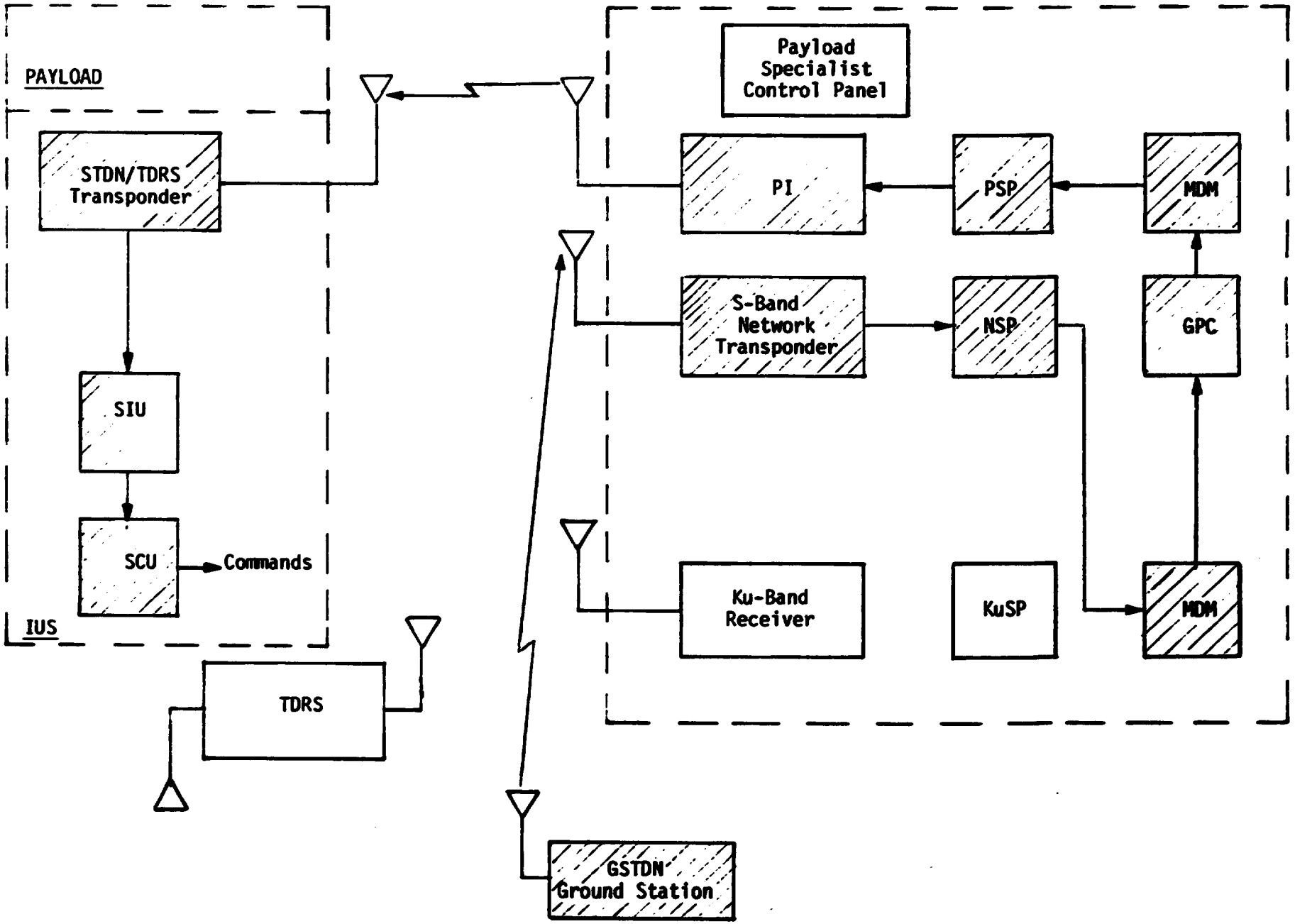

Figure 6. Attached/Detached IUS RF Command Link STDN/TDRS Commands (NASA Mode)

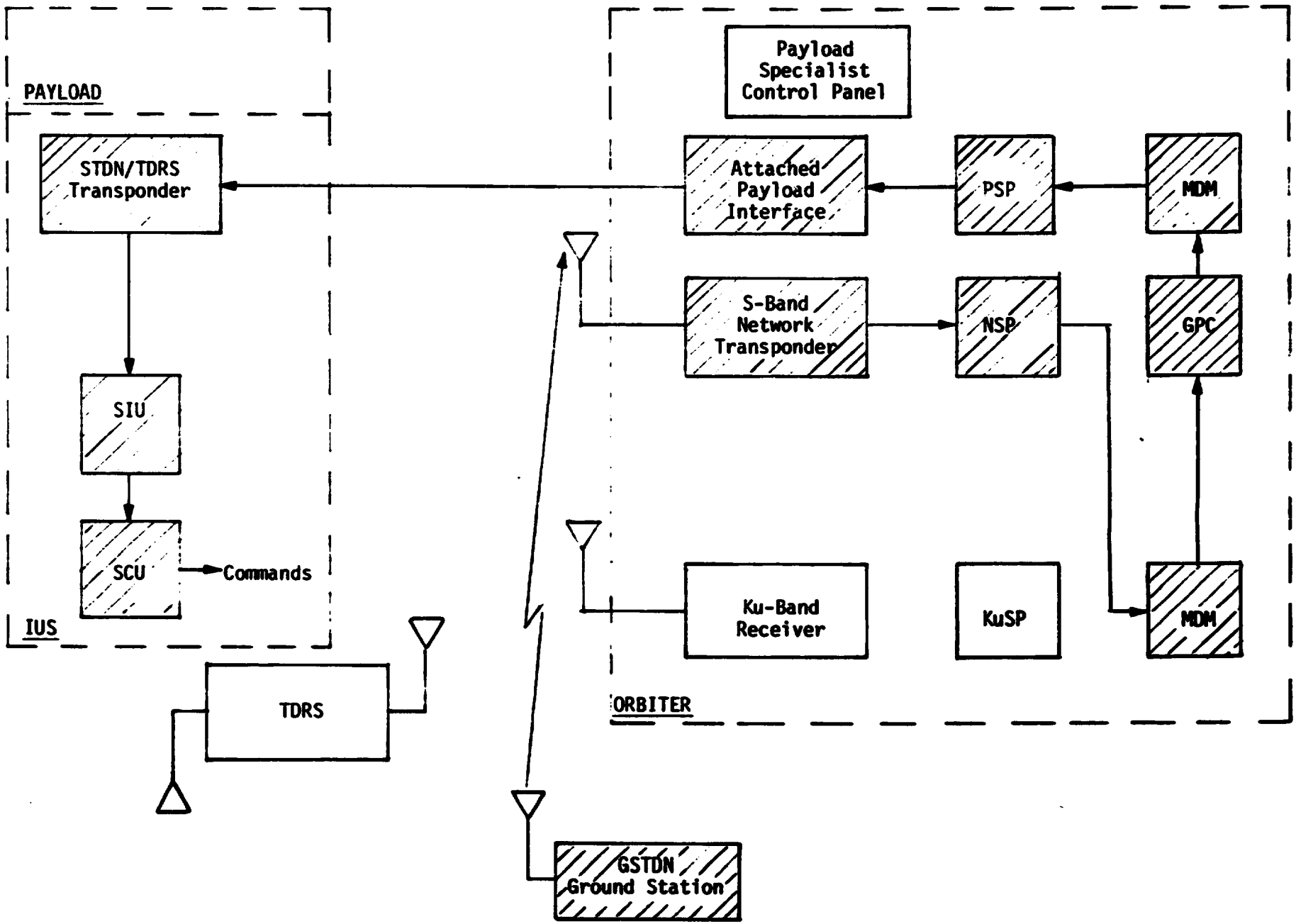

Figure 7. Attached IUS Hard-Line Command Link. STDN/TDRS Commands (NASA Mode)

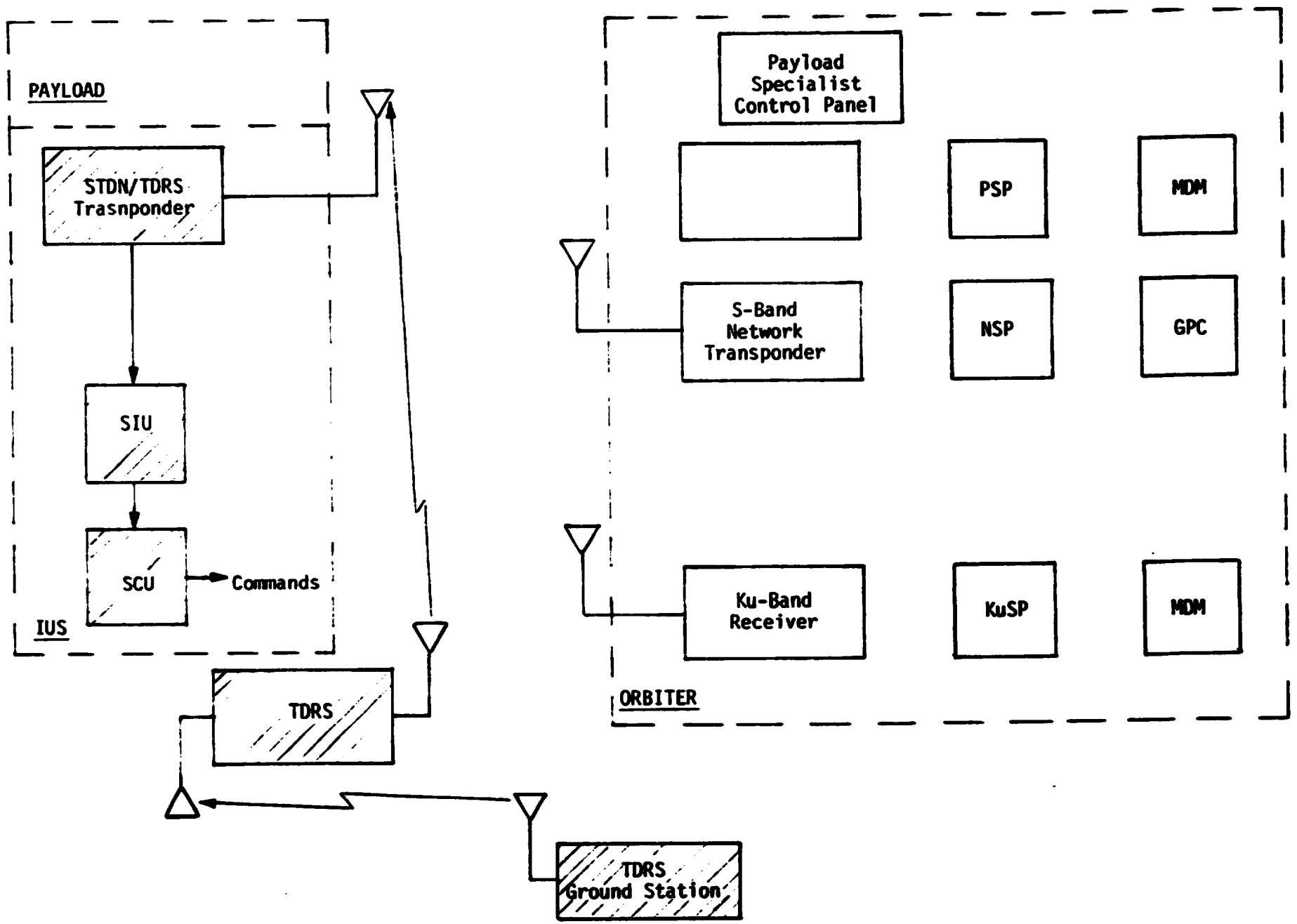

Figure 8. Attached/Detached IUS RF Command Link STDN/TDRS Commands (NASA Mode)

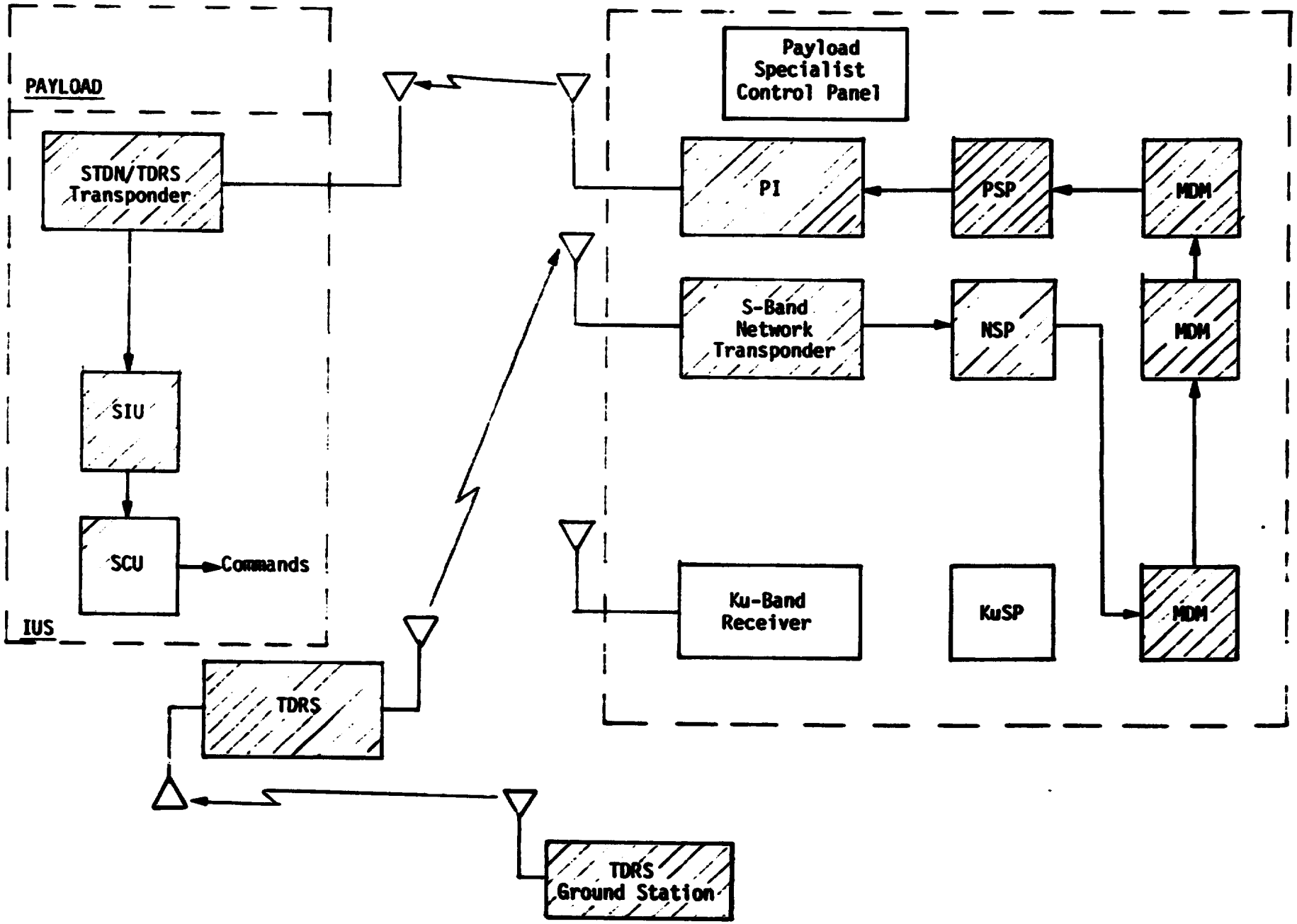

Figure 9. Attached/Detached IUS RF Command Link STDN/TDRS Commands (NASA Model)

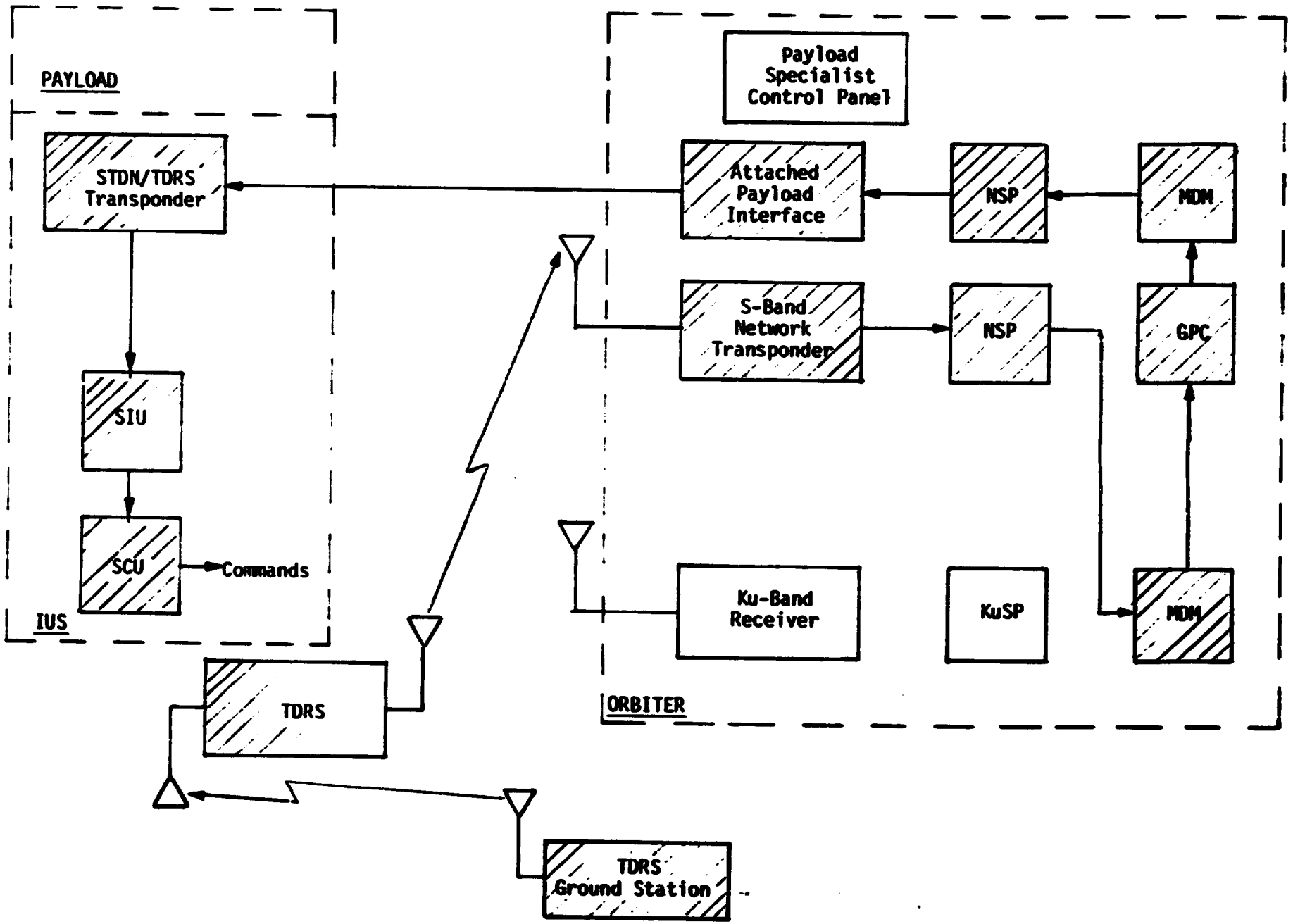

Figure 10. Attached IUS Hard-Line Command Link STDN/TDRS Commands (NASA Mode)

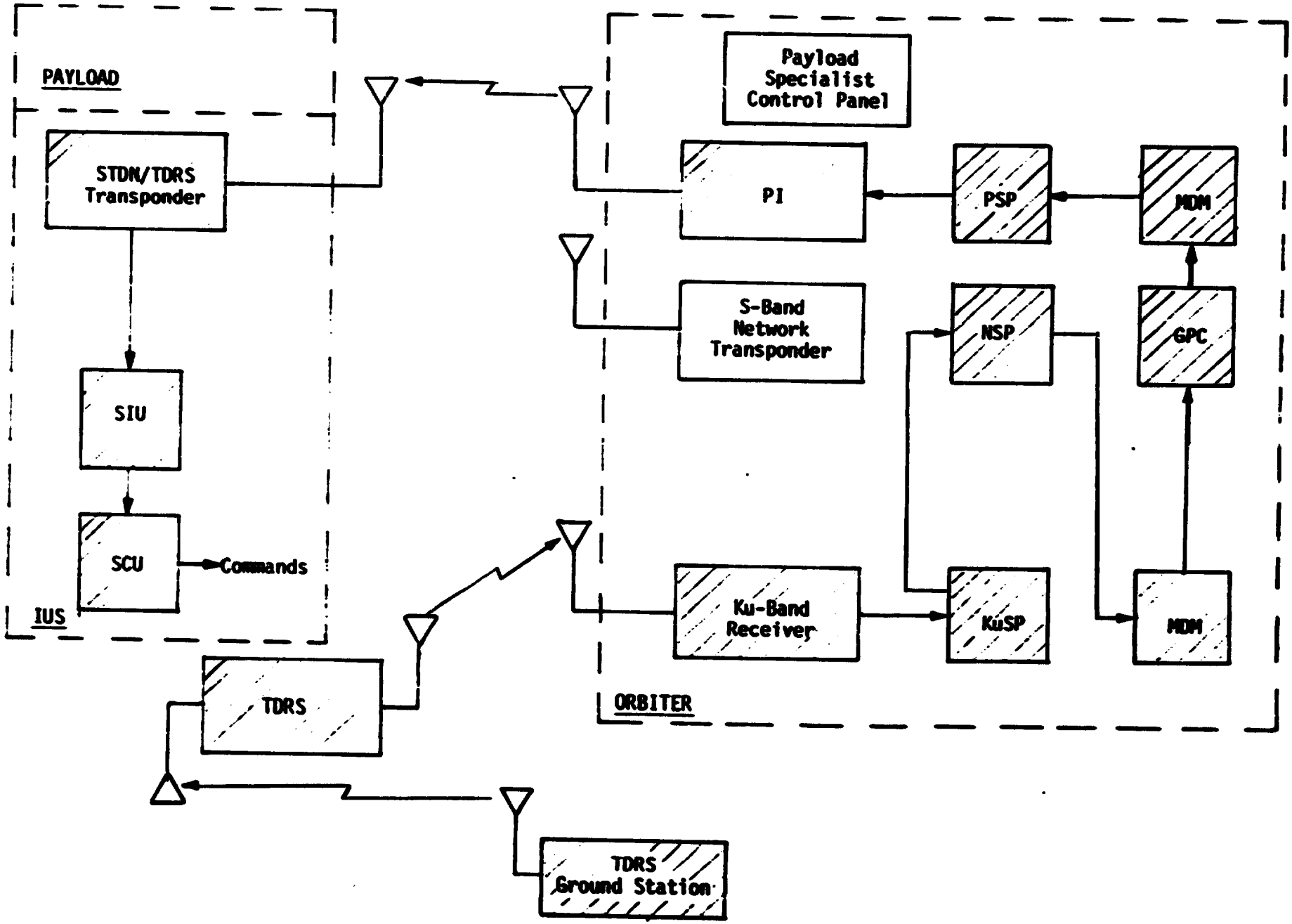

Figure 11. Attached/Detached IUS RF Command Link STDN/TDRS Command (NASA Mode)

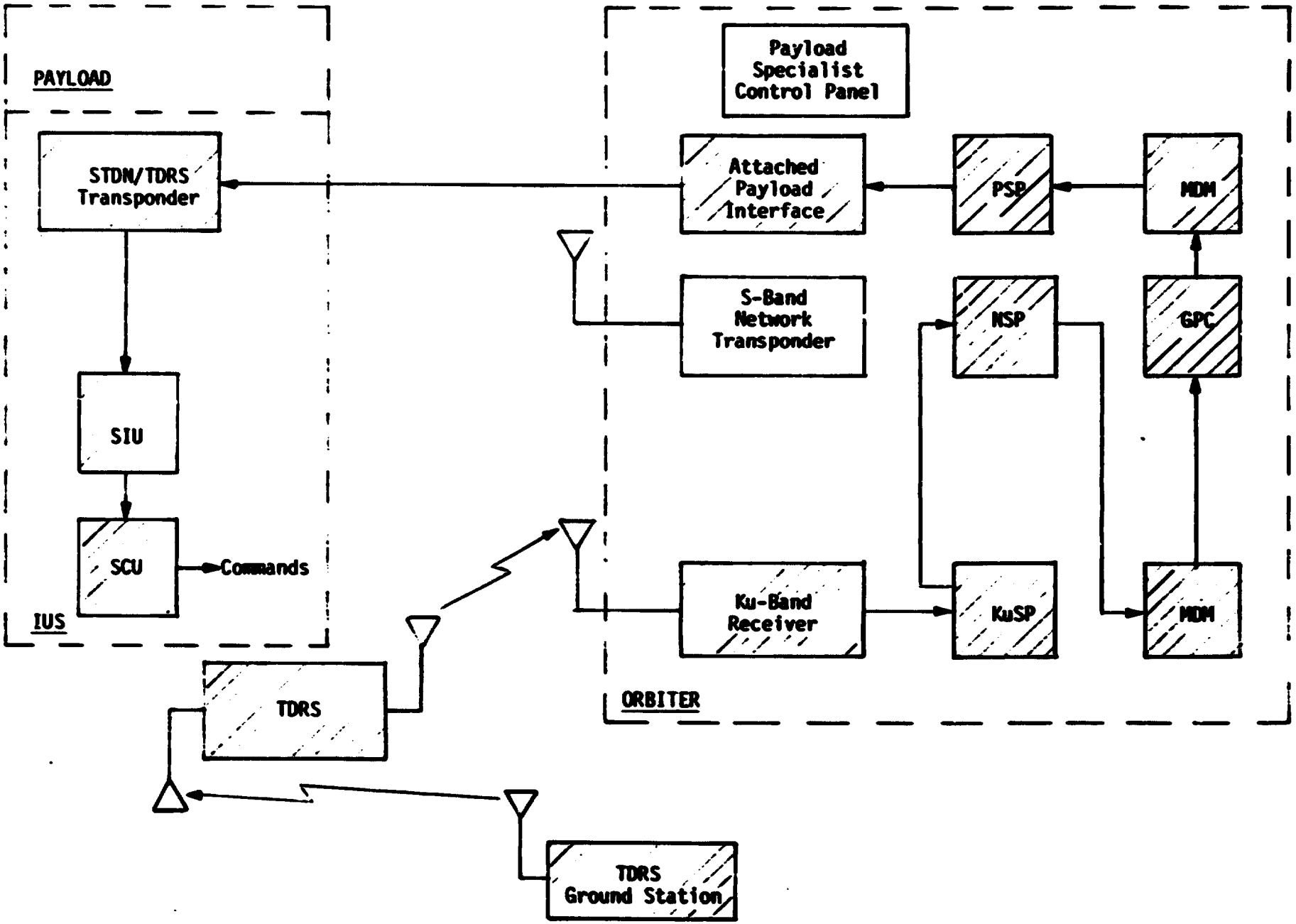

Figure 12. Attached IUS Hard-Line Command Link STDN/TDRS Commands (NASA Mode)

ADDENDUM C

END-TO-END DOD OR SGLS TELEMETRY SIGNAL PATHS

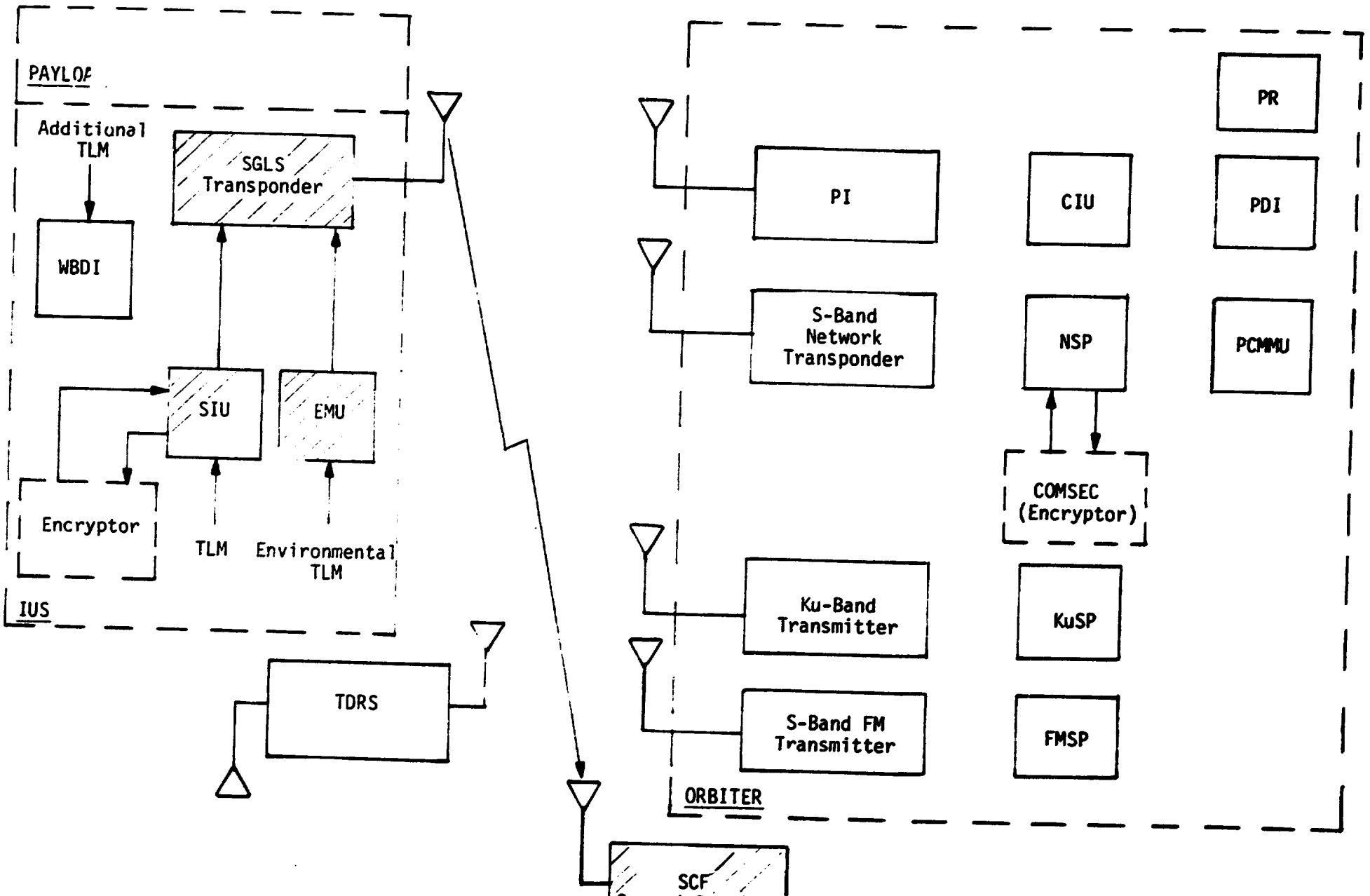

Figure 1. Attached/Detached IUS RF Telemetry Link SGLS Telemetry (DOD Mode)

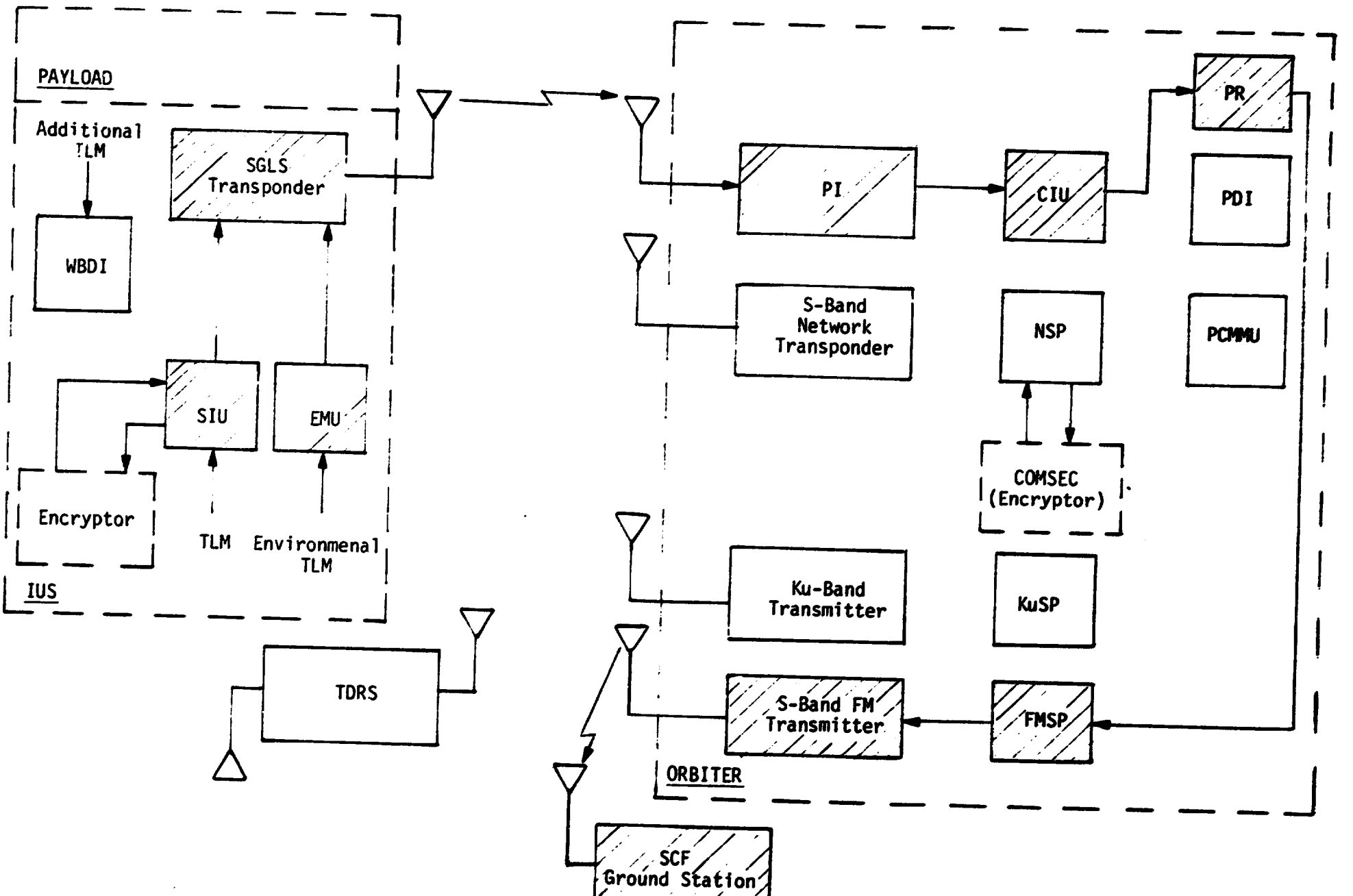

Figure 2. Attached/Detached IUS Telemetry Link
SGLS Telemetry (DOD (Mode)

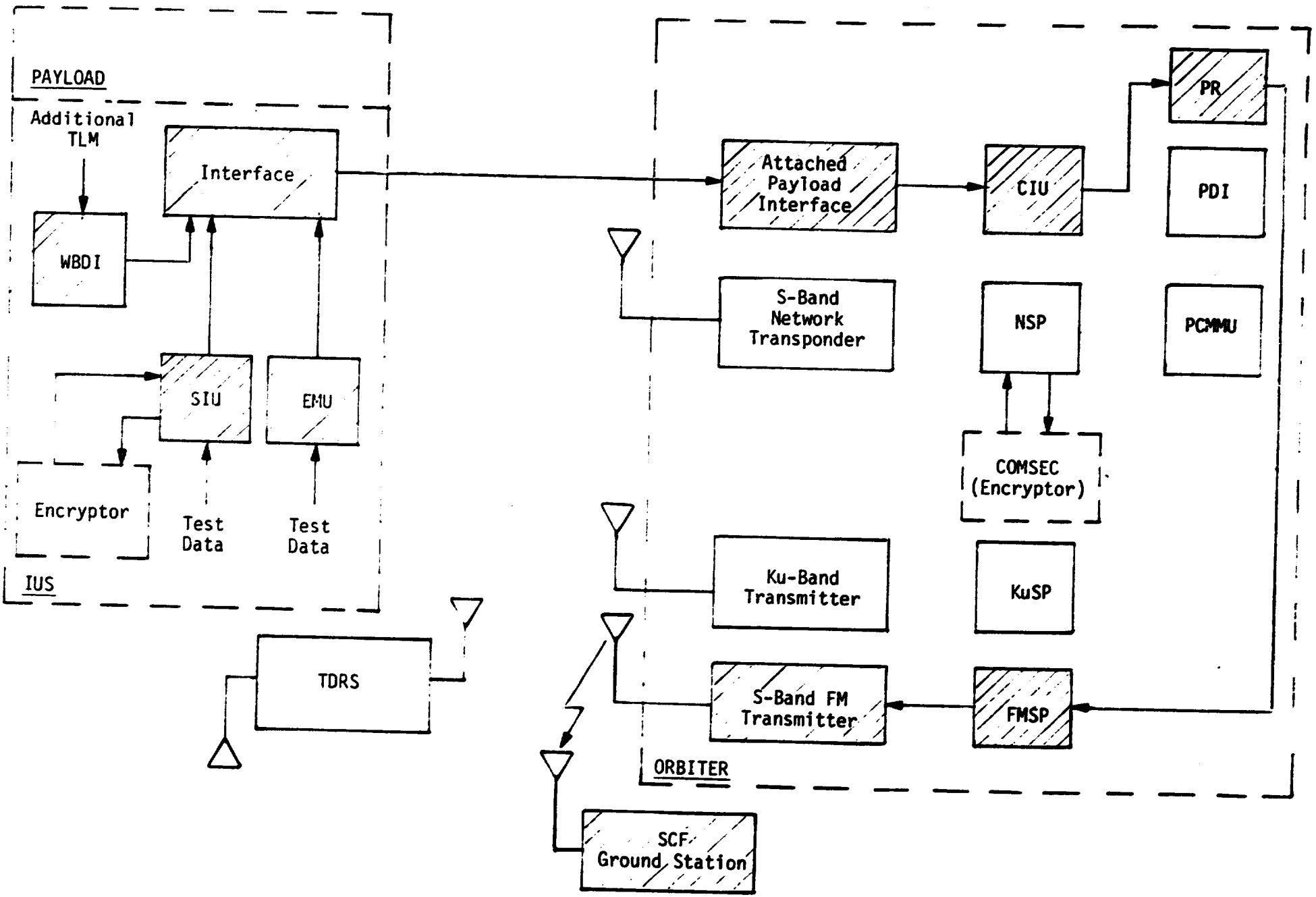

Figure 3. Attached IUS Hard-Line Telemetry Link
SGLS Telemetry (DOD Mode)

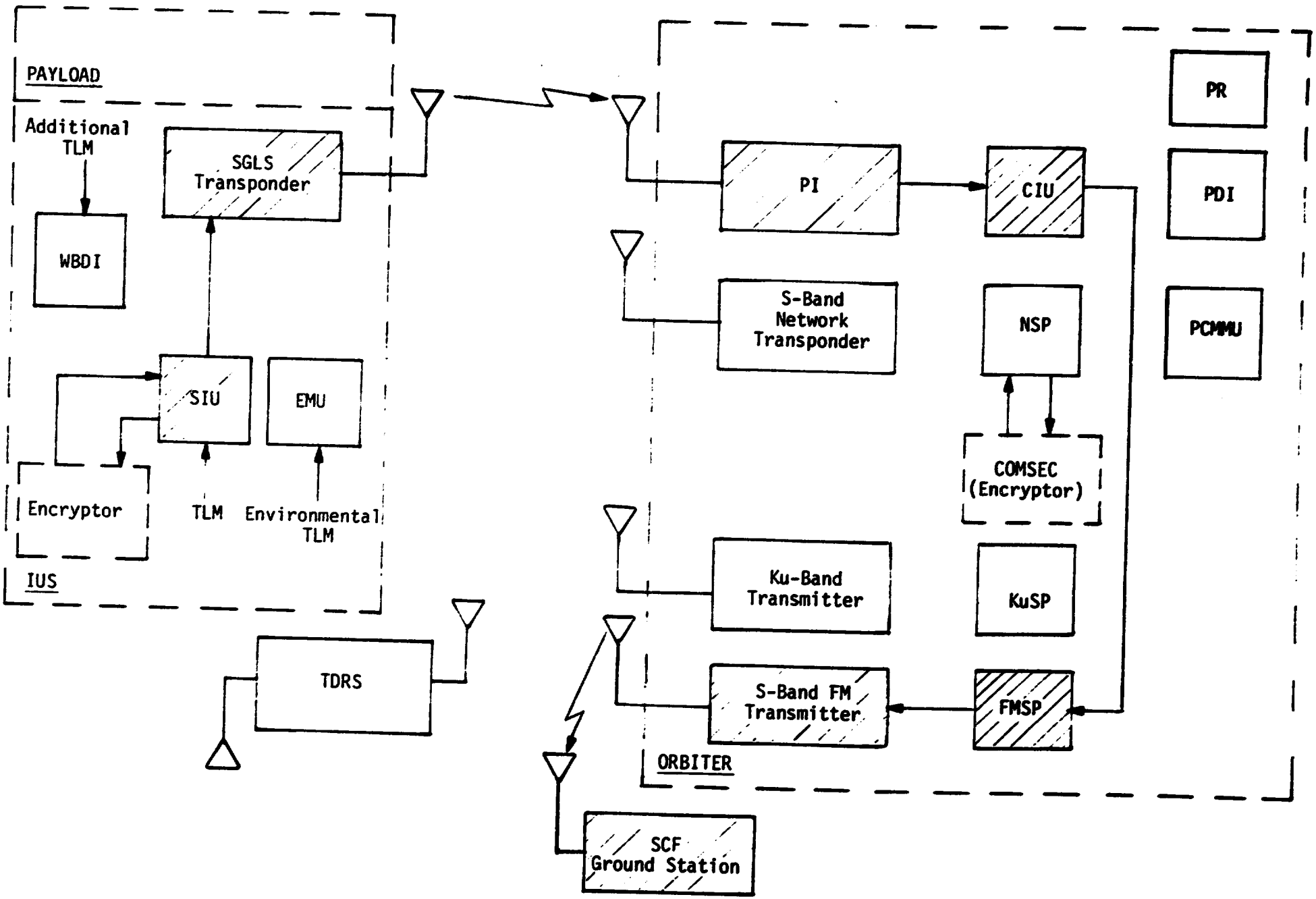

Figure 4. Attached/Detached IUS RF Telemetry Link SGLS Telemetry (DOD Mode)

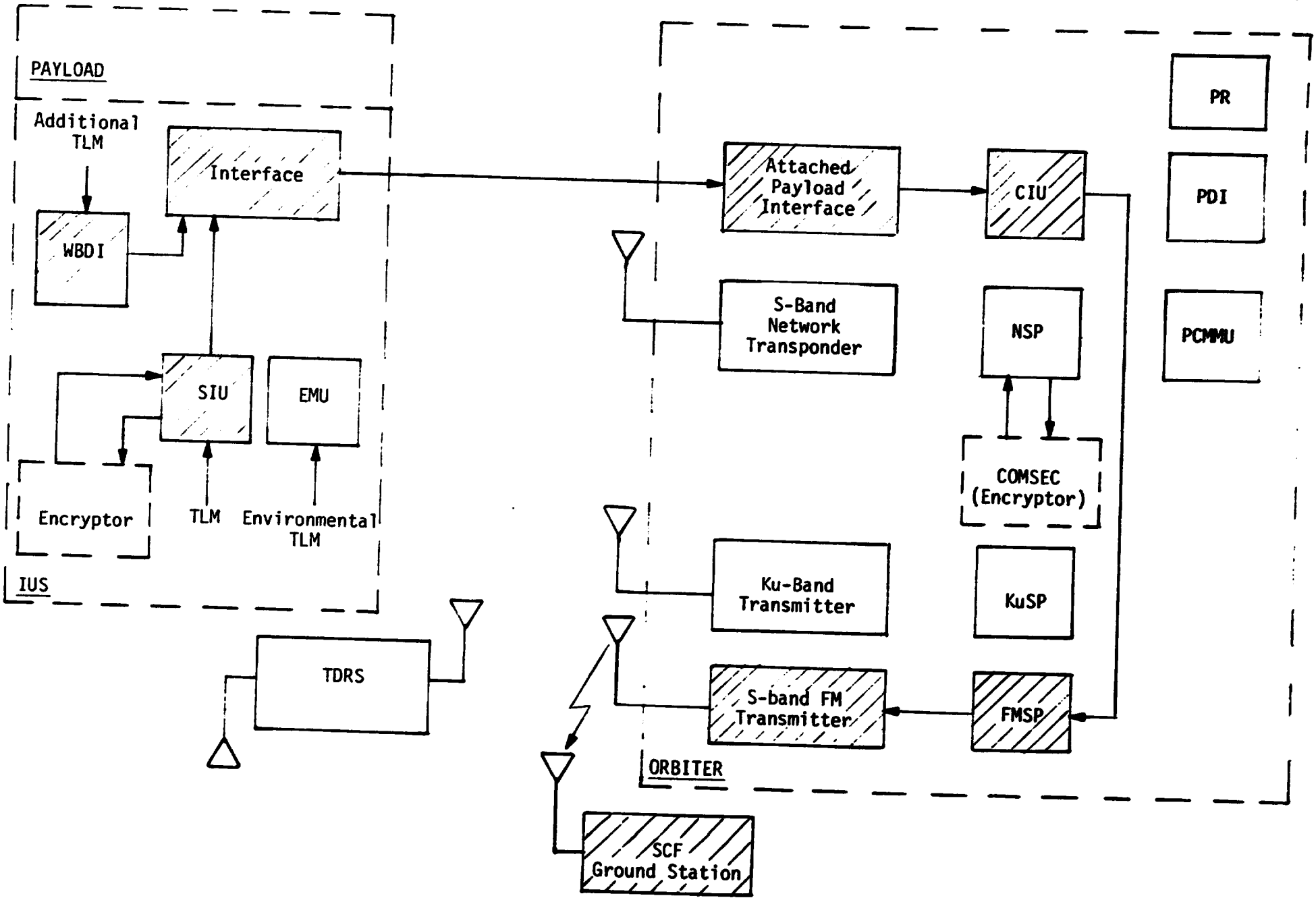

Figure 5. Attached IUS Hard-Line Telemetry Link SGLS Telemetry (DOD Mode)

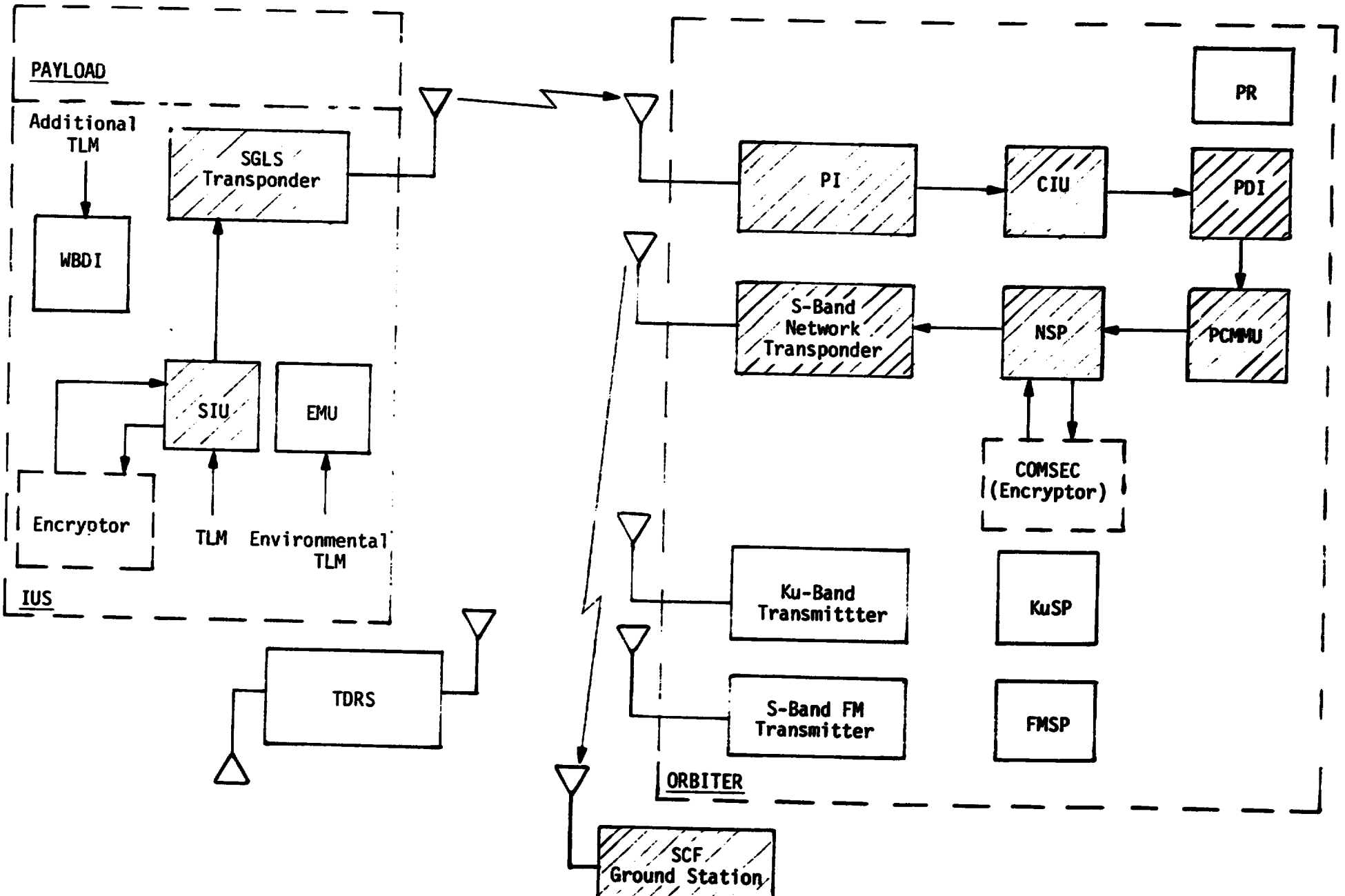

Figure 6. Attached/Detached IUS RF Telemetry Link
SGLS Telemetry (DOD Mode)

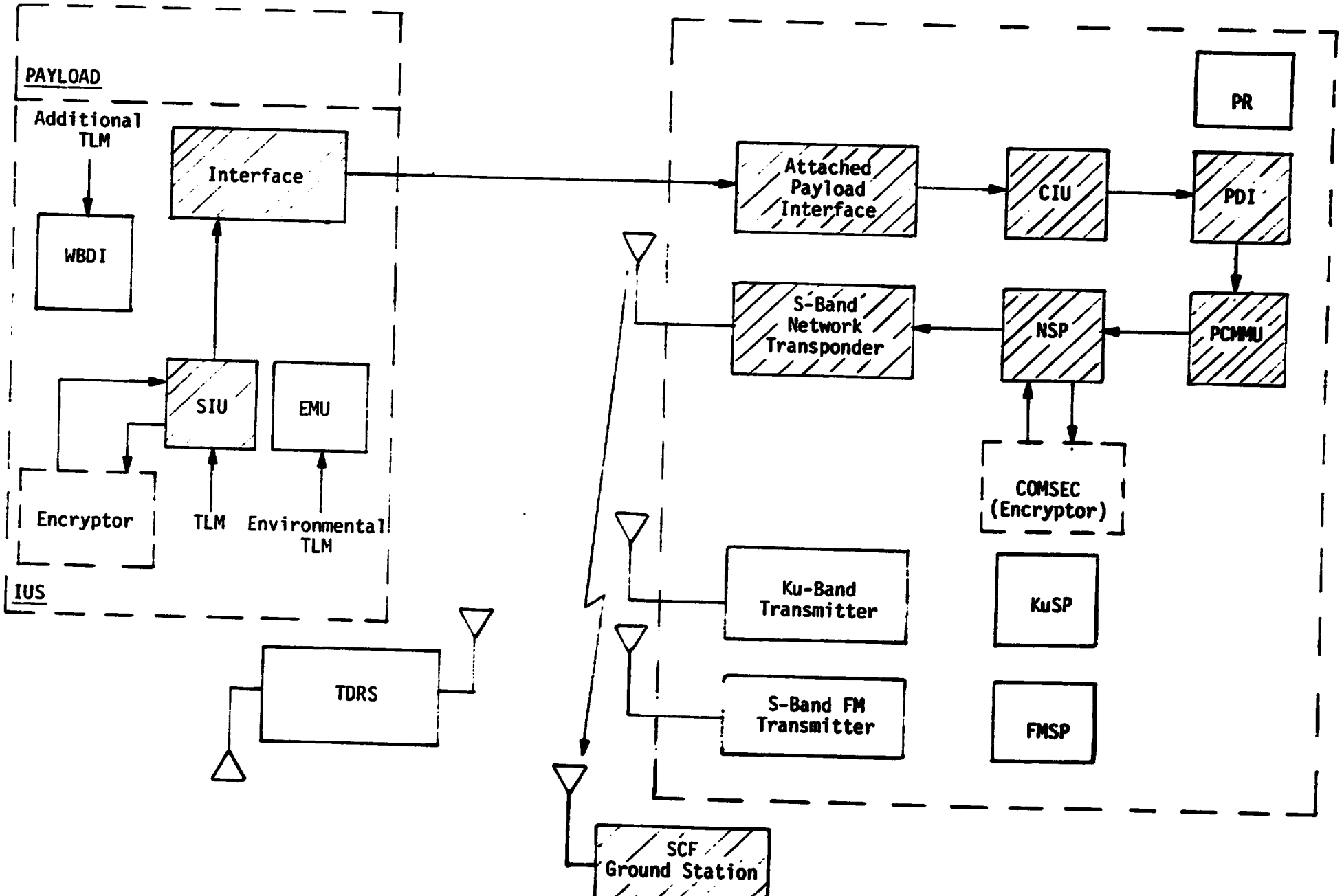

Figure 7. Attached IUS Hard-Line Telemetry Link SGLS Telemetry (DOD Mode)

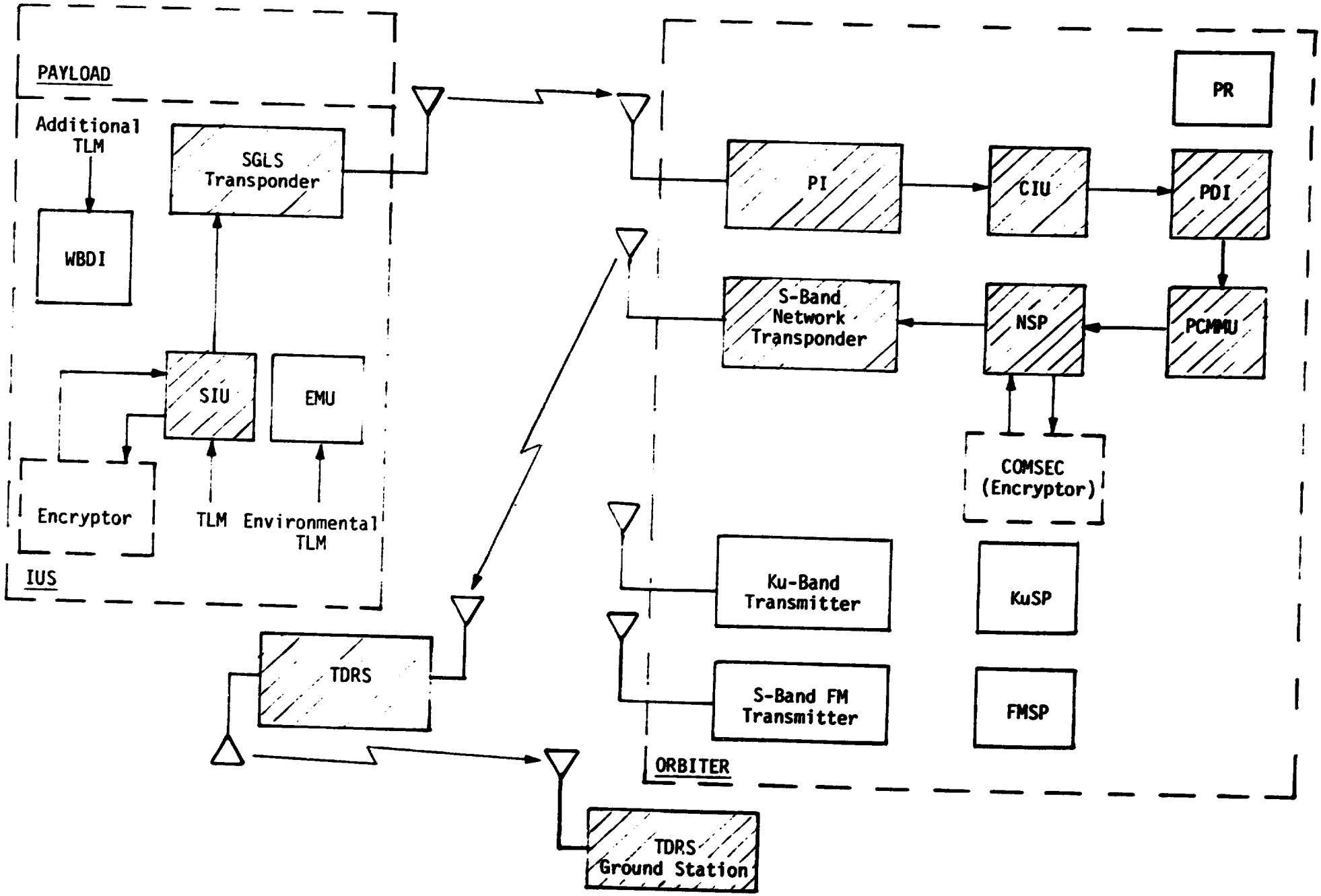

Figure 8. Attached/Detached IUS RF Telemetry Link SGLS Telemetry (DOD Mode)

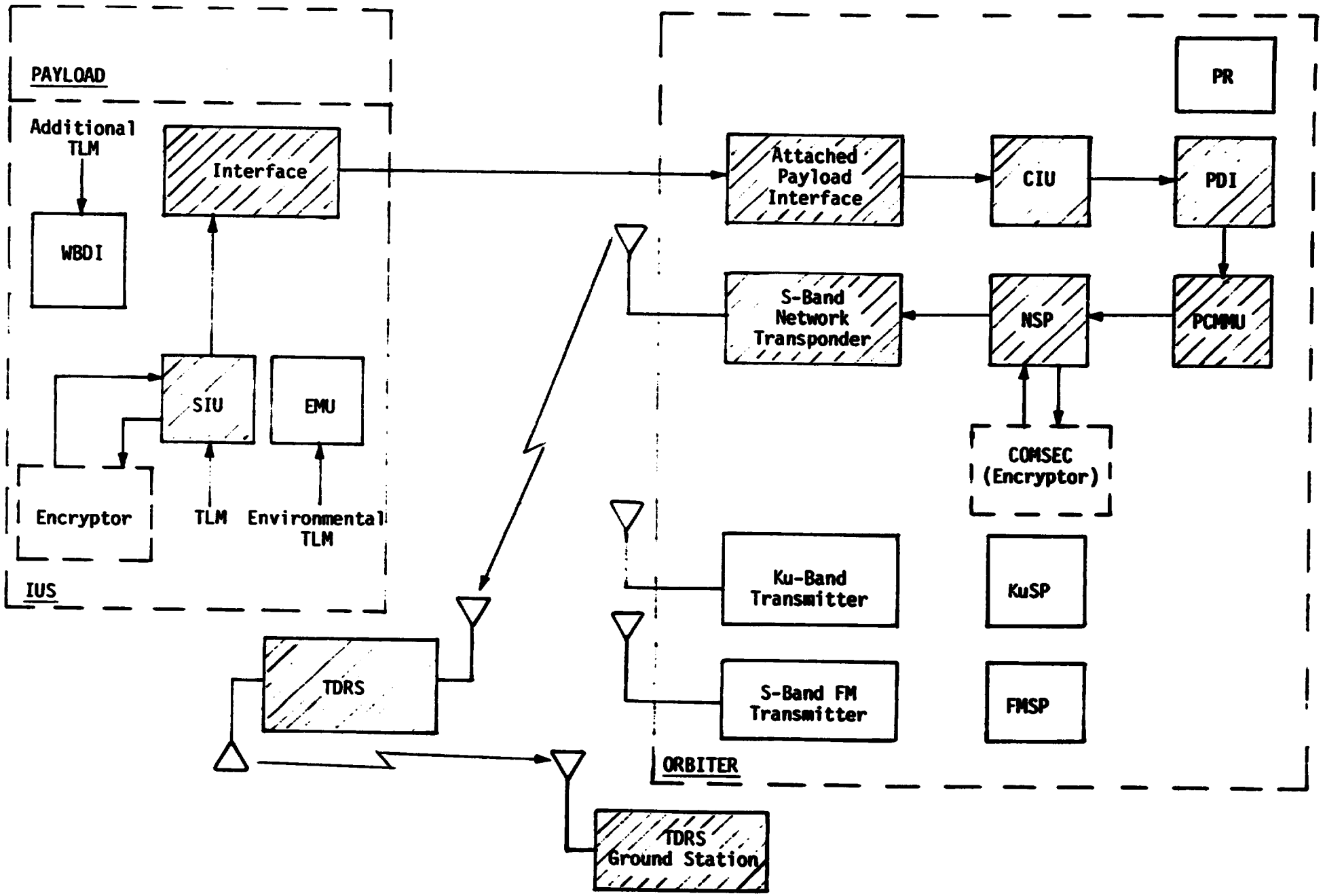

Figure 9. Attached IUS Hard-Line Telemetry Link SGLS Telemetry (DOD Mode)

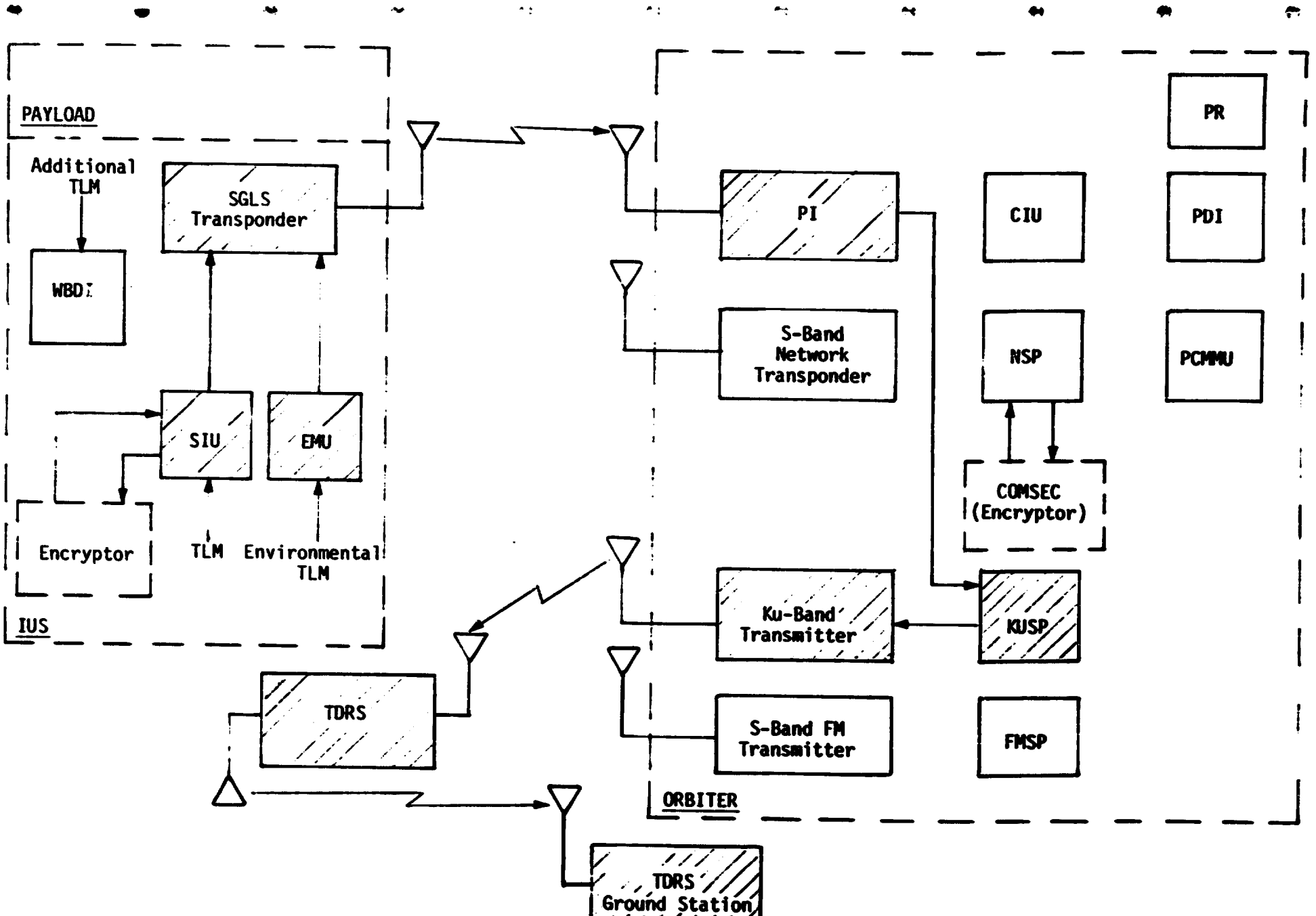

Figure 10. Attached/Detached IUS RF Telemetry Link SGLS Telemetry (DOD Mode)

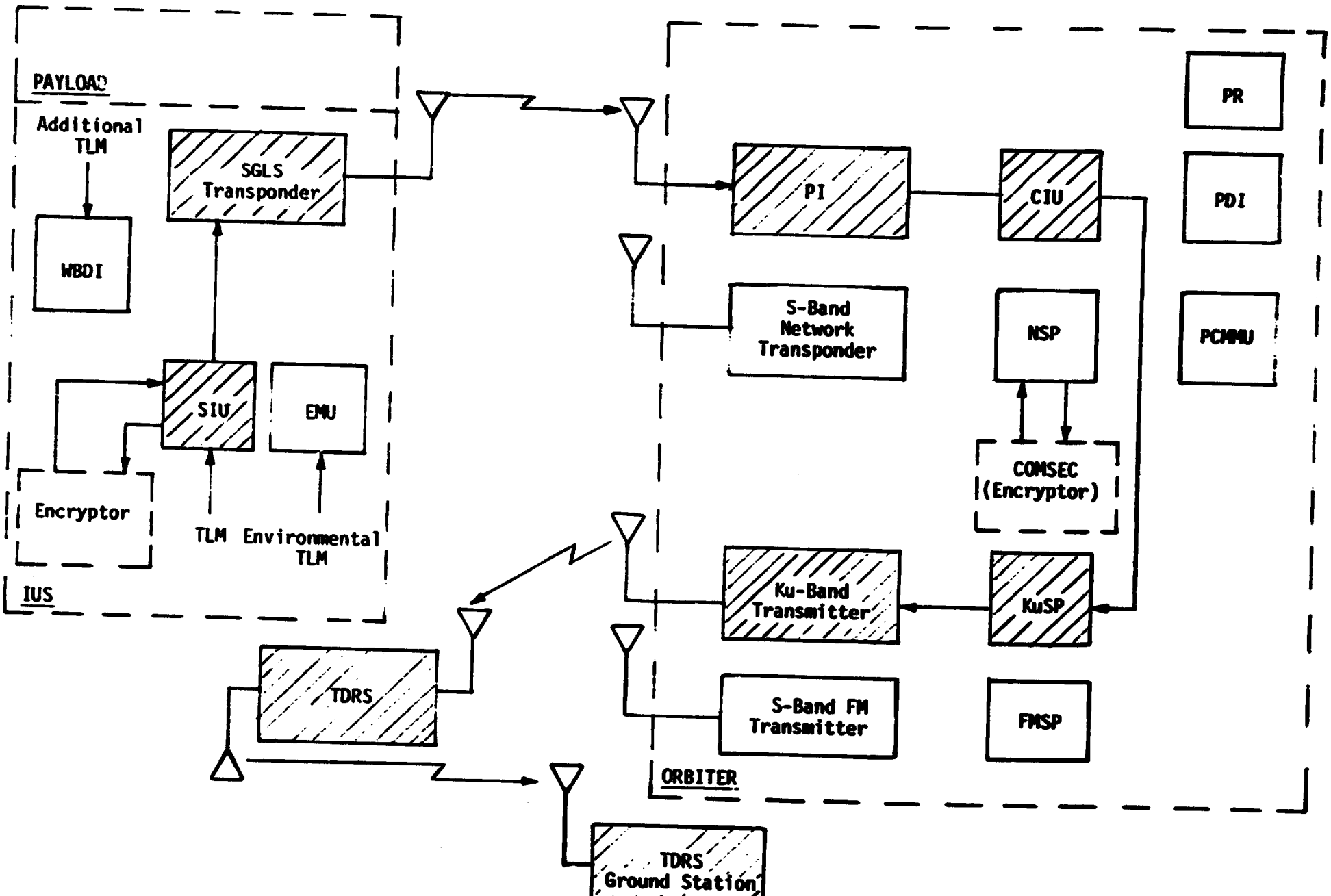

Figure 11. Attached/Detached IUS RF Telemetry Link SGLS Telemetry (DOD Mode)

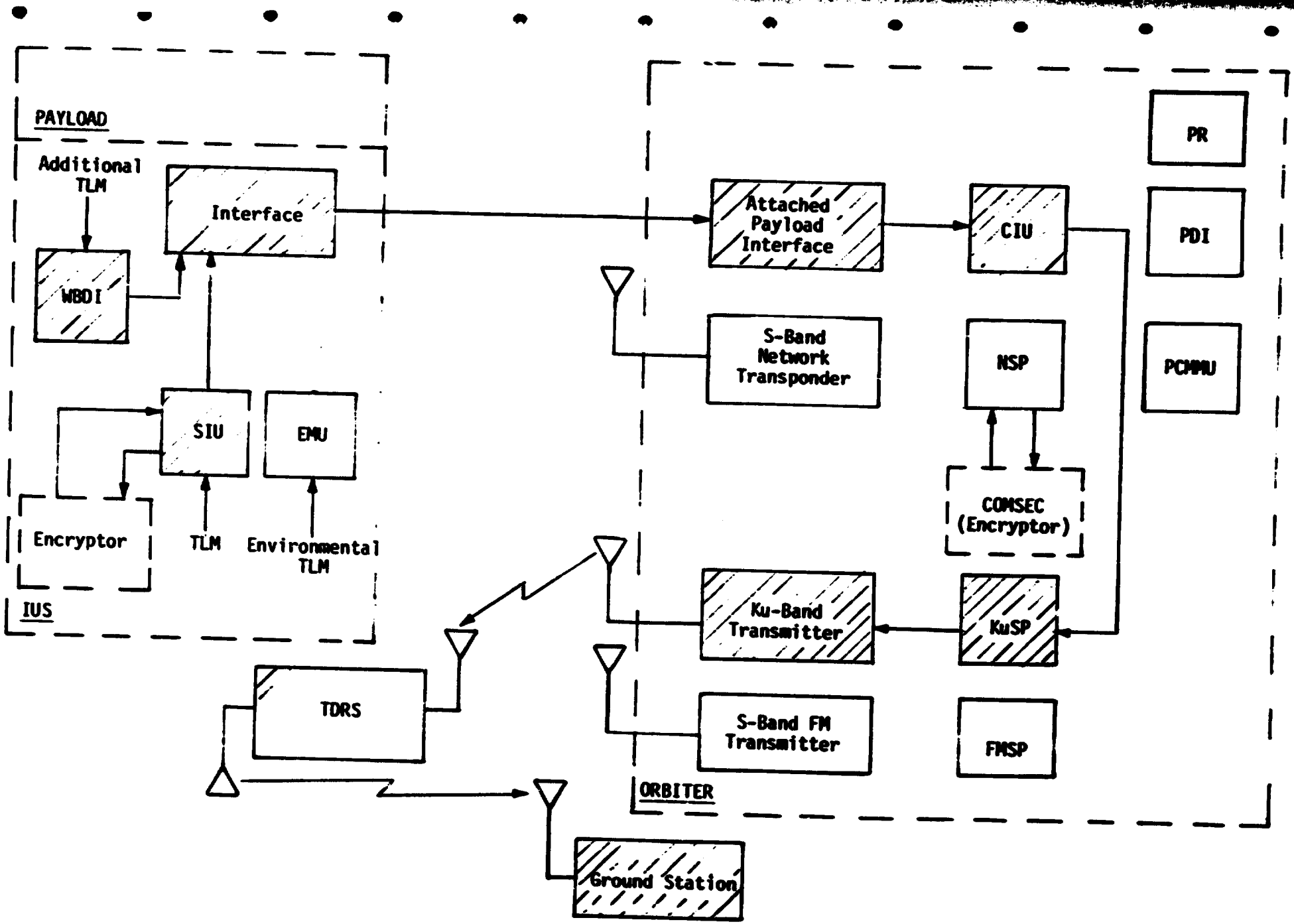

Figure 12. Attached IUS Hard-Line Telemetry Link SGLS Telemetry (DOD Mode)

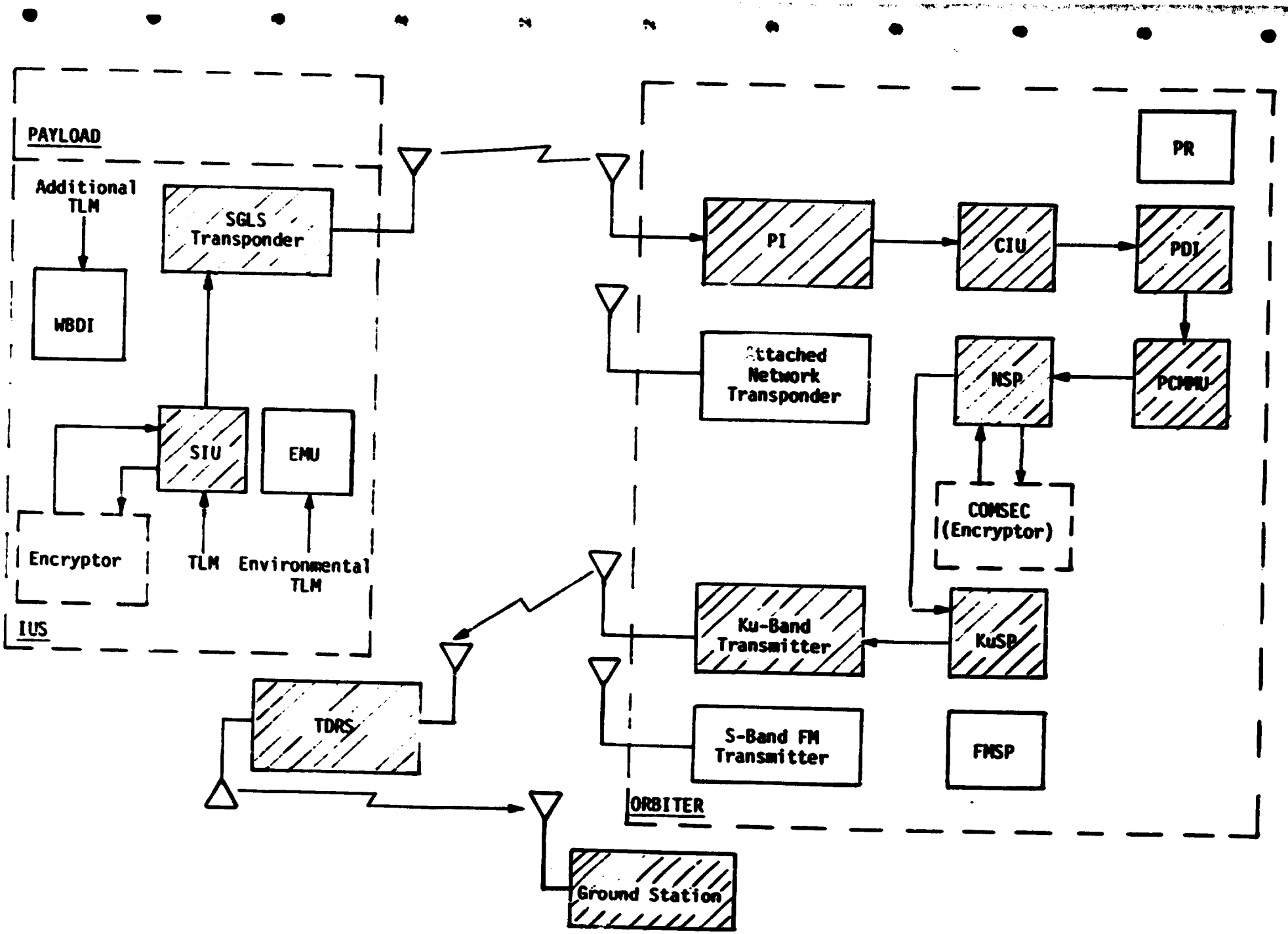

Figure 13. Attached/Detached IUS RF Telemetry Link SGLS Telemetry (DOD Mode)

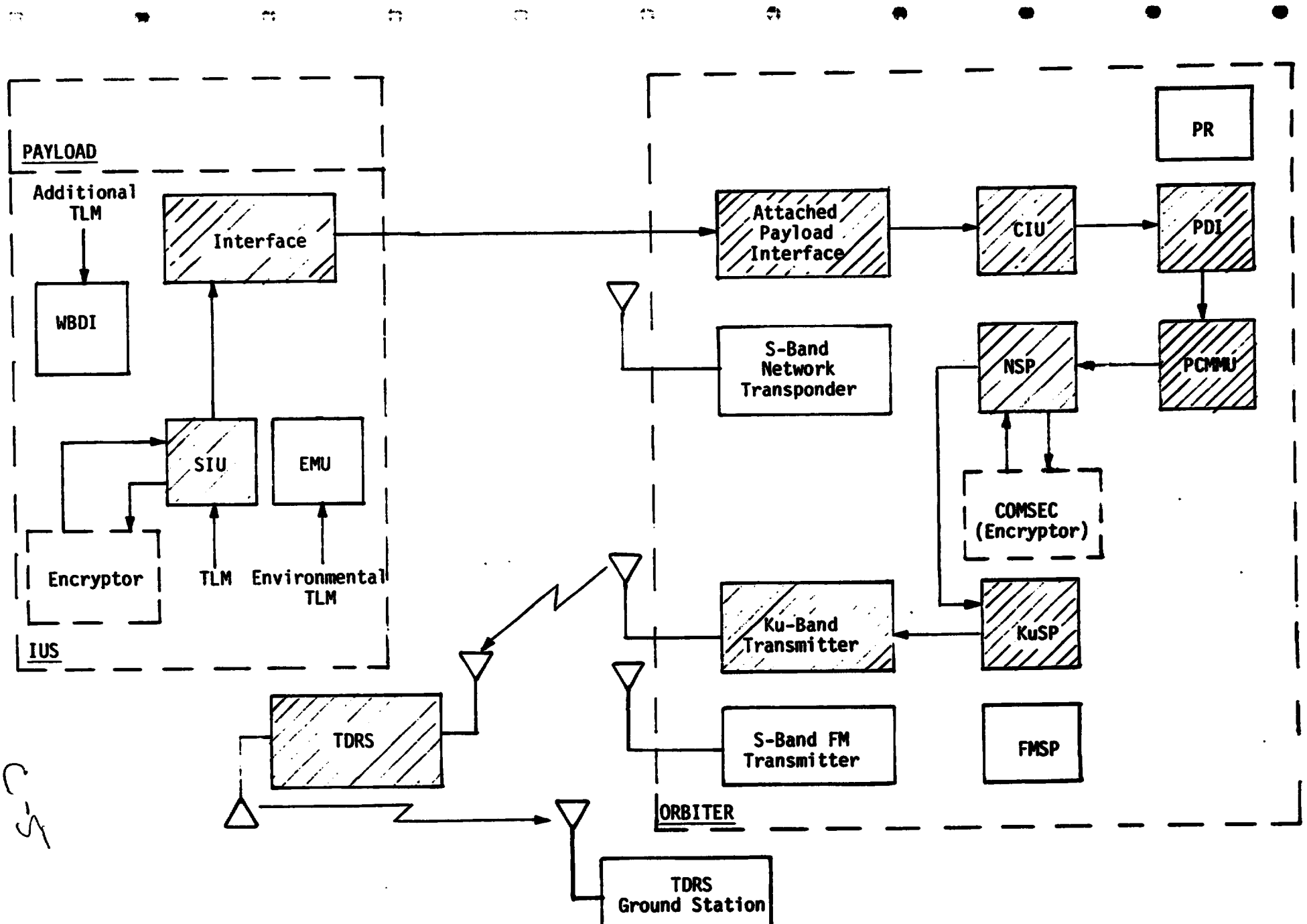

Figure 14. Attached IUS Hard-Line Telemetry Link
SGLS Telemetry (DOD Mode)

ADDENDUM D

END-TO-END NASA OR STDN/TDRS TELEMETRY SIGNAL PATHS

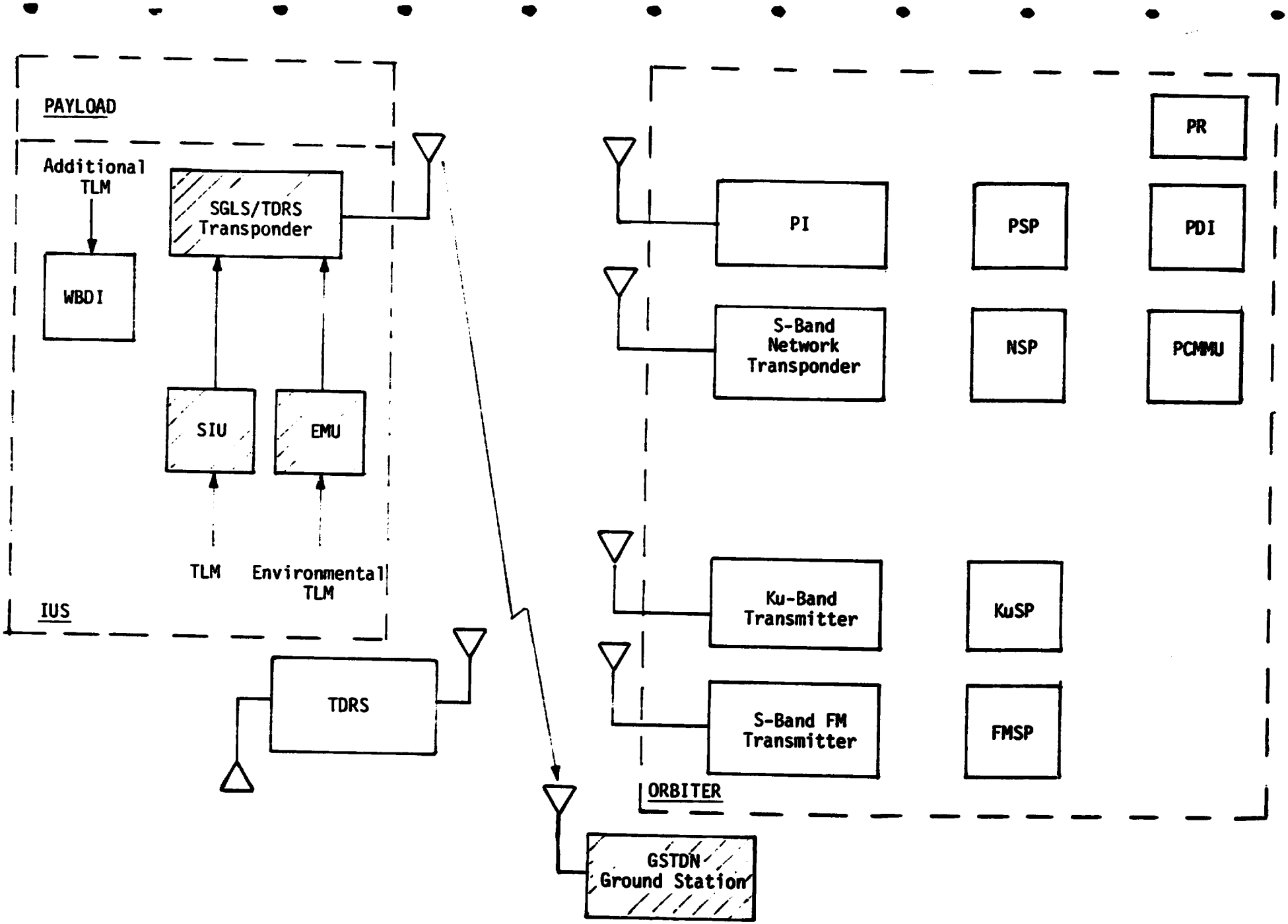

Figure 1. Attached/Detached IUS RF Telemetry Link STDN/TDRS Telemetry (NASA Mode)

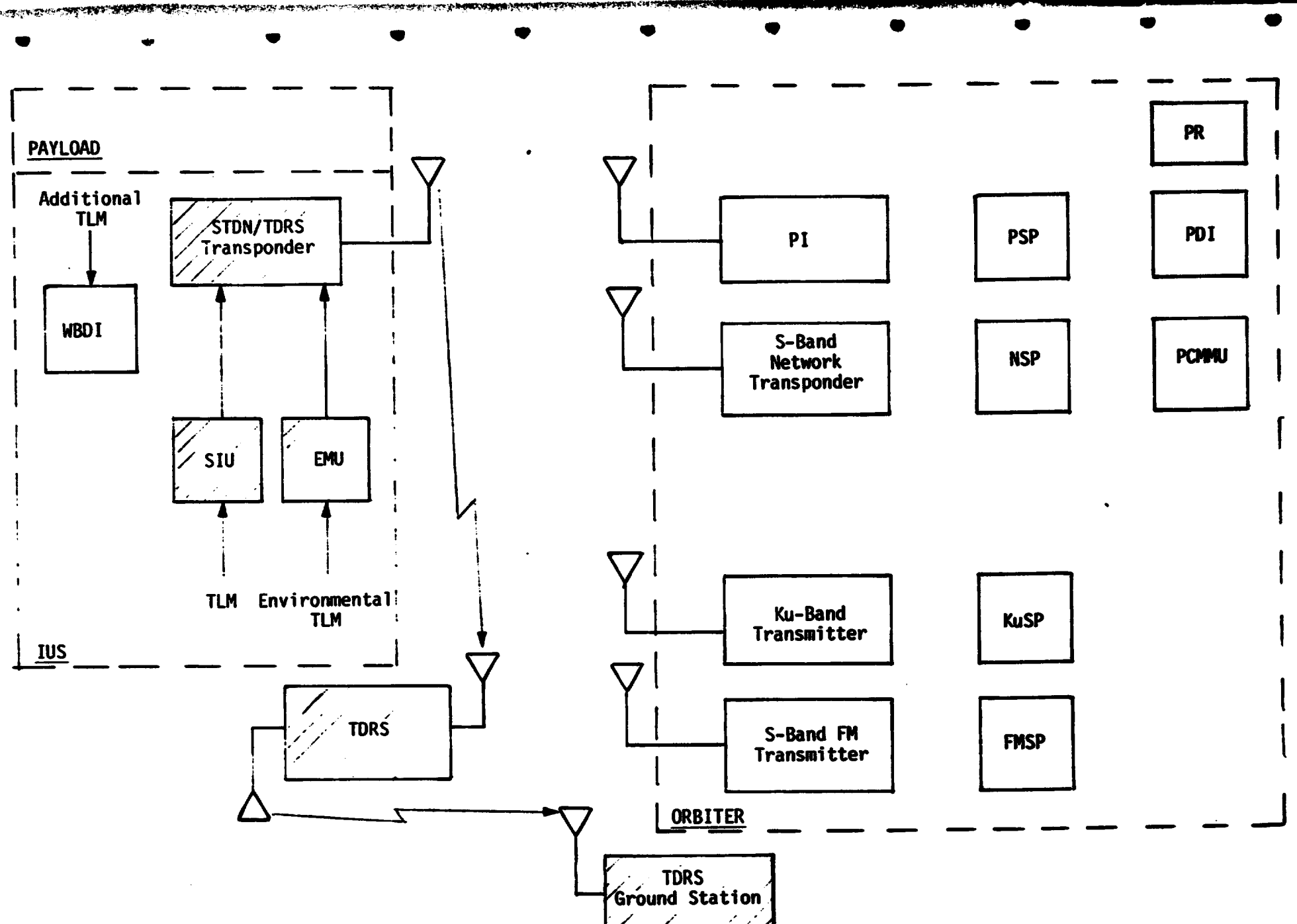

Figure 2. Attached/Detached IUS RF Telemetry Link
STDN/TDRS Telemetry (NASA Mode)

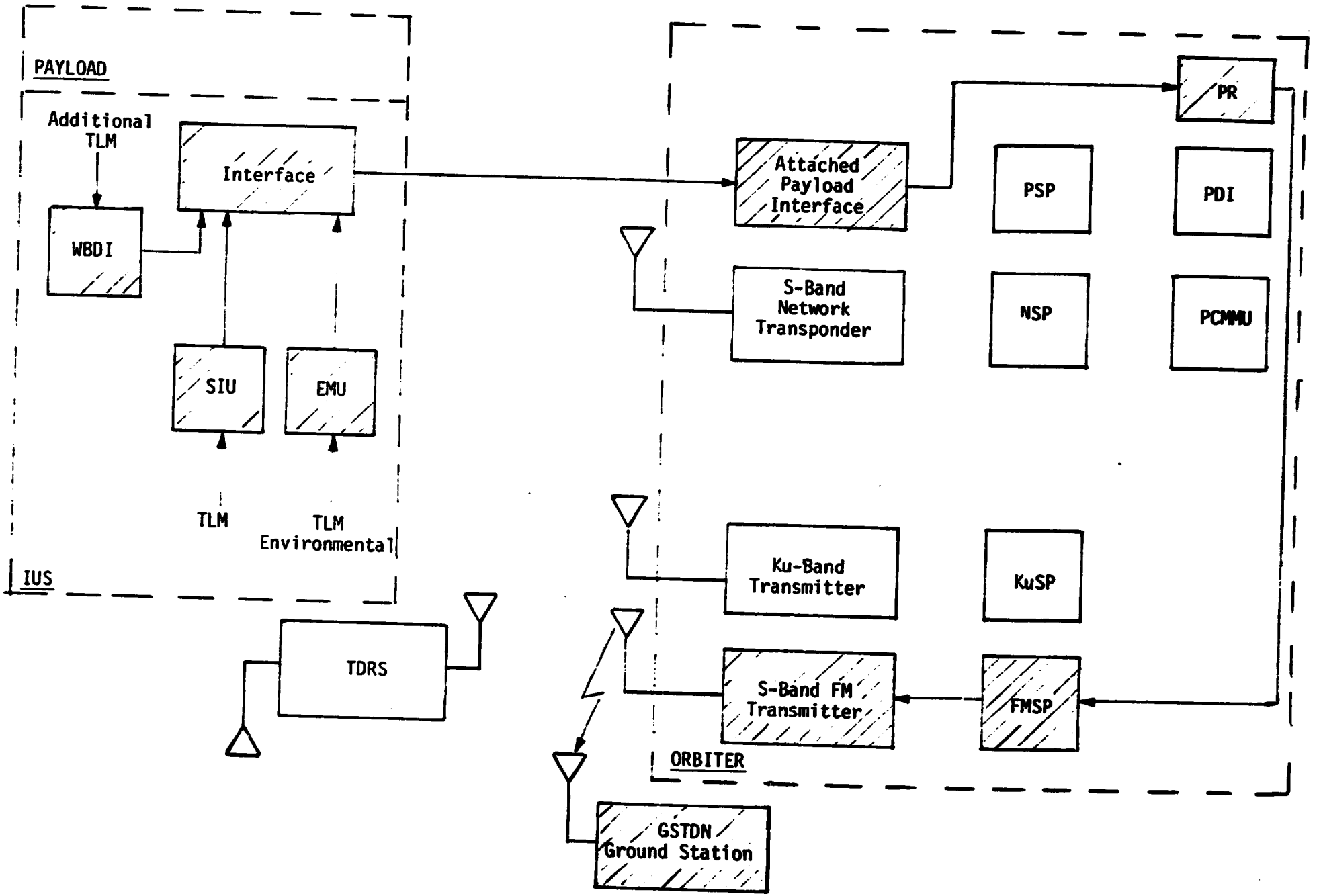

Figure 3. Attached IUS Hard-Line Telemetry Link STDN/TDRS Telemetry (NASA Mode)

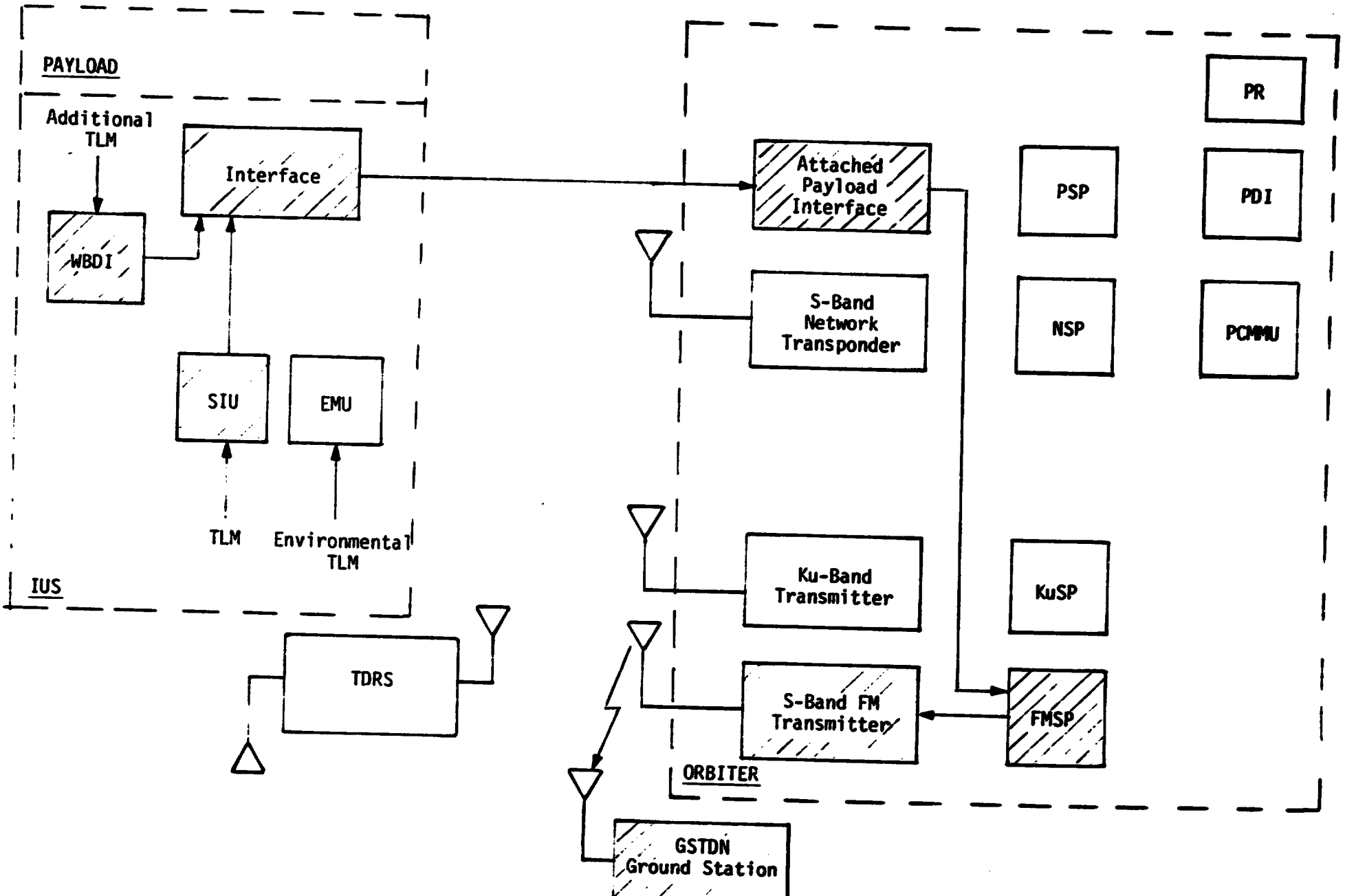

Figure 4. Attached IUS Hard-Line Telemetry Link STDN/TDRS Telemetry (NASA Mode)

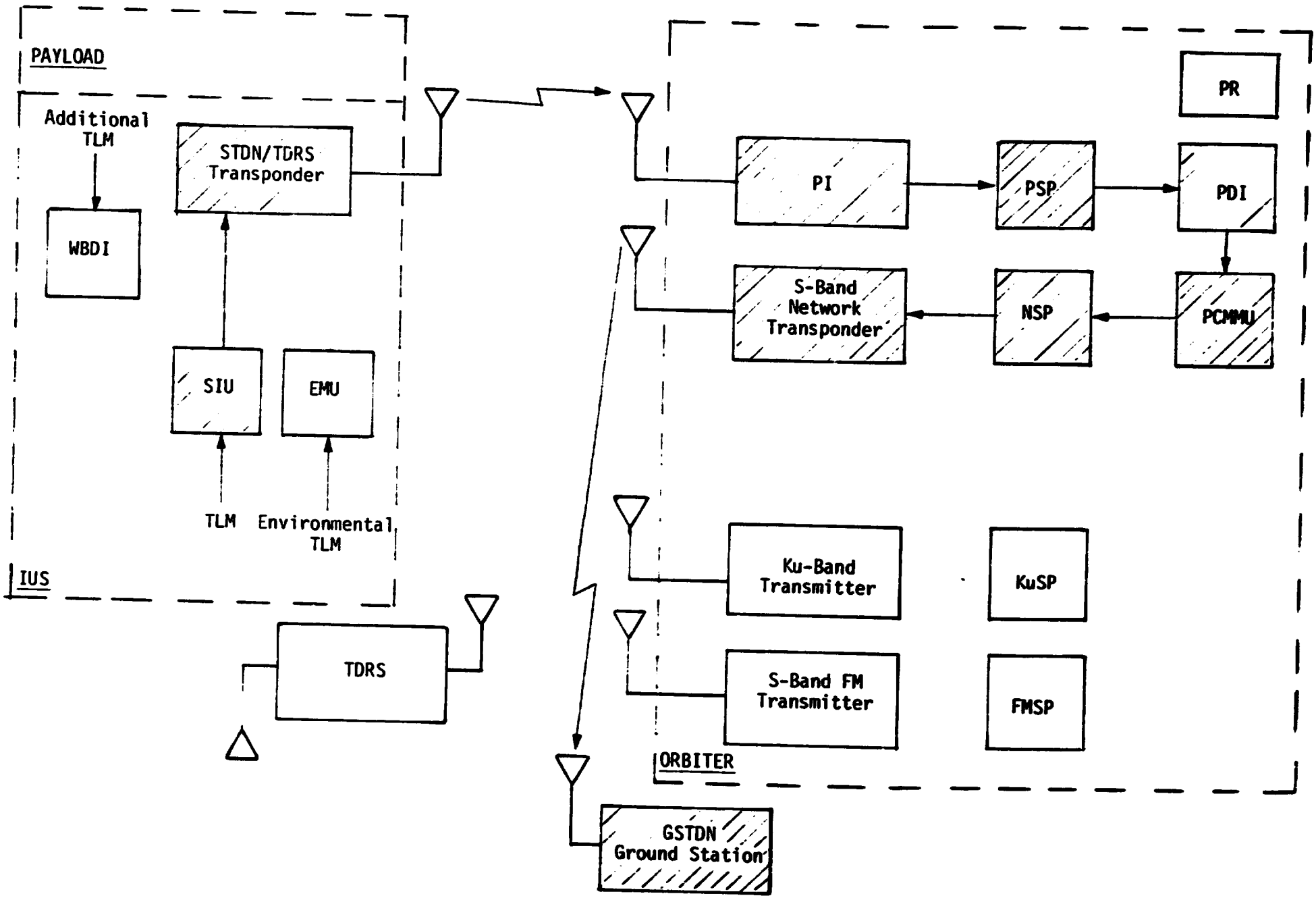

Figure 5. Attached/Detached IUS RF Telemetry Link
STDN /TDRS Telemetry (NASA Mode)

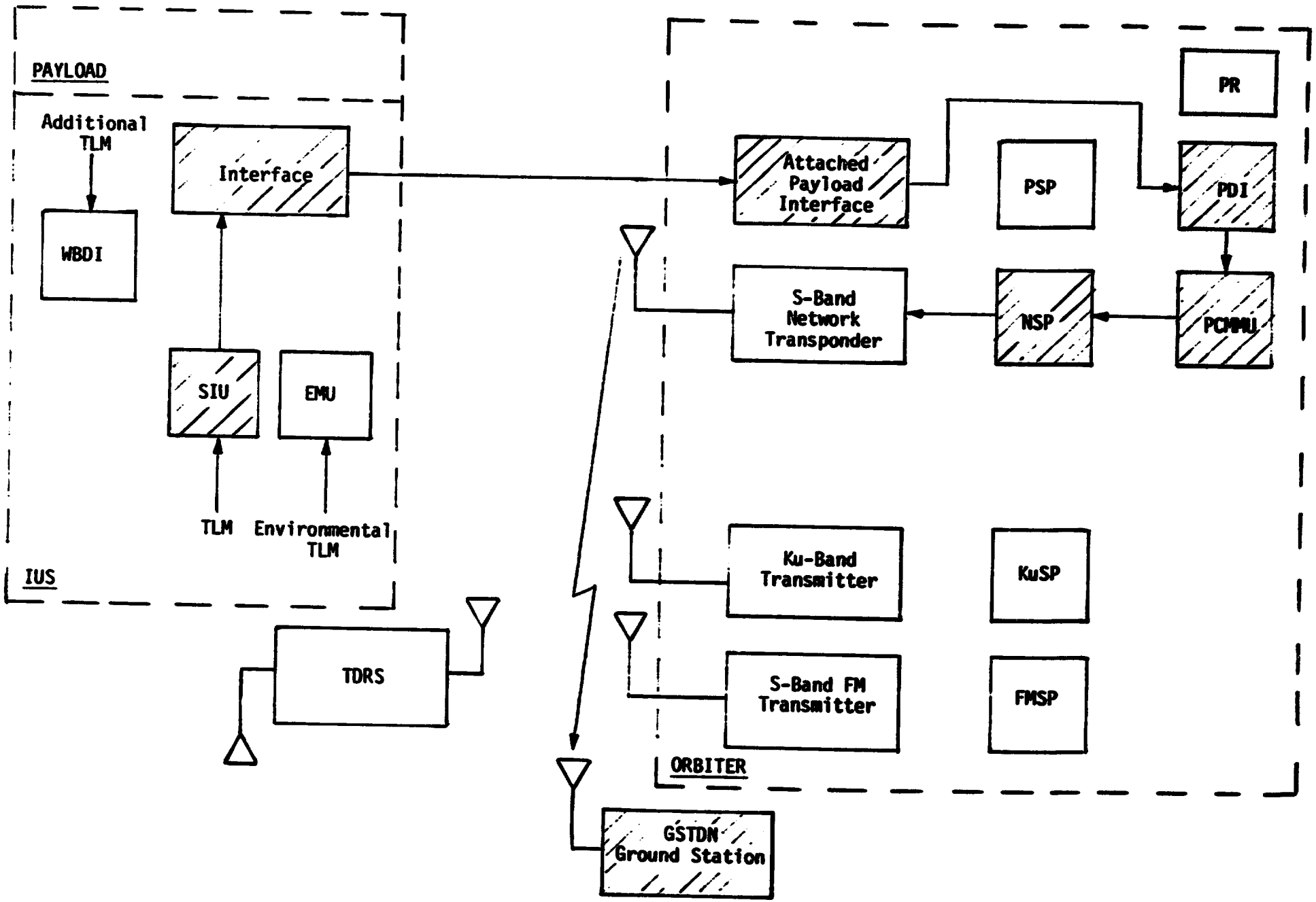

Figure 6. Attached IUS Hard-Line Telemetry Link STDN/TDRS Telemetry (NASA Mode)

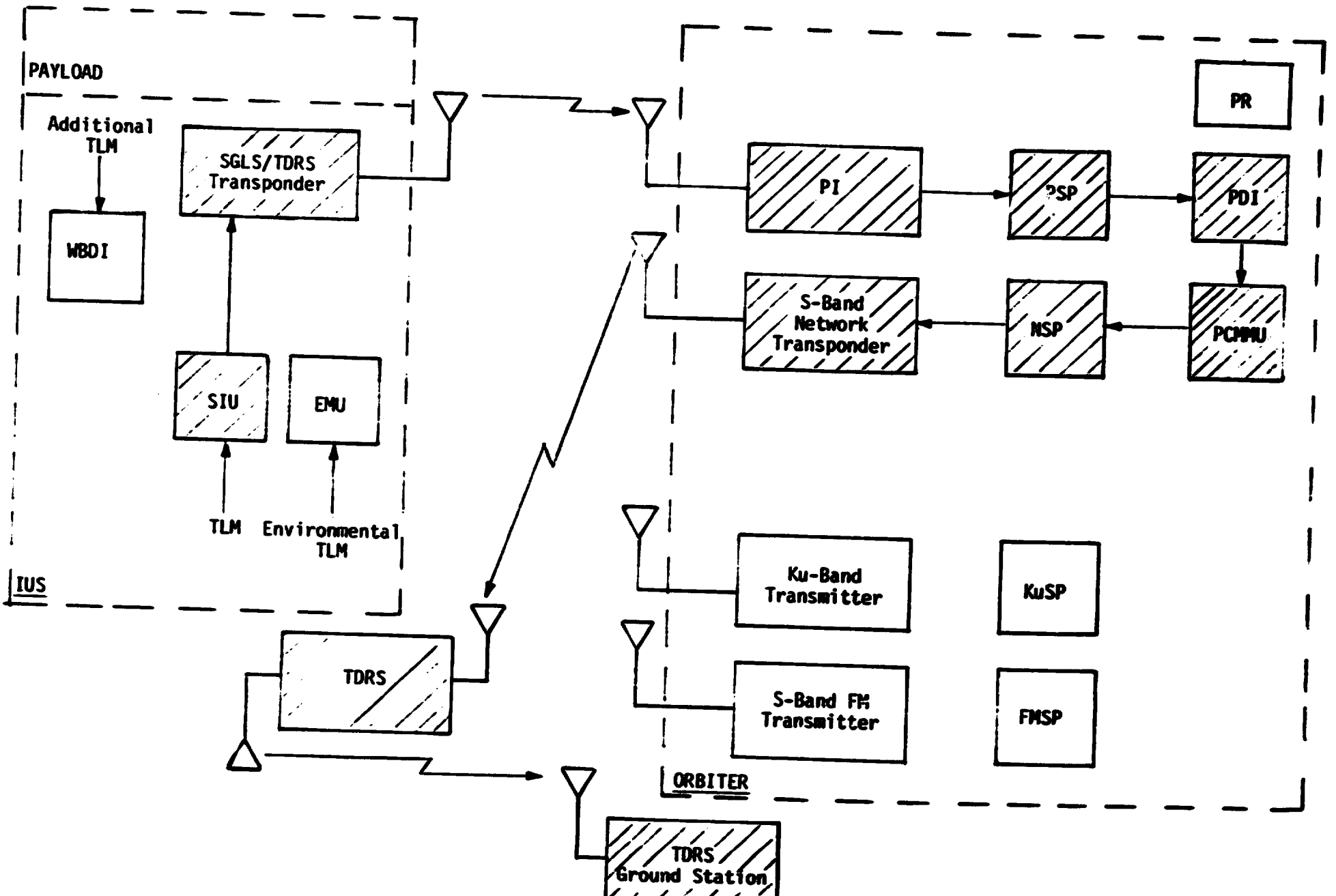

Figure 7. Attached/Detached IUS RF Telemetry Link STDN/TDRS Telemetry (NASA Mode)

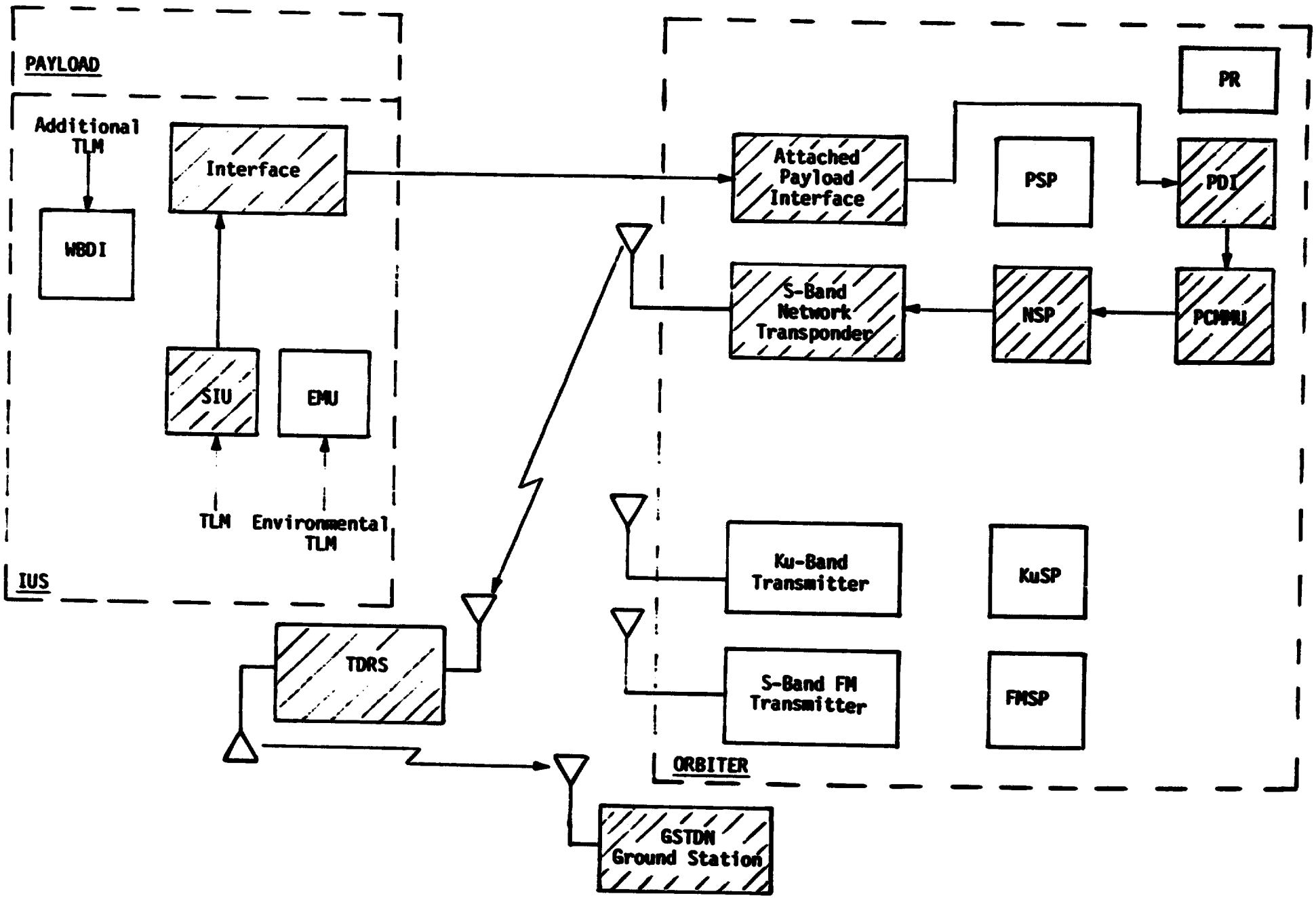

Figure 8. Attached IUS Hard-Line Telemetry Link STDN/TDRS Telemetry (NASA Mode)

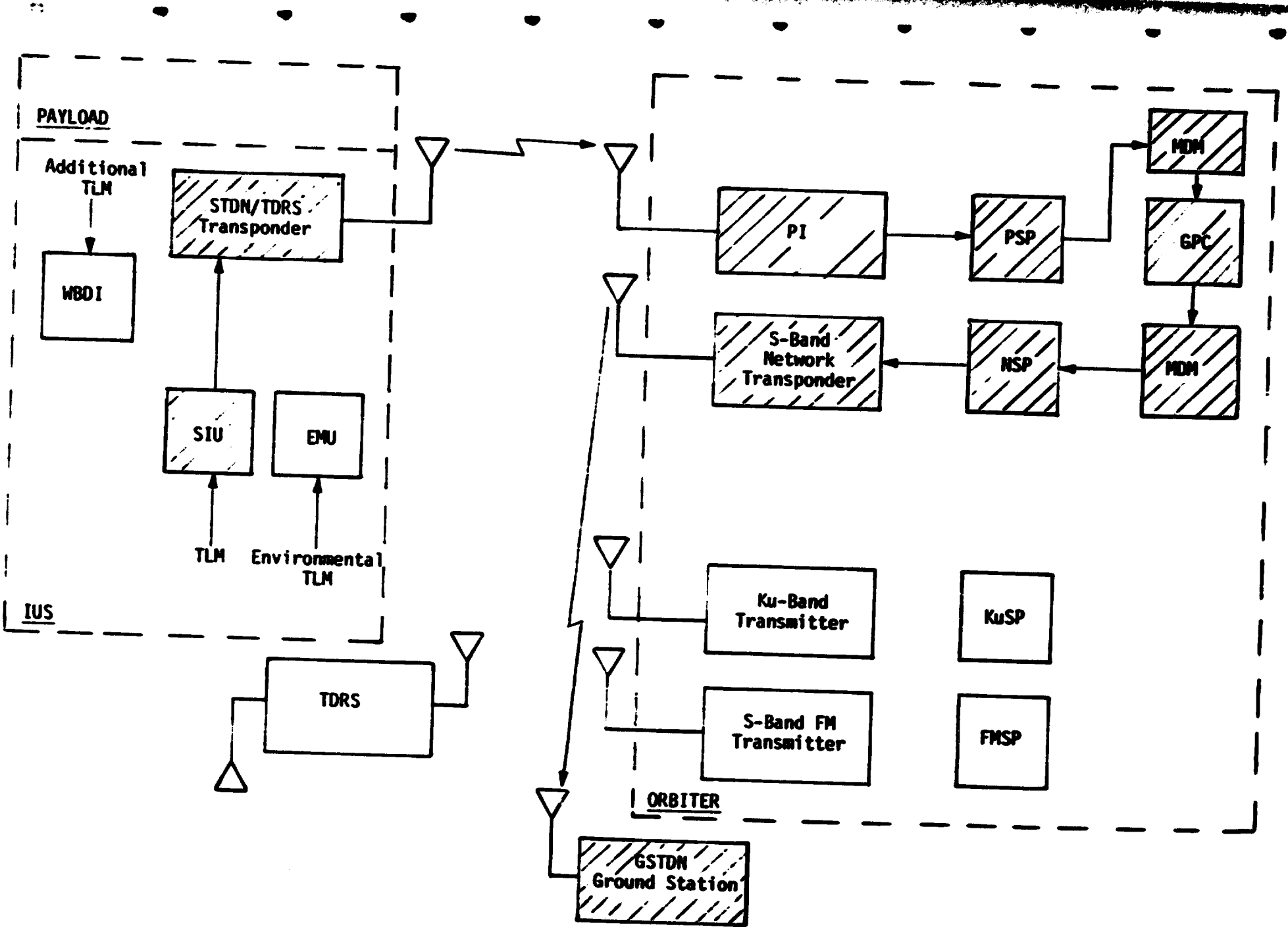

Figure 9. Attached/Detached IUS RF Telemetry Link STDN/TDRS Telemetry (NASA Mode)

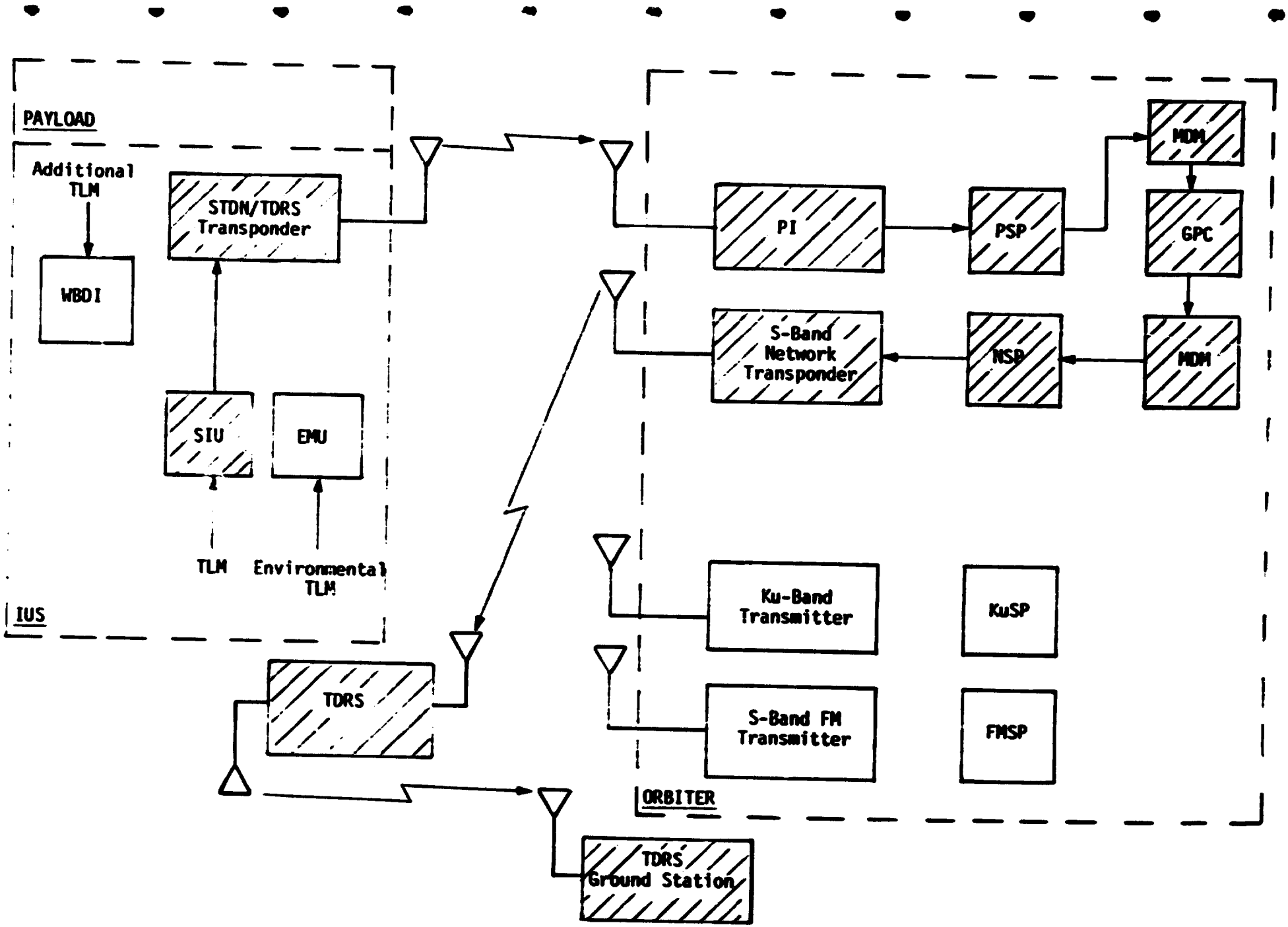

Figure 10. Attached/Detached IUS RF Telemetry Link STDN/TDRS Telemetry (NASA Mode)

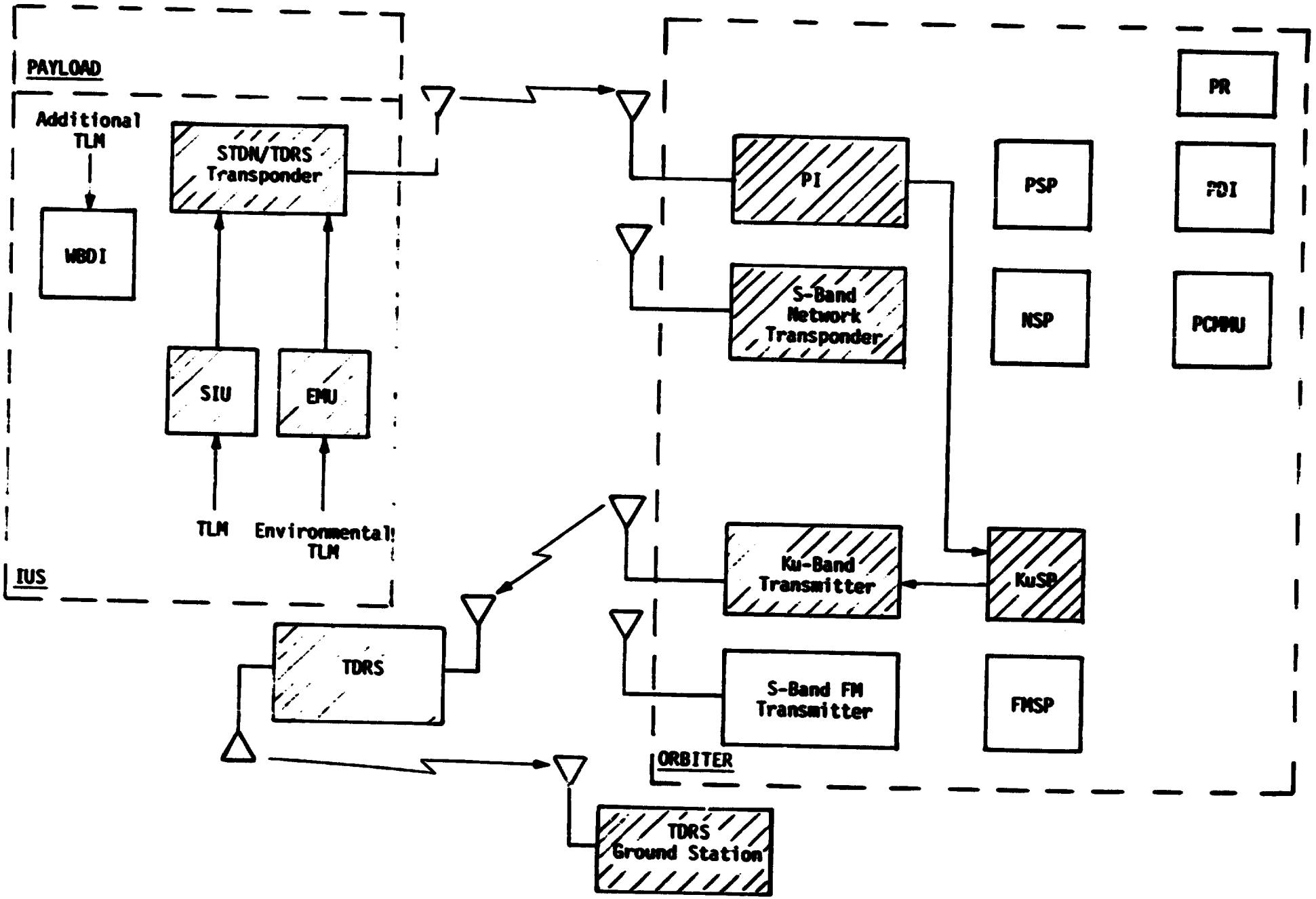

Figure 11. Attached/Detached IUS RF Telemetry Link STDN/TDRS Telemetry (NASA Mode)

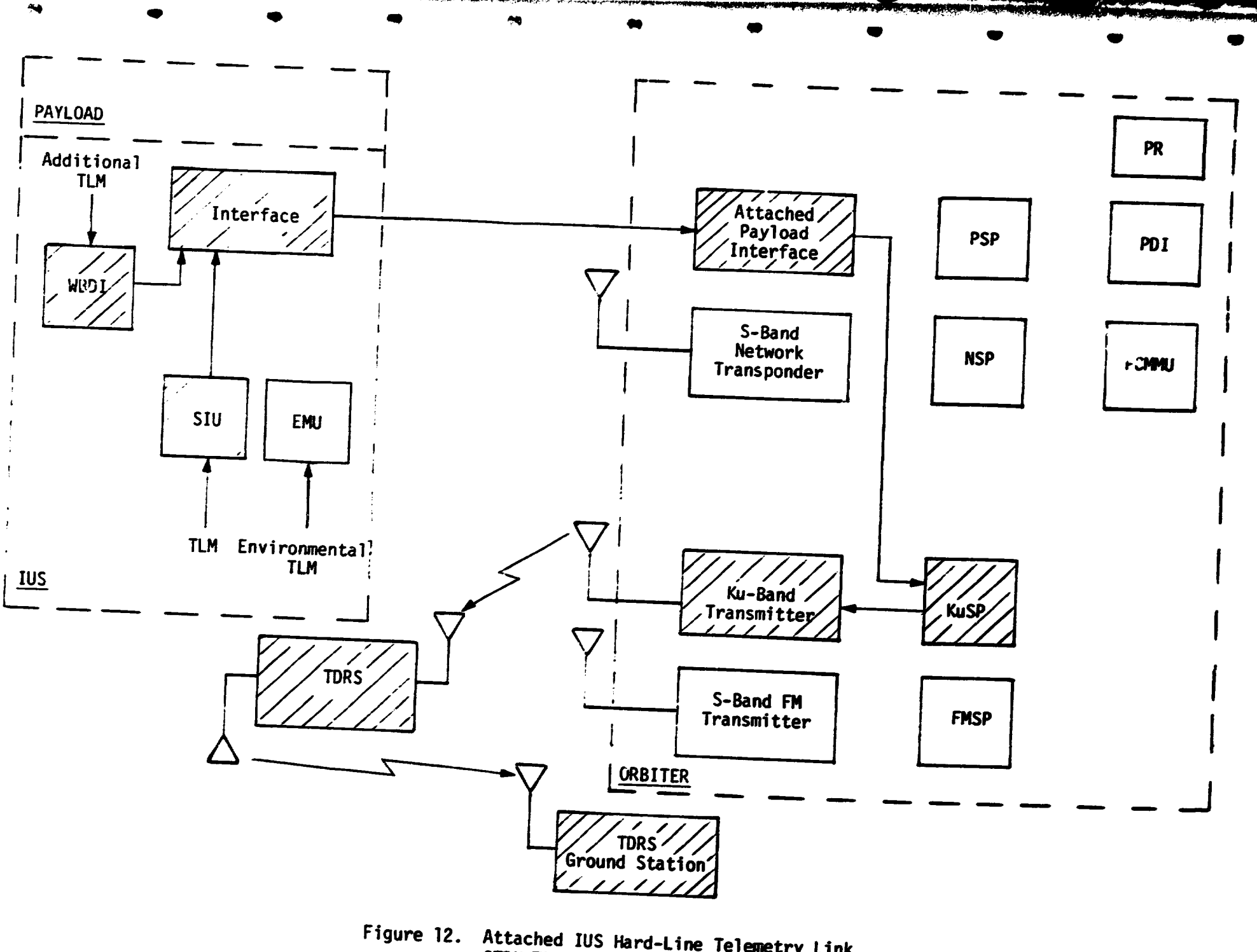

Figure 12. Attached IUS Hard-Line Telemetry Link STDN/TDRS Telemetry (NASA Mode)

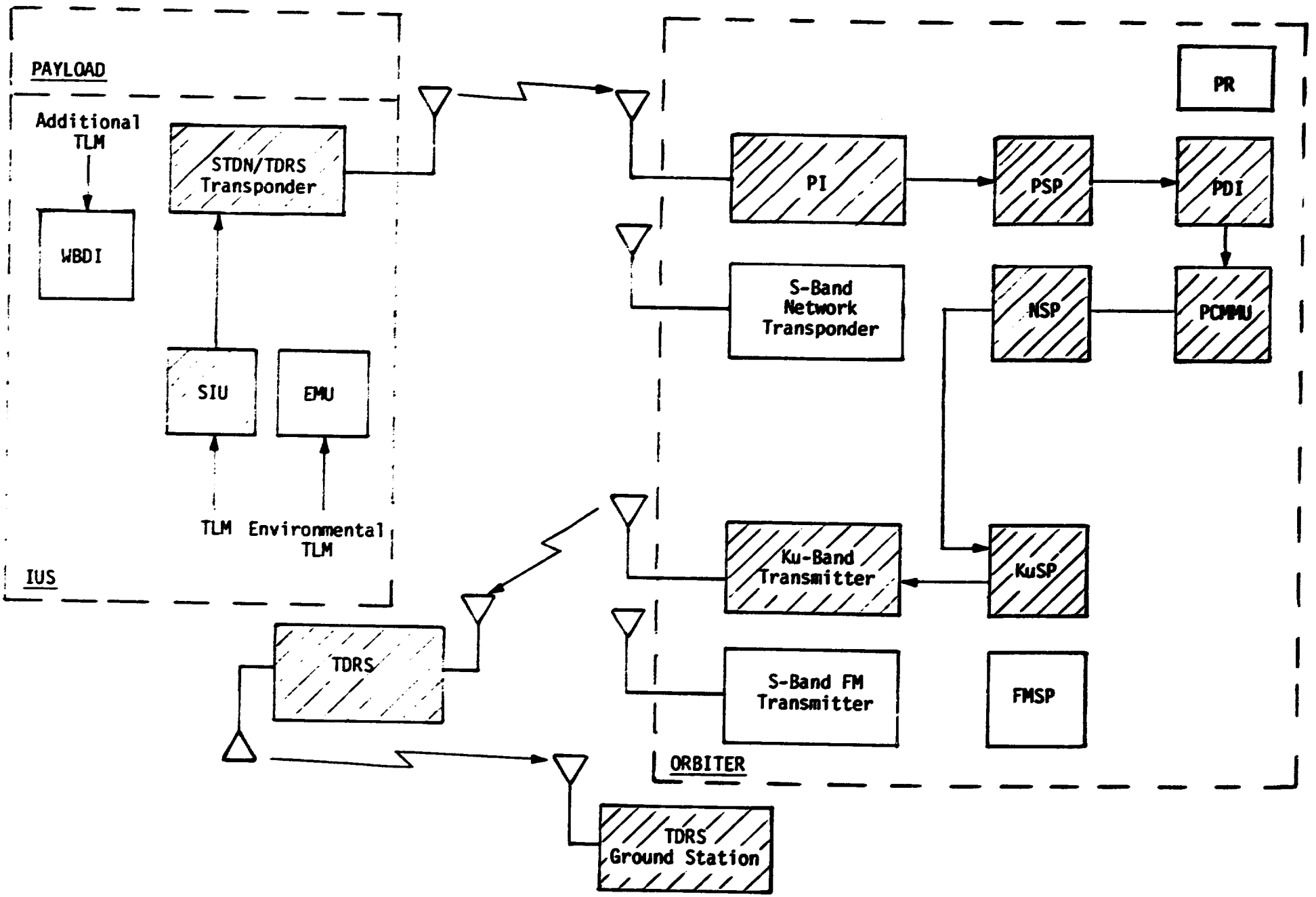

Figure 13. Attached/Detached IUS RF Telemetry Link STDN/TDRS Telemetry (NASA Mode)

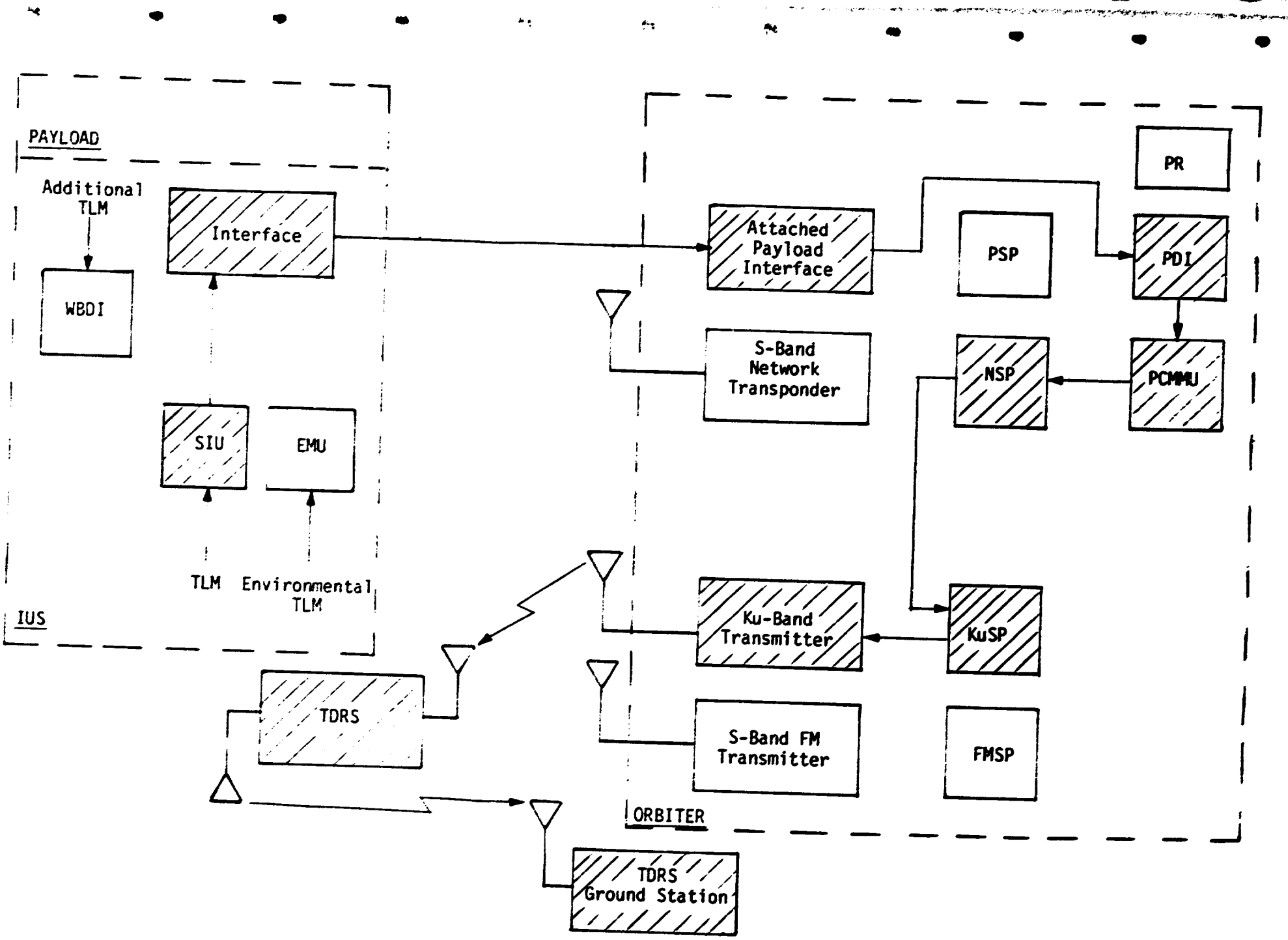

Figure 14. Attached IUS Hard-Line Telemetry Link STDN/TDRS Telemetry (NASA Mode)

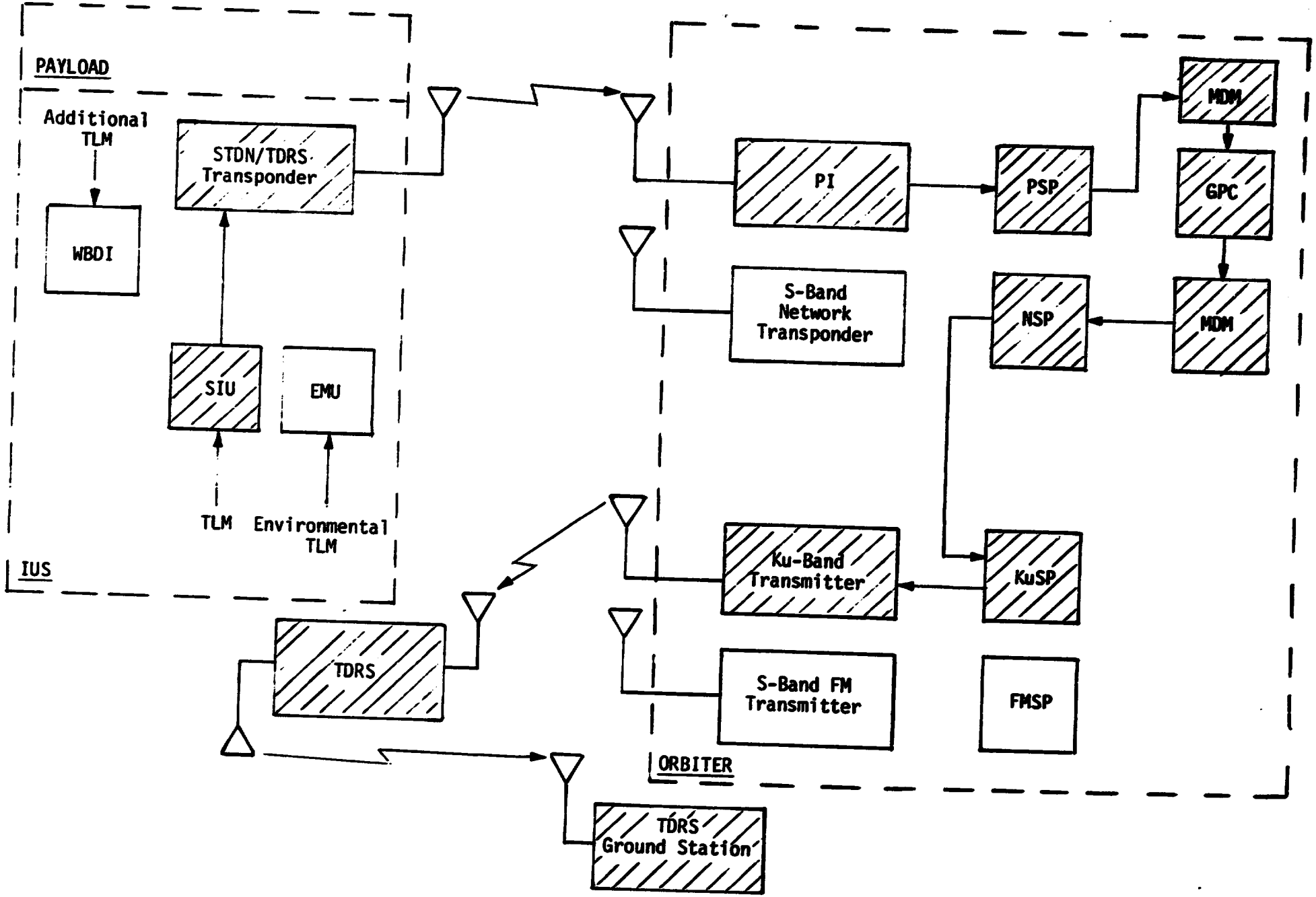

Figure 15. Attached/Detached IUS RF Telemetry Link STDN/TDRS Telemetry (NASA Mode)

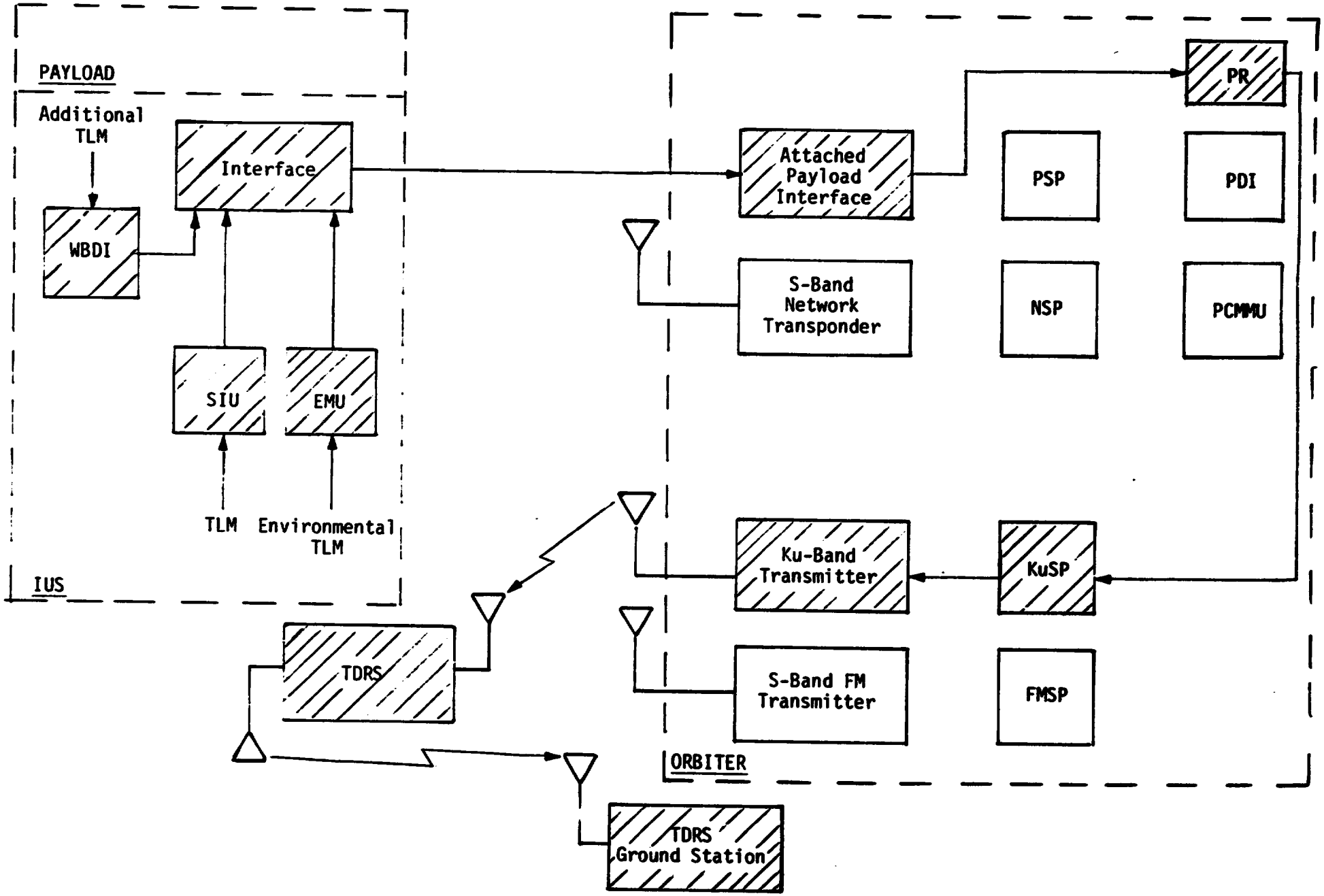

Figure 16. Attached IUS Hard-Line Telemetry Link STDN/TDRS Telemetry (NASA Mode)

APPENDIX E

MEAN TIME TO CYCLE SLIP PERFORMANCE OF POLARITY-TYPE COSTAS LOOPS

By

Marvin K. Simon

October 1979

1.0 INTRODUCTION

The polarity-type or hard-limited in-phase channel Costas loop (Figure 1) has recently received considerable attention [1-6] because of its many desirable attributes, primarily those relating to the reduction of unwanted DC voltages at the error control point of the loop (VCO input). This reduction of DC offset voltages, produced primarily in the multiplier and amplifier circuits associated with the loop gain and filter circuits, comes about because of the replacement of the "third multiplier" with a chopper-type device. While previous studies have focused on the true and false lock tracking performance of the loop [1-4] and its unaided and sweep-aided acquisition behavior [5-6], the threshold performance of the loop, as characterized by its mean time to slip a cycle, has not as yet been evaluated.

This appendix attempts to fill this void by presenting an analysis of the mean time to cycle slip performance of the polarity-type Costas loop from which the threshold loop signal-to-noise ratio can be determined. As in previous analyses, specific closed-form results will be obtained for NRZ and Manchester data formats and single-pole (RC) arm filters in the loop. The numerical results obtained will be compared with those for a conventional (analog third multiplier) Costas loop whose mean time to cycle slip behavior resembles that of a phase-locked loop (PLL). [7].

2.0 MEAN TIME TO CYCLE SLIP OF A FIRST-ORDER SYNCHRONOUS CONTROL SYSTEM (SCS) IN THE ABSENCE OF FREQUENCY DETUNING

We begin by considering the mean time to cycle slip behavior of a generalized first-order tracking loop referred to in [7] as a first-order synchronous control system (SCS). For such a loop, it was shown [7, Chapter 9] that the first moment of the first passage time of the loop phase error $\varphi(t)$ to the boundaries $\varphi_{\ell 1}$ or $\varphi_{\ell 2}$, given the initial condition $\varphi(0) = \varphi_0$, is given by

$$W_L\tau(\varphi_\ell|\varphi_0) = \frac{\rho'}{2} \int_{\varphi_{\ell 1}}^{\varphi_{\ell 2}} \int_{\varphi_{\ell 1}}^{\varphi} \left[C(0) - u(x - \varphi_0)\right] \exp\left[U_0(x) - U_0(\varphi)\right] dx d\varphi \quad (1)$$

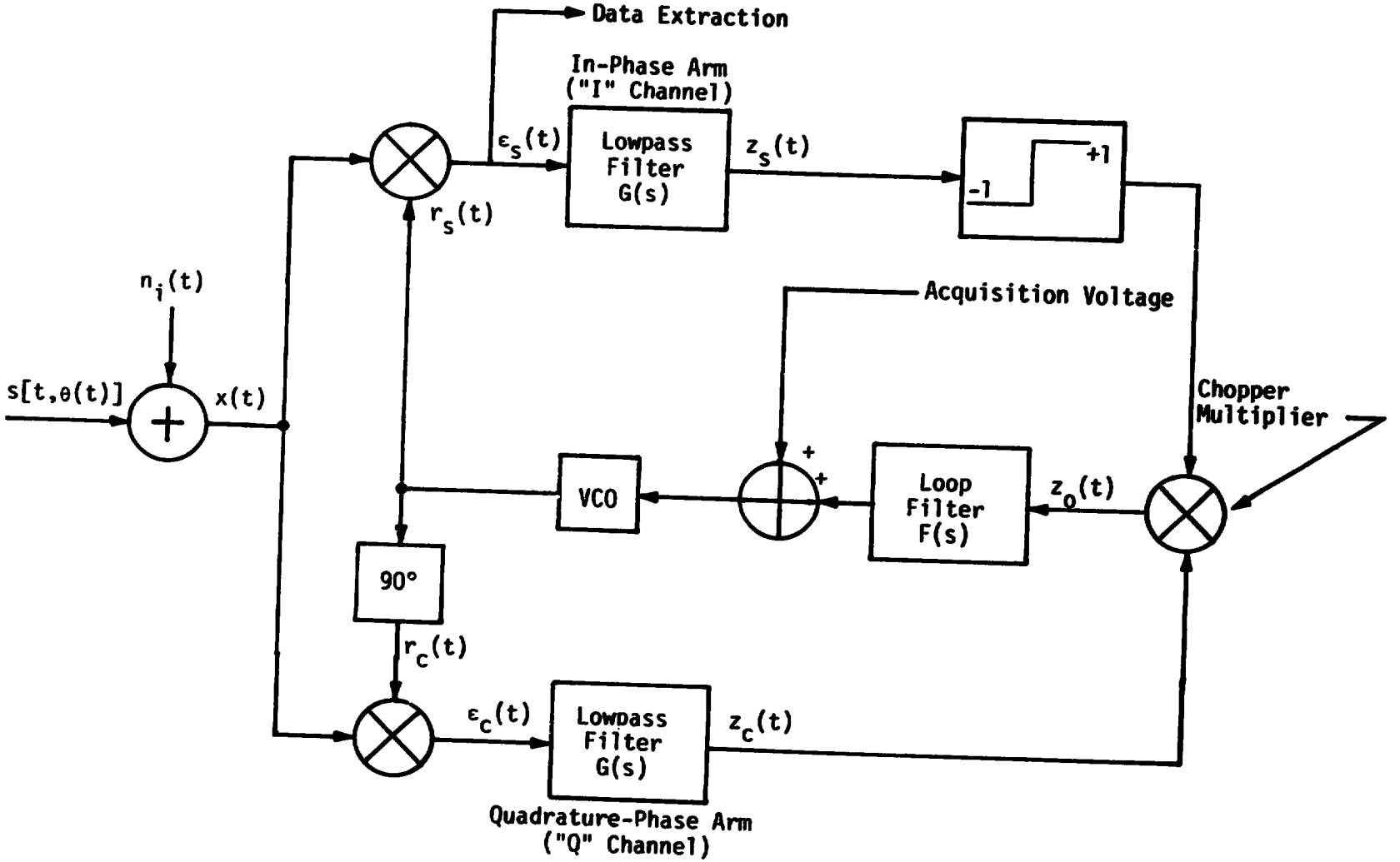

Figure 1. Costas Loop Functional Diagram with Hard-Limited In-Phase Channel

where

$$C(0) = \frac{\int_{\varphi_{\ell 1}}^{\varphi_{\ell 2}} u(x - \varphi_0) \exp[U_0(x)]dx}{\int_{\varphi_{\ell 1}}^{\varphi_{\ell 2}} \exp[U_0(x)]dx}$$

$U_0(\phi) = -\rho'\gamma\phi + \rho'\int^{\phi} g(x)\,dx$ = loop potential function

ρ' = effective loop signal-to-noise ratio

γ = loop detuning (in rad/sec) normalized to the loop gain $= \Lambda_0/AK$

$g(x)$ = equivalent loop nonlinearity (S-curve) normalized to unit slope at $x = 0$.

W_L = two-sided loop noise bandwidth

and

$u(x)$ = the unit step function. (2)

For the special case of zero detuning ($\gamma = 0$) and boundaries $\varphi_{\ell 1} = \varphi_0 - 2\pi$ and $\varphi_{\ell 2} = \varphi_0 + 2\pi$, the result of (1) can be considerably simplified. In particular, noting that, since $g(x)$ is periodic with period 2π, $U_0(\phi)$ and $\exp[U_0(\phi)]$ are also periodic with the same period; hence

$$\int_{\varphi_0-2\pi}^{\varphi_0+2\pi} \exp[U_0(x)]dx = 2\int_{\varphi_0}^{\varphi_0+2\pi} \exp[U_0(x)]dx \quad (3)$$

and

$$C(0) = \frac{\int_{\varphi_0}^{\varphi_0+2\pi} \exp[U_0(x)]dx}{\int_{\varphi_0-2\pi}^{\varphi_0+2\pi} \exp[U_0(x)]dx} = \frac{1}{2} \quad (4)$$

Furthermore, (1) can be broken into three terms, namely,

$$W_L\tau(2\pi|\varphi_0) = \frac{\rho'}{2}\int_{\varphi_0}^{\varphi_0+2\pi}\int_{\varphi_0-2\pi}^{\varphi_0} C(0)\exp[U_0(x)-U_0(\varphi)]dxd\varphi$$

$$+\frac{\rho'}{2}\int_{\varphi_0}^{\varphi_0+2\pi}\int_{\varphi_0}^{\varphi}[C(0)-1]\exp[U_0(x)-U_0(\varphi)]dxd\varphi$$

$$+\frac{\rho'}{2}\int_{\varphi_0-2\pi}^{\varphi_0}\int_{\varphi_0-2\pi}^{\varphi} C(0)\exp[U_0(x)-U_0(\varphi)]dxd\varphi \qquad (5)$$

which, using (4), becomes, upon simplification,

$$W_L\tau(2\pi|\varphi_0) = \frac{\rho'}{4}\int_{\varphi_0}^{\varphi_0+2\pi}\exp[-U_0(x)]dx\int_{\varphi_0}^{\varphi_0+2\pi}\exp[U_0(y)dy] \qquad (6)$$

For a sinusoidal PLL, i..., $g(\phi) = \sin\phi$, we have that $U_0(\phi) = -\rho'\cos\phi$ and

$$\int_{\varphi_0}^{\varphi_0+2\pi}\exp[\pm U_0(\phi)]d\phi = \int_{\varphi_0}^{\varphi_0+2\pi}\exp[\mp\rho'\cos\phi]d\phi = 2\pi I_0(\rho') \qquad (7)$$

where $I_0(x)$ is the zero-order modified Bessel function of the first kind. Substituting (7) into (6) gives the well-known result [7,8],

$$W_L\tau(2\pi|\varphi_0) = \pi^2\rho' I_0^2(\rho') \qquad (8)$$

independent of φ_0. Also, for this loop, $\rho' = \rho$, where $\rho = 2S/N_0W_L$ is the actual loop signal-to-noise ratio with S denoting signal power in watts and N_0 denoting single-sided noise spectral density in watts/Hz.

Since a conventional Costas loop tracks the doubled phase error $\phi = 2\phi$, whose potential function $U_0(\phi)$ of (2) is of the identical form as that for the phase error ϕ associated with the sinusoidal PLL, the mean

time to cycle slip is again given by (8) with, however, ρ' now related to ρ by

$$\rho' = \frac{\rho}{4}\mathscr{A}_L \tag{9}$$

In (9), the factor $\mathscr{A}_L$ (≤ 1) is the squaring loss associated with the SxN and NxN terms in the output of the loop's third multiplier. Characterization of $\mathscr{A}_L$ in terms of such parameters as the ratio of two-sided arm filter bandwidth B_i to data rate R and bit energy-to-noise ratio S/N_0R can be found in [9].

3.0 MEAN TIME TO CYCLE SLIP OF FIRST-ORDER POLARITY-TYPE COSTAS LOOP IN THE ABSENCE OF FREQUENCY DETUNING

As was true for the conventional Costas loop, the polarity-type Costas loop tracks the doubled phase error $\phi = 2\phi$. Thus, the loop potential function in the absence of frequency detuning becomes

$$U_0(\phi) = \rho' \int^{\phi} g(x)\, dx \tag{10}$$

where g(x) has been previously evaluated [5]. In particular, for RC arm filters in the loop with radian cutoff frequency ω_c and two-sided noise bandwidth $B_i = \omega_c/2$, the following results, which correspond respectively to NRZ and Manchester format data of rate $R = 1/T$, apply:

$$g(x) = \frac{f(x)}{\tilde{\alpha}} \tag{11}$$

$$\tilde{\alpha} = \text{effective limiter suppression factor} = \left.\frac{df(x)}{dx}\right|_{x=0}$$

NRZ Data

$$\tilde{\alpha}_{NRZ} = \frac{1}{2}\left\{\frac{2}{\omega_c T}\int_0^{\tanh \omega_c T/2}\left(\frac{y}{1-y^2}\right)\operatorname{erf}\left[\sqrt{\frac{\rho_i}{2}}y\right]dy + \operatorname{erf}\sqrt{\frac{\rho_i}{2}}\right\}$$

$$f(x) = \sin\frac{x}{2}\left\{\frac{2}{\omega_c T}\int_0^{\tanh \omega_c T/2}\left(\frac{y}{1-y^2}\right)\operatorname{erf}\left[\sqrt{\frac{\rho_i}{2}}y\cos\frac{x}{2}\right]dy\right\}$$

$$\rho_i = \frac{2S}{N_0 B_i} = \frac{2(E_b/N_0)}{B_i/R} \quad ; \quad E_b = ST \tag{12}$$

Manchester Data

$$\tilde{\alpha}_{MANCH} = \frac{1}{2}\left\{\frac{2}{\omega_c T}\int_0^{\tanh \omega_c T/2}\left(\frac{y}{1-y^2}\right)\operatorname{erf}\left[\sqrt{\frac{\rho_i}{2}}y\right]dy + \frac{4}{\omega_c T}\int_0^{\tanh \omega_c T/4}\left(\frac{y}{1-y^2}\right)\operatorname{erf}\left[\sqrt{\frac{\rho_i}{2}}y\right]dy\right\}$$

$$f(x) = \sin\frac{x}{2}\left\{\frac{2}{\omega_c T}\int_0^{\tanh \omega_c T/2}\left(\frac{y}{1-y^2}\right)\operatorname{erf}\left[\sqrt{\frac{\rho_i}{2}}y\cos\frac{x}{2}\right]dy + \frac{4}{\omega_c T}\int_0^{\tanh \omega_c T/4}\left(\frac{y}{1-y^2}\right)\operatorname{erf}\left[\sqrt{\frac{\rho_i}{2}}y\cos\frac{x}{2}\right]dy\right\} \tag{13}$$

Substituting (11) [in combination with (12) or (13)] into (10) and recognizing that

$$\int \sin\frac{x}{2}\operatorname{erf}\left[A\cos\frac{x}{2}\right]dx = -2\left[\cos\frac{x}{2}\operatorname{erf}\left(A\cos\frac{x}{2}\right) + \frac{1}{\sqrt{\pi}A}\exp\left(-A^2\cos^2\frac{x}{2}\right)\right] \tag{14}$$

gives the loop potential functions:

NRZ Data

$$U_0(\phi) = -\frac{2\rho'}{a_{NRZ}}\left\{\left(\frac{2}{\omega_c T}\right)\cos\frac{\phi}{2}\int_0^{\tanh \omega_c T/2}\left(\frac{y}{1-y^2}\right)\operatorname{erf}\left[\sqrt{\frac{\rho_i}{2}}\,y\cos\frac{\phi}{2}\right]dy\right.$$

$$+\left(\frac{2}{\omega_c T}\right)\frac{1}{\sqrt{\pi\rho_i/2}}\int_0^{\tanh \omega_c T/2}\left(\frac{1}{1-y^2}\right)\exp\left[-\frac{\rho_i}{2}y^2\cos^2\frac{\phi}{2}\right]dy$$

$$+\cos\frac{\phi}{2}\operatorname{erf}\left[\sqrt{\frac{\rho_i}{2}}\cos\frac{\phi}{2}\right]$$

$$\left.+\frac{1}{\sqrt{\pi\rho_i/2}}\exp\left[-\frac{\rho_i}{2}\cos^2\frac{\phi}{2}\right]\right\} \qquad (15)$$

Manchester Data

$$U_0(\phi) = -\frac{2\rho'}{a_{MANCH}}\left\{\left(\frac{2}{\omega_c T}\right)\cos\frac{\phi}{2}\int_0^{\tanh \omega_c T/2}\left(\frac{y}{1-y^2}\right)\operatorname{erf}\left[\sqrt{\frac{\rho_i}{2}}\,y\cos\frac{\phi}{2}\right]dy\right.$$

$$+\left(\frac{2}{\omega_c T}\right)\frac{1}{\sqrt{\pi\rho_i/2}}\int_0^{\tanh \omega_c T/2}\left(\frac{1}{1-y^2}\right)\exp\left[-\frac{\rho_i}{2}y^2\cos^2\frac{\phi}{2}\right]dy$$

$$+\left(\frac{4}{\omega_c T}\right)\cos\frac{\phi}{2}\int_0^{\tanh \omega_c T/4}\left(\frac{y}{1-y^2}\right)\operatorname{erf}\left[\sqrt{\frac{\rho_i}{2}}\,y\cos\frac{\phi}{2}\right]dy$$

$$\left.+\left(\frac{4}{\omega_c T}\right)\frac{1}{\sqrt{\pi\rho_i/2}}\int_0^{\tanh \omega_c T/4}\left(\frac{1}{1-y^2}\right)\exp\left[-\frac{\rho_i}{2}y^2\cos^2\frac{\phi}{2}\right]dy\right\} \qquad (16)$$

Finally, substitution of (15) or (16) into (6) allows computation of the mean time to cycle slip.

Figures 2 and 3 are illustrations of $W_L\tau(2\pi|\varphi_0)$ versus effective loop signal-to-noise ratio ρ' (in dB) for fixed values of B_i/R and E_b/N_0 as a parameter. Figure 2 represents the results for NRZ data and

Figure 2. Polarity-Type Costas Loop--Normalized Mean Time to Cycle Slip versus Effective Loop SNR with Bit Energy-to-Noise Spectral Density as a Parameter; NRZ Data, RC Arm Filter; Ratio of Two-Sided Arm Filter Bandwidth to Data Rate = $B_1/R = 3.0$

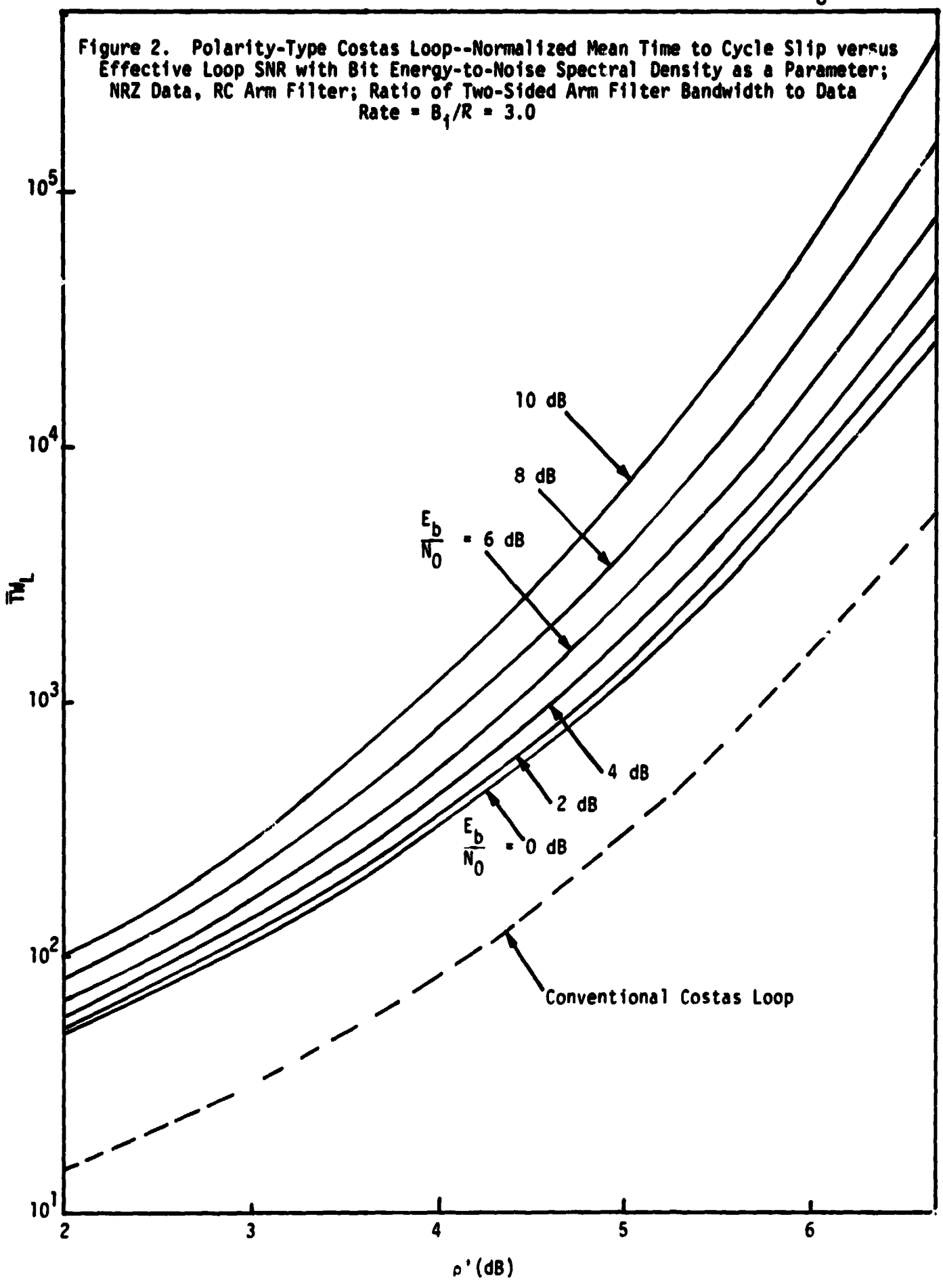

Figure 3. Polarity-Type Costas Loop--Normalized Mean Time to Cycle Slip versus Effective Loop SNR with Bit Energy-to-Noise Spectral Density as a Parameter; Manchester Data, RC Arm Filter; Ratio of Two-Sided Arm Filter Bandwidth to Data Rate = $B_1/R = 6.0$

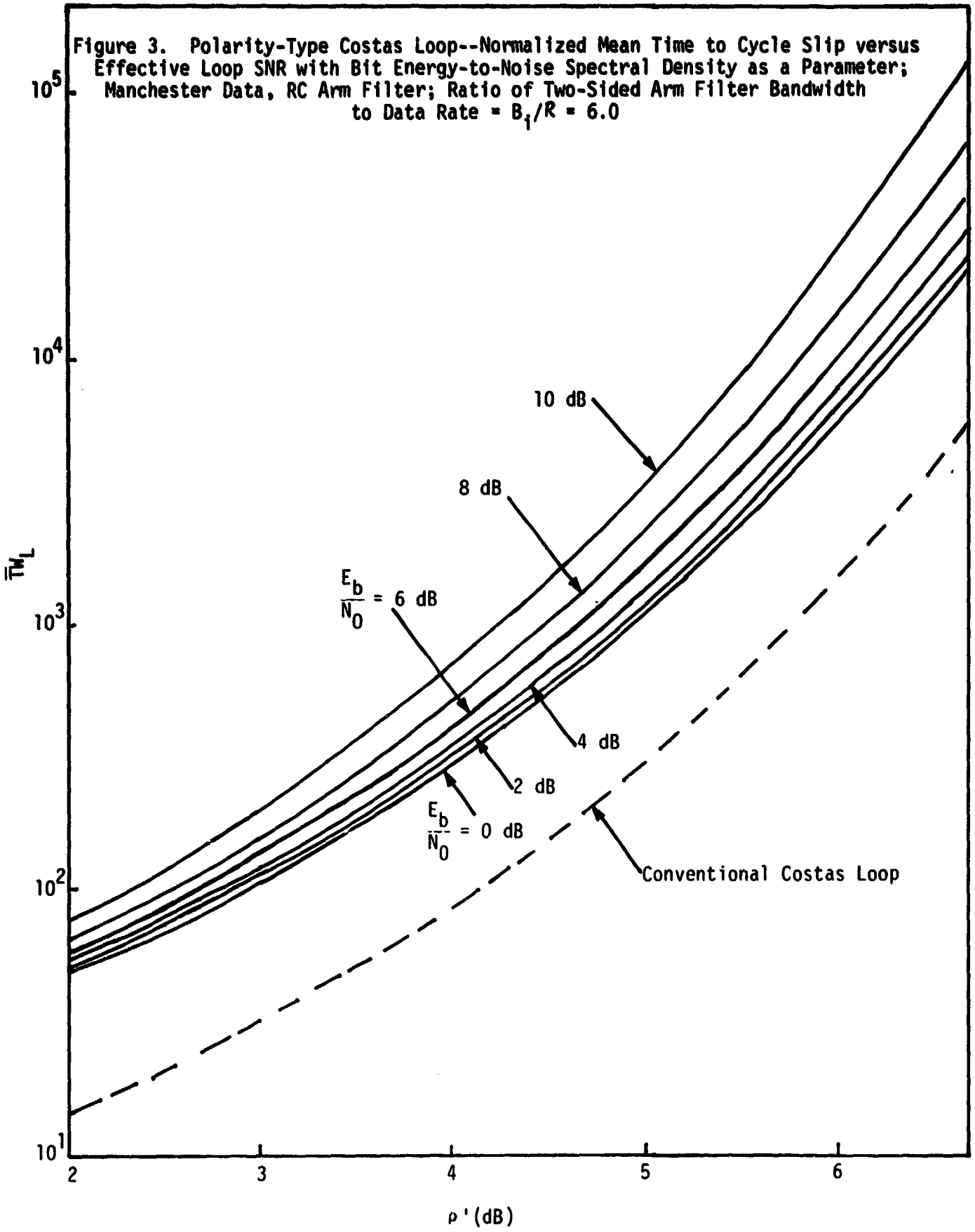

Figure 3, the corresponding results for Manchester data. The value of B_i/R selected in each case is chosen as that which optimizes* the tracking performance of the loop as measured by its mean-square tracking jitter. Also, indicated (in dashed lines) on these figures is the corresponding mean time to cycle slip performance of the conventional Costas loop as computed from (8). This performance curve is independent of E_b/N_0 and data format, and thus appears the same on both figures.

We observe that, for either NRZ or Manchester data and any value of E_b/N_0, the polarity-type Costas loop outperforms the conventional Costas loop (has a lower value of threshold loop signal-to-noise ratio ρ_0' for a given mean time to cycle slip and threshold loop bandwidth W_{L0}). More specifically, over the range of E_b/N_0 values chosen in the figures, the threshold is reduced (relative to the conventional loop) by about 1-2 dB for NRZ data and about 1-1.5 dB for Manchester data.

To complete the picture, we must again relate ρ' to the actual loop signal-to-noise ratio ρ. The appropriate relationship is still given by (9); however, the squaring loss evaluation is different and cannot be computed exactly in closed form.

Several approaches for obtaining approximate closed-form expressions for $\mathscr{L}$ with the expressions themselves are given in [1] for NRZ data and [2] for Manchester data. As was true for the conventional Costas loop, these expressions for $\mathscr{L}$ are parameterized by B_i/R and E_b/N_0.

4.0 MEAN TIME TO CYCLE SLIP OF SECOND-ORDER LOOPS

For a second-order SCS with imperfect integrating loop filter, the exact computation of mean time to cycle slip is extremely difficult, if not impossible. For large ρ, an approximate expression analogous to (1) has been derived in [7] and is given by

---

*The values of B_i/R which optimize the loop's tracking performance are actually functions of E_b/N_0 [1,2]. However, the variation of $(B_i/R)_{opt}$ with E_b/N_0 is small over the range of E_b/N_0 values considered in Figures 2 and 3; thus, a compromise fixed value has been selected in each case.

$$W_L\tau(\varphi_\ell|\varphi_0) = \left(\frac{r+1}{r}\right)^2 \frac{\rho'}{2} \int_{\varphi_{\ell 1}}^{\varphi_{\ell 2}} \int_{\varphi_{\ell 1}}^{\varphi} [C(0) - u(x-\varphi_0)] \exp[U_0(x) - U_0(\varphi)]\, dx d\varphi \tag{17}$$

where

$$U_0(\phi) = -\rho'\gamma\phi + \rho'\left(\frac{r+1}{r}\right)\int^{\phi} g(x)\, dx - \frac{\rho'\phi^2}{2r} \tag{18}$$

and $r \triangleq 4\zeta^2$, where ζ is the loop damping factor. In the absence of loop detuning ($\gamma = 0$) and boundaries $\varphi_{\ell 1} = \varphi_0 - 2\pi$ and $\varphi_{\ell 2} = \varphi_0 + 2\pi$, (17) can be approximately* simplified to

$$W_L\tau(2\pi|\varphi_0) = \left(\frac{r+1}{r}\right)^2 \frac{\rho'}{4} \int_{\varphi_0}^{\varphi_0+2\pi} \exp[-U_0(x)]\, dx \int_{\varphi_0}^{\varphi_0+2\pi} \exp[U_0(y)]\, dy \tag{19}$$

Simulation results [10] for a sinusoidal PLL with $r = 4$, $\varphi_0 = 0$ and γ as a parameter are compared in [7] with theoretical results calculated from (17). The comparison [7, Figure 10-21] reveals reasonably good agreement even for small values of $\rho' = \rho$. Thus, we may assume that (19) is a reasonably good approximation for an arbitrary second-order SCS (e.g., a second-order polarity-type Costas loop) even for small values of ρ'.

---

*The approximation here has to do with the fact that, because of the last term in (18), $U_0(\phi)$ is, even for $\gamma = 0$, not periodic in ϕ. However, for large ρ', this latter term can be approximated as $(\rho'/r\sigma_g^2)\int^{\phi} g(x)\, dx$ (thus making $U_0(\phi)$ periodic again) insofar as the reduction of (17) to (19). Here σ_g^2 is the variance (mean-squared value) of $g(\phi)$ with respect to the probability density function of ϕ.

REFERENCES

1. Simon, M. K., "Tracking Performance of Costas Loops with Hard-Limited In-Phase Channels," IEEE Transactions on Communications, Vol. COM-26, No. 4, April 1978, pp. 420-432.

2. Helgeson, R. J., "PSP Subcarrier Demodulator Tracking Performance Analysis/Manchester Data," TRW IOC SCTE-50-78-458/RJH, August 31, 1978.

3. Simon, M. K., "False Lock Performance of Costas Loops with Hard-Limited In-Phase Channel," IEEE Transactions on Communications, Vol. COM-26, No. 1, January 1978, pp. 23-34.

4. Simon, M. K. "On the False Lock Behavior of Polarity-Type Costas Loops with Manchester Coded Input," NTC'77 Conference Record, pp. 30:1-1 to 30:1-5.

5. Simon, M. K., "Unaided Frequency Acquisition Performance of Polarity-Type Costas Loops with Imperfect Integrating Loop Filters," Section 5.5 of "Shuttle Orbiter S-Band Communications Equipment Design Evaluation," Axiomatix Report No. R7901-3, under Contract No. NAS 9-15514A, January 20, 1979.

6. Simon, M. K., "Acquisition Time Performance of Polarity-Type Costas Loops Operating in the Frequency Search Mode," Appendix A of Axiomatix Report No. R7806-1, under Contract No. NAS 9-15515, June 1, 1978.

7. Lindsey, W. C., Synchronization Systems in Communication and Control, Prentice-Hall, Inc., Englewood Cliffs, N.J., 1973.

8. Viterbi, A. J., Principles of Coherent Communications, McGraw-Hill Book Co., N.Y, N.Y., 1966.

9. Simon, M. K., and Lindsey, W. C., "Optimum Performance of Suppressed Carrier Receivers with Costas Loop Tracking," IEEE Transactions on Communications, Vol. COM-25, No. 2, February 1977, pp. 215-227.

10. Holmes, J., "A Simulation Study of the First Slip Times Versus the Static Phase Offset for First- and Second-Order Phase-Locked Loops," JPL Space Program Summary, #37-58, Vol. II, pp.29-32.

APPENDIX F

THE EFFECTS OF A DITHER FILTER ON THE PSEUDONOISE CODE TRACKING PERFORMANCE OF A NONCOHERENT TAU-DITHER (TIME-SHARED) LOOP

By

Marvin K. Simon

November 1979

1.0 INTRODUCTION

The IUS-TDRSS transponder incorporates a noncoherent tau-dither (time-shared) loop for pseudonoise code tracking. It has been suggested that an additional filter (herein called the dither filter) be added to the conventional tau-dither loop configuration just prior to the post-dither multiplier with the express purpose of limiting the total (signal-plus-noise) power into this multiplier (see Figure 1).

A previous analysis [1] of the loop modified as above showed that using a dither filter possessing the first and third harmonics of the square-wave dither signal caused an increase in mean-square tracking jitter (timing error variance) of about 23% over the conventional tau-dither loop which employs no dither signal filtering. This result was based upon the fact that the dither filter affected only the equivalent signal component (SxS) of the loop filter input. Alternately stated, it was assumed that the dither filter had no effect on the equivalent noise components (SxN and NxN) of this same loop filter input signal. This is an incorrect assumption.

Following the approach taken in [2], this appendix attempts to correct the theoretical results of [1] by including the effects of the dither filter on the above-mentioned noise components. In particular, it will be demonstrated that the additional SxS distortion (power loss) caused by the addition of the dither filter is partially compensated by an attendant reduction in SxN and NxN power, thus resulting in an even smaller performance degradation than that predicted in [1]. For a dither filter which again passes only the first and third harmonics of the dither signal, it will be shown that the increase in mean-square tracking jitter caused by the addition of this filter to the loop is only about 11%, rather than 23%. In either event, the conclusion is, as was previously stated, that the addition of a dither filter imposes a negligible tracking performance penalty relative to the potential advantage gained in terms of total power reduction into the post-dither multiplier.

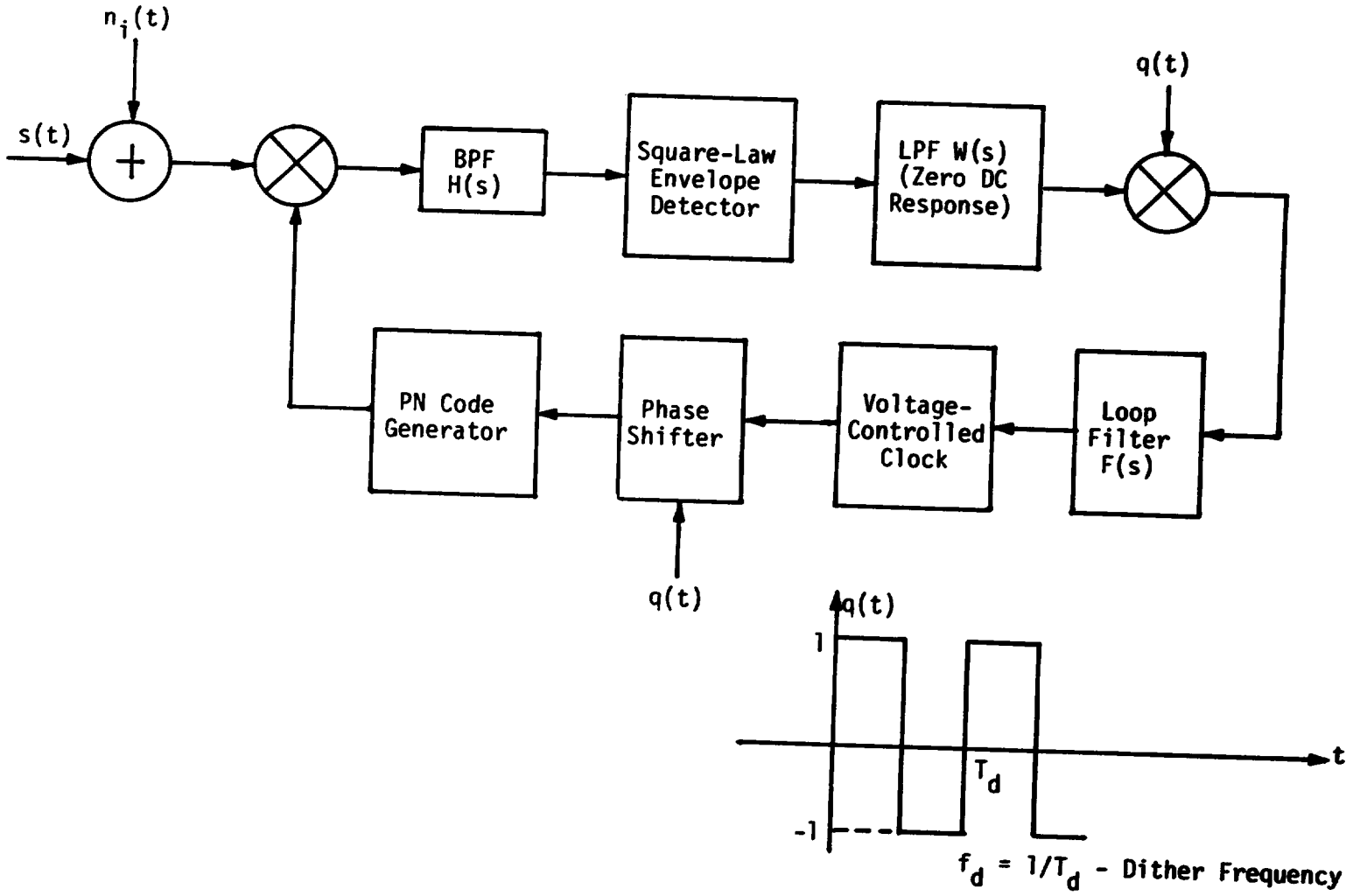

Figure 1. A Noncoherent "One-Δ" τ-Dither Loop with Dither Filter

2.0 TAU-DITHER LOOP MODEL

Consider the noncoherent tau-dither loop with dither filter W(s) illustrated in Figure 1 whose operation is described as follows. The received signal-plus-noise is alternately correlated with advanced and retarded versions of the locally generated PN code to produce an error signal which, when bandpass filtered, envelope detected, dither filtered and alternately inverted in synchronism by the square-wave signal q(t), drives the voltage-controlled clock (VCC) through the loop filter F(s). The VCC in turn drives the PN code generator from which the PN reference sequence is obtained. When the advance (and retard) interval is equal to one-half a PN code chip, the loop is commonly referred to as a "one-Δ" loop, where Δ denotes the length (in seconds) of a PN code chip.

For the purpose of analysis, it can be shown, analogous to the equivalence noted in [3] that, when the dither frequency is low relative to the noise bandwidth of the bandpass filter (the usual case of interest), the tau-dither loop has the equivalent loop model illustrated in Figure 2. The received signal x(t) is the sum of signal s(t) plus additive noise $n_i(t)$, where

$$s(t) = \sqrt{2S}\, s_{PN}(t-\tau_d)\, m(t-\tau_d) \cos[\omega_0 t + \theta(t)] \qquad (1)$$

and $n_i(t)$ has the bandpass representation

$$n_i(t) = \sqrt{2}\left\{N_c(t) \cos[\omega_0 t + \theta(t)] - N_s(t) \sin[\omega_0 t + \theta(t)]\right\} \qquad (2)$$

where

S = the average signal power

$s_{PN}(t-\tau_d)$ = the received PN sequence with transmission delay τ_d,

$m(t-\tau_d)$ = the data modulation in the presence of the same delay

ω_0 = the carrier radian frequency

$\theta(t) \triangleq \theta_0 + \Omega_0 t$ = the unknown carrier phase

The noise processes $N_c(t)$ and $N_s(t)$ are approximately statistically independent, stationary, lowpass white Gaussian noise processes with single-sided noise spectral density N_0 W/Hz and one-sided bandwidth $B \ll \omega_0/2\pi$.

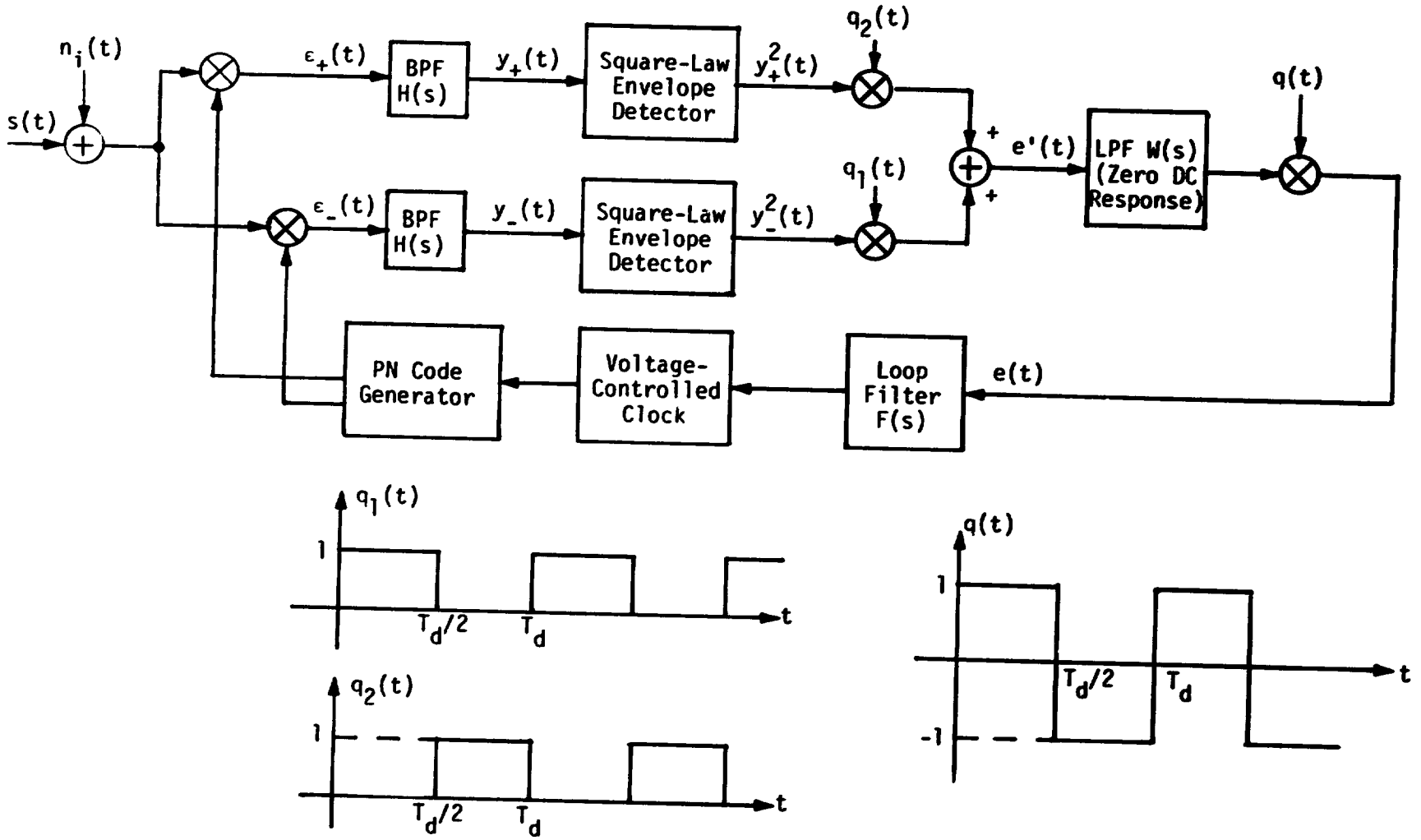

Figure 2. An Equivalent Loop Model for the τ-Dither Loop with Dither Filter

If the advanced and retarded PN reference signals are given by, respectively, $s_{PN}(t-\hat{\tau}_d+\Delta/2)$ and $s_{PN}(t-\hat{\tau}_d-\Delta/2)$, where $\hat{\tau}_d$ denotes the loop's estimate of τ_d, then the corresponding cross-correlator (phase detector) outputs become

$$\begin{aligned}\epsilon_{\pm}(t) &= \sqrt{2S}\,K_m\,m(t-\tau_d)\,\overline{s_{PN}(t-\tau_d)\,s_{PN}\left(t-\hat{\tau}_d\pm\frac{\Delta}{2}\right)}\,\cos[\omega_0 t+\theta(t)] \\ &\quad+\sqrt{2S}\,K_m\,m(t-\tau_d)\,s_{PN}(t-\tau_d)\left[s_{PN}\left(t-\hat{\tau}_d\pm\frac{\Delta}{2}\right)\right. \\ &\qquad\left.-\,\overline{s_{PN}(t-\tau_d)\,s_{PN}\left(t-\hat{\tau}_d\pm\frac{\Delta}{2}\right)}\right]\cos[\omega_0 t+\theta(t)] \\ &\quad+K_m\,s_{PN}\left(t-\hat{\tau}_d\pm\frac{\Delta}{2}\right)n_i(t) \qquad (3)\end{aligned}$$

with K_m denoting the phase detector gain and the overbar referring to statistical expectation. For larger PN code period p, we have that (see Figure 3)

$$R_{PN_+}\left(\frac{\tau_e}{\Delta}\right)\triangleq\overline{s_{PN}(t-\tau_d)\,s_{PN}\left(t-\hat{\tau}_d+\frac{\Delta}{2}\right)}=\begin{cases}0\;;\;\dfrac{\tau_e}{\Delta}\le-\dfrac{3}{2}\\[2ex]\dfrac{3}{2}+\dfrac{\tau_e}{\Delta}\;;\;-\dfrac{3}{2}\le\dfrac{\tau_e}{\Delta}\le-\dfrac{1}{2}\\[2ex]\dfrac{1}{2}-\dfrac{\tau_e}{\Delta}\;;\;\left|\dfrac{\tau_e}{\Delta}\right|\le\dfrac{1}{2}\\[2ex]0\;;\;\dfrac{\tau_e}{\Delta}>\dfrac{1}{2}\end{cases}$$

$$R_{PN_-}\left(\frac{\tau_e}{\Delta}\right)\triangleq\overline{s_{PN}(t-\tau_d)\,s_{PN}\left(t-\hat{\tau}_d-\frac{\Delta}{2}\right)}=R_{PN_+}\left(\frac{\tau_e}{\Delta}-1\right)$$

$$R_{PN_\pm}\left(\frac{\tau_e}{\Delta}\right)=R_{PN_\pm}\left(\frac{\tau_e}{\Delta}+np\right)\quad;\qquad n=\pm1,\pm2,\pm3,\ldots \qquad (4)$$

where $\tau_e\triangleq\tau_d-\hat{\tau}_d$ denotes the delay error.

Letting $H_\ell(s)$ denote the lowpass equivalent of the bandpass filter transfer function H(s) and

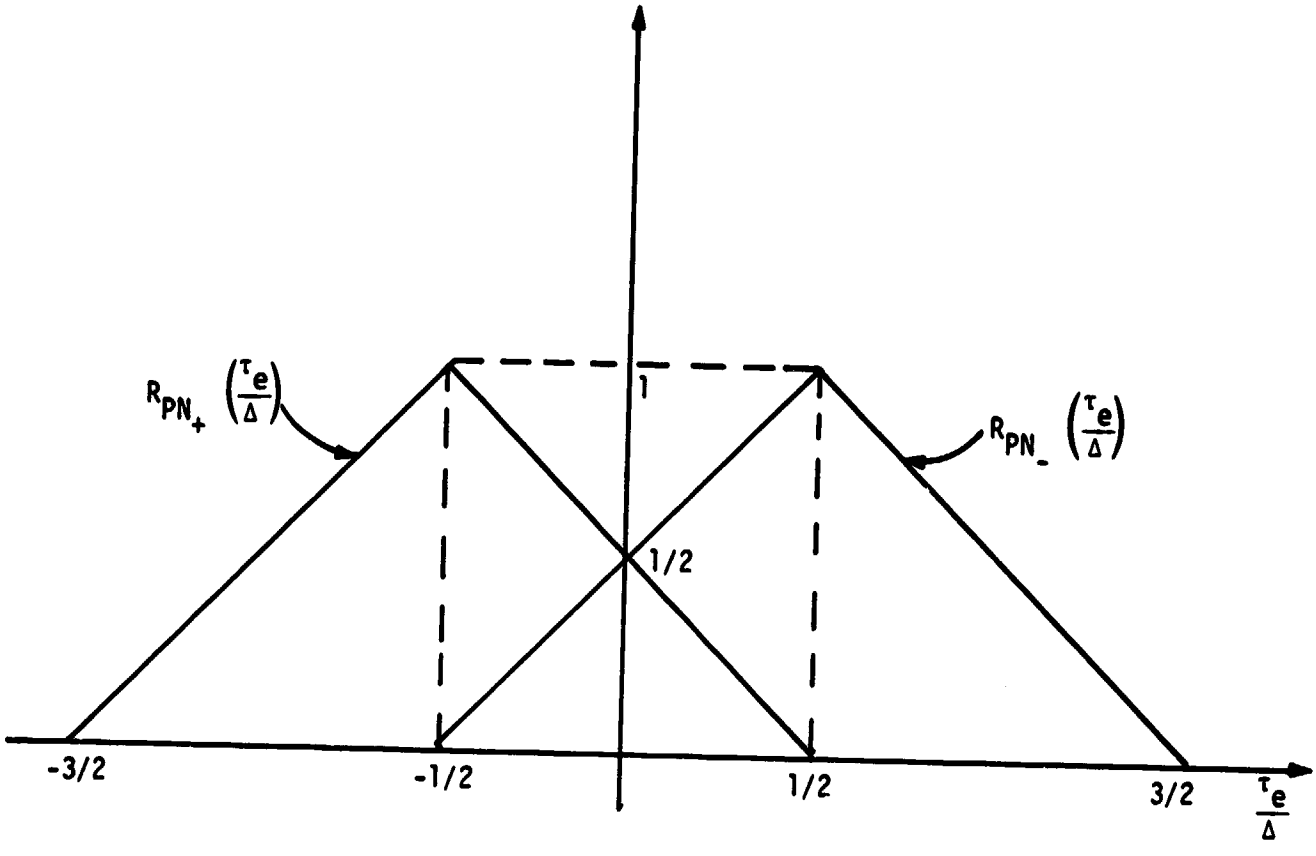

Figure 3. Advanced and Retarded PN Correlation Functions

$$s_{\Delta_\pm}(t-\tau_d, \tau_e) \triangleq s_{PN}(t-\tau_d)\, s_{PN}\left(t-\hat{\tau}_d \pm \frac{\Delta}{2}\right) - \overline{s_{PN}(t-\tau_d)\, s_{PN}\left(t-\hat{\tau}_d \pm \frac{\Delta}{2}\right)}$$

denote the PN code self-noise processes, then combining (2) and (3), we get (see Figure 2)

$$\begin{aligned} y_\pm(t) = {} & \sqrt{2S}\, K_m\, \hat{m}(t-\tau_d)\, R_{PN_\pm}\left(\frac{\tau_e}{\Delta}\right) \cos[\omega_0 t + \theta(t)] \\ & + \sqrt{2S}\, K_m\, \hat{s}_{\Delta_\pm}(t-\tau_d, \tau_e) \cos[\omega_0 t + \theta(t)] \\ & + \sqrt{2}\, K_m\, \hat{N}_{c_\pm}(t) \cos[\omega_0 t + \theta(t)] \\ & - \sqrt{2}\, K_m\, \hat{N}_{s_\pm}(t) \sin[\omega_0 t + \theta(t)] \end{aligned} \tag{5}$$

where*

$$\begin{aligned} \hat{m}(t) &= H_\ell(p)\, m(t) \\ \hat{s}_{\Delta_\pm}(t, \tau_e) &= H_\ell(p) \left[m(t)\, s_{\Delta_\pm}(t, \tau_e)\right] \\ \hat{N}_{c_\pm}(t) &= H_\ell(p) \left[s_{PN}\left(t-\tau_d \pm \frac{\Delta}{2}\right) N_c(t)\right] \\ \hat{N}_{s_\pm}(t) &= H_\ell(p) \left[s_{PN}\left(t-\tau_d \pm \frac{\Delta}{2}\right) N_s(t)\right] . \end{aligned} \tag{6}$$

When the single-sided loop bandwidth B_L is much less than the PN code chip rate $1/\Delta$ (most cases of practical interest), the effect of the PN code self-noise on loop performance can, to a first approximation, be neglected [4]. Thus, ignoring the self-noise term in (5) and the second harmonic terms produced by the square-law envelope detectors, we find that the input to the dither filter is given by

*In what follows, we shall write differential equations in compact form by introducing the Heaviside operator $p \triangleq d/dt$.

$$e'(t) \triangleq y_-^2(t)\, q_1(t) + y_+^2(t)\, q_2(t)$$

$$= SK_m^2\, \hat{m}^2(t-\tau_d)\left[q_1(t)\, R_{PN_-}^2\left(\frac{\tau_e}{\Delta}\right) + q_2(t)\, R_{PN_+}^2\left(\frac{\tau_e}{\Delta}\right)\right]$$

$$+ K_m^2\, n_e'\left(t; \frac{\tau_e}{\Delta}\right) \tag{7}$$

where

$$n_e'\left(t; \frac{\tau_e}{\Delta}\right) = q_1(t)\left[\hat{N}_{c_-}^2(t) + \hat{N}_{s_-}^2(t)\right] + q_2(t)\left[\hat{N}_{c_+}^2(t) + \hat{N}_{s_+}^2(t)\right]$$

$$+ 2\sqrt{S}\,\hat{m}(t-\tau_d)\left\{q_1(t)\, R_{PN_-}\left(\frac{\tau_e}{\Delta}\right)\hat{N}_{c_-}(t)\right.$$

$$\left. + q_2(t)\, R_{PN_+}\left(\frac{\tau_e}{\Delta}\right)\hat{N}_{c_+}(t)\right\} \tag{8}$$

Recognizing that $q_1(t) - q_2(t) = q(t)$ and $q_1(t) + q_2(t) = 1$, (7) simplifies to

$$e'(t) = SK_m^2\, \hat{m}^2(t-\tau_d)\, g'\left(\frac{\tau_e}{\Delta}; t\right) + K_m^2\, n_e'\left(t; \frac{\tau_e}{\Delta}\right) \tag{9}$$

where

$$g'\left(\frac{\tau_e}{\Delta}; t\right) \triangleq q_1(t)\, R_{PN_-}^2\left(\frac{\tau_e}{\Delta}\right) + q_2(t)\, R_{PN_+}^2\left(\frac{\tau_e}{\Delta}\right)$$

$$= \frac{1}{2} f_+\left(\frac{\tau_e}{\Delta}\right) + \frac{q(t)}{2} f_-\left(\frac{\tau_e}{\Delta}\right) \tag{10}$$

with (see Figure 4)

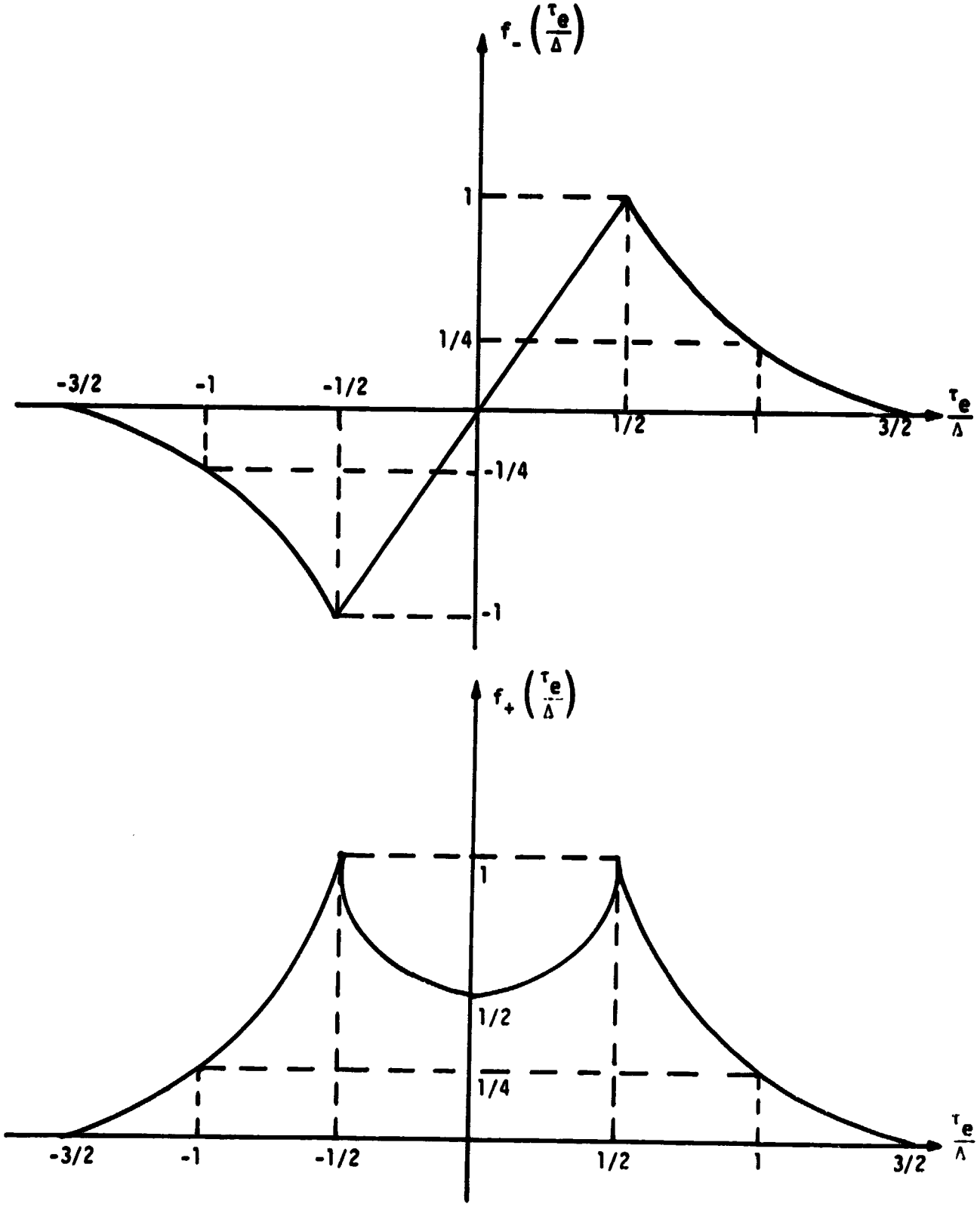

Figure 4. The Difference and Sum of the Squared PN Correlation Functions

$$f_-\left(\frac{\tau_e}{\Delta}\right) \triangleq R^2_{PN_-}\left(\frac{\tau_e}{\Delta}\right) - R^2_{PN_+}\left(\frac{\tau_e}{\Delta}\right) = \begin{cases} 0 \; ; \; \frac{\tau_e}{\Delta} \leq -\frac{3}{2} \\ -\left(\frac{3}{2}+\frac{\tau_e}{\Delta}\right)^2 \; ; \; -\frac{3}{2} \leq \tau_e \leq -\frac{1}{2} \\ 2\,\frac{\tau_e}{\Delta} \; ; \; \left|\frac{\tau_e}{\Delta}\right| \leq \frac{1}{2} \\ \left(\frac{3}{2}-\frac{\tau_e}{\Delta}\right)^2 \; ; \; \frac{1}{2} \leq \frac{\tau_e}{\Delta} \leq \frac{3}{2} \\ 0 \; ; \; \frac{\tau_e}{\Delta} \geq \frac{3}{2} \end{cases}$$

$$f_-\left(\frac{\tau_e}{\Delta}\right) = f_-\left(\frac{\tau_e}{\Delta} + np\right) \quad ; \quad n = \pm 1, \pm 2, \pm 3, \ldots \tag{11}$$

and

$$f_+\left(\frac{\tau_e}{\Delta}\right) \triangleq R^2_{PN_+}\left(\frac{\tau_e}{\Delta}\right) + R^2_{PN_-}\left(\frac{\tau_e}{\Delta}\right) = \begin{cases} 0 \; ; \; \frac{\tau_e}{\Delta} \leq -\frac{3}{2} \\ \left(\frac{3}{2}+\frac{\tau_e}{\Delta}\right)^2 \; ; \; -\frac{3}{2} \leq \frac{\tau_e}{\Delta} \leq -\frac{1}{2} \\ \frac{1}{2} + 2\left(\frac{\tau_e}{\Delta}\right)^2 \; ; \; \left|\frac{\tau_e}{\Delta}\right| \leq \frac{1}{2} \\ \left(\frac{3}{2}-\frac{\tau_e}{\Delta}\right)^2 \; ; \; \frac{1}{2} \leq \frac{\tau_e}{\Delta} \leq \frac{3}{2} \\ 0 \; ; \; \frac{\tau_e}{\Delta} \geq \frac{3}{2} \end{cases}$$

$$f_+\left(\frac{\tau_e}{\Delta}\right) = f_+\left(\frac{\tau_e}{\Delta} + np\right) \quad ; \quad n = \pm 1, \pm 2, \pm 3, \ldots \tag{12}$$

Passing e(t) through the dither filter and post-multiplying by the square-wave dither signal q(t) produces the loop error signal e(t) at the loop filter input, namely,

$$e(t) = q(t)[W(p)\, e'(t)] \; . \tag{13}$$

The instantaneous (normalized) delay estimate $\hat{\tau}_d/\Delta$ of the PN code generator output is related to e(t) by

$$\frac{\hat{\tau}_d}{\Delta} = \frac{K_{VCC}F(p)}{p} e(t) \tag{14}$$

where F(s) is the loop filter transfer function and K_{VCC} is the gain of the voltage-controlled clock which gates the PN code generator. Thus, combining (9), (13) and (14) and letting $K \triangleq K_m^2 K_{VCC}$ denote the loop gain, the stochastic integro-differential equation of operation of Figure 1 becomes

$$\frac{\hat{\tau}_d}{\Delta} = \frac{KF(p)}{p}\left\{q(t)\, W(p)\left[S\hat{m}^2(t-\tau_d)\, g'\left(\frac{\tau_e}{\Delta}\,;\, t\right) + n_e'\left(t\,;\,\frac{\tau_e}{\Delta}\right)\right]\right\} \tag{15}$$

or

$$\frac{\tau_e}{\Delta} = \frac{\tau_d}{\Delta} - \frac{KF(p)}{p}\left\{q(t)\, W(p)\left[S\,\hat{m}^2(t-\tau_d)\, g'\left(\frac{\tau_e}{\Delta}\,;\, t\right) + n_e'\left(t\,;\,\frac{\tau_e}{\Delta}\right)\right]\right\} \tag{16}$$

3.0 EVALUATION OF THE EQUIVALENT LOOP NONLINEARITY

The equivalent loop nonlinearity is defined as the SxS term at the loop filter input and is obtained from (16) as

$$g\left(\frac{\tau_e}{\Delta}\right) \triangleq \overline{< q(t)\, W(p)\left[S\hat{m}^2(t-\tau_d)\, g'\left(\frac{\tau_e}{\Delta}\,;\, t\right)\right] >} \tag{17}$$

where < > denotes time-averaging. Since the modulation m(t) and the dither signal are, in general, noncoherent, the time averaging is separable. Thus, since

$$\overline{< \hat{m}^2(t-\tau_d) >} \triangleq D_m = \int_{-\infty}^{\infty} S_m(f)\left|H_\ell(j2\pi f)\right|^2 df \tag{18}$$

with $S_m(f)$ the power spectral density of m(t), then (17) simplifies to

$$g\left(\frac{\tau_e}{\Delta}\right) = \frac{SD_m}{2} < q(t)W(p)\left[f_+\left(\frac{\tau_e}{\Delta}\right) + q(t)\, f_-\left(\frac{\tau_e}{\Delta}\right)\right] > \tag{19}$$

where we have also made use of (10).

Since the dither filter has zero dc response, then

$$W(p)\, f_+\left(\frac{\tau_e}{\Delta}\right) = 0 \tag{20}$$

Furthermore, letting $\tilde{q}(t)$ denote the dither filtered square-wave, i.e.,

$$\tilde{q}(t) \triangleq W(p)\, q(t) = \int_{-\infty}^{\infty} q(\tau)\, w(t-\tau)\, d\tau \tag{21}$$

then (19) further simplifies to

$$g\left(\frac{\tau_e}{\Delta}\right) = \frac{SD_m}{2} f_-\left(\frac{\tau_e}{\Delta}\right) < q(t)\, \tilde{q}(t) > = \frac{\gamma SD_m}{2} f_-\left(\frac{\tau_e}{\Delta}\right) \tag{22}$$

where [1]

$$\gamma \triangleq < q(t)\, \tilde{q}(t) > = \frac{1}{T_d}\int_0^{T_d} q(t)\, \tilde{q}(t)\, dt \tag{23}$$

is the signal degradation factor due to the dither filter.

If, as in [1], we assume that the dither filter W(s) is such as to pass only the 1, 3, 5, ..., Nth harmonics in q(t), then clearly

$$\tilde{q}(t) = \sum_{n=1,3,\ldots}^{N} \left(\frac{4}{n\pi}\right) \sin \frac{2\pi n}{T_d}\, t \tag{24}$$

and from (23),

$$\gamma = \frac{1}{T_d}\int_0^{T_d}\left(\sum_{n=1,3,\ldots}^{\infty}\left(\frac{4}{n\pi}\right)\sin\frac{2\pi n}{T_d}t\right)\left(\sum_{n=1,3,\ldots}^{N}\left(\frac{4}{n\pi}\right)\sin\frac{2\pi n}{T_d}t\right)dt$$

$$= \frac{8}{\pi^2}\sum_{n=1,3,\ldots}^{N}\frac{1}{n^2} \qquad (25)$$

Also, since

$$\sum_{n=1,3,\ldots}^{\infty}\frac{1}{n^2} = \frac{\pi^2}{8}\ , \qquad (26)$$

then $\lim_{N\to\infty}\gamma = 1$, as it should.

4.0 STATISTICAL CHARACTERIZATION OF THE EQUIVALENT ADDITIVE NOISE

What remains is to determine the power spectral density $N_e(\tau_e/\Delta)$ of the delta-correlated process (see (16))

$$n_e\left(t\ ;\ \tau_e/\Delta\right) \triangleq q(t)\left[W(p)\ n_e'\left(t\ ;\ \tau_e/\Delta\right)\right]\ ,\ \text{i.e.,} \qquad (27)$$

$$N_e\left(\frac{\tau_e}{\Delta}\right) = 2\int_{-\infty}^{\infty} R_e\left(\tau\ ;\ \frac{\tau_e}{\Delta}\right)\,d\tau \qquad (28)$$

where

$$R_e\left(\tau\ ;\ \frac{\tau_e}{\Delta}\right) \triangleq \overline{\left\langle n_e\left(t\ ;\ \frac{\tau_e}{\Delta}\right) n_e\left(t+\tau;\ \frac{\tau_e}{\Delta}\right)\right\rangle} \qquad (29)$$

Substituting (8) into (27) and introducing the simplifying notation

$$\hat{N}_-^{\,2}(t) = \hat{N}_{c_-}^{\,2}(t) + \hat{N}_{s_-}^{\,2}(t)$$

$$\hat{N}_+^{\,2}(t) = \hat{N}_{c_+}^{\,2}(t) + \hat{N}_{s_+}^{\,2}(t) \qquad (30)$$

gives

$$n_e\left(t; \frac{\tau_e}{\Delta}\right) = q(t)\int_{-\infty}^{\infty} q_1(y)\,\hat{N}_-^2(y)\,w(t-y)\,dy + q(t)\int_{-\infty}^{\infty} q_2(y)\,\hat{N}_+^2(y)\,w(t-y)\,dy + 2\sqrt{S}\,R_{PN_-}\left(\frac{\tau_e}{\Delta}\right) q(t)\int_{-\infty}^{\infty} \hat{m}(y-\tau_d)\,q_1(y)\,\hat{N}_{c_-}(y)\,w(t-y)\,dy + 2\sqrt{S}\,R_{PN_+}\left(\frac{\tau_e}{\Delta}\right) q(t)\int_{-\infty}^{\infty} \hat{m}(y-\tau_d)\,q_2(y)\,\hat{N}_{c_+}(y)\,w(t-y)\,dy \quad (31)$$

In order to evaluate the statistical average required in (29), we first note the following:

$$(1)\quad \overline{\hat{N}_-^2(y)\,\hat{N}_-^2(x)} = \overline{\hat{N}_+^2(y)\,\hat{N}_+^2(x)} = 4R_{\hat{N}}^2(x-y) + 4R_{\hat{N}}^2(0)$$

$$(2)\quad \overline{\hat{N}_-^2(y)\,\hat{N}_+^2(x)} = \overline{\hat{N}_+^2(y)\,\hat{N}_-^2(x)} = 4R_{\hat{N}}^2(0)$$

$$(3)\quad \overline{\hat{N}_{c_-}(y)\,\hat{N}_{c_-}(x)} = \overline{\hat{N}_{c_+}(y)\,\hat{N}_{c_+}(x)} = R_{\hat{N}}(x-y) \quad (32)$$

where

$$R_{\hat{N}}(\tau) = \frac{N_0}{2}\int_{-\infty}^{\infty} |H_\ell(j2\pi f)|^2\, e^{j2\pi f\tau}\,df \quad (33)$$

Thus, from (29), (31) and (32), we obtain, after combining like items,

$$R_e\left(\tau; \frac{\tau_e}{\Delta}\right) = \langle q(t)q(t+\tau)\int_{-\infty}^{\infty}\int_{-\infty}^{\infty} [q_1(y)q_1(x) + q_2(y)q_2(x)]\,w(t-y)w(t+\tau-x) \times 4R_{\hat{N}}^2(x-y)\,dxdy\rangle$$
$$+ \langle q(t)q(t+\tau)\left(4R_{\hat{N}}^2(0)\right)\int_{-\infty}^{\infty}\int_{-\infty}^{\infty} [q_1(y)q_1(x) + q_2(y)q_2(x) + q_1(y)q_2(x) + q_2(y)q_1(x)] \times w(t-y)\,w(t+\tau-x)\,dxdy\rangle$$
$$+ 4S\,\langle q(t)q(t+\tau)\int_{-\infty}^{\infty}\int_{-\infty}^{\infty}\left[R_{PN_-}^2\left(\frac{\tau_e}{\Delta}\right)q_1(y)q_1(x) + R_{PN_+}^2\left(\frac{\tau_e}{\Delta}\right)q_2(y)q_2(x)\right] \times R_{\hat{m}}(x-y)\,R_{\hat{N}}(x-y)\,w(t-y)\,w(t+\tau-x)\,dxdy\rangle \quad (34)$$

where

$$R_{\hat{m}}(\tau) = \int_{-\infty}^{\infty} S_m(f)\ |H_\ell(j2\pi f)|^2\ e^{j2\pi f\tau}\ df \tag{35}$$

In order to readily evaluate (34), we must introduce some simplifying assumptions. Since $1/T_d << B_i$, where B_i denotes the two-sided noise bandwidth of the equivalent lowpass filter $H_\ell(s)$, i.e.,

$$B_i = \int_{-\infty}^{\infty} |H_\ell(j2\pi f)|^2\ df \tag{36}$$

and since the data rate of the modulation m(t) is on the order of B_i, then insofar as the integrations in (34) are concerned, we can approximate $R_{\hat{N}}^2(\tau)$ and $R_{\hat{m}}(\tau)\ R_{\hat{N}}(\tau)$ by appropriately scaled delta functions, namely,

$$R_{\hat{N}}^2(\tau) = \frac{N_*}{2}\ \delta(\tau)$$

$$R_{\hat{m}}(\tau)\ R_{\hat{N}}(\tau) = \frac{N_{**}}{2}\ \delta(\tau) \tag{37}$$

where, from (33) and (35),

$$\frac{N_*}{2} = \int_{-\infty}^{\infty} R_{\hat{N}}^2(\tau)d\tau = \left(\frac{N_0}{2}\right)^2 \int_{-\infty}^{\infty} |H_\ell(j2\pi f)|^4\ df$$

$$\frac{N_{**}}{2} = \int_{-\infty}^{\infty} R_{\hat{N}}(\tau)R_{\hat{m}}(\tau)d\tau = \frac{N_0}{2} \int_{-\infty}^{\infty} S_m(f)|H_\ell(j2\pi f)|^4\ df \tag{38}$$

Substituting (37) and the definition of $\tilde{q}(t)$ in (21) into (34) results in

$$R_e\left(\tau;\frac{\tau_e}{\Delta}\right) = 2N_* < q(t)q(t+\tau)\int_{-\infty}^{\infty}\left[q_1^2(y)+q_2^2(y)\right] w(t-y)\, w(t+\tau-y)dy > + 4R_N^2(0)$$

$$x < q(t)q(t+\tau)\left[\tilde{q}_1(t)\tilde{q}_1(t+\tau)+\tilde{q}_2(t)\tilde{q}_2(t+\tau)+\tilde{q}_1(t)\tilde{q}_2(t+\tau)\right.$$

$$\left.+\tilde{q}_2(t)\tilde{q}_1(t+\tau)\right] >$$

$$+ 2SN_{**} < q(t)q(t+\tau)\int_{-\infty}^{\infty}\left[R_{PN_-}^2\left(\frac{\tau_e}{\Delta}\right) q_1^2(y) + R_{PN_+}^2\left(\frac{\tau_e}{\Delta}\right) q_2^2(y)\right]$$

$$x\, w(t-y)\, w(t+\tau-y)\, dy > \qquad (39)$$

Furthermore, since (see Figure 2) $q_i^2(y) = q_i(y)$; $i = 1,2$ and

$$\tilde{q}_1(t)\tilde{q}_1(t+\tau) + \tilde{q}_2(t)\tilde{q}_2(t+\tau)$$

$$+ \tilde{q}_1(t)\tilde{q}_2(t+\tau) + \tilde{q}_2(t)\tilde{q}_1(t+\tau) = \left[\tilde{q}_1(t)+\tilde{q}_2(t)\right]\left[\tilde{q}_1(t+\tau)+\tilde{q}_2(t+\tau)\right]$$

$$= \left[\frac{\tilde{q}(t)}{2} - \frac{\tilde{q}(t)}{2}\right]\left[\frac{\tilde{q}(t+\tau)}{2} - \frac{\tilde{q}(t+\tau)}{2}\right]$$

$$= 0 \qquad (40)$$

then (39) simplifies still further to

$$R_e\left(\tau;\frac{\tau_e}{\Delta}\right) = 2\left[N_* + SN_{**}\, R_{PN_-}^2\left(\frac{\tau_e}{\Delta}\right)\right] < q(t)q(t+\tau)\int_{-\infty}^{\infty} q_1(y)w(t-y)w(t+\tau-y)dy >$$

$$+ 2\left[N_* + SN_{**}\, R_{PN_+}^2\left(\frac{\tau_e}{\Delta}\right)\right] < q(t)q(t+\tau)\int_{-\infty}^{\infty} q_2(y)w(t-y)w(t+\tau-y)dy > \qquad (41)$$

To get the equivalent noise spectral density $N_e(\tau_e/\Delta)$ of (28), we must now integrate (41) on τ between $-\infty$ and ∞. Performing this integration on the first term in (41) requires evaluation of

$$< q(t)\int_{-\infty}^{\infty}\left[\int_{-\infty}^{\infty} q(t+\tau)\, w(t+\tau-y)d\tau\right] q_1(y)\, w(t-y)\, dy > \qquad (42)$$

From the definition of $\tilde{q}(t)$ in (21), the inner-bracketed quantity in (42) is recognized to be $-\tilde{q}(-y)$. Thus, (42) becomes

$$< q(t)\int_{-\infty}^{\infty}[-\tilde{q}(-y)]\, q_1(y)\, w(t-y)\, dy > \qquad (43)$$

Assuming, as before, that the dither filter W(s) is such as to pass all odd harmonics of $\tilde{q}(t)$ (or $q_1(t)$ or $q_2(t)$) up through the Nth, then, from (24), we have that

$$-\tilde{q}(-t) = \tilde{q}(t) \tag{44}$$

and

$$-\tilde{q}(-y)q_1(y) = \tilde{q}(t)\left[\frac{1+q(y)}{2}\right] = \frac{1}{2}\tilde{q}(y) + \frac{1}{2}\tilde{q}(y)q(y) \tag{45}$$

The integral required in (43) is the result of passing (45) through the dither filter. Clearly, the first term of (45) passes through unchanged. The second term of (45) contains only even harmonics of $1/T_d$ which, when passed through the dither filter, retains all of these even harmonics up through the Nth, but not including zero (since the filter has zero dc response). Finally, multiplying by q(t) and time averaging gives the result required in (43). For the dither-filtered second term in (45), the above multiplication by q(t) will again produce odd harmonics of $1/T_d$, all of whose time average is zero. Thus, this term does not contribute to (43). The first term of (45), then, yields the only contribution, namely,

$$< \tilde{q}(t) \int_{-\infty}^{\infty} [-\tilde{q}(-y)]\, q_1(y)\, w(t-y)dy > = < \frac{1}{2}\tilde{q}(t)q(t) > = \frac{\gamma}{2} \tag{46}$$

where γ is defined in (23). Substituting (46) into the first term of (41), integrated on τ between $-\infty$ and ∞, gives the first component of $N_e(\tau_e/\Delta)$, namely,

$$N_{e_1}\left(\frac{\tau_e}{\Delta}\right) = 4\left[N_* + SN_{**}\, R_{PN\_}{}^2\left(\frac{\tau_e}{\Delta}\right)\right]\left(\frac{\gamma}{2}\right) \tag{47}$$

The second term of (41), when integrated on τ between $-\infty$ and ∞ requires evaluation of (43) with $q_1(y)$ replaced by $q_2(y)$. Since, however, $q_2(y) = (1-q(y))/2$, then the result of (45) is again valid if the second

term is subtracted rather than added. However, since, as shown above, this second term ultimately produces no contribution to the desired result, its sign is unimportant and, thus, the component of $N_e(\tau_e/\Delta)$ due to the second term in (41) is also given by an expression similar to (47), namely,

$$N_{e_2}\left(\frac{\tau_e}{\Delta}\right) = 4\left[N_* + SN_{**}\, R_{PN_+}{}^2\left(\frac{\tau_e}{\Delta}\right)\right]\left(\frac{\gamma}{2}\right) \tag{48}$$

Finally, adding (47) and (48) and making use of (12) gives the desired result

$$N_e\left(\frac{\tau_e}{\Delta}\right) = \gamma\left[4N_* + 2SN_{**}\, f_+\left(\frac{\tau_e}{\Delta}\right)\right] \tag{49}$$

The result of (49) can be expressed in terms of previously defined [2] notation for a tau-dither loop without the dither filter. In particular, letting

$$K_L = \frac{\int_{-\infty}^{\infty} |H_\ell(j2\pi f)|^4\, df}{\int_{-\infty}^{\infty} |H_\ell(j2\pi f)|^2\, df}$$

$$K_D = \frac{\int_{-\infty}^{\infty} |S_m(f)|H_\ell(j2\pi f)|^4\, df}{\int_{-\infty}^{\infty} S_m(f)|H_\ell(j2\pi f)|^2\, df} \tag{50}$$

then, together with (18) and (36), the noise spectral densities N_* and N_{**} of (38) become

$$N_* = \frac{N_0{}^2}{2} B_i\, K_L$$

$$N_{**} = N_0 D_m K_D \tag{51}$$

Substituting (51) into (49) gives

$$N_e\left(\frac{\tau_e}{\Delta}\right) = 2\gamma S N_0 D_m\left[\frac{K_L}{\rho_1 D_m} + f_+\left(\frac{\tau_e}{\Delta}\right) K_D\right] \tag{52}$$

where

$$\rho_1 = \frac{S}{N_0 B_1} \tag{53}$$

denotes the signal-to-noise ratio in this bandpass bandwidth.

5.0 LINEAR ANALYSIS OF TRACKING PERFORMANCE

When the equivalent loop signal-to-noise ratio is large, the tracking performance of the tau-dither loop can be determined by linearizing $g(\tau_e/\Delta)$ of (22). In particular, since $f_-(\tau_e/\Delta) = 2\tau_e/\Delta$ in its linear region, then from (22)

$$g\left(\frac{\tau_e}{\Delta}\right) \approx \gamma S D_m\left(\frac{\tau_e}{\Delta}\right) . \tag{54}$$

Under this assumption and further assuming that $\dot{\tau}_d = 0$, one can write down, by inspection of (16), an expression for the mean-squared tracking jitter, viz.,

$$\left(\frac{\sigma_t}{\Delta}\right)^2 = \frac{\overline{N_e\left(\frac{\tau_e}{\Delta}\right) B_L}}{(\gamma S D_m)^2} , \tag{55}$$

which, upon substitution of (52) and (12), becomes

$$\left(\frac{\sigma_t}{\Delta}\right)^2 = \frac{1}{\gamma\rho}\left\{\frac{K_D + 2\dfrac{K_L}{\rho_1 D_m}}{D_m\left[1 - \dfrac{4}{\rho}\left(\dfrac{K_D}{D_m}\right)\right]}\right\} ; \quad \rho = \frac{S}{N_0 B_L} \tag{56}$$

or, to a first approximation,

$$\left(\frac{\sigma_t}{\Delta}\right)^2 = \frac{1}{\gamma\rho}\left\{\frac{K_D + 2\dfrac{K_L}{\rho_i D_m}}{D_m}\right\} = \frac{1}{\gamma\rho\mathcal{L}_L} \tag{57}$$

where $\mathcal{L}_L$ is the "squaring loss" of the tau-dither loop and is given by

$$\mathcal{L}_L = \frac{D_m}{K_D + \dfrac{2K_L}{\rho_i D_m}} \tag{58}$$

The result in (57), when compared with the corresponding result* in [2] for the tau-dither loop without dither filter, clearly shows that the <u>effective signal-to-noise ratio degradation due to the addition of the dither filter is a factor equal to γ</u>. A similar result is obtained in (1) except that, there, the signal-to-noise ratio degradation factor is shown to be γ^2. The discrepancy stems from the fact that, in [1], the dither filter effect on the SxN and NxN components was ignored.

As an example, suppose that the dither filter passes only the first and third harmonics of q(t). Then, letting N = 3 in (25), we get

$$\gamma = \frac{8}{\pi^2}\left(1 + \frac{1}{9}\right) = \frac{80}{9\pi^2} \tag{59}$$

or

$$\frac{1}{\gamma} = \frac{9\pi^2}{80} = 1.11 \tag{60}$$

Thus, the dither filter causes an increase in mean-square timing jitter of 11%. Based on the results of [1], the jitter increase factor would be $1/\gamma^2 = 1.23$, or an increase of 23% relative to that of the loop without a dither filter.

---

*When the assumption of large $B_i T_d$ is imposed on the results in [2], K_D' and K_L' achieve their upper bounds as in (58) of [2], and (56) of [2] reduces to (57) of above without the factor $1/\gamma$.

REFERENCES

1. Holmes, J. K., "Time-Shared Code Loop Performance Including an Additional Filter," TRW Interoffice Correspondence 7324.1-053-79, April 26, 1979.

2. Simon, M. K., "Noncoherent Pseudonoise Code Tracking Performance of Spread Spectrum Receivers," IEEE Transactions on Communications, Vol. COM-25, No. 3, March 1977, pp. 327-345.

3. Hartmann, H. P., "Analysis of a Dithering Loop for PN Code Tracking of Binary Signals," IEEE Transactions on Space Electronics and Telemetry, Vol. SET-9, No. 1, March 1963, pp. 1-8.